

**The Development of Chemical Tools to Study Cell-Cell Communication and
Virulence in Gram-Positive Bacteria**

By
Korbin H. J. West

A dissertation submitted in partial fulfillment of
the degree requirements for the degree of

Doctor of Philosophy
(Chemistry)

at the
UNIVERSITY OF WISCONSIN-MADISON
2021

Date of final oral examination: May 27, 2021

The dissertation is approved by the following members of the Final Oral Committee:

Helen E. Blackwell, Professor, Chemistry

Samuel H. Gellman, Professor, Chemistry

David M. Lynn, Professor, Chemical and Biological Engineering

Andrew R. Buller, Assistant Professor, Chemistry

*A day once dawned, and it was beautiful
A day once dawned from the ground,
Then the night she fell
And the air was beautiful,
The night she fell all around.*

*So look see the days
The endless coloured ways
And go play the game that you learnt
From the morning.*

*And now we rise
And we are everywhere,
And now we rise from the ground,
And see she flies
And she is everywhere,
See she flies all round,
So look see the sights
The endless summer nights
And go play the game that you learnt
From the morning.*

–Nick Drake

Reproduced by permission of Bryter Music / Blue Raincoat Music

The Development of Chemical Tools to Study Cell-Cell Communication and Virulence in Gram-Positive Bacteria

Korbin H. J. West

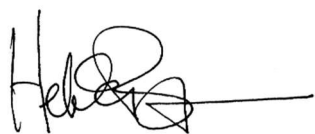
Under the supervision of Professor Helen E. Blackwell

At the University of Wisconsin–Madison

Abstract

Over the past 40 years, quorum sensing (QS)—a type of chemical communication used by common bacteria—has been shown to play an increasingly important role in bacterial communities. QS mediates a wide array of bacterial group behaviors such as initiating infection, mediating symbiosis, and adapting to environmental stimuli. A common QS pathway used by many Gram-positive bacteria is the accessory gene regulator (*agr*) system, which has been recognized as a key regulator of virulence in several clinically relevant pathogens. Activation of *agr* QS and its downstream regulation is dependent upon the production and reception of a peptide signal known as the autoinducing peptide (AIP). Interfering with this signaling process using non-native chemical modulators that target the various components of *agr* represents an approach to attenuate *agr* QS activity and alter associated bacterial phenotypes. There currently is a dearth of potent and efficacious chemical modulators for the majority of *agr* systems. Moreover, many of these synthetic ligands have been only examined *in vitro*, and many questions remain about the modes by which bacteria use *agr* QS *in vivo* and the methods by which to best leverage these chemical modulators to reduce bacterial virulence.

In this thesis, I describe my work to create, develop, and apply chemical tools to investigate *agr* QS in three important pathogens. I performed structure-activity relationship (SAR) analyses on the native AIP signal of *Listeria monocytogenes* and uncovered the most potent *agr* agonists and antagonists of its *agr* system to date. These modulators can strongly promote or inhibit biofilm formation, a critical virulence phenotype in *L. monocytogenes*, demonstrating the utility of chemical control of *agr* activity. Structural and SAR studies of the AIPs from *Staphylococcus epidermidis* revealed new structural insights into modulator potency and efficacy, as well as enabling the development of the first agonists capable of activating multiple AgrC receptors. Lastly, I characterized degradable polymeric materials loaded with potent *Staphylococcus aureus agr* antagonists and demonstrated their ability to attenuate infection in a murine model. The studies presented herein represent significant advances towards developing chemical tools to probe and control *agr* QS in important Gram-positive bacteria.



Helen E. Blackwell, Ph.D.

Acknowledgements

When I was first starting my venture into graduate school, I was prepared for a lot of hard work over many years. It is a clear expectation that coming into a PhD program you'll spend a lot of time and effort trying to solve difficult problems, failing over and over again, and maybe succeeding every now and then. Looking back over my time though, I never would have expected that I would enjoy the journey as much as I did. There really is no substitute for the "eureka!" moment that you get when, after many months or years of work on a project, you finally uncover a major missing piece of your project or successfully show your compound works the way you want it to. That said, I know these moments are possible only because of the phenomenal network of friends, co-workers, collaborators, and mentors that have supported me during my time in graduate school.

I first want to thank the many wonderful lab members I have worked with over the years—each has had a positive impact on my time here. The Blackwell lab has consistently been filled with intelligent, talented, and compassionate scientists, and moreover folks who make coming to work each day fun. Graduate school would have been much tougher without the positive and supportive atmosphere you all bring to the lab. While I know it is a running gag in the lab that I'm a robot who likes nothing, I can now openly admit that I count many of you as close friends. I dearly miss the times where we could enjoy a Friday night happy hour at the Library, have group meals at restaurants, and general goofing off when outside of lab.

Even though our time together was rather short, I'm incredibly appreciative of Matt O'Reilly, Michelle Boursier, and Josh Combs for welcoming me into their office as

a new member and showing me that doing top-notch science doesn't mean you have to be boring. I also want to thank Tian Yang and Joseph Vasquez, who taught me so much in my early years and encouraged me when things weren't always going smoothly at the beginning of my projects. I'm grateful to other senior members like Betty Slinger, Kayleigh Nyffeler, Daniel Manson, and Matt Styles who, despite working on very different systems, were always willing to help troubleshoot when I had problems and offer creative ideas and solutions for my projects.

To the junior students I've had the pleasure of working with—Cassie Doody, Maggie McEwan, Tom Polaske, Kate Zhao, Emma Eisenbraun, Emma Santa, Jordan York, Lupe Aguirre-Figueroa, and the many undergrads we've had over the years—it's been so wonderful to see you all develop as scientists. You'd be surprised how much senior students learn from junior members. So many times, one of you asked me a question or said something that made me reconsider my perspective on how something fundamentally works. In the same vein, I want to thank those I have personally worked close with and mentored: Stella Ma, Emma Eisenbraun, Wenqi Shen, and Erin Fehrman. I can verify that it is true that you learn so much just by trying to teach someone else. It has been an immensely rewarding experience seeing you all grow into independent researchers, and I am eagerly looking forward to what you achieve in the future.

In addition to my own lab members, I've also had many great collaborators that have been fundamental to my projects. I first want to thank Dr. Dan Pensinger and Prof. JD Sauer for teaching me so much about *Listeria* biology, as well as Dr. Trisha Tucholski and Prof. Ying Ge for helping identify the native *Listeria* AIP. The help I

received for you four helped me set the foundation that the rest of the *Listeria* project was built on. I also want to thank Curran Gahan and Prof. David Lynn for their help in creating and characterizing different compound-loaded materials. I've learned so much about materials chemistry through this collaboration and I think our collaboration will help push the envelope of practical applications of quorum sensing. Similarly, I want to thank Patricia Kierski, Dr. Diego Calderon, Prof. Charles Czuprynski, and Prof. Jonathan McAnulty for their help in teaching me how to test our compounds and materials in mice. I had absolutely no experience with *in vivo* models, and through their patience, guidance, and insights I have become so much more aware of the power and complexity of *in vivo* models. I am also grateful to my committee members, Prof. Sam Gellman, Prof. David Lynn, and Prof. Andrew Buller, for their critical feedback on my proposals and presentations, thoughtful and encouraging discussions about results and possible next steps, and for constantly challenging me to be a better scientist.

More than anyone else on campus, though, I have to thank my advisor Prof. Helen Blackwell. Despite not having any relevant synthetic or microbiology research background, she welcomed me into her lab and gave me the opportunity to show her what I could do. Her support allowed me to gain innumerable skills and pursue groundbreaking projects, and her wealth of knowledge could always point me towards success when I was unsure how to interpret results or doubting my path forward. Most of all, I am grateful for Helen's ability to foster a culture of incredibly high standards in her students while simultaneously encouraging a healthy relationship between work and life. Her mentorship these past five years has had a major influence on the scientist I am today.

Finally, I must thank those in my life outside of UW–Madison. My closest friends from my undergraduate days—Tom Blaich, Cameron Stepler, Lane Owen, and Tim Livolsi—have been steadfast allies since we’ve met many years ago and have always been there when I needed them. My family has always supported my academic pursuits, especially my grandparents. They all have entertained my (surely annoying) thousands of questions, and I thank them for buying me books chock-full of random facts, driving me to my many extra-curricular activities, and just giving me the freedom to follow my interests. Lastly, I must thank my wife Liv. I’m very grateful that when we first started dating, you were willing to join me wherever I chose for graduate school. I couldn’t imagine doing this thing without you. Thank you for your constant love and support when things were going well in lab and when they weren’t, and for making the “life” part in “work/life balance” worth it. I’m so excited to see what life has in store for us next.

Table of Contents

Abstract.....	ii
Acknowledgements.....	iv
Table of Contents.....	viii
List of Figures, Tables, Schemes, and Equations.....	xiii
Chapter 1: Characterization, Development, and Application of Chemical Tools to Probe the <i>agr</i> Quorum Sensing System.....	1
Abstract.....	2
1.1 Introduction	3
1.1.1 <i>Brief introduction of bacterial quorum sensing</i>	3
1.1.2 <i>Behaviors under quorum sensing control</i>	5
1.2 Common Gram-positive Quorum Sensing Systems.....	9
1.2.1 <i>Overview of Gram-positive quorum sensing</i>	9
1.2.2 <i>The <i>agr</i> QS system</i>	10
1.2.3 <i>The ComQXPA and ComABCDE QS systems</i>	12
1.2.4 <i>The RNPP QS systems</i>	13
1.3 The <i>agr</i> QS System in Detail.....	14
1.3.1 <i>Brief history of the <i>agr</i> QS system</i>	14
1.3.2 <i>The AgrD propeptide</i>	15
1.3.3 <i>AgrB processing of AgrD</i>	17
1.3.4 <i>Additional AgrD processing to produce the mature AIP</i>	20
1.3.5 <i>AgrC receptor sensing the AIP signal</i>	22
1.3.6 <i>AgrA interactions with DNA</i>	27
1.4 Chemical Control of the <i>agr</i> System.....	29
1.4.1 <i>Chemical modulators as tools to probe QS</i>	29
1.4.2 <i>AIP biosynthesis modulators</i>	30
1.4.3 <i>Targeted AIP sequestration and degradation</i>	32
1.4.4 <i>AgrC receptor modulators</i>	33
1.4.5 <i>AgrA modulators</i>	39
1.4.6 <i>Looking ahead: remaining questions about the role of <i>agr</i> QS in vivo and the modes by which chemical modulators can be applied to probe complex systems</i>	41
1.5 Thesis Outline	44
1.5.1 <i>Dissertation overview</i>	44
1.5.2 <i>Summary of Chapter 2: A Native Autoinducing Peptide Signal Reveals Highly Efficacious Inhibitors and Activators of <i>Listeria monocytogenes</i> Quorum Sensing and Biofilm Formation</i>	45
1.5.3 <i>Summary of Chapter 3: Conformational Switch to a β-turn in a Staphylococcal Quorum Sensing Signal Peptide Causes a Dramatic Increase in Potency</i>	46
1.5.4 <i>Summary of Chapter 4: Non-Native Peptides Capable of Pan-Activating the <i>agr</i> Quorum Sensing System across Multiple Specificity Groups of <i>Staphylococcus epidermidis</i></i>	47

1.5.5	<i>Summary of Chapter 5: Sustained Release of a Synthetic Autoinducing Peptide Mimetic Strongly Attenuates MRSA Infections In Vivo</i>	48
1.5.6	<i>Summary of Chapter 6: Future Directions</i>	49
1.5.7	<i>Summary of Appendix I: Chemical Control of Quorum Sensing in E. coli: Identification of Small Molecule Modulators of SdiA and Mechanistic Characterization of a Covalent Inhibitor</i>	50
1.6	References.....	51

Chapter 2: A Native Autoinducing Peptide Reveals Highly Efficacious Inhibitors and Activators of *Listeria monocytogenes* Quorum Sensing and Biofilm

Formation	70
Abstract.....	71
2.1 Introduction	73
2.2 Results and Discussion	79
2.2.1 <i>Synthesis confirms the native L. monocytogenes AIP structure</i>	79
2.2.2 <i>Construction of L. monocytogenes agr-dependent GFP reporter strains</i>	80
2.2.3 <i>L. monocytogenes agr is insensitive to other native AIPs and closely related analogs</i>	82
2.2.4 <i>Thioester AIPs have improved potency over homodetic peptide</i>	84
2.2.5 <i>Altering the AIP exocyclic tail length causes only minor effects on activity</i>	86
2.2.6 <i>Alanine and D-amino acid scans reveal general SARs for native AIP</i>	87
2.2.7 <i>Design and biological evaluation of first-generation AIP analogs</i>	90
2.2.8 <i>Combinatorial substitutions reveal a route to antagonism</i>	94
2.2.9 <i>Chemical control of biofilm formation with agr modulators</i>	98
2.3 Summary and Conclusions	99
2.4 Materials and Methods.....	101
2.4.1 <i>Reagents, strains, and general methods</i>	101
2.4.2 <i>Peptide synthesis</i>	102
2.4.3 <i>Fluorescence reporter assay protocol</i>	102
2.4.4 <i>Biofilm assay protocol</i>	103
2.5 Supplemental Information	105
2.5.1 <i>Additional experimental procedures</i>	105
2.5.2 <i>LC-MS/MS analysis of bacterial supernatant</i>	113
2.5.3 <i>The S→N acyl shift of the 5-mer thioester</i>	114
2.5.4 <i>Non-cognate AIP activity in L. monocytogenes agr reporter strains</i>	116
2.5.5 <i>Dose response activity data of L. monocytogenes AIP analogs</i>	119
2.5.6 <i>Lead L. monocytogenes AIP analogs and native AIP assayed in S. aureus agr-I reporter assays</i>	123
2.5.7 <i>Bacterial strains, plasmids, and primers</i>	124
2.5.8 <i>Dose response curves of peptides</i>	125
2.5.9 <i>Peptide HPLC and MS characterization</i>	143
2.6 Acknowledgements	162
2.7 References.....	163

Chapter 3: Conformational Switch to a β-turn in a Staphylococcal Quorum Sensing Signal Peptide Causes a Dramatic Increase in Potency	170
Abstract.....	171
3.1 Introduction	173
3.2 Results and Discussion.....	177
3.2.1 <i>Selection of peptides for structural analyses</i>	177
3.2.2 <i>NMR analyses</i>	179
3.2.3 <i>Structural comparison of AIP-I to the antagonist t-AIP-I</i>	179
3.2.4 <i>Structural comparison of AIP-I to the antagonist AIP-I V3A</i>	181
3.2.5 <i>Structural comparison of AIP-I to agonists with increased potency</i>	183
3.2.6 <i>Structural comparison of AIP-I to the antagonist AAA</i>	187
3.2.7 <i>Structures of S. epidermidis AIP-II and AIP-III</i>	188
3.2.8 <i>Comparison of the most potent AgrC-I agonist and antagonist</i>	190
3.2.9 <i>Exploration of the β-turn motif through new analogs</i>	192
3.3 Summary and Conclusions	197
3.4 Supplemental Information	201
3.4.1 <i>Experimental procedures</i>	201
3.4.2 <i>NMR spectra for 3-D solution-phase structures</i>	209
3.4.3 <i>3J coupling constants for 3-D solution-phase structures</i>	236
3.4.4 <i>Chemical shift assignment for 3-D solution-phase structures</i>	239
3.4.5 <i>ROE constraint statistics</i>	242
3.4.6 <i>Additional images of structure ensembles</i>	247
3.4.7 <i>Validation using MolProbity</i>	252
3.4.8 <i>MS and analytical HPLC data for β-turn modifying analogs</i>	260
3.4.9 <i>AgrC-I dose-response assay data for new analogs</i>	264
3.4.10 <i>NMR spectra for select β-turn modifying analogs</i>	267
3.4.11 <i>Chemical shift assignments for select β-turn modifying analogs</i>	276
3.4.12 <i>TALOS-N predictions for AIP-I and AIP-I D1AS6A</i>	278
3.4.13 <i>Comparative chemical shift analysis for select β-turn modifying analogs</i>	280
3.5 Acknowledgements	284
3.6 References.....	285

Chapter 4: Non-Native Peptides Capable of Pan-Activating the agr Quorum Sensing System across Multiple Specificity Groups of Staphylococcus epidermidis	292
Abstract.....	293
4.1 Introduction	295
4.2 Results and Discussion.....	299
4.2.1 <i>Overview of methods and analysis of reported SARs for agr agonism by group-I S. epidermidis AIP</i>	299
4.2.2 <i>SARs for agr agonism by group-II and group-III S. epidermidis AIPs</i>	304
4.2.3 <i>Design and biological characterization of multi-group agonist scaffolds</i>	308
4.2.4 <i>Multi-group agonists promote PSM production in S. epidermidis</i> ...	311

4.2.5	<i>Design and characterization of second-generation multi-group agonist scaffolds</i>	312
4.3	Summary and Conclusions	314
4.4	Supplemental Information	316
4.4.1	<i>Experimental procedures and methods</i>	316
4.4.2	<i>Activity data for AIP-II analogs in group-II and group-III reporters</i> ..	321
4.4.3	<i>Chimeric peptide scaffolds and activity data</i>	330
4.4.4	<i>S. epidermidis PSM production with multi-group agonist Cmr1 S7A</i>	355
4.4.5	<i>HPLC and MS characterization of AIP-II analogs, AIP-III analogs, chimera analogs, and PSMs</i>	356
4.5	Acknowledgements	379
4.6	References.....	380
Chapter 5: Sustained Release of a Synthetic Autoinducing Peptide Mimetic Strongly Attenuates MRSA Infections <i>In Vivo</i>		385
	Abstract.....	386
5.1	Introduction	387
5.2	Results and Discussion.....	389
5.2.1	<i>Ex vivo screening reveals two stable and highly potent synthetic inhibitors of agr</i>	389
5.2.2	<i>Bolus delivery of tr AIP-III D2A substantially reduces abscess formation in a murine dermonecrosis model</i>	394
5.2.3	<i>tr AIP-III D2A attenuates infection when released from PLG microparticles</i>	396
5.3	Summary and Conclusions	402
5.4	Materials and Methods.....	404
5.4.1	<i>Reagents, strains, and general methods</i>	404
5.4.2	<i>Instrumentation and related considerations</i>	404
5.4.3	<i>Fluorescence-based bacterial reporter assay</i>	405
5.4.4	<i>Ex vivo tissue sequestration assay</i>	405
5.4.5	<i>Fabrication of tr AIP-III D2A-loaded PLG microparticles</i>	406
5.4.6	<i>Characterization of peptide loading of PLG microparticles</i>	407
5.4.7	<i>Characterization of peptide-loaded PLG microparticle release profiles</i>	407
5.4.8	<i>Murine abscess infection model</i>	407
5.5	Supporting Information	409
5.5.1	<i>Additional experiments and figures related to in vitro and ex vivo compound analysis</i>	409
5.5.2	<i>Mouse abscess data for wild-type S. aureus lab strain and Δagr strain</i>	413
5.5.3	<i>Additional microparticle characterization</i>	414
5.5.4	<i>Images of all Day 7 lesions from mice in abscess experiments</i>	419
5.6	Acknowledgements	422
5.7	References.....	423
Chapter 6: Future Directions		429
	Abstract.....	430

6.1	Introduction	431
6.2	Projects Focused on <i>L. monocytogenes</i>	431
6.2.1	<i>Continued AIP SAR studies in L. monocytogenes</i>	431
6.2.2	<i>Utilizing L. monocytogenes agr modulators to examine virulence phenotypes in culture</i>	432
6.2.3	<i>Incorporating L. monocytogenes agr antagonists into materials to reduce biofilm on surfaces</i>	433
6.3	Projects Focused on <i>S. epidermidis</i>	435
6.3.1	<i>Approaches to improve efficacy of multi-group agonists in S. epidermidis</i>	435
6.4	Projects to Explore Modulation of <i>agr</i> Activity <i>In Vivo</i>	436
6.4.1	<i>Screening agr modulators ex vivo to characterize key structural features for sequestration/degradation</i>	436
6.4.2	<i>Sustained release of agr activators to reduce Staphylococcal biofilms in a murine implant infection model</i>	437
6.5	Projects to explore new approaches to probe <i>agr</i> QS.....	438
6.5.1	<i>Incorporation of photoreactive amino acids to identify AgrD protein partners and ligand-binding sites of AgrC</i>	438
6.5.2	<i>Using AIP intein technology to rapidly generate new agr modulators</i>	439
6.6	References.....	440

Appendix I: Chemical Control of Quorum Sensing in *E. coli*: Identification of Small Molecule Modulators of SdiA and Mechanistic Characterization of a Covalent Inhibitor..... 442

	Abstract.....	443
I.1	Introduction	445
I.2	Results and Discussion.....	450
I.2.1	<i>Selection of a small molecule library for screening in SdiA_{EC}</i>	450
I.2.2	<i>Development of a cell-based reporter assay of SdiA_{EC} transcriptional activity</i>	451
I.2.3	<i>SdiA_{EC} can be activated by a broad range of AHLs but is inhibited by few</i>	452
I.2.4	<i>The promiscuity of SdiA is conserved</i>	453
I.2.5	<i>Structure-activity relationships for SdiA_{EC} agonism</i>	454
I.2.6	<i>Antagonism assay data in SdiA_{EC}</i>	458
I.2.7	<i>Compound 11 reacts with C232 of SdiA_{EC}</i>	461
I.2.8	<i>11 reduces SdiA dependent survival of E. coli in acidic media</i>	467
I.2.9	<i>Implications</i>	468
I.3	Summary and Conclusions	470
I.4	Supporting Information	471
I.4.1	<i>Chemical and biological methods</i>	471
I.4.2	<i>Additional figures and tables</i>	477
I.4.3	<i>Synthesis of GEE/HSL compounds</i>	505
I.4.4	<i>NMR spectra for new compounds</i>	514
I.5	Acknowledgements	528
I.6	References.....	529

List of Figures, Tables, Schemes, and Equations

Chapter 1: Characterization, Development, and Application of Chemical Tools to Probe the <i>agr</i> Quorum Sensing System.....	1
Figure 1.1 A generic QS system.	4
Figure 1.2 Some common QS signals used in Gram-negative and Gram-positive bacteria.	5
Figure 1.3 Many Gram-positive QS systems can be categorized by using either a histidine kinase receptor or an intracellular receptor.	10
Figure 1.4 Processing of AgrD to produce mature AIP.	18
Figure 1.5 The mechanism of AgrC activation.	24
Figure 1.6 Small molecule modulators of <i>agr</i> activity, categorized by target..	32
Figure 1.7 Peptidic modulators of <i>agr</i> activity, categorized by target.	36
Figure 1.8 Potential uses of chemical probes to explore <i>agr</i> QS in vivo.	43
Chapter 2: A Native Autoinducing Peptide Reveals Highly Efficacious Inhibitors and Activators of <i>Listeria monocytogenes</i> Quorum Sensing and Biofilm Formation.....	70
Figure 2.1 The <i>L. monocytogenes agr</i> quorum sensing system.....	75
Figure 2.2 Validation of the <i>agr</i> -dependent GFP reporter strains.....	82
Figure 2.3 Examining effects of tail-length modifications of AIP.....	87
Table 2.1 Activity data for native <i>L. monocytogenes</i> AIP and analogs thereof in <i>agr</i> reporter assays.	89
Figure 2.4 Summary of substitutions made to <i>L. monocytogenes</i> AIP to investigate SAR trends of individual amino acids.....	91
Table 2.2 Reporter assay activity data for select first- and second-generation analogs of <i>L. monocytogenes</i> AIP.....	93
Figure 2.5 Activity of key antagonists against wild-type reporter.....	97
Figure 2.6 AIP analogs can modulate biofilm formation through controlled <i>agr</i> activity.	99
Figure 2.7 Summary of SAR findings of the <i>L. monocytogenes</i> AIP.	101
Scheme 2.S1 Solid-phase synthesis of standard thioester AIP analogs.....	108
Scheme 2.S2 Solid-phase synthesis of acetylated AIP analogs.....	110
Scheme 2.S3 AIP amide synthesis.....	112
Figure 2.S1 LC-MS/MS results matches a native AIP in <i>L. monocytogenes</i> supernatant to hexapeptide standard.....	113
Figure 2.S2 The proposed S→N shift in the 5-mer thioester to produce a homodetic peptide.....	114
Figure 2.S3 Multiple sequence alignment of <i>agrD</i> genes from different <i>Listeria</i> species.....	116
Table 2.S1 Agonism activity of native and proposed AIPs and AIP analogs of other bacterial species in the Δ <i>agrD</i> <i>L. monocytogenes agr</i> reporter strain.	117
Table 2.S2 Antagonism activity table of native and proposed AIPs and AIP analogs of other species in the wild-type <i>L. monocytogenes agr</i> reporter strain.....	118

Table 2.S3	Dose response agonism activity table of <i>L. monocytogenes</i> AIP analogs with varying exocyclic tail length in the $\Delta agrD$ <i>L. monocytogenes agr</i> reporter strain.	119
Table 2.S4	Dose response antagonism activity table of <i>L. monocytogenes</i> AIP analogs with varying exocyclic tail length in the wild-type <i>L. monocytogenes agr</i> reporter strain	120
Table 2.S5	Dose response agonism activity table of alanine and D-amino acid scan analogs in the $\Delta agrD$ <i>L. monocytogenes agr</i> reporter strain.	120
Table 2.S6	Dose response antagonism activity table of alanine and D-amino acid scan analogs in the wild-type <i>L. monocytogenes agr</i> reporter strain.	121
Table 2.S7	Dose response agonism activity table of first-generation analogs in the $\Delta agrD$ <i>L. monocytogenes agr</i> reporter strain.	121
Table 2.S8	Dose response antagonism activity table of first-generation analogs in the wild-type <i>L. monocytogenes agr</i> reporter strain.....	122
Table 2.S9	Dose response agonism activity table of second-generation analogs in the $\Delta agrD$ <i>L. monocytogenes agr</i> reporter strain.	122
Table 2.S10	Dose response antagonism activity table of second-generation analogs and ambuic acid in the wild-type <i>L. monocytogenes agr</i> reporter strain.....	123
Figure 2.S4	Dose response antagonism activity of the <i>L. monocytogenes</i> native AIP, AIP M4dM, and KdCdM in the <i>S. aureus agr-I</i> fluorescent reporter strain AH1677.....	123
Table 2.S11	Dose response antagonism activity table of <i>L. monocytogenes</i> AIP and analogs in the <i>S. aureus agr-I</i> fluorescent reporter strain AH1677.	124
Table 2.S12	Bacterial strains and plasmids used in this study.	124
Table 2.S13	Primers used in this study.	125
Table 2.A	MS spectral data, HPLC retention times, and purity data of synthesized peptides.....	143
Chapter 3: Conformational Switch to a β-turn in a Staphylococcal Quorum Sensing Signal Peptide Causes a Dramatic Increase in Potency		170
Figure 3.1	Schematic of the QS process in <i>S. epidermidis</i>	174
Figure 3.2	Structures of the native <i>S. epidermidis</i> AIP signals (I–III) and AIP-I analogs examined in this study.	175
Table 3.1	Structures and cell-based reporter activities in AgrC-I of the peptides evaluated in this study.	178
Figure 3.3	Representative structures of AIP-I and t-AIP-I.	181
Figure 3.4	Structure of AIP-I V3A.....	182
Figure 3.5	Representative structures of AIP-I D1A and AIP-I D1AS6A.....	185
Figure 3.6	Structure of AAA and overlay with AIP-I.....	188
Figure 3.7	Representative structures of AIP-II and AIP-III.....	189
Figure 3.8	Overlay of AIP-I D1AS6A and AAA.....	191
Figure 3.9	Structural modifications of lead agonist AIP-I D1AS6A and lead antagonist AAA to provide β -turn modifying analogs.	193

Figure 3.10	Group-I AgrC activity dose-response curves of β -turn modifying analogs.	194
Figure 3.11	Model for AgrC-I activation by AIP-I.	199
Scheme 3.S1	Solid-phase synthesis of β -turn modifying analogs.	203
Scheme 3.S2	Solid-phase synthesis of depsipeptides.	206
Table 3.S1	Important 3J coupling constants of AIP-I in Hz.	236
Table 3.S2	Important 3J coupling constants of t-AIP-I in Hz.	236
Table 3.S3	Important 3J coupling constants of AIP-I V3A in Hz.	236
Table 3.S4	Important 3J coupling constants of AIP-I D1A in Hz.	237
Table 3.S5	Important 3J coupling constants of AIP-I D1AS6A in Hz.	237
Table 3.S6	Important 3J coupling constants of AIP-I D1AV3AS6S (AAA) in Hz.	237
Table 3.S7	Important 3J coupling constants of AIP-II in Hz.	238
Table 3.S8	Important 3J coupling constants of AIP-III in Hz.	238
Table 3.S9	Assignments for AIP-I.	239
Table 3.S10	Assignments for t-AIP-I.	239
Table 3.S11	Assignments for AIP-I V3A.	239
Table 3.S12	Assignments for AIP-I D1A.	240
Table 3.S13	Assignments for AIP-I D1AS6A.	240
Table 3.S14	Assignments for AIP-I D1AV3AS6A (AAA).	240
Table 3.S15	Assignments for AIP-II.	241
Table 3.S16	Assignments for AIP-III.	241
Figure 3.S1	Heavy atom ensemble of the 20 lowest-energy structures for AIP-I.	247
Figure 3.S2	Heavy atom ensemble of the 20 lowest-energy structures for t-AIP-I.	247
Figure 3.S3	Heavy atom ensemble of the 20 lowest-energy structures for AIP-I V3A.	248
Figure 3.S4	Heavy atom ensemble of the 20 lowest-energy structures for AIP-I D1A.	248
Figure 3.S5	Heavy atom ensemble of the 20 lowest-energy structures for AIP-I D1AS6A.	249
Figure 3.S6	Heavy atom ensemble of the 20 lowest-energy structures for AIP-I D1AV3AS6A (AAA).	249
Figure 3.S7	Heavy atom ensemble of the 20 lowest-energy structures for AIP-II.	250
Figure 3.S8	Heavy atom ensemble of the 20 lowest-energy structures for AIP-III.	250
Figure 3.S9	Overlay of the macrocycles from AAA, AIP-II, and AIP-III.	251
Table 3.S17	MS spectral data, HPLC retention times, and purity data for the β -turn modifying analogs.	260
Table 3.S18	Cell-based reporter activities in AgrC-I of agonist AIP-I D1AS6A, antagonist AAA, and the β -turn modifying peptide analogs.	266
Table 3.S19	Assignments for AIP-I.	276
Table 3.S20	Assignments for AIP-I D1AS6A.	276
Table 3.S21	Assignments for AIP-I D1AS6dA.	277

Table 3.S22	Assignments for AIP-I D1AS6A [N-MeF8].....	277
Table 3.S23	Torsion angle analysis for AIP-I	278
Table 3.S24	Torsion angle analysis for AIP-I D1AS6A	278
Table 3.S25	Calculated NMR chemical shift differences between AIP-I D1AS6A and either AIP-I D1AS6dA or AIP-I D1AS6A [N-MeF8].	280
Equation 3.S1	Calculation of the mean for proton chemical shift differences.	281
Equation 3.S2	Standard deviation calculation for proton chemical shift differences.....	281
Equation 3.S3	Determination of the cutoff value for significant proton shifts differences.....	281
Equation 3.S4	Calculation of the mean for carbon chemical shift differences.....	281
Equation 3.S5	Standard deviation calculation for carbon chemical shift differences.....	281
Equation 3.S6	Determination of the cutoff value for significant carbon shifts differences.....	281
Chapter 4: Non-Native Peptides Capable of Pan-Activating the <i>agr</i> Quorum Sensing System across Multiple Specificity Groups of <i>Staphylococcus epidermidis</i>		
		292
Figure 4.1	A simplified diagram of the <i>agr</i> QS system in <i>S. epidermidis</i>	297
Figure 4.2	Summary of SAR trends for activation of the three <i>S. epidermidis</i> AgrC receptors by their cognate AIPs.	301
Table 4.1	Selected activity data for native <i>S. epidermidis</i> AIPs and key analogs from SAR studies in corresponding reporter strains.	303
Figure 4.3	Structures of the three AIP chimeric scaffolds (Cmr 1–3).	309
Table 4.2	Agonism activity data for native AIPs, chimera scaffolds, and identified multi-group agonists.	310
Figure 4.4	Representative portions of HPLC traces of samples of <i>S. epidermidis</i> cultures showing the PSM peaks.....	312
Table 4.3	Potency data for pairs of AIP analogs where the only sequence difference is a C-terminal phenylalanine or leucine.....	314
Scheme 4.S1	Solid-phase synthesis of standard thioester AIP analogs.	319
Table 4.S1	Summary of agonism and antagonism dose-response data for AIP-II based analogs in <i>S. epidermidis</i> AH2673 (group-II).....	325
Table 4.S2	Summary of agonism and antagonism dose-response data for AIP-III based analogs in <i>S. epidermidis</i> AH3409 (group-III).....	329
Figure 4.S1	<i>S. epidermidis</i> group-I agonism screen of chimeric peptides.	331
Figure 4.S2	<i>S. epidermidis</i> group-I antagonism screen of chimeric peptides.	332
Figure 4.S3	<i>S. epidermidis</i> group-II agonism screen of chimeric peptides.	332
Figure 4.S4	<i>S. epidermidis</i> group-II antagonism screen of chimeric peptides.	333
Figure 4.S5	<i>S. epidermidis</i> group-III agonism screen of chimeric peptides.	333
Figure 4.S6	<i>S. epidermidis</i> group-III antagonism screen of chimeric peptides.	334
Figure 4.S7	Summary heatmap of single-point agonism activity of chimeric analogs in groups-I–III.....	335

Table 4.S3	Summary of agonism dose-response data for select non-chimera peptides.	336
Table 4.S4	Summary of agonism dose-response data for select Cmr1 peptides.	337
Table 4.S5	Summary of agonism dose-response data for select Cmr2 peptides.	338
Table 4.S6	Summary of agonism dose-response data for select Cmr3 peptides.	339
Table 4.S7	Summary of antagonism dose-response data for select non-chimera peptides.	345
Table 4.S8	Summary of antagonism dose-response data for select Cmr1 peptides.	346
Table 4.S9	Summary of antagonism dose-response data for select Cmr2 peptides.	347
Table 4.S10	Summary of antagonism dose-response data for select Cmr3 peptides.	348
Figure 4.S8	HPLC traces of PSM production restoration by Cmr1 S7A in groups-I-III.	355
Table 4.A	MS and HPLC data for the <i>S. epidermidis</i> AIP-II analogs synthesized in this study.	356
Table 4.B	MS and HPLC data for the <i>S. epidermidis</i> AIP-III analogs synthesized in this study.	357
Table 4.C	MS and HPLC data for the <i>S. epidermidis</i> chimera analogs synthesized in this study.	358
Table 4.D	MS and HPLC data for the <i>S. epidermidis</i> PSM α , PSM β , and PSM γ isolated from group-I (RP62A) cellular supernatant.	359

Chapter 5: Sustained Release of a Synthetic Autoinducing Peptide Mimetic Strongly Attenuates MRSA Infections *In Vivo* 385

Figure 5.1	Chemical structures and potency values for QS inhibitors evaluated in this study.	390
Figure 5.2	Time course of <i>S. aureus agr</i> activity for compounds incubated with mouse tissue.	392
Figure 5.3	Abscess attenuation due to tr AIP-III D2A delivered as a bolus in solution or delivered in 1 mg of PLG microparticles.	396
Figure 5.4	Characterization of PLG microparticles loaded with tr AIP-III D2A.	398
Figure 5.5	Side-by-side comparison of abscess formation after treatment with tr AIP-III D2A in solution vs PLG microparticles.	401
Figure 5.S1	A schematic of <i>ex vivo</i> experimental system to examine compound activity incubated at 10,000-fold IC ₅₀ in presence of mouse tissue.	409
Figure 5.S2	Activity of <i>S. aureus agr</i> -I fluorescence reporter strain when exposed to supernatant of AIP-III D4A incubated in PBS in the presence or absence of mouse tissue sample.	410

Figure 5.S3	Activity of AIP-III D4A in <i>S. aureus agr-I</i> fluorescent reporter strain when exposed to either heat denatured mouse tissue or a control tissue.....	411
Figure 5.S4	Examination of interactions of AIP-III D4A and tr AIP-III D2A with ApoB as analyzed via analytical RP-HPLC.....	412
Figure 5.S5	Infection abscess analysis of mice inoculated with wild-type and Δagr <i>S. aureus</i>	413
Figure 5.S6	PLG microparticle size histogram as measured by SEM.	414
Figure 5.S7	HPLC standard curve for tr-AIP III D2A.....	415
Equation 5.S1	Four-parameter logistic regression model.....	416
Equation 5.S2	Equation to determine compound concentration from <i>agr</i> activity.....	416
Figure 5.S8	Dose-response inhibition curve for tr AIP-III D2A.....	417
Figure 5.S9	Activity of supernatants isolated over time in release experiments from tr AIP-III D2A loaded PLG microparticles.....	418
Chapter 6: Future Directions.....		429
Figure 6.1	Covalent attachment of AIP analogs to surfaces.....	434
Appendix I: Chemical Control of Quorum Sensing in <i>E. coli</i>: Identification of Small Molecule Modulators of SdiA and Mechanistic Characterization of a Covalent Inhibitor.....		442
Figure I.1	AHL-mediated LuxI/LuxR-type QS overview.....	446
Figure I.2	Activity heatmap of AHL and AHL analogs in various LuxR-type receptors.....	453
Table I.1	Selected SdiA _{EC} agonism dose-response assay data.....	455
Figure I.3	Dose response curves of 11 and 15.....	459
Figure I.4	Crystal Structure of SdiA _{EC} and MS analysis of 11 with SdiA _{EC} . .	462
Figure I.5	Structural features of analogues of 11.	465
Figure I.6	Dose response curves of analogues of 11.....	465
Figure I.7	Survival of WT or $\Delta sdiA$ <i>E. coli</i> in an acid challenge assay.....	468
Figure I.S1	Chemical structures of library screened in this study.....	477
Table I.S1	Details of prior small molecule screens with other LuxR-type receptors.....	478
Table I.S2	Strains, plasmids, and primers used in this study.	479
Figure I.S2	Characterization of <i>E. coli</i> SdiA _{EC} reporter strains.	480
Table I.S3	Primary single-concentration SdiA _{EC} agonism and antagonism screening data in the JLD271-SdiA _{EC} WT reporter.	481
Table I.S4	Secondary single-concentration SdiA _{EC} agonism screening data in the JLD271-SdiA _{EC} WT reporter.....	485
Figure I.S3	Plots of trends in SAR for AHL and PHL SdiA _{EC} agonism in the JLD271-SdiA _{EC} WT reporter.....	487
Figure I.S4	SdiA _{EC} agonism dose-response curve plots for compounds in Table I.1 in the main text.....	488
Table I.S5	SdiA _{EC} agonism and antagonism dose-response assay data for compounds 11 and 15 in the JLD271-SdiA _{EC} WT reporter.	492

Figure I.S5	Plots of bacterial growth in the presence of compounds 2, 11, and 15.....	493
Figure I.S6	Dose-response competition curves for compounds 11 and 2.	494
Figure I.S7	Chromatographic and SDS-PAGE data for SdiA _{EHEC} H ₆	495
Figure I.S8	Representative nano-ESI FTICR mass spectra and MS/MS sequence tables for SdiA _{EHEC} H ₆ treated with compound.....	496
Figure I.S9	Mass spectral data for SdiA _{EHEC} H ₆ incubated with compound 11 or compounds 11 + 2 in cells.....	497
Figure I.S10	Quantification of the relative amounts of SdiA _{EHEC} H ₆ and ¹¹ SdiA _{EHEC} H ₆	498
Figure I.S11	Fragmentation of SdiA _{EHEC} H ₆ proteoforms for MS/MS.	499
Figure I.S12	Dose-response plots for compound 11 in the <i>E. coli</i> SdiA _{EC} C232A mutant reporter strain.....	500
Table I.S6	SdiA _{EC} agonism and antagonism dose-response assay data for GEE/HSL library.....	501
Figure I.S13	GEE/HSL library dose-response curve plots.....	503
Figure I.S14	<i>E. coli</i> acid-challenge assay supporting data.	504

Chapter 1:
Characterization, Development, and Application of Chemical Tools to
Probe the *agr* Quorum Sensing System

Contributions: K. H. J. West wrote the chapter. H. E. Blackwell assisted in writing.

Abstract

This introductory chapter provides an overview of bacterial quorum sensing (QS), its functions, and common QS systems utilized by Gram-positive bacteria. A brief general overview of QS is followed by a comprehensive description of the known functions and molecular mechanisms of the accessory gene regulator (*agr*) QS system used by many Gram-positive bacteria. We next discuss the virtues of chemical control of QS and describe efforts by our research laboratory and others to identify, develop, and apply chemical modulators of *agr* activity. Finally, we outline the remaining chapters in this thesis that describe recent work pursued in our laboratory to understand *agr* QS through chemical modulation of this pathway in three important Gram-positive pathogens.

1.1 Introduction

1.1.1 *Brief introduction of bacterial quorum sensing*

A common misconception about bacteria is that, since they are unicellular organisms, individual bacteria operate entirely independently of one another. While it is true that each bacterium has all the necessary components and capabilities to perform the tasks essential for life, bacteria also have evolved ways to coordinate, collaborate, and otherwise interact with one another through chemical communication systems that allow them to accomplish complex and group-beneficial tasks that individuals could not achieve alone. This chemical-mediated cell-cell communication phenomenon is known as quorum sensing (QS), as it relies upon a threshold population density (i.e., a quorum) of bacteria to produce sufficient chemical signal for receptors to sense the signal and activate the downstream response (Figure 1.1). In the generic quorum sensing process, bacteria synthesize signaling molecules at a low basal level and export these signals into their local environment; if many bacteria in close proximity to one another are each producing this signal (or if they live in a confined environment), the local concentration of the signal reaches a threshold level and can productively bind to and activate cognate receptor proteins. Upon activation, these receptors trigger changes in the gene expression, often upregulating the QS machinery for signal synthesis and sensing in a positive feedback loop, and these alterations in gene expression leads to changes in bacterial behavior. Since the signaling molecules only activate their cognate receptors when there is a sufficiently high density of bacteria nearby, the entire population simultaneously then undergoes these behavioral changes.

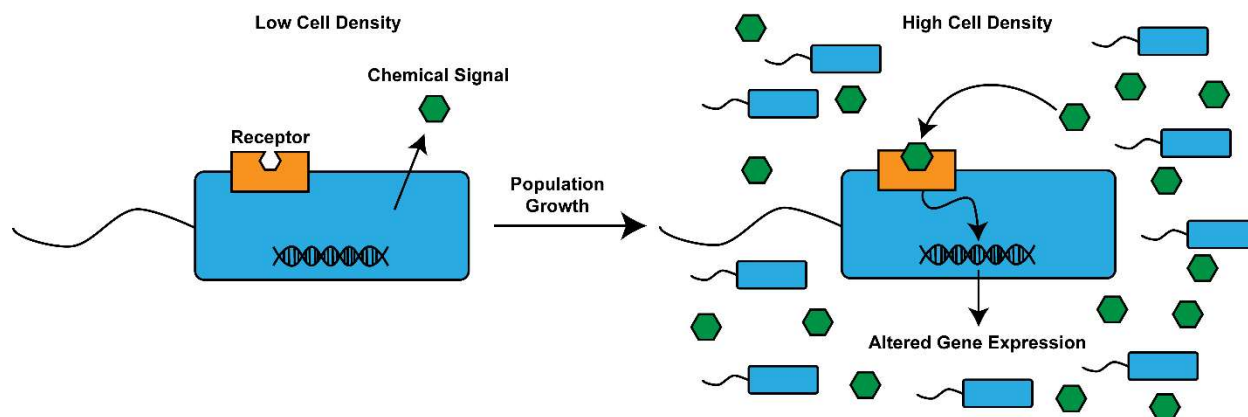


Figure 1.1 A generic QS system. At low cell densities, bacteria will produce chemical signal, but the local concentration is too low for productive receptor binding. At high cell density, the signal concentration will pass the threshold necessary for productive binding, activating the receptor and initiating gene expression changes in the population.

QS was first uncovered in the 1970s as the autoinduction system behind the bioluminescent behavior exhibited by *Vibrio fischeri* during exponential growth.¹ After a decade of work studying the system, the structure of the signaling molecule was revealed to be *N*-(3-oxohexanoyl)-L-homoserine lactone (known as OHHL).² In the years since, it has determined that this small molecule is synthesized by the LuxI protein from *S*-adenosyl-L-methionine and an acylated acyl carrier protein,³ and that upon reaching its threshold concentration OHHL binds to an intracellular receptor LuxR and initiate gene expression changes.⁴ Similar small molecules known collectively as *N*-acyl homoserine lactones (AHLs) have been found in many other Gram-negative bacteria with corresponding synthase (LuxI-type) and receptor (LuxR-type) proteins, with some species such as *Pseudomonas aeruginosa* having multiple LuxI/LuxR-type systems that create a complex web of inter-regulation.⁴⁻⁵ LuxR-type receptors are often very selective for their cognate signal, as even subtle differences in structure can prevent activity,⁶ leading to the hypothesis that QS is utilized as a method for

intraspecies communication to gauge the local population. While AHL-based QS was the first system characterized, in the decades since its discovery many additional QS architectures have been uncovered (Figure 1.2).

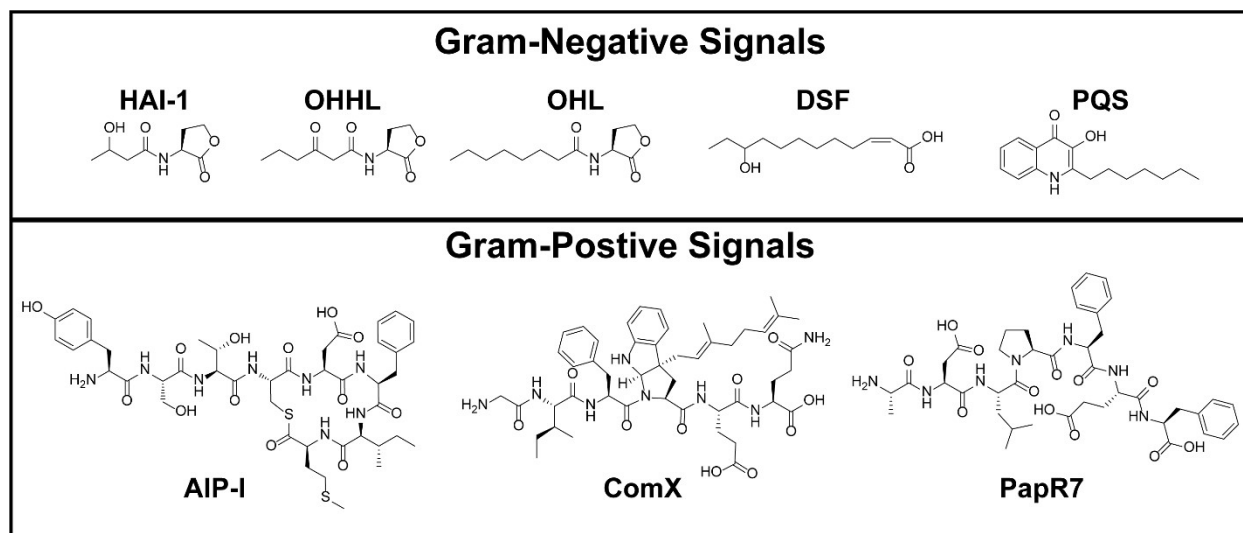


Figure 1.2 Some common QS signals used in Gram-negative and Gram-positive bacteria.

1.1.2 Behaviors under quorum sensing control

Bacteria are generally believed to use QS to gauge their own species' local population and behave accordingly depending on cell number. At low population densities (QS inactive), bacteria express certain genes and exhibit individual behaviors focused on survival, such as avoiding detection by the immune system. At high population densities (QS activated), the larger quorum of bacteria can now coordinate expression of different genes and switch to performing more energetically costly behaviors that will benefit the greater population, such as breaking down more complex nutrient sources or producing antimicrobial agents to kill competitors, among many other activities. In addition to these “canonical” intraspecies QS phenomena, there has

been growing evidence that bacteria use QS systems to regulate their behavior in other scenarios that bacteria encounter in nature. Due to QS systems sharing similar scaffolds for their signaling molecules (like the AHLs scaffold described above), non-native signals can bind to other receptors and maintain some activity (whether agonistic or antagonistic). This cross-activity has been found to occur between the QS signals produced by species co-isolated *in vivo*,⁷⁻⁸ suggesting that their individual QS systems could also be used as a form of interspecies communication. Moreover, some LuxR-type receptors known as orphan or “solo” receptors have no known corresponding LuxI-type synthase (and thus no cognate AHL signal is known) and instead respond to a wide variety of AHLs, suggesting that this non-canonical usage of QS can be quite common.⁹ The importance of interspecies QS activity in mixed microbial environments is a growing interest in the field.¹⁰⁻¹²

In addition to possible interspecies communication, QS circuits can be used to sense an individual bacterium’s local environment. If an individual bacterium is enclosed in a small compartment, for example, the local concentration of the QS signal will increase to a high level and could activate its receptor without the need for a large population. Boedicker *et al.* has shown that a single bacterium can activate QS when confined in a microfluidic compartment,¹³ and Carnes *et al.* similarly demonstrated QS activation within phagosomes.¹⁴ The activation of QS outside of large populations has led some to re-define the phenomenon as “diffusion sensing.”¹⁵ In diffusion sensing, these systems function not as ways to gauge the population of bacteria but rather as methods to determine how quickly secreted molecules diffuse away from the cell. If the concentration of the autoinducer is low enough that it does not bind the receptor, the

compound is diffusing away and, therefore, other products will also diffuse away. To optimize the efficiency of their exoproducts, such as enzymes that degrade complex nutrients, bacteria use these systems to only activate the production of these exoproducts when there is limited diffusion (i.e., when the autoinducer does not diffuse away and instead productively binds the receptor).¹⁵ This description can better describe how other environmental factors, such as flow, can modulate QS activity through increased or decreased diffusion, regardless of the size of the compartment or the population. However, this description fails to incorporate the social elements that have been characterized in these systems (*vide supra*). This has led some to present unifying hypotheses, such as “efficiency sensing,”¹⁶ that incorporate elements from both QS and diffusion sensing. Others have argued that focusing on the terminology leads to confusion and competition rather than focusing research efforts on more fully cataloging all the individual factors that contribute to the overall phenomenon.¹⁷ While the field has largely settled on using QS as the general term to describe these systems, it is critical to realize no single factor completely describes the complexity of these systems and researchers should carefully examine the role all these factors play when describing and characterizing bacterial behavior in response to signaling molecules.¹⁷

Regardless of whether QS systems are activated by large populations of the same species, different species, or just a single organism in a small space, bacterial QS systems are often key regulators of gene expression. Studies estimate between 5–25% of bacterial genomes are influenced by QS activity.¹⁸⁻²¹ With such a wide effect on the genome, the resulting phenotypic changes upon QS activation vary considerably from species to species. Some bacteria use QS to mediate symbiotic relationships. As

mentioned above, QS was first discovered in *V. fischeri* due to its regulation of bioluminescence.¹ Isolated from the light organ of the Hawaiian bobtail squid, *V. fischeri* uses QS to camouflage the squid from predators and prey in exchange for nutrients and colonization.²²⁻²⁴ Other symbiotic relationships have been found to be facilitated by QS-regulated behavior, such as *Rhizobia* species that fix nitrogen in legume root nodules.²⁵

QS can also regulate an array of defensive mechanisms as well, such as controlling bacterial competence (uptake of foreign DNA) to gain new resistances through horizontal gene transfer²⁶ or sporulation to extend lifespan under harsh conditions.²⁷ The most notable defensive phenotype under QS control is the production of biofilm, which are protective extracellular layers composed of exopolysaccharides, nucleic acids, proteins, and lipids. The physical barrier of biofilm can shield bacteria from antimicrobial agents or immune cells, with reports estimating a biofilm growth state provides up to 1,000 times more protection from antibacterial agents over a planktonic growth state.²⁸⁻³⁰ In some species, QS activation will initiate biofilm production,³¹⁻³³ while in others QS activation initiates dispersal of biofilms.³⁴⁻³⁵

Lastly, and perhaps of the greatest interest over the past several decades, the virulence of many common pathogens is regulated by QS. Upon QS activation, bacteria can produce a variety of different agents to attack competitors or their host. To eliminate nearby microbial competition, a number of bacteria produce bacteriocins, antimicrobial peptides, and other antibiotics when their respective QS systems are activated.³⁶⁻⁴¹ In terms of larger targets, bacterial QS is often essential for invasion and infection in plants and animals. AHL-based QS is extensively used by many plant pathogens (reviewed by von Bodman et al.⁴²), such as the Tra system in *Agrobacterium tumefaciens* to induce

crown gall tumors through transferring tumor-inducing DNA transfer into plant cell chromosomes⁴³ or the Exp system of *Pectobacterium carotovora* to cause soft rot in various plants through the secretion of exoenzymes to degrade plant cell walls.⁴⁴ Similar behaviors are seen in animal pathogens as well, with QS controlling the production and secretion of myriad exoenzymes, toxins, and biosurfactants to attack host cells.^{27, 32, 45-50} These trends follow into animals models where QS-deficient mutants of various pathogens have severely attenuated invasion and infection phenotypes.^{32, 50-53} With the many facets of bacterial behavior under QS regulation, considerable research has been pursued to start to detail both the fundamental mechanics of QS as well as to develop an understanding of how disruption of these systems can affect phenotypes.

1.2 Common Gram-positive Quorum Sensing Systems

1.2.1 Overview of Gram-positive quorum sensing

Generally, Gram-positive bacteria have been found to use higher molecular weight peptide pheromones in their QS systems as opposed to small molecule signals. These peptide-driven QS systems can be classified into two superfamilies by their signal and receptor pair. The first superfamily consists of systems that utilize long and/or modified peptides signals that bind to membrane-bound histidine kinase receptors (Figure 1.3A). The most characterized system in this superfamily—and of all Gram-positive QS systems in general—is the accessory gene regulator (*agr*) system, which is distributed across the Firmicutes and generally utilizes a macrocyclic peptide known as the autoinducing peptide (AIP) as the signaling molecule.⁵⁴⁻⁵⁵ The *agr* QS

system is the focus of this thesis. We give a brief overview here, but we will return to the *agr* system in much greater detail later in the chapter.

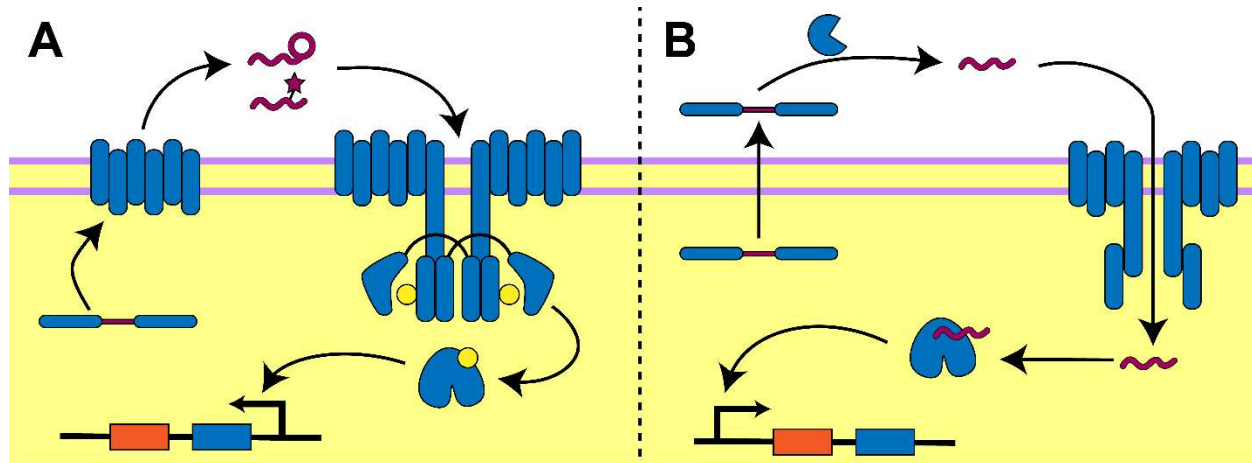


Figure 1.3 Many Gram-positive QS systems can be categorized by using either a histidine kinase receptor or an intracellular receptor. (A) A propeptide signal is modified at least in part by a membrane bound protein. These modified signals are then exported and possibly further processed by other factors to produce the mature signal. These modified peptide signals then bind to a histidine kinase, initiating a phosphoryl transfer to a response regulator that can bind DNA to change gene expression. (B) A propeptide is exported out of the cell and is processed by extracellular proteases to produce the small, linear peptide signal. These are transported back into the cell and bind intracellular receptors, inducing changes in transcription.

1.2.2 The *agr* QS system

The prototypical *agr* system was first characterized in *Staphylococcus aureus* and is comprised of four protein components, AgrA–D.⁵⁶⁻⁵⁷ The AgrD polypeptide is a precursor to the AIP signaling molecule and is produced at a low basal level within the cell. AgrD is processed by AgrB, a membrane peptidase, which cleaves the C-terminal portion of AgrD and cyclizes the new C-terminus to a conserved cysteine to form a thioester linkage.⁵⁸ The thiolactone AgrD is hypothesized to be secreted to the extracellular matrix and to have its N-terminal domain cleaved to produce the mature

AIP signal (often between 5–12 amino acids in length), although the mechanics by which this occurs is still not well-understood.⁵⁹⁻⁶⁰ Once reaching a sufficiently high local concentration, the AIP signal binds the transmembrane AgrC histidine kinase receptor, initiating *trans*-autophosphorylation and phosphorelay to the intracellular AgrA response regulator.⁶¹ Activated AgrA then binds to DNA as a transcription factor, upregulating the *agr* operon in a positive feedback loop at the P2 promoter and other loci (most notably at the P3 promoter in *S. aureus* to produce the regulatory RNAIII, a main effector of virulence).⁶¹⁻⁶²

Across Gram-positive bacteria, there is substantial variation in the *agr* genes. The greatest diversity within the *agr* operon is found in the hypervariable region that spans parts of *agrB*, all of *agrD*, and parts of *agrC*.⁶³ The diversity of AgrD leads to unique AIP signals, and thus the domains needed to produce it (AgrB) and sense it (AgrC) have been tuned accordingly.^{55, 57} These different *agr* systems are often shared by all members of a genus or a species. However, sometimes strains of a single species may have divergent *agr* systems as well. Strains with identical *agr* genes are then classified as members of the same *agr* specificity group (often denoted with Roman numerals, e.g., *agr*-I). These different *agr* specificity groups often have complex cross-activity networks, where the AIP of one group may activate or inhibit the AgrC receptor of a different group. This cross-activity is common in many QS systems, and has led many labs to characterize these relationships between groups and investigate their potential ecological importance in nature. In addition, there are other interesting deviations from the prototypical *agr* systems, as some species have multiple *agr* loci^{48, 53} or utilize alternate two-component systems to sense the AIP signal.⁶⁴

1.2.3 The ComQXPA and ComABCDE QS systems

The ComQXPA QS system, found in *Bacillus subtilis* and some related species,⁶⁵ utilizes an isoprenylated, small (~5–10 residues) peptide pheromone known as ComX⁶⁶ to regulate over >150 genes and control competence.⁶⁷ ComX is initially produced as a propeptide that is modified by ComQ, isoprenylating a conserved tryptophan of ComX,⁶⁸⁻⁶⁹ and exported out the cell. The mature ComX signal binds and activates the ComP histidine kinase, subsequently activating the response regulator ComA to alter gene expression. While the C-terminal end of ComP and ComA are well-conserved, ComQ, ComX, and the N-terminal portion of ComP differ from system to system, leading to unique signal-receptor pairs.²⁶ Interestingly, there is no known positive feedback loop for the ComQXPA system (i.e., ComA does not upregulate the *com* operon), deviating from the standard QS feedback loop to rapidly amplify signal to induce gene expression changes. Nonetheless, the ComQXPA system appears to respond in a similar fashion through other means, with recent studies pointing towards an ultra-sensitive response to detection.⁷⁰

A similarly named QS system, ComABCDE, has been characterized in the Streptococci and involves a long (~20 residues) unmodified pheromone called the competence stimulating peptide (CSP) to regulate competence, biofilm, and bacteriocin production among other behaviors.^{40, 71} The CSP sequence is not well conserved across species;⁷² however, its precursor, the ComC polypeptide, has a well conserved N-terminal leader sequence with a Gly-Gly motif. This double glycine motif is important for recognition by the ABC transporter/protease ComAB and cleaves ComC during export out of the cell to produce the CSP.^{40, 73-74} Depending on the species, the C-

terminus of the CSP can also be trimmed by extracellular protease SepM.⁷⁵ The mature, extracellular CSP can then bind to the ComD histidine kinase. As the CSP sequence varies from species, the ComD receptor also has significant variation in the domains proposed to bind CSP.⁷⁶ The activated ComD receptor phosphorylates the response regulator ComE to alter gene expression levels, most notably *sigX* that encodes for the alternative sigma factor that regulates competence and bacteriocin production.⁷³

1.2.4 The RNPP QS systems

The second superfamily of Gram-positive QS systems is the RNPP family, so named after the founding receptors of Rap, NprR, PlcR, and PrgX. This family of QS circuits involves small, unmodified peptides as pheromones that are imported into the cell and bind cytoplasmic receptors (Figure 1.3B).⁷⁷ RNPP systems are found in a number of *Bacillus* species, but also in other species such as *Enterococcus faecalis*.⁷³ A precursor to the signaling peptide is secreted out of the cell, where it undergoes processing by proteases into the mature oligopeptides that are usually under 10 residues in length.⁷⁸ Once matured, the extracellular peptide is actively transported by an oligopeptide permease (Opp) into the cytoplasm.⁷⁹ The peptide pheromones then bind to their intracellular receptors, which are characterized by tandem-repeats of a 34-residue motif known as tetratrico peptide repeats (TRPs).^{77-78, 80} Multiple TRP domains form a bundle that facilitates oligomerization and other protein-protein interactions.⁸⁰ Productive binding of the peptide signals induces conformational changes in the receptors through the TRP domains to allow for gene expression changes.⁸¹ However, the mechanisms by which the individual receptors mediate regulation varies; some

receptors directly bind to DNA, while others indirectly affect transcription through sterically blocking promoters or dephosphorylating other response regulators.^{73, 78, 82-83} Studies of the RNPP family has largely focused on identifying the active peptide pheromone, characterizing the key residues for activity, and probing how peptide binding alters receptor interactions with DNA and other proteins.⁸³

1.3 The *agr* QS System in Detail

1.3.1 Brief history of the *agr* QS system

As described above, the *agr* system is a prevalent QS circuit found in many Gram-positive bacteria. The system is best characterized in *S. aureus*, where it was initially discovered and studied. Many seminal works published by the Novick laboratory in the late 20th century laid the foundation of our current understanding of the *agr* system. The first key study was in 1986, where the *agr* system was discovered and named due to its regulation of accessory genes, like exoprotein genes.⁸⁴ In a series of elegant studies in the mid-1990s, Novick and others characterized the autocatalytic properties of the P2 promoter for the *agr* operon,⁸⁵ determined that the P3 promoter initiates transcription of the main Staphylococci *agr* regulatory effector molecule RNAIII,⁸⁶ identified the macrocyclic AIPs to be the *agr* signaling molecules,⁴⁷ and observed variant AIPs from different *S. aureus* strains that exhibited *agr* cross-activity.⁸⁷ Entering the 21st century, the core functions of the four *agr* proteins had been characterized in *S. aureus*, but many of their mechanisms of actions were still not well-understood.⁸⁸ In the years since, studies have progressively delineated more of the intricate molecular details of how the *agr* proteins function and their relationships with

the AIP signal in *S. aureus*, and several forays into examining the *agr* systems of other organisms have been launched. A more detailed description of each *agr* protein, with a primary focus on the Staphylococci, is provided below.

1.3.2 *The AgrD propeptide*

The AgrD polypeptide is the precursor to the AIP molecule. Full length AgrD is approximately 50 amino acid residues long and is sectioned into three domains: an N-terminal leader sequence, a middle portion containing the AIP sequence, and a C-terminal recognition sequence. The N-terminal leader sequence forms an amphipathic helix that stabilizes and directs AgrD to the membrane to facilitate association with AgrB.⁸⁹ The exact conservation for most residues does not seem to be as important, as there is substantial deviation in the sequence between organisms and even within species subgroups. Only a single glycine residue is fully conserved in AgrD in the Staphylococci, and this glycine is only sometimes present in other genera.⁵⁷ In mutational studies of the *S. aureus* AgrD-I, substitution of this conserved glycine prevented cleavage by AgrB, completely blocking AIP production.⁹⁰ Generally though, it seems maintaining the amphipathic nature of the sequence is the only requisite feature, as replacement of the sequence with an artificial amphipathic sequence still allows for AIP synthesis.⁸⁹ The native N-terminal sequence can also be shortened to an extent, but this in turn reduces the amount of AIP produced.⁸⁹ Interestingly, like many amphipathic peptide sequences, the N-terminal sequence has been reported to have cytolytic activity against human cells and enhance virulence *in vivo*.⁹¹⁻⁹² In these same studies, the N-terminal domain was identified in the supernatant of *S. aureus* cultures,⁹¹⁻

⁹² suggesting the N-terminal domain and its cytolytic activity may play additional biological roles in virulence after delivery of AgrD to AgrB for processing.

The AIP sequence contained within AgrD has the greatest diversity across the Staphylococci and Gram-positive bacteria in general, and the unique AIP sequences are often used to differentiate different *agr* specificity groups for a species. Within AIP sequences, there are only a few features that are common to most sequences. The most notable element between AIPs is the high conservation of a cysteine that is used to make the thioester linkage to the C-terminus after AgrB processing. The macrocycle is critical for activity, as linear forms of the AIPs are usually inactive.⁸⁷ Some species, such as *Staphylococcus intermedius*, instead substitute cysteine for serine and create ester macrocycles that otherwise function identically to the cysteine-containing AIPs in their native systems.^{57, 93} Another commonality between AIPs is that most contain five amino acids in their macrocycle, although some *agr*-like systems in *E. faecalis*⁹⁴ and some *Clostridia* species have larger macrocycles.^{57, 95} Lastly, most AIPs have additional residues outside the macrocycle that make up an exocyclic tail, but a few have been reported without exocyclic tails, such as *Lactobacillus plantarum*⁹⁶ and some *Clostridia* species.⁹⁵ Without an exocyclic tail, the N-terminus of the mature AIP signals are adjacent to the thioester linkage and can undergo an S→N acyl shift in physiological pH to produce homodetic peptides. Chemical species corresponding to this S→N acyl shift product have been recently identified in *Clostridia* supernatants,⁹⁵ suggesting that these homodetic peptides might be the active signaling molecules in these *agr* systems. It remains unclear whether this S→N acyl shift occurs in other organisms outside *Clostridia* but could become yet another facet of AIP diversity in *agr* systems.

Of the three domains of AgrD, the C-terminal domain is the most conserved in the Staphylococci, with many residues immediately following the AIP sequence fully conserved.⁵⁷ This conservation appears important for activity, as informed by C-terminal truncation studies of AgrD-I in *S. aureus*. Removal of the poorly-conserved, final few residues of AgrD did not affect AgrD cleavage by AgrB, but removal of any highly conserved residues negatively impacted cleavage and/or eliminated production of any mature AIP.⁹⁷ Similarly, *S. aureus* AgrD-I mutants with random single substitutions at these residues also had drastically impaired or negligible AIP biosynthesis.⁹⁰ Together, these results indicate that the C-terminal domain likely functions as a recognition domain for AgrB processing. Looking to the AgrD sequences in other organisms, the C-terminal domain is not as well-conserved as it is in the Staphylococci: only a couple proline and leucine residues are commonly found in most AgrD sequences.⁵⁷ In general, however, the domain is populated by multiple charged residues making it hydrophilic, although it is unclear whether this feature is important for function.⁵⁷ While there have been no additional genetic studies following up on the role of C-terminal residues in other *agr* systems to our knowledge, it is likely that these C-terminal domains function similarly to the *S. aureus* AgrD C-terminal domain and have each been tuned to be recognized by their native AgrB peptidases.

1.3.3 *AgrB* processing of *AgrD*

AgrB is the second component critical for the biosynthesis of the AIP signal. AgrB is a membrane-bound endopeptidase that cleaves the C-terminal recognition domain of AgrD and forms the macrocyclic linkage from the sidechain of the conserved

cysteine (or occasional serine) to the new C-terminus of AgrD. Topology models predict AgrB to contain multiple transmembrane segments (although studies differ on the number of passes).^{58, 97} While the hydrophobic properties of these segments appear to be consistent, sequence alignments across organisms show considerable variation in residue identity.⁵⁷ Despite a lack of conservation, many AgrB mutants were poorly tolerated in a random mutagenesis study, often destabilizing AgrB or preventing peptidase activity even when distant from the active site, suggesting a possible role for these sites in the recognition of AgrD.⁹⁰ Interestingly, a number of mutants were capable of cleaving AgrD, but there were no detectable levels of the mature AIP signal, possibly indicating an additional and still uncharacterized role for AgrB during AgrD processing.⁹⁰

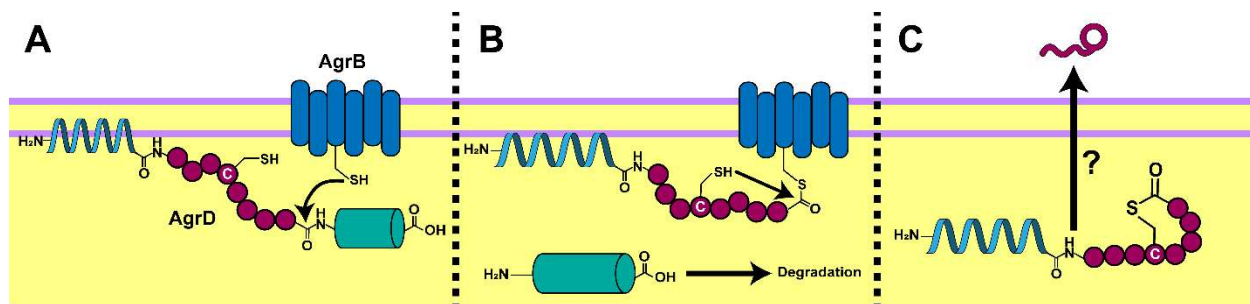


Figure 1.4 Processing of AgrD to produce mature AIP. (A) The N-terminal domain of AgrD localizes to the membrane, and the AgrD C-terminal domain is recognized and cleaved by AgrB. (B) The conserved AgrD cysteine exchanges with the bridging thioester between AgrD and AgrB, creating a macrocycle. The free C-terminal domain of AgrD is rapidly degraded. (C) After AgrB processing, uncharacterized partners transport and cleave the N-terminal domain of the modified AgrD to produce the mature AIP signal.

The active site of AgrB is composed of a cysteine and histidine that are both fully conserved in all known AgrB sequences.⁵⁷ These two residues form a catalytic dyad that gives rise to peptidase activity.⁹⁸ When the C-terminal domain of AgrD is

recognized by AgrB, the AgrB conserved cysteine attacks the scissile bond between the AgrD AIP and C-terminal domains, forming a thioester linkage to the N-terminal half of AgrD (Figure 1.4A).⁹⁷ This results in an AgrB-AgrD intermediate and a free AgrD C-terminal domain. The AgrB-AgrD intermediate is short-lived as the AgrD cysteine exchanges with the AgrB cysteine thioester and is released as a macrocyclic AgrD (Figure 1.4B). Mutational studies which replace the AgrD cysteine with an alanine prevented this rapid exchange, and the AgrB-AgrD intermediate could be isolated.⁹⁷ Despite this process being energetically unfavorable (from the stable amide bond in full length AgrD to the thioester bond in the final product), *in vitro* thermodynamic studies utilizing AgrB liposomes and AgrD have shown the AgrD macrocycle to be the major product.⁹⁹ These studies also revealed this processing is reversible in cells, but is driven forward likely by the rapid degradation of the AgrD C-terminal domain after cleavage.⁹⁹

While there is variation in the AgrB sequences even between *agr* specificity groups of a single species, studies have shown that AgrB proteins can process non-cognate AgrD peptides. In the earliest identification of *agr* specificity groups, it was demonstrated that AgrB-I and AgrB-III of *S. aureus* could produce active peptides (as determined by β -lactamase activity) from AgrD-III and AgrD-I, respectively.⁸⁷ Additionally, the *S. aureus* AgrB-I could produce an active peptide from the AgrD sequence of *Staphylococcus lugdunensis* and vice versa; however, the *S. aureus* AgrB-II and AgrD-II could neither process nor be processed by any other *agr* components tested, demonstrating this cross-processing is not universal.⁸⁷ A later study examined chimeric AgrB proteins containing different segments of AgrB-I and AgrB-II from *S. aureus*,¹⁰⁰ designed to interchange domains according to the predicted topology models

at the time.⁵⁸ While some chimeras could only process AgrD-I or AgrD-II, some chimeras could process both AgrD sequences to produce AIP-I and AIP-II.¹⁰⁰ Interestingly, some of these chimeras even outperformed the wild-type AgrB-I in production of AIP-I.¹⁰⁰ While these studies show that cross-processing is possible, the mechanism by which these chimeras facilitate processing of non-cognate AgrD sequences is unclear, as these studies only determined if active peptide signal was produced.¹⁰⁰ These studies did not inform on whether the domain swapping changes how AgrD is recognized, cleaved, or cyclized, or other downstream modifications of AgrD; additional studies elucidating these mechanistic changes could give new insights into AgrB processing.

1.3.4 Additional AgrD processing to produce the mature AIP

After the cyclization of AgrD by AgrB, the modified AgrD needs to be transported outside of the cell and have the N-terminal domain cleaved to produce the mature AIP (Figure 1.4C). Neither the order nor the source of these processing steps is well-understood, although the presence of the N-terminal domain of AgrD in supernatants⁹¹⁻⁹² suggests transport occurs first. Early studies of AgrB put forth the hypothesis it was responsible for all of AgrD processing and transport,⁵⁸ but no studies in the subsequent years have provided evidence for its ability to transport AgrD or cleave the N-terminal domain *in vitro*,^{90, 97-99} so it is likely that other protein partners are key to these additional processing steps. Cross-linking studies of AgrB failed to elucidate any interacting protein partners;⁹⁸ consequently, researchers instead turned to identifying possible partner proteins through interaction with AgrD mimics or by identifying genes that

interfere with *agr* activity using transposon libraries. To our knowledge, no transporters of modified AgrD (or AIP) have been identified to date.

As for proteins that cleave the N-terminal domain of AgrD, a few have been reported but none have been shown to have direct interactions with AgrD. The first study in 2007 by Kavanaugh *et al.* reported that type-I signal peptidase SpsB, a housekeeping protein in *S. aureus*, could cleave short peptide sequences corresponding to the cleavage site of AgrD-I.⁵⁹ While SpsB could cleave these peptides at the correct site, the ability of SpsB to cleave the full-length macrocyclic AgrD-I was never verified nor was the peptidase activity of SpsB demonstrated with other AgrD sequences.⁵⁹ While unpublished, preliminary data from the Muir lab suggested SpsB could not cleave the macrocyclic AgrD-II, bringing into question the role of SpsB for all *S. aureus agr* systems.¹⁰¹ More recently, two reports detail that *S. aureus* knockout mutants of a membrane peptidase MroQ have diminished *agr* activity.¹⁰²⁻¹⁰³ Supernatant analysis revealed that while these mutants can produce small amounts of AIP, the AIP levels are substantially less than wild-type production (approximately 50-fold reduced).¹⁰²⁻¹⁰³ The overexpression of *agrBD* in the $\Delta mroQ$ strain restored some AIP production, suggesting MroQ plays a role in optimizing AgrD processing and/or export.¹⁰³ While these works characterize specific proteins that contribute to AIP biosynthesis, it is also possible these final modifications are not performed by specialized proteins and instead can be done by multiple housekeeping proteins found in many bacteria. This possibility would explain the mechanisms by which synthetic constructs of the *S. aureus agr* system in *Escherichia coli* and *Bacillus megaterium* can produce AIPs (e.g., when provided *agrBD* genes).¹⁰⁴⁻¹⁰⁵ It is important to note, however,

that while these heterologous systems produced bioactive AIPs as determined by fluorescent *agr* reporter assays, mass spectrometry data to confirm that these AIPs were of the correct length were not reported.¹⁰⁴⁻¹⁰⁵ Regardless of whether the final modification steps are performed by specific or general actors, additional biochemical work is clearly needed to better elucidate the final steps of AgrD processing in *S. aureus* and characterize this pathway in other organisms.

1.3.5 *AgrC* receptor sensing the AIP signal

AIPs are sensed by a two-component signal transduction system comprised of AgrC and AgrA, functioning as the histidine protein kinase (HPK) receptor and response regulator, respectively. AgrC receptors are active as homodimers and belong to the HPK₁₀ subfamily; many of their unique structural features and deviations in relation to this subfamily and HPKs in general have been reviewed previously⁵⁷ and will not be discussed here in detail. AgrC is comprised of an N-terminal sensor domain embedded into the membrane, a linker domain, and a cytoplasmic C-terminal histidine kinase (HK) domain (Figure 1.5A). AIP activation of AgrC triggers *trans*-autophosphorylation of the HK domain and subsequent phosphorelay to AgrA.

The N-terminal sensor domain of AgrC, as its name implies, is the site for AIP binding. Sequence alignments indicate this domain is not well-conserved across Gram-positive bacteria and is within the hypervariable region along with AgrD and portions of AgrB,⁶³ suggesting that the sensor domain co-evolved with AgrD and AgrB to make and sense its own unique cognate AIP.⁵⁷ The short linker domain, recently named the “S Helix,”¹⁰⁶ is critical for signal transduction, and is similarly not well-conserved across *agr*

systems.⁶¹ As the C-terminal HK domain of AgrC lies outside of the hypervariable region, it is more highly-conserved than the other domains across *agr* systems and particularly in the Staphylococci,^{57, 87} and is comprised of two subdomains, a dimerization and histidine phosphorylation (DHP) subdomain and a catalytic, ATP-binding (CA) subdomain. The DHP portion forms a four-helix bundle in the AgrC homodimer. Upon AIP activation of AgrC, the CA subdomain catalyzes phosphorylation of a conserved histidine in the DHP subdomain. Importantly, this occurs in *trans*: the CA subdomain of one monomer binds ATP and transfers a phosphoryl to the histidine in the DHP subdomain of the opposite monomer (i.e., *trans*-autophosphorylation).¹⁰⁷ The phosphorylated histidine can then transfer the phosphoryl to a conserved aspartic acid of AgrA to initiate transcriptional regulation.⁵⁷

While the exact binding epitopes have not yet been identified, studies of AgrC mutants and chimeras in *S. aureus* have identified that AIP binding is largely mediated by various residues in the extracellular loops of the AgrC N-terminal domain¹⁰⁸⁻¹¹⁰ and hydrophobic patches on the AIPs.¹¹¹ Many AgrC sensor domain mutants and chimeras displayed altered activity profiles; some of these had broadened activity towards non-cognate, native AIPs,^{108-109, 112} were activated by linear forms of the AIPs,¹¹¹ had constitutive activity in the absence of AIPs,¹¹² or could even mode-switch, in which they were no longer antagonized but rather agonized by a specific AIP.¹⁰⁸

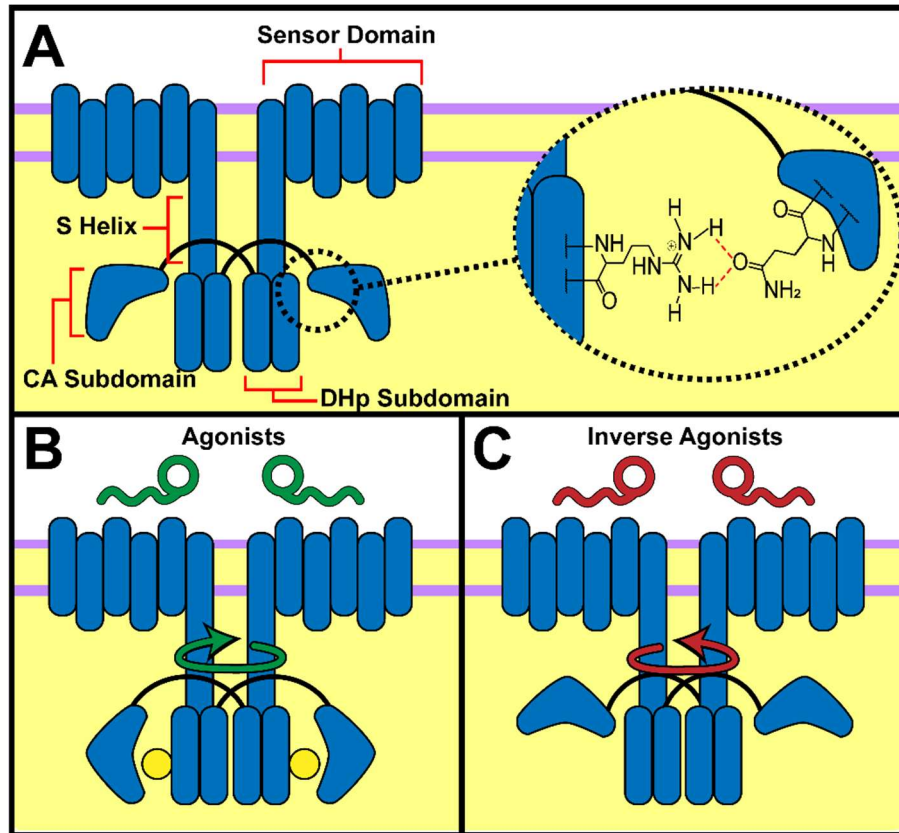


Figure 1.5 The mechanism of AgrC activation. (A) The N-terminal sensor domain links to the S Helix that transduces the signal through rotation of the DHp subdomain. Rotation of the DHp subdomain can alter a hydrogen bond (inset) between the DHp subdomain and the CA subdomain, either enabling or preventing the CA subdomain to catalyze phosphorylation. (B) Binding of agonists initiate a counter-clockwise rotation of the S Helix and freeing the CA subdomain for phosphorylation. (C) Inverse agonists induce clockwise rotation, sequestering the CA subdomain and inhibiting phosphorylation.

Once the AgrC sensor domain is activated by an AIP ligand, it must then transduce the signal to the HK domain. Beautiful biochemical studies to elucidate and characterize this transduction system have been performed the Muir laboratory, most recently utilizing their AgrC nanodisc technology (AgrC dimers stabilized by insertion into lipid bilayer discs), which has greatly facilitated *in vitro* study of AgrC. For example, with a fluorescently labeled AIP probe (FAM-AIP-I), binding affinity of AIPs with AgrCs nanodiscs could be determined (e.g., apparent K_D values of 63 and 160 nM were

determined for AIP-I and AIP-II with a preformed FAM-AIP-I: AgrC-I complex).⁶¹ Using the nanodisc format, phosphorylation of AgrC could be quantified readily using isotopically-labeled ATP, allowing for more detailed characterization of AIP and AIP analog activity on AgrC. Assessing phosphorylation activity of AIPs-I–IV on AgrC-I revealed that AIP-I and AIP-IV were agonists, AIP-II was an inverse agonist (as it lowered phosphorylation relative to vehicle control), and AIP-III was a neutral antagonist (as it matched vehicle control levels).⁶¹ Partial agonists could also be identified, as seen with a truncated analog of AIP-I (tr-AIP-I).⁶¹ These differing activity profiles suggested a complex system of signal transduction capable of sending a spectrum of activating or inhibitory signals.

While many HK-type proteins utilize a HAMP, PAS, or GAF domain for signal transduction,¹¹³ AgrC has no such domains and instead uses the S Helix linker to transduce its signal. The strong helical properties of the S Helix provides the foundation for transduction. Using a series of truncated S Helix domains fused to a GCN4 protein, Wang *et al.* demonstrated that the conformational rotation of the helix imparted phosphorylation activity.⁶¹ Furthermore, using S Helix mutants with cysteine residues at various locations on the helix, they demonstrated the S Helix rotated in full-length AgrC by measuring disulfide formation of the cysteine residues across the dimer interface.⁶¹ When assessing AIP ligand activity *in vitro* using the nanodisc system, AIP-I induced a counter-clockwise rotation and an increase in phosphorylation, while the inverse agonist AIP-II induced a clockwise rotation and a decrease in phosphorylation (Figure 1.5B–C), suggesting the activity profile of AIPs induce different rotations of the S Helix and give rise to the observed AgrC activity.⁶¹

This signal transduction via the S Helix occurs symmetrically and in *trans* throughout the AgrC dimer as demonstrated with a series of AgrC heterodimers that complement each other's defects.¹⁰⁷ For example, heterodimers of AgrC mutants with inactivated kinase domains (AgrC_{Kin}) and AgrC mutants with removed histidine phosphorylation sites (AgrC_{His}) were still active *in vitro*, suggesting the histidine on the AgrC_{Kin} protomer was phosphorylated through the AgrC_{His} protomer.¹⁰⁷ Similar complementary results occurred when the heterodimers were formed between wild-type and inactivated sensor-domain mutants,¹⁰⁷ and even heterodimers formed with AgrC-I and AgrC-II resulting in both units being phosphorylated upon addition of either AIP-I or AIP-II.⁵⁶ A few mutations in the DHp subdomain could result in constitutively active AgrC monomers, and heterodimers between these constitutive mutants and wild-type AgrC displayed ligand-independent phosphorylation.¹⁰⁷ Later AgrC nanodisc studies revealed that an arginine in the DHp domain forms a hydrogen-bond to a glutamine residue in the CA subdomain of the opposite monomer (Figure 1.5A, inset), preventing the CA subdomain from phosphorylating the histidine until this hydrogen-bond is disrupted upon ligand-induced conformational changes.¹⁰⁶ Thus, substitutions of these residues or surrounding residues can disrupt these hydrogen-bonds and can permanently release the CA subdomain for ligand-independent, constitutive activity.^{107, 112, 114}

Taking these collective *in vitro* data for AgrC receptors together, the working model that best describes the mechanism of AgrC activity is as follows. The binding of AIPs to the N-terminal sensor domain triggers differential conformational changes in the S Helix linker domain. With agonists, the counter-clockwise rotation of the linker domain helices likely breaks the hydrogen bond between the DHp and CA subdomains and

facilitates histidine phosphorylation and subsequent phosphorelay to AgrA. Partial agonists likely induce counter-clockwise rotations of smaller magnitudes, resulting in increased but not full accessibility of the histidine for phosphorylation. Neutral antagonists maintain the basal phosphorylation rate, suggesting negligible effects on the CA subdomain sequestration and therefore they likely do not substantially rotate the S-helix. Finally, inverse agonists are hypothesized to induce clockwise helical rotations that strengthen the hydrogen-bonding interaction between the DHp and CA subdomains, reducing phosphorylation activity below basal levels. While these mechanistic studies have only been performed in the *S. aureus* AgrC receptors, Wang *et al.* have shown that the S-Helix linker region is present between the last transmembrane helix of the N-terminal domain and the start of the DHp subdomain in many members of the HPK₁₀ subfamily.⁶¹ This common linker region and the overall higher conservation of the AgrC C-terminal domain would suggest that other AgrC receptors likely function in similar manners. The nanodisc technology theoretically should be applicable to *in vitro* studies of any AgrC receptor, opening up new avenues to examine their similarities and differences in the future.

1.3.6 *AgrA interactions with DNA*

The AgrA protein is the response regulator in the AgrC:AgrA two component system and the source of the observed regulatory changes upon *agr* activity. Of the four *agr* proteins, AgrA is the only one not in the hypervariable region and accordingly is far better conserved.⁶³ As an example, while there is substantial divergence between the other *agr* proteins in the *S. aureus agr* specificity groups, AgrA is fully conserved across

the species. The N-terminal domain contains the conserved aspartic acid phosphorylation site; its phosphorylation induces AgrA dimerization, and the C-terminal domains of the complex then bind DNA. While most response regulators utilize a helix-turn-helix (HTH) domain for DNA binding, AgrA is a part of the LytTR family of response regulators that bind DNA differently.¹¹⁵ LytTR domains bind a small consensus sequence, where loop regions of LytTR domains interact with three subsequent grooves (two major, 1 minor) of DNA and induce a characteristic bend in the DNA.¹¹⁵ One residue involved in DNA binding, Arg-233 in *S. aureus agr-I*, is 100% conserved in more than 200 AgrA sequences.¹¹⁶ Moreover, many residues surrounding this arginine are also 100% conserved, suggesting all AgrA proteins bind DNA similarly.¹¹⁶

With the LytTR DNA binding domain, the AgrA dimer binds promoter regions such as the P2 promoter for the *agr* operon and the P3 promoter for RNAIII transcription. Surprisingly, *in vitro* studies have demonstrated AgrA does not require phosphorylation for DNA binding activity, as electrophoretic mobility shift (EMSA) assays show interactions of AgrA with the P2 and P3 promoters when incubated in the absence of a phosphate donor.⁶² Phosphorylation of AgrA did enhance its affinity for the promoters, and greater affinity was observed for the P2 promoter over P3 in *S. aureus*.⁶² The enhanced affinity for P2 is hypothesized to assist with the autoinduction loop, amplifying the response prior to activating the main effector molecule RNAIII under the control of the P3 promoter. In addition to the P2 and P3 promoters, there is also a P1 promoter upstream of *agrA* that AgrA is hypothesized to bind to, but has not been experimentally verified.¹¹⁷ In the Staphylococci, AgrA is also known to bind promoters responsible for production of phenol-soluble modulins (PSMs), biosurfactants that

structure and disperse biofilms among other functions.¹¹⁸ While AgrA-dependent transcription of RNAIII is critical to *agr*-dependent genetic regulation in the Staphylococci due to the large regulon under RNAIII control,⁸⁶ it is unclear how widespread the P3 promoter and the regulatory RNAIII molecule is in other bacteria with *agr* systems. For example, despite detailed searching for homologues, no corresponding RNAIII has been found in *Listeria monocytogenes*¹¹⁹ or *Clostridia difficile*.¹²⁰ In these species, AgrA must bind to more promoters or induce expression of other regulatory RNAs in order to regulate gene expression upon activation, although to date no studies have identified any such promoters or regulatory RNAs.

1.4 Chemical Control of the *agr* System

1.4.1 Chemical modulators as tools to probe QS

Initially, the phenomenon we know today as QS was originally known as “autoinduction” as the native signaling molecules were found to activate production of their biosynthetic machinery and cognate receptors. However, early in the studies of AHL-based LuxI/LuxR-type QS, instances of cross-activity from non-cognate AHLs was observed, making “autoinduction” a less precise descriptor for the entire system and eventually “quorum sensing” was accepted as the general term. Moreover, in addition to non-native AHLs having activity, many entirely synthetic AHL analogs not known to be naturally produced by any species were active in LuxR-type receptors.¹²¹⁻¹³⁰ The activity of synthetic QS signal analogs was revealed to occur in many QS systems, and these compounds represent powerful chemical tools to modulate bacterial group behavior. The ability to control QS phenotypes with chemical modulators inspired many labs,

including our own, to design and synthesize compounds to probe QS systems. In addition to molecules that mimic the native QS signal, many have successfully found novel and structurally diverse scaffolds that target various components of QS machinery through discovery-based screening of commercial libraries and collections of natural product isolates.¹³¹⁻¹⁴² Lead compounds revealed in these screens often have improved chemical stability and solubility relative to signal mimics, along with additional handles for further synthetic modification.¹⁴³

Chemical probes can allow for the modulation of biological pathways at a variety of levels through agonists, partial agonists, and antagonists, with each able to be used with both spatial and temporal control.¹⁴⁴⁻¹⁴⁶ Wielding finely tuned probes with a spectrum of activity, researchers can probe deeper into many fundamental aspects of biology that genetic knockouts, with their simple binary “on-off” outputs, cannot offer.¹⁴⁷⁻¹⁴⁸ Such chemical probes can facilitate the study of the complex regulation circuits controlled by QS activity, the mechanisms by which the protein components function both individually and together, and how bacteria may utilize QS in their natural environments.

1.4.2 *AIP biosynthesis modulators*

One mechanism to chemically modulate *agr* activity would be to target the machinery that synthesizes the AIP molecules. While it is conceivable there are molecules that could enhance the rate of AIP production by catalyzing interactions between AgrD and AgrB or the other uncharacterized components that process and/or transport AgrD, none such molecules have been discovered. Screening for compounds

that alter the activity of this machinery has produced a single inhibitory molecule, the natural product ambuic acid (Figure 1.6a).¹⁴⁹ Initially discovered in 2009 from a screen of fungal metabolites to inhibit production of the *E. faecalis* AIP, ambuic acid is active against a number of Staphylococci and members of the *Listeria* genus.^{138, 149} Currently, the mechanism by which ambuic acid blocks AIP biosynthesis is not understood. The potency of ambuic acid varies in the different species, with IC₅₀ values ranging from single-digit micromolar in *E. faecalis* to hundreds of micromolar in some Staphylococci, and intriguingly also for *agr* specificity groups within a species (*S. epidermidis agr*-I, 15 μ M; *agr*-II and *agr*-III, >200 μ M).¹³⁸ This varying potency within the same species suggests ambuic targets AgrD or AgrB, as presumably the other components for additional processing and transport would be similar between *agr* specificity groups. Additional research to investigate the mechanism of action for ambuic acid could more fully reveal the source of its specificity, and perhaps give insight into development of new AIP biosynthesis modulators that could selectively or universally target other *agr* systems.

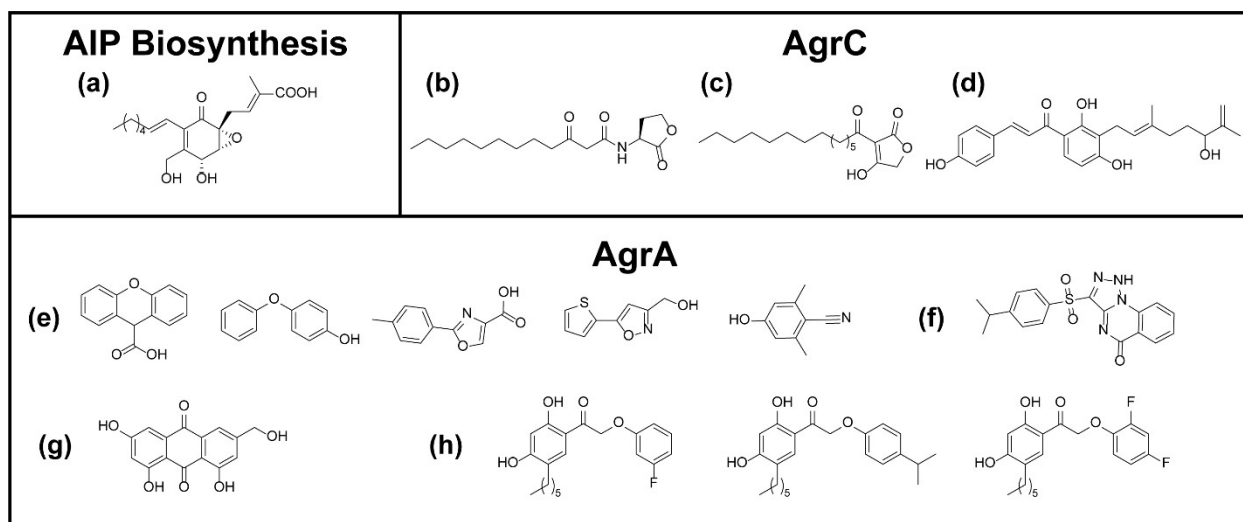


Figure 1.6 Small molecule modulators of *agr* activity, categorized by target.

1.4.3 Targeted AIP sequestration and degradation

Methods to capture the AIP after production and secretion, preventing AgrC activation and thereby QS, have also been successful. In the early 2000s, it was reported that *agr* activity (via RNAIII) was severely repressed in the presence of serum,¹⁵⁰ leading others to investigate if any specific serum components could be interacting with components of the *agr* system. Peterson *et al.* hypothesized that the hydrophobic interactions that dictate AIP-AgrC binding^{108, 111} could be intercepted by lipoproteins in plasma.¹⁵¹ They went on to demonstrate that serum protein Apolipoprotein B (ApoB) binds *S. aureus* AIP-I through surface plasmon resonance, suggesting that this binding event could sequester AIPs away from AgrC and cause the observed reduction in *agr* activity.¹⁵¹ They also showed that mice with low levels of ApoB had severe *S. aureus* infections when compared to wild-type mice, but this susceptibility vanished when using Δagr *S. aureus* strains, indicating a strong physiological connection between ApoB and *agr* activity *in vivo*.¹⁵¹ Subsequent studies

would show that the N-terminal portion of ApoB is necessary and sufficient for this effect,¹⁵² and that protection can be broadened to cover all *S. aureus* AIPs when ApoB is combined with oxidized low density lipoproteins.¹⁵³ These results suggest that ApoB may contribute to the host-defense against *S. aureus*, but it remains unclear whether ApoB can bind AIPs from other organisms.

In addition to these barriers to *agr* activity in hosts, others have developed monoclonal antibodies that bind to AIPs and effectively prevent these peptides from acting as QS signals, thereby “quenching” this quorum. Park *et al.* designed a novel hapten based on *S. aureus* AIP-IV and were able to discover an antibody, AP4-24H11, that tightly bound AIP-IV with high specificity over the other native *S. aureus* AIPs.¹⁵⁴ Subsequent *in vitro* evaluation demonstrated AP4-24H11 altered virulence factor production in cultures, suggesting the antibody successfully bound AIP-IV prior to binding and activating AgrC.¹⁵⁴ Furthermore, AP4-244H11 was found to block *S. aureus* infection in an *in vivo* mouse model.¹⁵⁴ Despite these promising results, additional studies utilizing AP4-24H11 or the development of other novel AIP-targeting antibodies have not been reported.

1.4.4 *AgrC* receptor modulators

Of the various strategies to target *agr* activity with chemical probes, AgrC modulation has been the most pursued approach to date. Targeting AgrC offers a number of key advantages. First, the native interaction between the AIP ligand and the AgrC receptor provides a starting platform from which many non-native synthetic modulators have been discovered and developed. As the sensor domain of AgrC is

extracellular, modulators do not have to be membrane permeable which greatly increases the structural diversity of molecules and enables additional functionalization of probes (such as covalent attachment of antibiotics,¹⁵⁵ fluorescent probes,¹⁵⁵⁻¹⁵⁸ moieties for affinity pull-down,¹⁵⁷ or attachment to surfaces¹⁵⁹). Additionally, as the sensor domain is typically highly selective for specific AIP signals, the receptor is capable of distinguishing between signals allowing for selective activation or inhibition; that said, this selectivity can be overcome as many pan-active molecules have also been reported. Lastly, while chemical inhibition of the other *agr* components can be accomplished, chemical activation of the *agr* system can currently only be achieved via AgrC.

The first reported and most characterized AgrC modulators to date are native AIP signals and their peptide analogs. After observing cross-activity between the native AIPs of *S. aureus* and other organisms,^{87, 160} many groups, including our laboratory, began to detail the structure-activity relationships (SARs) between AIPs and AgrCs that give rise to *agr* agonism and antagonism. Studies in many organisms have shown that assessing the activity of AIP analogs in which individual amino acid residues were systematically replaced with alanine or D-amino acids was a reliable and efficient method to build fundamental SARs.^{51, 94, 157, 161-165} Often, a single amino acid substitution was sufficient to mode-switch the native AIP signal into a strong antagonist with low nanomolar potency (e.g., *S. aureus* AIP-I D5A; Figure 1.7a);^{161, 163-164} otherwise, truncation of the exocyclic tail was another common route towards AgrC inhibition, although generally these were less potent (e.g., truncated *S. aureus* AIP-II; Figure 1.7b).^{157, 162-163} These methods in isolation or combined have produced potent

antagonists of *agr* activity that are often active towards multiple *agr* groups, with our lab developing the inhibitor AIP-III D4A that has sub-nanomolar potency in all four *S. aureus* *agr* groups, representing the most potent *agr* antagonist reported to date (Figure 1.7c).¹⁶³ While generally more rare than inhibitory compounds, AIP analogs with improved agonism activity or potency have also been discovered through similar means.^{51, 161, 164, 166-167} Very recently, our lab has developed chimeric AIP analogs (e.g., Cmr1 S7A; Figure 1.7d) that agonize multiple *agr* groups in *S. epidermidis*, suggesting that the development of pan-group AgrC agonists is possible.¹⁶⁷ To date, the only molecules demonstrated to agonize AgrC receptors are based on AIP scaffolds, highlighting the importance of these synthetic AIP analog agonists.

From these AIP analogs, novel peptidomimetic scaffolds have been developed and have desirable qualities over standard peptide AgrC modulators. Subtle deviations from standard peptides with non-canonical amino acids (ncAAs) has enabled deeper investigation into the SARs of AIP analogs. Using diaminopropionic acid, lactam macrocyclic AIPs were developed; while lactam versions of the native AIPs appear to drastically reduce agonism potency,^{51, 168-169} we have shown that the incorporation of this amide linkage into inhibitors not only greatly improves their hydrolytic stability over standard thioester AIPs but also largely maintains their high antagonism potencies.¹⁶⁸ Various peptoids based on AIPs (i.e., containing *N*-alkyl glycine residues) can antagonize AgrC, although these are generally not as potent as peptidic molecules.¹⁷⁰⁻¹⁷¹ Recent work in our lab has demonstrated that the component parts of peptide modulators can be condensed and simplified into minimal, small-molecule-like scaffolds with enhanced aqueous solubility while maintaining potency and efficacy.¹⁷²⁻¹⁷³

Development of this minimal scaffold has produced a *S. aureus* pan-group AgrC inhibitor named Bnc3 with low- to sub-nanomolar potency while only containing a single standard amino acid (Figure 1.7e).¹⁷³

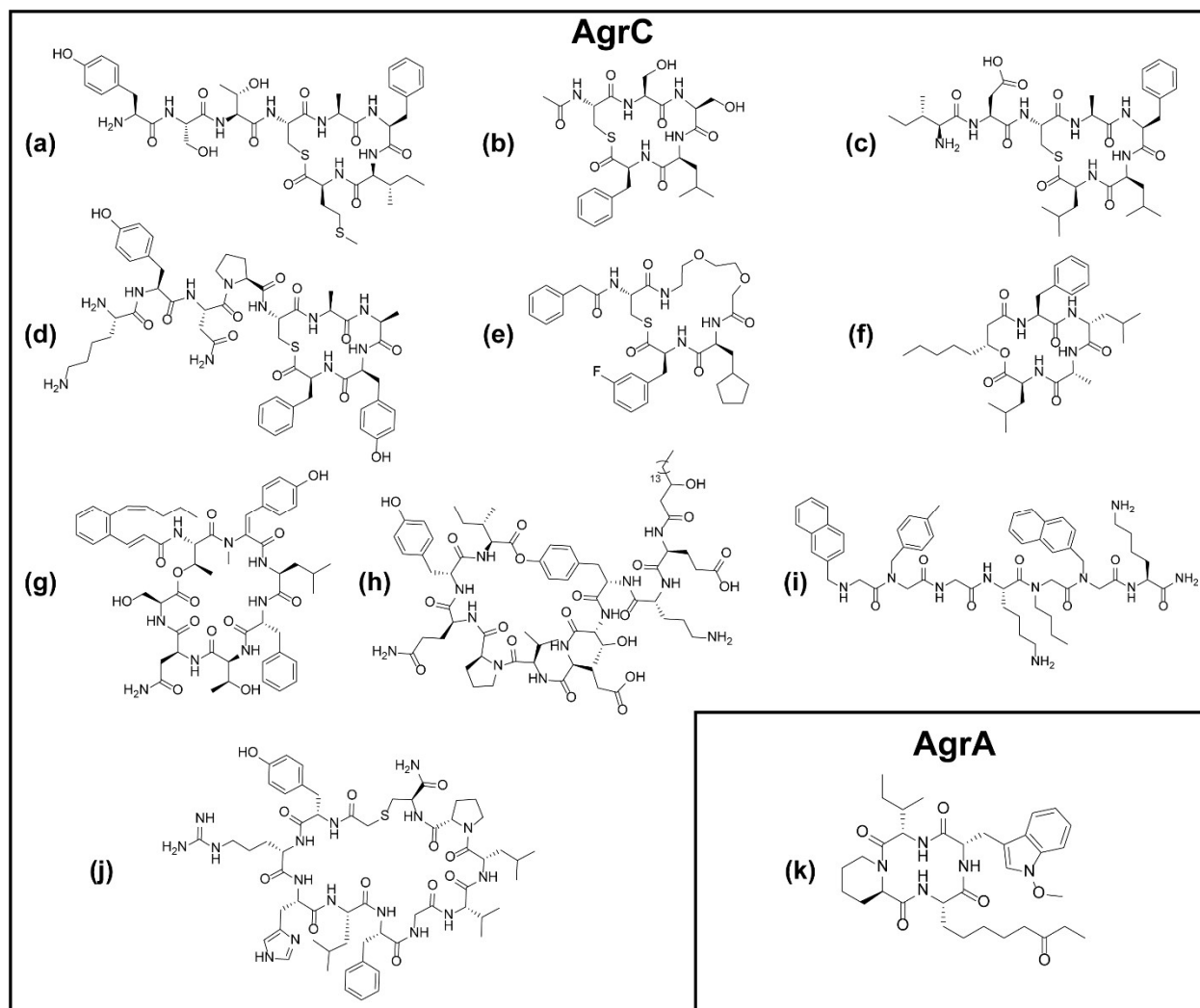


Figure 1.7 Peptidic modulators of *agr* activity, categorized by target.

Beyond AgrC modulators based on native AIP scaffolds, a number of other naturally occurring peptides unrelated to the *agr* system have been discovered to also antagonize AgrC. Solonomide compounds, or nonribosomal cyclodepsipeptides

produced by *Photobacterium halotolerans*, are structurally similar to AIPs, containing identically sized macrocycles (albeit with a lactone linkage instead of a thioester linkage) and multiple hydrophobic residues.¹⁴⁰ Solonamide B (Figure 1.7f) has been shown to directly compete with native AIPs for AgrC binding and has pan-inhibitory activity across the *S. aureus agr* groups,¹⁴⁰ and analogs based on Solonamide B have been developed with increased potency (although not as potent as previously discussed AIP mimics).¹⁷⁴⁻¹⁷⁵ Other cyclodepsipeptides also have been shown to inhibit *agr* activity with low micromolar potency, such as WS9326A (Figure 1.7g), WS9326B, and cochimicin II/III isolated from actinomycetes cultures.¹⁷⁶ These compounds have larger macrocycles than those found in AIPs, but are hypothesized to also interact with AgrC.¹⁷⁶ Probiotic *Bacillus* species can produce macrocyclic lipoproteins known as fengycins that contain a number of non-canonical amino acids, D-amino acids, and a β -hydroxy-fatty acid tail.¹⁴² Fengycins, such as β -OH-C17-fengycin B (Figure 1.7h), have been shown to protect against *S. aureus* infection through competition with native AIPs for AgrC binding, and are active against multiple *S. aureus agr* groups as well as *S. epidermidis*.¹⁴² While most naturally-occurring AgrC modulators are peptides, there are a few small molecule ligands as well. Interestingly, native AHL molecules from Gram-negative species (e.g., 3-oxo-dodecanoyl homoserine lactone; Figure 1.6b) or AHL analogs (e.g., 3-acyltetronic acids; Figure 1.6c) have been shown to inhibit AgrC.¹⁷⁷ Many of these compounds exhibited non-competitive inhibition, suggesting an allosteric binding site to inhibit AgrC activity with low micromolar potency.¹⁷⁷ No follow up studies have been performed with AHLs to explore this possibility further. Lastly, xanthoangelol B, a natural product isolated from a Japanese herb, can also inhibit AgrC activity (Figure

1.6d); however, experiments demonstrated this molecule can inhibit other histidine kinases, suggesting xanthoangelol B has a broad HK inhibitor rather than a specific AgrC inhibitor.¹⁷⁸

In recent years, discovery-based methods have identified several novel, synthetic scaffolds that target AgrC. Screening a combinatorial library of peptomers (i.e., peptide-peptoid hybrids), Karathanasi *et al.* identified linear peptidomimetics that compete with native AIPs to inhibit AgrC activity.¹⁷⁹ Their lead peptomers, G3 (Figure 1.7i) and A3, could inhibit AgrC at low micromolar concentrations, and are thought to adopt a pseudo-macrocyclic structure in solution.¹⁷⁹ While these peptomers are less potent than the other non-AIP-based macrocyclic peptides discussed above, their activity suggests linear peptidomimetics that mimic macrocyclic interactions could be further developed to target AgrC without the need for difficult cyclization reactions. That said, macrocyclization provides additional structural rigidity and contacts that are known to be important for high potency, as well as providing protection from proteolysis. Recent advances in macrocyclic peptide synthesis has allowed for incredibly diverse libraries to be generated quickly¹⁸⁰⁻¹⁸² that are relevant to the *agr* QS system. Xie *et al.* have used the RaPID mRNA display system to discover novel and competitive macrocyclic peptide inhibitors of AgrC that target multiple *agr* groups in *S. aureus* (e.g., QQ-3; Figure 1.7j).¹³⁶ Although not examined to date, applications of these macrocyclic peptide generating technologies should enable rapid discovery of AgrC modulators in other organisms.

1.4.5 *AgrA* modulators

While AgrC has been the most characterized biological target for *agr* modulators, many molecules have been discovered to target the response regulator AgrA. After the 3D structure of the DNA binding domain of AgrA was determined by X-ray crystallography, several groups screened for synthetic compounds that can potentially interact with the receptor:DNA binding interface. Screening of drug fragments by Leonard *et al.* has revealed multiple scaffolds with affinity for AgrA *in vitro* (Figure 1.6e); NMR and *in silico* docking data suggested these molecules bind to a shallow hydrophobic groove in AgrA, and this interaction disrupted DNA binding as evidenced by EMSAs.¹¹⁶ Follow-on studies demonstrate some of these compounds were efficacious at reducing virulence gene expression in cultures of *S. aureus*.¹⁴¹ While these drug fragments are not particularly potent at present (requiring high micromolar to low millimolar concentrations for efficacy),¹¹⁶ they present fertile scaffolds for continued development into more potent small molecule inhibitors of AgrA. Using *agr*-dependent fluorescent reporter strains, other studies screening sizable small molecule libraries for activity against *agr* led to the identification of a molecule known as savirin (*S. aureus* virulence inhibitor; Figure 1.6f), which similarly disrupts DNA binding of AgrA as determined by EMSAs.¹³⁹ Interestingly, despite high conservation of AgrA between *S. aureus* and *S. epidermidis* (88% identity), savirin is reported to selectively inhibit *S. aureus* with an IC₅₀ of 83 μM.¹³⁹ Computational docking data suggests savirin interacts with a few residues in a hydrophobic cleft (near the cleft proposed by Leonard *et al.*)¹¹⁶ of *S. aureus* AgrA, and that differences in these residues between *S. aureus* and *S. epidermidis* give rise to the selectivity of savirin.¹³⁹ Additional studies by the same group

that identified savirin revealed the natural product ω -hydroxyemodin (OHM; Figure 1.6g), which similarly targets the AgrA DNA binding interface.¹⁸³

In addition to experimental small molecule screening in the laboratory, virtual screening studies have also successfully identified AgrA inhibitory scaffolds. After an initial virtual screen of 90,000 small molecules from the National Cancer Institute for those capable of docking into the phosphorylation site of the N-terminal domain of AgrA, Khodaverdian *et al.* validated the activity of around 100 compounds to inhibit AgrA DNA binding *in vitro* with EMSAs, along with performing similar searches in commercial compound databases to find other potential hits.¹⁸⁴ The authors identified a number of biaryl compounds, including previously FDA-approved drugs,¹⁸⁴ and subsequent SAR studies have demonstrated some of their lead compounds (Figure 1.6h) could curb virulent phenotypes in *S. aureus* as well as sensitize *S. aureus* to antibiotics.¹⁸⁴⁻¹⁸⁶ Unfortunately, despite virtually screening for compounds that target the phosphorylation site in the N-terminal domain of AgrA, it is unclear whether these molecules actually prevent AgrA phosphorylation, as the authors suggest these molecules might also bind in the DNA-binding domain¹⁸⁴ analogous to the other AgrA inhibitors discussed above.

Outside of small molecules, other inhibitors of AgrA activity have been discovered and developed. When Parlet *et al.* discovered that some cyclic, modified tetrapeptide fungal metabolites inhibited *agr* activity (e.g., apicidin; Figure 1.7k), they initially expected these molecules would target AgrC due to sharing many common qualities with other known AgrC modulators—i.e., cyclic, peptidic, and largely hydrophobic.¹³⁷ Surprisingly, these apicidins appear to target AgrA, as the authors demonstrate dose-dependent inhibition of P3-dependent luminescence in a *S. aureus*

reporter strain that constitutively produces AgrA in the absence of *agrB*, *agrD*, and *agrC*.¹³⁷ The exact mechanism by which apicidins inhibit AgrA is not yet understood.¹³⁷ Finally, Da *et al.* have inhibited AgrA activity through designing antisense peptide locked nucleic acids (PLNAs) that target *agrA* mRNA.¹⁸⁷ Two PLNAs were designed to bind to regions of the predicted secondary structure of *agrA* mRNA and then conjugated to a cell-penetrating peptide sequence. These PLNAs reduced *agrA* and downstream *RNAIII* transcription at low micromolar concentrations and were subsequently shown to alleviate virulence phenotypes *in vitro* and *in vivo*.¹⁸⁷ To our knowledge, this report is the first to target *agr* activity through directly disrupting translation of the *agr* components, and this approach could be used to selectively target any *agr* system that has been sequenced.

1.4.6 Looking ahead: remaining questions about the role of agr QS in vivo and the modes by which chemical modulators can be applied to probe complex systems

While it is clear from the many studies in *S. aureus*, and to a lesser extent in other organisms, that *agr* QS controls a large number of genes and downstream phenotypes *in vitro*, we are still far from understanding the intricacies of *agr* QS in physiologically and ecologically relevant settings. For example, the temporal role of *agr* QS during the stages of infection is not well understood. Knockout mutants, while informing on the necessity of the *agr* system for establishing an infection, fail to describe how the *agr* system contributes to virulence *in vivo* over the course of an infection. By controlling the timing at which bacteria are exposed to *agr* activators or inhibitors (e.g., prior to, during, or after infection), researchers can start to understand the role of *agr* in

infection development. While Sully *et al.* has shown that their AgrA inhibitor savirin can strongly reduce abscess formation when co-injected with *S. aureus* in a dermonecrosis mouse model, efficacy is drastically reduced when savirin is delivered 24 or 48 hours after *S. aureus*.¹³⁹ Studies investigating the effects of chemical *agr* agonists and antagonists in the early stages of infection could be highly informative to elucidate the temporal relationship between *agr* activity and abscesses formation.

Whereas *agr* activity in the early stages of infection are likely key to acute infections, very little is known about the role of *agr* QS in chronic infections. Often, clinical isolates of *S. aureus* from chronic infections are deficient in *agr* QS, but as noted above *agr* QS is often required to establish infections, suggesting that spontaneous *agr*-deficient mutants could emerge sometime after acute infection is established *in vivo* that eventually lead to chronic infections.¹⁸⁸ Some researchers hypothesize that the increased immune response during QS activation in various species creates selective pressure that can drive QS-deficient mutants over time *in vivo*;¹⁸⁹ accordingly, studies that investigate the effects of long-term QS activation or inhibition through sustained exposure to *agr* modulators may help elucidate the pathways by which these mutants emerge (Figure 1.8A). Interestingly, while QS is historically defined as a coordinated, population-wide change in genetic regulation, recent research in *agr* QS suggests distinct spatial zones of increased or decreased *agr* activity for genetically-identical cells in a bacterial population.¹⁹⁰ These differences in *agr* activity could persist and give rise to differentiated cells more poised for either chronic or acute infections.¹⁹⁰ Spatial control of *agr* QS using chemical modulators with wild-type and genetic knockout

mutants could enable researchers to better characterize these differentiation events that may lead to chronic infection.

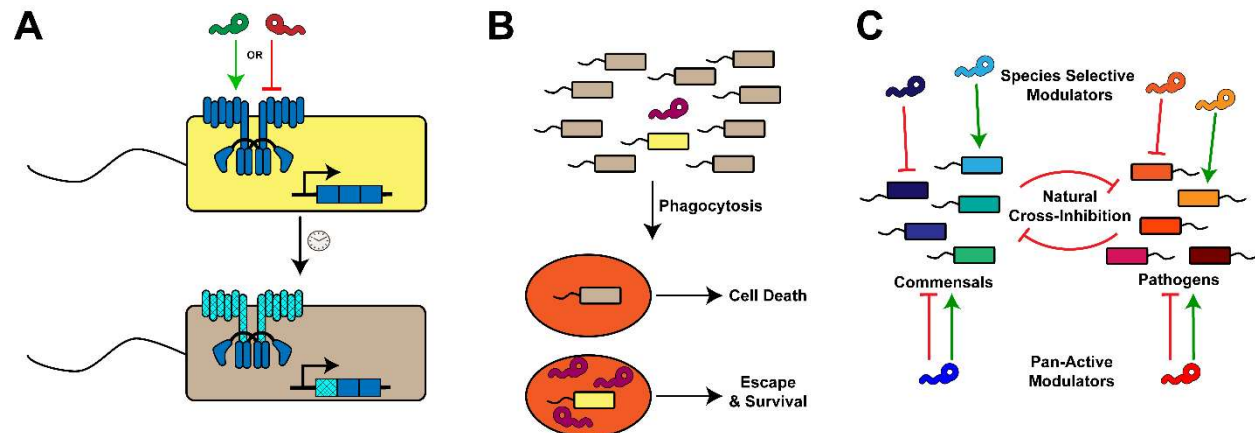


Figure 1.8 Potential uses of chemical probes to explore *agr* QS in vivo. (A) Long-term dosing of wild-type bacteria (yellow bacteria) with agonists or antagonists could produce mutants with altered or non-functional *agr* QS (grey bacteria). (B) Small numbers of *agr*-active bacteria in populations of *agr*-null bacteria cannot activate QS extracellularly, but could activate in a phagosome (orange) to escape while *agr*-null bacteria are killed. (C) Using selective or pan-active modulators to agonize or antagonize QS of commensals and pathogens can elucidate the role of *agr* QS cross activity in physiological settings.

In addition to delineating the pathways and conditions by which *agr*-deficient mutants emerge in wild-type bacteria, chemical *agr* modulators also could assist in characterizing reversions. Recent studies have shown that within *agr*-deficient *S. aureus* cultures there are small populations that can revert back to normal *agr* QS.¹⁹¹ While the number of these variant cells is insufficient to activate *agr* activity in extracellular spaces, in a small compartment these variants could re-initiate *agr* activity. This could occur in a phagosome during host immune responses (others have previously shown wild-type *S. aureus* activate *agr* QS in phagosomes)¹⁴ and suggests these variants may serve as a strategy to ensure survival and provide a way to continue

infection (Figure 1.8B).¹⁹¹ Chemical inhibition of these phase variants could prevent *agr* activation in a phagosome, disrupting this hypothesized insurance strategy.

Finally, *agr* QS is also not well-understood in the context of mixed microbial communities. The prevalence of cross-activity between *agr* systems suggests *agr* QS may be used to block *agr* activity of other organisms, allowing individual groups to establish dominance and/or prevent colonization of pathogens. Multiple commensal Staphylococci in the human microbiome produce AIPs that can potently block *S. aureus* *agr* activity (such as *S. caprae* or *S. simulans*), suggesting these types of interactions may be important for commensal protection against pathogens in humans.^{8, 192-193} Using selective or pan-activators to agonize commensal *agr* systems or selective inhibitors to antagonize pathogenic *agr* systems in mixed systems would facilitate characterizing the mechanisms by which pathogens colonize hosts and whether commensal *agr* QS contributes to host protection (Figure 1.8C).

1.5 Thesis Outline

1.5.1 Dissertation overview

At the time I joined the Blackwell Lab in 2016, there were multiple areas of *agr* QS that I could choose to investigate and try to push forward. Many *agr* systems had been identified across Gram-positive bacteria over the years, but very few had been thoroughly investigated outside of *S. aureus*. For several important Gram-positive organisms, such as *L. monocytogenes* and members of the *Clostridia* species, only a handful of fundamental studies had been reported detailing *agr* knockout mutants or preliminary AIP signal identifications. While there was a growing foundation of

knowledge of *agr* in some organisms like *S. epidermidis* and *E. faecalis* arising from early AIP SAR studies, deeper characterization of AIP-AgrC interactions and more specialized modulators were needed to probe if such chemical approaches could be applied to control behavior in these species. Finally, even with the comparative wealth of mechanistic knowledge in the *S. aureus* system and highly potent AIP mimics that inhibit AgrC, only a few labs had characterized the effects of *agr* inhibition in *in vivo* infection models. Over the past five years since I joined the Blackwell lab, I have contributed to further each of these fronts by: (1) exploring the under-characterized *agr* system in *L. monocytogenes*, (2) developing and characterizing novel chemical modulators with increased potency and efficacy in *S. epidermidis*, and (3) designing and evaluating degradable polymeric materials containing *agr* inhibitors to control *S. aureus* virulence *in vivo*. I summarize each of my efforts below.

1.5.2 Summary of Chapter 2: A Native Autoinducing Peptide Signal Reveals Highly Efficacious Inhibitors and Activators of Listeria monocytogenes Quorum Sensing and Biofilm Formation

Despite some initial studies that detailed effects of *agr* activity in *L. monocytogenes* with genetic knockout mutants, very little research has been reported that explores chemical approaches to probe the *L. monocytogenes agr* system. Importantly, at the outset of my research, there was confusion in the field about the native AIP, as multiple groups had reported conflicting structures. We sought to identify the native *L. monocytogenes* AIP ourselves, and we confirmed a 6-mer AIP structure that was in agreement with another past report. Using new *agr*-dependent fluorescent

reporter strains, we determined that the *L. monocytogenes agr* system is highly selective for its native AIP, as many non-cognate AIPs fails to activate or inhibit *agr* activity. Using the native AIP scaffold, we synthesized and assayed analogs to build SARs for *agr* activation (presumably by targeting AgrC), and utilized those structure-function data to develop potent and efficacious agonists and antagonists of the system. We validated the activity of these *agr* modulators in biofilm assays using wild-type *L. monocytogenes*, demonstrating that *agr* is an attractive target to combat a key virulence phenotype used by this pathogen to persist and avoid eradication in industry. These ligands represent the most potent and efficacious modulators for *L. monocytogenes agr*, with our agonists outperforming the native signal and our antagonists outperforming the known *agr* inhibitors in *L. monocytogenes*, and serve as scaffolds for further development and investigation of *L. monocytogenes* virulence.

1.5.3 Summary of Chapter 3: Conformational Switch to a β -turn in a Staphylococcal Quorum Sensing Signal Peptide Causes a Dramatic Increase in Potency

In a prior SAR study of AIP-I in *S. epidermidis*, our lab had described the activity of the native *S. epidermidis* AIPs against AgrC-I, and discovered agonists with increased potency over the native AIP-I for AgrC-I as well as pan-group antagonists that inhibited three *S. epidermidis agr* groups. In this past work, we used NMR spectroscopy to characterize the solution-phase conformations of these modulators, giving key structural insights into the activity profiles that we observed in cell-based fluorescent reporter assays. In our most potent modulators, we noticed the re-occurring presence of a β -turn motif in the compound macrocycles. While structural analogs that could

reinforce this β -turn displayed similar potencies, analogs that disrupted the hydrogen-bonding required for this β -turn had drastically reduced potency. Chemical shift analysis revealed these disrupted β -turn analogs had key structural deviations from their parent compounds near the β -turn, suggesting that the β -turn motif is critical for high potency with AgrC-I. The structure-function insights from these studies should inform the development of new chemical modulators of *S. epidermidis*.

1.5.4 Summary of Chapter 4: Non-Native Peptides Capable of Pan-Activating the *agr* Quorum Sensing System across Multiple Specificity Groups of *Staphylococcus epidermidis*

Our previous investigations of *S. epidermidis* AIPs and SARs for AgrC agonism/antagonism had focused on the *agr*-I group, and in this Chapter we turn to characterizing the SARs of the native AIP-II and AIP-III with their cognate receptors AgrC-II and AgrC-III, respectively. Surveying the known SARs for the three native AIPs, we noticed significant overlap in how AIPs are recognized and agonize their cognate receptors. We hypothesized we could design novel chimeric peptides that blend aspects of the three native AIPs and that agonize all three AgrC receptors simultaneously. Such compounds could be extremely useful for blocking biofilm formation in *S. epidermidis*, as the *agr* system represses biofilm formation (and thus *agr* agonism inhibits biofilm formation). We synthesized multiple scaffolds and analogs to identify multi-group *agr* agonists, finding two analogs which we call Cmr1 and Cmr1 S7A. We validated these multi-group agonists could induce phenotypes downstream of *agr* activation, as our multi-group agonists increased production of PSMs in the three *agr* specificity group

strains. These multi-group agonists are the first synthetic compounds demonstrated to activate multiple *agr* groups in any of the Staphylococci, and provide a key first step to developing potent and efficacious pan-group agonists.

1.5.5 Summary of Chapter 5: Sustained Release of a Synthetic Autoinducing Peptide Mimetic Strongly Attenuates MRSA Infections In Vivo

Many studies have demonstrated that chemical inhibition of *agr* activity in *S. aureus* can attenuate virulence phenotypes *in vitro*. However, there is still much to be understood about the role of *agr* activity *in vivo*. Chemical tools and strategies to probe *agr in vivo* are few as (i) many reported small molecule *agr* inhibitors lack known SAR to tune specificity, (ii) AIP mimics, which are generally the most potent modulators and can be tuned to be selective or pan-active, are hydrolytically unstable, have poor aqueous solubilities, and have largely not been studied *in vivo*, and (iii) the animal host can sequester or degrade inhibitors, necessitating large amounts of compound for efficacy. In this Chapter, we determined that certain scaffolds of AIP mimics can resist sequestration and degradation effects, and that these AIP mimics can be released from poly(lactic-co-glycolic acid) (PLGA) polymers to extend inhibition over long time periods. Our lead inhibitor was efficacious in reducing abscess formation in a *S. aureus* dermonecrosis mouse infection model when administered as a solution or loaded into PLGA microspheres. Critically, the compound loaded microsphere enables nanogram quantities of compound to attenuate infection, drastically improving over previous reports that utilize microgram quantities for similar results. The modular nature of both PLGA materials and the AIP mimics facilitate *in vivo* studies not only for *S. aureus*, but also for any other *agr* systems with known *agr* modulators.

1.5.6 Summary of Chapter 6: Future Directions

The results described in Chapters 2–5 create new opportunities for research into *agr* systems. In this chapter, I first propose new areas to continue exploring within the projects described above as well as offer novel project ideas to investigate *agr* QS. I describe follow up experiments in *L. monocytogenes*, exploring additional SARs of our novel agonists and antagonists to improve efficacy and potency. Our existing *L. monocytogenes* modulators or new ones discovered in future SAR studies could be utilized in a variety of applications, such as more closely detailing how *agr* activity affects the ability of *L. monocytogenes* to invade cells and spread. Next, I propose new SAR studies to expand our chimeric multi-group agonists in *S. epidermidis*, focusing on a few residues that we hypothesize to be key to improving agonism efficacy in the three *agr* groups. After this, I discuss deeper characterization of the structural-dependence of AIP sequestration *ex vivo* and propose novel applications of our compound-loaded materials to investigate *agr* activity in a variety of scenarios. I end the Chapter with a pair of novel project proposals: the first that seeks to utilize photoreactive amino acids to identify missing partners in AgrD processing and the AgrC binding site, and the second that seeks to develop new methods to generate AIP analogs rapidly.

1.5.7 Summary of Appendix I: Chemical Control of Quorum Sensing in E. coli: Identification of Small Molecule Modulators of SdiA and Mechanistic Characterization of a Covalent Inhibitor

This appendix details some of the collaborative work that I performed with Blackwell lab members who study AHL-based QS in Gram-negative bacteria. *E. coli* uses an orphan LuxR-type receptor known as SdiA to sense AHLs in its local environment. Interestingly, SAR studies of AHL analogs demonstrates SdiA is exceptionally promiscuous when compared to other LuxR-type receptors, and this is likely key to its activation of acid-resistance that is required *in vivo*. While most AHL analogs could activate SdiA, a few had inhibitory activity. We characterized the mechanism of action of one covalent inhibitor, providing new insights into how LuxR-type receptors can be targeted for covalent inhibition.

1.6 References

1. Nealson, K. H.; Platt, T.; Hastings, J. W., Cellular control of the synthesis and activity of the bacterial luminescent system. *J. Bacteriol.* **1970**, *104* (1), 313-22.
2. Eberhard, A.; Burlingame, A. L.; Eberhard, C.; Kenyon, G. L.; Nealson, K. H.; Oppenheimer, N. J., Structural identification of autoinducer of *Photobacterium fischeri* luciferase. *Biochemistry* **1981**, *20* (9), 2444-9.
3. Watson, W. T.; Minogue, T. D.; Val, D. L.; von Bodman, S. B.; Churchill, M. E. A., Structural Basis and Specificity of Acyl-Homoserine Lactone Signal Production in Bacterial Quorum Sensing. *Mol. Cell* **2002**, *9* (3), 685-694.
4. Fuqua, W. C.; Winans, S. C.; Greenberg, E. P., Quorum sensing in bacteria: the LuxR-LuxI family of cell density-responsive transcriptional regulators. *J. Bacteriol.* **1994**, *176* (2), 269-75.
5. Miller, M. B.; Bassler, B. L., Quorum sensing in bacteria. *Annu. Rev. Microbiol.* **2001**, *55*, 165-99.
6. Gray, K. M.; Passador, L.; Iglewski, B. H.; Greenberg, E. P., Interchangeability and specificity of components from the quorum-sensing regulatory systems of *Vibrio fischeri* and *Pseudomonas aeruginosa*. *J. Bacteriol.* **1994**, *176* (10), 3076-80.
7. Lewenza, S.; Visser, M. B.; Sokol, P. A., Interspecies communication between *Burkholderia cepacia* and *Pseudomonas aeruginosa*. *Can. J. Microbiol.* **2002**, *48* (8), 707-16.
8. Brown, M. M.; Kwiecinski, J. M.; Cruz, L. M.; Shahbandi, A.; Todd, D. A.; Cech, N. B.; Horswill, A. R., Novel Peptide from Commensal *Staphylococcus simulans* Blocks Methicillin-Resistant *Staphylococcus aureus* Quorum Sensing and Protects Host Skin from Damage. *Antimicrob. Agents Chemother.* **2020**, *64* (6), e00172-20.
9. Venturi, V.; Ahmer, B. M., Editorial: LuxR Solos are Becoming Major Players in Cell-Cell Communication in Bacteria. *Front. Cell. Infect. Microbiol.* **2015**, *5*, 89.
10. Abisado, R. G.; Benomar, S.; Klaus, J. R.; Dandekar, A. A.; Chandler, J. R., Bacterial Quorum Sensing and Microbial Community Interactions. *mBio* **2018**, *9* (3).
11. Wintermute, E. H.; Silver, P. A., Dynamics in the mixed microbial concourse. *Genes Dev.* **2010**, *24* (23), 2603-14.

12. Whiteley, M.; Diggle, S. P.; Greenberg, E. P., Progress in and promise of bacterial quorum sensing research. *Nature* **2017**, *551* (7680), 313-320.
13. Boedicker, J. Q.; Vincent, M. E.; Ismagilov, R. F., Microfluidic confinement of single cells of bacteria in small volumes initiates high-density behavior of quorum sensing and growth and reveals its variability. *Angew. Chem. Int. Ed. Engl.* **2009**, *48* (32), 5908-11.
14. Carnes, E. C.; Lopez, D. M.; Donegan, N. P.; Cheung, A.; Gresham, H.; Timmins, G. S.; Brinker, C. J., Confinement-induced quorum sensing of individual *Staphylococcus aureus* bacteria. *Nat. Chem. Biol.* **2010**, *6* (1), 41-5.
15. Redfield, R., Is quorum sensing a side effect of diffusion sensing? *Trends Microbiol.* **2002**, *10* (8), 365-370.
16. Hense, B. A.; Kuttler, C.; Muller, J.; Rothballer, M.; Hartmann, A.; Kreft, J. U., Does efficiency sensing unify diffusion and quorum sensing? *Nat. Rev. Microbiol.* **2007**, *5* (3), 230-9.
17. West, S. A.; Winzer, K.; Gardner, A.; Diggle, S. P., Quorum sensing and the confusion about diffusion. *Trends Microbiol.* **2012**, *20* (12), 586-94.
18. Wagner, V. E.; Bushnell, D.; Passador, L.; Brooks, A. I.; Iglewski, B. H., Microarray analysis of *Pseudomonas aeruginosa* quorum-sensing regulons: effects of growth phase and environment. *J. Bacteriol.* **2003**, *185* (7), 2080-95.
19. Schuster, M.; Lostroh, C. P.; Ogi, T.; Greenberg, E. P., Identification, timing, and signal specificity of *Pseudomonas aeruginosa* quorum-controlled genes: a transcriptome analysis. *J. Bacteriol.* **2003**, *185* (7), 2066-79.
20. Khmel, I. A., Quorum-sensing regulation of gene expression: Fundamental and applied aspects and the role in bacterial communication. *Microbiology* **2006**, *75* (4), 390-397.
21. Joint, I.; Allan Downie, J.; Williams, P., Bacterial conversations: talking, listening and eavesdropping. An introduction. *Philos. Trans. R. Soc. Lond. B Biol. Sci.* **2007**, *362* (1483), 1115-7.
22. McFall-Ngai, M., Hawaiian bobtail squid. *Curr. Biol.* **2008**, *18* (22), R1043-4.
23. Nyholm, S. V.; McFall-Ngai, M. J., The Winnowing: Establishing the Squid-*Vibrio* Symbiosis. *Nat. Rev. Microbiol.* **2004**, *2* (8), 632-42.
24. Dunlap, P. V.; Kita-Tsukamoto, K.; Waterbury, J. B.; Callahan, S. M., Isolation and characterization of a visibly luminous variant of *Vibrio fischeri* strain ES114

- from the sepiolid squid *Euprymna scolopes*. *Arch. Microbiol.* **1995**, *164* (3), 194-202.
25. Gonzalez, J. E.; Marketon, M. M., Quorum sensing in nitrogen-fixing rhizobia. *Microbiol. Mol. Biol. Rev.* **2003**, *67* (4), 574-92.
 26. Tortosa, P.; Logsdon, L.; Kraigher, B.; Itoh, Y.; Mandic-Mulec, I.; Dubnau, D., Specificity and genetic polymorphism of the *Bacillus* competence quorum-sensing system. *J. Bacteriol.* **2001**, *183* (2), 451-60.
 27. Li, J.; Chen, J.; Vidal, J. E.; McClane, B. A., The Agr-like quorum-sensing system regulates sporulation and production of enterotoxin and beta2 toxin by *Clostridium perfringens* type A non-food-borne human gastrointestinal disease strain F5603. *Infect. Immun.* **2011**, *79* (6), 2451-9.
 28. Davies, D., Understanding biofilm resistance to antibacterial agents. *Nat. Rev. Drug Discov.* **2003**, *2* (2), 114-22.
 29. Mah, T.-F. C.; O'Toole, G. A., Mechanisms of biofilm resistance to antimicrobial agents. *Trends Microbiol.* **2001**, *9* (1), 34-39.
 30. Rumbaugh, K. P.; Sauer, K., Biofilm dispersion. *Nat. Rev. Microbiol.* **2020**, *18* (10), 571-586.
 31. De Kievit, T. R.; Gillis, R.; Marx, S.; Brown, C.; Iglewski, B. H., Quorum-sensing genes in *Pseudomonas aeruginosa* biofilms: their role and expression patterns. *Appl. Environ. Microbiol.* **2001**, *67* (4), 1865-73.
 32. Riedel, C. U.; Monk, I. R.; Casey, P. G.; Waidmann, M. S.; Gahan, C. G.; Hill, C., AgrD-dependent quorum sensing affects biofilm formation, invasion, virulence and global gene expression profiles in *Listeria monocytogenes*. *Mol. Microbiol.* **2009**, *71* (5), 1177-89.
 33. Huber, B.; Riedel, K.; Hentzer, M.; Heydorn, A.; Gotschlich, A.; Givskov, M.; Molin, S.; Eberl, L., The cep quorum-sensing system of *Burkholderia cepacia* H111 controls biofilm formation and swarming motility. *Microbiology (Reading)* **2001**, *147* (Pt 9), 2517-2528.
 34. Vuong, C.; Gerke, C.; Somerville, G. A.; Fischer, E. R.; Otto, M., Quorum-sensing control of biofilm factors in *Staphylococcus epidermidis*. *J. Infect. Dis.* **2003**, *188* (5), 706-18.
 35. Boles, B. R.; Horswill, A. R., Agr-mediated dispersal of *Staphylococcus aureus* biofilms. *PLoS Pathog.* **2008**, *4* (4), e1000052.

36. Quadri, L. E. N., Regulation of antimicrobial peptide production by autoinducer-mediated quorum sensing in lactic acid bacteria. *Antonie Leeuwenhoek* **2002**, *82*, 133-145.
37. Brurberg, M. B.; Nes, I. F.; Eijsink, V. G., Pheromone-induced production of antimicrobial peptides in *Lactobacillus*. *Mol. Microbiol.* **1997**, *26* (2), 347-60.
38. Liu, X.; Bimerew, M.; Ma, Y.; Muller, H.; Ovadis, M.; Eberl, L.; Berg, G.; Chernin, L., Quorum-sensing signaling is required for production of the antibiotic pyrrolnitrin in a rhizospheric biocontrol strain of *Serratia plymuthica*. *FEMS Microbiol. Lett.* **2007**, *270* (2), 299-305.
39. Duerkop, B. A.; Varga, J.; Chandler, J. R.; Peterson, S. B.; Herman, J. P.; Churchill, M. E.; Parsek, M. R.; Nierman, W. C.; Greenberg, E. P., Quorum-sensing control of antibiotic synthesis in *Burkholderia thailandensis*. *J. Bacteriol.* **2009**, *191* (12), 3909-18.
40. Shanker, E.; Federle, M. J., Quorum Sensing Regulation of Competence and Bacteriocins in *Streptococcus pneumoniae* and *mutans*. *Genes (Basel)* **2017**, *8* (1).
41. McClean, K. H.; Winson, M. K.; Fish, L.; Taylor, A.; Chhabra, S. R.; Camara, M.; Daykin, M.; Lamb, J. H.; Swift, S.; Bycroft, B. W.; Stewart, G.; Williams, P., Quorum sensing and *Chromobacterium violaceum*: exploitation of violacein production and inhibition for the detection of N-acylhomoserine lactones. *Microbiology (Reading)* **1997**, *143* (Pt 12), 3703-3711.
42. Von Bodman, S. B.; Bauer, W. D.; Coplin, D. L., Quorum sensing in plant-pathogenic bacteria. *Annu. Rev. Phytopathol.* **2003**, *41*, 455-82.
43. Zhang, L.; Murphy, P. J.; Kerr, A.; Tate, M. E., *Agrobacterium* conjugation and gene regulation by N-acyl-L-homoserine lactones. *Nature* **1993**, *362* (6419), 446-8.
44. Jones, S.; Yu, B.; Bainton, N. J.; Birdsall, M.; Bycroft, B. W.; Chhabra, S. R.; Cox, A. J.; Golby, P.; Reeves, P. J.; Stephens, S., The lux autoinducer regulates the production of exoenzyme virulence determinants in *Erwinia carotovora* and *Pseudomonas aeruginosa*. *The EMBO Journal* **1993**, *12* (6), 2477-2482.
45. Azimi, S.; Klementiev, A. D.; Whiteley, M.; Diggle, S. P., Bacterial Quorum Sensing During Infection. *Annu. Rev. Microbiol.* **2020**, *74*, 201-219.
46. Rasko, D. A.; Sperandio, V., Anti-virulence strategies to combat bacteria-mediated disease. *Nat. Rev. Drug Discov.* **2010**, *9* (2), 117-28.

47. Ji, G.; Beavis, R. C.; Novick, R. P., Cell density control of staphylococcal virulence mediated by an octapeptide pheromone. *Proc. Natl. Acad. Sci. U. S. A.* **1995**, *92* (26), 12055-9.
48. Darkoh, C.; DuPont, H. L.; Norris, S. J.; Kaplan, H. B., Toxin synthesis by *Clostridium difficile* is regulated through quorum signaling. *mBio* **2015**, *6* (2), e02569.
49. Cheung, G. Y.; Joo, H. S.; Chatterjee, S. S.; Otto, M., Phenol-soluble modulins--critical determinants of staphylococcal virulence. *FEMS Microbiol. Rev.* **2014**, *38* (4), 698-719.
50. Pearson, J. P.; Feldman, M.; Iglewski, B. H.; Prince, A., *Pseudomonas aeruginosa* cell-to-cell signaling is required for virulence in a model of acute pulmonary infection. *Infect. Immun.* **2000**, *68* (7), 4331-4.
51. Mayville, P.; Ji, G.; Beavis, R.; Yang, H.; Goger, M.; Novick, R. P.; Muir, T. W., Structure-activity analysis of synthetic autoinducing thiolactone peptides from *Staphylococcus aureus* responsible for virulence. *Proc. Natl. Acad. Sci. U. S. A.* **1999**, *96* (4), 1218-23.
52. Papaioannou, E.; Utari, P. D.; Quax, W. J., Choosing an appropriate infection model to study quorum sensing inhibition in *Pseudomonas* infections. *Int. J. Mol. Sci.* **2013**, *14* (9), 19309-40.
53. Darkoh, C.; Odo, C.; DuPont, H. L., Accessory Gene Regulator-1 Locus Is Essential for Virulence and Pathogenesis of *Clostridium difficile*. *mBio* **2016**, *7* (4).
54. Wuster, A.; Babu, M. M., Conservation and evolutionary dynamics of the agr cell-to-cell communication system across firmicutes. *J. Bacteriol.* **2008**, *190* (2), 743-6.
55. Gray, B.; Hall, P.; Gresham, H., Targeting agr- and agr-Like quorum sensing systems for development of common therapeutics to treat multiple gram-positive bacterial infections. *Sensors (Basel)* **2013**, *13* (4), 5130-66.
56. Novick, R. P.; Geisinger, E., Quorum Sensing in Staphylococci. *Annu. Rev. Genet.* **2008**, *42*, 541-64.
57. Thoendel, M.; Kavanaugh, J. S.; Flack, C. E.; Horswill, A. R., Peptide Signaling in the Staphylococci. *Chem. Rev.* **2011**, *111* (1), 117-51.
58. Zhang, L.; Gray, L.; Novick, R. P.; Ji, G., Transmembrane topology of AgrB, the protein involved in the post-translational modification of AgrD in *Staphylococcus aureus*. *J. Biol. Chem.* **2002**, *277* (38), 34736-42.

59. Kavanaugh, J. S.; Thoendel, M.; Horswill, A. R., A role for type I signal peptidase in *Staphylococcus aureus* quorum sensing. *Mol. Microbiol.* **2007**, *65* (3), 780-98.
60. Wang, B.; Muir, T. W., Regulation of Virulence in *Staphylococcus aureus*: Molecular Mechanisms and Remaining Puzzles. *Cell Chem. Biol.* **2016**, *23* (2), 214-224.
61. Wang, B.; Zhao, A.; Novick, R. P.; Muir, T. W., Activation and inhibition of the receptor histidine kinase AgrC occurs through opposite helical transduction motions. *Mol. Cell* **2014**, *53* (6), 929-40.
62. Koenig, R. L.; Ray, J. L.; Maleki, S. J.; Smeltzer, M. S.; Hurlburt, B. K., *Staphylococcus aureus* AgrA binding to the RNAIII-agr regulatory region. *J. Bacteriol.* **2004**, *186* (22), 7549-55.
63. Dufour, P.; Jarraud, S.; Vandenesch, F.; Greenland, T.; Novick, R. P.; Bes, M.; Etienne, J.; Lina, G., High genetic variability of the agr locus in *Staphylococcus* species. *J. Bacteriol.* **2002**, *184* (4), 1180-6.
64. Li, J.; McClane, B. A., Evidence That VirS Is a Receptor for the Signaling Peptide of the *Clostridium perfringens* Agr-like Quorum Sensing System. *mBio* **2020**, *11* (5).
65. Dogsa, I.; Choudhary, K. S.; Marsetic, Z.; Hudaiberdiev, S.; Vera, R.; Pongor, S.; Mandic-Mulec, I., ComQXPA quorum sensing systems may not be unique to *Bacillus subtilis*: a census in prokaryotic genomes. *PLoS One* **2014**, *9* (5), e96122.
66. Okada, M.; Sato, I.; Cho, S. J.; Iwata, H.; Nishio, T.; Dubnau, D.; Sakagami, Y., Structure of the *Bacillus subtilis* quorum-sensing peptide pheromone ComX. *Nat. Chem. Biol.* **2005**, *1* (1), 23-4.
67. Comella, N.; Grossman, A. D., Conservation of genes and processes controlled by the quorum response in bacteria: characterization of genes controlled by the quorum-sensing transcription factor ComA in *Bacillus subtilis*. *Mol. Microbiol.* **2005**, *57* (4), 1159-74.
68. Bacon Schneider, K.; Palmer, T. M.; Grossman, A. D., Characterization of comQ and comX, two genes required for production of ComX pheromone in *Bacillus subtilis*. *J. Bacteriol.* **2002**, *184* (2), 410-9.
69. Oslizlo, A.; Stefanic, P.; Dogsa, I.; Mandic-Mulec, I., Private link between signal and response in *Bacillus subtilis* quorum sensing. *Proc. Natl. Acad. Sci. U. S. A.* **2014**, *111* (4), 1586-91.

70. Dogsa, I.; Spacapan, M.; Dragos, A.; Danevcic, T.; Pandur, Z.; Mandic-Mulec, I., Peptide signaling without feedback in signal production operates as a true quorum sensing communication system in *Bacillus subtilis*. *Commun Biol* **2021**, *4* (1), 58.
71. Li, Y. H.; Tang, N.; Aspiras, M. B.; Lau, P. C.; Lee, J. H.; Ellen, R. P.; Cvitkovitch, D. G., A quorum-sensing signaling system essential for genetic competence in *Streptococcus mutans* is involved in biofilm formation. *J. Bacteriol.* **2002**, *184* (10), 2699-708.
72. Whatmore, A. M.; Barcus, V. A.; Dowson, C. G., Genetic diversity of the streptococcal competence (com) gene locus. *J. Bacteriol.* **1999**, *181* (10), 3144-54.
73. Cook, L. C.; Federle, M. J., Peptide pheromone signaling in *Streptococcus* and *Enterococcus*. *FEMS Microbiol. Rev.* **2014**, *38* (3), 473-92.
74. Ishii, S.; Yano, T.; Hayashi, H., Expression and characterization of the peptidase domain of *Streptococcus pneumoniae* ComA, a bifunctional ATP-binding cassette transporter involved in quorum sensing pathway. *J. Biol. Chem.* **2006**, *281* (8), 4726-31.
75. Hossain, M. S.; Biswas, I., An extracellular protease, SepM, generates functional competence-stimulating peptide in *Streptococcus mutans* UA159. *J. Bacteriol.* **2012**, *194* (21), 5886-96.
76. Pozzi, G.; Masala, L.; Iannelli, F.; Manganelli, R.; Havarstein, L. S.; Piccoli, L.; Simon, D.; Morrison, D. A., Competence for genetic transformation in encapsulated strains of *Streptococcus pneumoniae*: two allelic variants of the peptide pheromone. *J. Bacteriol.* **1996**, *178* (20), 6087-90.
77. Declerck, N.; Bouillaut, L.; Chaix, D.; Rugani, N.; Slamti, L.; Hoh, F.; Lereclus, D.; Arold, S. T., Structure of PlcR: Insights into virulence regulation and evolution of quorum sensing in Gram-positive bacteria. *Proc. Natl. Acad. Sci. U. S. A.* **2007**, *104* (47), 18490-5.
78. Aggarwal, C.; Federle, M. J., Peptide Pheromones and Their Protein Receptors: Cellular Signaling in Gram-Positive Bacteria. In *Molecular Life Sciences*, 2014; pp 1-14.
79. Gominet, M.; Slamti, L.; Gilois, N.; Rose, M.; Lereclus, D., Oligopeptide permease is required for expression of the *Bacillus thuringiensis* plcR regulon and for virulence. *Mol. Microbiol.* **2001**, *40* (4), 963-75.
80. D'Andrea, L. D.; Regan, L., TPR proteins: the versatile helix. *Trends Biochem. Sci* **2003**, *28* (12), 655-62.

81. Grenha, R.; Slamti, L.; Nicaise, M.; Refes, Y.; Lereclus, D.; Nessler, S., Structural basis for the activation mechanism of the PlcR virulence regulator by the quorum-sensing signal peptide PapR. *Proc. Natl. Acad. Sci. U. S. A.* **2013**, *110* (3), 1047-52.
82. Do, H.; Kumaraswami, M., Structural Mechanisms of Peptide Recognition and Allosteric Modulation of Gene Regulation by the RRNPP Family of Quorum-Sensing Regulators. *J. Mol. Biol.* **2016**, *428* (14), 2793-804.
83. Rocha-Estrada, J.; Aceves-Diez, A. E.; Guarneros, G.; de la Torre, M., The RNPP family of quorum-sensing proteins in Gram-positive bacteria. *Appl. Microbiol. Biotechnol.* **2010**, *87* (3), 913-23.
84. Recsei, P.; Kreiswirth, B.; O'Reilly, M.; Schlievert, P.; Gruss, A.; Novick, R. P., Regulation of exoprotein gene expression in *Staphylococcus aureus* by agr. *Mol. Gen. Genet.* **1986**, *202* (1), 58-61.
85. Novick, R. P.; Projan, S. J.; Kornblum, J.; Ross, H. F.; Ji, G.; Kreiswirth, B.; Vandenesch, F.; Moghazeh, S., The agr P2 operon: an autocatalytic sensory transduction system in *Staphylococcus aureus*. *Mol. Gen. Genet.* **1995**, *248*, 446-458.
86. Novick, R. P.; Ross, H. F.; Projan, S. J.; Kornblum, J.; Kreiswirth, B.; Moghazeh, S., Synthesis of staphylococcal virulence factors is controlled by a regulatory RNA molecule. *EMBO J.* **1993**, *12* (10), 3967-3975.
87. Ji, G.; Beavis, R.; Novick, R. P., Bacterial interference caused by autoinducing peptide variants. *Science* **1997**, *276* (5321), 2027-30.
88. Novick, R. P., Autoinduction and signal transduction in the regulation of staphylococcal virulence. *Mol. Microbiol.* **2003**, *48* (6), 1429-49.
89. Zhang, L.; Lin, J.; Ji, G., Membrane anchoring of the AgrD N-terminal amphipathic region is required for its processing to produce a quorum-sensing pheromone in *Staphylococcus aureus*. *J. Biol. Chem.* **2004**, *279* (19), 19448-56.
90. Thoendel, M.; Horswill, A. R., Random mutagenesis and topology analysis of the autoinducing peptide biosynthesis proteins in *Staphylococcus aureus*. *Mol. Microbiol.* **2013**, *87* (2), 318-37.
91. Schwartz, K.; Sekedat, M. D.; Syed, A. K.; O'Hara, B.; Payne, D. E.; Lamb, A.; Boles, B. R., The AgrD N-terminal leader peptide of *Staphylococcus aureus* has cytolytic and amyloidogenic properties. *Infect. Immun.* **2014**, *82* (9), 3837-44.

92. Gonzalez, D. J.; Corriden, R.; Akong-Moore, K.; Olson, J.; Dorrestein, P. C.; Nizet, V., N-terminal ArgD peptides from the classical *Staphylococcus aureus* Agr system have cytotoxic and proinflammatory activities. *Chem. Biol.* **2014**, *21* (11), 1457-62.
93. Ji, G.; Pei, W.; Zhang, L.; Qiu, R.; Lin, J.; Benito, Y.; Lina, G.; Novick, R. P., *Staphylococcus intermedius* produces a functional agr autoinducing peptide containing a cyclic lactone. *J. Bacteriol.* **2005**, *187* (9), 3139-50.
94. Nishiguchi, K.; Nagata, K.; Tanokura, M.; Sonomoto, K.; Nakayama, J., Structure-activity relationship of gelatinase biosynthesis-activating pheromone of *Enterococcus faecalis*. *J. Bacteriol.* **2009**, *191* (2), 641-50.
95. Molloy, E. M.; Dell, M.; Hansch, V. G.; Dunbar, K. L.; Feldmann, R.; Oberheide, A.; Seyfarth, L.; Kumpfmuller, J.; Horch, T.; Arndt, H. D.; Hertweck, C., Enzyme-Primed Native Chemical Ligation Produces Autoinducing Cyclopeptides in *Clostridia*. *Angew. Chem. Int. Ed. Engl.* **2021**.
96. Sturme, M. H.; Nakayama, J.; Molenaar, D.; Murakami, Y.; Kunugi, R.; Fujii, T.; Vaughan, E. E.; Kleerebezem, M.; de Vos, W. M., An agr-like two-component regulatory system in *Lactobacillus plantarum* is involved in production of a novel cyclic peptide and regulation of adherence. *J. Bacteriol.* **2005**, *187* (15), 5224-35.
97. Thoendel, M.; Horswill, A. R., Identification of *Staphylococcus aureus* AgrD residues required for autoinducing peptide biosynthesis. *J. Biol. Chem.* **2009**, *284* (33), 21828-38.
98. Qiu, R.; Pei, W.; Zhang, L.; Lin, J.; Ji, G., Identification of the putative staphylococcal AgrB catalytic residues involving the proteolytic cleavage of AgrD to generate autoinducing peptide. *J. Biol. Chem.* **2005**, *280* (17), 16695-704.
99. Wang, B.; Zhao, A.; Novick, R. P.; Muir, T. W., Key driving forces in the biosynthesis of autoinducing peptides required for staphylococcal virulence. *Proc. Natl. Acad. Sci. U. S. A.* **2015**, *112* (34), 10679-84.
100. Zhang, L.; Ji, G., Identification of a staphylococcal AgrB segment(s) responsible for group-specific processing of AgrD by gene swapping. *J. Bacteriol.* **2004**, *186* (20), 6706-13.
101. Wang, B. Reconstitution and Mechanistic Studies on the Staphylococcal agr Quorum Sensing Circuit. The Rockefeller University, Student Theses and Dissertations, 2016.
102. Marroquin, S.; Gimza, B.; Tomlinson, B.; Stein, M.; Frey, A.; Keogh, R. A.; Zapf, R.; Todd, D. A.; Cech, N. B.; Carroll, R. K.; Shaw, L. N., MroQ Is a Novel Abi-

- Domain Protein That Influences Virulence Gene Expression in *Staphylococcus aureus* via Modulation of Agr Activity. *Infect. Immun.* **2019**, *87* (5).
103. Cosgriff, C. J.; White, C. R.; Teoh, W. P.; Grayczyk, J. P.; Alonzo, F., 3rd, Control of *Staphylococcus aureus* Quorum Sensing by a Membrane-Embedded Peptidase. *Infect. Immun.* **2019**, *87* (5).
 104. Marchand, N.; Collins, C. H., Peptide-based communication system enables *Escherichia coli* to *Bacillus megaterium* interspecies signaling. *Biotechnol. Bioeng.* **2013**, *110* (11), 3003-12.
 105. Marchand, N.; Collins, C. H., Synthetic Quorum Sensing and Cell-Cell Communication in Gram-Positive *Bacillus megaterium*. *ACS Synth Biol* **2016**, *5* (7), 597-606.
 106. Xie, Q.; Zhao, A.; Jeffrey, P. D.; Kim, M. K.; Bassler, B. L.; Stone, H. A.; Novick, R. P.; Muir, T. W., Identification of a Molecular Latch that Regulates Staphylococcal Virulence. *Cell Chem. Biol.* **2019**, *26* (4), 548-558 e4.
 107. George Cisar, E. A.; Geisinger, E.; Muir, T. W.; Novick, R. P., Symmetric signalling within asymmetric dimers of the *Staphylococcus aureus* receptor histidine kinase AgrC. *Mol. Microbiol.* **2009**, *74* (1), 44-57.
 108. Jensen, R. O.; Winzer, K.; Clarke, S. R.; Chan, W. C.; Williams, P., Differential recognition of *Staphylococcus aureus* quorum-sensing signals depends on both extracellular loops 1 and 2 of the transmembrane sensor AgrC. *J. Mol. Biol.* **2008**, *381* (2), 300-9.
 109. Geisinger, E.; George, E. A.; Chen, J.; Muir, T. W.; Novick, R. P., Identification of ligand specificity determinants in AgrC, the *Staphylococcus aureus* quorum-sensing receptor. *J. Biol. Chem.* **2008**, *283* (14), 8930-8.
 110. Lina, G.; Jarraud, S.; Ji, G.; Greenland, T.; Pedraza, A.; Etienne, J.; Novick, R. P.; Vandenesch, F., Transmembrane topology and histidine protein kinase activity of AgrC, the agr signal receptor in *Staphylococcus aureus*. *Mol. Microbiol.* **1998**, *28* (3), 655-62.
 111. Wright, J. S., 3rd; Lyon, G. J.; George, E. A.; Muir, T. W.; Novick, R. P., Hydrophobic interactions drive ligand-receptor recognition for activation and inhibition of staphylococcal quorum sensing. *Proc. Natl. Acad. Sci. U. S. A.* **2004**, *101* (46), 16168-73.
 112. Geisinger, E.; Muir, T. W.; Novick, R. P., agr receptor mutants reveal distinct modes of inhibition by staphylococcal autoinducing peptides. *Proc. Natl. Acad. Sci. U. S. A.* **2009**, *106* (4), 1216-21.

113. Bhate, M. P.; Molnar, K. S.; Goulian, M.; DeGrado, W. F., Signal transduction in histidine kinases: insights from new structures. *Structure* **2015**, *23* (6), 981-94.
114. Wang, B.; Zhao, A.; Xie, Q.; Olinares, P. D.; Chait, B. T.; Novick, R. P.; Muir, T. W., Functional Plasticity of the AgrC Receptor Histidine Kinase Required for Staphylococcal Virulence. *Cell Chem. Biol.* **2017**, *24* (1), 76-86.
115. Sidote, D. J.; Barbieri, C. M.; Wu, T.; Stock, A. M., Structure of the *Staphylococcus aureus* AgrA LytTR domain bound to DNA reveals a beta fold with an unusual mode of binding. *Structure* **2008**, *16* (5), 727-35.
116. Leonard, P. G.; Bezar, I. F.; Sidote, D. J.; Stock, A. M., Identification of a hydrophobic cleft in the LytTR domain of AgrA as a locus for small molecule interactions that inhibit DNA binding. *Biochemistry* **2012**, *51* (50), 10035-43.
117. Rajasree, K.; Fasim, A.; Gopal, B., Conformational features of the *Staphylococcus aureus* AgrA-promoter interactions rationalize quorum-sensing triggered gene expression. *Biochem Biophys Rep* **2016**, *6*, 124-134.
118. Queck, S. Y.; Jameson-Lee, M.; Villaruz, A. E.; Bach, T. H.; Khan, B. A.; Sturdevant, D. E.; Ricklefs, S. M.; Li, M.; Otto, M., RNAIII-independent target gene control by the agr quorum-sensing system: insight into the evolution of virulence regulation in *Staphylococcus aureus*. *Mol. Cell* **2008**, *32* (1), 150-8.
119. Autret, N.; Raynaud, C.; Dubail, I.; Berche, P.; Charbit, A., Identification of the agr locus of *Listeria monocytogenes*: role in bacterial virulence. *Infect. Immun.* **2003**, *71* (8), 4463-71.
120. Martin, M. J.; Clare, S.; Goulding, D.; Faulds-Pain, A.; Barquist, L.; Browne, H. P.; Pettit, L.; Dougan, G.; Lawley, T. D.; Wren, B. W., The agr locus regulates virulence and colonization genes in *Clostridium difficile* 027. *J. Bacteriol.* **2013**, *195* (16), 3672-81.
121. Eberhard, A.; Widrig, C. A.; McBath, P.; Schineller, J. B., Analogs of the autoinducer of bioluminescence in *Vibrio fischeri*. *Arch. Microbiol.* **1986**, *146* (1), 35-40.
122. Schaefer, A. L.; Hanzelka, B. L.; Eberhard, A.; Greenberg, E. P., Quorum sensing in *Vibrio fischeri*: probing autoinducer-LuxR interactions with autoinducer analogs. *J. Bacteriol.* **1996**, *178* (10), 2897-901.
123. Reverchon, S.; Chantegrel, B.; Deshayes, C.; Doutheau, A.; Cotte-Pattat, N., New synthetic analogues of N -acyl homoserine lactones as agonists or antagonists of transcriptional regulators involved in bacterial quorum sensing. *Bioorg. Med. Chem. Lett.* **2002**, *12* (8), 1153-1157.

124. Smith, K. M.; Bu, Y.; Suga, H., Induction and Inhibition of *Pseudomonas aeruginosa* Quorum Sensing by Synthetic Autoinducer Analogs. *Chem. Biol.* **2003**, *10* (1), 81-89.
125. Persson, T.; Hansen, T. H.; Rasmussen, T. B.; Skinderso, M. E.; Givskov, M.; Nielsen, J., Rational design and synthesis of new quorum-sensing inhibitors derived from acylated homoserine lactones and natural products from garlic. *Org. Biomol. Chem.* **2005**, *3* (2), 253-62.
126. Geske, G. D.; O'Neill, J. C.; Blackwell, H. E., N-phenylacetanoyl-L-homoserine lactones can strongly antagonize or superagonize quorum sensing in *Vibrio fischeri*. *ACS Chem. Biol.* **2007**, *2* (5), 315-9.
127. Geske, G. D.; O'Neill, J. C.; Miller, D. M.; Mattmann, M. E.; Blackwell, H. E., Modulation of bacterial quorum sensing with synthetic ligands: systematic evaluation of N-acylated homoserine lactones in multiple species and new insights into their mechanisms of action. *J. Am. Chem. Soc.* **2007**, *129* (44), 13613-25.
128. McInnis, C. E.; Blackwell, H. E., Thiolactone modulators of quorum sensing revealed through library design and screening. *Bioorg. Med. Chem.* **2011**, *19* (16), 4820-8.
129. Palmer, A. G.; Streng, E.; Jewell, K. A.; Blackwell, H. E., Quorum sensing in bacterial species that use degenerate autoinducers can be tuned by using structurally identical non-native ligands. *ChemBioChem* **2011**, *12* (1), 138-47.
130. Amara, N.; Mashlach, R.; Amar, D.; Krief, P.; Spieser, S. A.; Bottomley, M. J.; Aharoni, A.; Meijler, M. M., Covalent inhibition of bacterial quorum sensing. *J. Am. Chem. Soc.* **2009**, *131* (30), 10610-9.
131. Muh, U.; Schuster, M.; Heim, R.; Singh, A.; Olson, E. R.; Greenberg, E. P., Novel *Pseudomonas aeruginosa* quorum-sensing inhibitors identified in an ultra-high-throughput screen. *Antimicrob. Agents Chemother.* **2006**, *50* (11), 3674-9.
132. Muh, U.; Hare, B. J.; Duerkop, B. A.; Schuster, M.; Hanzelka, B. L.; Heim, R.; Olson, E. R.; Greenberg, E. P., A structurally unrelated mimic of a *Pseudomonas aeruginosa* acyl-homoserine lactone quorum-sensing signal. *Proc. Natl. Acad. Sci. U. S. A.* **2006**, *103* (45), 16948-52.
133. Ishii, S.; Fukui, K.; Yokoshima, S.; Kumagai, K.; Beniyama, Y.; Kodama, T.; Fukuyama, T.; Okabe, T.; Nagano, T.; Kojima, H.; Yano, T., High-throughput Screening of Small Molecule Inhibitors of the *Streptococcus* Quorum-sensing Signal Pathway. *Sci. Rep.* **2017**, *7* (1), 4029.

134. Borlee, B. R.; Geske, G. D.; Blackwell, H. E.; Handelsman, J., Identification of synthetic inducers and inhibitors of the quorum-sensing regulator LasR in *Pseudomonas aeruginosa* by high-throughput screening. *Appl. Environ. Microbiol.* **2010**, *76* (24), 8255-8.
135. Christensen, Q. H.; Grove, T. L.; Booker, S. J.; Greenberg, E. P., A high-throughput screen for quorum-sensing inhibitors that target acyl-homoserine lactone synthases. *Proc. Natl. Acad. Sci. U. S. A.* **2013**, *110* (34), 13815-20.
136. Xie, Q.; Wiedmann, M. M.; Zhao, A.; Pagan, I. R.; Novick, R. P.; Suga, H.; Muir, T. W., Discovery of quorum quenchers targeting the membrane-embedded sensor domain of the *Staphylococcus aureus* receptor histidine kinase, AgrC. *Chem. Commun. (Camb.)* **2020**, *56* (76), 11223-11226.
137. Parlet, C. P.; Kavanaugh, J. S.; Crosby, H. A.; Raja, H. A.; El-Elimat, T.; Todd, D. A.; Pearce, C. J.; Cech, N. B.; Oberlies, N. H.; Horswill, A. R., Apicidin Attenuates MRSA Virulence through Quorum-Sensing Inhibition and Enhanced Host Defense. *Cell Rep.* **2019**, *27* (1), 187-198 e6.
138. Todd, D. A.; Parlet, C. P.; Crosby, H. A.; Malone, C. L.; Heilmann, K. P.; Horswill, A. R.; Cech, N. B., Signal Biosynthesis Inhibition with Ambuic Acid as a Strategy To Target Antibiotic-Resistant Infections. *Antimicrob. Agents Chemother.* **2017**, *61* (8), e00263-17.
139. Sully, E. K.; Malachowa, N.; Elmore, B. O.; Alexander, S. M.; Femling, J. K.; Gray, B. M.; DeLeo, F. R.; Otto, M.; Cheung, A. L.; Edwards, B. S.; Sklar, L. A.; Horswill, A. R.; Hall, P. R.; Gresham, H. D., Selective chemical inhibition of agr quorum sensing in *Staphylococcus aureus* promotes host defense with minimal impact on resistance. *PLoS Pathog.* **2014**, *10* (6), e1004174.
140. Nielsen, A.; Mansson, M.; Bojer, M. S.; Gram, L.; Larsen, T. O.; Novick, R. P.; Frees, D.; Frokiaer, H.; Ingmer, H., Solonamide B inhibits quorum sensing and reduces *Staphylococcus aureus* mediated killing of human neutrophils. *PLoS One* **2014**, *9* (1), e84992.
141. Bezar, I. F.; Mashruwala, A. A.; Boyd, J. M.; Stock, A. M., Drug-like Fragments Inhibit agr-Mediated Virulence Expression in *Staphylococcus aureus*. *Sci. Rep.* **2019**, *9* (1), 6786.
142. Piewngam, P.; Zheng, Y.; Nguyen, T. H.; Dickey, S. W.; Joo, H. S.; Villaruz, A. E.; Glose, K. A.; Fisher, E. L.; Hunt, R. L.; Li, B.; Chiou, J.; Pharkjaksu, S.; Khongthong, S.; Cheung, G. Y. C.; Kiratisin, P.; Otto, M., Pathogen elimination by probiotic *Bacillus* via signalling interference. *Nature* **2018**, *562* (7728), 532-537.

143. Manson, D. E.; O'Reilly, M. C.; Nyffeler, K. E.; Blackwell, H. E., Design, Synthesis, and Biochemical Characterization of Non-Native Antagonists of the *Pseudomonas aeruginosa* Quorum Sensing Receptor LasR with Nanomolar IC50 Values. *ACS Infect. Dis.* **2020**, *6* (4), 649-661.
144. Arrowsmith, C. H.; Audia, J. E.; Austin, C.; Baell, J.; Bennett, J.; Blagg, J.; Bountra, C.; Brennan, P. E.; Brown, P. J.; Bunnage, M. E.; Buser-Doepner, C.; Campbell, R. M.; Carter, A. J.; Cohen, P.; Copeland, R. A.; Cravatt, B.; Dahlin, J. L.; Dhanak, D.; Edwards, A. M.; Frederiksen, M.; Frye, S. V.; Gray, N.; Grimshaw, C. E.; Hepworth, D.; Howe, T.; Huber, K. V.; Jin, J.; Knapp, S.; Kotz, J. D.; Kruger, R. G.; Lowe, D.; Mader, M. M.; Marsden, B.; Mueller-Fahrnow, A.; Muller, S.; O'Hagan, R. C.; Overington, J. P.; Owen, D. R.; Rosenberg, S. H.; Roth, B.; Ross, R.; Schapira, M.; Schreiber, S. L.; Shoichet, B.; Sundstrom, M.; Superti-Furga, G.; Taunton, J.; Toledo-Sherman, L.; Walpole, C.; Walters, M. A.; Willson, T. M.; Workman, P.; Young, R. N.; Zuercher, W. J., The promise and peril of chemical probes. *Nat. Chem. Biol.* **2015**, *11* (8), 536-41.
145. Bunnage, M. E.; Chekler, E. L.; Jones, L. H., Target validation using chemical probes. *Nat. Chem. Biol.* **2013**, *9* (4), 195-9.
146. Zorn, J. A.; Wells, J. A., Turning enzymes ON with small molecules. *Nat. Chem. Biol.* **2010**, *6* (3), 179-188.
147. Workman, P.; Collins, I., Probing the probes: fitness factors for small molecule tools. *Chem. Biol.* **2010**, *17* (6), 561-77.
148. Antolin, A. A.; Workman, P.; Al-Lazikani, B., Public resources for chemical probes: the journey so far and the road ahead. *Future Med. Chem.* **2021**, *13* (8), 731-747.
149. Nakayama, J.; Uemura, Y.; Nishiguchi, K.; Yoshimura, N.; Igarashi, Y.; Sonomoto, K., Ambuic acid inhibits the biosynthesis of cyclic peptide quormones in gram-positive bacteria. *Antimicrob. Agents Chemother.* **2009**, *53* (2), 580-6.
150. Yarwood, J. M.; McCormick, J. K.; Paustian, M. L.; Kapur, V.; Schlievert, P. M., Repression of the *Staphylococcus aureus* accessory gene regulator in serum and *in vivo*. *J. Bacteriol.* **2002**, *184* (4), 1095-101.
151. Peterson, M. M.; Mack, J. L.; Hall, P. R.; Alsup, A. A.; Alexander, S. M.; Sully, E. K.; Sawires, Y. S.; Cheung, A. L.; Otto, M.; Gresham, H. D., Apolipoprotein B Is an innate barrier against invasive *Staphylococcus aureus* infection. *Cell Host Microbe* **2008**, *4* (6), 555-66.
152. Elmore, B. O.; Triplett, K. D.; Hall, P. R., Apolipoprotein B48, the Structural Component of Chylomicrons, Is Sufficient to Antagonize *Staphylococcus aureus* Quorum-Sensing. *PLoS One* **2015**, *10* (5), e0125027.

153. Hall, P. R.; Elmore, B. O.; Spang, C. H.; Alexander, S. M.; Manifold-Wheeler, B. C.; Castleman, M. J.; Daly, S. M.; Peterson, M. M.; Sully, E. K.; Femling, J. K.; Otto, M.; Horswill, A. R.; Timmins, G. S.; Gresham, H. D., Nox2 modification of LDL is essential for optimal apolipoprotein B-mediated control of agr type III *Staphylococcus aureus* quorum-sensing. *PLoS Pathog.* **2013**, *9* (2), e1003166.
154. Park, J.; Jagasia, R.; Kaufmann, G. F.; Mathison, J. C.; Ruiz, D. I.; Moss, J. A.; Meijler, M. M.; Ulevitch, R. J.; Janda, K. D., Infection control by antibody disruption of bacterial quorum sensing signaling. *Chem. Biol.* **2007**, *14* (10), 1119-27.
155. Tsuchikama, K.; Shimamoto, Y.; Anami, Y., Truncated Autoinducing Peptide Conjugates Selectively Recognize and Kill *Staphylococcus aureus*. *ACS Infect. Dis.* **2017**, *3* (6), 406-410.
156. Kratochvil, M. J.; Yang, T.; Blackwell, H. E.; Lynn, D. M., Nonwoven Polymer Nanofiber Coatings That Inhibit Quorum Sensing in *Staphylococcus aureus*: Toward New Nonbactericidal Approaches to Infection Control. *ACS Infect. Dis.* **2017**, *3* (4), 271-280.
157. Lyon, G. J.; Wright, J. S.; Muir, T. W.; Novick, R. P., Key determinants of receptor activation in the agr autoinducing peptides of *Staphylococcus aureus*. *Biochemistry* **2002**, *41* (31), 10095-104.
158. Kratochvil, M. J.; Tal-Gan, Y.; Yang, T.; Blackwell, H. E.; Lynn, D. M., Nanoporous Superhydrophobic Coatings that Promote the Extended Release of Water-Labile Quorum Sensing Inhibitors and Enable Long-Term Modulation of Quorum Sensing in *Staphylococcus aureus*. *ACS Biomater. Sci. Eng.* **2015**, *1* (10), 1039-1049.
159. Kim, M. K.; Zhao, A.; Wang, A.; Brown, Z. Z.; Muir, T. W.; Stone, H. A.; Bassler, B. L., Surface-attached molecules control *Staphylococcus aureus* quorum sensing and biofilm development. *Nat. Microbiol.* **2017**, *2*, 17080.
160. Otto, M.; Echner, H.; Voelter, W.; Gotz, F., Pheromone cross-inhibition between *Staphylococcus aureus* and *Staphylococcus epidermidis*. *Infect. Immun.* **2001**, *69* (3), 1957-60.
161. McDowell, P.; Affas, Z.; Reynolds, C.; Holden, M. T.; Wood, S. J.; Saint, S.; Cockayne, A.; Hill, P. J.; Dodd, C. E.; Bycroft, B. W.; Chan, W. C.; Williams, P., Structure, activity and evolution of the group I thiolactone peptide quorum-sensing system of *Staphylococcus aureus*. *Mol. Microbiol.* **2001**, *41* (2), 503-12.
162. Lyon, G. J.; Mayville, P.; Muir, T. W.; Novick, R. P., Rational design of a global inhibitor of the virulence response in *Staphylococcus aureus*, based in part on

- localization of the site of inhibition to the receptor-histidine kinase, AgrC. *Proc. Natl. Acad. Sci. U. S. A.* **2000**, *97* (24), 13330-5.
163. Tal-Gan, Y.; Stacy, D. M.; Foegen, M. K.; Koenig, D. W.; Blackwell, H. E., Highly potent inhibitors of quorum sensing in *Staphylococcus aureus* revealed through a systematic synthetic study of the group-III autoinducing peptide. *J. Am. Chem. Soc.* **2013**, *135* (21), 7869-82.
164. Yang, T.; Tal-Gan, Y.; Paharik, A. E.; Horswill, A. R.; Blackwell, H. E., Structure-Function Analyses of a *Staphylococcus epidermidis* Autoinducing Peptide Reveals Motifs Critical for AgrC-type Receptor Modulation. *ACS Chem. Biol.* **2016**, *11* (7), 1982-91.
165. Gordon, C. P.; Olson, S. D.; Lister, J. L.; Kavanaugh, J. S.; Horswill, A. R., Truncated Autoinducing Peptides as Antagonists of *Staphylococcus lugdunensis* Quorum Sensing. *J. Med. Chem.* **2016**, *59* (19), 8879-8888.
166. McBrayer, D. N.; Gantman, B. K.; Cameron, C. D.; Tal-Gan, Y., An Entirely Solid Phase Peptide Synthesis-Based Strategy for Synthesis of Gelatinase Biosynthesis-Activating Pheromone (GBAP) Analogue Libraries: Investigating the Structure-Activity Relationships of the *Enterococcus faecalis* Quorum Sensing Signal. *Org. Lett.* **2017**, *19* (12), 3295-3298.
167. West, K. H. J.; Shen, W.; Eisenbraun, E. L.; Yang, T.; Vasquez, J. K.; Horswill, A. R.; Blackwell, H. E., Non-Native Peptides Capable of Pan-Activating the agr Quorum Sensing System across Multiple Specificity Groups of *Staphylococcus epidermidis*. *ACS Chem. Biol.* **2021**.
168. Tal-Gan, Y.; Ivancic, M.; Cornilescu, G.; Yang, T.; Blackwell, H. E., Highly Stable, Amide-Bridged Autoinducing Peptide Analogues that Strongly Inhibit the AgrC Quorum Sensing Receptor in *Staphylococcus aureus*. *Angew. Chem. Int. Ed. Engl.* **2016**, *55* (31), 8913-7.
169. Lyon, G. J.; Wright, J. S.; Christopoulos, A.; Novick, R. P.; Muir, T. W., Reversible and specific extracellular antagonism of receptor-histidine kinase signaling. *J. Biol. Chem.* **2002**, *277* (8), 6247-53.
170. Fowler, S. A.; Stacy, D. M.; Blackwell, H. E., Design and synthesis of macrocyclic peptomers as mimics of a quorum sensing signal from *Staphylococcus aureus*. *Org. Lett.* **2008**, *10* (12), 2329-32.
171. Tal-Gan, Y.; Stacy, D. M.; Blackwell, H. E., N-Methyl and peptoid scans of an autoinducing peptide reveal new structural features required for inhibition and activation of AgrC quorum sensing receptors in *Staphylococcus aureus*. *Chem. Commun. (Camb.)* **2014**, *50* (23), 3000-3.

172. Vasquez, J. K.; Tal-Gan, Y.; Cornilescu, G.; Tyler, K. A.; Blackwell, H. E., Simplified AIP-II Peptidomimetics Are Potent Inhibitors of *Staphylococcus aureus* AgrC Quorum Sensing Receptors. *ChemBioChem* **2017**, *18* (4), 413-423.
173. Vasquez, J. K.; Blackwell, H. E., Simplified Autoinducing Peptide Mimetics with Single-Nanomolar Activity Against the *Staphylococcus aureus* AgrC Quorum Sensing Receptor. *ACS Infect. Dis.* **2019**, *5* (4), 484-492.
174. Baldry, M.; Kitir, B.; Frokiaer, H.; Christensen, S. B.; Taverne, N.; Meijerink, M.; Franzyk, H.; Olsen, C. A.; Wells, J. M.; Ingmer, H., The agr Inhibitors Solonamide B and Analogues Alter Immune Responses to *Staphylococcus aureus* but Do Not Exhibit Adverse Effects on Immune Cell Functions. *PLoS One* **2016**, *11* (1), e0145618.
175. Hansen, A. M.; Peng, P.; Baldry, M.; Perez-Gassol, I.; Christensen, S. B.; Vinther, J. M. O.; Ingmer, H.; Franzyk, H., Lactam hybrid analogues of solonamide B and autoinducing peptides as potent *S. aureus* AgrC antagonists. *Eur. J. Med. Chem.* **2018**, *152*, 370-376.
176. Desouky, S. E.; Shojima, A.; Singh, R. P.; Matsufuji, T.; Igarashi, Y.; Suzuki, T.; Yamagaki, T.; Okubo, K.; Ohtani, K.; Sonomoto, K.; Nakayama, J., Cyclodepsipeptides produced by actinomycetes inhibit cyclic-peptide-mediated quorum sensing in Gram-positive bacteria. *FEMS Microbiol. Lett.* **2015**, *362* (14).
177. Murray, E. J.; Crowley, R. C.; Truman, A.; Clarke, S. R.; Cottam, J. A.; Jadhav, G. P.; Steele, V. R.; O'Shea, P.; Lindholm, C.; Cockayne, A.; Chhabra, S. R.; Chan, W. C.; Williams, P., Targeting *Staphylococcus aureus* quorum sensing with nonpeptidic small molecule inhibitors. *J. Med. Chem.* **2014**, *57* (6), 2813-9.
178. Mizar, P.; Arya, R.; Kim, T.; Cha, S.; Ryu, K. S.; Yeo, W. S.; Bae, T.; Kim, D. W.; Park, K. H.; Kim, K. K.; Lee, S. S., Total Synthesis of Xanthoangelol B and Its Various Fragments: Toward Inhibition of Virulence Factor Production of *Staphylococcus aureus*. *J. Med. Chem.* **2018**, *61* (23), 10473-10487.
179. Karathanasi, G.; Bojer, M. S.; Baldry, M.; Johannessen, B. A.; Wolff, S.; Greco, I.; Kilstrup, M.; Hansen, P. R.; Ingmer, H., Linear peptidomimetics as potent antagonists of *Staphylococcus aureus* agr quorum sensing. *Sci. Rep.* **2018**, *8* (1), 3562.
180. Passioura, T.; Suga, H., A RaPID way to discover nonstandard macrocyclic peptide modulators of drug targets. *Chem. Commun. (Camb.)* **2017**, *53* (12), 1931-1940.
181. Wang, X. S.; Chen, P. C.; Hampton, J. T.; Tharp, J. M.; Reed, C. A.; Das, S. K.; Wang, D. S.; Hayatshahi, H. S.; Shen, Y.; Liu, J.; Liu, W. R., A Genetically

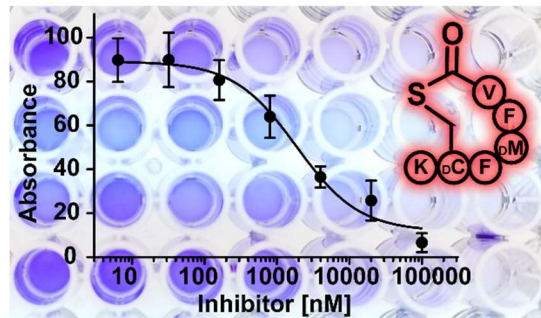
- Encoded, Phage-Displayed Cyclic-Peptide Library. *Angew. Chem. Int. Ed. Engl.* **2019**, *58* (44), 15904-15909.
182. Simonetti, L.; Ivarsson, Y., Genetically Encoded Cyclic Peptide Phage Display Libraries. *ACS Cent Sci* **2020**, *6* (3), 336-338.
 183. Daly, S. M.; Elmore, B. O.; Kavanaugh, J. S.; Triplett, K. D.; Figueroa, M.; Raja, H. A.; El-Elimat, T.; Crosby, H. A.; Femling, J. K.; Cech, N. B.; Horswill, A. R.; Oberlies, N. H.; Hall, P. R., omega-Hydroxyemodin limits *Staphylococcus aureus* quorum sensing-mediated pathogenesis and inflammation. *Antimicrob. Agents Chemother.* **2015**, *59* (4), 2223-35.
 184. Khodaverdian, V.; Pesho, M.; Truitt, B.; Bollinger, L.; Patel, P.; Nithianantham, S.; Yu, G.; Delaney, E.; Jankowsky, E.; Shoham, M., Discovery of antivirulence agents against methicillin-resistant *Staphylococcus aureus*. *Antimicrob. Agents Chemother.* **2013**, *57* (8), 3645-52.
 185. Yu, G.; Kuo, D.; Shoham, M.; Viswanathan, R., Combinatorial synthesis and in vitro evaluation of a biaryl hydroxyketone library as antivirulence agents against MRSA. *ACS Comb Sci* **2014**, *16* (2), 85-91.
 186. Kuo, D.; Yu, G.; Hoch, W.; Gabay, D.; Long, L.; Ghannoum, M.; Nagy, N.; Harding, C. V.; Viswanathan, R.; Shoham, M., Novel quorum-quenching agents promote methicillin-resistant *Staphylococcus aureus* (MRSA) wound healing and sensitize MRSA to beta-lactam antibiotics. *Antimicrob. Agents Chemother.* **2015**, *59* (3), 1512-8.
 187. Da, F.; Yao, L.; Su, Z.; Hou, Z.; Li, Z.; Xue, X.; Meng, J.; Luo, X., Antisense locked nucleic acids targeting *agrA* inhibit quorum sensing and pathogenesis of community-associated methicillin-resistant *Staphylococcus aureus*. *J. Appl. Microbiol.* **2017**, *122* (1), 257-267.
 188. Traber, K. E.; Lee, E.; Benson, S.; Corrigan, R.; Cantera, M.; Shopsin, B.; Novick, R. P., *agr* function in clinical *Staphylococcus aureus* isolates. *Microbiology* **2008**, *154* (Pt 8), 2265-2274.
 189. LaSarre, B.; Federle, M. J., Exploiting quorum sensing to confuse bacterial pathogens. *Microbiol. Mol. Biol. Rev.* **2013**, *77* (1), 73-111.
 190. Garcia-Betancur, J. C.; Goni-Moreno, A.; Horger, T.; Schott, M.; Sharan, M.; Eikmeier, J.; Wohlmuth, B.; Zerneck, A.; Ohlsen, K.; Kuttler, C.; Lopez, D., Cell differentiation defines acute and chronic infection cell types in *Staphylococcus aureus*. *Elife* **2017**, *6*.

191. Gor, V.; Takemura, A. J.; Nishitani, M.; Higashide, M.; Medrano Romero, V.; Ohniwa, R. L.; Morikawa, K., Finding of Agr Phase Variants in *Staphylococcus aureus*. *mBio* **2019**, *10* (4).
192. Peng, P.; Baldry, M.; Gless, B. H.; Bojer, M. S.; Espinosa-Gongora, C.; Baig, S. J.; Andersen, P. S.; Olsen, C. A.; Ingmer, H., Effect of Co-inhabiting Coagulase Negative Staphylococci on *S. aureus* agr Quorum Sensing, Host Factor Binding, and Biofilm Formation. *Front. Microbiol.* **2019**, *10*, 2212.
193. Paharik, A. E.; Parlet, C. P.; Chung, N.; Todd, D. A.; Rodriguez, E. I.; Van Dyke, M. J.; Cech, N. B.; Horswill, A. R., Coagulase-Negative Staphylococcal Strain Prevents *Staphylococcus aureus* Colonization and Skin Infection by Blocking Quorum Sensing. *Cell Host Microbe* **2017**, *22* (6), 746-756 e5.

Chapter 2:
**A Native Autoinducing Peptide Reveals Highly Efficacious Inhibitors
and Activators of *Listeria monocytogenes* Quorum Sensing and
Biofilm Formation**

Contributions: K. H. J. West designed and conducted the experiments and wrote the chapter. S. V. Ma assisted in peptide preparation and assisted in writing. D. A. Pensinger and J. D. Sauer assisted in construction of fluorescent reporter strains. T. Tucholski and Y. Ge assisted in identification of native signal. Z. Hayouka assisted in preparation of peptides. H. E. Blackwell guided research and assisted in writing.

Abstract



Bacteria can use chemical signals to assess their local population density in a cell-to-cell communication process called quorum sensing (QS). Many of these bacteria are common human pathogens, including Gram-positive bacteria that utilize small macrocyclic autoinducing peptide (AIP) signals. *Listeria monocytogenes*, an important food-borne pathogen, uses the *agr* system to regulate a variety of virulence factors and biofilm formation, yet we know little about the specific roles of *agr* in *Listeria* infection and its persistence in various environments. As QS is controlled by chemical signals, chemical agonists and antagonists capable of intercepting this signaling pathway represent powerful tools to explore mechanism and block deleterious bacterial behaviors at high cell densities. Herein, we report the first such peptide tools to explore QS in *Listeria*. We confirmed the structure of a native *L. monocytogenes* AIP, used it as a scaffold to synthesize a collection of non-native AIP mimics, and evaluated their activity in cell-based *agr* reporter assays. The structure-activity relationships (SARs) gathered from these studies guided the design of a suite of novel AIP analogs, including agonists with increased potency relative to the native AIP and an antagonist capable of reducing *agr* activity to basal levels. Interestingly, both the lead *agr* agonist and antagonist in *L. monocytogenes* were also capable of antagonizing *agr* signaling in the related pathogen *Staphylococcus aureus*, further extending their utility. Perhaps most

notably, the lead antagonist was able to reduce wild-type *L. monocytogenes* biofilm formation by over 90%. This study represents an important first step in the application of chemical methods to modulate QS and concomitant virulence outcomes in *L. monocytogenes*.

2.1 Introduction

Listeria monocytogenes is a Gram-positive bacterium responsible for the foodborne illness listeriosis, which can cause severe infections in the immunocompromised, the young, the aged, and pregnant women.¹ Although listeriosis comprises only 0.1% of foodborne illnesses, this disease alone is responsible for nearly one-fifth of all foodborne illness-related deaths.¹⁻² Despite increased awareness and testing, *L. monocytogenes* continues to plague the food industry, and food recalls have increased significantly in recent years.³ The notoriety of *L. monocytogenes* stems from multiple sources: its ubiquity in the environment, its high resistance and adaptability to environmental stressors, and its unique intracellular lifecycle.⁴⁻⁸ *L. monocytogenes* is able to escape the phagosome and survive in host cells, reproduce within the usually toxic cytosol, and use host cellular machinery to propel itself within the host cell and invade neighboring cells, allowing the bacteria to spread with relatively little immune surveillance. Due to the intracellular lifecycle of *L. monocytogenes*, antibiotics and other drugs must enter host cells to combat infection, which limits treatment options and often their efficacy.⁹ New tools to curb the virulence and spread of *L. monocytogenes* would represent a significant advance toward curtailing infections.

Similar to other common bacterial pathogens, many virulent traits exhibited by *L. monocytogenes* are controlled in part by quorum sensing (QS), a method of bacterial cell-cell communication mediated by chemical signals that allows for the detection of population density and coordination of group behaviors at high cell densities.¹⁰⁻¹² Work over the last 20 years has shown that close structural mimics of these QS signals can be used as chemical tools to either agonize or antagonize QS and thereby modify

bacterial community behavior.^{11, 13-17} The potential to attenuate virulent behavior of pathogens with QS modulators is promising and, given the rise of antibiotic resistance, makes QS inhibition (or activation for certain pathogens or traits) a highly attractive target for preventing or treating bacterial infections.¹⁸⁻¹⁹

QS in *L. monocytogenes* is mediated by the accessory gene regulator (*agr*) system. This QS system is used by other Gram-positive bacteria such as the Staphylococci, and consists of four components—AgrA-D—and the autoinducing peptide (AIP) signal (Figure 2.1A).²⁰⁻²² The polypeptide AgrD is produced at a basal rate within the cell and consists of an N-terminal amphipathic helix, a signal precursor sequence centered around a conserved cysteine, and a C-terminal recognition domain.²³ AgrB, a membrane-bound peptidase, recognizes and cleaves the C-terminal domain of AgrD, then cyclizes the peptide by forming a thioester linkage between the conserved cysteine of AgrD and the new C-terminus.²⁴ In a manner still not fully understood, AgrD is further processed and exported from the cell as the mature AIP signal. As the bacterial population grows and produces AIP in a given environment, the extracellular AIP concentration reaches a certain local threshold that will activate the two-component signaling system formed by AgrC and AgrA. AgrC is a transmembrane receptor histidine kinase that, upon binding of AIP, *trans*-autophosphorylates and subsequently transfers the phosphoryl group to the intracellular response regulator AgrA.²⁵ Phosphorylation then activates AgrA to dimerize, bind to various promoters, and upregulate the *agr* locus as well as other loci.²⁰

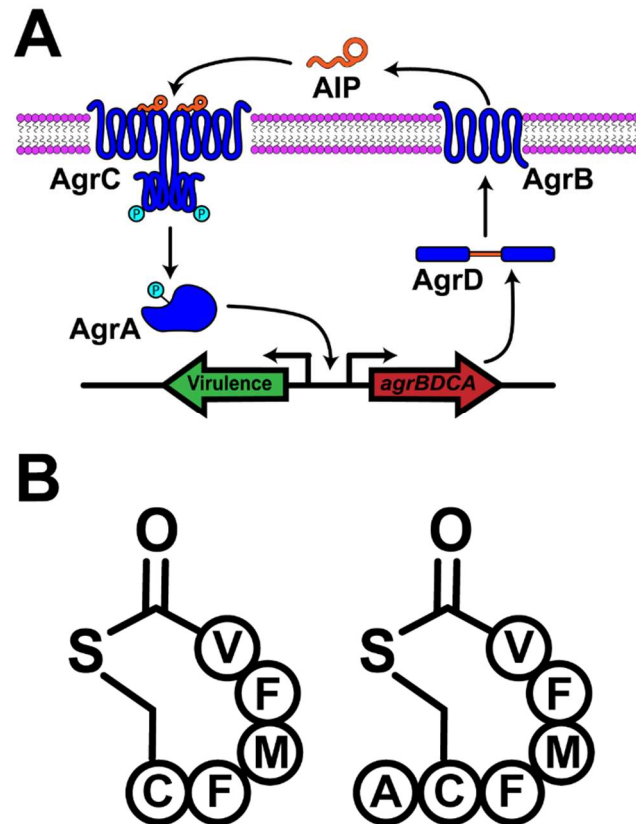


Figure 2.1 The *L. monocytogenes* *agr* quorum sensing system. A) A simplified overview of the *agr* system. P = phosphorylated residues formed upon activation. B) The primary amino acid sequence of the previously reported structures for the *L. monocytogenes* AIP in one letter amino acid abbreviations. Left, the 5-mer reported by Zetzmann et al.²⁶ Right, the 6-mer reported by Todd et al.²⁷

The *agr* system in *L. monocytogenes* has seen far less study relative to related systems in other bacteria (e.g., *Staphylococcus aureus*),²⁸ yet it is known to be vital to the ability of *L. monocytogenes* to persist in the environment as well as to infect hosts. In terms of persistence, *L. monocytogenes* mutants lacking various components of the *agr* system have critical defects in their ability to survive in soil,²⁹⁻³⁰ adapt to different temperatures when transitioning between saprophytic and *in vivo* states,³¹ and adhere and form biofilms on abiotic surfaces such as glass or steel.^{10, 32-34} For host infection, while it has been widely understood that the master virulence regulator PrfA controls the

various factors that *L. monocytogenes* uses for infection and spread (such as internalins, chitinases, listeriolysin O, phospholipases, actin polymerases, etc.),³⁵⁻³⁶ the production of many of these virulence factors, including PrfA, has been found to be down-regulated in Δagr strains of *L. monocytogenes*.^{1, 10, 21, 31-32, 37-39} In addition, these Δagr strains display attenuated virulence in mice infection models.^{10, 21} While many questions remain with regard to the timing, regulation, and targets of the *agr* system, the results of these past studies provide strong support for the role of *agr* in the pathogenicity of *L. monocytogenes*.^{10, 21}

Chemical agonists and antagonists of the *agr* system in *L. monocytogenes* would represent powerful tools to investigate QS in *L. monocytogenes* and develop methods to combat both its persistence and virulence. Such compounds remain largely unexplored. In fact, the native AIP used by *L. monocytogenes* is still open to debate, underscoring the current lack of molecular details with regard to *agr* signaling in this pathogen. To our knowledge, there have only been two reports that describe molecules that appear to directly affect the *L. monocytogenes agr* system. The first report by Zetzmann et al. showed that macrocyclic peptides based on the AgrD sequence can influence *L. monocytogenes agr* activity as measured using a luminescence-based ($P_{agr-lux}$) reporter. In this study, the authors asserted that the pentapeptide R5T0 (hereafter referred to as “5-mer”; Figure 2.1B, left) is the native AIP of *L. monocytogenes* due to the identification of this compound in the supernatant of *E. coli* expressing the *L. monocytogenes agrBD* components, and its agonizing activity in *L. monocytogenes agr* reporter strains when chemically synthesized.²⁶ The second report by Todd et al. demonstrated that ambuic acid, a fungal metabolite, is a micromolar

inhibitor of AIP production in a variety of Gram-positive bacteria, including *L. monocytogenes*, and likely targets AgrBD.²⁷ However, in contrast to the report by Zetzmann et al., Todd et al. concluded that a hexapeptide (hereafter referred to as “6-mer”; Figure 2.1B, right) was the native AIP for *L. monocytogenes* upon HPLC-MS analysis of the supernatant of wild-type *L. monocytogenes* EGD-e. This result was further bolstered by an earlier report of a peptide with a matching mass to the 6-mer produced by the closely related species *L. innocua* that contains an AgrD sequence identical to that of *L. monocytogenes*.⁴⁰ Todd et al. note that they were unable to detect the 5-mer that Zetzmann et al. identified from the heterologous *E. coli* system. There have been no additional reports by either group or others that resolve this discrepancy, and none of the compounds from these two reports have been shown to modulate any virulent phenotype of wild-type *L. monocytogenes*.

For QS modulation to be a viable approach to attenuate virulence in *L. monocytogenes*, we first need to better characterize the structure of the native AIP signal. With this structure in hand, we could then delineate the parts of the signal critical to function, and develop structure-activity relationships (SARs) that govern *agr* activation (via AgrC). Such SAR data for native AIPs have been used successfully to generate non-native AIP analogs capable of strongly inhibiting the *agr* systems in *S. aureus* and *S. epidermidis*.^{13, 41-42} In the current study, we sought to explore this approach in *L. monocytogenes* and, critically, determine whether exogenous ligands capable of *agr* modulation can effectively regulate downstream virulence phenotypes in this pathogen.

Herein, we report confirmation of the identity of a native *L. monocytogenes* AIP signal and the discovery of highly efficacious, synthetic *L. monocytogenes agr* antagonists and agonists. We isolated a native AIP from *L. monocytogenes* supernatant, confirmed its identity via HPLC-MS/MS and independent chemical synthesis, and demonstrated its bioactivity in a new *L. monocytogenes agr* reporter strain. We then performed a systematic structure-function analysis of the native AIP through the synthesis of a suite of peptide analogs and assessed their ability to activate and inhibit the *agr* system using the *L. monocytogenes* reporter strain. These studies led to the discovery of peptide agonists with enhanced potency over the native AIP signal and informed the design of peptide antagonists capable of fully inhibiting wild-type *L. monocytogenes agr* QS. In addition to having high efficacy, our lead antagonist also has improved potency over the previously reported small molecule inhibitor of the *L. monocytogenes agr* system, ambuic acid. Interestingly, both our lead *agr* agonist and antagonist in *L. monocytogenes* were also capable of antagonizing *agr* signaling in the related pathogen *Staphylococcus aureus*, further extending their utility and underscoring mechanistic differences between the AgrC receptors in these two bacteria. Perhaps most notably, our lead antagonist was able to drastically attenuate *L. monocytogenes* biofilm formation, demonstrating for the first time the potential for *agr* modulators to control a key virulence phenotype in this important pathogen. These compounds represent powerful chemical tools to interrogate fundamental questions surrounding the role of QS in the different lifestyles of *L. monocytogenes*, as well as in applied studies to develop new anti-virulence and anti-biofilm strategies to control infection and fouling.

2.2 Results and Discussion

2.2.1 Synthesis confirms the native *L. monocytogenes* AIP structure

As noted above, two structures have been reported for the *L. monocytogenes* native AIP, but the proposed structures differ in exocyclic tail length.²⁶⁻²⁷ We sought to remedy this discrepancy by comparing bacterial supernatant to chemically synthesized peptide standards using LC-MS/MS. Using solid-phase peptide synthesis, we first synthesized the 6-mer peptide as it had been reported by two separate research groups as the native AIP (in two different *Listeria* species but with identical AgrD sequences).^{27, 40} We analyzed the 6-mer peptide with HPLC-MS/MS (see SI for methods), then compared it to supernatant from a spent culture of *L. monocytogenes* EGD-e (grown for 20 h to achieve a quorate density to naturally produce AIP). We observed a peak in the *L. monocytogenes* supernatant that matched the retention time, molecular ion, and mass fragmentation patterns of the 6-mer peptide standard (Figure 2.S1), providing strong support for the 6-mer peptide as a native AIP for *L. monocytogenes* (Figure 2.1B) and corroborating the report by Todd et al.²⁷

We also synthesized the 5-mer, the structure posited by Zetzmann *et al.* as the native *L. monocytogenes* AIP,²⁶ in order to perform a similar HPLC-MS/MS analysis as for the 6-mer. However, we observed this compound to rapidly rearrange through a S→N shift (Figure 2.S2) at pH 7 to yield a homodetic peptide with nearly full conversion within 3 h at room temperature (see SI for analytical HPLC traces monitoring conversion). A recent report identified similar homodetic peptides based on AgrD sequences in *Clostridia* supernatants, and these peptides were posited to be the active QS signals in these species.⁴³ Our subsequent studies (see below) revealed this 5-mer

homodetic peptide is a less potent than the parent 5-mer thioester and drastically less potent than the 6-mer in cell-based *agr* agonism assays. It is conceivable that multiple AIPs could be derived from a single AgrD sequence, leading to the formation of the 5-mer thioester (that converts to the homodetic peptide) in addition to the 6-mer in *L. monocytogenes*, due to differential cleavage of AgrD. However, we note that AIPs of multiple lengths from a single *agr* locus have not been reported in any bacterial species to date.^{22, 28} Given that we isolated the 6-mer peptide from bacterial supernatant, corroborating the studies of Todd et al.,²⁷ and its dramatically stronger potency than the 5-mer homodetic peptide, hereafter we refer to the 6-mer as a native AIP of *L. monocytogenes*.

2.2.2 Construction of *L. monocytogenes* *agr*-dependent GFP reporter strains

In order to facilitate profiling the native AIP and analogs for *agr* activity, we designed and constructed two *L. monocytogenes* reporter strains that allow for *agr* activity to be monitored by production of green fluorescent protein (GFP, see SI for detailed methods). Briefly, a plasmid containing the *agr* promoter region fused upstream of *gfp* was transformed into wild-type (EGD-e) and $\Delta agrD$ *L. monocytogenes* strains. The wild-type reporter naturally produces its own AIP and is able to activate AgrC, which will subsequently phosphorylate AgrA for productive binding to DNA and trigger the production of GFP (Figure 2.2A). The $\Delta agrD$ reporter, lacking the ability to produce its own AIP, cannot trigger substantial production of GFP alone. However, adding exogenous AIP to the $\Delta agrD$ reporter results in an increase of fluorescence, indicating *agr* activity has been restored.

We utilize these two reporters to inform on agonism and antagonism activity of analogs of the native *L. monocytogenes* AIP. In the $\Delta agrD$ reporter, the agonism activity of an AIP analog is determined by its ability to increase fluorescence relative to a 1 μ M AIP control (see Methods for normalization procedure). In turn, in the wild-type reporter, the antagonism activity of an AIP analog is determined by its ability to decrease fluorescence relative to a vehicle control. Based on the close structural similarity of the native AIP to the analogs in this study, it is likely that analogs that increase *agr* activity are functioning by directly binding and activating AgrC analogous to the native AIP, and that analogs with *agr* inhibitory activity likely function by competing with the native AIP for binding to AgrC, but lack some or all the correct contacts to activate AgrC.

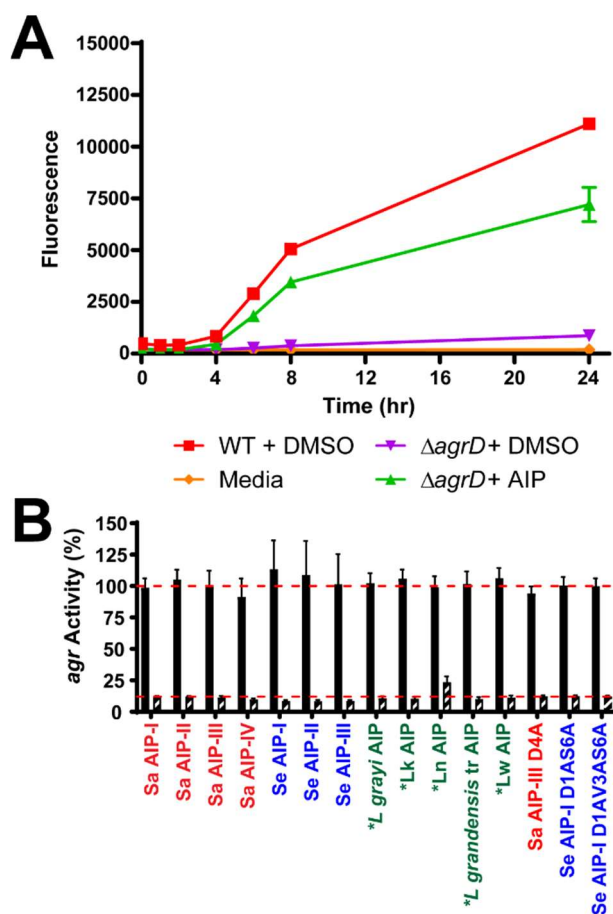


Figure 2.2 Validation of the agr-dependent GFP reporter strains. (A) Activity of reporter strains with vehicle or with native *L. monocytogenes* AIP over time. Data from a single representative data set. (B) Single-point screen of non-cognate native AIPs and analogs in the *L. monocytogenes* reporters, with * signifying putative AIPs. Red compounds originate from *S. aureus* (Sa), blue originate from *S. epidermidis* (Se), and green originate from various *Listeria* AgrD sequences (Lk denotes *L. kieliensis*, Ln denotes *L. newyorkensis*, and Lw denotes *L. weihenstephanensis*; see SI). All compounds assayed at 10 μ M for antagonism in the wild-type reporter (black bars) or for agonism in the $\Delta agrD$ reporter (striped bars). Red dashed lines signify activity levels of wild-type (top) and $\Delta agrD$ (bottom) reporters with vehicle control.

2.2.3 *L. monocytogenes* agr is insensitive to other native AIPs and closely related analogs

In other Gram-positive bacteria, native AIPs from different strains and species often have cross-activity with non-self AgrC receptors.⁴⁴⁻⁴⁷ This cross-activity has revealed useful scaffolds to explore structure-activity relationships (SARs) for AIP

agonism and antagonism in a particular AgrC, along with insights into the promiscuity and selectivity of these receptors.^{42, 48-49} We therefore explored the activity of a set of native AIPs and close analogs active in *Staphylococcus aureus* and *S. epidermidis* for any cross-activity in our *L. monocytogenes* reporters. None of these peptides had substantial activity in either reporter as agonists or antagonists (Figure 2.2B; Tables 2.S1–2.S2).

We questioned if this lack of activity was due to these Staphylococci AIPs being quite structurally distinct than the native *L. monocytogenes* AIP, so we next turned to assessing more closely related AIPs by examining putative AIPs from other species in the *Listeria* genus. The *Listeria* genus is split into two clades, *Listeria sensu stricto* and *Listeria sensu lato*.⁵⁰⁻⁵¹ All the species within *Listeria sensu stricto*, including *L. monocytogenes*, share a well-conserved AgrD sequence (Figure 2.S3) and most notably an identical sequence surrounding the conserved cysteine in the AIP region, suggesting identical native AIPs. However, the genomic data available for *Listeria sensu lato* show these members all have relatively distinct AgrD sequences (Figure 2.S3). We synthesized peptides corresponding to putative AIPs from each *Listeria* species, assuming an identical macrocycle size and exocyclic tail length (with the exception of *L. grandensis*; synthetic difficulties due to its exocyclic cysteine caused us to examine the acetylated truncated peptide instead), and screened these in our *L. monocytogenes* reporter strains (Figure 2.2B). Similar to the Staphylococci AIPs, none of the putative AIPs from other *Listeria* species displayed any activity in *L. monocytogenes*, as either agonists or antagonists. We were particularly surprised that the *L. grayi* putative AIP lacked activity, as it only differed by the *L. monocytogenes* AIP at two positions (the

second and fifth endocyclic positions). These results suggest that *L. monocytogenes* AgrC does not readily accommodate peptides that differ from its cognate AIP. These data are in contrast to Staphylococci AgrCs that are generally capable of binding structurally diverse non-cognate AIPs, as evidenced by the large set of non-native peptide inhibitors and activators reported to date.¹⁷ In fact, we tested several of these lead compounds from *S. aureus* (AIP-III D4A) and *S. epidermidis* (AIP-I D1AS6A and AIP-I D1AV3AS6A) in the *L. monocytogenes* reporters and found they were all inactive (Figure 2.2B), underscoring the different activity profile for the *L. monocytogenes* AgrC receptor. A systematic investigation of the *L. monocytogenes* AIP structure was thus necessary to elucidate the SARs that dictate its activity in AgrC.

2.2.4 Thioester AIPs have improved potency over homodetic peptide

To launch our SAR investigations, we first examined the activity differences between the native AIP, the 5-mer thioester, and the *S*→*N* 5-mer homodetic peptide product in our *agr* fluorescent reporters (see full activity data sets in Tables 2.S3–2.S4). In terms of efficacy, none of these peptides exhibited antagonistic activity and all could fully or nearly fully agonize *agr*. In terms of potency, there were more interesting differences. Compared to the native AIP that had an EC₅₀ of 29.7 nM, the 5-mer thioester had a modest four-fold loss in potency with an EC₅₀ of 107 nM (Table 2.1). The *S*→*N* 5-mer homodetic peptide, however, was over 60-fold less potent than the native AIP and 17-fold less potent than the 5-mer thioester, suggesting this rearrangement significantly impacted compound potency (Table 2.1). As the 5-mer thioester likely converts to the *S*→*N* 5-mer *in situ*, this could result in the lowered potency observed for

the 5-mer thioester relative to the native AIP. To prevent the $S \rightarrow N$ exchange, we synthesized a 5-mer thioester with an acetylated N-terminus (Ac-5-mer). The acetylation reduced maximal activation relative to the free N-terminal 5-mer but halved the potency to an EC_{50} of 46.6 nM that is more similar to the potency of the native AIP (Table 2.1, Tables 2.S3–2.S4), indicative that the rearrangement contributed to the lower potency of the 5-mer thioester.

Considering that (1) the 5-mer thioester fully converted to the $S \rightarrow N$ 5-mer product within a few hours *in vitro* and (2) the cell-based reporter assay is 24 h long, the observed potency difference between the thioester and $S \rightarrow N$ versions of the 5-mer is certainly intriguingly. We speculate that the 5-mer thioester may be longer lived in cell culture versus *in vitro*, possibly through interactions with AgrC protecting the thioester bond from this rearrangement. In addition, the ability of AgrC to be activated by both the thioester-containing AIPs and the homodetic peptide is noteworthy. The ability to be agonized by both scaffolds has been observed previously in *Clostridia* although, unlike our results above in *Listeria*, the *Clostridia* homodetic peptides were more potent and efficacious than the thioester-containing peptides.⁴³ Regardless of which scaffold is more potent or efficacious, the activity of homodetic peptides against *agr* systems in multiple genera warrants further investigation into the prevalence of homodetic peptide activity in *agr* systems. In the case of *L. monocytogenes*, though, the dramatic potency loss of the $S \rightarrow N$ 5-mer product suggests that homodetic peptides, despite improved hydrolytic stability from the amide linkage over the thioester, would be a poor scaffold from which to develop *agr* modulators in *L. monocytogenes* and were not pursued further for derivatization.

2.2.5 Altering the AIP exocyclic tail length causes only minor effects on activity

We next examined *L. monocytogenes* AIP analogs with increasing exocyclic tail lengths (1–10 residue tails; Figure 2.3A). The residues added correspond to the N-terminal residues adjacent to the AIP sequence in AgrD. While previous work by Zetzmann et al. had shown that differing tail lengths of AIP analogs in *L. monocytogenes* affected activity using a luminescence *agr* reporter,²⁶ potency and efficacy data were not reported. Surprisingly, analysis of these analogs in our own *L. monocytogenes agr* GFP reporters demonstrated that tail length changes had negligible effects on potency and all analogs maintained substantial, if not full, agonism activity (Figure 2.3B, see Tables 2.S3–2.S4 and SI for full dose-response data and curves). The 7- and 8-mer peptides were the least active agonists, maintaining 70% efficacy and were only two-fold less potent than the native AIP. Examining these peptides in the wild-type reporter revealed these compounds were partial agonists (i.e., compounds that agonize the $\Delta agrD$ reporter and antagonize the wild-type reporter to similar levels of overall *agr* activity) and were the only peptides from this set with appreciable antagonistic activity. Overall, these results were unexpected, as previous SAR studies of AIPs in other organisms have shown that altering or removing the exocyclic tail can have dramatic results on activity, often mode-switching agonists to antagonists of varying potencies.^{42, 49, 52} The lack of substantial activity changes upon varying the tail length suggests that the ligand contacts required for AgrC binding and activation by the 6-mer AIP are largely unaffected by additions to its tail and suggest the key contacts are present within the macrocycle.

abolished agonism activity and had no noticeable antagonism. The lack of either agonism or antagonism activity suggests that removal of these phenylalanine sidechains impairs the ability of these peptides to bind AgrC effectively, implicating Phe3 and Phe5 as playing critical roles in the AIP-AgrC binding event. This result aligns with previous studies investigating AIP-AgrC interactions in other bacteria, in which ligand binding was shown to be largely facilitated by bulky and hydrophobic endocyclic residues (as supported by both in cell-based and *in vitro* assays).⁵³⁻⁵⁵ We observed that the remaining two alanine substitutions—i.e., in AIP M4A and AIP V6A—both decrease in agonism efficacy (50 and 30% loss, respectively; Table 2.1) and potency (66- and 8-fold, respectively; Table 2.1) compared to the native AIP suggesting that, while these side chains do contribute to full activation of AgrC, they are ultimately non-essential for activity. While only four Ala-containing analogs were examined here, it was intriguing to note that none of these analogs were capable of substantially inhibiting the wild-type *agr* reporter. In other *agr* and related peptide-based QS systems, a single alanine substitution can often mode-switch a native peptide signal into an exquisitely potent antagonist (e.g., AIP-III D4A in *S. aureus*),^{13, 42, 52, 56-58} so the lack of antagonists revealed in this alanine scan suggests the mechanism of AgrC agonism in *L. monocytogenes* is different than in these other organisms.

Table 2.1 Activity data for native *L. monocytogenes* AIP and analogs thereof in *agr* reporter assays. See Methods for details of strains and data normalization method. 95% CI values can be found in SI.

Compound	Sequence	EC ₅₀ (nM)	Max Activation Observed (%)	IC ₅₀ (nM)	Max Inhibition Observed (%)
AIP (6-mer)	A-(C-F-M-F-V)	29.7	114	-- ^a	NA ^b
5-mer	(C-F-M-F-V)	107	105	-- ^a	1.15
S→N 5-mer	(C-F-M-F-V)	1820	89.7	-- ^a	0.81
Ac-5-mer	Ac-(C-F-M-F-V)	46.3	75.3	-- ^a	6.39
AIP F3A	A-(C- A -M-F-V)	-- ^a	9.72	-- ^a	3.65
AIP M4A	A-(C-F- A -F-V)	1980	53.5	-- ^a	7.85
AIP F5A	A-(C-F-M- A -V)	-- ^a	6.37	-- ^a	NA ^b
AIP V6A	A-(C-F-M-F- A)	241	69.0	-- ^a	15.0
AIP A1dA	dA -(C-F-M-F-V)	96.9	58.8	-- ^a	15.2
AIP C2dC	A-(dC -F-M-F-V)	106	41.0	3970	48.4
AIP F3dF	A-(C- dF -M-F-V)	-- ^a	6.63	-- ^a	14.7
AIP M4dM	A-(C-F- dM -F-V)	10.2	111	-- ^a	3.99
AIP F5dF	A-(C-F-M- dF -V)	2180	72.3	-- ^a	2.71
AIP V6dV	A-(C-F-M-F- dV)	883	72.9	-- ^a	NA ^b

^aDose response did not converge. ^bNA = inactive.

Next we replaced each residue in the *L. monocytogenes* AIP with its D-amino acid analog, and we observed that this stereochemical inversion yielded many analogs with reduced agonism efficacy and potency. The only largely inactive peptide was AIP F3dF which, when coupled with the previously discussed inactivity of AIP F3A, further supports that Phe3 likely plays a critical role in AIP-AgrC interactions. Similarly, while AIP F5dF did maintain some agonism activity, it lost two orders of magnitude in potency, again underscoring the importance of Phe5 for AIP activity. The D-amino acid substitutions at Ala1 and Val6 both reduced efficacy and potency, yet not to the extent as the D-phenylalanine analogs. Inverting the remaining two positions, Cys2 and Met4, had perhaps more interesting outcomes. First, by inverting the stereochemistry of Cys2

and therefore the relative orientation of the AIP thiolactone bridge, the resulting peptide AIP C2dC exhibited a modest three-fold loss in agonism potency in the $\Delta agrD$ reporter. Moreover, AIP C2dC was able to antagonize wild-type reporter to nearly 50% of its maximum activity, indicative of a partial agonist activity profile. We note that the antagonistic activity of AIP C2dC is substantially greater than any of the other analogs we have detailed thus far. The large reduction in agonism activity by AIP C2dC suggests that the local conformation surrounding the thioester bond plays an important role in activation of AgrC. Secondly, incorporation of D-Met to yield AIP M4dM caused three-fold *increase* in agonism potency relative to the native AIP, representing the first peptide with heightened potency uncovered so far. We used the findings from these preliminary alanine and D-amino acid scans (namely, the requirement for the Phe3 and Phe5 side chain, and the effects of inversion at Cys2 and Met4) to guide our antagonist and agonist development as described below.

2.2.7 Design and biological evaluation of first-generation AIP analogs

Several additional analogs the *L. monocytogenes* AIP were designed (Figure 2.4), synthesized, and screened in the wild-type and $\Delta agrD$ reporters (select analog activity data in Table 2.2, full data sets in Tables 2.S7–2.S8) with the goal of developing a stronger set of SAR data. We first focused on synthesizing analogs to probe how the exocyclic Ala1 contributes to activity with four sidechains of varying polarity, charge, and steric bulk. Three of the analogs—AIP A1P, AIP A1T, and AIP A1K—were partial agonists that leveled off to around 75% *agr* activity in both agonism and antagonism assays. The remaining analog, AIP A1V, maintained the full activity of the parent AIP

with four-fold enhanced potency, similar to AIP M4dM described above. Altogether however, the relatively minor activity changes despite rather large structural differences to the side chain in these analogs suggests this exocyclic position is quite tolerant to substitution.

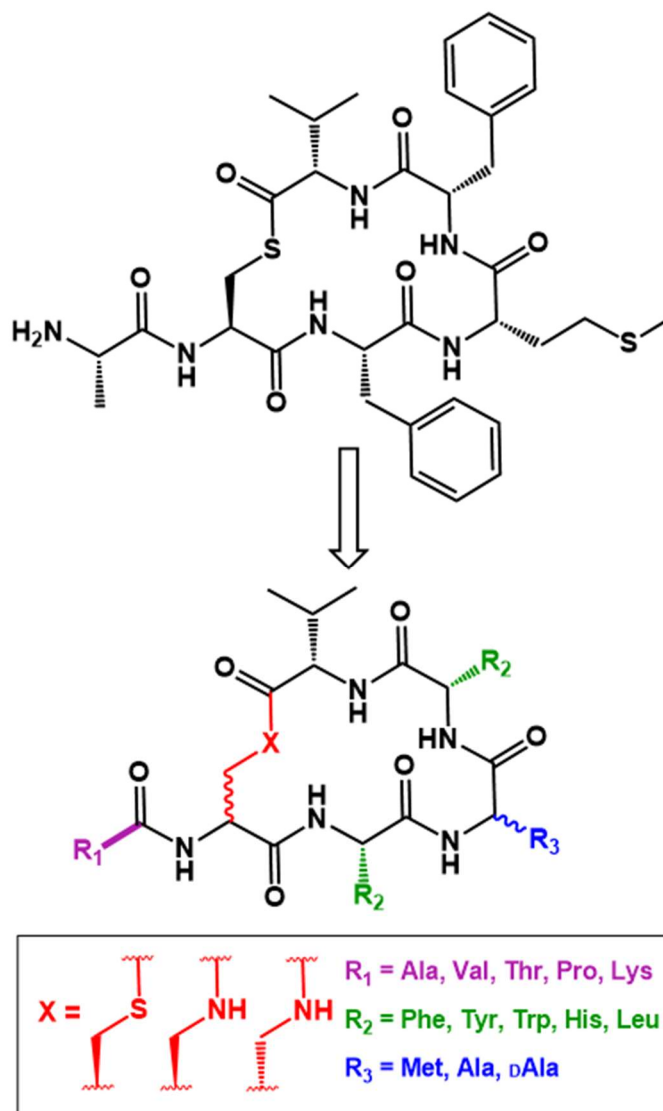


Figure 2.4 Summary of substitutions made to *L. monocytogenes* AIP to investigate SAR trends of individual amino acids.

As our initial alanine and D-phenylalanine analogs of Phe3 and Phe5 had large efficacy and potency losses suggesting important roles in the binding event with AgrC, we next turned to examining substitutions that better maintain some of L-phenylalanine's properties—bulky, hydrophobic, aromatic—with the hypothesis that these may be better tolerated. The hydrophobic substitutions (tyrosine, leucine, tryptophan) in the Phe3 position were able to maintain some activity, agonizing to 40–60% and antagonizing to around 30% (Table 2.2). While these analogs were certainly an improvement over the inactive alanine or D-phenylalanine analogs, these new peptides still suffered over 10-fold potency losses. Alternatively, we explored maintaining aromaticity while changing hydrophobicity by replacement of Phe3 with histidine; interestingly, while this analog was devoid of any observable agonism, it did exhibit minor antagonistic activity (albeit with low potency). The same set of substitutions were also examined in Phe5. The Phe5 analogs overall were able to agonize to similar levels as the Phe3 analogs, but with even more severe potency losses and the analogs had no observable antagonism. These conservative substitutions in Phe3 and Phe5 demonstrate that, while strict adherence to L-phenylalanine is not necessary to induce some level of activation of AgrC, even subtle deviations of the side chain properties can drastically affect the activity of the resulting compound.

Table 2.2 Reporter assay activity data for select first- and second-generation analogs of *L. monocytogenes* AIP. See Methods for data normalization. 95% CI values can be found in SI.

Compound	Sequence	EC ₅₀ (nM)	Max Activation Observed (%)	IC ₅₀ (nM)	Max Inhibition Observed (%)
AIP	A-(C-F-M-F-V)	29.7	114	-- ^a	NA ^b
<i>Select First Generation Analogs</i>					
AIP A1K	K-(C-F-M-F-V)	22.9	80.0	233	31.3
AIP A1V	V-(C-F-M-F-V)	7.67	109	-- ^a	1.63
AIP C2Dap	A-(D ap-F-M-F-V)	342	92.9	-- ^a	5.32
AIP C2dDap	A-(d Dap-F-M-F-V)	-- ^a	14.3	-- ^a	19.3
AIP F3Y	A-(C-Y-M-F-V)	518	47.4	3460	33.4
AIP F3H	A-(C- H -M-F-V)	-- ^a	12.4	-- ^a	24.9
AIP M4dA	A-(C-F- d A-F-V)	455	82.0	-- ^a	9.54
AIP F5Y	A-(C-F-M-Y-V)	5620	44.4	-- ^a	6.61
AIP F5H	A-(C-F-M- H -V)	-- ^a	7.13	-- ^a	2.19
<i>Second Generation Analogs</i>					
AIP A1K/C2dC	K-(d C-F-M-F-V)	-- ^a	10.2	4440	30.7
AIP A1K/M4dM	K-(C-F- d M-F-V)	4.18	74.1	-- ^a	20.2
AIP C2dC/M4dM	A-(d C-F- d M-F-V)	24.1	35.7	242	64.8
KdCdM	K-(d C-F- d M-F-V)	-- ^a	8.10	1400	92.6

^aDose response did not converge. ^bNA = not active.

After seeing the increased potency of AIP M4dM relative to the native AIP, we were curious if this could be replicated with any D-amino acid at this position. While our initial alanine scan demonstrated that substituting Met4 for L-alanine (AIP M4A) resulted in a low potency agonist (Table 2.2), inverting the stereochemistry to D-alanine (AIP M4dA) improved potency about four-fold. The similar potency increases seen from the two pairs of substitutions (a three-fold increase going from L-methionine to D-methionine and a four-fold increase going from L-alanine and D-alanine) would suggest the D-stereochemistry is largely the driving force for the enhanced agonism potency. Given the proximity of Met4 to its neighbors Phe3 and Phe5, the D-stereochemistry at Met4

could better orient this trio of hydrophobic sidechains for optimal contacts with AgrC; structural studies of the native AIP and these analogs could illuminate how these D-amino acids contribute to the improved potency and are ongoing.

We further investigated the thioester linkage in new analogs, as since AIP C2dC displayed significant antagonism, we were curious if other substitutions could produce or alter antagonistic activity. Using L-2,3-diaminopropionic acid (Dap), we synthesized an AIP analog where the thioester linkage was replaced with an amide linkage (AIP C2Dap; Table 2.2). AIP C2Dap failed to antagonize AgrC, and instead largely retained the efficacy of the native AIP at the cost of a 10-fold loss in potency. This activity profile indicates the sulfur is not essential for the activation mechanism, but does influence potency. Our lab has reported similar potency losses when converting the thioester to an amide in *S. aureus* AIP-based antagonists.⁵⁹⁻⁶⁰ Lastly, given that we observed partial agonism upon stereochemical inversion of the cysteine (in AIP C2dC), we were curious if a peptide that incorporated D-Dap would perform similarly. Intriguingly, while AIP C2dDap did slightly antagonize in the wild-type reporter, this analog appeared to have little or no agonism activity in the $\Delta agrD$ reporter, suggesting it is a true AgrC antagonist and not a partial agonist. While this activity profile could be beneficial in designing an antagonist for the system, we decided not to pursue amide analogs further due to their weak potencies overall.

2.2.8 Combinatorial substitutions reveal a route to antagonism

Despite characterizing over 30 analogs at this point, our efforts exploring SARs of the native AIP through single substitutions had yet to produce an efficacious

antagonist. We hypothesized that we could rationally design an antagonist with improved activity through combinatorial substitutions and focused on a set of three to start. First, the A1K substitution, while only inhibiting the wild-type reporter by 30%, still maintains high potency in AgrC agonism assays. Next, the C2dC substitution was able to antagonize *agr* activity to 50% at the cost of some potency. Lastly, the M4dM substitution yielded a three-fold enhancement in agonism potency relative to the native AIP with no significant change in efficacy. We combined these substitutions using the native AIP scaffold to synthesize double-substitution analogs as well as a triple-substitution analog and profiled their activity in the *L. monocytogenes agr* reporter strains (Table 2.2, Tables 2.S9–2.S10).

First surveying the double substitutions, when the two antagonistic substitutions, A1K and C2dC, were combined, the resulting analog AIP A1K/C2dC was unable to agonize the $\Delta agrD$ reporter and instead displayed antagonism in the wild-type assay (Table 2.2). Its low potency, however, prevented characterizing its IC₅₀ over the concentration ranges tested. Next, we reasoned that the agonism potency increase from the M4dM substitution could carry over when combined with the two other substitutions. This was indeed the case, as the double substitution analog AIP A1K/M4dM was a five-fold more potent agonist than AIP A1K while maintaining a similar partial agonism profile. Likewise, combining M4dM with C2dC in AIP C2dC/M4dM yielded marked improvements in potency for both agonism (four-fold) and antagonism (16-fold) activities relative to AIP C2dC. This potency increase also allowed for the antagonism curve of AIP C2dC/M4dM to flatten out at 65% inhibition, signifying the most efficacious antagonist we had identified so far. These consistent potency

increases by incorporation of D-Met4 further cements the critical role it must play in AIP analog:AgrC interactions.

We then combined these three features—the low antagonistic activity of A1K, the strong antagonistic activity of C2dC, and the high agonism potency of M4dM—into a triple substitution analog AIP A1K/C2dC/M4dM that we named KdCdM. Similar to the AIP A1K/C2dC analog, KdCdM shows no observable activation in the $\Delta agrD$ reporter; however, now with the incorporation D-Met4, KdCdM was the first analog we found that could fully antagonize the wild-type *L. monocytogenes agr* reporter to basal activity levels (Figure 2.5A). In addition to its high efficacy, KdCdM is also 15-fold more potent than the only other characterized antagonist of the *L. monocytogenes agr* system, ambuic acid, as determined by our reporters (Figure 2.5B, Table 2.S10). The strong activity of KdCdM is further enhanced by its clearer mechanism of inhibition (almost certainly targeting AgrC) relative to ambuic acid. The activity profile of KdCdM appears to largely be the sum of the single substitution's activity profiles—the lack of apparent cooperative or uncooperative effects between these three substitutions may suggest that their individual structural effects are localized and do not largely affect the global conformation of the peptide.

While we had observed that *L. monocytogenes* is unresponsive to AIPs and analogs from other organisms (*vide supra*), we were curious if KdCdM or any of our other *L. monocytogenes agr* modulators identified herein were active in other species. We elected *S. aureus* for further experiments. Dose response experiments in a *S. aureus agr-I* reporter system⁶¹ revealed that that the *L. monocytogenes* native AIP, our more potent agonist AIP M4dM, and our antagonist KdCdM could all antagonize *S.*

aureus agr-I activity with high nanomolar potency (Figure 2.S4, Table 2.S11). These results indicate that, while the *L. monocytogenes* AgrC appears to be more selective in terms of AIP analog modulators, peptide activity in *L. monocytogenes* AgrC and other AgrCs is not mutually exclusive. Moreover, these findings provide new scaffolds for the design of *agr* antagonists with activities that expand beyond one species.

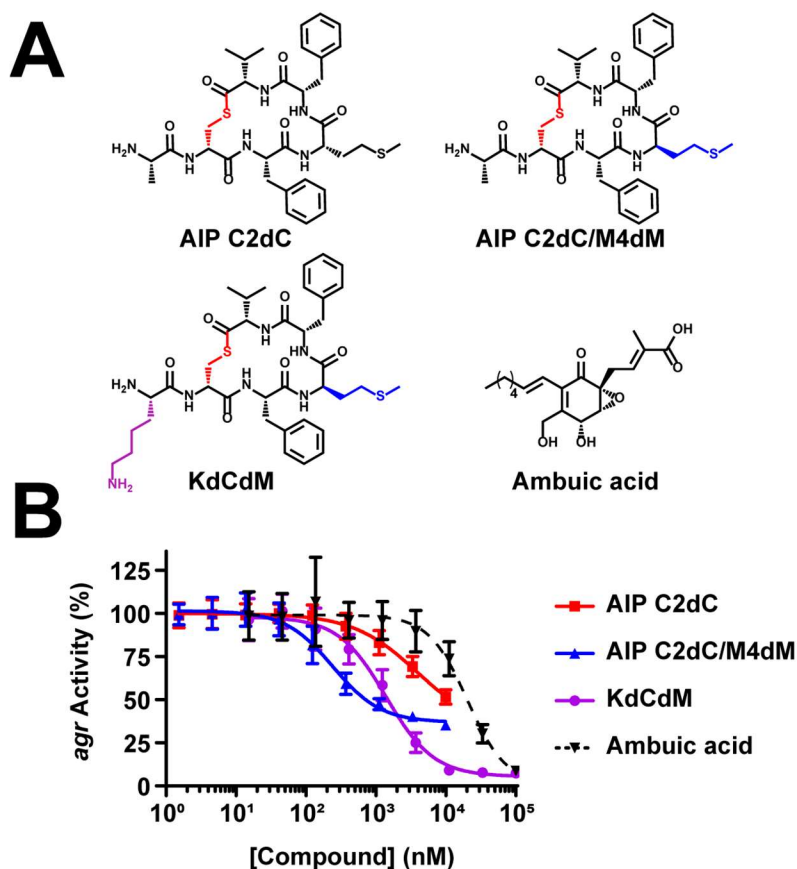


Figure 2.5 Activity of key antagonists against wild-type reporter. (A) Structures of AIP analog antagonists leading to lead antagonist KdCdM and previously reported small molecule inhibitor, ambuic acid. (B) Dose response assay activity data of antagonists.

2.2.9 Chemical control of biofilm formation with *agr* modulators

As highlighted above, biofilm formation is a critical virulence phenotype that allows *L. monocytogenes* to persist and spread through harsh conditions, and attenuating biofilm formation has been a major focus in *L. monocytogenes* research.⁶²⁻⁶³ As $\Delta agrD$ strains have attenuated biofilm formation, this suggests *agr* activation promotes biofilm production.¹⁰ We therefore hypothesized that our *agr* agonists should restore biofilm production in $\Delta agrD$ strains, while *agr* antagonists should reduce biofilm in wild-type strains. Indeed, incubating *L. monocytogenes* $\Delta agrD$ with the native AIP or our synthetic agonist AIP M4dM restored a substantial amount of biofilm production when compared to vehicle controls (Figure 2.6A). In turn, wild-type biofilm formation was reduced by 90% when incubated with the KdCdM antagonist (Figure 2.6B). Moreover, this effect was dose-dependent (Figure 2.6C) and revealed a very similar IC₅₀ value (1.86 μ M) when compared to our fluorescence reporter data (1.40 μ M), further supporting a strong connection between biofilm formation and *agr* activity in *L. monocytogenes*. Interestingly, we note that the level of biofilm produced by wild-type *L. monocytogenes* in the presence KdCdM was significantly lower than the $\Delta agrD$ control. This finding could indicate KdCdM acts as an inverse agonist. These biofilm assay data are the first to demonstrate attenuation of *L. monocytogenes* biofilm formation using a synthetic *agr* modulator and serve to highlight the potential chemical ligands to control phenotypes linked to QS in this important human pathogen.

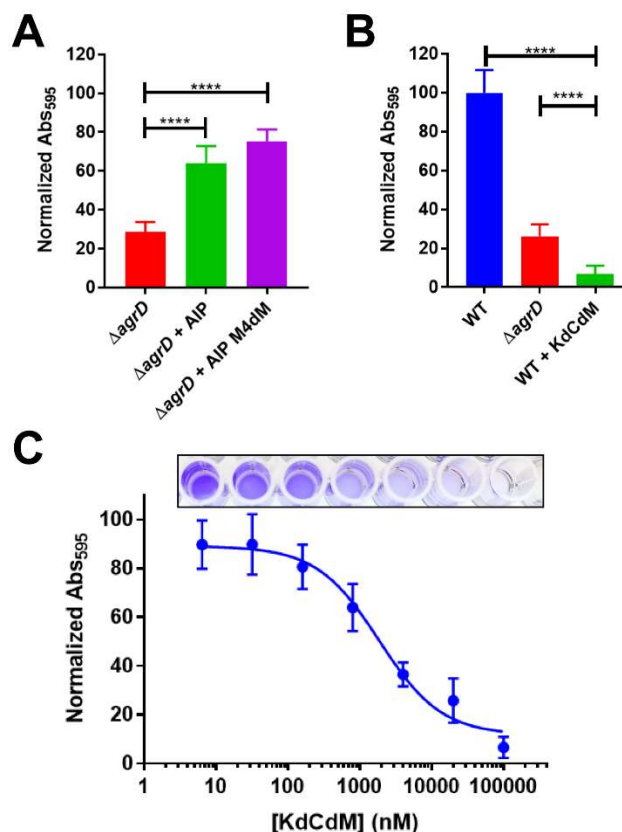


Figure 2.6 AIP analogs can modulate biofilm formation through controlled *agr* activity. A) 10 μ M AIP and AIP M4dM increase biofilm formation of Δ *agrD* strain. B) 100 μ M KdCdM reduces biofilm of wild-type (WT) strain. C) Dose-response effect of KdCdM on WT biofilm formation with representative biofilm wells overlaid. See Methods for data normalization. **** indicates $p < 0.0001$ as determined by ANOVA.

2.3 Summary and Conclusions

The ubiquity and adaptability of *L. monocytogenes* make it a difficult organism to combat, and, coupled with an increasing number of infection cases in recent years,³ it is clear that new tools to further our understanding of virulence in this pathogen would benefit both the healthcare and food industries. The *agr* QS system has been shown to regulate a number of key virulence behaviors in *L. monocytogenes* yet remains poorly understood. In this study, we describe a set of new chemical tools that target *L. monocytogenes agr* QS and are based on its native AIP sequence. First, we

successfully identified a hexapeptide from bacterial supernatant that matched a chemically-synthesized standard, confirming the structure of the native AIP previously reported.²⁷ In addition, we constructed robust *agr*-dependent GFP reporter strains that accelerated the characterization of the native AIP and AIP analogs, and can be used to characterize other *agr* system modulators as we demonstrated with ambuic acid. The SARs gathered on the native *L. monocytogenes* AIP revealed multiple key features that dictate the activity of analogs (Figure 2.7), such as the Phe3 and Phe5 residues being critical for activity or the incorporation of D-amino acids can enhance potency in the case of Met4 or induce substantial antagonism in the case of Cys2. This SAR survey discovered multiple agonists more potent than the native AIP and, while individual substitutions could not fully antagonize *agr* activity, rational combination of substitutions eventually led to the discovery of KdCdM, the most potent *agr* antagonist in *L. monocytogenes* reported to date. While *L. monocytogenes* was unresponsive to native AIPs and analogs from other bacterial species, these new AIP analogs described here were also found to antagonize *S. aureus agr* activity, expanding the known set of scaffolds to alter *agr* activity in *S. aureus* and providing a foundation for the development of potential pan-genera *agr* antagonists.

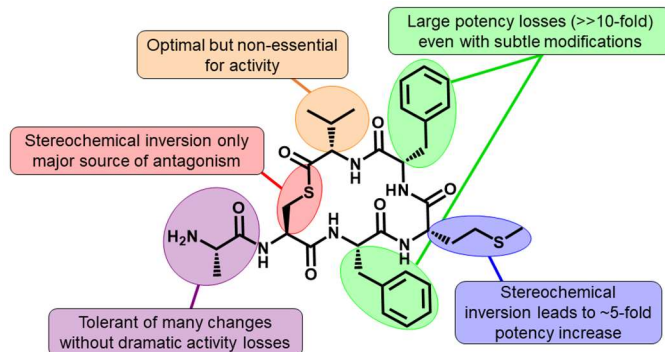


Figure 2.7 Summary of SAR findings of the *L. monocytogenes* AIP.

Another key finding of this study was that these *agr* modulators could be applied to control *L. monocytogenes* virulence phenotypes, as agonists restored biofilm production in an *agr* mutant while our lead antagonists decimated wild-type biofilms. The compounds and insights gained from this study of the *L. monocytogenes agr* system should enable future work to investigate the modes by which chemical control of *agr* can disrupt mechanisms of persistence and virulence of this common pathogen. For example, preemptive application of *agr* antagonists to surfaces could limit biofilm formation that plagues the food industry, and *agr* modulators could be used in culture to elucidate the mechanisms by which the *agr* system leads to *L. monocytogenes* invasion of eukaryotic cells. Ongoing studies will focus on such applications and exploring the activity of these peptides in related bacteria.

2.4 Materials and Methods

2.4.1 Reagents, strains, and general methods

All standard reagents were purchased from commercial sources and used according to sources' instructions. Strains, plasmids, and primers are summarized in

Tables 2.S12–2.S13. For standard methods, *L. monocytogenes* strains EGD-e and $\Delta agrD$ were cultured in brain heart infusion (BHI, from Teknova), while the corresponding fluorescent reporter strains were grown in BHI supplemented with 10 $\mu\text{g}/\text{mL}$ chloramphenicol. Similarly, the fluorescent *S. aureus agr* reporter strain AH1677 was also grown in BHI supplemented with 10 $\mu\text{g}/\text{mL}$ chloramphenicol. For biofilm assays, *L. monocytogenes* EGD-e and $\Delta agrD$ biofilms were grown in Lysogeny Broth (LB, from Research Products International). Overnight cultures were grown in 3 mL of media (with antibiotic if appropriate) at 37 °C with 200 rpm shaking unless noted otherwise.

2.4.2 Peptide synthesis

L. monocytogenes AIP analogs were synthesized on solid-phase resin, purified using reverse-phase high-performance liquid chromatography (HPLC), and characterized using high-resolution mass spectrometry (HRMS) and analytical HPLC, following previously characterized methods.^{54, 59} Additional experimental and characterization details can be found in the Supporting Information documents.

2.4.3 Fluorescence reporter assay protocol

For *L. monocytogenes* QS (*agr*) reporter assays, peptide stock solutions in DMSO (1 mM) were serially diluted in DMSO, and 2 μL of solution was added to each well in a black 96-well plate (polystyrene microtiter plate, Costar). Agonism assays utilized the $\Delta agrD$ reporter strain, with 2 μL of 100 μM AIP (final concentration 1 μM) as a positive control and 2 μL of DMSO as a negative control. Antagonism assays utilized

the EGD-e reporter strain, with 2 μ L of DMSO as a positive control. In both assays, wells containing only BHI media served as negative controls for normalization. An overnight culture of bacteria was diluted 1:50 in fresh BHI, then 198 μ L were transferred to each well (excluding the media control wells). Plates were then incubated at 37 °C for 24 hours with shaking at 200 rpm. Fluorescence of GFP (excitation at 500 nm, emission at 540 nm) and OD₆₀₀ of each well was measured using BioTek Synergy 2 plate reader. Measurements were processed by subtracting background fluorescence (BHI media), correcting by OD₆₀₀, and then normalized. Agonism assays were normalized to media controls (0%) and 1 μ M AIP controls (100%). Antagonism assays were normalized to media controls (0%) and DMSO vehicle controls (100%). *S. aureus agr* reporter strain assays were performed as previously described in strain AH1677.⁶⁰ Non-linear regression curves were fitted to the data sets in GraphPad Prism 7 by using variable slope (four-parameter) dose-response analysis to obtain potency, efficacy, and statistical information about the activity of tested peptides. Each peptide was tested with three technical replicates and three biological replicates. All data derived from fluorescent reporter strains are represented with data points signifying the mean and error bars signifying the standard deviation from all replicates.

2.4.4 Biofilm assay protocol

Biofilms assays were adapted from previous reports and protocols.⁶⁴⁻⁶⁵ Overnight cultures of *L. monocytogenes* EGD-e and $\Delta agrD$ were grown in BHI, then diluted 1:100 in LB. For single-point assays, 2 μ L of agonists or antagonists at an appropriate concentration were added to wells in a clear 96-well microtiter plates. For dose-

response assays, a stock solution of the select peptide were serially diluted in DMSO, then 2 μL of each concentration were transferred to the appropriate wells. Then, 198 μL of bacteria were added to their respective wells, using $\Delta agrD$ for agonist wells and EGD-e for antagonist wells. In each plate, additional vehicle controls for baseline biofilm formation of EGD-e and $\Delta agrD$ strains (2 μL of DMSO) were included, as well as a media control (200 μL of LB). Plates were incubated at room temperature for 24 hours statically, at which point plates were inverted over a glass waste container and gently shaken to remove planktonic bacteria. The wells were gently washed with 200 μL of PBS twice, inverting again over the waste container to remove liquid. Then, 200 μL of 0.1% crystal violet solution (in water) were added to each well and incubated for 30 minutes. The wells were then washed with 200 μL of PBS three more times and left to air dry for 15 minutes. Remaining crystal violet was solubilized by the addition of 100 μL of 95% ethanol in water solution, pipetting up and down to mix, incubated for 10 minutes, then absorbance was read at 595 nm. Absorbance data was processed by normalizing to the EGD-e vehicle control (100%) and the LB media control (0%). Non-linear regression curves were fitted to the data sets in GraphPad Prism 7 by using variable slope (four-parameter) dose-response analysis to obtain potency, efficacy, and statistical information about the activity of tested peptides. Each well was tested with four technical replicates and three biological replicates. All data derived from crystal violet biofilm assays are represented with data points signifying the mean and error bars signifying the standard deviation from all replicates.

2.5 Supplemental Information

2.5.1 Additional experimental procedures

Construction of biological reporter strains

A DNA sequence was designed and purchased from Integrated DNA Technologies to contain an EagI recognition site, the P_{II} promoter of the *agr* system, the 3' UTR of *hly*, super folder GFP, and a Sall recognition site. The DNA was digested with EagI and Sall, cloned into an EagI/Sall-cut pAM401 plasmid resulting in the plasmid pAM401-KW1, and then transformed into *Escherichia coli* XL1-Blue competent cells. The insertion into pAM401 was confirmed using Kapa polymerase and primers DAP337 and DAP338, and additional confirmation via commercial sequencing. Purified plasmid was transformed into the conjugative *E. coli* S17 strain, which was used to conjugate to *Listeria monocytogenes* EGD-e and EGD-e $\Delta agrD$ to generate the *agr*-GFP reporter strains EGD-e:pAM401-KW1 and EGD-e $\Delta agrD$:pAM401-KW1. Conjugation was verified using primers DAP337 and DAP338.

Instrumentation

Reverse-phase high performance liquid chromatography (RP-HPLC) was carried out on a Shimadzu system equipped with a SLC-10Avp controller, a LC-10AT pump, a FCV-ALvp solvent mixer, and a SPC-10MAvp UV/Vis diode array detector. Peptides were purified using a semi-preparative Kromasil Eternity C18 column (10 mm x 250 mm, 5 μ m particle size with 100 Å pore size) with a 5 mL/min flow rate. Peptide purity was assessed on an analytical Kromasil Eternity C18 column (4.6 mm x 250 mm, 5 μ m particle size with 100 Å pore size) with a 1 mL/min flow rate. Solvent A = 18 M Ω water +

0.1% trifluoroacetic acid (TFA); solvent B = acetonitrile + 0.1% TFA. Peptide identity was determined using mass spectrometry (MS). MALDI-TOF MS data were obtained using a Bruker microflex LRF spectrometer equipped with a 337 nm laser and a reflectron. Exact mass (EM) MS data were obtained using a Thermo Q Exactive Plus ESI-Q-IT (orbitrap) mass spectrometer.

Native AIP isolation and characterization

Overnight cultures of *L. monocytogenes* EGD-e were grown in BHI, centrifuged at 3000 rpm for 15 min at 4 °C, and 5 mL aliquots of the supernatant were lyophilized. A scoop of lyophilized supernatant was re-constituted in 1.5 mL of 18 MΩ water, vortexed, chilled at 4 °C for one hour, and then centrifuged at 15000 rpm for 10 min. The supernatant was removed, and the pellet was reconstituted in 25% acetonitrile in water with 0.1% formic acid and analyzed by LC-MS/MS by injection on a Bruker Q-TOF MS (Maxis II) instrument with electrospray ionization and a C18 column (250 μm i.d., 250 mm long). For comparison, synthetic peptide standards were diluted in 25% acetonitrile in water with 0.1% formic acid and injected on the instrument.

Standard thioester AIP analog peptide synthesis

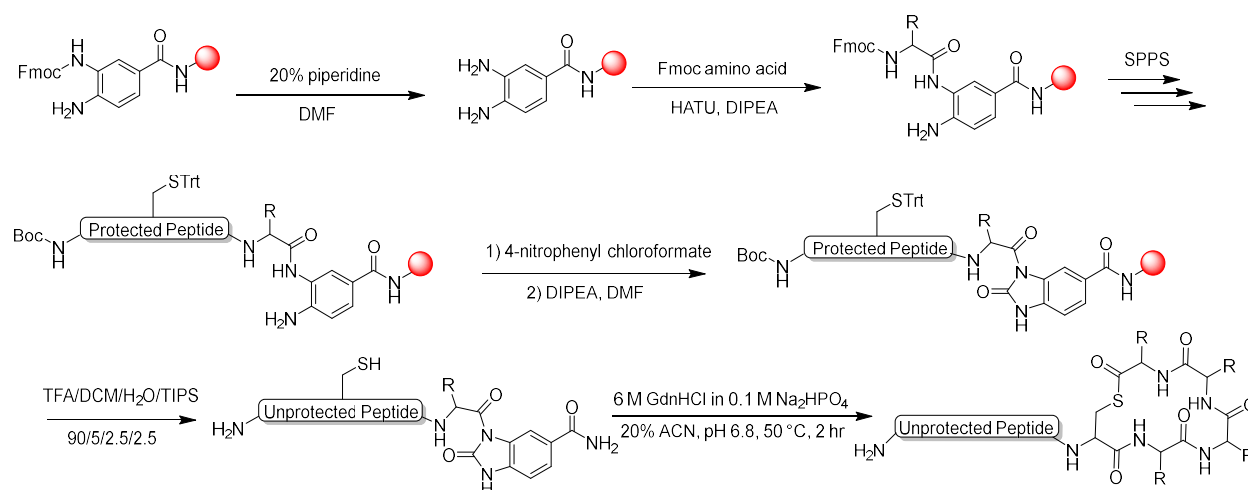
Standard thioester AIP peptides were synthesized accordingly to previous protocols (shown in Scheme S1).^{54, 66} Briefly, approximately 30 mg (0.0147 mmol, 1 eq.) of Fmoc Dawson Dbz AM resin was swelled in a vessel of DCM for at least 40 min, then subsequently washed with DCM (2 mL ×3) and DMF (2 mL ×3). The washed resin was then deprotected with 20% piperidine in DMF (2 mL ×3 for 5, 5,

and 10 minutes) while shaking the vessel. After washing the resin with DMF (2 mL \times 3), the first amino acid for loading was prepared. The appropriate *N* $^{\alpha}$ -Fmoc protected amino acid (4 eq.), HATU (4 eq.), and DIPEA (8 eq.) were dissolved in 2 mL DMF, incubated for 5 min, and added to the deprotected resin. The resin was allowed to couple with the amino acid for 1 hr while shaking. The resin was washed with DMF (2 mL \times 3), then deprotected and coupled to the next *N* $^{\alpha}$ -Fmoc protected amino acid (0.5 hr coupling time), and the process repeated for the remaining amino acids. The final amino acid was *N* $^{\alpha}$ -Boc-protected instead of *N* $^{\alpha}$ -Fmoc protected. Proceeding from the final coupling, the resin was washed with DMF (2 mL \times 3) and then DCM (2 mL \times 3).

Next, 4-nitrophenylchloroformate (4 eq.) was dissolved in 2 mL of DCM and added to the resin, and the resulting slurry was shaken for 30 min. The solution was drained and an additional 2 mL of 4-nitrophenylchloroformate in DCM was added to resin and shaken for another 30 min. After washing with DCM (2 mL \times 3), the resin was incubated with shaking with 5.5% DIPEA in DMF (2 mL \times 3, 10 min per round). After the final incubation, the resin was washed with DMF (2 mL \times 3), DCM (2 mL \times 3), and then Et₂O (2 mL \times 3). The washed resin was dried under N₂ and then under vacuum. The peptide was simultaneously deprotected and cleaved from the resin using 2 mL of 90/5/2.5/2.5 TFA/DCM/H₂O/ triisopropylsilane (TIPS) solution while shaking for 2 hr. The solution was filtered from the resin, then the resin was washed with another 2 mL of the cleavage solution and filtered again. The solution was isolated, mixed with 40 mL of Et₂O, chilled at -20 °C for at least 1 hr to precipitate the peptide, and then centrifuged using a Beckman-Coulter Allegra 6R with a GH-

3.8 rotor at 3500 rpm for 30 min at 4 °C. The supernatant was decanted, and the pellet dissolved in 6 mL of 25% ACN in H₂O and lyophilized.

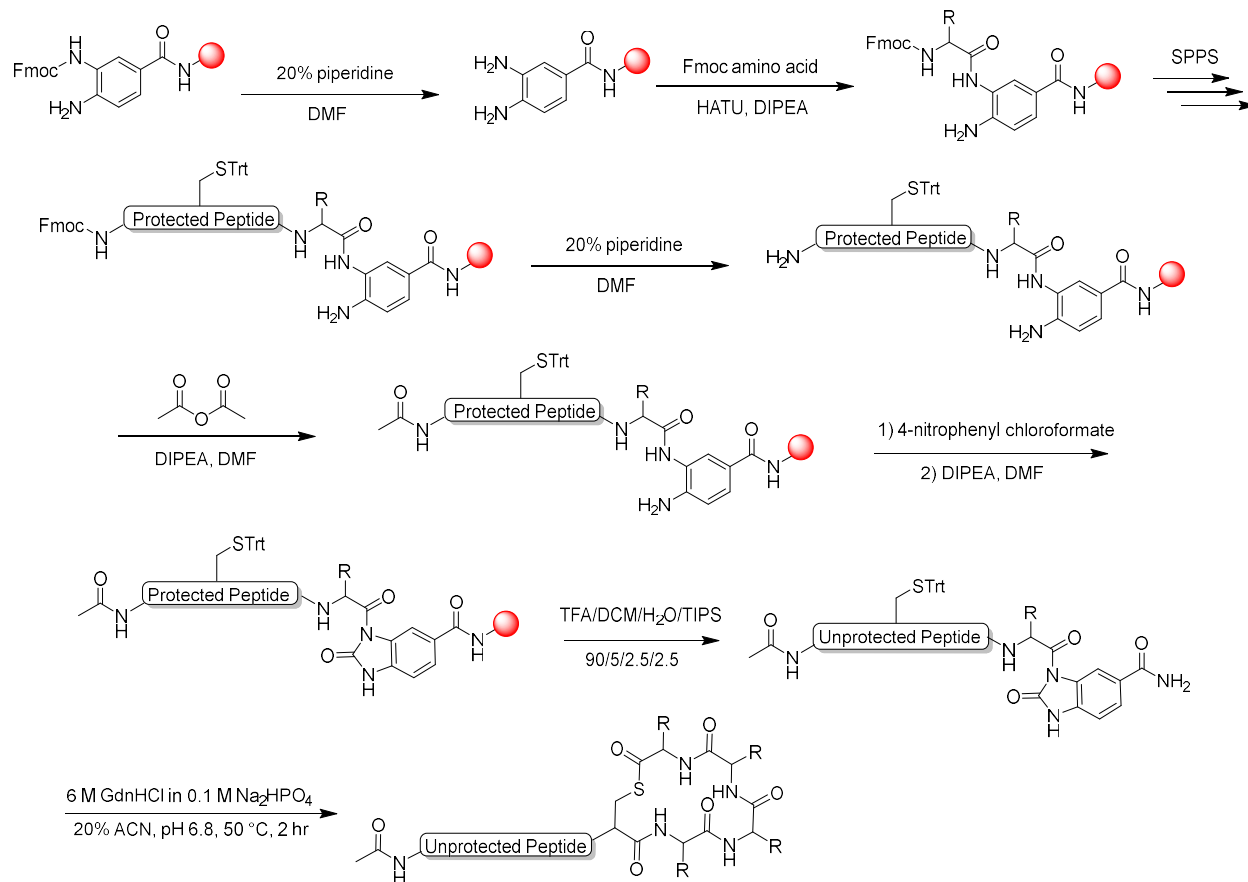
The crude, lyophilized peptide was reconstituted in 25% ACN in H₂O, passed through a 0.22 μm filter, and purified by RP-HPLC. Fractions were collected and analyzed using MALDI-MS, and those with peaks matching that of the linear peptides were kept and lyophilized. Purified linear peptides were cyclized in 3 mL of cyclization buffer (20% ACN, 80% 6 M guanidinium chloride in 0.1 M Na₂PO₄, pH 6.8) for 2 hr at 50 °C with shaking. Following cyclization, solutions were passed through 0.22 μm filter, diluted with 1 mL of H₂O, and purified by RP-HPLC. Fractions were again analyzed with MALDI-MS to identify those with cyclized peptide, and those fractions were submitted for high-resolution mass measurement and analytical RP-HPLC to assess final purity.



Scheme 2.S1 Solid-phase synthesis of standard thioester AIP analogs.

Acetylated AIP analog peptide synthesis

Synthesis of AIP analogs with an acetylated N-terminus followed the same protocol for standard AIP synthesis as described above with the exception of the final amino acid coupling (Scheme S2). Instead of a N^α -Boc-protected amino acid, a standard N^α -Fmoc-protected amino acid was used. After this coupling, the resin was washed with DMF (2 mL \times 3), and the Fmoc group was deprotected using 20% piperidine (2 mL \times 3 for 5, 5, and 10 min). Next, acetic anhydride (10 eq.) and DIPEA (7 eq.) were dissolved in 2 mL of DMF and added to the resin to shake for 15 min. The resin was then washed with DMF (2 mL \times 3) and DCM (2 mL \times 3). After this point, the synthesis followed the protocol for standard AIP analogs beginning at the addition of 4-nitrophenylchloroformate.



Scheme 2.S2 Solid-phase synthesis of acetylated AIP analogs.

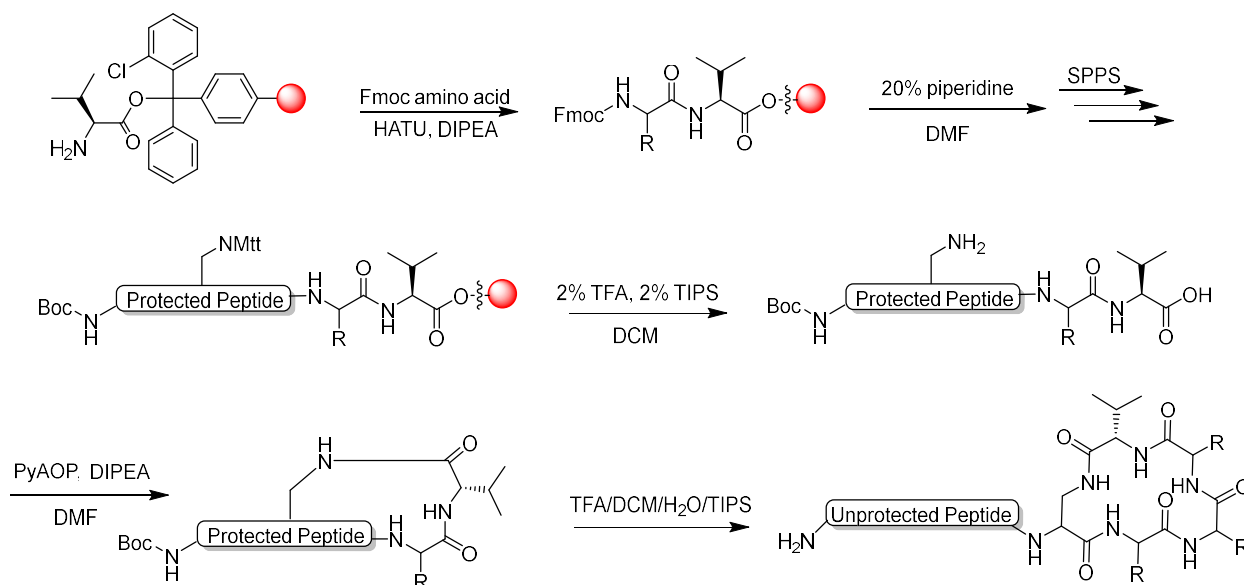
AIP amide peptide synthesis

AIP analogs where the thioester bond was replaced with an amide linkage were synthesized on pre-loaded L-valine 2-chlorotrityl resin (0.74 mmol/g) using standard Fmoc/tBu procedures and adapted from previous reports (Scheme S3).⁵⁹ Briefly, approximately 50 mg of resin (0.037 mmol, 1 eq.) was swelled in DCM for 40 min in a reaction vessel. Resin was washed with DMF (2 mL ×3), and then the next amino acid was prepared as above for standard AIP synthesis. The rest of linear peptide synthesis followed the protocol for standard AIP synthesis, with the exception of using longer coupling times (all amino acids coupled for at least 1 hr) and using *N*^α-Fmoc-*N*^β-4-Mtt-diaminopropionic acid (Dap) or its D-amino acid

equivalent for amide linkages instead of the usual N^α -Fmoc-S-Trt-cysteine for the appropriate linkage amino acid. After the final N^α -Boc-protected amino acid was coupled, the resin was washed with DMF (2 mL \times 3) and then DCM (2 mL \times 3).

Next, to facilitate partial deprotection and cleavage from the resin, 2 mL of 2% TFA/2% TIPS in DCM was added to the resin and shaken for 2 min, the solution was collected in a 50 mL round-bottom flask, and the process was repeated four more times. The resin was washed with DCM (2 mL \times 3), and the solution collected in the same round-bottom flask. The solvent was removed using a rotary evaporator, leaving an oil. The oil was dissolved in 3 mL of ACN, then diluted with 3 mL of H₂O and lyophilized. To cyclize the partially deprotected peptide, PyAOP (2 eq.) and DIPEA (4 eq.) were dissolved in 5 mL of DCM and added to the lyophilized peptide and stirred for 24 hr at RT. The solvent was removed using rotary evaporation, leaving an oil.

To fully deprotect the peptide, 5 mL of a 90/5/2.5/2.5 TFA/DCM/H₂O/TIPS solution was added to the round-bottom flask and stirred for 2 hr. The solution was then transferred to a 50 mL falcon tube, mixed with 40 mL of cold Et₂O, and chilled in a -20 °C freezer overnight to precipitate the peptide. The crude peptide was centrifuged following the standard AIP synthesis protocol, the solvent decanted, and the pellet dissolved in 50% ACN in H₂O and lyophilized. The lyophilized peptide was reconstituted in 25% ACN in H₂O and purified by RP-HPLC. MALDI-MS confirmed which fractions contained desired peptides, and these fractions were submitted for high-resolution mass measurement and analytical RP-HPLC to confirm purity.



Scheme 2.S3 AIP amide synthesis.

Inducing *S*→*N* conversion of 5-mer thioester

Approximately 200 μL of a 1 mM stock solution of 5-mer thioester in DMSO was lyophilized and resuspended in 1 mL of 50% ACN in water, diluted with 1 mL of 50% ACN in PBS (pH 7.4), and set to stir vigorously at room temperature. At set time points, 60 μL aliquots were diluted with 200 μL pure water and analyzed using analytical RP-HPLC. The reaction appeared almost complete after 3 hours, and at 4 hours the solution was purified on semi-preparative RP-HPLC. MALDI-MS confirmed which fractions contained desired peptides, and these fractions were submitted for high-resolution mass measurement and analytical RP-HPLC to confirm purity.

2.5.2 LC-MS/MS analysis of bacterial supernatant

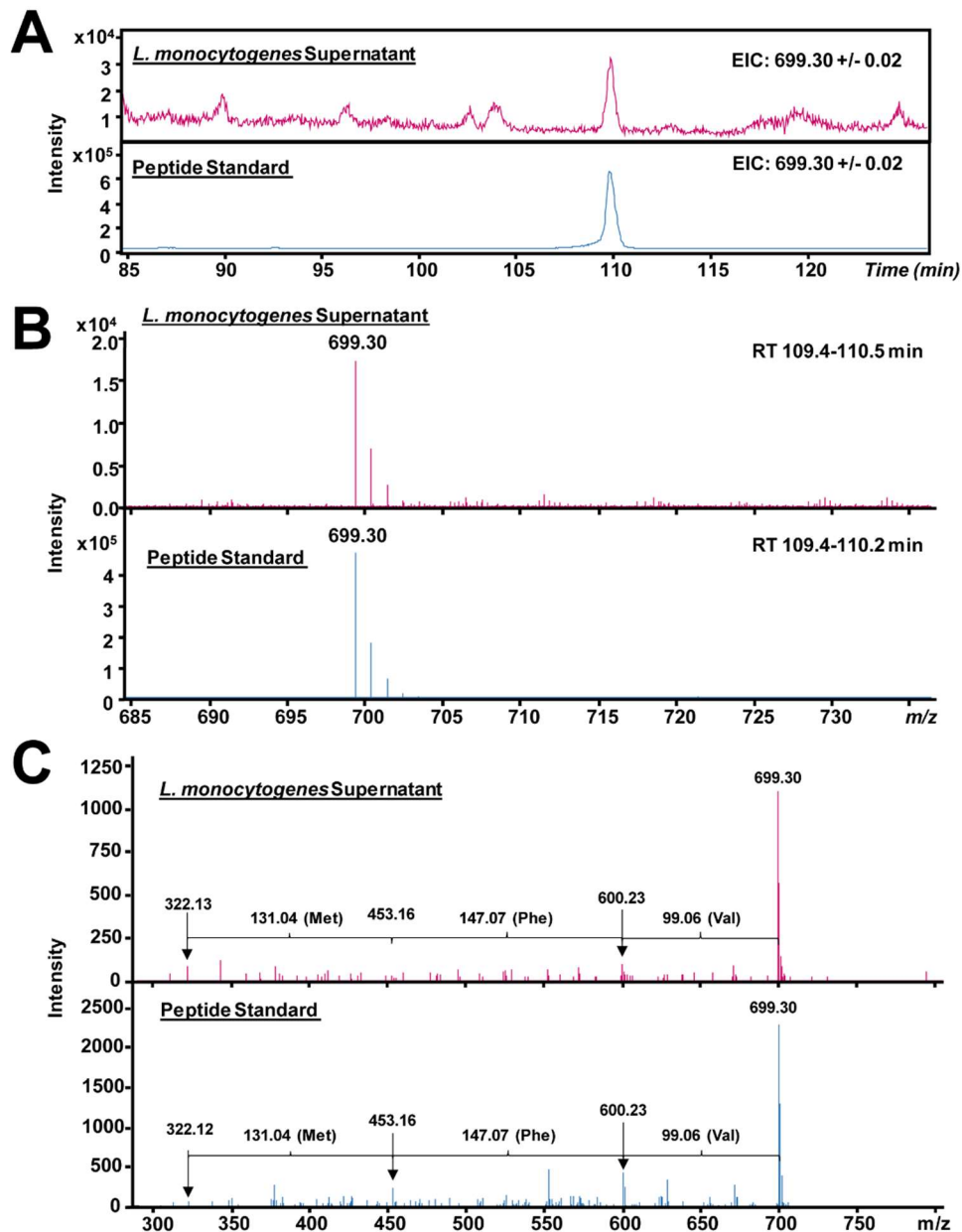


Figure 2.S1 LC-MS/MS results matches a native AIP in *L. monocytogenes* supernatant to hexapeptide standard. (A) Extracted ion chromatograms (EICs) for 699.30 +/- 0.2 m/z for the wild-type (WT) supernatant (magenta) and peptide standard mixture (blue). (B) Mass spectra averaged over the peak retention time (RT) for WT and peptide standard mixture. MS/MS results showing fragmentation of the native AIP in *L. monocytogenes* supernatant matches with that of the 6-mer standard. MS/MS spectra for the 6-mer peptide standard (blue, energy 23 eV, RT 110.4 min) and the native AIP from *L. monocytogenes* supernatant (magenta, energy 20 eV, RT 110.0 min).

2.5.3 The S→N acyl shift of the 5-mer thioester

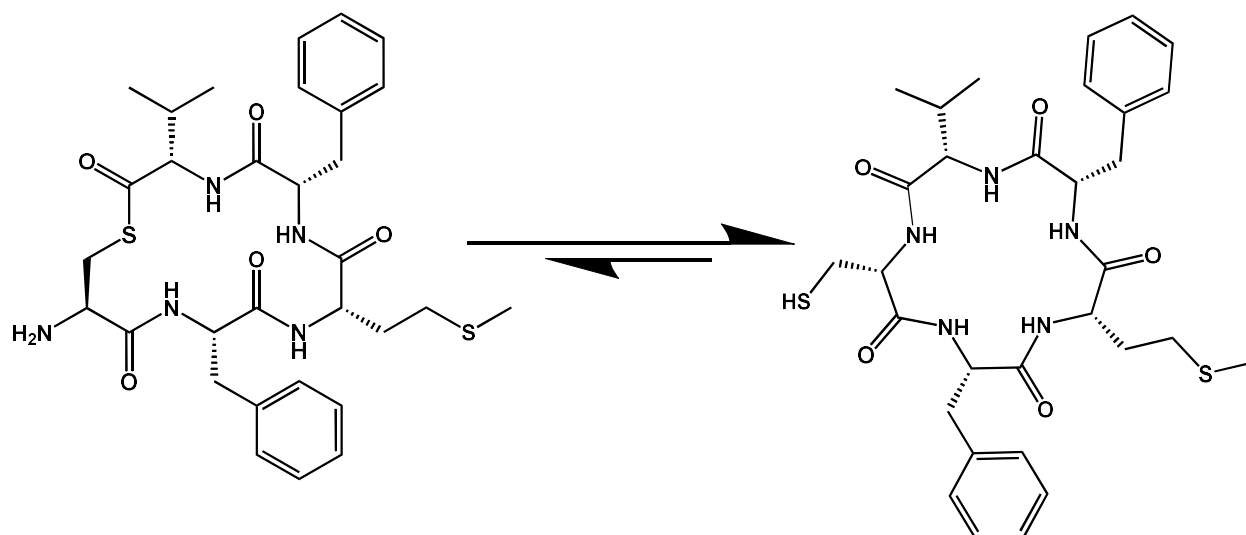
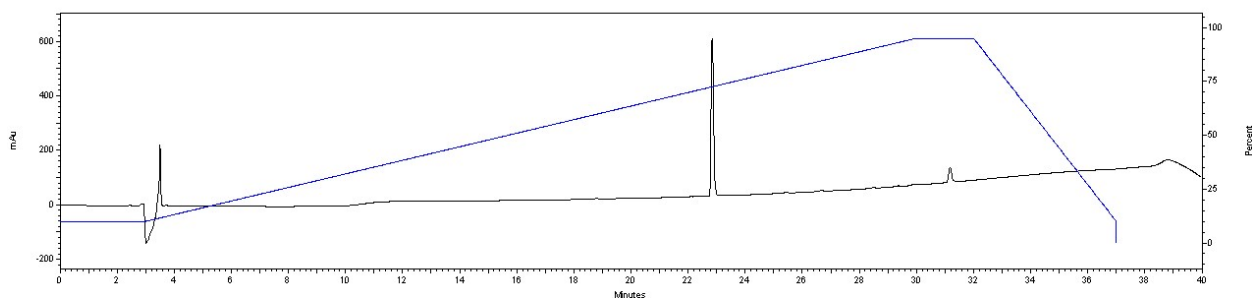


Figure 2.S2 The proposed S→N shift in the 5-mer thioester to produce a homodetic peptide. The free N-terminus in the uncapped *L. monocytogenes* 5-mer peptide likely undergoes an S→N acyl shift in aqueous conditions at physiological pH.

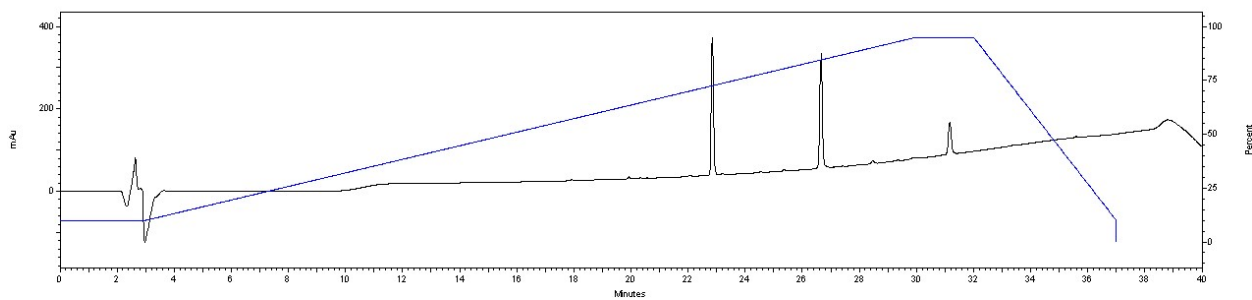
Monitoring $S \rightarrow N$ reaction progress by analytical HPLC

The 5-mer thioester has a retention time 22.81 min, and within one hour of stirring at pH 7 in room temperature, nearly half had converted into the $S \rightarrow N$ product with a retention time of 26.71 min. By hour 3, nearly all of the 5-mer thioester had converted, and the reaction was stopped after 4 hours to be purified on semi-preparative HPLC.

t=0 hr



t=1 hr



t=3 hr

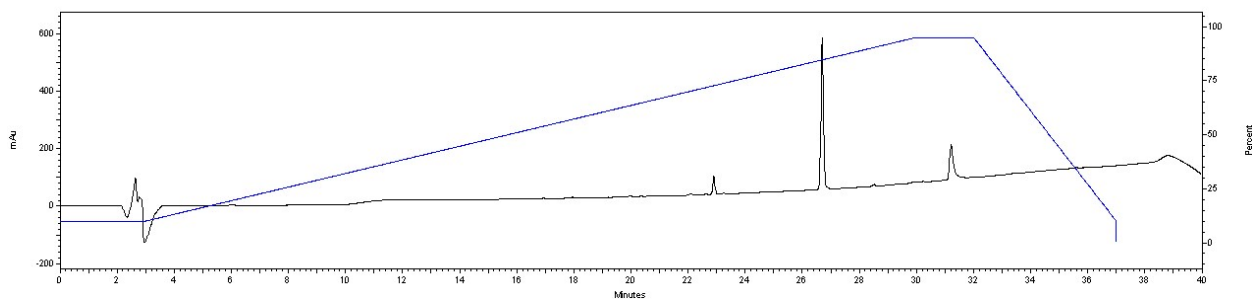


Table 2.S1 Agonism activity of native and proposed AIPs and AIP analogs of other bacterial species in the $\Delta agrD$ *L. monocytogenes agr* reporter strain. Lm = *L. monocytogenes*; Sa = *Staphylococcus aureus*; Se = *S. epidermidis*. See text for details of assay and strain.

Compound	Sequence	EC ₅₀ (nM)	EC ₅₀ 95 CI (nM)	Max Activation (%)
Lm AIP	A-(C-F-M-F-V)	29.6	20.0 to 40.0	114
Lm AIP F3S	A-(C-S-M-F-V)	---- ^a	---- ^a	16.1
Lm AIP V6A	A-(C-F-M-F-A)	241	192 to 307	69.0
Sa AIP-I	Y-S-T-(C-D-F-I-M)	---- ^b	---- ^b	12.2
Sa AIP-II	G-V-N-A-(C-S-S-L-F)	---- ^b	---- ^b	12.0
Sa AIP-III	I-N-(C-D-F-L-L)	---- ^b	---- ^b	11.3
Sa AIP-IV	Y-S-T-(C-Y-F-I-M)	---- ^b	---- ^b	9.81
Sa AIP-III D4A	I-N-(C-A-F-L-L)	---- ^b	---- ^b	12.3
Se AIP-I	D-S-V-(C-A-S-Y-F)	---- ^b	---- ^b	8.65
Se AIP-II	N-A-S-K-Y-N-P-(C-S-N-Y-L)	---- ^b	---- ^b	8.45
Se AIP-III	N-A-A-K-Y-N-P-(C-A-S-Y-L)	---- ^b	---- ^b	8.73
Se AIP-I D1AS6A	A-S-V-(C-A-A-Y-F)	---- ^b	---- ^b	12.4
Se AIP-I D1AV3AS6A	A-S-A-(C-A-A-Y-F)	---- ^b	---- ^b	12.1
<i>L. grandensis</i> tr AIP	Ac-(C-V-G-F-V)	---- ^b	---- ^b	10.1
<i>L. grayi</i> AIP	A-(C-S-M-F-A)	---- ^a	---- ^a	10.7
<i>L. kieliensis</i> AIP	S-(C-V-G-L-S)	---- ^b	---- ^b	10.4
<i>L. newyorkensis</i> AIP	S-(C-F-L-I-F)	---- ^b	---- ^b	23.6
<i>L. weihenstephanensis</i> AIP	S-(C-V-L-H-L)	---- ^b	---- ^b	11.2

^aCurve not converged. ^bFrom single point data only, no potency data available.

Table 2.S2 Antagonism activity table of native and proposed AIPs and AIP analogs of other species in the wild-type *L. monocytogenes agr* reporter strain.

Lm = *L. monocytogenes*; Sa = *Staphylococcus aureus*; Se = *S. epidermidis*. See text for details of assay and strain.

Compound	Sequence	IC ₅₀ (nM)	IC ₅₀ 95 CI (nM)	Max Inhibition (%)
Lm AIP	A-(C-F-M-F-V)	---- ^a	---- ^a	2.66
Lm AIP F3S	A-(C-S-M-F-V)	---- ^a	---- ^a	16.3
Lm AIP V6A	A-(C-F-M-F-A)	---- ^a	---- ^a	15.0
Sa AIP-I	Y-S-T-(C-D-F-I-M)	---- ^b	---- ^b	1.29
Sa AIP-II	G-V-N-A-(C-S-S-L-F)	---- ^b	---- ^b	0
Sa AIP-III	I-N-(C-D-F-L-L)	---- ^b	---- ^b	0.64
Sa AIP-IV	Y-S-T-(C-Y-F-I-M)	---- ^b	---- ^b	8.56
Sa AIP-III D4A	I-N-(C-A-F-L-L)	---- ^b	---- ^b	5.87
Se AIP-I	D-S-V-(C-A-S-Y-F)	---- ^b	---- ^b	0
Se AIP-II	N-A-S-K-Y-N-P-(C-S-N-Y-L)	---- ^b	---- ^b	0
Se AIP-III	N-A-A-K-Y-N-P-(C-A-S-Y-L)	---- ^b	---- ^b	0
Se AIP-I D1AS6A	A-S-V-(C-A-A-Y-F)	---- ^b	---- ^b	0
Se AIP-I D1AV3AS6A	A-S-A-(C-A-A-Y-F)	---- ^b	---- ^b	0.06
<i>L. grandensis</i> tr AIP	Ac-(C-V-G-F-V)	---- ^b	---- ^b	0
<i>L. grayi</i> AIP	A-(C-S-M-F-A)	---- ^a	---- ^a	0.42
<i>L. kieliensis</i> AIP	S-(C-V-G-L-S)	---- ^b	---- ^b	0
<i>L. newyorkensis</i> AIP	S-(C-F-L-I-F)	---- ^b	---- ^b	0.96
<i>L. weihenstephanensis</i> AIP	S-(C-V-L-H-L)	---- ^b	---- ^b	0

^aCurve not converged. ^bFrom single point data only, no potency data available.

2.5.5 Dose response activity data of *L. monocytogenes* AIP analogs

Table 2.S3 Dose response agonism activity table of *L. monocytogenes* AIP analogs with varying exocyclic tail length in the $\Delta agrD$ *L. monocytogenes agr* reporter strain. See text for details of assay and strain.

Compound	Sequence	EC ₅₀ (nM)	EC ₅₀ 95 CI (nM)	Max Activation (%)
AIP	A-(C-F-M-F-V)	29.7	20.0 to 40.0	114
5-mer	(C-F-M-F-V)	107 ^a	92.1 to 125	105
S→N 5-mer	(C-F-M-F-V)	1820 ^a	1250 to 3440	89.7
Ac-5-mer	Ac-(C-F-M-F-V)	46.3	37.1 to 56.8	75.3
7-mer	K-A-(C-F-M-F-V)	61.7	53.2 to 71.2	64.6
8-mer	S-K-A-(C-F-M-F-V)	68.6	57.2 to 81.8	71.5
9-mer	M-S-K-A-(C-F-M-F-V)	23.5	19.1 to 28.2	93.6
10-mer	S-M-S-K-A-(C-F-M-F-V)	21.5	17.7 to 25.4	110
11-mer	S-S-M-S-K-A-(C-F-M-F-V)	14.3	9.05 to 19.4	111
12-mer	D-S-S-M-S-K-A-(C-F-M-F-V)	43.4	31.9 to 56.3	116
13-mer	A-D-S-S-M-S-K-A-(C-F-M-F-V)	29.0	21.6 to 36.9	108
14-mer	V-A-D-S-S-M-S-K-A-(C-F-M-F-V)	39.9	32.5 to 47.9	105
15-mer	K-V-A-D-S-S-M-S-K-A-(C-F-M-F-V)	22.2	16.4 to 28.4	122

^aCurve not converged

Table 2.S4 Dose response antagonism activity table of *L. monocytogenes* AIP analogs with varying exocyclic tail length in the wild-type *L. monocytogenes agr* reporter strain. See text for details of assay and strain.

Compound	Sequence	IC ₅₀ (nM)	IC ₅₀ 95 CI (nM)	Max Inhibition (%)
AIP	A-(C-F-M-F-V)	---- ^a	---- ^a	2.66
5-mer	(C-F-M-F-V)	---- ^a	---- ^a	1.15
S→N 5-mer	(C-F-M-F-V)	---- ^a	---- ^a	0.81
Ac-5-mer	Ac-(C-F-M-F-V)	---- ^a	---- ^a	6.39
7-mer	K-A-(C-F-M-F-V)	866	641 to 1260	38.3
8-mer	S-K-A-(C-F-M-F-V)	842	554 to 1430	29.4
9-mer	M-S-K-A-(C-F-M-F-V)	416	192 to 1390	8.89
10-mer	S-M-S-K-A-(C-F-M-F-V)	---- ^a	---- ^a	0
11-mer	S-S-M-S-K-A-(C-F-M-F-V)	---- ^a	---- ^a	3.90
12-mer	D-S-S-M-S-K-A-(C-F-M-F-V)	---- ^a	---- ^a	0.26
13-mer	A-D-S-S-M-S-K-A-(C-F-M-F-V)	---- ^a	---- ^a	0
14-mer	V-A-D-S-S-M-S-K-A-(C-F-M-F-V)	---- ^a	---- ^a	0
15-mer	K-V-A-D-S-S-M-S-K-A-(C-F-M-F-V)	---- ^a	---- ^a	0.23

^aCurve not converged

Table 2.S5 Dose response agonism activity table of alanine and D-amino acid scan analogs in the $\Delta agrD$ *L. monocytogenes agr* reporter strain. See text for details of assay and strain.

Compound	Sequence	EC ₅₀ (nM)	EC ₅₀ 95 CI (nM)	Max Activation (%)
AIP F3A	A-(C-A-M-F-V)	---- ^a	---- ^a	9.72
AIP M4A	A-(C-F-A-F-V)	1980	1480 to 3060	53.5
AIP F5A	A-(C-F-M-A-V)	---- ^a	---- ^a	6.37
AIP V6A	A-(C-F-M-F-A)	241	192 to 307	69.0
AIP A1dA	dA-(C-F-M-F-V)	96.9	74.3 to 125	58.8
AIP C2dC	A-(dC-F-M-F-V)	106	89.7 to 124	41.0
AIP F3dF	A-(C-dF-M-F-V)	---- ^a	---- ^a	6.63
AIP M4dM	A-(C-F-dM-F-V)	10.2	8.99 to 11.6	111
AIP F5dF	A-(C-F-M-dF-V)	2180	1770 to 2910	72.3
AIP V6dV	A-(C-F-M-F-dV)	883	784 to 1010	72.9

^aCurve not converged

Table 2.S6 Dose response antagonism activity table of alanine and D-amino acid scan analogs in the wild-type *L. monocytogenes agr* reporter strain. See text for details of assay and strain.

Compound	Sequence	IC ₅₀ (nM)	IC ₅₀ 95 CI (nM)	Max Inhibition (%)
AIP F3A	A-(C-A-M-F-V)	---- ^a	---- ^a	3.65
AIP M4A	A-(C-F-A-F-V)	---- ^a	---- ^a	7.85
AIP F5A	A-(C-F-M-A-V)	---- ^a	---- ^a	0
AIP V6A	A-(C-F-M-F-A)	---- ^a	---- ^a	15.0
AIP A1dA	dA-(C-F-M-F-V)	---- ^a	---- ^a	15.2
AIP C2dC	A-(dC-F-M-F-V)	3970	1910 to 25800	48.4
AIP F3dF	A-(C-dF-M-F-V)	---- ^a	---- ^a	14.7
AIP M4dM	A-(C-F-dM-F-V)	---- ^a	---- ^a	3.99
AIP F5dF	A-(C-F-M-dF-V)	---- ^a	---- ^a	2.71
AIP V6dV	A-(C-F-M-F-dV)	---- ^a	---- ^a	0

^aCurve not converged

Table 2.S7 Dose response agonism activity table of first-generation analogs in the $\Delta agrD$ *L. monocytogenes agr* reporter strain. See text for details of assay and strain.

Compound	Sequence	EC ₅₀ (nM)	EC ₅₀ 95 CI (nM)	Max Activation (%)
AIP A1P	P-(C-F-M-F-V)	29.0	20.6 to 38.1	76.8
AIP A1T	T-(C-F-M-F-V)	35.2	28.4 to 42.4	88.1
AIP A1K	K-(C-F-M-F-V)	22.9	19.8 to 26.1	80.0
AIP A1V	V-(C-F-M-F-V)	7.67	5.21 to 10.7	109
AIP C2Dap	A-(Dap-F-M-F-V)	342	312 to 376	92.9
AIP C2dDap	A-(dDap-F-M-F-V)	---- ^a	---- ^a	14.3
AIP F3Y	A-(C-Y-M-F-V)	518	383 to 766	47.4
AIP F3L	A-(C-L-M-F-V)	693	505 to 1070	37.6
AIP F3H	A-(C-H-M-F-V)	---- ^a	---- ^a	12.4
AIP F3W	A-(C-W-M-F-V)	414	357 to 487	60.6
AIP M4dA	A-(C-F-dA-F-V)	455	383 to 556	82.0
AIP F5Y	A-(C-F-M-Y-V)	5620	3260 to 19200	44.4
AIP F5L	A-(C-F-M-L-V)	2060	1630 to 2820	64.8
AIP F5H	A-(C-F-M-H-V)	---- ^a	---- ^a	7.13
AIP F5W	A-(C-F-M-W-V)	1130	810 to 1860	85.8

^aCurve not converged

Table 2.S8 Dose response antagonism activity table of first-generation analogs in the wild-type *L. monocytogenes agr* reporter strain. See text for details of assay and strain.

Compound	Sequence	IC ₅₀ (nM)	IC ₅₀ 95 CI (nM)	Max Inhibition (%)
AIP A1P	P-(C-F-M-F-V)	611	322 to 1740	23.7
AIP A1T	T-(C-F-M-F-V)	420	204 to 1020	11.7
AIP A1K	K-(C-F-M-F-V)	233	148 to 403	31.3
AIP A1V	V-(C-F-M-F-V)	---- ^a	---- ^a	1.63
AIP C2Dap	A-(Dap-F-M-F-V)	---- ^a	---- ^a	5.32
AIP C2dDap	A-(dDap-F-M-F-V)	---- ^a	---- ^a	19.3
AIP F3Y	A-(C-Y-M-F-V)	3460	1860 to 77700	33.4
AIP F3L	A-(C-L-M-F-V)	3600	2300 to 13600	33.4
AIP F3H	A-(C-H-M-F-V)	---- ^a	---- ^a	24.9
AIP F3W	A-(C-W-M-F-V)	2180	1190 to 15700	27.1
AIP M4dA	A-(C-F-dA-F-V)	---- ^a	---- ^a	9.54
AIP F5Y	A-(C-F-M-Y-V)	---- ^a	---- ^a	6.61
AIP F5L	A-(C-F-M-L-V)	---- ^a	---- ^a	8.97
AIP F5H	A-(C-F-M-H-V)	---- ^a	---- ^a	2.19
AIP F5W	A-(C-F-M-W-V)	---- ^a	---- ^a	8.43

^aCurve not converged

Table 2.S9 Dose response agonism activity table of second-generation analogs in the *ΔagrD L. monocytogenes agr* reporter strain. See text for details of assay and strain.

Compound	Sequence	EC ₅₀ (nM)	EC ₅₀ 95 CI (nM)	Max Activation (%)
AIP A1K/C2dC	K-(dC-F-M-F-V)	---- ^a	---- ^a	10.2
AIP A1K/M4dM	K-(C-F-dM-F-V)	4.18	3.18 to 5.36	74.1
AIP C2dC/M4dM	A-(dC-F-dM-F-V)	24.1	20.9 to 27.5	35.7
AIP A1K/C2dC/M4dM	K-(dC-F-dM-F-V)	---- ^a	---- ^a	8.10

^aCurve not converged

Table 2.S10 Dose response antagonism activity table of second-generation analogs and ambuic acid in the wild-type *L. monocytogenes agr* reporter strain.
See text for details of assay and strain.

Compound	Sequence	IC ₅₀ (nM)	IC ₅₀ 95 CI (nM)	Max Inhibition (%)
AIP A1K/C2dC	K-(DC-F-M-F-V)	4440	3050 to 165000	30.7
AIP A1K/M4dM	K-(C-F-DM-F-V)	---- ^a	---- ^a	20.2
AIP C2dC/M4dM	A-(DC-F-DM-F-V)	242	190 to 317	64.8
AIP A1K/C2dC/M4dM	K-(DC-F-DM-F-V)	1400	1150 to 1680	92.6
Ambuic acid	---- ^b	20300	14900 to 38100	91.2

^aCurve not converged, ^bNot a peptide.

2.5.6 Lead *L. monocytogenes* AIP analogs and native AIP assayed in *S. aureus agr-I* reporter assays

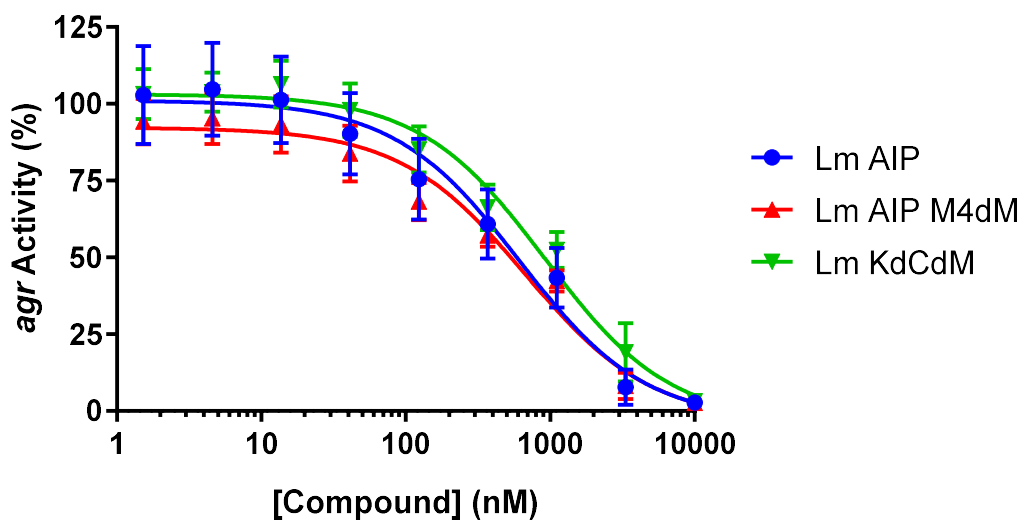


Figure 2.S4 Dose response antagonism activity of the *L. monocytogenes* native AIP, AIP M4dM, and KdCdM in the *S. aureus agr-I* fluorescent reporter strain AH1677.

Table 2.S11 Dose response antagonism activity table of *L. monocytogenes* AIP and analogs in the *S. aureus agr-I* fluorescent reporter strain AH1677. See text for details of assay and strain.

Compound	Sequence	IC ₅₀ (nM)	IC ₅₀ 95 CI (nM)	Max Inhibition (%)
AIP	A-(C-F-M-F-V)	615	413 to 912	97.2
AIP M4dM	A-(C-F-DM-F-V)	674	506 to 896	97.3
KdCdM	K-(DC-F-DM-F-V)	922	707 to 1200	96.8

2.5.7 Bacterial strains, plasmids, and primers

Table 2.S12 Bacterial strains and plasmids used in this study.

Strain/plasmid	Characteristics	Reference/source
<u>Strains</u>		
<i>L. monocytogenes</i> EGD-e	Wild-type <i>L. monocytogenes</i> lab strain	
<i>L. monocytogenes</i> EGD-e $\Delta agrD$	In-frame deletion of <i>agrD</i> in EGD-e background	Reference ¹⁰
<i>L. monocytogenes</i> EGD-e:pAM401-KW1	EGD-e with plasmid for <i>agr</i> -dependent GFP expression	This study
<i>L. monocytogenes</i> EGD-e $\Delta agrD$:pAM401-KW1	EGD-e $\Delta agrD$ with plasmid for <i>agr</i> -dependent GFP expression	This study
<i>E. coli</i> XL1-Blue	Cloning host strain	Agilent
<i>E. coli</i> S17	Plasmid conjugation strain	Reference ⁶⁸
<i>S. aureus</i> AH1677	USA300 LAC strain with plasmid for <i>agr</i> -dependent YFP expression	Reference ⁶¹
<u>Plasmids</u>		
pAM401	<i>E. coli</i> - <i>Listeria</i> shuttle vector, Cm ^r	Reference ⁶⁹
pAM401-KW1	Super folder <i>gfp</i> under control of <i>L. monocytogenes agr</i> promoter inserted into pAM401	This study

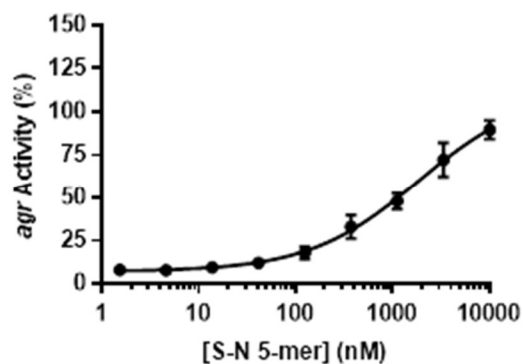
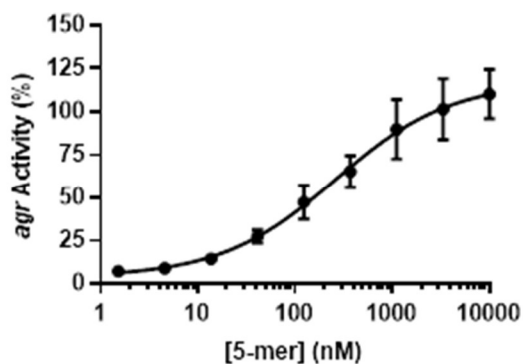
Table 2.S13 Primers used in this study.

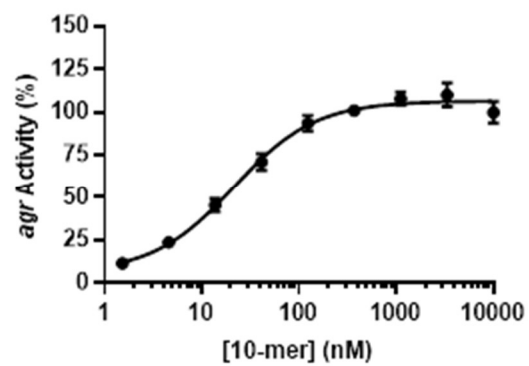
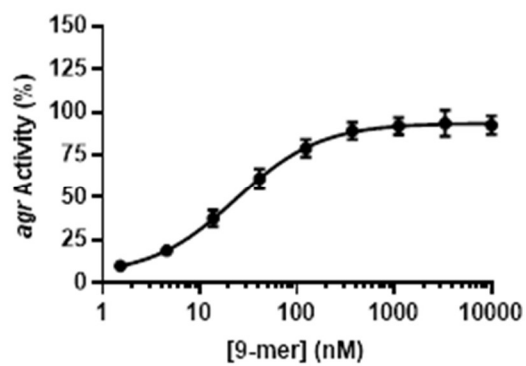
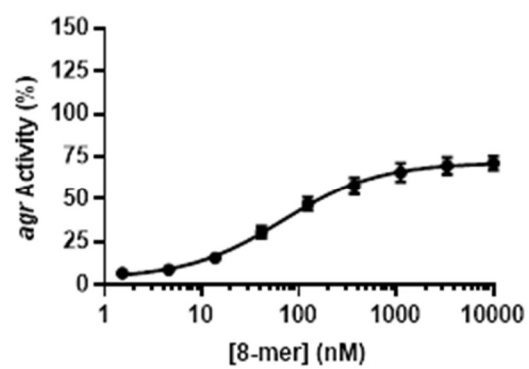
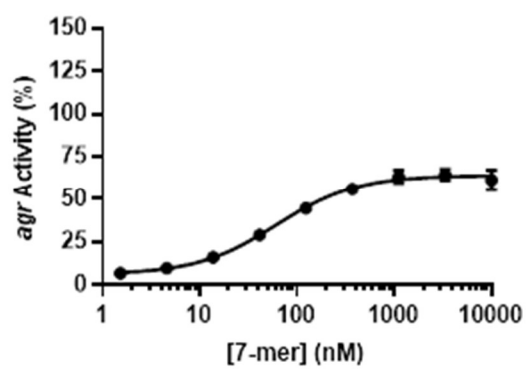
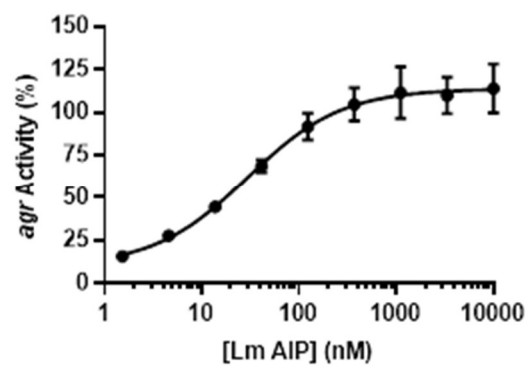
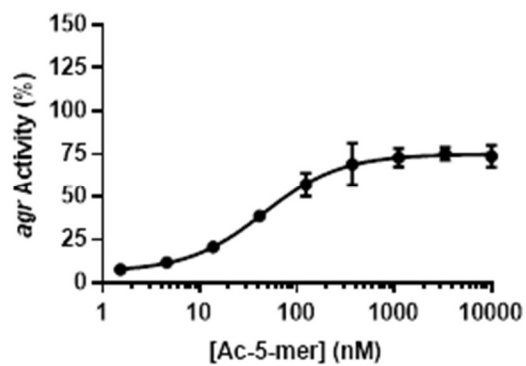
Primer	Sequence	Characteristics	Reference/source
DAP337	AAT CCA TGC CAA CCC GTT CCA TGT	Forward primer to verify pAM401 insert	This study
DAP338	ACG CAT CGT GGC CGG CAT C	Reverse primer to verify pAM401 insert	This study

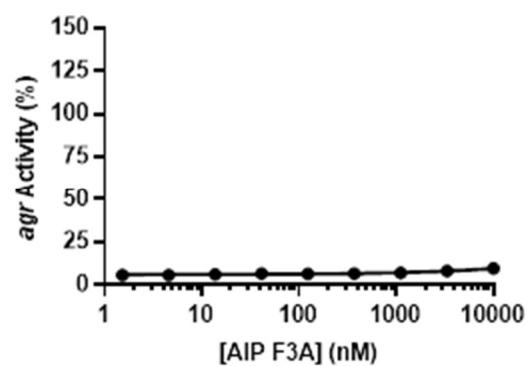
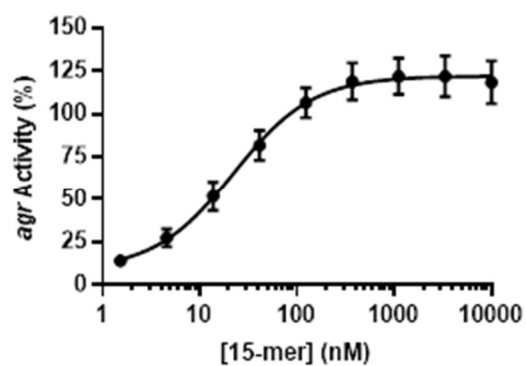
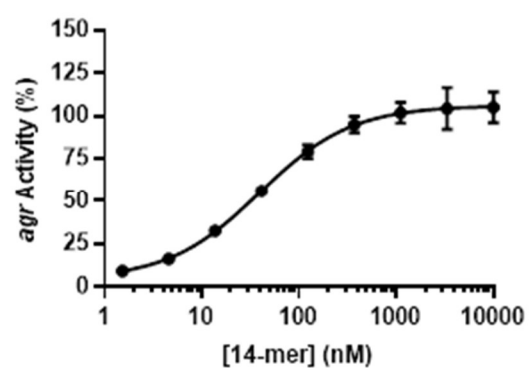
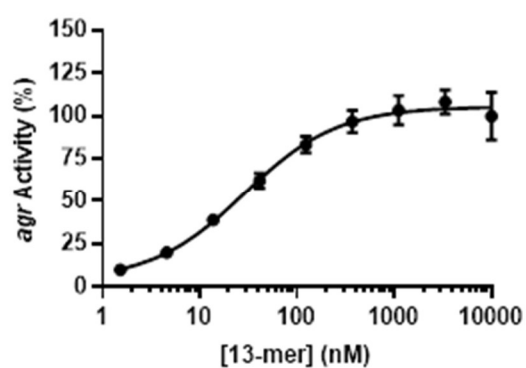
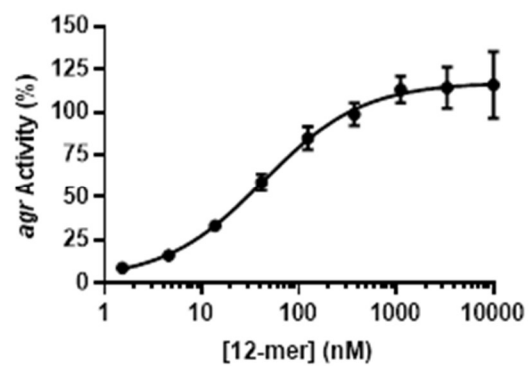
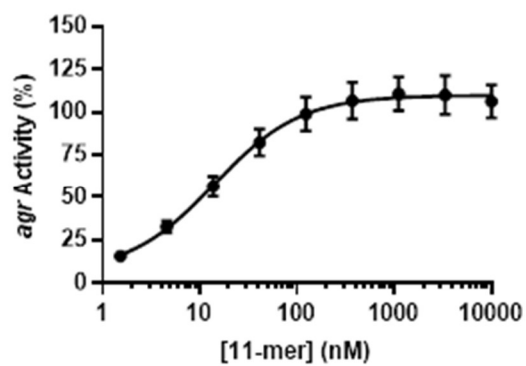
2.5.8 Dose response curves of peptides

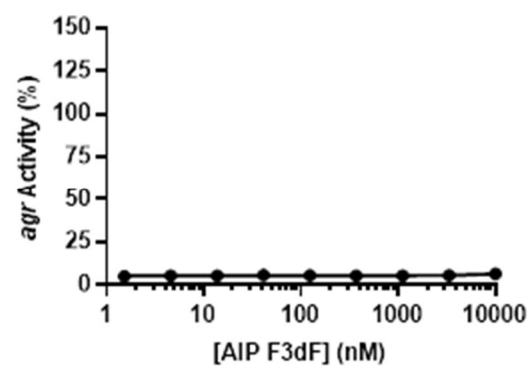
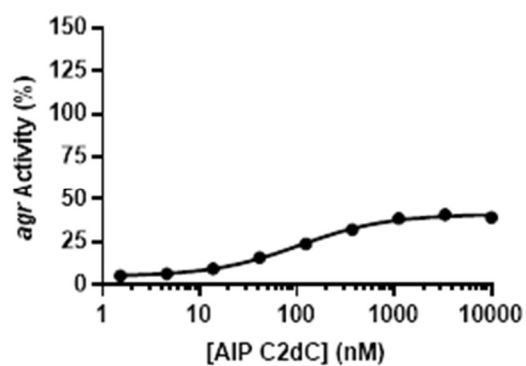
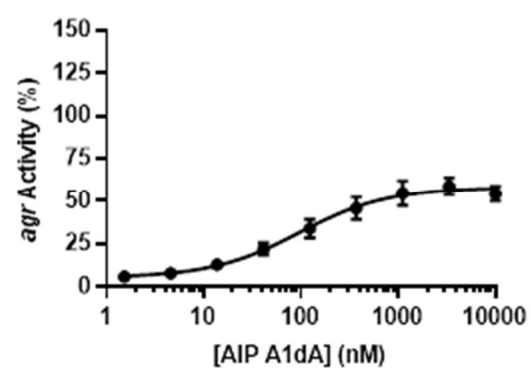
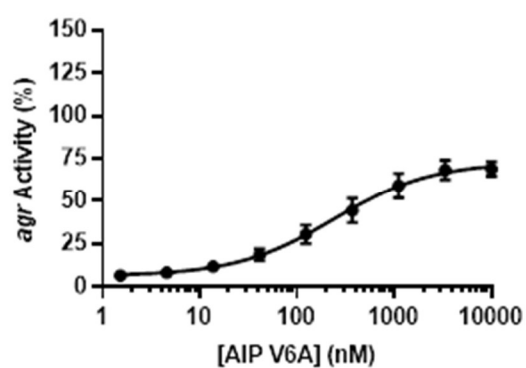
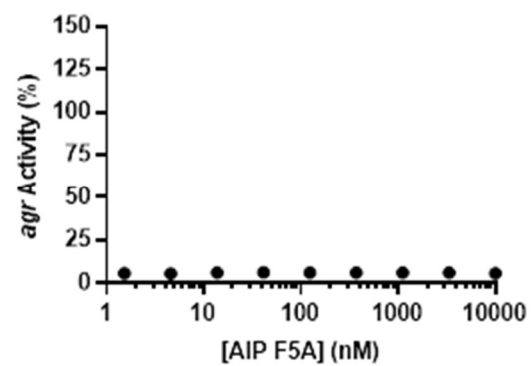
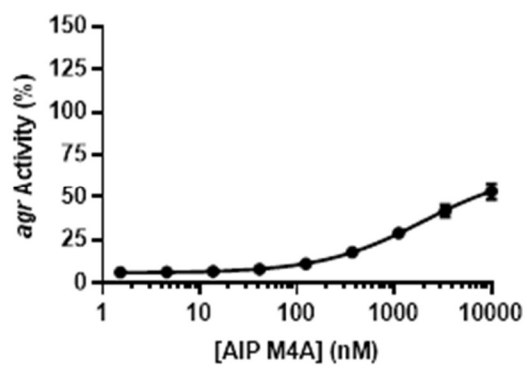
Agonism Assays Dose Response Curves

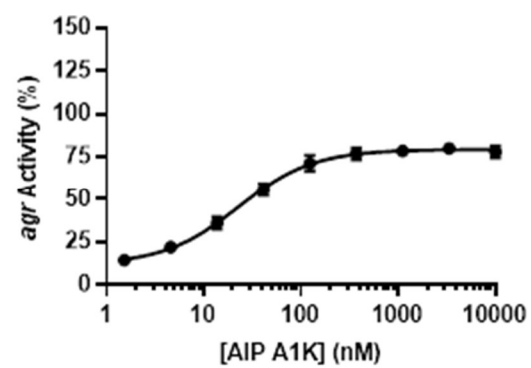
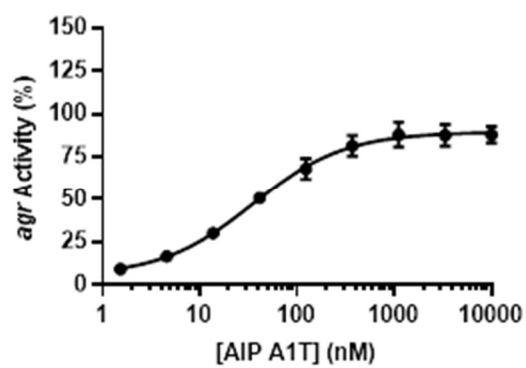
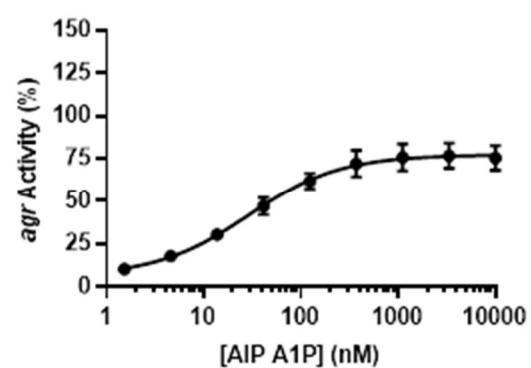
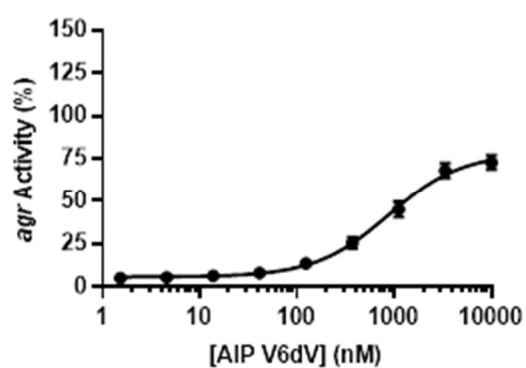
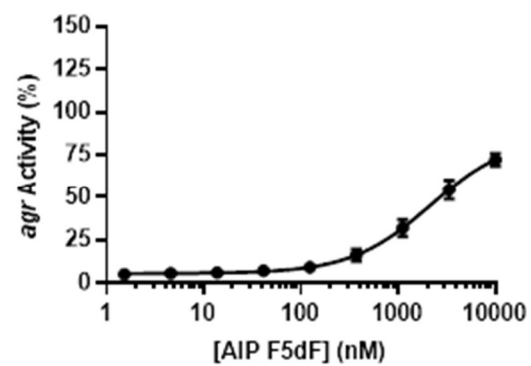
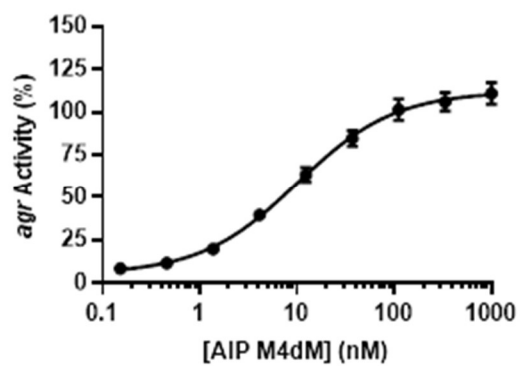
Compounds tested over range of concentrations in $\Delta agrD$ fluorescent reporter strain. Data points signify mean values for each concentration with error bars represent standard deviation of mean over three biological replicates, each with three technical replicates.

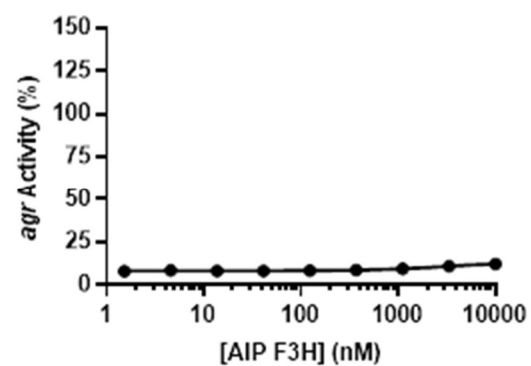
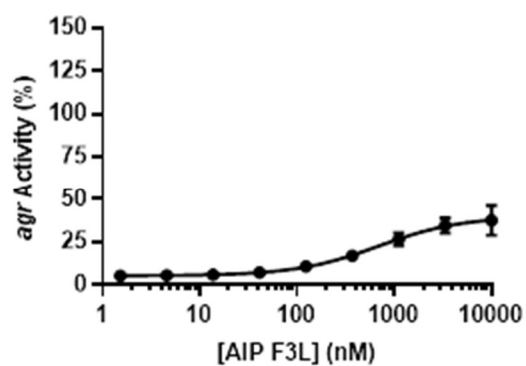
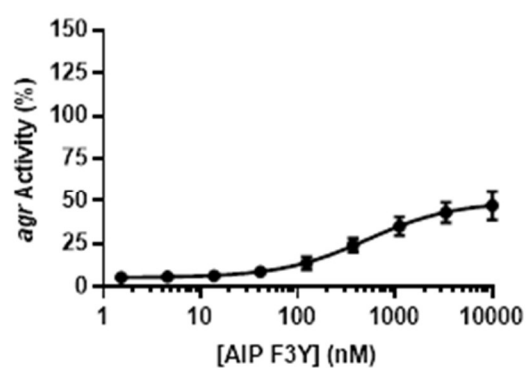
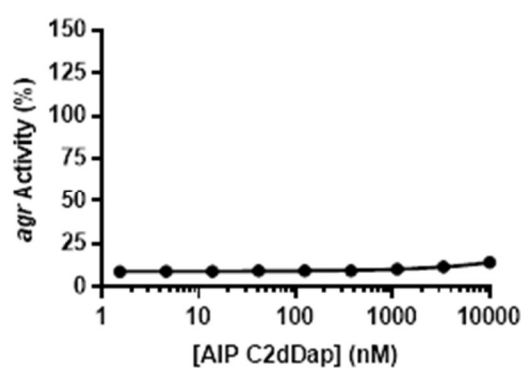
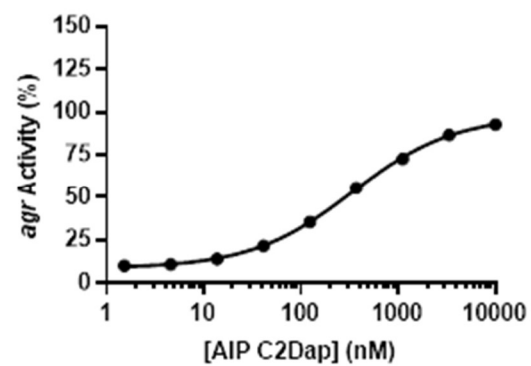
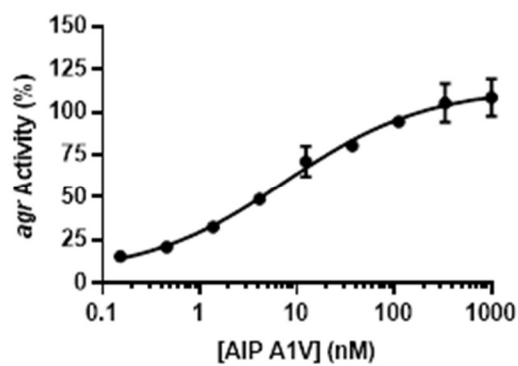


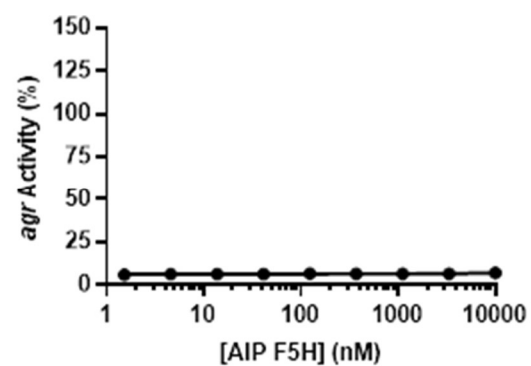
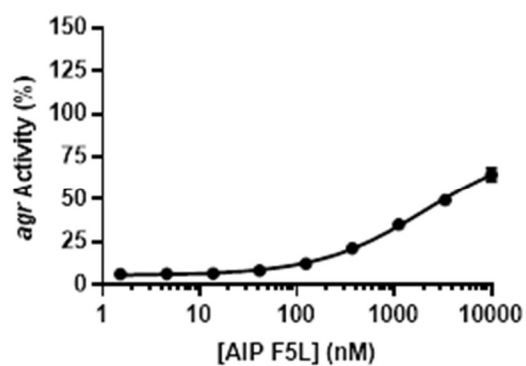
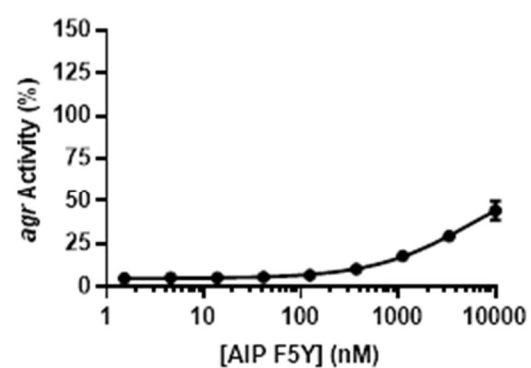
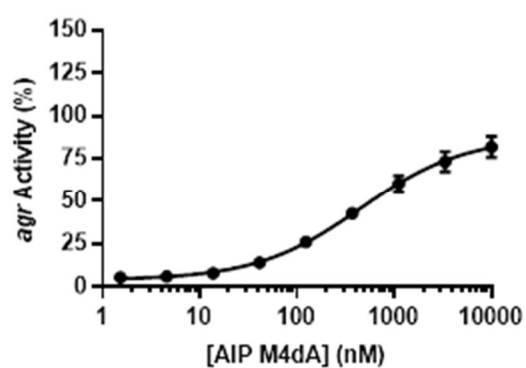
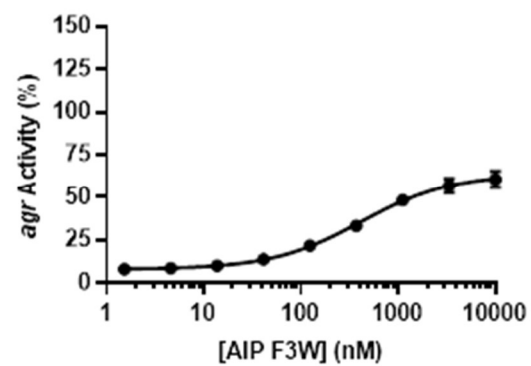
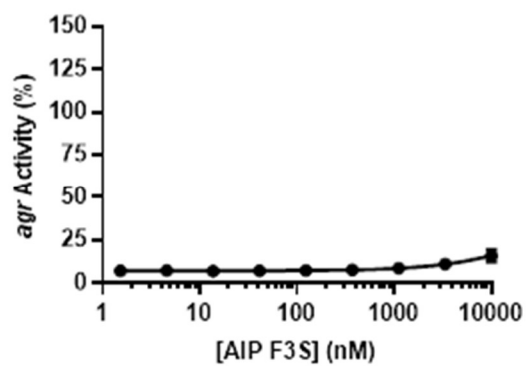


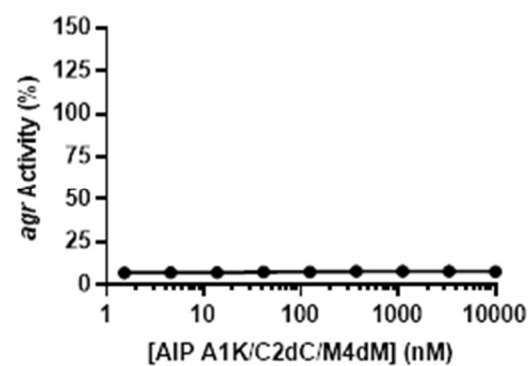
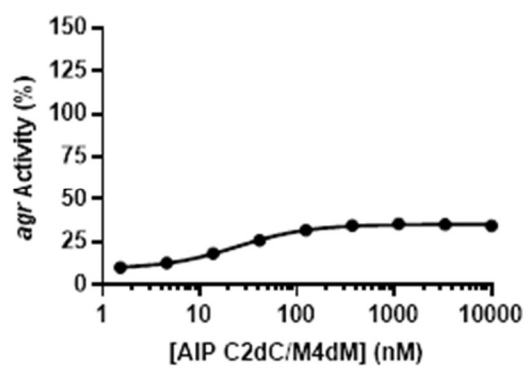
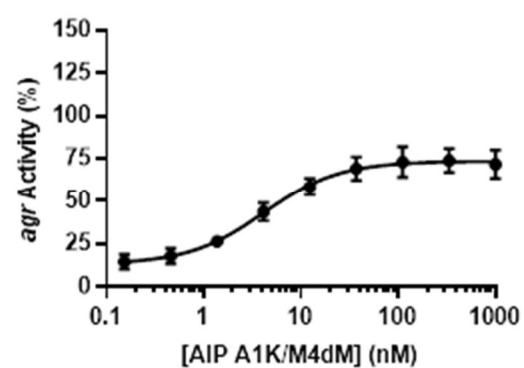
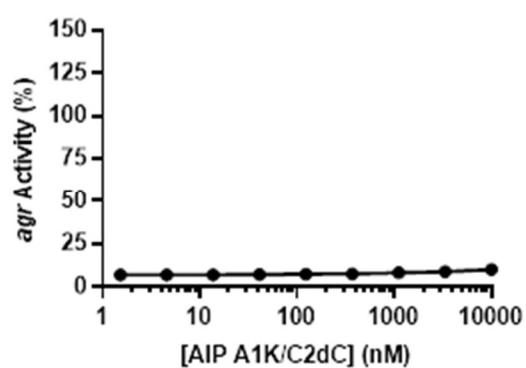
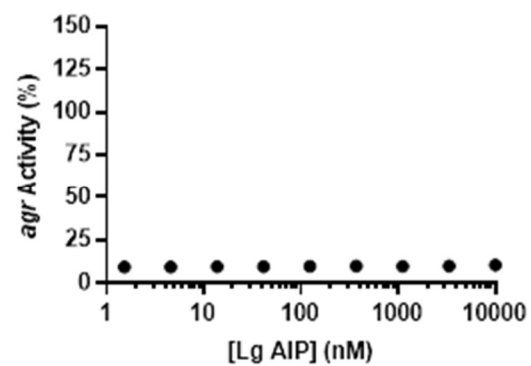
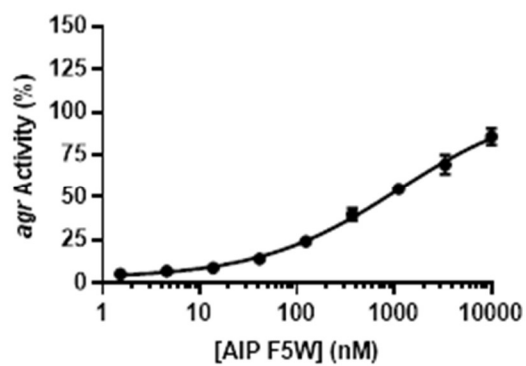


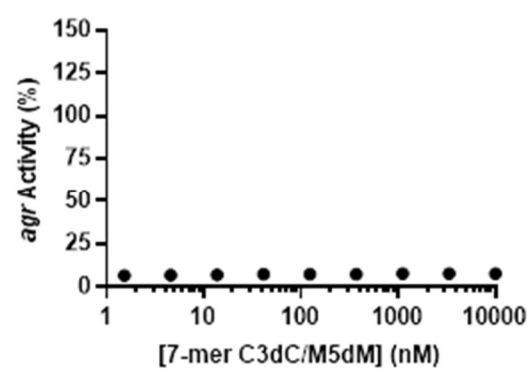
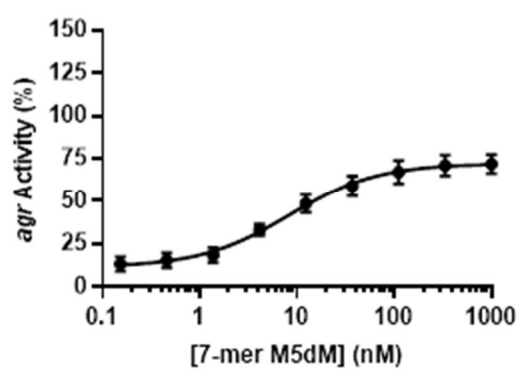
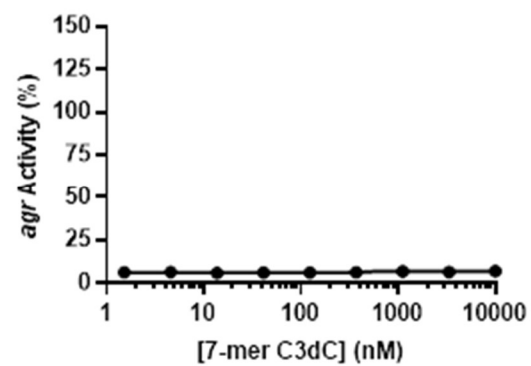
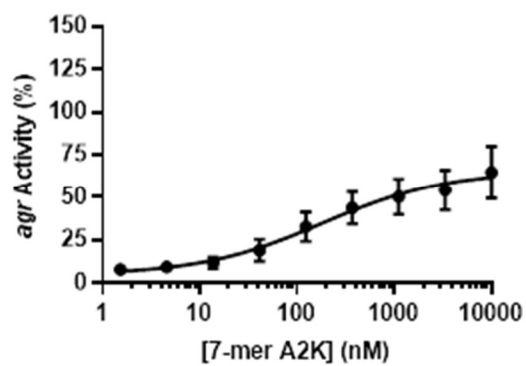






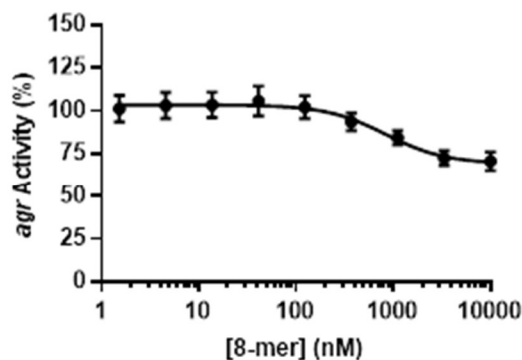
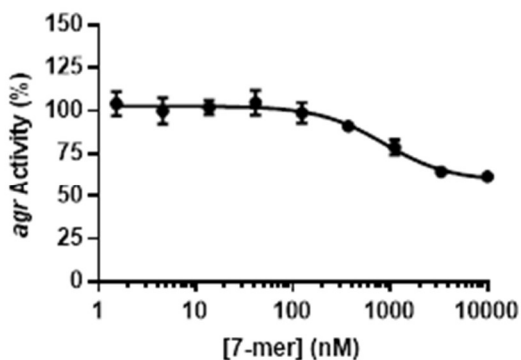
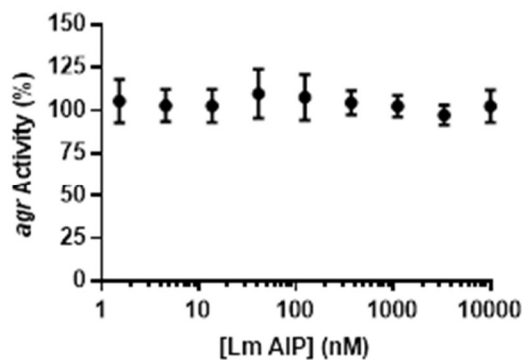
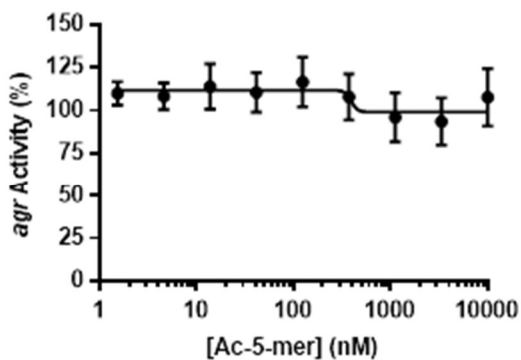
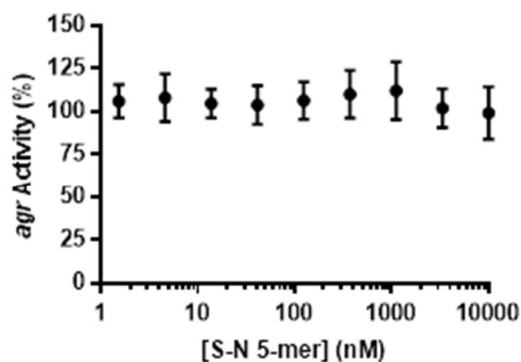
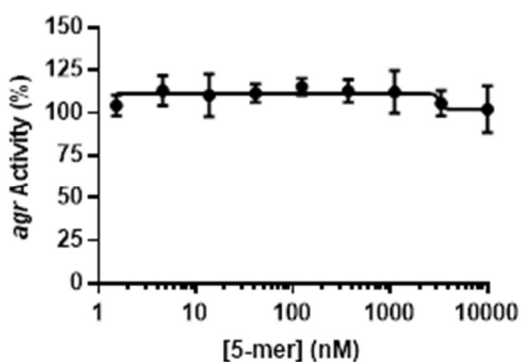


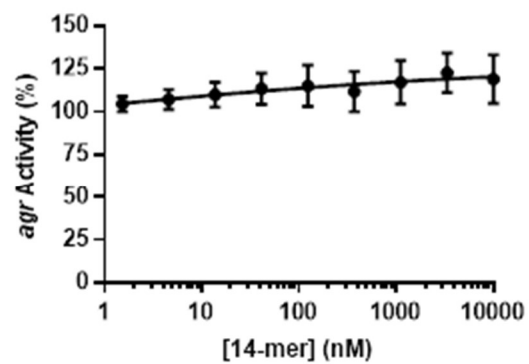
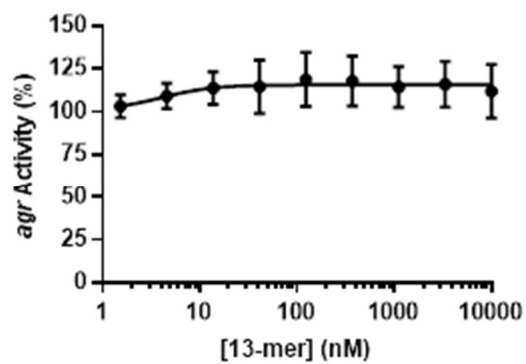
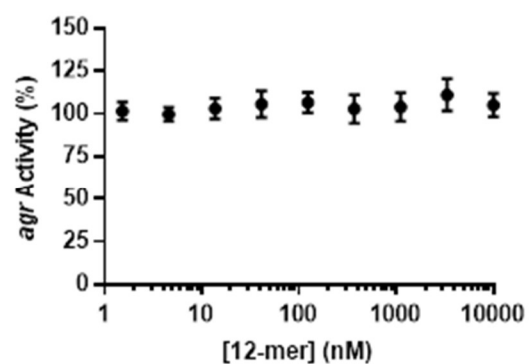
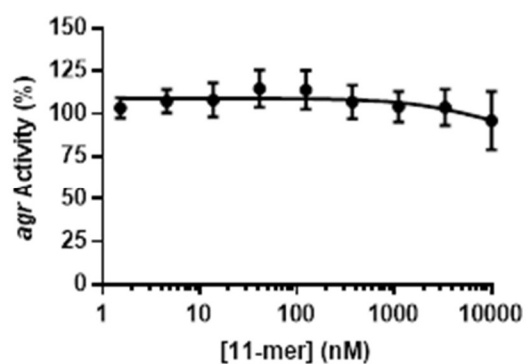
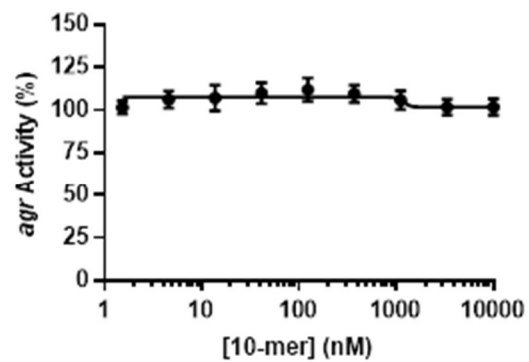
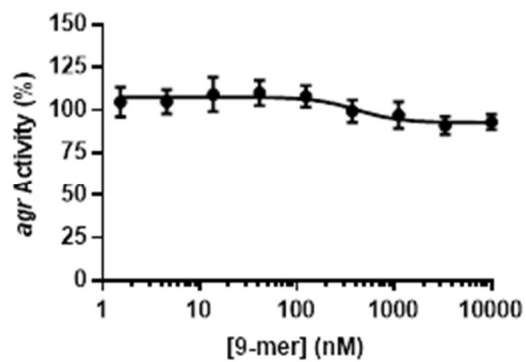


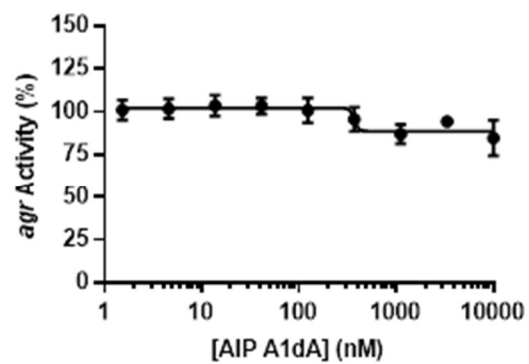
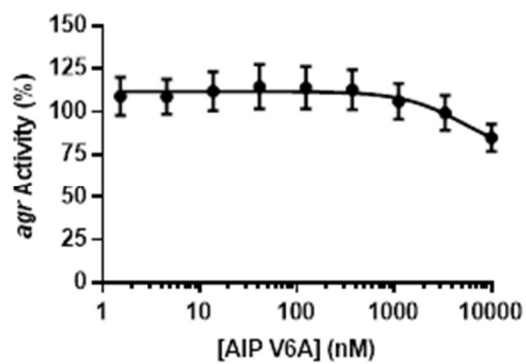
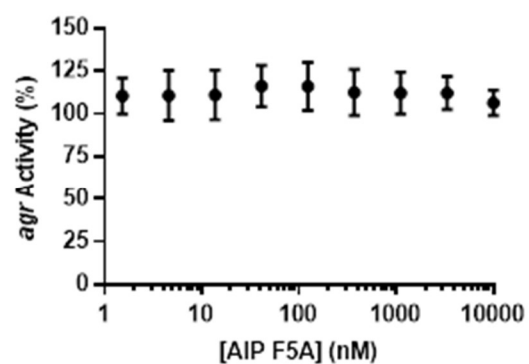
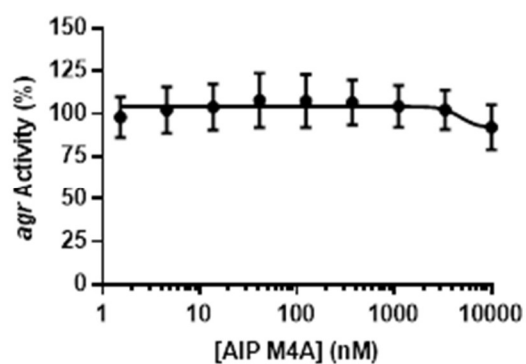
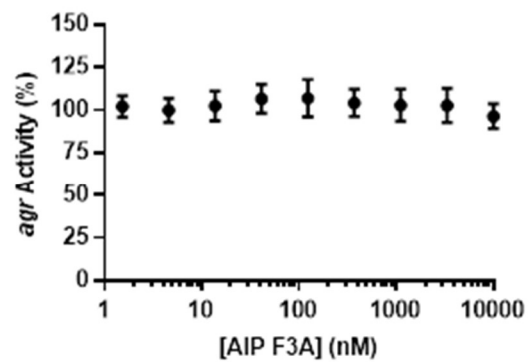
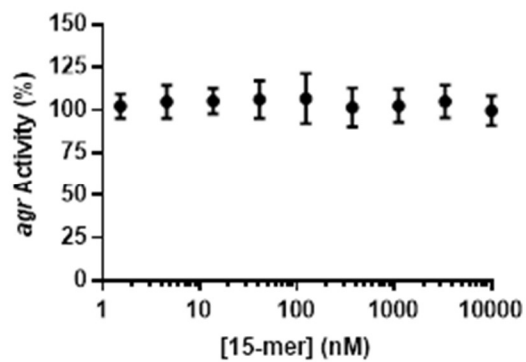


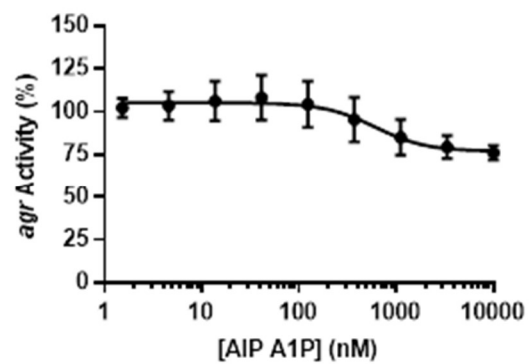
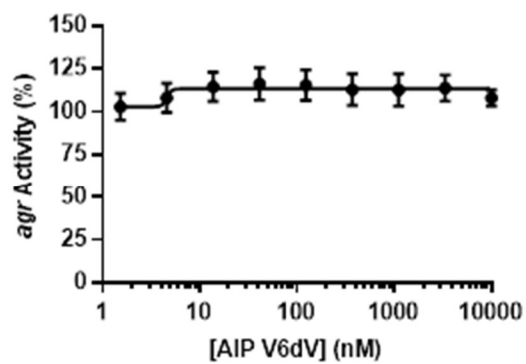
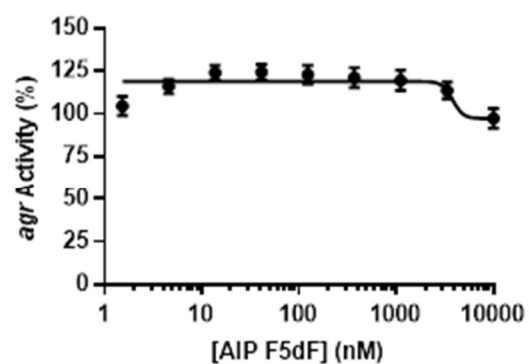
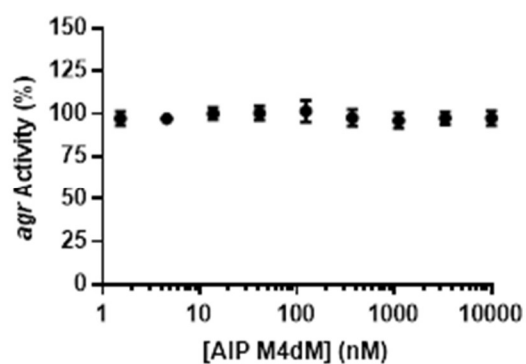
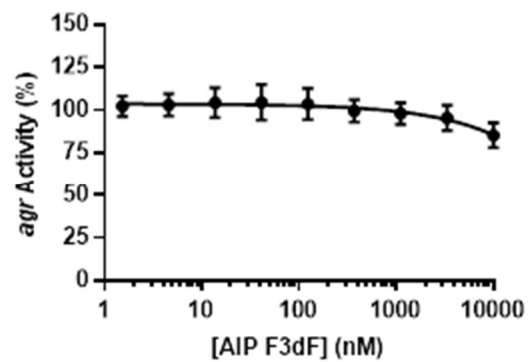
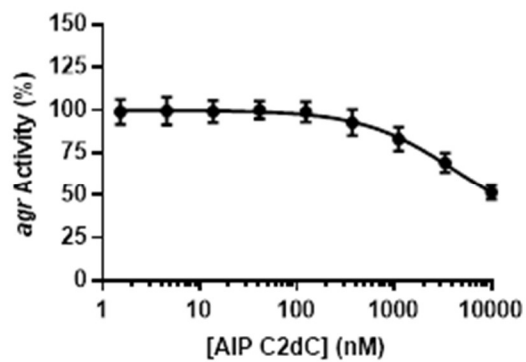
Antagonism Assays Dose Response Curves

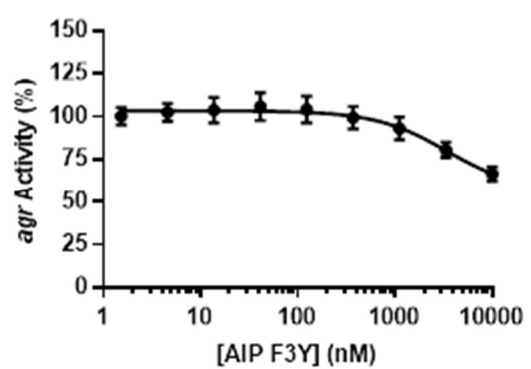
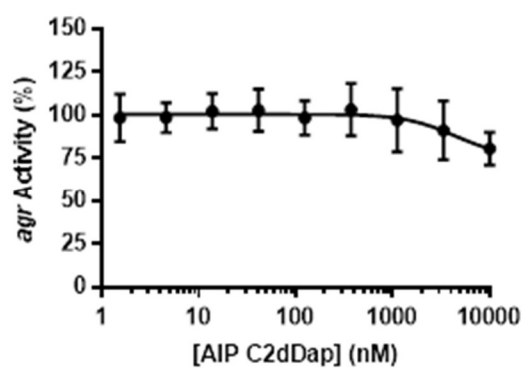
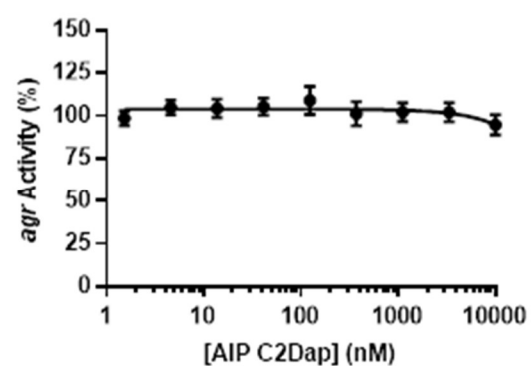
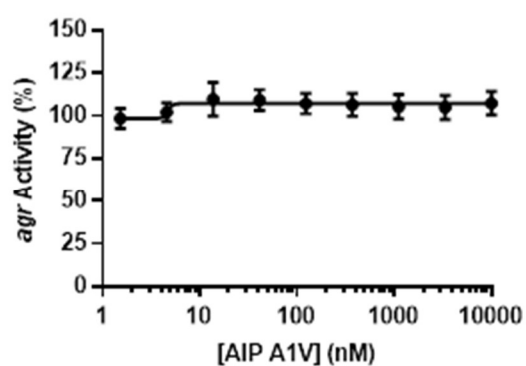
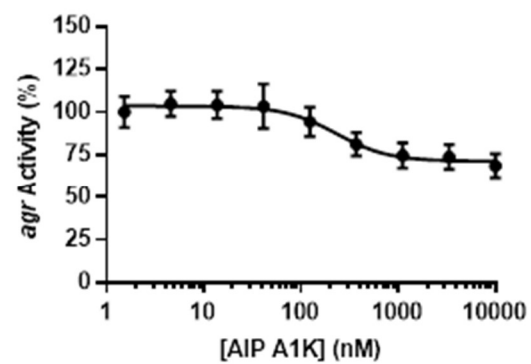
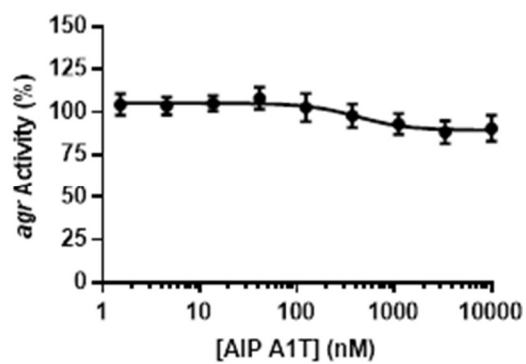
Compounds tested over range of concentrations in wild-type fluorescent reporter strain. Data points signify mean values for each concentration with error bars represent standard deviation of mean over three biological replicates, each with three technical replicates.

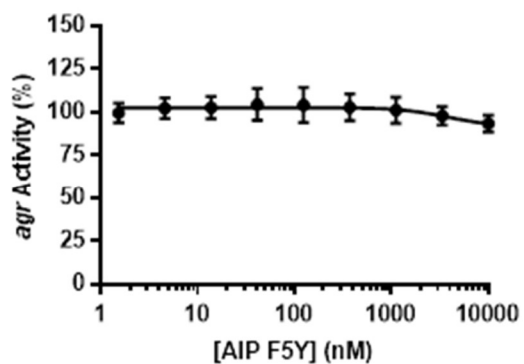
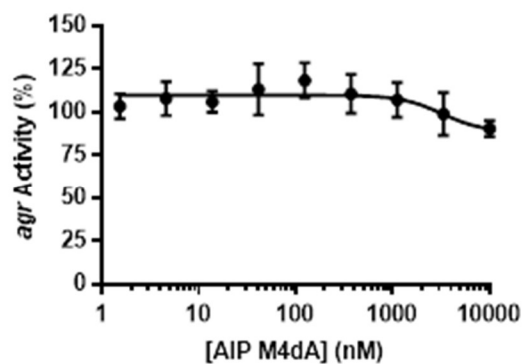
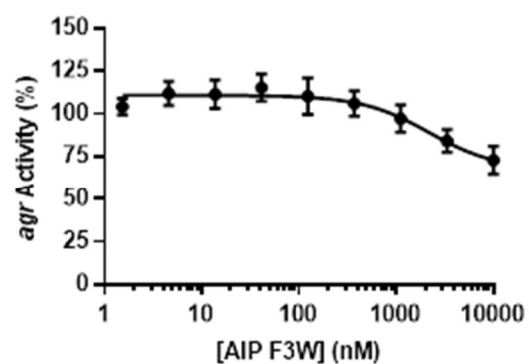
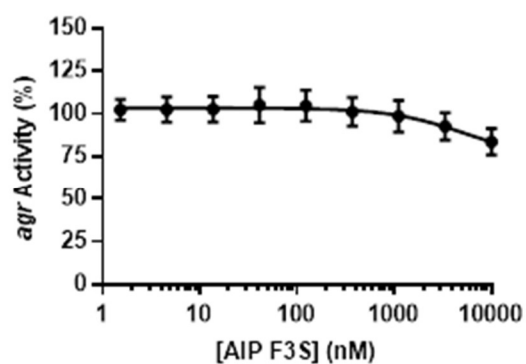
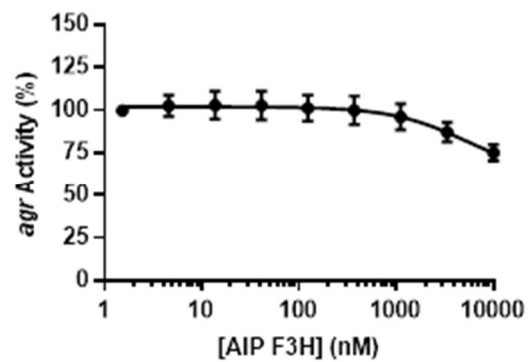
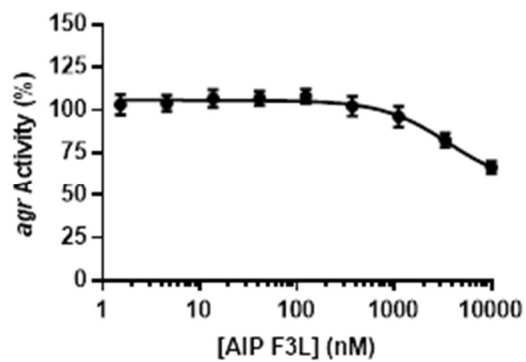


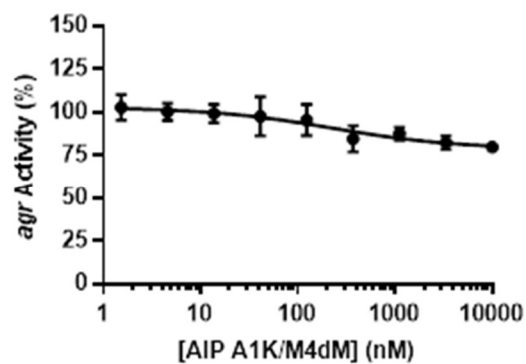
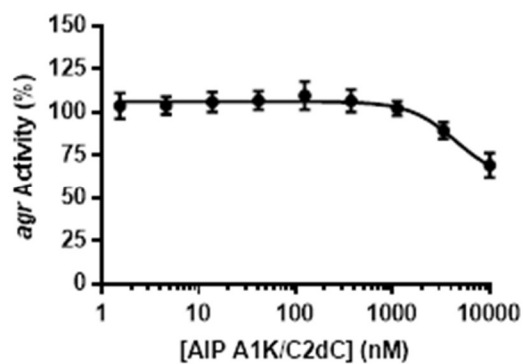
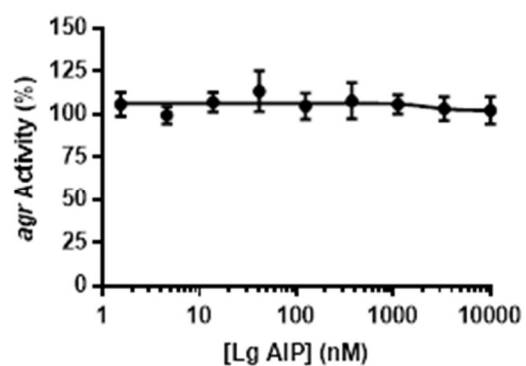
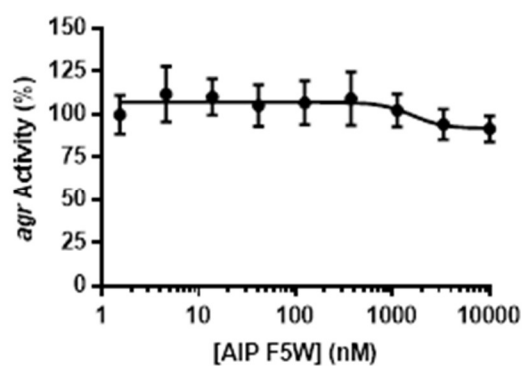
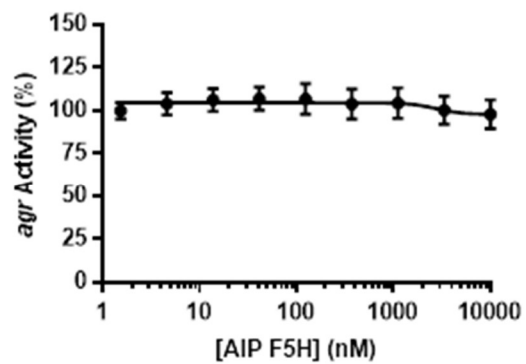
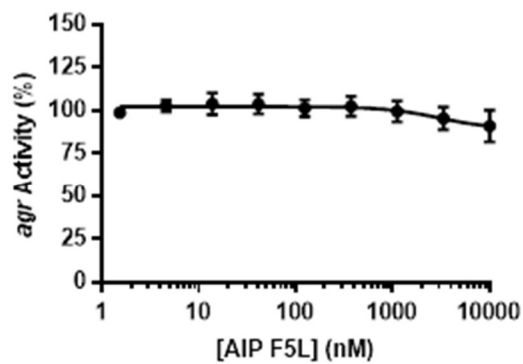


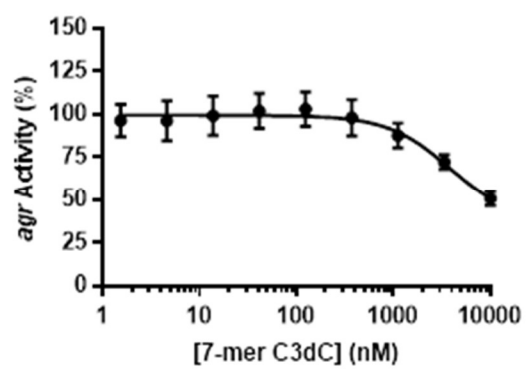
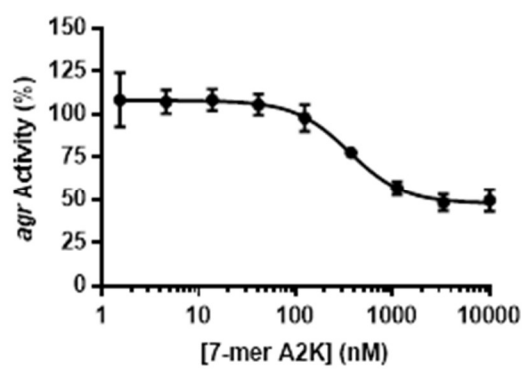
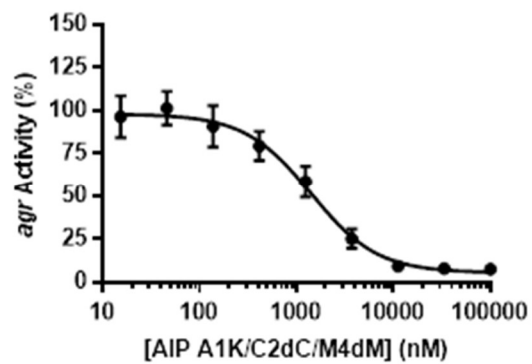
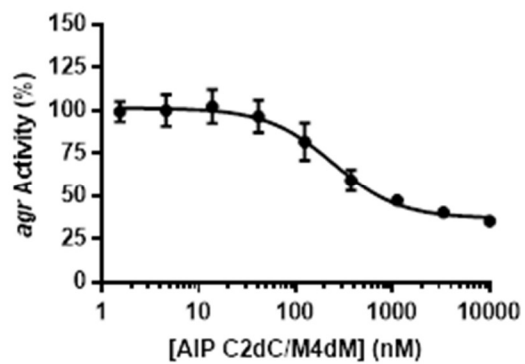


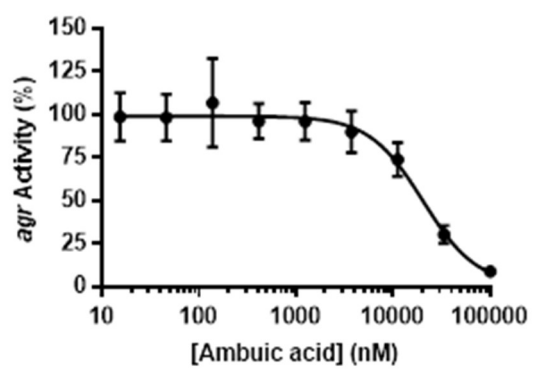
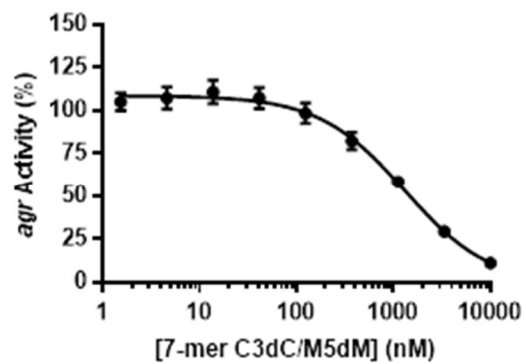
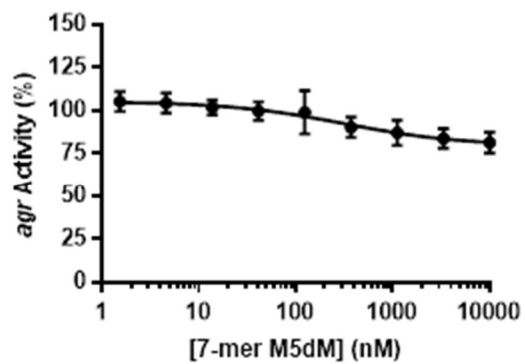












2.5.9 Peptide HPLC and MS characterization

Table 2.A MS spectral data, HPLC retention times, and purity data of synthesized peptides.

peptide	calculated m/z [M+H] ⁺ (Da)	observed m/z [M+H] ⁺ (Da)	Δm (ppm)	retention time (min)	HPLC trace purity (%, 220 nm)
Ac-5-mer	670.2728	670.2725	0.4	26.69	96.9
AIP	699.2993	699.2997	0.6	22.59	>99
7-mer	827.3943	827.394	0.4	22.37	97.7
8-mer	914.4263	914.4276	1.4	20.95	92.3
9-mer	1045.4668	1045.4679	1.1	21.25	94.3
10-mer	566.753 ^a	566.7532 ^a	0.4	21.16	93.2
11-mer	610.2691 ^a	610.2682 ^a	1.5	20.94	97.9
12-mer	667.7825 ^a	667.7828 ^a	0.4	20.86	98.4
13-mer	703.3011 ^a	703.3015 ^a	0.6	20.78	96.5
14-mer	752.8353 ^a	752.8357 ^a	0.5	20.89	98.2
15-mer	816.8828 ^a	816.8826 ^a	0.2	20.28	96.4
AIP F3A	623.268	623.2679	0.2	20.35	99.0
AIP M4A	661.2779	611.2774	0.8	21.39	>99
AIP F5A	623.268	623.2684	0.6	19.50	99.0
AIP V6A	671.268	671.2682	0.3	21.04	98.8
AIP A1dA	699.2993	699.2998	0.7	22.74	97.5
AIP C2dC	699.2993	699.2995	0.3	22.19	97.9
AIP F3dF	699.2993	699.2996	0.4	21.78	98.2
AIP M4dM	699.2993	699.2993	<0.1	22.24	96.2
AIP F5dF	699.2993	699.2999	0.9	22.04	96.2
AIP V6dV	699.2993	699.2995	0.3	22.14	98.1
AIP A1P	725.315	725.3145	0.7	23.09	98.6
AIP A1T	729.3099	729.3099	<0.1	22.45	98.6
AIP A1K	756.3572	756.3572	<0.1	26.07	98.6
AIP A1V	727.3306	727.3315	1.2	28.34	96.5
AIP C2Dap (AIP amide)	682.3381	682.3381	<0.1	22.25	95.2

^aMass calculated and observed as [M+2H]²⁺. ^bMass calculated and observed as [M+Na]⁺.

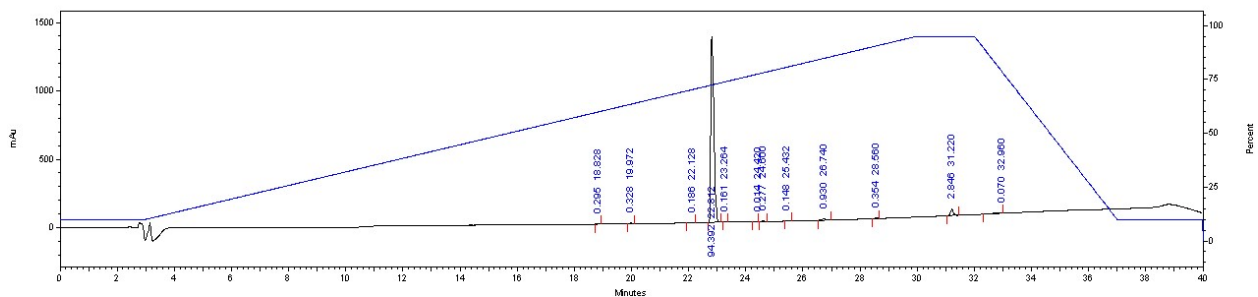
Table 2.A (continued) MS spectral data, HPLC retention times, and purity data of synthesized peptides.

peptide	calculated m/z [M+H] ⁺ (Da)	observed m/z [M+H] ⁺ (Da)	Δm (ppm)	retention time (min)	HPLC trace purity (%, 220 nm)
AIP C2dDap (AIP D-amide)	682.33813	682.3386	0.7	25.90	96.2
AIP F3Y	715.2942	715.2958	2.2	26.02	96.4
AIP F3L	665.315	665.3159	1.4	27.28	98.3
AIP F3H	689.2898	689.2892	0.9	18.74	95.4
AIP F3S	639.2629	639.2628	0.2	19.70	97.0
AIP F3W	738.3102	738.3089	1.8	22.57	98.8
AIP M4dA	639.2959	639.2967	1.3	26.04	96.4
AIP F5Y	715.2942	715.2959	2.4	25.26	98.6
AIP F5L	665.315	665.3149	0.2	22.22	96.4
AIP F5H	689.2898	689.2899	0.1	22.05	97.8
AIP F5W	738.3102	738.3112	1.4	22.25	>99
AIP A1K/C2dC	756.3572	756.3574	0.3	25.59	97.3
AIP A1K/M4dM	756.3572	756.357	0.3	25.87	97.4
AIP C2dC/M4dM	699.2993	699.2999	0.9	26.96	97.0
AIP A1K/C2dC/M4dM	756.3572	756.3568	0.5	25.45	98.5
7-mer A2K	884.4521	884.452	0.1	19.91	>99
7-mer C3dC	827.3943	827.3937	0.7	25.22	97.3
7-mer M5dM	827.3943	827.3937	0.7	20.76	98.2
7-mer C3dC/M5dM	827.3943	827.3939	0.5	20.23	>99
<i>L. grandensis</i> tr AIP	548.25373	548.2532	1.0	25.72	98.4
<i>L. grayi</i> AIP	611.2316	611.232	0.7	22.98	>99
<i>L. kieliensis</i> AIP	547.2545	547.2541	0.7	19.35	>99
<i>L. newyorkensis</i> AIP	711.3535 ^b	711.3535 ^b	<0.1	29.12	>99
<i>L. weihenstephanensis</i> AIP	653.3439	653.3436	0.5	21.29	>99

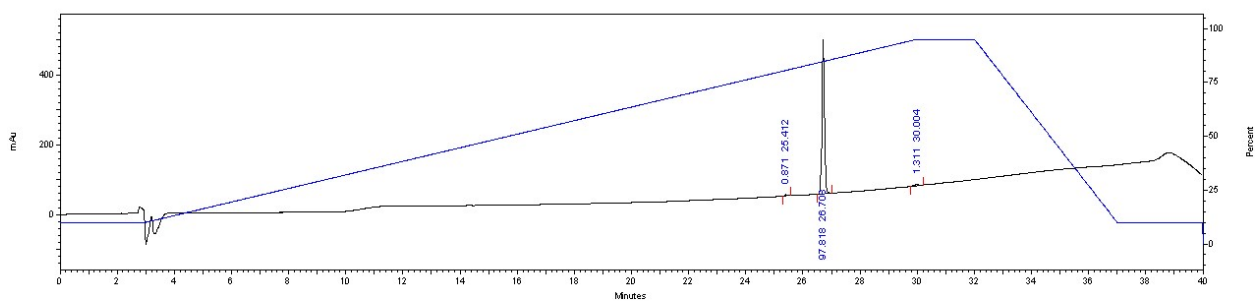
^aMass calculated and observed as [M+2H]²⁺. ^bMass calculated and observed as [M+Na]⁺.

Analytical HPLC traces for synthesized peptides

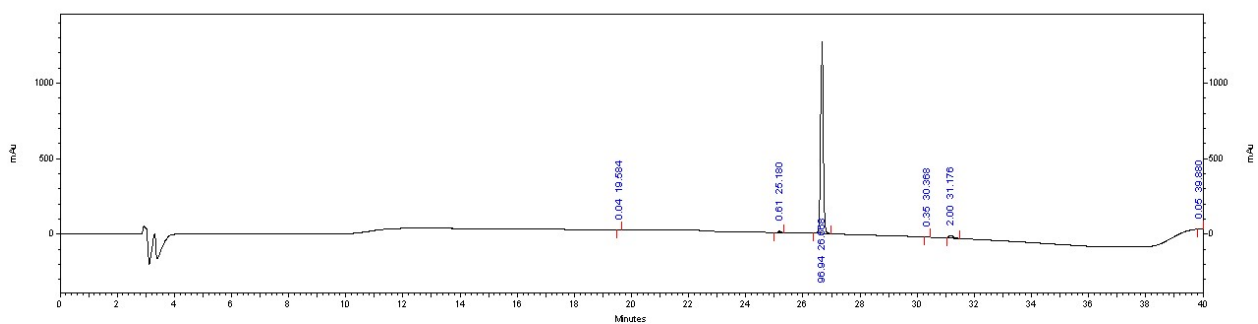
5-mer



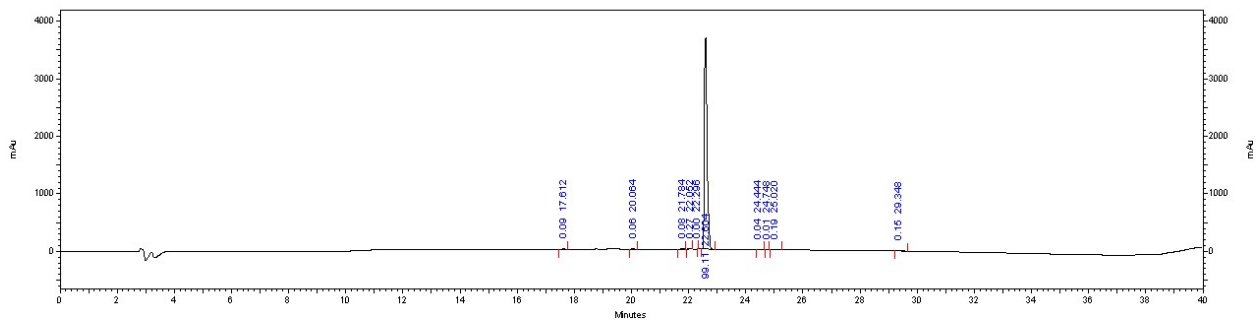
S→N 5mer



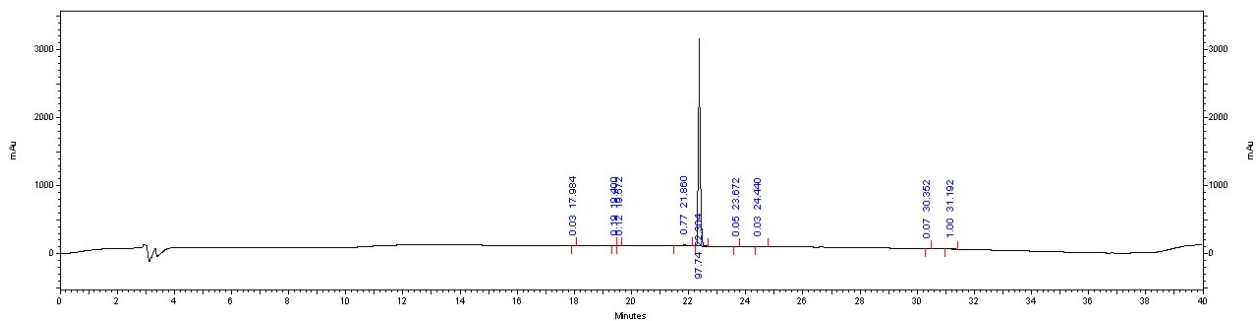
Ac-5-mer



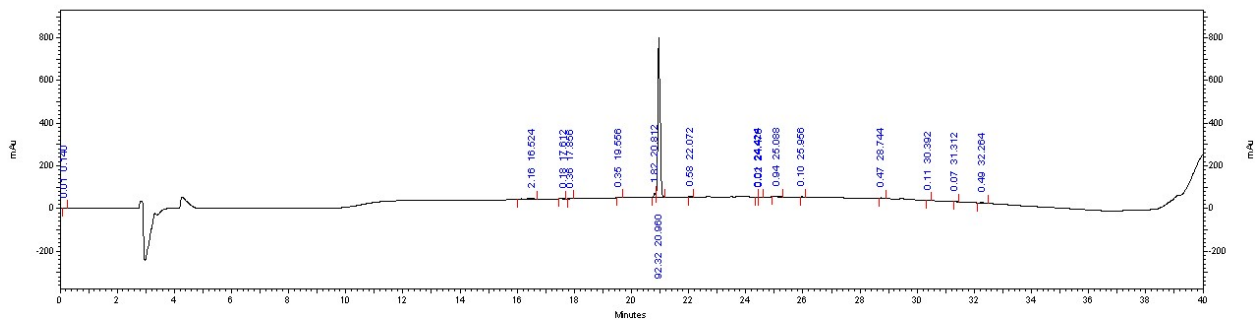
AIP (6-mer)



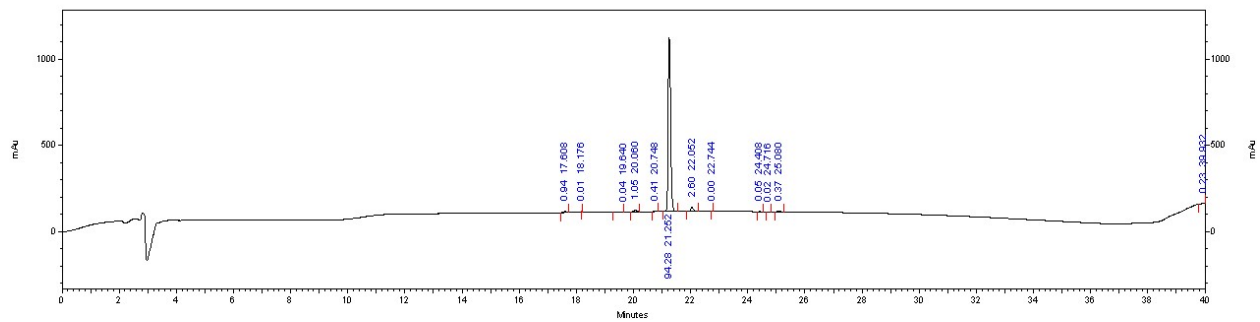
7-mer



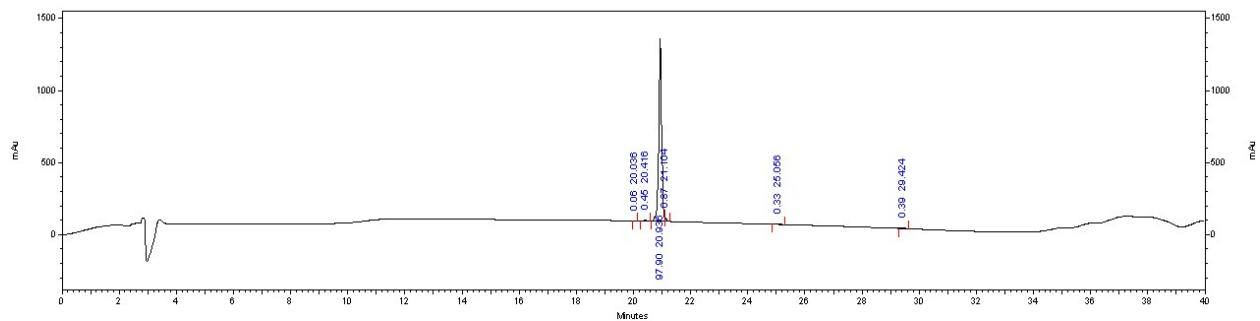
8-mer



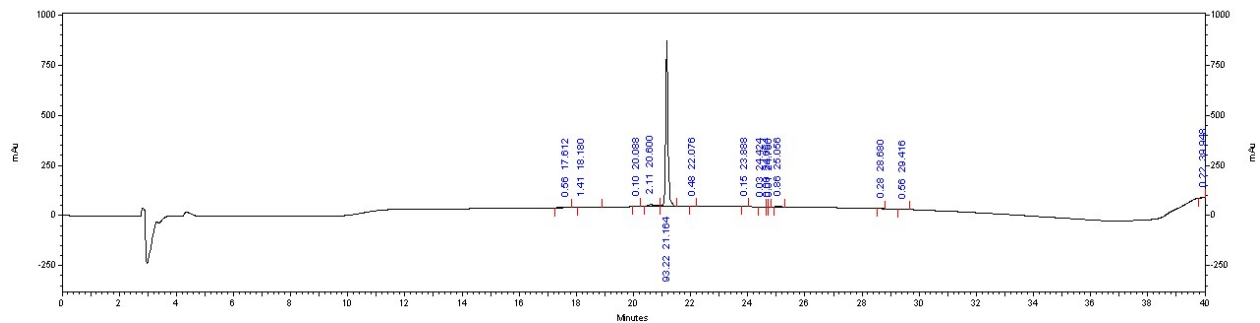
9-mer



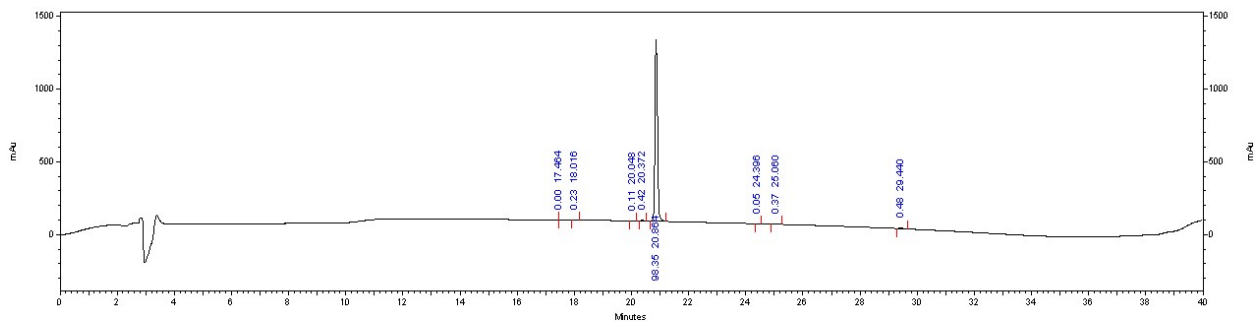
10-mer



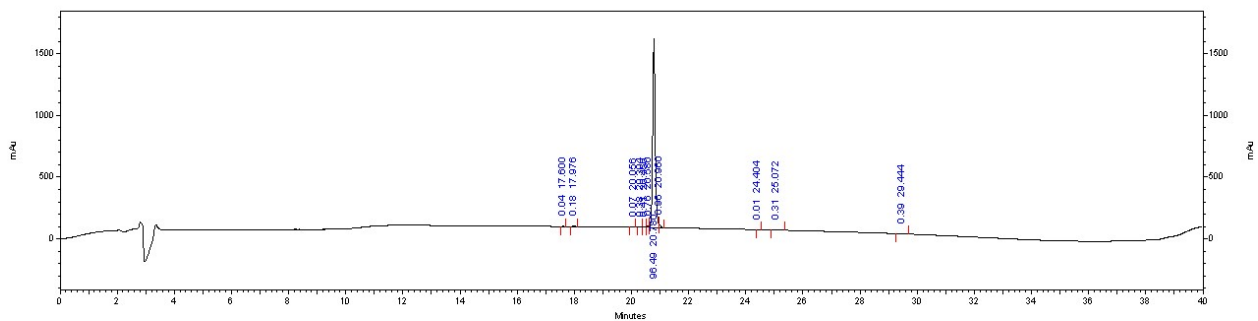
11-mer



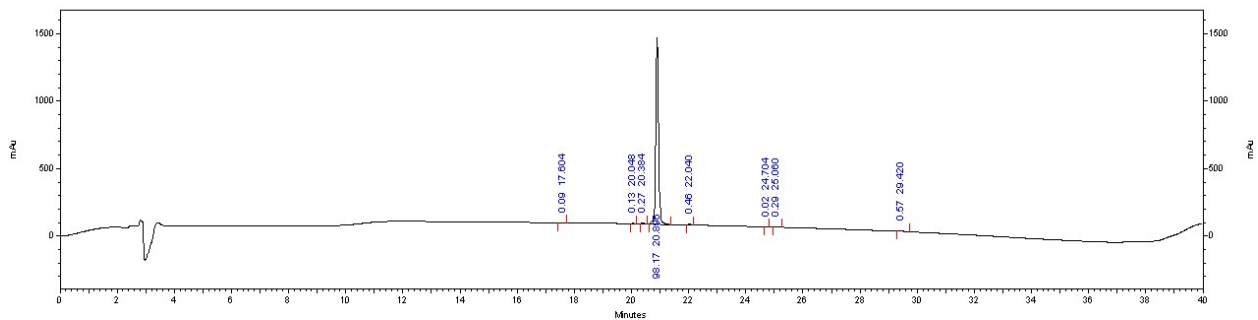
12-mer



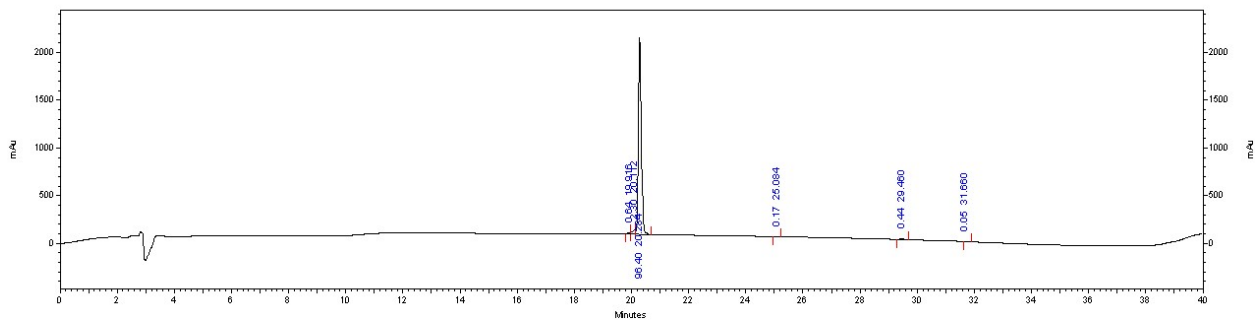
13-mer



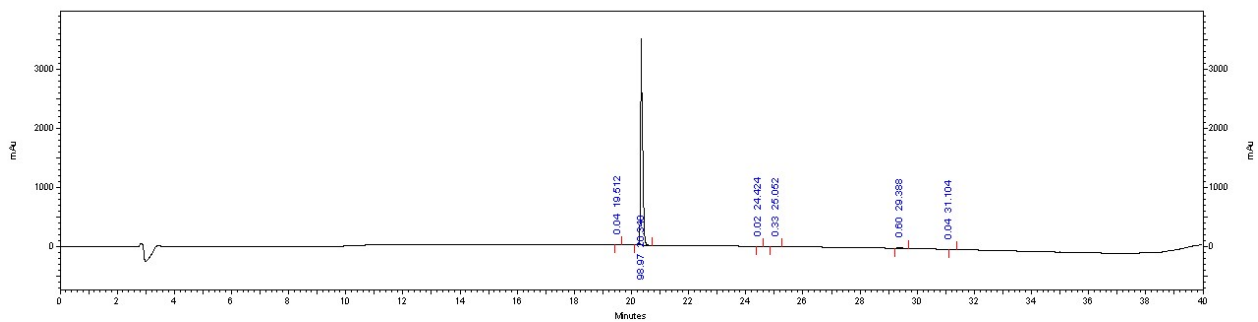
14-mer



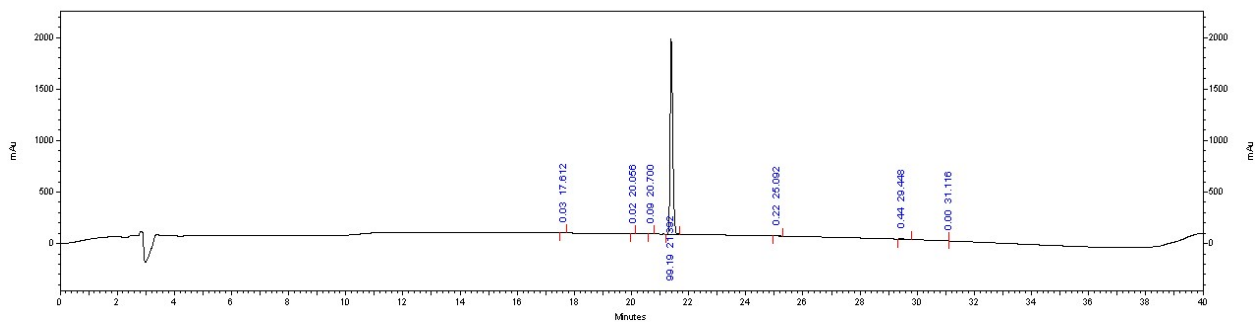
15-mer



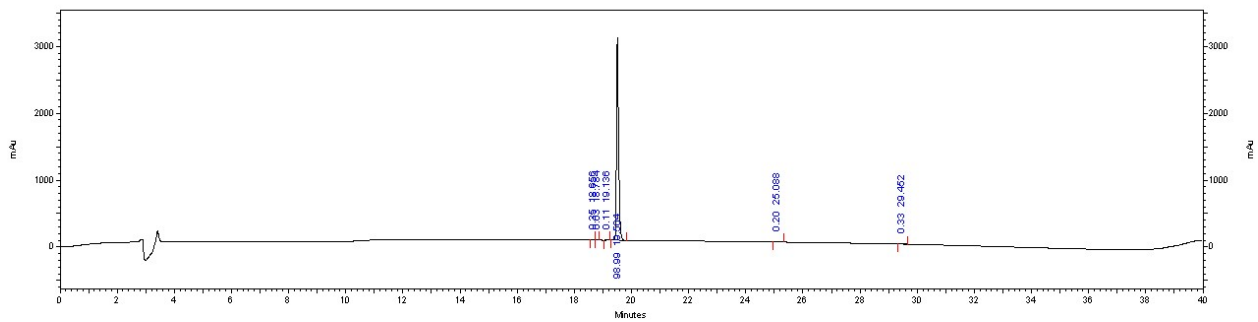
AIP F3A



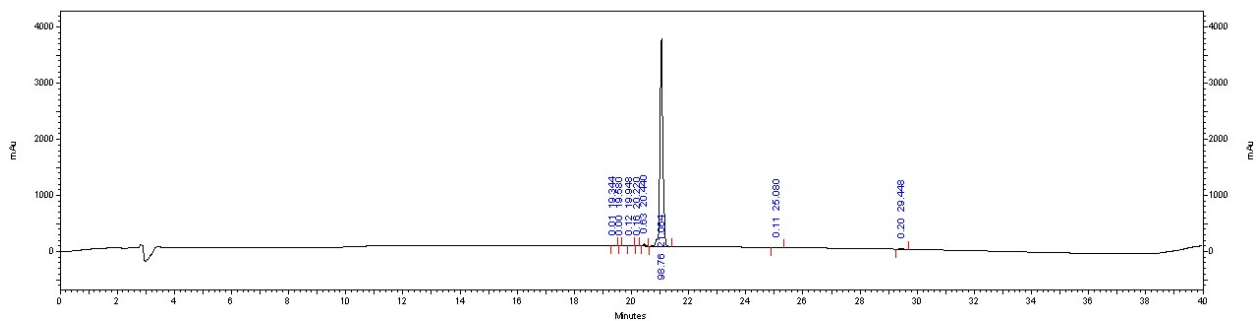
AIP M4A



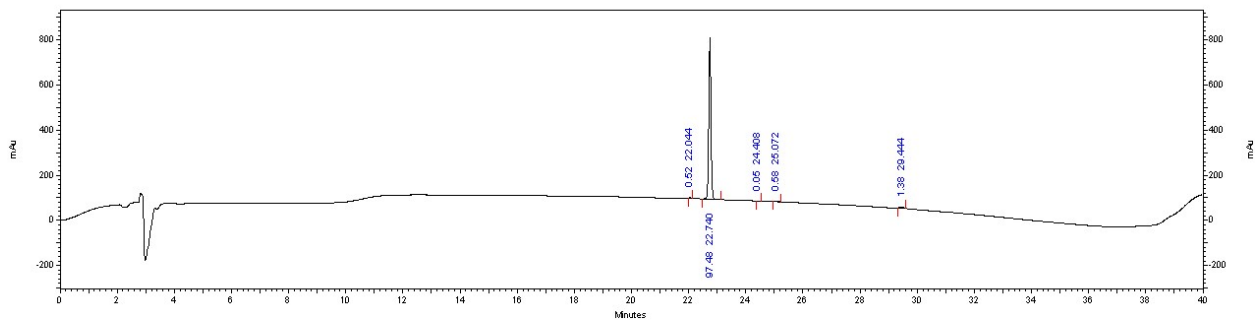
AIP F5A



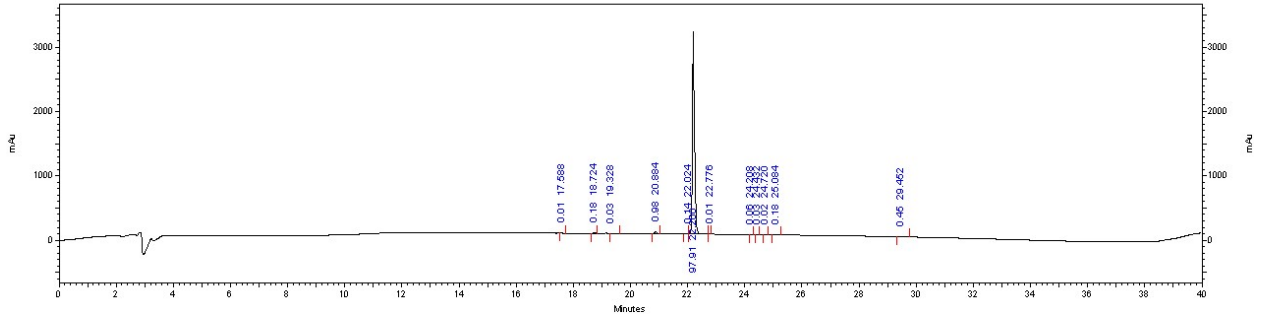
AIP V6A



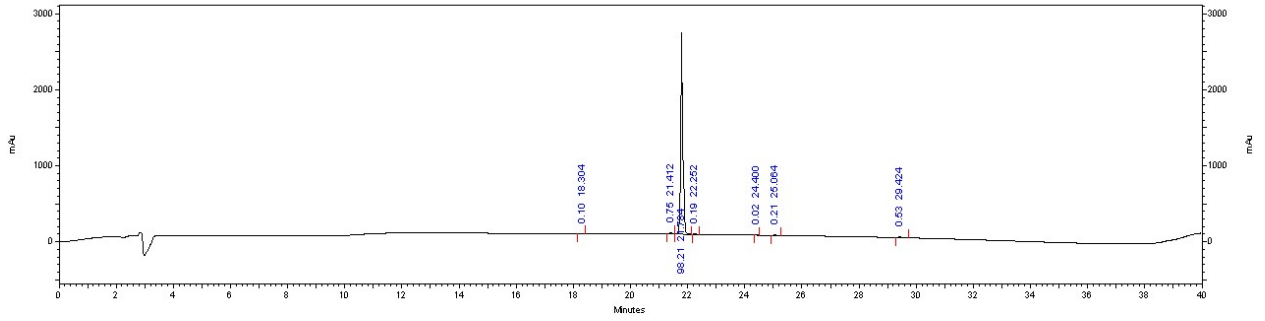
AIP A1dA



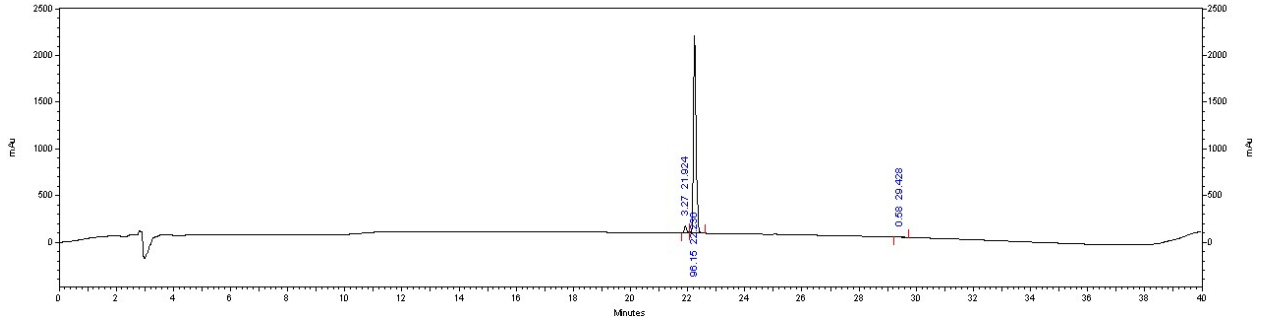
AIP C2dC



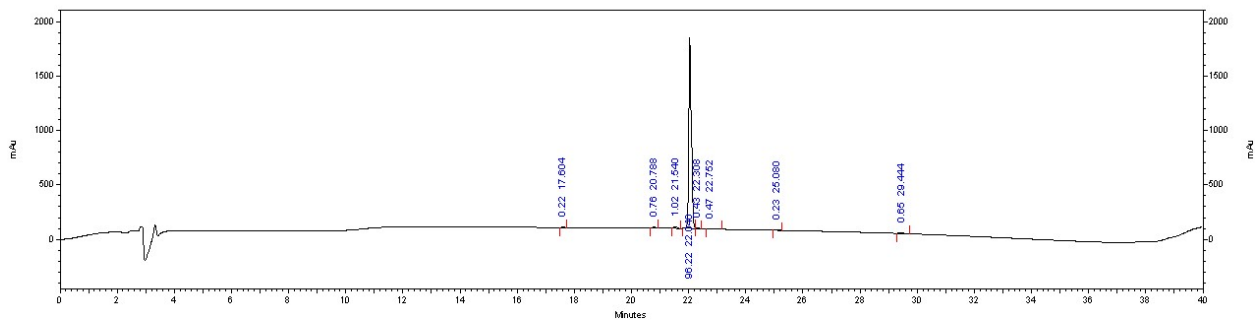
AIP F3dF



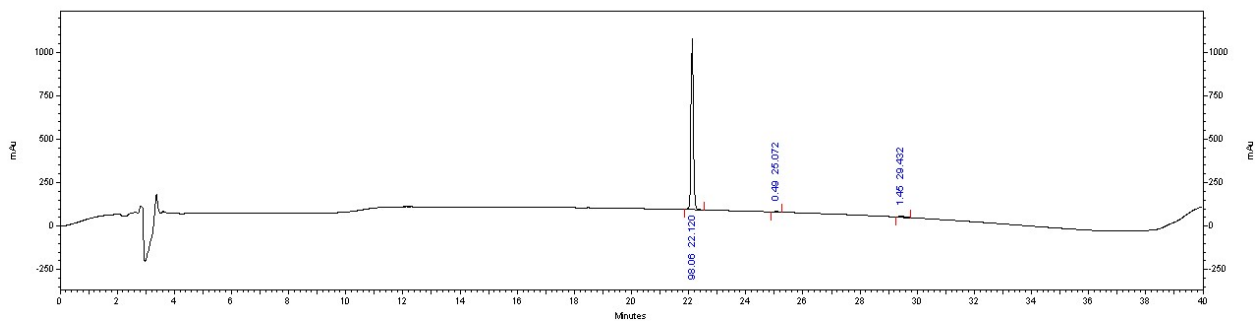
AIP M4dM



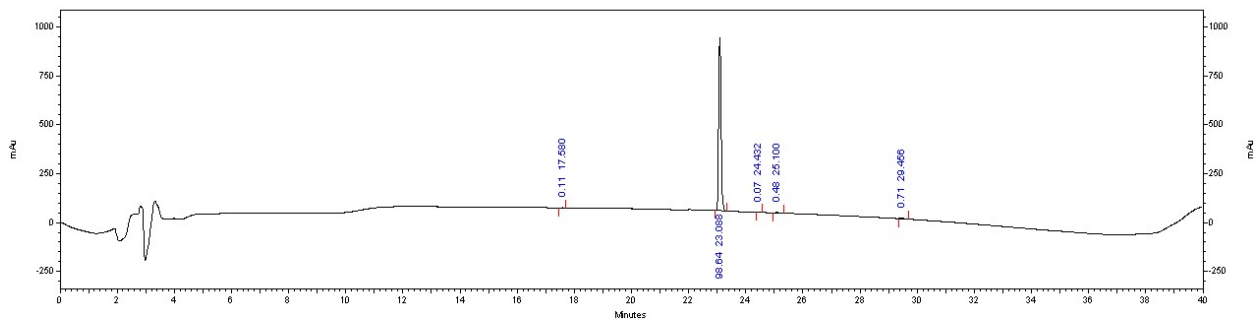
AIP F5dF



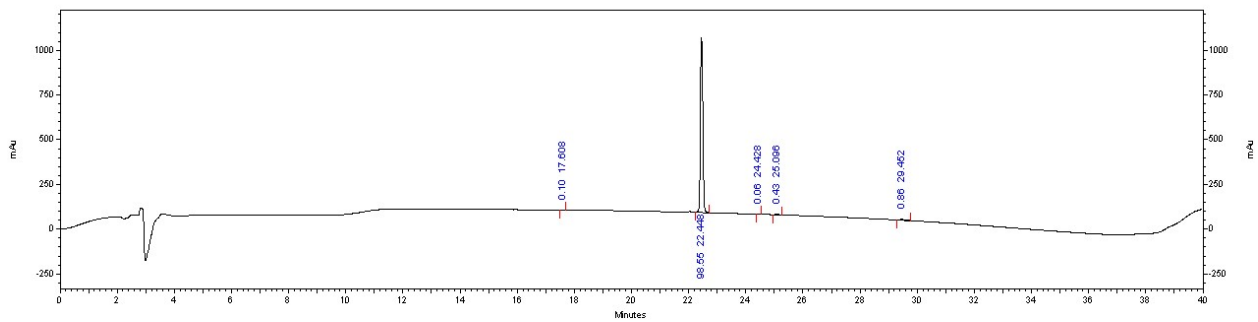
AIP V6dV



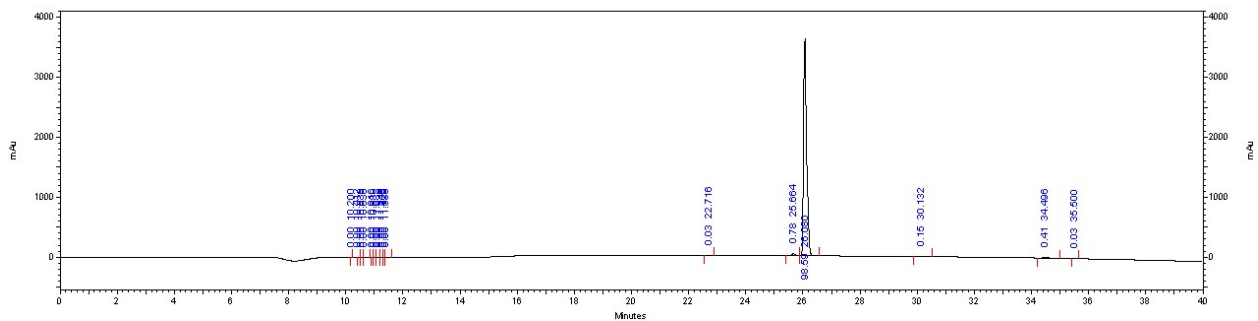
AIP A1P



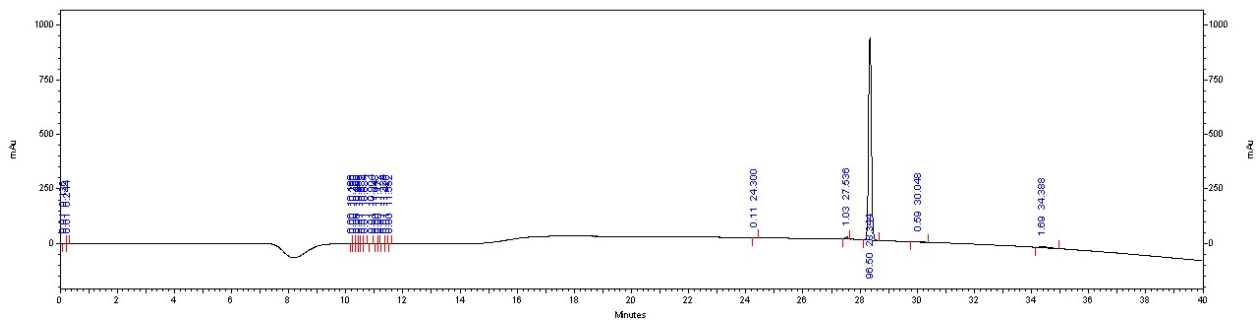
AIP A1T



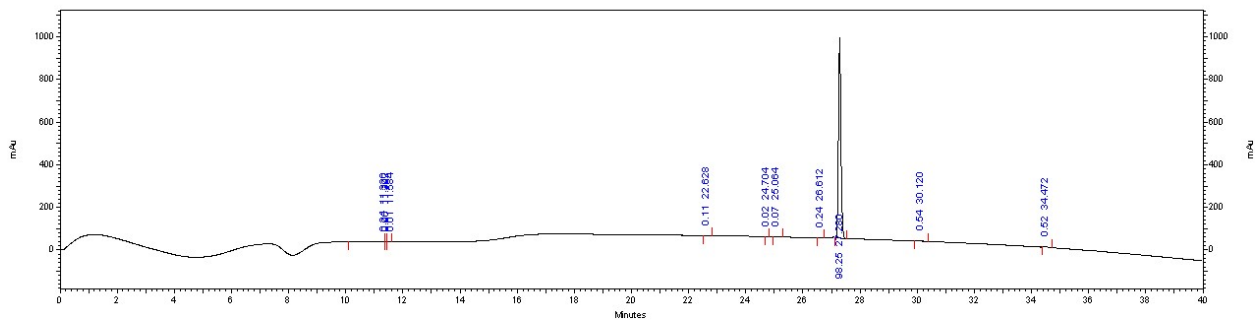
AIP A1K



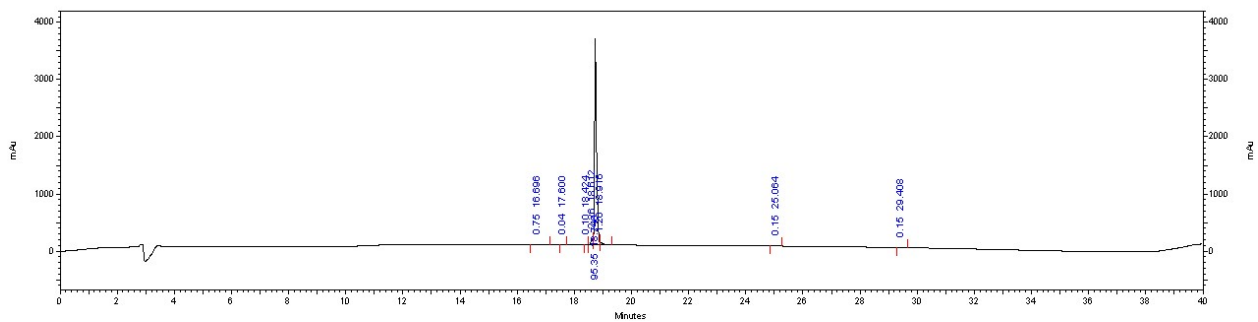
AIP A1V



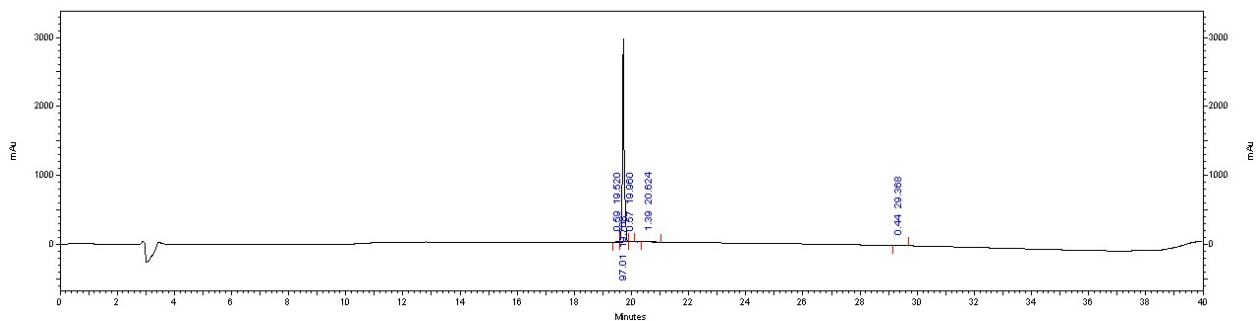
AIP F3L



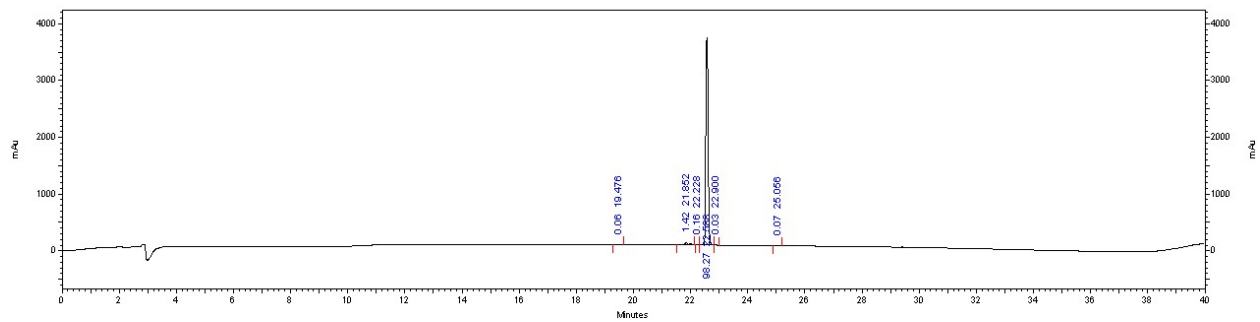
AIP F3H



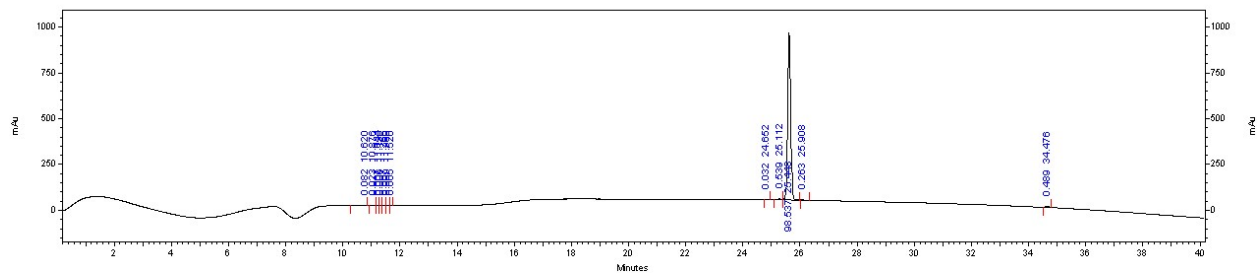
AIP F3S



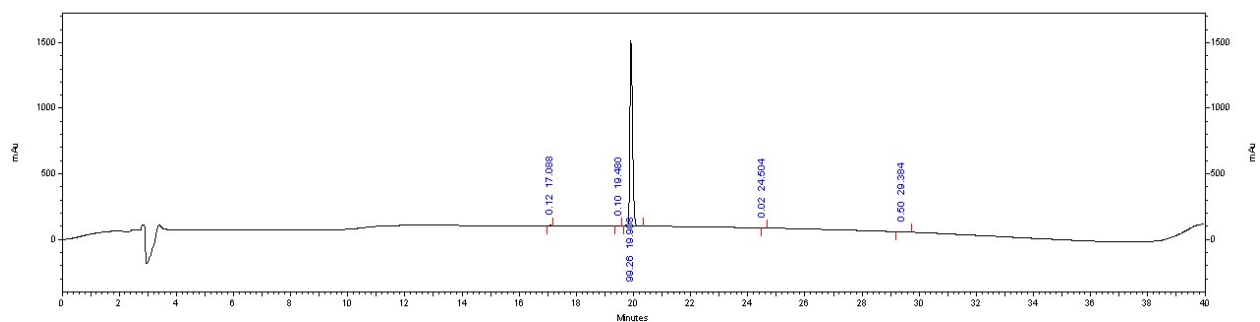
AIP F3W



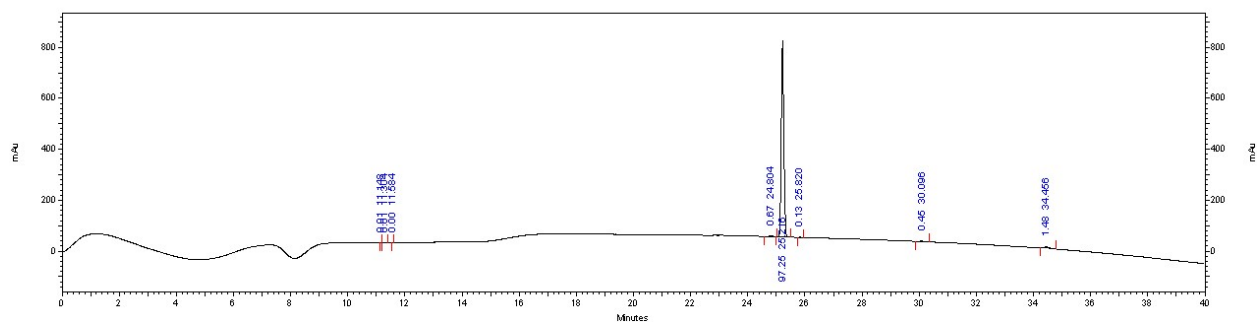
AIP A1K/C2dC/M4dM



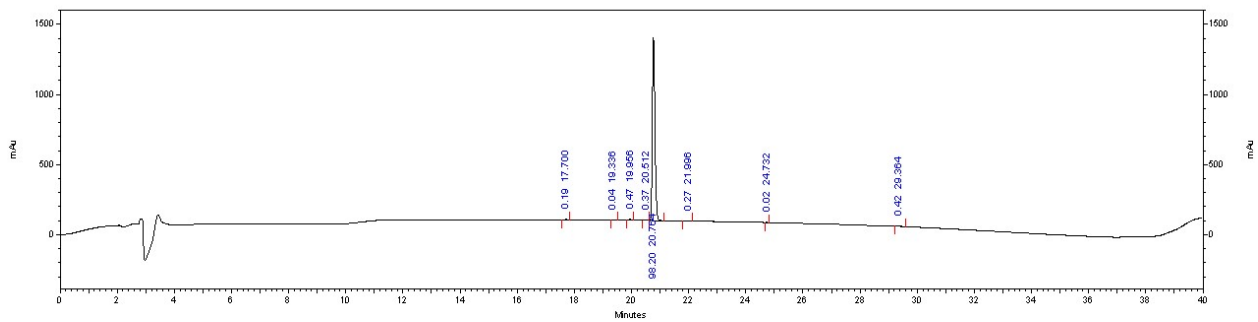
7-mer A2K



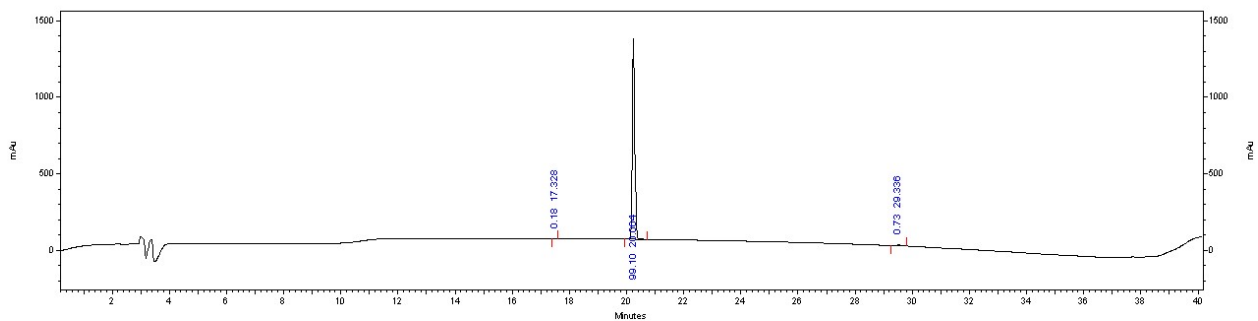
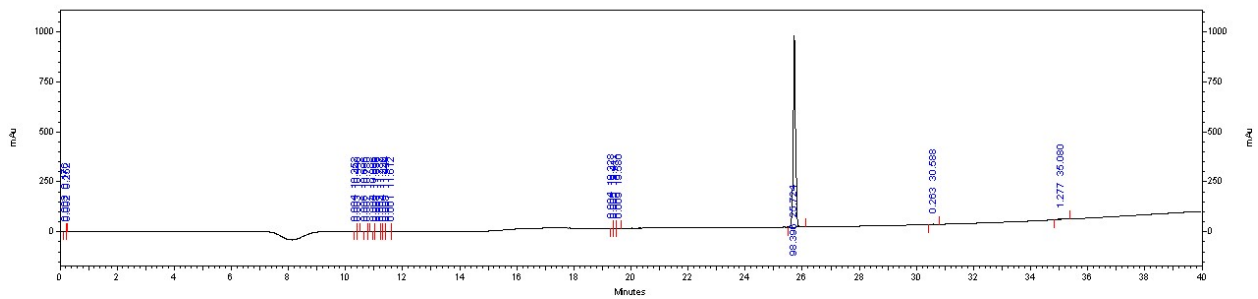
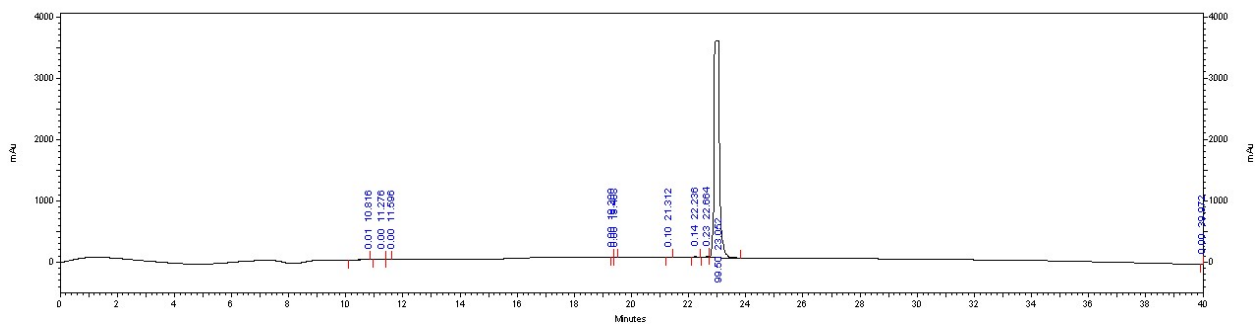
7-mer C3dC



7-mer M5dM



7-mer C3dC/M5dM

*L. grandensis* tr AIP*L. grayi* AIP

2.6 Acknowledgements

H.E.B. thanks the NSF for generous support of this research (CHE-1708714). K.H.J.W. and T.T. were supported in part by the UW–Madison NIH Chemistry–Biology Interface Training Program (T32 GM008505). MS facilities in the Department of Chemistry were supported by the NIH (1S10 OD020022-1) and a gift from P. Bender. We thank C. Riedel for providing EGD-e and $\Delta agrD$ strains.

2.7 References

1. Radoshevich, L.; Cossart, P., *Listeria monocytogenes*: towards a complete picture of its physiology and pathogenesis. *Nat. Rev. Microbiol.* **2018**, *16* (1), 32-46.
2. Scallan, E.; Hoekstra, R. M.; Angulo, F. J.; Tauxe, R. V.; Widdowson, M. A.; Roy, S. L.; Jones, J. L.; Griffin, P. M., Foodborne illness acquired in the United States—major pathogens. *Emerg. Infect. Dis.* **2011**, *17* (1), 7-15.
3. Page, E. T., Trends in Food Recalls: 2004-13, EIB-191. U.S.D.A., Ed. Economic Research Service: 2018.
4. Vivant, A. L.; Garmyn, D.; Piveteau, P., *Listeria monocytogenes*, a down-to-earth pathogen. *Front. Cell. Infect. Microbiol.* **2013**, *3*, 87.
5. Freitag, N. E.; Port, G. C.; Miner, M. D., *Listeria monocytogenes* - from saprophyte to intracellular pathogen. *Nat. Rev. Microbiol.* **2009**, *7* (9), 623-8.
6. Farber, J. M.; Peterkin, P. I., *Listeria monocytogenes*, a Food-Borne Pathogen. *Microbiol. Rev.* **1991**, *55* (3), 476-511.
7. Gandhi, M.; Chikindas, M. L., *Listeria*: A foodborne pathogen that knows how to survive. *Int. J. Food Microbiol.* **2007**, *113* (1), 1-15.
8. Tilney, L. G.; Portnoy, D. A., Actin filaments and the growth, movement, and spread of the intracellular bacterial parasite, *Listeria monocytogenes*. *J. Cell Biol.* **1989**, *109* (4 Pt 1), 1597-608.
9. Hof, H.; Nichterlein, T.; Kretschmar, M., Management of listeriosis. *Clin. Microbiol. Rev.* **1997**, *10* (2), 345-57.
10. Riedel, C. U.; Monk, I. R.; Casey, P. G.; Waidmann, M. S.; Gahan, C. G.; Hill, C., AgrD-dependent quorum sensing affects biofilm formation, invasion, virulence and global gene expression profiles in *Listeria monocytogenes*. *Mol. Microbiol.* **2009**, *71* (5), 1177-89.
11. Rutherford, S. T.; Bassler, B. L., Bacterial quorum sensing: its role in virulence and possibilities for its control. *Cold Spring Harb. Perspect. Med.* **2012**, *2* (11), a012427.
12. Camilli, A.; Bassler, B. L., Bacterial small-molecule signaling pathways. *Science* **2006**, *311* (5764), 1113-6.
13. Tal-Gan, Y.; Stacy, D. M.; Foegen, M. K.; Koenig, D. W.; Blackwell, H. E., Highly potent inhibitors of quorum sensing in *Staphylococcus aureus* revealed through a

- systematic synthetic study of the group-III autoinducing peptide. *J. Am. Chem. Soc.* **2013**, *135* (21), 7869-82.
14. Mayville, P.; Ji, G.; Beavis, R.; Yang, H.; Goger, M.; Novick, R. P.; Muir, T. W., Structure-activity analysis of synthetic autoinducing thiolactone peptides from *Staphylococcus aureus* responsible for virulence. *Proc. Natl. Acad. Sci. U. S. A.* **1999**, *96* (4), 1218-23.
 15. Palmer, A. G.; Streng, E.; Blackwell, H. E., Attenuation of virulence in pathogenic bacteria using synthetic quorum-sensing modulators under native conditions on plant hosts. *ACS Chem. Biol.* **2011**, *6* (12), 1348-56.
 16. Mattmann, M. E.; Blackwell, H. E., Small molecules that modulate quorum sensing and control virulence in *Pseudomonas aeruginosa*. *J. Org. Chem.* **2010**, *75* (20), 6737-46.
 17. Horswill, A. R.; Gordon, C. P., Structure-Activity Relationship Studies of Small Molecule Modulators of the Staphylococcal Accessory Gene Regulator. *J. Med. Chem.* **2020**, *63* (6), 2705-2730.
 18. Rasko, D. A.; Sperandio, V., Anti-virulence strategies to combat bacteria-mediated disease. *Nat. Rev. Drug Discov.* **2010**, *9* (2), 117-28.
 19. Dickey, S. W.; Cheung, G. Y. C.; Otto, M., Different drugs for bad bugs: antivirulence strategies in the age of antibiotic resistance. *Nat. Rev. Drug Discov.* **2017**, *16* (7), 457-471.
 20. Thoendel, M.; Kavanaugh, J. S.; Flack, C. E.; Horswill, A. R., Peptide Signaling in the Staphylococci. *Chem. Rev.* **2011**, *111* (1), 117-51.
 21. Autret, N.; Raynaud, C.; Dubail, I.; Berche, P.; Charbit, A., Identification of the agr locus of *Listeria monocytogenes*: role in bacterial virulence. *Infect. Immun.* **2003**, *71* (8), 4463-71.
 22. Wang, B.; Muir, T. W., Regulation of Virulence in *Staphylococcus aureus*: Molecular Mechanisms and Remaining Puzzles. *Cell Chem. Biol.* **2016**, *23* (2), 214-224.
 23. Thoendel, M.; Horswill, A. R., Identification of *Staphylococcus aureus* AgrD residues required for autoinducing peptide biosynthesis. *J. Biol. Chem.* **2009**, *284* (33), 21828-38.
 24. Wang, B.; Zhao, A.; Novick, R. P.; Muir, T. W., Key driving forces in the biosynthesis of autoinducing peptides required for staphylococcal virulence. *Proc. Natl. Acad. Sci. U. S. A.* **2015**, *112* (34), 10679-84.

25. Wang, B.; Zhao, A.; Novick, R. P.; Muir, T. W., Activation and inhibition of the receptor histidine kinase AgrC occurs through opposite helical transduction motions. *Mol. Cell* **2014**, *53* (6), 929-40.
26. Zetzmann, M.; Sanchez-Kopper, A.; Waidmann, M. S.; Blombach, B.; Riedel, C. U., Identification of the agr Peptide of *Listeria monocytogenes*. *Front. Microbiol.* **2016**, *7*, 989.
27. Todd, D. A.; Parlet, C. P.; Crosby, H. A.; Malone, C. L.; Heilmann, K. P.; Horswill, A. R.; Cech, N. B., Signal Biosynthesis Inhibition with Ambuic Acid as a Strategy To Target Antibiotic-Resistant Infections. *Antimicrob. Agents Chemother.* **2017**, *61* (8), e00263-17.
28. Gray, B.; Hall, P.; Gresham, H., Targeting agr- and agr-Like quorum sensing systems for development of common therapeutics to treat multiple gram-positive bacterial infections. *Sensors (Basel)* **2013**, *13* (4), 5130-66.
29. Vivant, A. L.; Garmyn, D.; Gal, L.; Hartmann, A.; Piveteau, P., Survival of *Listeria monocytogenes* in Soil Requires AgrA-Mediated Regulation. *Appl. Environ. Microbiol.* **2015**, *81* (15), 5073-84.
30. Vivant, A. L.; Garmyn, D.; Gal, L.; Piveteau, P., The Agr communication system provides a benefit to the populations of *Listeria monocytogenes* in soil. *Front. Cell. Infect. Microbiol.* **2014**, *4*, 160.
31. Garmyn, D.; Augagneur, Y.; Gal, L.; Vivant, A. L.; Piveteau, P., *Listeria monocytogenes* differential transcriptome analysis reveals temperature-dependent Agr regulation and suggests overlaps with other regulons. *PLoS One* **2012**, *7* (9), e43154.
32. Rieu, A.; Weidmann, S.; Garmyn, D.; Piveteau, P.; Guzzo, J., Agr system of *Listeria monocytogenes* EGD-e: role in adherence and differential expression pattern. *Appl. Environ. Microbiol.* **2007**, *73* (19), 6125-33.
33. Rieu, A.; Briandet, R.; Habimana, O.; Garmyn, D.; Guzzo, J.; Piveteau, P., *Listeria monocytogenes* EGD-e biofilms: no mushrooms but a network of knitted chains. *Appl. Environ. Microbiol.* **2008**, *74* (14), 4491-7.
34. Chang, Y.; Gu, W.; Fischer, N.; McLandsborough, L., Identification of genes involved in *Listeria monocytogenes* biofilm formation by mariner-based transposon mutagenesis. *Appl. Microbiol. Biotechnol.* **2012**, *93* (5), 2051-62.
35. Freitag, N. E.; Rong, L.; Portnoy, D. A., Regulation of the *prfA* Transcriptional Activator of *Listeria monocytogenes*: Multiple Promoter Elements Contribute to Intracellular Growth and Cell-to-Cell Spread. *Infect. Immun.* **1993**, *61* (6), 2537-2544.

36. de las Heras, A.; Cain, R. J.; Bielecka, M. K.; Vazquez-Boland, J. A., Regulation of *Listeria* virulence: PrfA master and commander. *Curr. Opin. Microbiol.* **2011**, *14* (2), 118-27.
37. Pinheiro, J.; Lisboa, J.; Pombinho, R.; Carvalho, F.; Carreaux, A.; Brito, C.; Pontinen, A.; Korkeala, H.; Dos Santos, N. M. S.; Morais-Cabral, J. H.; Sousa, S.; Cabanes, D., MouR controls the expression of the *Listeria monocytogenes* Agr system and mediates virulence. *Nucleic Acids Res.* **2018**, *46* (18), 9338-9352.
38. Chaudhuri, S.; Gantner, B. N.; Ye, R. D.; Cianciotto, N. P.; Freitag, N. E., The *Listeria monocytogenes* ChiA chitinase enhances virulence through suppression of host innate immunity. *mBio* **2013**, *4* (2), e00617-12.
39. Paspaliari, D. K.; Mollerup, M. S.; Kallipolitis, B. H.; Ingmer, H.; Larsen, M. H., Chitinase expression in *Listeria monocytogenes* is positively regulated by the Agr system. *PLoS One* **2014**, *9* (4), e95385.
40. Nakayama, J.; Uemura, Y.; Nishiguchi, K.; Yoshimura, N.; Igarashi, Y.; Sonomoto, K., Ambuic acid inhibits the biosynthesis of cyclic peptide quorumones in gram-positive bacteria. *Antimicrob. Agents Chemother.* **2009**, *53* (2), 580-6.
41. McDowell, P.; Affas, Z.; Reynolds, C.; Holden, M. T.; Wood, S. J.; Saint, S.; Cockayne, A.; Hill, P. J.; Dodd, C. E.; Bycroft, B. W.; Chan, W. C.; Williams, P., Structure, activity and evolution of the group I thiolactone peptide quorum-sensing system of *Staphylococcus aureus*. *Mol. Microbiol.* **2001**, *41* (2), 503-12.
42. Yang, T.; Tal-Gan, Y.; Paharik, A. E.; Horswill, A. R.; Blackwell, H. E., Structure-Function Analyses of a *Staphylococcus epidermidis* Autoinducing Peptide Reveals Motifs Critical for AgrC-type Receptor Modulation. *ACS Chem. Biol.* **2016**, *11* (7), 1982-91.
43. Molloy, E. M.; Dell, M.; Hansch, V. G.; Dunbar, K. L.; Feldmann, R.; Oberheide, A.; Seyfarth, L.; Kumpfmuller, J.; Horch, T.; Arndt, H. D.; Hertweck, C., Enzyme-Primed Native Chemical Ligation Produces Autoinducing Cyclopeptides in *Clostridia*. *Angew. Chem. Int. Ed. Engl.* **2021**.
44. Ji, G.; Beavis, R.; Novick, R. P., Bacterial interference caused by autoinducing peptide variants. *Science* **1997**, *276* (5321), 2027-30.
45. Otto, M.; Echner, H.; Voelter, W.; Gotz, F., Pheromone cross-inhibition between *Staphylococcus aureus* and *Staphylococcus epidermidis*. *Infect. Immun.* **2001**, *69* (3), 1957-60.

46. Brown, M. M.; Kwiecinski, J. M.; Cruz, L. M.; Shahbandi, A.; Todd, D. A.; Cech, N. B.; Horswill, A. R., Novel Peptide from Commensal *Staphylococcus simulans* Blocks Methicillin-Resistant *Staphylococcus aureus* Quorum Sensing and Protects Host Skin from Damage. *Antimicrob. Agents Chemother.* **2020**, *64* (6), e00172-20.
47. Williams, M. R.; Costa, S. K.; Zaramela, L. S.; Khalil, S.; Todd, D. A.; Winter, H. L.; Sanford, J. A.; O'Neill, A. M.; Liggins, M. C.; Nakatsuji, T.; Cech, N. B.; Cheung, A. L.; Zengler, K.; Horswill, A. R.; Gallo, R. L., Quorum sensing between bacterial species on the skin protects against epidermal injury in atopic dermatitis. *Sci. Transl. Med.* **2019**, *11* (490).
48. Lyon, G. J.; Mayville, P.; Muir, T. W.; Novick, R. P., Rational design of a global inhibitor of the virulence response in *Staphylococcus aureus*, based in part on localization of the site of inhibition to the receptor-histidine kinase, AgrC. *Proc. Natl. Acad. Sci. U. S. A.* **2000**, *97* (24), 13330-5.
49. Gordon, C. P.; Olson, S. D.; Lister, J. L.; Kavanaugh, J. S.; Horswill, A. R., Truncated Autoinducing Peptides as Antagonists of *Staphylococcus lugdunensis* Quorum Sensing. *J. Med. Chem.* **2016**, *59* (19), 8879-8888.
50. Orsi, R. H.; Wiedmann, M., Characteristics and distribution of *Listeria* spp., including *Listeria* species newly described since 2009. *Appl. Microbiol. Biotechnol.* **2016**, *100* (12), 5273-87.
51. Schardt, J.; Jones, G.; Muller-Herbst, S.; Schauer, K.; D'Orazio, S. E. F.; Fuchs, T. M., Comparison between *Listeria sensu stricto* and *Listeria sensu lato* strains identifies novel determinants involved in infection. *Sci. Rep.* **2017**, *7* (1), 17821.
52. Lyon, G. J.; Wright, J. S.; Muir, T. W.; Novick, R. P., Key determinants of receptor activation in the agr autoinducing peptides of *Staphylococcus aureus*. *Biochemistry* **2002**, *41* (31), 10095-104.
53. Wright, J. S., 3rd; Lyon, G. J.; George, E. A.; Muir, T. W.; Novick, R. P., Hydrophobic interactions drive ligand-receptor recognition for activation and inhibition of staphylococcal quorum sensing. *Proc. Natl. Acad. Sci. U. S. A.* **2004**, *101* (46), 16168-73.
54. Tal-Gan, Y.; Ivancic, M.; Cornilescu, G.; Blackwell, H. E., Characterization of structural elements in native autoinducing peptides and non-native analogues that permit the differential modulation of AgrC-type quorum sensing receptors in *Staphylococcus aureus*. *Org. Biomol. Chem.* **2016**, *14* (1), 113-21.
55. Johnson, J. G.; Wang, B.; Debelouchina, G. T.; Novick, R. P.; Muir, T. W., Increasing AIP Macrocycle Size Reveals Key Features of agr Activation in *Staphylococcus aureus*. *ChemBioChem* **2015**, *16* (7), 1093-100.

56. Duan, C.; Zhu, L.; Xu, Y.; Lau, G. W., Saturated alanine scanning mutagenesis of the pneumococcus competence stimulating peptide identifies analogs that inhibit genetic transformation. *PLoS One* **2012**, *7* (9), e44710.
57. Yang, Y.; Koirala, B.; Sanchez, L. A.; Phillips, N. R.; Hamry, S. R.; Tal-Gan, Y., Structure-Activity Relationships of the Competence Stimulating Peptides (CSPs) in *Streptococcus pneumoniae* Reveal Motifs Critical for Intra-group and Cross-group ComD Receptor Activation. *ACS Chem. Biol.* **2017**, *12* (4), 1141-1151.
58. Bikash, C. R.; Tal-Gan, Y., Structure Activity Relationship Study of the XIP Quorum Sensing Pheromone in *Streptococcus mutans* Reveal Inhibitors of the Competence Regulon. *ACS Chem. Biol.* **2020**, *15* (10), 2833-2841.
59. Tal-Gan, Y.; Ivancic, M.; Cornilescu, G.; Yang, T.; Blackwell, H. E., Highly Stable, Amide-Bridged Autoinducing Peptide Analogues that Strongly Inhibit the AgrC Quorum Sensing Receptor in *Staphylococcus aureus*. *Angew. Chem. Int. Ed. Engl.* **2016**, *55* (31), 8913-7.
60. Vasquez, J. K.; Blackwell, H. E., Simplified Autoinducing Peptide Mimetics with Single-Nanomolar Activity Against the *Staphylococcus aureus* AgrC Quorum Sensing Receptor. *ACS Infect. Dis.* **2019**, *5* (4), 484-492.
61. Kirchdoerfer, R. N.; Garner, A. L.; Flack, C. E.; Mee, J. M.; Horswill, A. R.; Janda, K. D.; Kaufmann, G. F.; Wilson, I. A., Structural basis for ligand recognition and discrimination of a quorum-quenching antibody. *J. Biol. Chem.* **2011**, *286* (19), 17351-8.
62. Rodriguez-Lopez, P.; Rodriguez-Herrera, J. J.; Vazquez-Sanchez, D.; Lopez Cabo, M., Current Knowledge on *Listeria monocytogenes* Biofilms in Food-Related Environments: Incidence, Resistance to Biocides, Ecology and Biocontrol. *Foods* **2018**, *7* (6).
63. Galie, S.; Garcia-Gutierrez, C.; Miguelez, E. M.; Villar, C. J.; Lombo, F., Biofilms in the Food Industry: Health Aspects and Control Methods. *Front. Microbiol.* **2018**, *9*, 898.
64. Zetzmann, M.; Okshevsky, M.; Endres, J.; Sedlag, A.; Caccia, N.; Auchter, M.; Waidmann, M. S.; Desvaux, M.; Meyer, R. L.; Riedel, C. U., DNase-Sensitive and -Resistant Modes of Biofilm Formation by *Listeria monocytogenes*. *Front. Microbiol.* **2015**, *6*, 1428.
65. Merritt, J. H.; Kadouri, D. E.; O'Toole, G. A., Growing and analyzing static biofilms. *Curr. Protoc. Microbiol.* **2005**, *Chapter 1*, Unit 1B 1.

66. Blanco-Canosa, J. B.; Dawson, P. E., An efficient Fmoc-SPPS approach for the generation of thioester peptide precursors for use in native chemical ligation. *Angew. Chem. Int. Ed. Engl.* **2008**, *47* (36), 6851-5.
67. Madeira, F.; Park, Y. M.; Lee, J.; Buso, N.; Gur, T.; Madhusoodanan, N.; Basutkar, P.; Tivey, A. R. N.; Potter, S. C.; Finn, R. D.; Lopez, R., The EMBL-EBI search and sequence analysis tools APIs in 2019. *Nucleic Acids Res.* **2019**, *47* (W1), W636-W641.
68. Simon, R.; Priefer, U.; Pühler, A., A Broad Host Range Mobilization System for In Vivo Genetic Engineering: Transposon Mutagenesis in Gram Negative Bacteria. *Biotechnology. (N. Y.)* **1983**, *1* (9), 784-791.
69. Wirth, R.; An, F. Y.; Clewell, D. B., Highly efficient protoplast transformation system for *Streptococcus faecalis* and a new *Escherichia coli*-*S. faecalis* shuttle vector. *J. Bacteriol.* **1986**, *165* (3), 831-6.

Chapter 3:

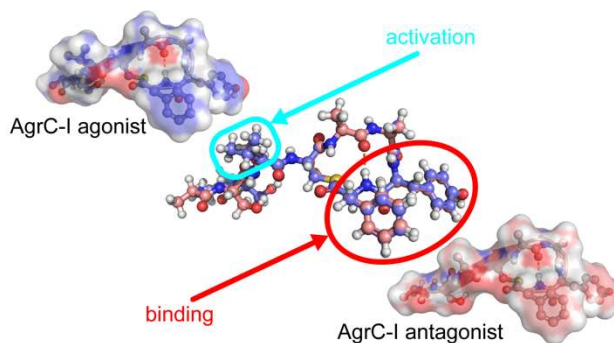
Conformational Switch to a β -turn in a Staphylococcal Quorum Sensing Signal Peptide Causes a Dramatic Increase in Potency

Contributions: J. K. Vasquez designed and conducted NMR experiments to characterize peptide 3-D conformations and wrote chapter sections on NMR analysis. K. H. J. West synthesized and assayed novel β -turn modifying peptides, assisted in NMR characterization, and wrote chapter sections on novel peptide activity. T. Yang assisted in NMR characterization. T. Polaske assisted in peptide preparation. G. Cornilescu and M. Tonelli assisted with technical expertise. H. E. Blackwell guided research and assisted in writing.

*This chapter is published under the same title:

Vasquez, J. K.; West, K. H. J.; Yang, T.; Polaske, T. J.; Cornilescu, G.; Tonelli, M.; Blackwell, H. E. Conformational switch to a β -turn in a Staphylococcal quorum sensing signal peptide causes a dramatic increase in potency. *J. Am. Chem. Soc.* **2020**, *142*, 750-761.

Abstract



We report the solution-phase structures of native signal peptides and related analogs capable of either strongly agonizing or antagonizing the AgrC quorum sensing (QS) receptor in the emerging pathogen *Staphylococcus epidermidis*. Chronic *S. epidermidis* infections are often recalcitrant to traditional therapies due to antibiotic resistance and formation of robust biofilms. The accessory gene regulator (*agr*) QS system plays an important role in biofilm formation in this opportunistic pathogen, and the binding of an autoinducing peptide (AIP) signal to its cognate transmembrane receptor (AgrC) is responsible for controlling *agr*. Small molecules or peptides capable of modulating this binding event are of significant interest as probes to investigate both the *agr* system and QS as a potential antivirulence target. We used NMR spectroscopy to characterize the structures of the three native *S. epidermidis* AIP signals and five non-native analogs with distinct activity profiles in the AgrC-I receptor from *S. epidermidis*. These studies revealed a suite of structural motifs critical for ligand activity. Interestingly, a unique β -turn was present in the macrocycles of the two most potent AgrC-I modulators—in both an agonist and an antagonist—that was distinct from the macrocycle conformation in the less-potent AgrC-I modulators and in the native AIP-I itself. This previously unknown β -turn provides a structural rationale for these ligands'

respective biological activity profiles. Development of analogs to reinforce the β -turn resulted in our first antagonist with subnanomolar potency in AgrC-I, while analogs designed to contain a disrupted β -turn were dramatically less potent relative to their parent compounds. Collectively, these studies provide new insights into the AIP:AgrC interactions crucial for QS activation in *S. epidermidis* and advance the understanding of QS at the molecular level.

3.1 Introduction

Staphylococcus epidermidis is a ubiquitous, skin-colonizing Gram-positive bacterium¹ that has emerged as an opportunistic pathogen in many hospital acquired infections.²⁻³ This bacterium is now a leading cause of biomedical device-associated infections due to its propensity to form robust biofilms on abiotic surfaces.³⁻⁸ This biofilm lifestyle, combined with its increasing antibiotic resistance, makes treating *S. epidermidis* infections with traditional antibacterial drugs difficult.^{2-3, 6, 9-11} Playing an important role in the pathogenesis of *S. epidermidis* infections is the accessory gene regulator (*agr*) system,¹²⁻¹⁷ a cell-cell communication system that allows the bacteria to sense population density and coordinate gene expression at high cell numbers to initiate group behaviors.¹⁸⁻¹⁹ This cell-cell signaling process is a type of quorum sensing (QS, Figure 3.1) and is mediated in *S. epidermidis* by a macrocyclic peptide pheromone called an autoinducing peptide (AIP).²⁰⁻²³ As the bacterial population density increases, so does the concentration of the AIP. Once a threshold concentration is reached, the AIP can productively bind with its cognate receptor AgrC, a transmembrane histidine kinase, which subsequently initiates the signaling cascade that leads to changes in gene expression.²²

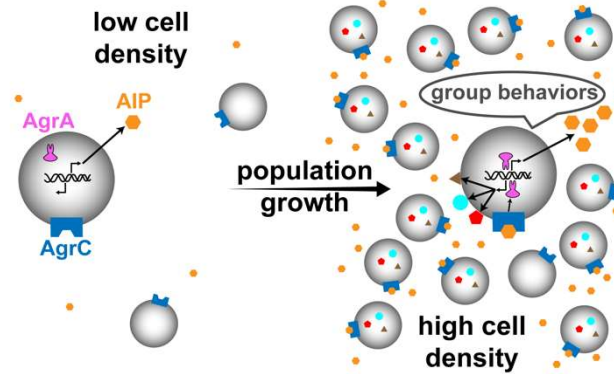


Figure 3.1 Schematic of the QS process in *S. epidermidis*. At low cell density, the QS signal (AIP) is produced at a low level. As the population grows, the corresponding AIP concentration increases until the AIP reaches a threshold level at which it productively binds to AgrC. This AIP:AgrC binding event then activates the response regulator AgrA to simultaneously amplify expression of *agr* and alter gene expression to drive group-beneficial behaviors.

As a number of phenotypes associated with *S. epidermidis* virulence, such as the production of phenol-soluble modulins and biofilms, are under the direct control of QS,^{11-14, 24-28} targeting the *agr* system represents an attractive approach for studying the role of QS in infection and even possibly attenuating *S. epidermidis* infections.^{25, 29-32} This strategy has been used in *Staphylococcus aureus*, a pathogen closely related to *S. epidermidis* with an analogous *agr* QS system, and prior studies by our lab and others have revealed several highly potent, non-native antagonists of the *agr* system in *S. aureus*.³³⁻⁴⁸ Similar to *S. aureus*, *S. epidermidis* has evolved into different *agr* specificity groups (I–III), each with a different AIP signal and some variability in the other components of the *agr* system (i.e., in proteins AgrB–D).^{30, 49} Interestingly, these AIP signals are also capable of either inhibiting or activating the receptors of the other *S. epidermidis* groups, motivating hypotheses about cross-group interactions mediated by QS. For example, AIP-II and AIP-III each inhibit AgrC-I, while AIP-I inhibits both AgrC-II and AgrC-III (AIP signals shown in Figure 3.2).³⁰ Synthetic ligands that selectively

activate or inhibit each of these receptors, or that pan-activate or pan-inhibit all receptors, would represent valuable chemical probes to interrogate the nature of such possible cross-group interactions, and to study *agr*-based QS in general.

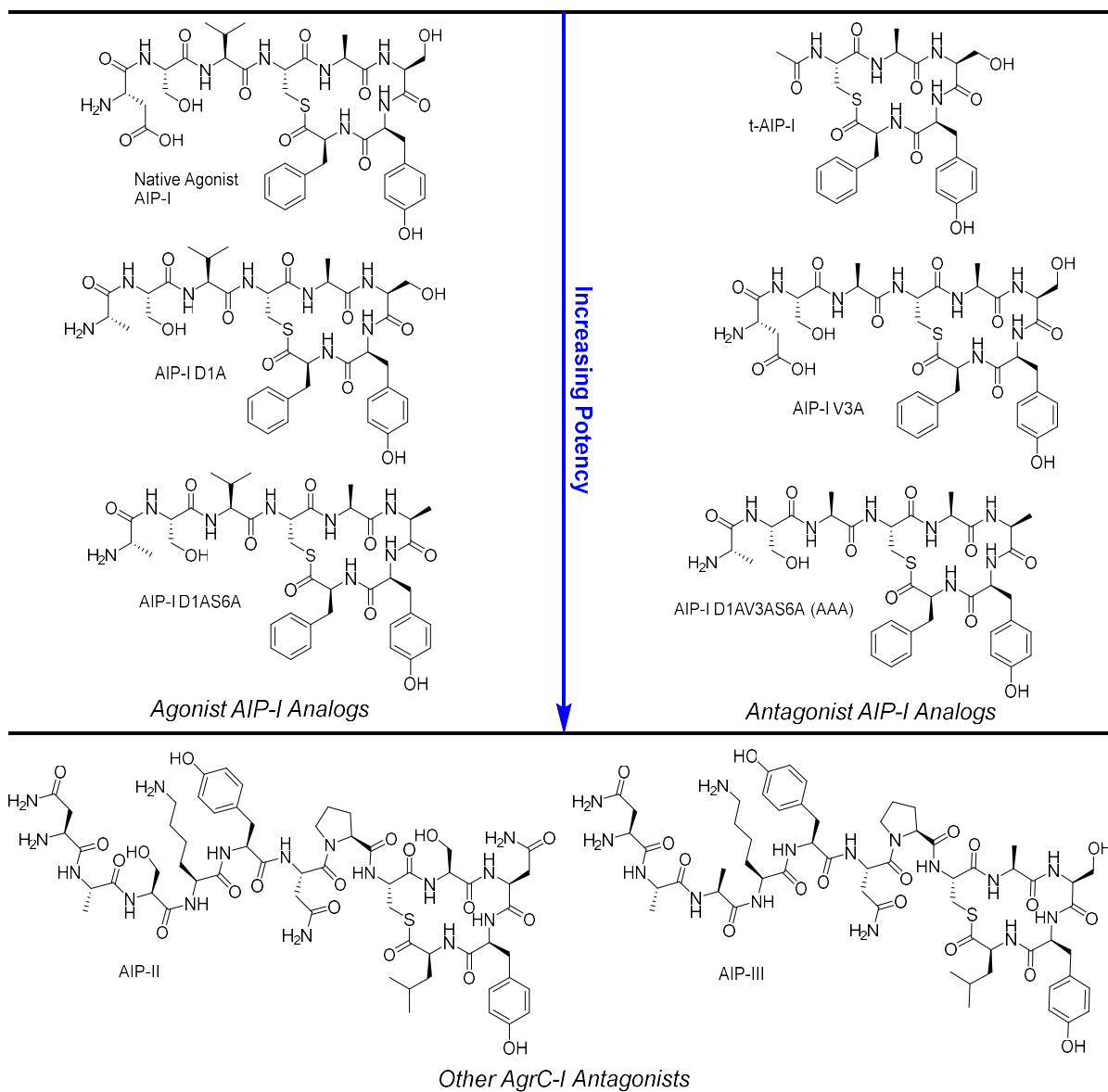


Figure 3.2 Structures of the native *S. epidermidis* AIP signals (I–III) and AIP-I analogs examined in this study. Relative potency in the QS receptor AgrC-I is indicated with the arrow for AIP-I analogs. Relative potencies indicated are from cell-based assays of AgrC-I activity reported in our previous work.⁵⁰

Recently, our laboratory performed a systematic study of the structure of the AIP-I signal from group-I *S. epidermidis*, and using cell-based assays reporting *agr* activity, delineated the structure-activity relationships (SARs) governing its ability to activate its cognate receptor, AgrC-I.⁵⁰ This study revealed the first set of non-native AIP analogs that are capable of potently agonizing or antagonizing the *agr* system in *S. epidermidis* (selected peptides shown in Figure 3.2). However, we lack an understanding of how these activity data connect to the three-dimensional (3-D) structures of these peptides. Such a connection, assuming that these small and rigidified macrocyclic peptides can adopt a similar conformation upon binding to AgrC-I, would illuminate the chemical features crucial to AgrC-I receptor agonism or antagonism by these peptides, and provide new insights into their mechanisms of action. To date, only the solution-phase structure of the *S. epidermidis* AIP-I has been reported in a mixed-solvent system,⁵¹ and the analysis of this structure focused on the motifs important for interaction with the *S. aureus* AgrC receptors, not with *S. epidermidis* AgrC-I. To the best of our knowledge, no structural information on any *S. epidermidis* AIP analogs has been reported.

Herein, we report the first detailed characterization of the 3-D solution-phase structures of the *S. epidermidis* AIP-I signal, several non-native AIP-I analogs capable of strongly modulating AgrC-I, and the *S. epidermidis* AIP-II and AIP-III signals using NMR spectroscopy. Comparison of these peptide structures revealed several features that we propose, when aligned with their cell-based activity profiles, to be critical to receptor binding and activation, including a β -turn motif that was present in the macrocycles of both the most potent agonist and the most potent antagonist ligands, yet lacking in less potent ligands, including the native AIP-I signal. Our structural data

suggest that a minimum of two endocyclic hydrophobic residues and the presence and specific orientation of a C-terminal hydrophobic group are necessary for activation of AgrC-I. Together, these structural analyses illuminate the mechanism of both AgrC-I agonism and antagonism by peptide ligands, and motivate new hypotheses on the modularity of the receptor-binding and receptor-activating motifs of AIP-I. A small set of second-generation analogs designed to strengthen or weaken the β -turn were synthesized based upon these findings, resulting in analogs with comparable or greatly diminished potency relative to the parent peptides, respectively. These studies also revealed the first AgrC-I antagonist with subnanomolar potency. The effects of these β -turn alterations on potency represent proof-of-concept and validation for structure-function studies such as this one.

3.2 Results and Discussion

3.2.1 Selection of peptides for structural analyses

To start, we selected a series of non-native AIP-I analogs from our previous study that displayed a range of agonistic and antagonistic activity in AgrC-I as determined utilizing a *S. epidermidis* GFP reporter strain (Figure 3.2; Table 3.1).⁵⁰ We chose two agonists that were more potent than the native AIP-I signal: AIP-I D1A, in which a single Asp to Ala modification gave a four-fold increase in potency, and AIP-I D1AS6A, in which the double Ala modification gave a 20-fold increase in potency. We envisioned that comparisons between these two AIP-I analogs and the native AIP-I could provide insights into how the Ala substitutions increased agonism potency. We also selected three AgrC-I antagonists that displayed moderate to strong antagonism

potencies (Table 3.1). This trio included t-AIP-I, in which the N-terminal tail was removed and the Cys residue was simply acetylated; AIP-I V3A, in which a single modification to the native AIP-I (Val to Ala) mode-switched its activity from agonist to antagonist; and the triple Ala modified peptide, AIP-I D1AV3AS6A (hereafter referred to as AAA), which is a highly potent antagonist with a single-digit nanomolar IC₅₀ value. As the *S. epidermidis* AIP-II and AIP-III signals are also relatively strong antagonists of AgrC-I (Table 3.1), we included these native peptides in our structural studies. To facilitate these comparative studies, we also chose to determine the NMR structure of the native AIP-I under comparable experimental conditions. All of these native and non-native peptides were prepared and purified to homogeneity using the methods in our prior study.⁵⁰

Table 3.1 Structures and cell-based reporter activities in AgrC-I of the peptides evaluated in this study.^a CI= 95% confidence interval.

peptide name	sequence	IC ₅₀ in nM, (95% CI)	EC ₅₀ in nM, (95% CI)
AIP-I	D-S-V-(C-A-S-Y-F)	–	196 (162–238)
AIP-I D1A	A-S-V-(C-A-S-Y-F)	–	49.3 (43.3–56.2)
AIP-I D1AS6A	A-S-V-(C-A-A-Y-F)	–	10.3 (6.18–17.2)
t-AIP-I	Ac-(C-A-S-Y-F)	192 (150–245)	–
AIP-I V3A	D-S-A-(C-A-S-Y-F)	51.9 (37.9–71.0)	–
AAA	A-S-A-(C-A-A-Y-F)	2.84 (1.95–4.11)	–
AIP-II	N-A-S-K-Y-N-P-(C-S-N-Y-L)	9.64 (7.99–11.6)	–
AIP-III	N-A-A-K-Y-N-P-(C-A-S-Y-L)	34.3 (31.4–37.4)	–

^aValues from reference 50.

3.2.2 NMR analyses

We used NMR spectroscopy to characterize the solution-phase structures of the peptides, using methods similar to our prior reports (see SI for full details).^{43, 51-52} The 1-D and 2-D (TOCSY and ROESY) NMR spectra were obtained on a 750 MHz spectrometer equipped with a cryoprobe at ambient temperature in H₂O/D₂O (95:5) except for AIP-I and t-AIP-I, which were dissolved in H₂O/CD₃CN (8:1 and 7:3, respectively) due to solubility limitations. Previous studies of similar *S. aureus* AgrC modulators showed that the presence of these amounts of acetonitrile did not cause significant structural changes relative to structures obtained in water alone.⁴³ The 1-D proton and 2-D TOCSY and ROESY spectra were used to determine chemical shifts via sequential assignments of each amino acid residue. Internuclear proton distances were determined from 2-D ROESY cross peaks and converted to distance constraint files. These files were used to calculate and refine 3-D structures using torsion angle simulated annealing through Xplor-NIH,⁵³⁻⁵⁴ and an ensemble of 20 lowest-energy structures was utilized to determine the most representative low energy structure (ensembles in SI Figures 3.S1–3.S8). Structure comparisons were performed with alignment fitting using PyMOL.⁵⁵

3.2.3 Structural comparison of AIP-I to the antagonist t-AIP-I

The NMR experimental results for AIP-I and t-AIP-I were compared first. Again, t-AIP-I lacks the N-terminal tail and is a moderate antagonist of AgrC-I (Table 3.1). Analogous ROESY cross peaks appeared in both spectra, with extremely similar coupling constants and chemical shifts for all analogous hydrogens (see SI; Tables

3.S1, 3.S2, 3.S9, and 3.S10). The ROEs observed for AIP-I revealed an almost identical macrocycle conformation compared to t-AIP-I, as illustrated in the overlay in Figure 3.3C. The structures align with an RMS difference of 0.3 Å for all analogous atoms. This close structural similarity between native AIP-I and the antagonist t-AIP-I suggests that while the tail in AIP-I has little impact on the structure of the macrocycle, it contains a contact critical for AgrC activation. When missing, as in t-AIP-I, the ligand is capable of competitively binding to AgrC-I yet fails to activate the receptor.

Several features from the comparative analyses of AIP-I and t-AIP-I are important and warrant discussion. First, Asp1 and Ser2 of the AIP-I tail do not have well-defined conformations (see ensembles in SI Figure 3.S1), despite the rigidified conformation of its macrocycle (Figure 3.3; SI Figure 3.S1). Second, the spectra suggest that the Ser in the macrocycle of both peptides adopts a conformation where the hydroxyl oxygen forms a hydrogen bond to the adjacent Tyr amide hydrogen. This finding is aligned with the well-established propensity of short, polar sidechains such as Ser and Thr for this interaction.⁵⁶⁻⁵⁷ The result of this hydrogen bond is the formation of a half-chair six-member ring, and we reason that this ring acts to stabilize the macrocycle. Third, our structures of AIP-I and t-AIP show the side chains of both of the endocyclic hydrophobic residues (Phe and Tyr) oriented away from the macrocycle to form a hydrophobic face (Figure 3.3). This observation supports the conclusions of prior SAR studies of AIPs in both *S. aureus* and *S. epidermidis* that implicate a hydrophobic face as critical for productive AgrC binding.^{36, 42, 50, 52, 58} Indeed, removal of these hydrophobic residues from the macrocycle completely ablates AIP-I activity.⁵⁰ Fourth, the Cys and Phe sidechains adopt well-defined rotational conformations, while the Tyr

sidechain appears to be less restricted. This last trend was observed for all the peptides studied in this work.

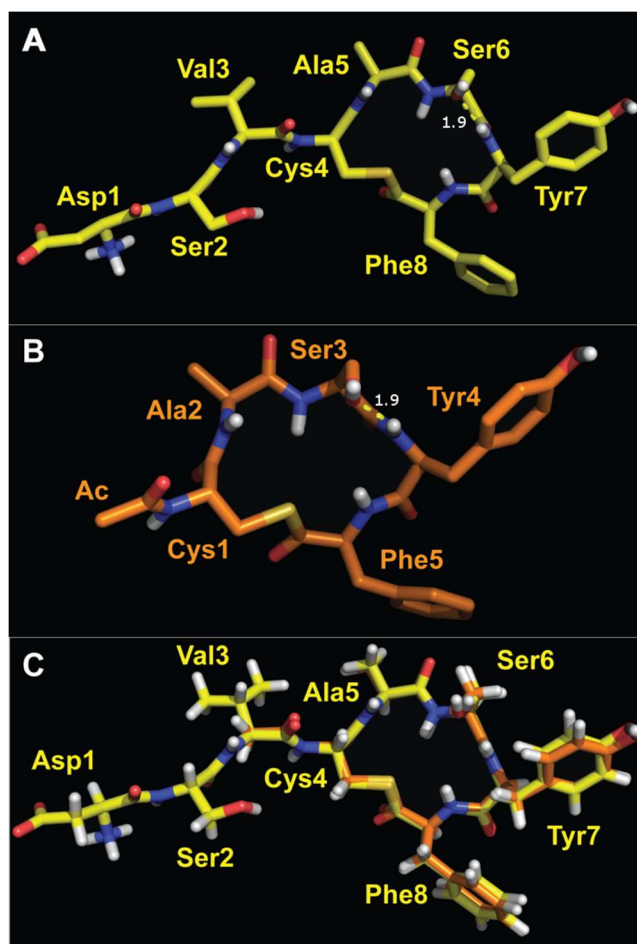


Figure 3.3 Representative structures of AIP-I and t-AIP-I. Conformations of AIP-I (A) and t-AIP-I (B). Oxygen is shown in red, nitrogen in blue, hydrogen in white, and sulfur in gold. (C) Overlay of AIP-I (in yellow) and t-AIP-I (in orange, with an all-atom RMS difference of 0.3 Å (72 atoms).

3.2.4 Structural comparison of AIP-I to the antagonist AIP-I V3A

We next compared the structure of native AIP-I to the antagonist AIP-I V3A (Figure 3.4), which is approximately four-fold more potent than t-AIP-I (Table 3.1) and has a single amino acid modification (Val to Ala) relative to native AIP-I.⁵⁰ This activity

mode-switch (agonist to antagonist) suggests that Val3 may play an important role in dictating the active conformation of the native signal or makes a crucial contact with the receptor. Interestingly, when examining the structure of AIP-I, Val3 is directed in the opposite direction of its endocyclic hydrophobic face (composed of Tyr7 and Phe8), as shown in Figures 3.3A, 3.3C.

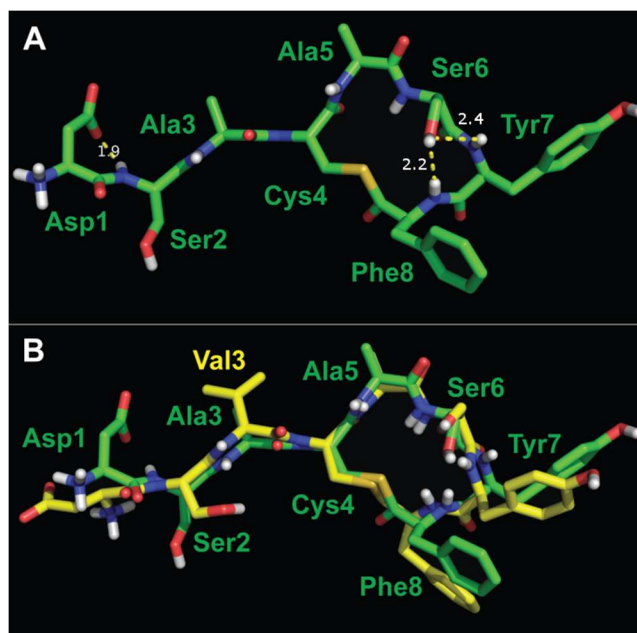


Figure 3.4 Structure of AIP-I V3A. (A) Representative structure of AIP-I V3A. Atom colors analogous to Figure 3.3. (B) Overlay of AIP-I (in yellow) and AIP-I V3A (in green), having an all-atom RMS difference of 2.1 Å (79 atoms) for residues 3–8.

The ensemble of AIP-I V3A from Xplor has the highest RMSD of the peptides analyzed in this study, but like AIP-I, the structure of the macrocycle and relative position of residue 3 were highly ordered while Asp1 and Ser2 were the most disordered (SI Figure 3.S3). Also similar to AIP-I, the hydrophobic residues (Phe8 and Tyr7) of AIP-I V3A were extended towards one face of the macrocycle and create a hydrophobic surface (Figure 3.4A), and the Ser6 hydroxyl to Tyr7 amide hydrogen bond

appears to be maintained as a stabilizing interaction of the macrocycle. While the isopropyl side chain of Val3 is replaced with a methyl side chain in AIP-I V3A, the orientation of the Ala side chain relative to the hydrophobic face of the macrocycle is conserved (Figure 3.4B). Therefore, the structures of native AIP-I and AIP-I V3A are highly similar, having an all-atom RMS difference for residues 3–8 (excluding the more disordered hydrophilic N-terminal residues) of 2.1 Å (79 atoms), and an RMS difference for the backbone of only 0.8 Å (24 atoms). In view of these data, we propose that the lack of the branched hydrophobic side chain of residue Val3 (as in AIP-I V3A) is the primary cause for switching AIP-I from an agonist to an antagonist, with little or no dependence on conformational changes. We reason that the Val3 side chain in AIP-I makes a key contact with AgrC-I that is essential for activation, and in its absence, AIP-I V3A competitively inhibits AgrC-I.

3.2.5 Structural comparison of AIP-I to agonists with increased potency

Next, we turned our attention to the structures of two non-native agonists of AgrC-I, AIP-I D1A and AIP-I D1AS6A (Figures 3.5A and 3.5B). Both analogs are more potent agonists than the native agonist AIP-I (Table 3.1), with AIP-I D1AS6A being the most potent non-native agonist targeting *S. epidermidis* AgrC-I reported to date.⁵⁰ Counterintuitively in view of their less polar primary structures, AIP-I D1A and AIP-I D1AS6A were found to be more soluble in water than AIP-I, and their corresponding NMR spectra reflected that difference with higher S/N. Regardless, representative structures of the native AIP-I and AIP-I D1A were found to be exceptionally similar (overlay in Figure 3.5C), having an all-atom RMS difference of 1.3 Å (99 atoms) and a

backbone-atom RMS difference of 0.5 Å (28 atoms). While the ROESY spectrum of AIP-I indicated disorder in Asp1 and Ser2 (see above), the ROESY spectrum of AIP-I D1A had more cross peaks related to Ala1 and Ser2, yielding a more defined structure from Xplor (SI Figure 3.S4). It seemed possible that this was simply due to the greater S/N of the AIP-I D1A sample, but a closer examination of the AIP-I spectrum revealed that other small ROE cross peaks were visible, suggesting the issue was not S/N, but rather a true disorder in Asp1 and Ser2. In view of their highly similar structures, we speculate that the more ordered tail of AIP-I D1A relative to AIP-I contributes to its heightened agonistic activity, presumably better positioning an activation motif therein.

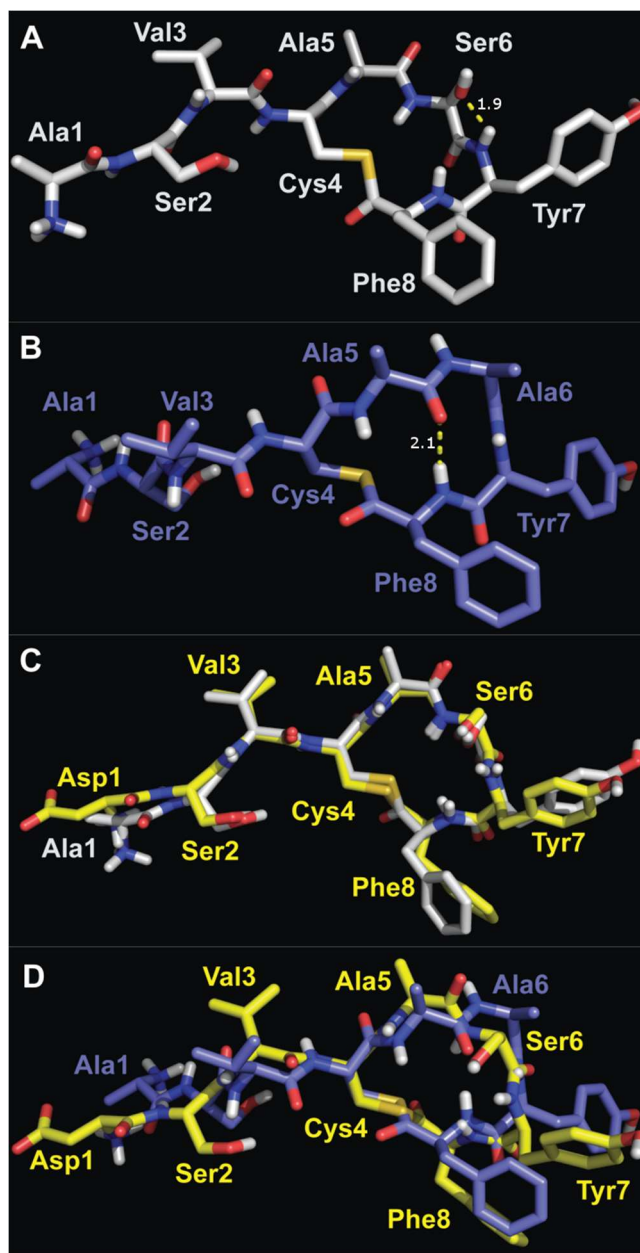


Figure 3.5 Representative structures of AIP-I D1A (A) and AIP-I D1AS6A (B). Atom colors analogous to Figure 3.3. The characteristic hydrogen bond of a β -turn is indicated, with $i+1$ $\phi = 63^\circ$ and $\psi = -88^\circ$, $i+2$ $\phi = -125^\circ$ and $\psi = 16^\circ$ (in B). (C) Overlay of AIP-I (in yellow) and AIP-I D1A (in white), with an all-atom RMS difference of 1.3 Å (99 atoms). (D) Overlay of AIP-I (in yellow) and AIP-I D1AS6A (in dark blue), with an all-atom RMS difference of 3.6 Å (97 atoms).

The structural similarity between AIP-I and the more potent agonist AIP-I D1AS6A, with an all-atom RMS difference of 3.6 Å (97 atoms), was less than that

between AIP-I and AIP-I D1A. The differences originate from conformational changes in the AIP-I D1AS6A macrocycle. AIP-I D1AS6A has an Ala residue in place of Ser6, and thus no hydrogen bond is possible between the Ser6 hydroxyl and Tyr7 amide hydrogen. Instead, the AIP-I D1AS6A macrocycle was observed to adopt a β -turn motif with the Ala5 carbonyl H-bonded to the Phe8 HN (Figure 3.5B). Analysis of the appropriate ϕ and ψ angles revealed the turn was a type II' β -turn.⁵⁹ The ROESY spectrum for AIP-I D1AS6A also featured several major differences in cross peaks that were analogous in the spectra of each of the other peptides compared up to this point. For example, in these latter spectra, an ROE existed between Ser6 H α and Ser6 NH that was calculated at 2.5 or 2.6 Å. In the spectrum of AIP-I D1AS6A, however, this ROESY cross peak was much more intense, with a calculated value of 2.2 Å. This difference indicates a dissimilar ϕ -dihedral angle at Ala6 in AIP-I D1AS6A. Additionally, what was observed as a moderate cross peak between Ser6 HN and Phe8 HN in the AIP-I D1A spectrum, which only differs by a single amino acid from AIP-I D1AS6A, was a weak cross peak between Ala6 HN and Phe8 HN in the AIP-I D1AS6A spectrum, indicating a difference in the plane of the amide bond of Ala5 and Ala6. This difference brings the carbonyl of the amide bond into the center of the AIP-I D1AS6A macrocycle, allowing for formation of the hydrogen bond to the Phe8 HN (Figure 3.5B). This hydrogen bond then stabilizes the β -turn in the macrocycle of AIP-I D1AS6A.

This alteration to the macrocycle in AIP-I D1AS6A caused a change in the way the exocyclic tail protrudes from the macrocycle, and brought the Val3 sidechain to the same face as the hydrophobic endocyclic sidechains. The tails of AIP-I and related analogs studied so far form a short β -strand that is connected to the macrocycle,

comprised of Ser2 to Ala5. As Ala5 in AIP-I D1AS6A has a major change in its conformation, the strand exiting the macrocycle is rotated by roughly 60° relative to AIP-I. Given that the hydrophobic sidechain of Val3 is strongly implicated as an effector of agonism in these peptides (see above), and also that AIP-I D1AS6A is 20-fold more potent than AIP-I and 5-fold more potent than AIP-I D1A, we reason that the macrocyclic fold *and* corresponding change of orientation of Val3 in AIP-I D1AS6A make this ligand more efficacious for binding and activating AgrC-I.

3.2.6 Structural comparison of AIP-I to the antagonist AAA

To further examine the relationships between the macrocycle conformation, the potency of the peptide, and the presence of the hydrophobic sidechain of Val3, we determined the structure of the most potent AgrC-I antagonist from our previous study, peptide AAA (Table 3.1). Xplor outputted a very ordered ensemble from the AAA constraint file (SI Figure 3.S6), and strikingly, a β -turn in the macrocycle was observed that was closely analogous to that of agonist AIP-I D1AS6A. Indeed, just as many ROESY cross peaks were analogous between the spectra of AIP-I, t-AIP-I, AIP-I V3A, and AIP-I D1A, the ROESY cross peaks of the antagonist AAA and the agonist AIP-I D1AS6A were equally analogous, with patterns suggesting the same type II' β -turn in the macrocycle and the same short β -strand exiting the macrocycle in a similar manner. A representative structure of AAA is shown in Figure 3.6A, with an overlay of AIP-I and AAA having a relatively large all-atom RMS difference of 3.4 Å (88 atoms) shown in Figure 3.6B. This overlay is suggestive that the antagonist AAA, like the agonist AIP-I D1AS6A, adopts a structure quite different from AIP-I.

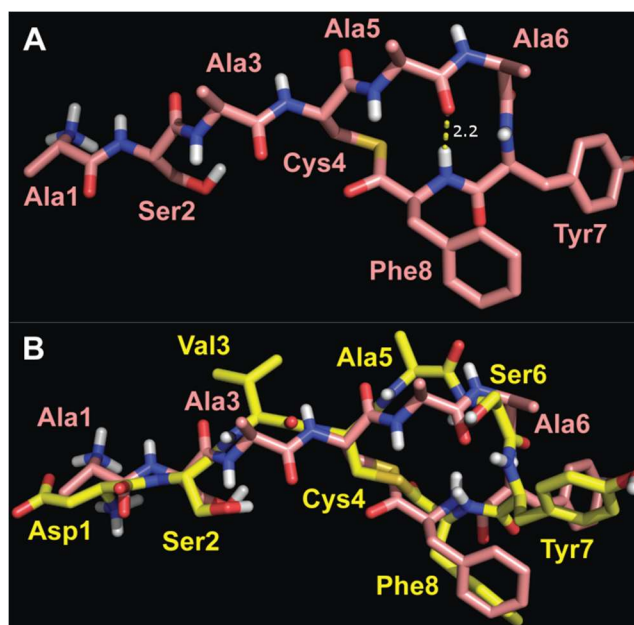


Figure 3.6 Structure of AAA and overlay with AIP-I. (A) Representative structure of AAA. Atom colors analogous to Figure 3.3. For the macrocycle β -turn, $i+1 \phi = 62^\circ$ and $\psi = -89^\circ$, $i+2 \phi = -123^\circ$ and $\psi = 18^\circ$. (B) Overlay of AIP-I and AAA, with an all-atom RMS difference of 3.4 Å (88 atoms). AIP-I is shown in yellow, and AAA is shown in pink.

3.2.7 Structures of *S. epidermidis* AIP-II and AIP-III

Because both native AIP-II and native AIP-III are also relatively potent AgrC-I antagonists, we investigated the structures of these two AIPs for comparison to the native AIP-I and antagonist AAA. AIP-II and AIP-III have similar primary sequences (Figure 3.2, Table 3.1), and their corresponding 2-D NMR spectra showed many similar cross peaks in the macrocycle region. However, a single amino acid difference in the tail sequence yielded a dramatic difference in the calculated tail structures. AIP-II has a sequence in its tail region (S-K-Y-N) that formed a β -turn (Figure 3.7A), indicated strongly by a robust series of cross peaks in the ROESY spectrum. In AIP-III, the corresponding sequence is A-K-Y-N, and the ROESY spectrum in this region instead indicated a β -stand from residue 2 through residue 9 within the ring, with no i to $i+3$

cross peaks analogous to the β -turn as indicated in AIP-II (Figure 3.7B). Overall, AIP-II was more globular, with the tail folding around the macrocycle but not quite contacting it, and AIP-III was more extended, with the strand of the tail pointing directly out from the ring. Additionally, in a comparison of the macrocycles, the plane of the amide bond between residue-10 (Asn in AIP-II and Ser in AIP-III) and Tyr11 was inverted by $\sim 180^\circ$ (Figure 3.7C).

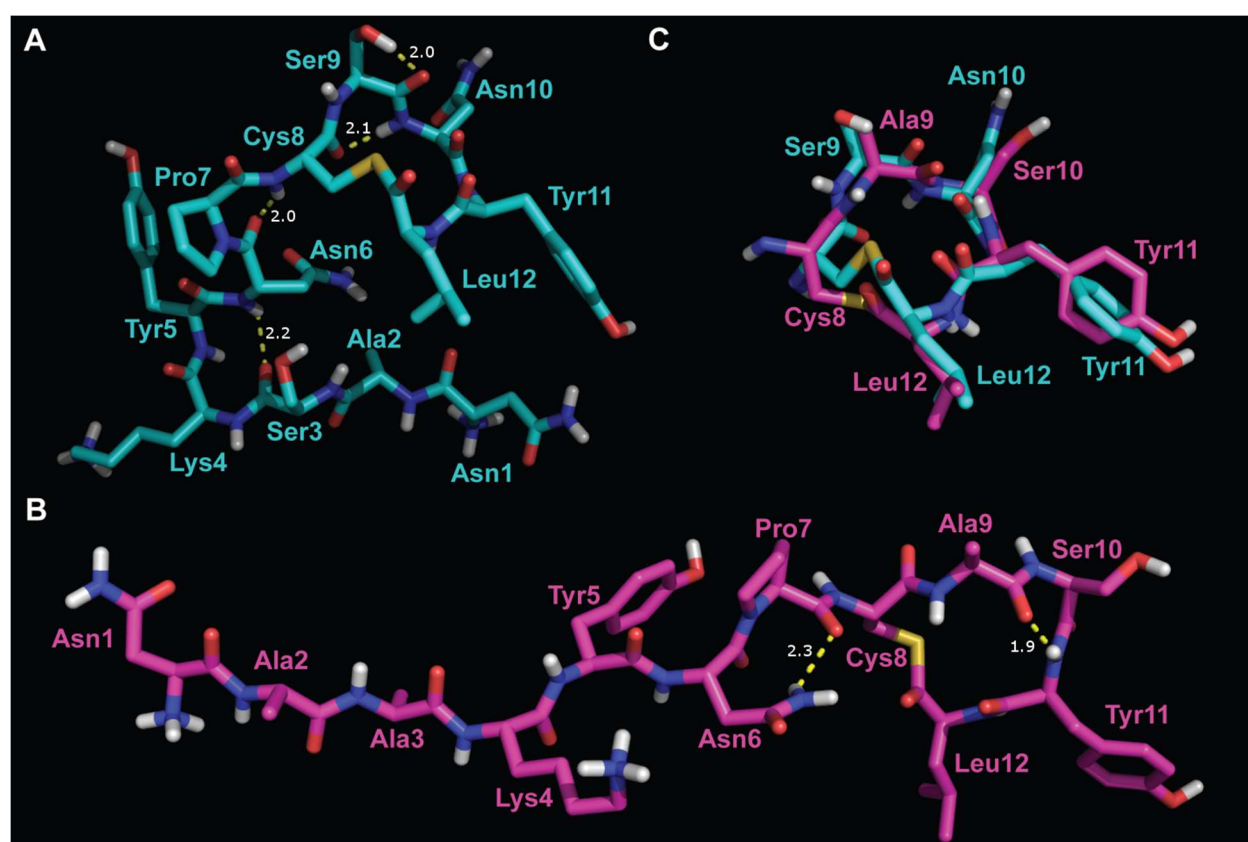


Figure 3.7 Representative structures of AIP-II (A) and AIP-III (B). Atom colors analogous to Figure 3.3. C: Overlay of AIP-II (cyan) and AIP-III (magenta) for the macrocycle only, with an all-atom RMS difference of 1.5 Å (68 atoms).

An alignment of the macrocycle of AIP-I with either AIP-II or AIP-III yields only modest overlap, having all-atom RMS differences of 2.2 Å (PyMOL fits 49 atoms) or 2.1

Å (PyMOL fits 52 atoms) respectively, for most-similar atom matching (results not shown), indicating that AIP-II and AIP-III have major 3-D structural differences in their macrocycles relative to AIP-I. In contrast, there is better overlap of the macrocycle of the antagonist AAA with that of AIP-II (all-atom RMS difference for macrocycle of 1.9 Å, of 49 atoms) and AIP-III (all-atom RMS difference of macrocycle of 1.2 Å, 50 atoms) (SI Figure 3.S9), which is in accord with all three peptides acting as AgrC-I antagonists. We return to this below.

3.2.8 Comparison of the most potent AgrC-I agonist and antagonist

Given the remarkable, and unexpected, similarity of the ROESY spectra of the most potent AgrC agonist AIP-I D1AS6A and the most potent AgrC antagonist AAA, a direct comparison of these two structures was warranted. The structural overlay is shown in Figure 3.8. Although the slight differences in ROE intensity from the spectra lead to subtle differences between the two structures, they are very similar overall, with an all-atom RMS difference of 1.0 Å (101 atoms) and a backbone RMS difference of 0.8 Å for all residues (32 atoms), or an all-atom RMS difference of just 0.2 Å (78 atoms) and a backbone RMS difference of just 0.1 Å (24 atoms) when considering only residues 3–8. To further validate the interpretation of these two solution NMR structures, they were each analyzed using MolProbity, and both AIP-I D1AS6A and AAA have very good relative clash and MolProbity scores (see MolProbity validation in SI).⁶⁰⁻⁶¹

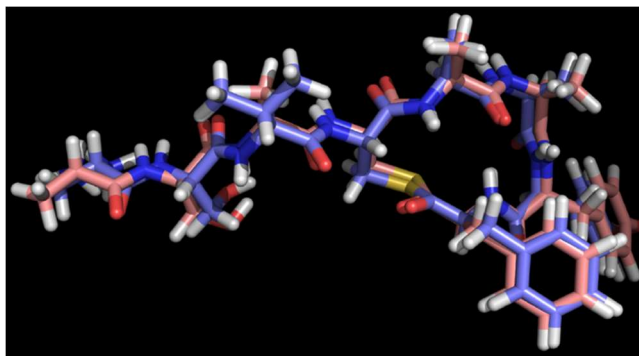


Figure 3.8 Overlay of AIP-I D1AS6A (dark blue) and AAA (pink). Overlay of the two structures has an all-atom RMS difference of 1.0 Å (101 atoms), and all-atom RMS difference for residues 3–8 of 0.2 Å (78 atoms). Atom colors analogous to Figure 3.3.

These structural data suggest that the β -turn in the macrocycles of AIP-I D1AS6A and AAA arranges them for optimal binding to AgrC-I relative to the macrocycle of the native ligand AIP-I, which lacks the same β -turn. We then speculate that the stabilizing Ser6 hydroxyl to Tyr7 amide hydrogen bond in the AIP-I macrocycle impairs it from adopting the optimal β -turn conformation for binding its own cognate receptor. This difference is correlated with the heightened potencies of AIP-I D1AS6A (as an agonist) and AAA (as an antagonist) relative to AIP-I (Table 3.1). The opposite activity profiles for AIP-I D1AS6A and AAA, despite their very similar structures, indicates that their only point of real structural divergence—the branched hydrophobic motif of the Val3 side chain—engages in critical interactions with the AgrC-I receptor, with its position dictated by the fold of the macrocycle. The Val3 sidechain is oriented more toward the hydrophobic endocyclic face of AIP-I D1AS6A relative to that of AIP-I, and this positioning of both Val3 and the hydrophobic face in AIP-I D1AS6A presumably facilitates receptor binding and activation. This model then implicates Val, and only Val positioned properly next to the ring, as essential for receptor activation. If the model is accurate, introducing a Val residue or other appropriate hydrophobic moiety next to a

different AIP macrocycle or even a β -turn mimetic could lead to new modulators that activate *S. epidermidis* AgrC-I.

3.2.9 Exploration of the β -turn motif through new analogs

We sought to further examine the importance of the β -turn motif for peptide:AgrC-I interactions in *S. epidermidis* and designed eight new analogs of AIP-I D1AS6A and AAA to modify the type II' β -turn. Substitution of Ala6 with D-Ala or Gly should strengthen the β -turn, and we hypothesized that, if the β -turn motif was indeed critical, such substitutions should either maintain or possibly enhance the agonism or antagonism potency of the two parent peptides.^{59, 62-63} Conversely, substitution of Phe8 with *N*-MePhe or phenyllactic acid (PLA) should destabilize the β -turn by removing the key hydrogen bond between the Ala5 carbonyl and Phe8 NH. We hypothesized that destabilization of the β -turn would reduce the potency of these new analogs relative to the parent peptides where the β -turn is intact. We synthesized new AIP-I D1AS6A and AAA analogs containing these modifications (shown in Figure 3.9) using standard methods and screened them in *agr* reporter assays (side-by-side with their parent peptides) in group-I *S. epidermidis* to allow for comparisons of their activity profiles (Figure 3.10, see SI for synthetic protocols and assay methods).⁵⁰

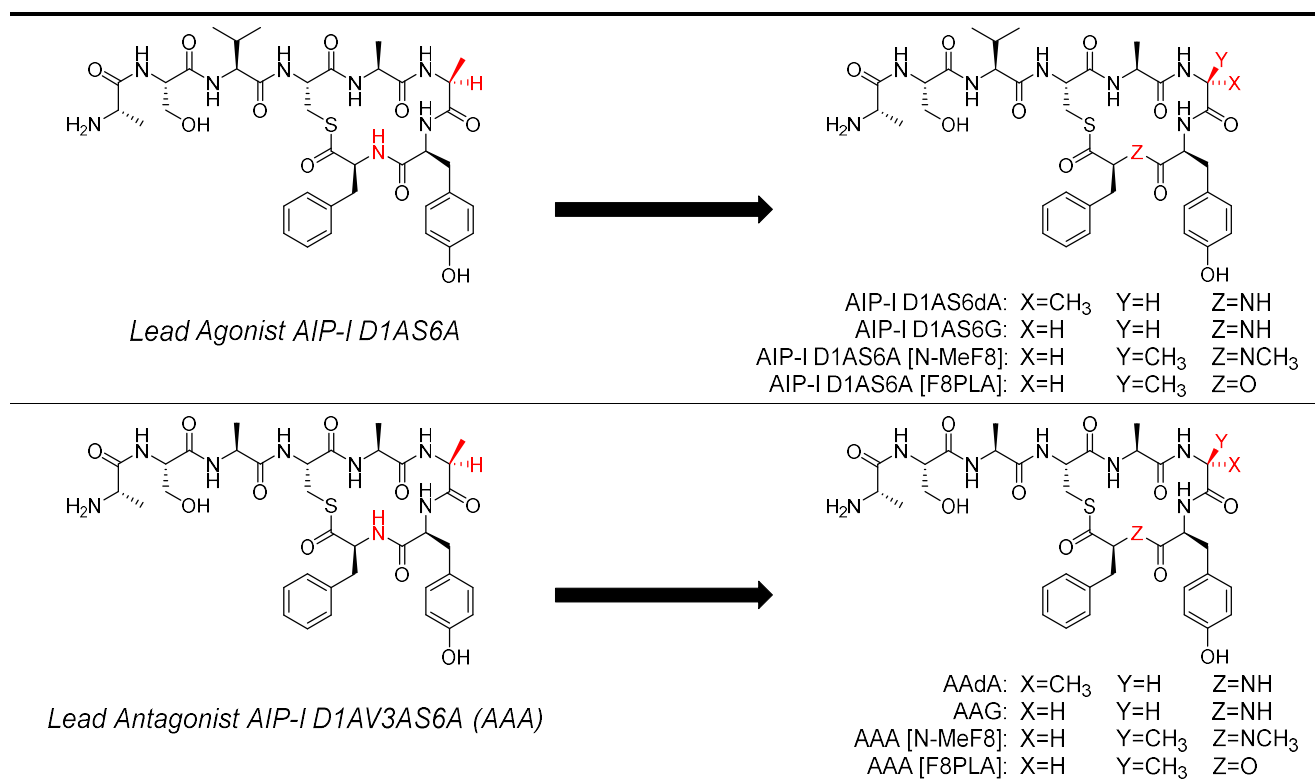


Figure 3.9 Structural modifications of lead agonist AIP-I D1AS6A and lead antagonist AAA to provide β -turn modifying analogs.

The dose-response assays for the new analogs with D-Ala and Gly substitutions, which should strengthen or maintain the β -turn, showed only slight changes in potency relative to their parent compounds. As the parents already contain the critical β -turn, this result is not altogether surprising. The AgrC-I agonism assays revealed AIP-I D1AS6G and AIP-I D1AS6dA to be ~2-fold and ~4 fold less potent, respectively, than the parent AIP-I D1AS6A (Figure 3.10A, see SI Table 3.S18 for potency data for all new analogs). These reductions in potency, especially for AIP-I D1AS6G, are relatively minor; indeed, both peptides are still highly active, with EC₅₀ values in the low nanomolar range. This only minor reduction in activity relative to AIP-I D1AS6A reinforces the β -turn as important for AgrC-I binding, and suggests that these particular type II' β -turn mimics

are simply not optimal for AgrC-I activation. Turning to the AgrC-I antagonism assay data, AAG and AAdA both maintained their high potencies, with IC₅₀ values comparable or lower than the parent AAA (Figure 3.10B). These results provide further support for the β -turn as a critical element for the interactions of these AIP-I analogs with AgrC-I. Moreover, they revealed the most potent AgrC-I antagonist that we have observed to date in *S. epidermidis* (AAdA), with a subnanomolar IC₅₀ value (0.908 nM).

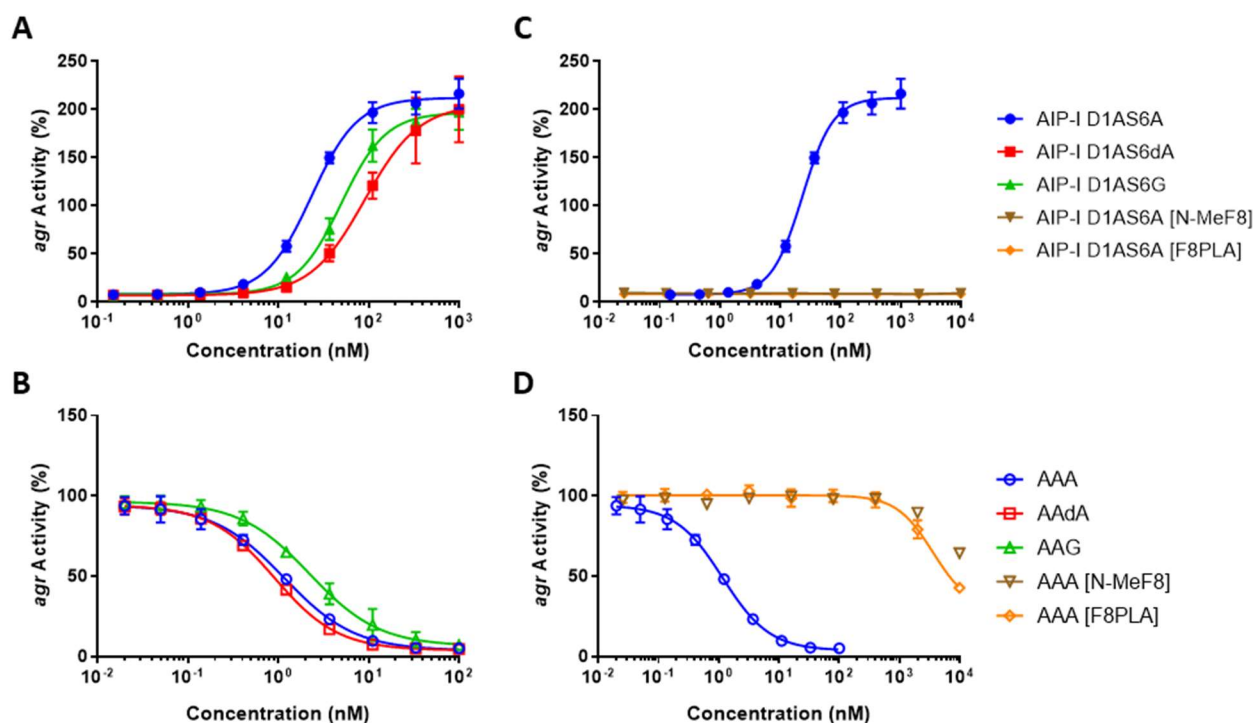


Figure 3.10 Group-I AgrC activity dose-response curves of β -turn modifying analogs. Agonism (closed shapes) and antagonism (open shapes) dose-response curves shown. Curves depicted for agonist (A) and antagonist (B) analogs designed to strengthen the β -turn, and agonists (C) and antagonists (D) designed to weaken the β -turn. The parent agonist (AIP-I D1AS6A) or antagonist (AAA) are shown alongside the new analogs (in blue) for comparison.

In contrast to the data for the D-Ala and Gly substituted analogs, the incorporation of *N*-MePhe and PLA, hypothesized to eliminate the key hydrogen bond

necessary for the β -turn, obliterated activity in AgrC-I relative to their parent compounds. Dose-response agonism assays of AIP-I D1AS6A [N-MeF8] and AIP-I D1AS6A [F8PLA] indicated a complete lack of activity (Figure 3.10C), while the antagonism assays of AAA [N-MeF8] and AAA [F8PLA] revealed a potency loss of over three orders of magnitude relative to the parent antagonist AAA (Figure 3.10D). These major shifts in potency due to the elimination of a single hydrogen bond strongly supports the importance of the β -turn for optimal binding interactions with AgrC-I.

To further examine the structures of these β -turn modified analogs and their activity profiles in AgrC-I, we performed additional 1-D and 2-D NMR experiments on a set of peptides with varying agonistic activities: AIP-I, AIP-I D1AS6A, AIP-I D1AS6dA, and AIP-I D1AS6A [N-MeF8]. AIP-I D1AS6A and its second-generation analogs were effective surrogates for the AAA family as well, as the chemical shifts of AIP-I D1AS6A and AAA were highly conserved and their solution NMR structures were analogous (again, both shown to adopt a type II' β -turn; see above). Chemical shifts are well-known to be sensitive to local structural changes in peptide/protein conformation, including the torsion angles used to classify β -turns.⁶⁴⁻⁶⁷ We initially sought to use NMR chemical shift data to generate backbone torsion angles using the established TALOS-N computer program,⁶⁸ in order to gauge similarities in the local conformations of the peptides.

We performed 1-D ^1H , 2-D TOCSY and 2-D ^1H - ^{13}C HSQC NMR experiments in D_2O on an 800 MHz spectrometer (see SI for full details of NMR experiments and data) on the family of peptides, and first inputted chemical shift data into TALOS-N for AIP-I and AIP-I D1AS6A to compare the software's predicted torsion angles to those

determined in our solution-phase NMR structures. We found that TALOS-N could not make torsion angle predictions for all the amino acids in these macrocyclic peptides, most likely because it relies on a training set based on natural linear peptides/proteins, and it was unable to predict torsion angles for all of the residues in the β -turn in AIP-I D1AS6A (see SI for the TALOS-N predictions and associated analysis). TALOS-N could make predictions with high confidence for residues in the exocyclic tails, and these predictions fell in the same regions of the Ramachandran plots as the observed torsion angles from the representative solution NMR structures, adding a second measure of validation for these NMR structures in addition to the validation with MolProbity (Tables 3.S23 and 3.S24). In view of this incomplete data set, however, we turned to comparative NMR chemical shift analysis, a technique commonly used for analyzing conformations of proteins and peptides,⁶⁵⁻⁶⁶ to identify putative structural changes between the agonist AIP-I D1AS6A and the two second-generation analogs, AIP-I D1AS6dA and AIP-I D1AS6A [N-MeF8].

We performed a systematic analysis of the $H\alpha$, $C\alpha$, $H\beta$, and $C\beta$ chemical shifts associated with each residue in AIP-I D1AS6A, AIP-I D1AS6dA, and AIP-I D1AS6A [N-MeF8] to obtain a gauge of their overall structural similarity (see SI for full assignments [Tables 3.S20–3.S22] and additional detailed text). A side-by-side comparison of the chemical shifts for AIP-I D1AS6A versus AIP-I D1AS6dA (Table 3.S25) revealed no significant changes in chemical shifts between the two peptides (i.e., no chemical shift change was greater than two standard deviations above the average shift difference).⁶⁹ This lack of significant chemical shift changes suggests that the conformation of AIP-I D1AS6dA is very similar to the parent AIP-I D1AS6A. This result correlates with the

comparable agonistic activities of the two peptides in the cell-based *agr* reporter assay. An analogous comparison was performed on the NMR data for AIP-I D1AS6A and its *N*-methyl amino acid, AIP-I D1AS6A [N-MeF8] (Table 3.S25). While there were only small differences in chemical shifts in many of the residues between the two peptides, in the residues near the β -turn there were four significant chemical shift changes between AIP-I D1AS6A and AIP-I D1AS6A [N-MeF8], signifying that the local conformation around these residues was perturbed.⁶⁹ These chemical shift changes suggest that the *N*-methyl amino acid modification not only removes the key hydrogen necessary for a β -turn hydrogen bond, but also causes changes in the local conformation of AIP-I D1AS6A [N-MeF8] relative to its parent AIP-I D1AS6A. This result correlates with the dramatic loss in agonistic activity for AIP-I D1AS6A [N-MeF8] relative to AIP-I D1AS6A in the cell-based *agr* reporter assay. These new NMR data and comparative analyses serve to support the claim that the structure of the macrocycle in this class of AIP-I mimics is critical to strong binding interactions with AgrC-I.

3.3 Summary and Conclusions

We have determined the 3-D structures of the three *S. epidermidis* AIPs (I–III) and five AIP-I analogs to gain insight into the modes by which these compounds activate and inhibit *S. epidermidis* AgrC-I. Comparisons of the solution-phase NMR structures revealed chemical features essential to AgrC-I agonism and antagonism (summarized in Figure 3.11). Specifically, we propose that the AIP macrocycle exhibits a hydrophobic face at the C-terminus that facilitates receptor binding, and that the positioning of that hydrophobic face is best facilitated by a type II' β -turn macrocycle that

is not present in native AIP-I. Instead, we found AIP-I has a dispensable stabilizing interaction in its macrocycle that we predict impairs adoption of the optimal conformation for binding its own cognate receptor. Additionally, a bulky hydrophobic group on the tail (e.g., Val3), oriented properly by the macrocycle, is the essential factor for AgrC-I receptor activation. Removal of this hydrophobic group, while maintaining the β -turn macrocycle, results in a highly potent AgrC-I antagonist (i.e., AAA). Removal of the tail altogether, as in t-AIP-I, yields a moderate antagonist with a macrocycle conformation analogous to the native AIP-I. We found the native AIP-II and AIP-III to adopt structures quite different from AIP-I, with each having highly different tail structures. Interestingly, both AIP-II and AIP-III are capable of antagonizing AgrC-I,^{30, 50} and have macrocycle conformations more similar to the β -turn motif of antagonist AAA, again suggesting that the most important features for binding to AgrC-I are hydrophobic residues in the macrocycle and a β -turn type macrocycle, while additional contacts made by the exocyclic tail may improve the AIP-I:AgrC-I binding interaction but are secondary to the macrocycle interactions. To further underscore the importance of the macrocyclic β -turn motif for peptide:AgrC-I binding, we found that analogs of AIP-I D1AS6A and AAA that reinforced the β -turn motif were also highly potent, with the antagonist AAdA having a subnanomolar IC₅₀ value and constituting, to our knowledge, the most potent AgrC antagonist in *S. epidermidis* to be reported. In turn, analogs in which β -turn formation was perturbed exhibited dramatic losses in potency, along with large perturbations of key NMR chemical shifts not present for other β -turn containing peptides, emphasizing the key role that the β -turn plays for AgrC-I binding.

The proposed models of AgrC-I agonism and antagonism are in agreement with the relative potencies of the AIP analogs observed in the cell-based reporter assay, strongly suggesting that the NMR structures and associated data reported herein are biologically relevant. We note that while the presence of two hydrophobic side chains near the C-terminus in conjunction with a type II' β -turn was sufficient for subnanomolar antagonism in *S. epidermidis*, such levels of antagonistic activity have been reserved for AIP analogs with at least three major hydrophobic groups and highly variable macrocyclic structures in the related bacterial species, *S. aureus*.⁵² These structural differences may contribute to the relatively weak cross-inhibition observed for the native AIP signals and related analogs between *S. aureus* and *S. epidermidis*.⁵⁰

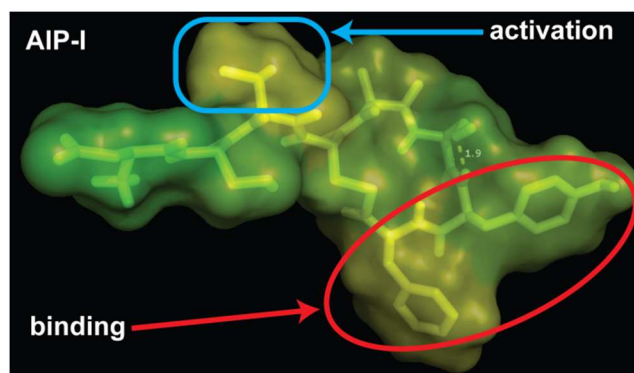


Figure 3.11 Model for AgrC-I activation by AIP-I. AIP-I is shown with a Connolly surface indicating relative hydrophobicity of residues, with yellow being most hydrophobic and green being most hydrophilic.

These structures and biological data for the native *S. epidermidis* AIPs and non-native AIP-I analogs are significant as they provide the first insights into the mechanism of AgrC receptor activation in in this emerging pathogen and shape our understanding of *agr*-type QS. These data and insights should also guide the design of new chemical probes to study QS in *S. epidermidis*, as we showcase through the synthesis and study

of β -turn modifying analogs herein. Indeed, the discovery of AAdA as a highly potent AgrC-I antagonist serves to validate structure-function studies such as this one. Looking to the future, because the primary mechanism by which *S. epidermidis* causes infection is biofilm formation and the activation of the *agr* system can reduce biofilm accumulation,^{12, 25, 27, 29} designing AIP analogs that can agonize all three AgrC receptors in *S. epidermidis* would be of great interest. Our structural studies suggest that, while the branched hydrophobic side chain of residue Val3 is crucial for receptor activation, the proper orientation of this side chain may not be dictated by any specific interactions between the side chain and the macrocycle. Consequently, we hypothesize that a Val residue, or another moiety with an adequately bulky hydrophobic group, could be introduced onto a type II' β -turn macrocycle mimetic, the AIP-II macrocycle, or AIP-III macrocycle, turning the resulting peptide into a highly potent activator for multiple AgrC receptors. Further simplified AgrC-I antagonists and agonists also could be identified using a method similar to that previously described for *S. aureus* AgrC receptors, where a number of different hydrophobic residues were substituted at the C-terminal region, and the other residues in the macrocycle were replaced with a single amino acid linker.^{43, 48} Studies toward these and related goals are ongoing and will be reported in due course.

3.4 Supplemental Information

3.4.1 Experimental procedures

Chemical reagents, strains, and general methods

All reagents and solvents were purchased from Sigma-Aldrich or Chem-Impex and used as obtained. Water (18 M Ω) was purified using a Barnstead Nanopure from Thermo Scientific. The majority of the peptides used in this study were previously synthesized in our laboratory,¹ and all were purified to homogeneity using established reverse-phase high performance liquid chromatography (RP-HPLC) methods on a Shimadzu instrument composed of SCL-10Avp controller, DGU-14A degasser, FCV-10ALvp solvent mixer, LC-10ATvp pump, CTO-10ASvp column oven with a 5 mL manual injection loop and Kromasil Eternity column (5 μ m 100 Å C18 packing of 10 mm \times 250 mm), SPD-M10Avp diode array detector, and FRC-10A fraction collector. Peptide masses were determined using a Bruker microflex LRF MALDI-TOF mass spectrometer. The *S. epidermidis* GFP agr group-I reporter strain AH3408² was generously donated by Prof. Alexander Horswill (University of Colorado Medical School) and cultured in Tryptic Soy Broth (TSB, from Sigma) supplemented with 10 μ g/mL of erythromycin.

Solid-phase peptide synthesis methods

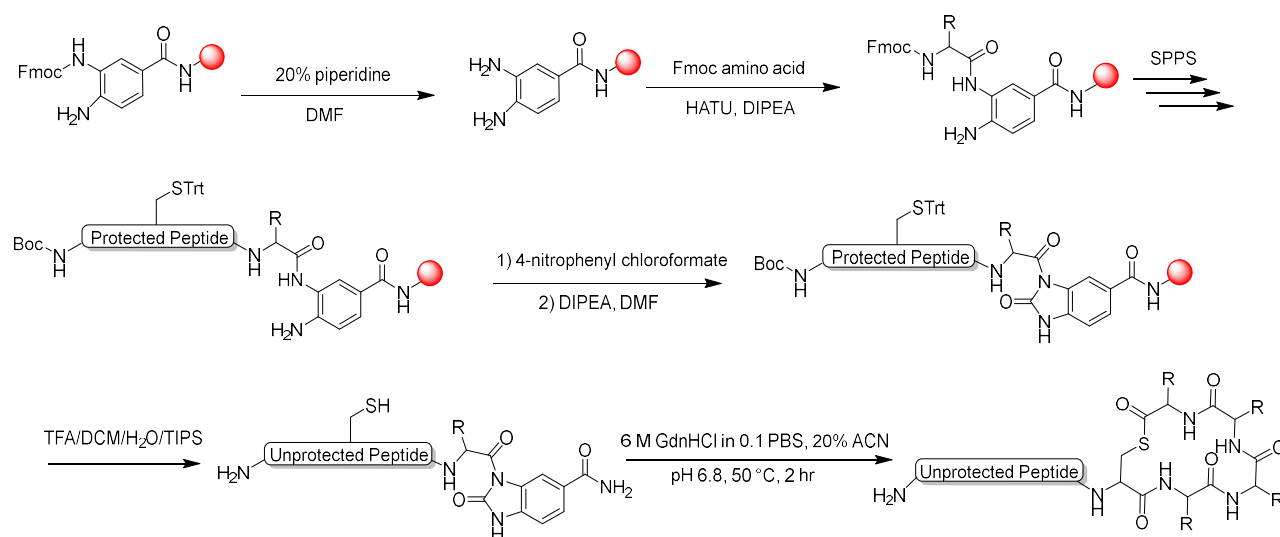
The β -turn modifying peptide analogs of AIP-I D1AS6A and AIP-I D1AV3AS6A (AAA), designed to examine the importance of the β -turn motif, were synthesized according to previously reported protocols (shown in Scheme 3.S1).⁵⁰ Approximately 30 mg (0.0147 mmol, 1 eq.) of Fmoc Dawson Dbz AM resin was swelled in DCM for 40 min in a fritted reactor vessel. The resin was washed with DCM (2 mL \times 3), DMF (2 mL \times 3),

and the Fmoc group deprotected with 20% piperidine in DMF (2 mL ×3; 5 min, 5 min, 10 min) while shaking. The deprotected resin was washed with DMF (2 mL ×3). *N*^α-Fmoc protected amino acid (4 eq.), HATU (4 eq.), and DIPEA (8 eq.) were dissolved in 2 mL DMF, incubated for 5 min, and added to the deprotected resin and shaken (1 h for the first amino acid, 0.5 h for the remaining amino acids). Deprotections and couplings were repeated to couple the remaining amino acids to the resin, with the final amino acid coupling using a Boc-protected amino acid instead of a Fmoc-protected amino acid.

Following the final Boc-protected amino acid coupling, the resin was washed with DMF (2 mL ×3) and DCM (2 mL ×3). Thereafter, 4-nitrophenyl chloroformate (4 eq.) dissolved in 2 mL of DCM was added to the vessel, and the slurry was shaken for 30 min. An additional 2 mL of 4-nitrophenyl chloroformate (4 eq.) in DCM was added to the vessel, and the slurry was shaken for another 30 min. The resin was washed with DCM (2 mL ×3) and treated with 2 mL of 5.5% DIPEA in DMF (10 min ×3). The resin was washed with DMF (2 mL ×3), DCM (2 mL ×3), and Et₂O (2 mL ×3), dried under N₂, and dried under vacuum. The peptide was cleaved from the resin (while also being deprotected) by treatment with 2 mL of 90/5/2.5/2.5 TFA/DCM/H₂O/triisopropylsilane (TIPS) and shaking for 2 h. The solution was filtered, mixed with 40 mL of Et₂O, chilled at -20 °C for 1 h to precipitate peptide, and centrifuged using a Beckman-Coulter Allegra 6R with a GH-3.8 rotor at 3500 rpm and 4 °C for 30 min. The supernatant was decanted, the pellet dissolved in 3 mL 50% ACN in H₂O, and lyophilized.

Lyophilized peptide was redissolved in 25% ACN in H₂O and purified by RP-HPLC. Fractions containing peptides were identified using MALDI MS and lyophilized. The lyophilized linear peptides were cyclized in 3 mL of cyclization buffer (20% ACN,

80% 6 M guanidinium chloride in 0.1 M Na₂PO₄, pH 6.8) while shaking at 50 °C for 2 h. The cyclized peptide was purified using RP-HPLC; fractions that contained cyclized peptide were identified by MALDI MS. Aliquots of the cyclized peptide fractions were submitted for high-resolution mass measurement and analytical RP-HPLC to check purity, while the remaining portions of the fractions were lyophilized in pre-massed vials to obtain final isolated yields of approximately 12–23%.



Scheme 3.S1 Solid-phase synthesis of β -turn modifying analogs.

Solid-phase *N*-methylated peptide synthesis methods

N-methylated analogs of AIP-I D1AS6A and AAA were synthesized and purified following the above peptide synthesis protocol with two exceptions. First, instead of using a standard *N*^α-Fmoc protected amino acid, an *N*^α-methyl, *N*^α-Fmoc protected amino acid was used to load the resin. Second, the coupling time to couple the following

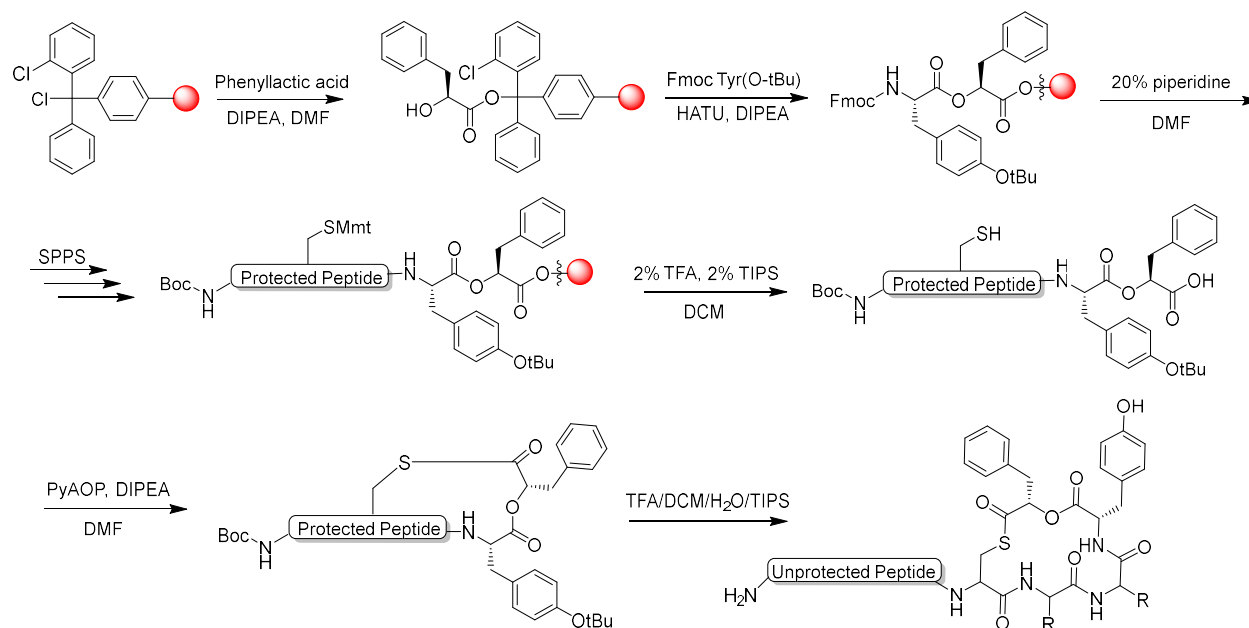
N^α-Fmoc protected amino acid was extended to 3 h. Final isolated yields of peptides ranged from approximately 5–16%.

Solid-phase depsipeptide synthesis methods

Depsipeptide analogs of AIP-I D1AS6A and AAA were synthesized by replacing Phe8 with L-phenyllactic acid (PLA) (shown in Scheme 3.S2). Approximately 100 mg (0.1 mmol, 1 eq.) of 2-chlorotrityl resin was swelled in DCM for 10 min in a fritted reactor vessel, and the resin was washed with DCM (2 mL ×3). To load PLA onto the resin, PLA (2 eq.) and DIPEA (4 eq.) were dissolved in 2 mL of DMF, added to the resin, and shaken for 30 min. The resin was washed with DCM (2 mL ×3), and then capped by incubating with 2 mL of a 15% MeOH/5% DIPEA in DCM solution for 10 min while shaking (×2). The resin was washed with DCM (2 mL ×3) and then with DMF (2 mL ×3). Thereafter, *N*^α-Fmoc-O-*t*Bu-L-tyrosine (4 eq.), HATU (4 eq.), and DIPEA (8 eq.) were dissolved in 2 mL of DMF, pre-incubated for 5 min, and then added to the PLA-loaded resin vessel and shaken for 16 h. The resin was then washed with DMF (2 mL ×3), then Fmoc deprotected with 2 mL of 20% piperidine in DMF ×3 (5 min, 5 min, 10 min) while shaking. The deprotected resin was washed with DMF (2 mL ×3). The next *N*^α-Fmoc protected amino acid (4 eq.), HATU (4 eq.), and DIPEA (8 eq.) were dissolved in 2 mL of DMF, pre-incubated for 5 min, and added to the deprotected resin and shaken for 30 min. Deprotections and couplings were repeated to couple the remaining amino acids to the resin, with the final amino acid coupling using a Boc-protected amino acid instead of a Fmoc-protected amino acid.

Following the final Boc-protected amino acid coupling, the resin was washed with DMF (2 mL ×3), DCM (2 mL ×3), MeOH (2 mL ×3), dried with N₂, and then dried under vacuum. The peptide was cleaved from the resin (while simultaneously deprotecting only the Cys4 thiol from its Mmt protecting group) using 5 mL of 2% TFA/2% TIPS in DCM solution, and shaking for 15 min. The solution was filtered into a 25 mL round-bottom flask, and the resin was treated with another 5 mL of 2% TFA/2% TIPS in DCM solution, shaken for another 15 min, and drained into a 25 mL round bottom flask. A small volume (~0.5 mL) of DMSO was added to the flask, and the DCM was removed under reduced pressure. The remaining approximately 0.5 mL of the peptide dissolved in DMSO was diluted with 25% ACN in water and purified on RP-HPLC. Fractions containing the partially-protected linear depsipeptides were identified by MALDI MS and lyophilized. Yields of partially-protected linear depsipeptides ranged from 1–2%.

The partially-protected linear depsipeptides (1 eq.) were cyclized with PyAOP (1.5 eq.) and DIPEA (2 eq.) in 0.5 mL DMF, stirring for 48 h in a 50 °C water bath. The solvent was removed by rotary evaporation under reduced pressure, and the cyclized, partially-protected depsipeptides were fully deprotected by stirring in 0.5 mL of a 90/5/2.5/2.5 TFA/DCM/H₂O/TIPS solution for 2 h. The solution was removed by rotary evaporation under reduced pressure, leaving a yellow oil. The oil then was diluted with water and purified by RP-HPLC, and fractions that contained cyclized depsipeptide were identified with MALDI MS. Aliquots of the cyclized depsipeptide fractions were submitted for high-resolution mass measurement and analytical RP-HPLC to check purity, while the remaining portions of the fractions were lyophilized in pre-massed vials to obtain isolated yields of approximately 21–58% (relative to linear starting material).



Scheme 3.S2 Solid-phase synthesis of depsipeptides.

Fluorescent *AgrC-I* reporter assay protocol

Peptides were evaluated for agr activity using the *S. epidermidis* GFP agr group-I reporter strain AH3408.³⁰ A culture of AH3408 was grown overnight at 37 °C with shaking at 200 rpm, after which it was diluted 1:50 in fresh TSB medium. Peptide stocks (1 mM) were serially diluted in DMSO, and 2 μ L aliquots were transferred to wells in triplicate within a black 96-well microtiter plate. For antagonism assays, 198 μ L of the diluted AH3408 culture were added to each well. For agonism assays, 2 μ L of a 2.5 μ M AAA stock solution (final concentration in plate: 25 nM) were added to each well to block agr activity, and subsequently 196 μ L of diluted AH3408 culture were transferred into each well. Separate from the test wells, each plate also included two controls: a vehicle control (wells containing only 2 or 4 μ L DMSO with dilute AH3408 culture for agonism or antagonism assays, respectively), and a media control (wells containing TSB medium only). Plates were incubated with shaking (200 rpm) at 37 °C for 24 h.

Fluorescence (excitation at 500 nm, emission at 540 nm) and the OD₆₀₀ of each well were measured using a BioTek Synergy 2 plate reader. Measurements were processed by subtracting background fluorescence (TSB medium), correcting to OD₆₀₀, and then normalizing using the respective DMSO control for the agonism and antagonism assays. Non-linear regression curves were fitted to the data sets with GraphPad Prism software (version 7) by using variable slope (four-parameter) dose-response analysis to obtain potency, efficacy, and statistical information about the activity profiles of the tested peptides.

NMR methods and spectral analyses

To obtain solution structures of key peptides, NMR experiments (1-D proton, 2-D TOCSY, and 2-D ROESY) and subsequent analyses of the spectral data were carried out using our previously reported methods.⁴³ In brief, peptides were dissolved in H₂O:D₂O (95:5), except for AIP-I which was dissolved in 12.5% CD₃CN in H₂O and t-AIP-I which was dissolved in 30% CD₃CN in H₂O at pH 5. Final concentrations of each peptide were at least 700 μM. These NMR spectra were obtained on a Bruker Avance-III 750 MHz spectrometer equipped with a TXI cryoprobe using standard pulse sequences at ambient temperature. Solvent suppression of the water peak was achieved using excitation sculpting, and chemical shifts in the spectra were referenced to residual H₂O at 4.79 ppm or CD₃CN at 1.94 ppm.

All spectra were analyzed using MestReNova 10 NMR processing software, with important ³J couplings and chemical shifts provided in Tables 3.S1–3.S16. Resonance assignments for each peptide, calculations of interproton distances from ROESY

crosspeak volumes, and the three-dimensional structure calculations and refinements were completed according to established methods.⁷⁰⁻⁷² ROE constraint specifics are provided below.

An average structure for each peptide was determined from an ensemble of the 20 lowest-energy structures from a set of 100 total structures obtained by torsion angle simulated annealing in Xplor-NIH.^{53-54, 73-77} During refinement, an initial constraint allowance of $\pm 20\%$ of each calculated ROE was used to determine initial structures with a soft potential. Final refinement was done with a constraint allowance of $\pm 10\%$ of each calculated ROE plus an additional 0.5 Å using a hard potential for the final structures. The average structure was used as a comparative tool, from which a representative structure with a small RMS difference from the average structure was selected from the low-energy ensemble. These representative structures are shown in the main text (Figures 3.3–3.8). Additional images are provided in Figures 3.S1–3.S9. Visual analysis, structure comparisons with alignment fitting, and presentation of the peptide structures were performed with PyMOL.⁵⁵ For consistent RMS fitting in PyMOL, degenerate hydrogens were numbered for consistent relative coordinates. Final representative structures were validated using MolProbity.⁶⁰⁻⁶¹

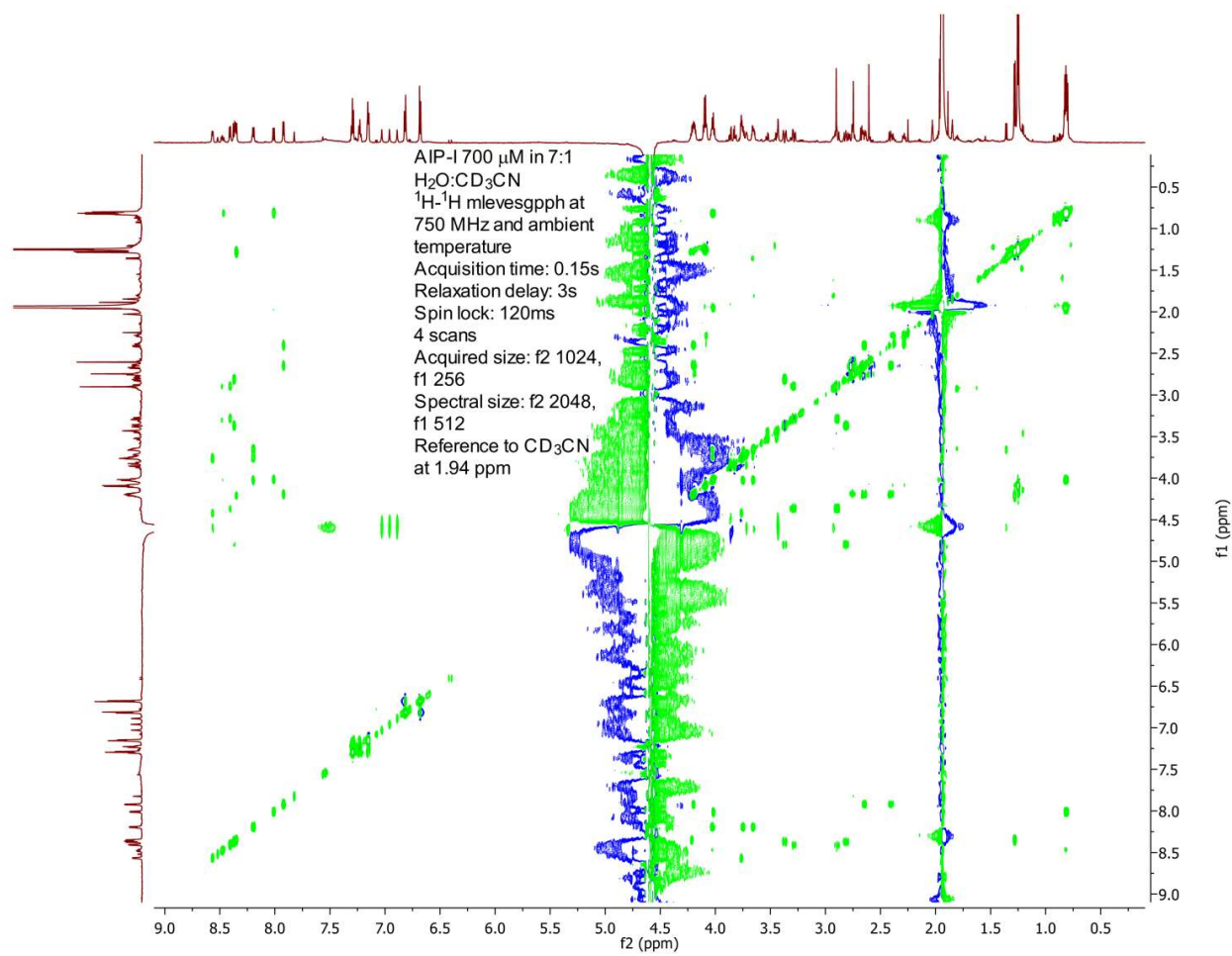
Additional NMR experiments (1-D proton, 2-D TOCSY, and 2-D ^1H - ^{13}C HSQC) were performed to compare the chemical shifts of select peptides. Peptides were dissolved in D_2O at pH 5, with the exception of AIP-I which was dissolved in 12.5% CD_3CN in D_2O at pH 5. Final concentrations of each peptide were at least 700 μM . Spectra were obtained on a Varian 800 MHz spectrometer with a HCN cryoprobe using standard pulse sequences at ambient temperature. Chemical shifts within the spectra

were referenced to a DMSO internal standard at 2.71 ppm (^1H) or 39.39 ppm (^{13}C). The chemical shift data for AIP-I and AIP-I D1AS6A were entered into the TALOS-N program in attempt to predict torsion angles (see additional discussion below).^{68, 78}

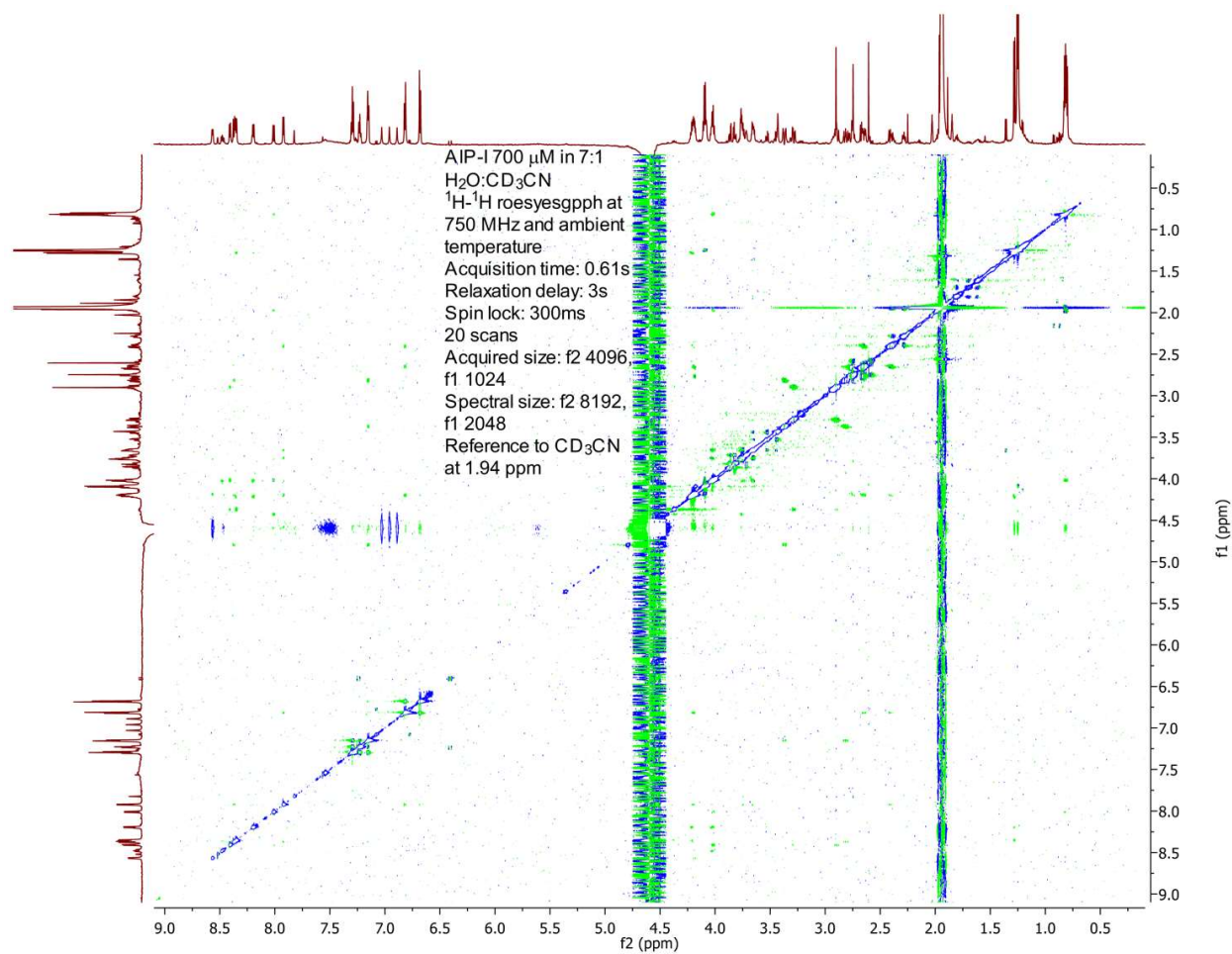
3.4.2 NMR spectra for 3-D solution-phase structures

One-dimensional proton, 2-D TOCSY, and 2-D ROESY NMR experiments were performed for each peptide as described in the experimental procedures above. Selected parameters for each experiment are included in each spectrum. For the 2-D experiments, blue indicates negative peak intensity and green indicates positive peak intensity.

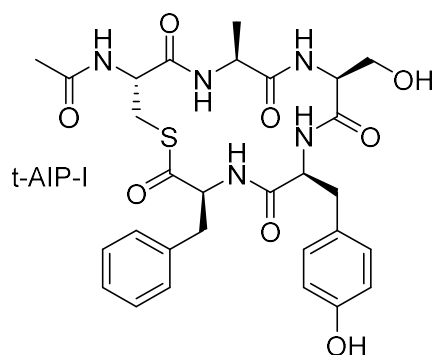
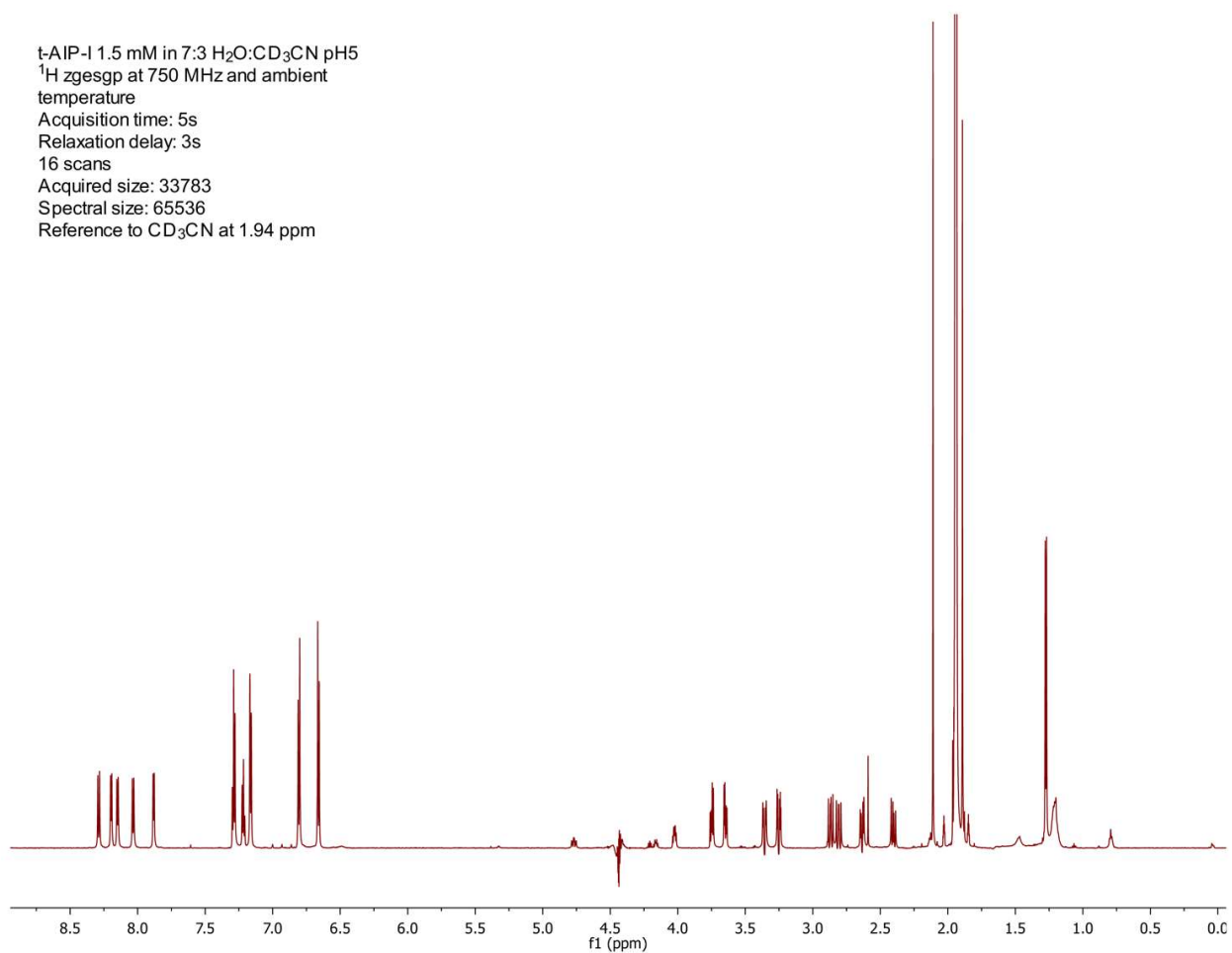
- *AIP-I* ^1H - ^1H TOCSY spectrum



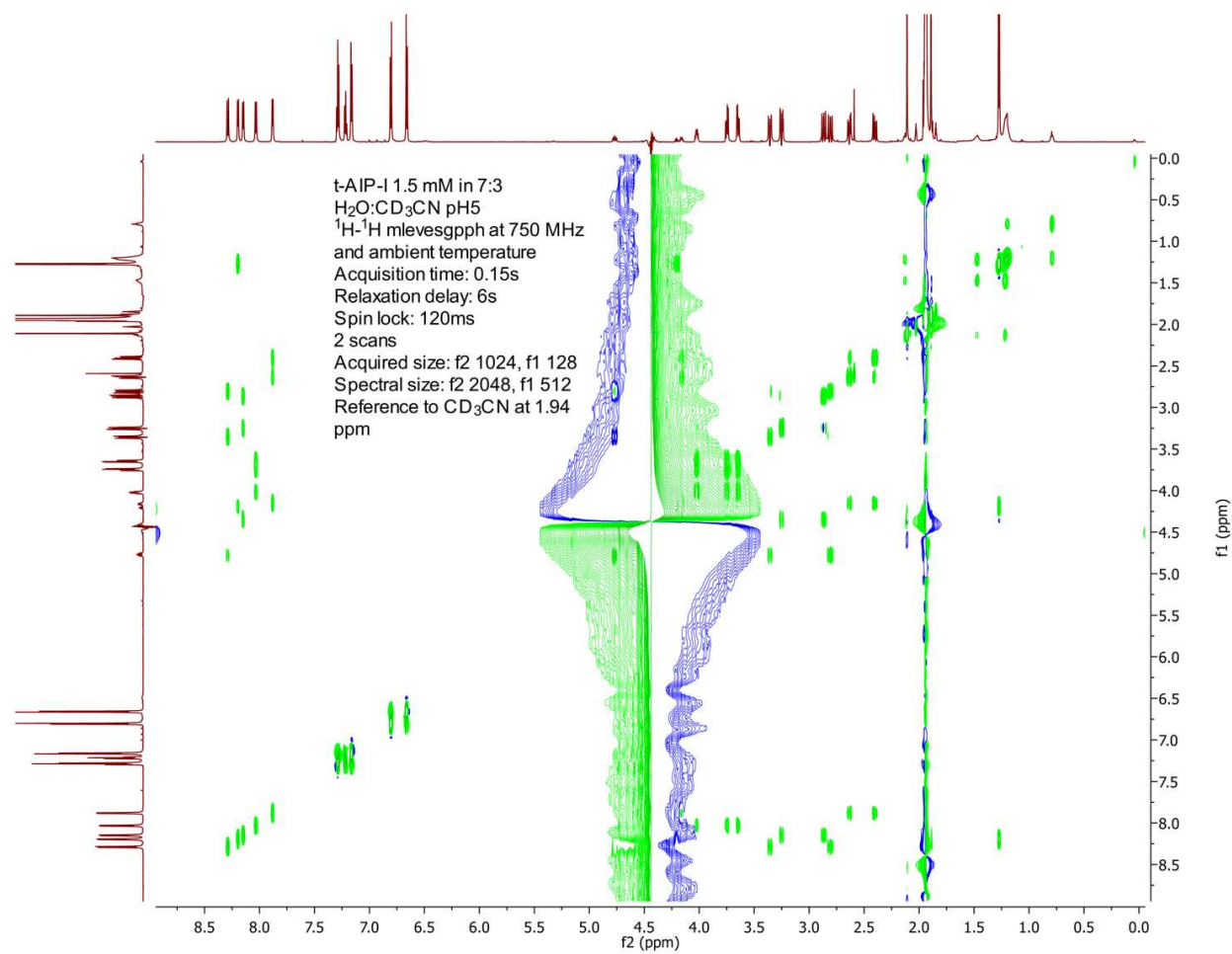
- AIP-I ^1H - ^1H ROESY spectrum



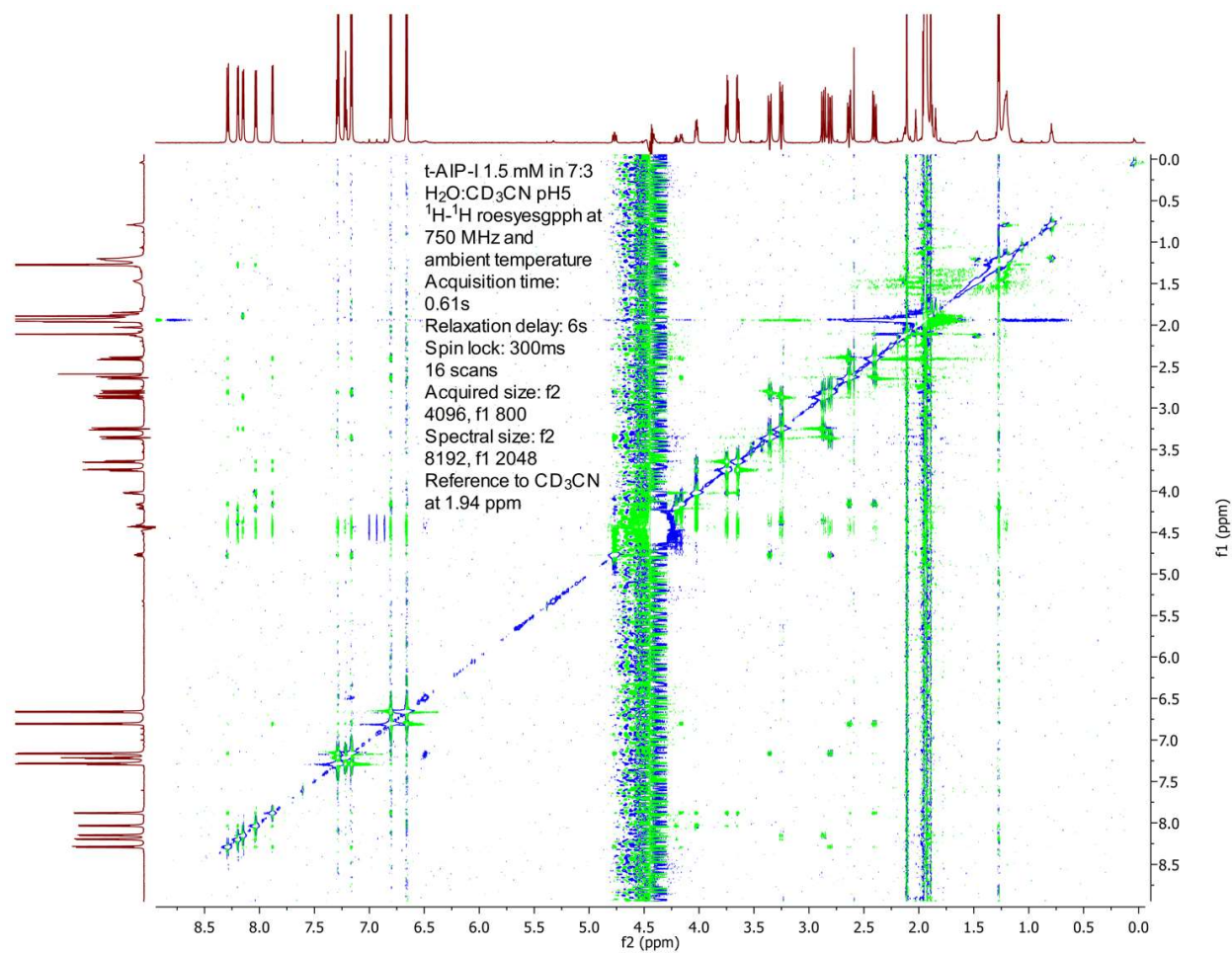
- *t*-AIP-I ¹H NMR spectrum (1.5 mM dissolved in 30% CD₃CN in H₂O, pH ~5 with HCl)



- *t*-AIP-I ^1H - ^1H TOCSY spectrum

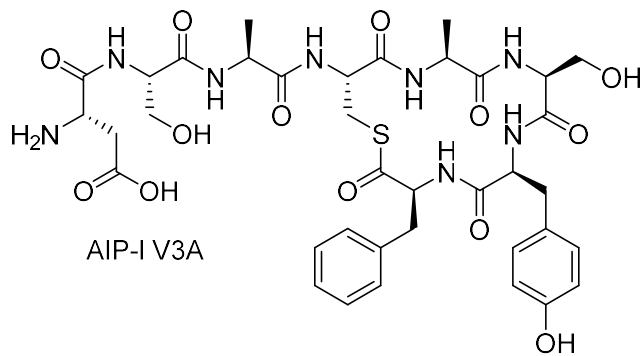
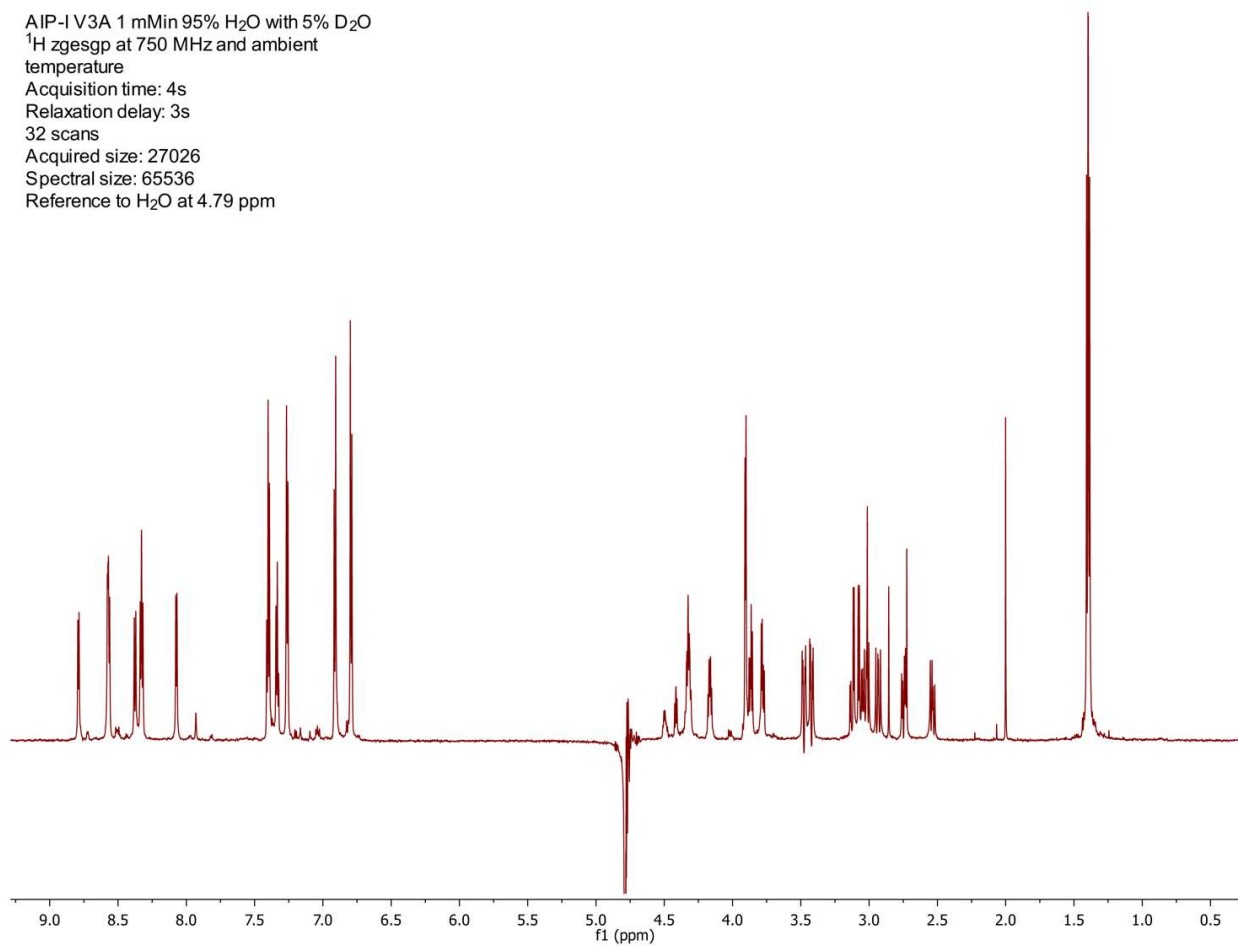


- *t*-AIP-I ^1H - ^1H ROESY spectrum

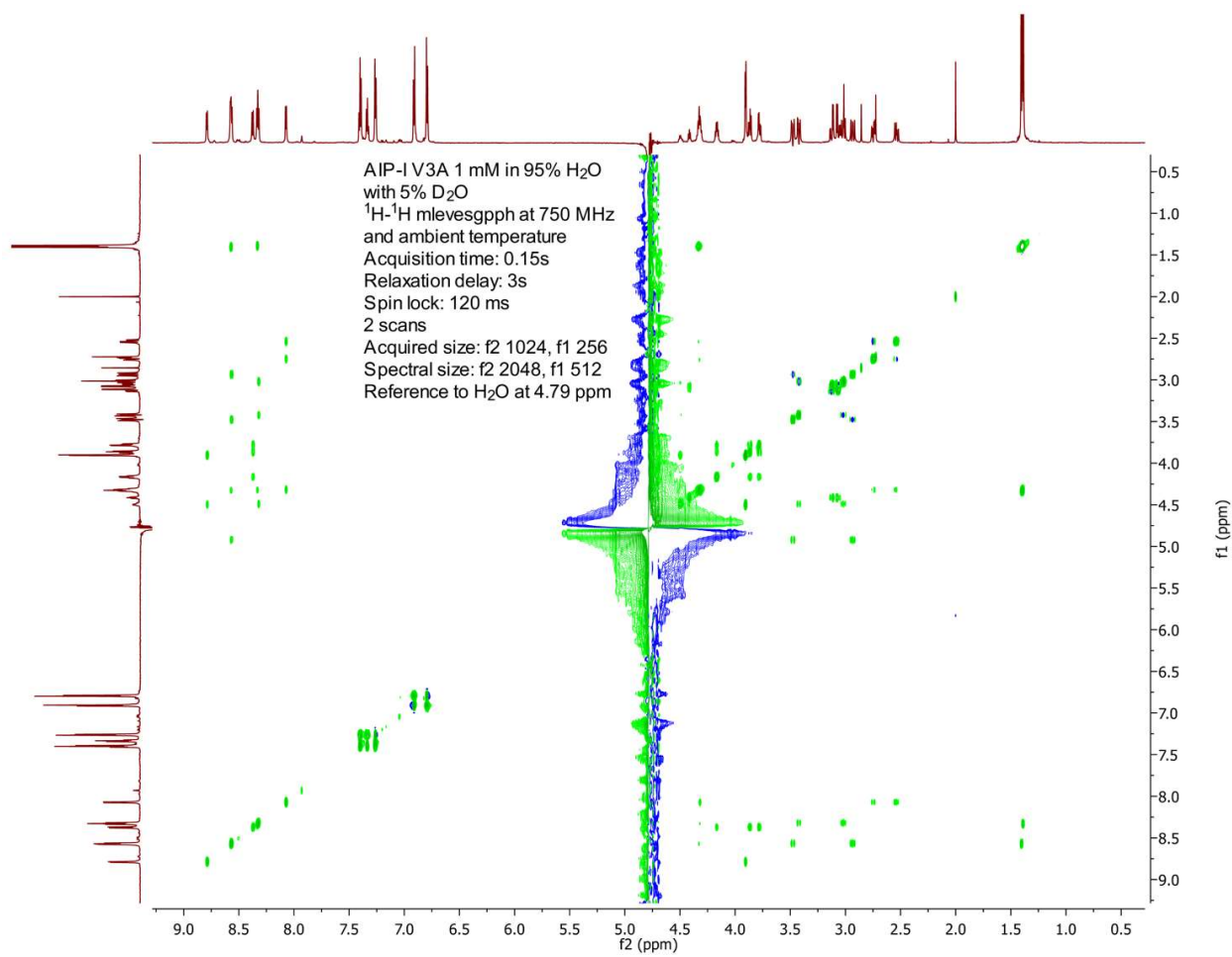


- *AIP-I V3A* ^1H spectrum (1 mM dissolved in 95% H_2O with 5% D_2O , pH ~6.5)

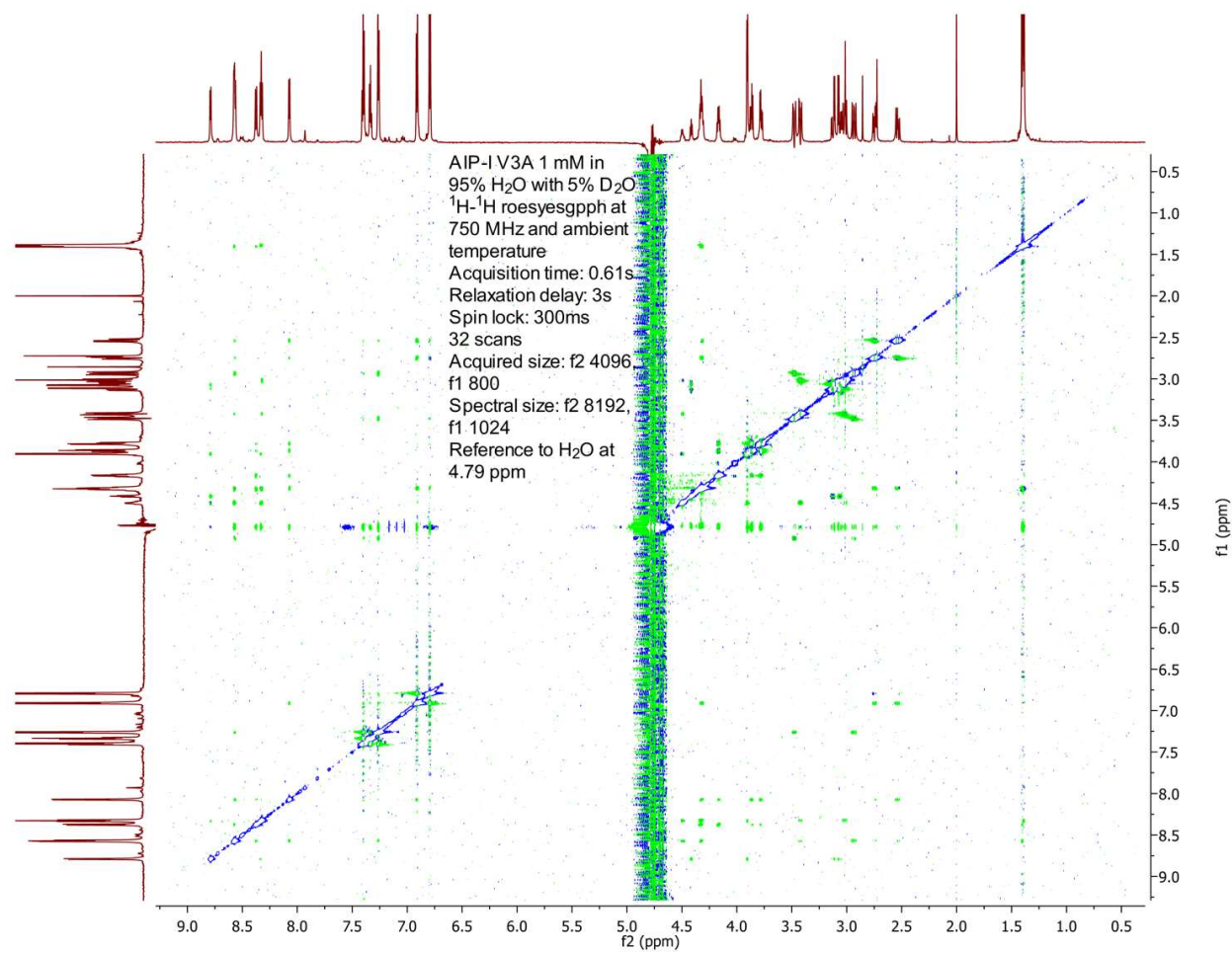
AIP-I V3A 1 mM in 95% H_2O with 5% D_2O
 ^1H zgpg30 at 750 MHz and ambient
temperature
Acquisition time: 4s
Relaxation delay: 3s
32 scans
Acquired size: 27026
Spectral size: 65536
Reference to H_2O at 4.79 ppm



- AIP-I V3A ^1H - ^1H TOCSY spectrum

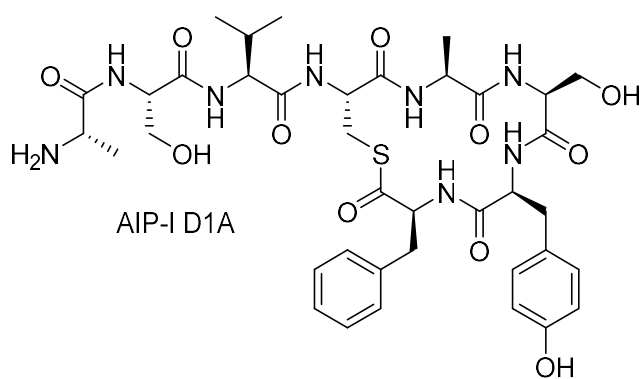
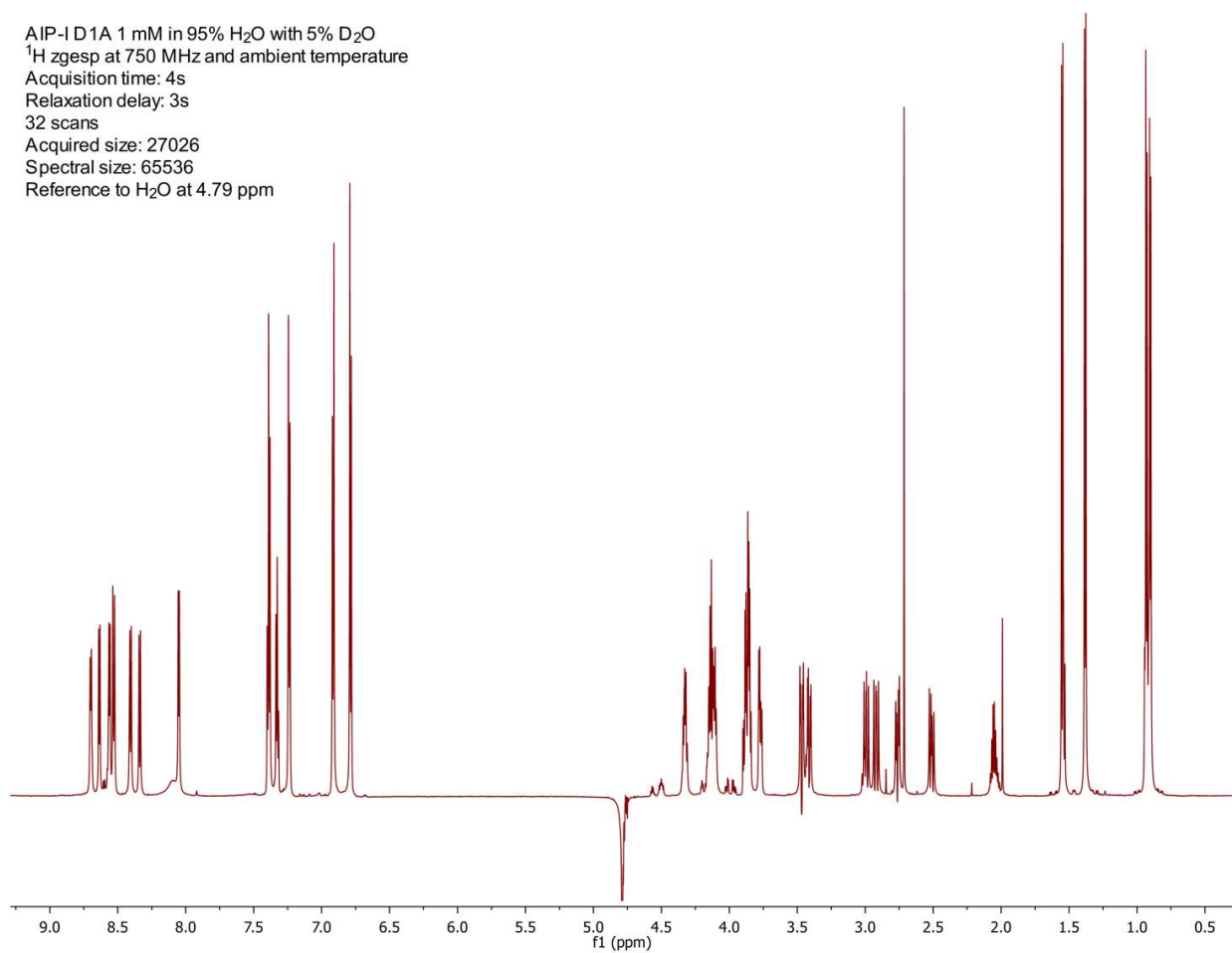


- *AIP-I V3A* ^1H - ^1H ROESY spectrum

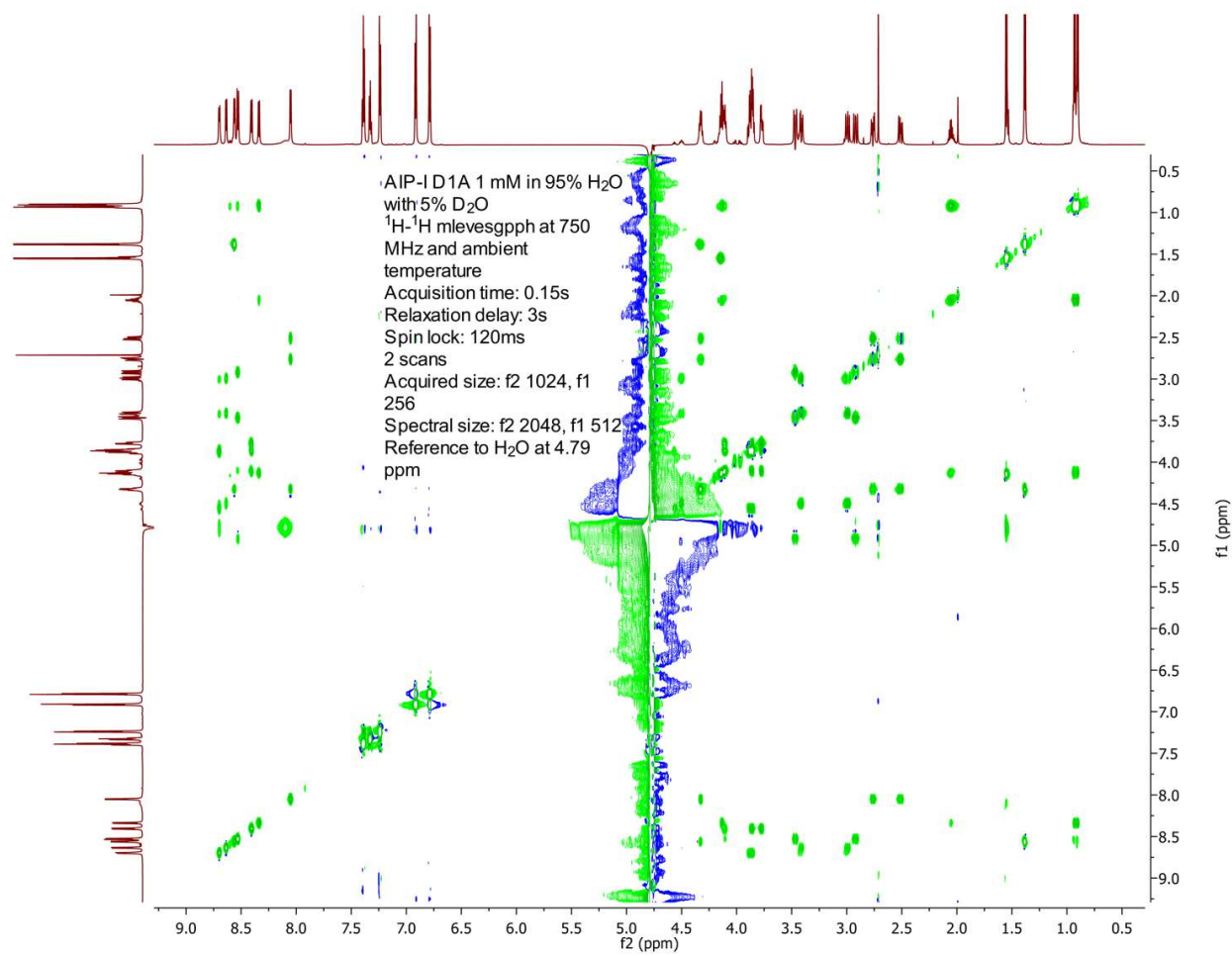


- *AIP-I D1A* ^1H NMR spectrum (1 mM dissolved in 95% H_2O with 5% D_2O , pH ~6.5)

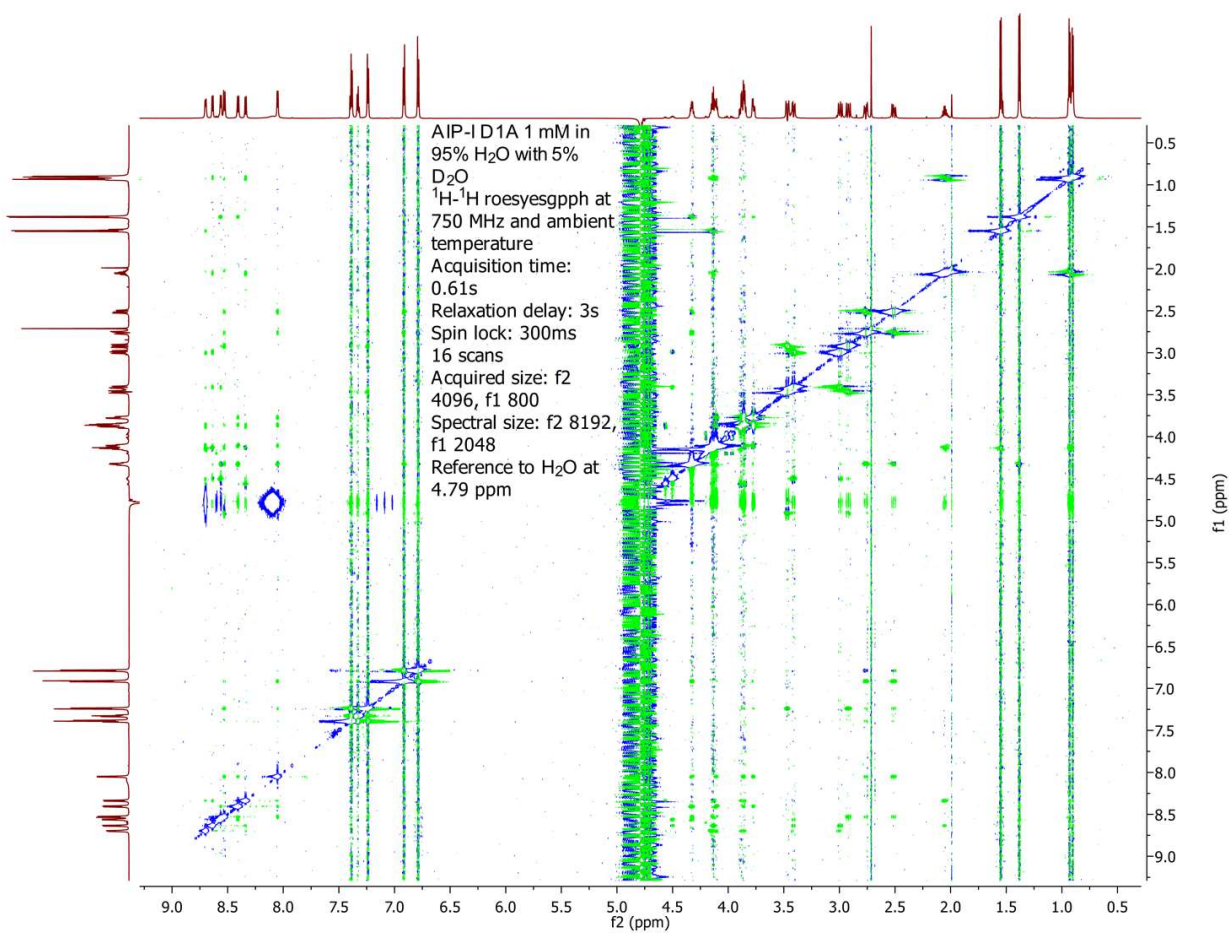
AIP-I D1A 1 mM in 95% H_2O with 5% D_2O
 ^1H zgspg at 750 MHz and ambient temperature
Acquisition time: 4s
Relaxation delay: 3s
32 scans
Acquired size: 27026
Spectral size: 65536
Reference to H_2O at 4.79 ppm



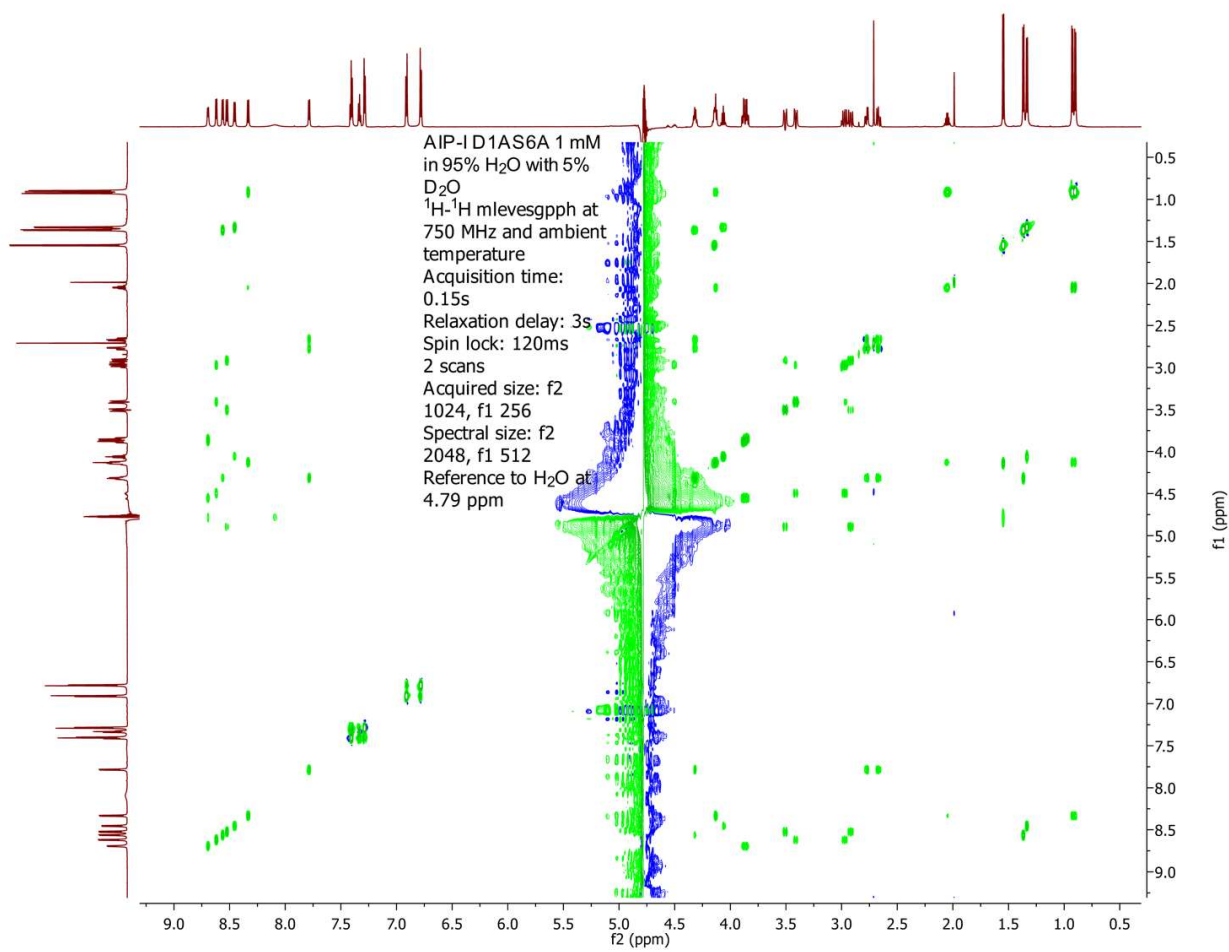
- AIP-I D1A ^1H - ^1H TOCSY spectrum



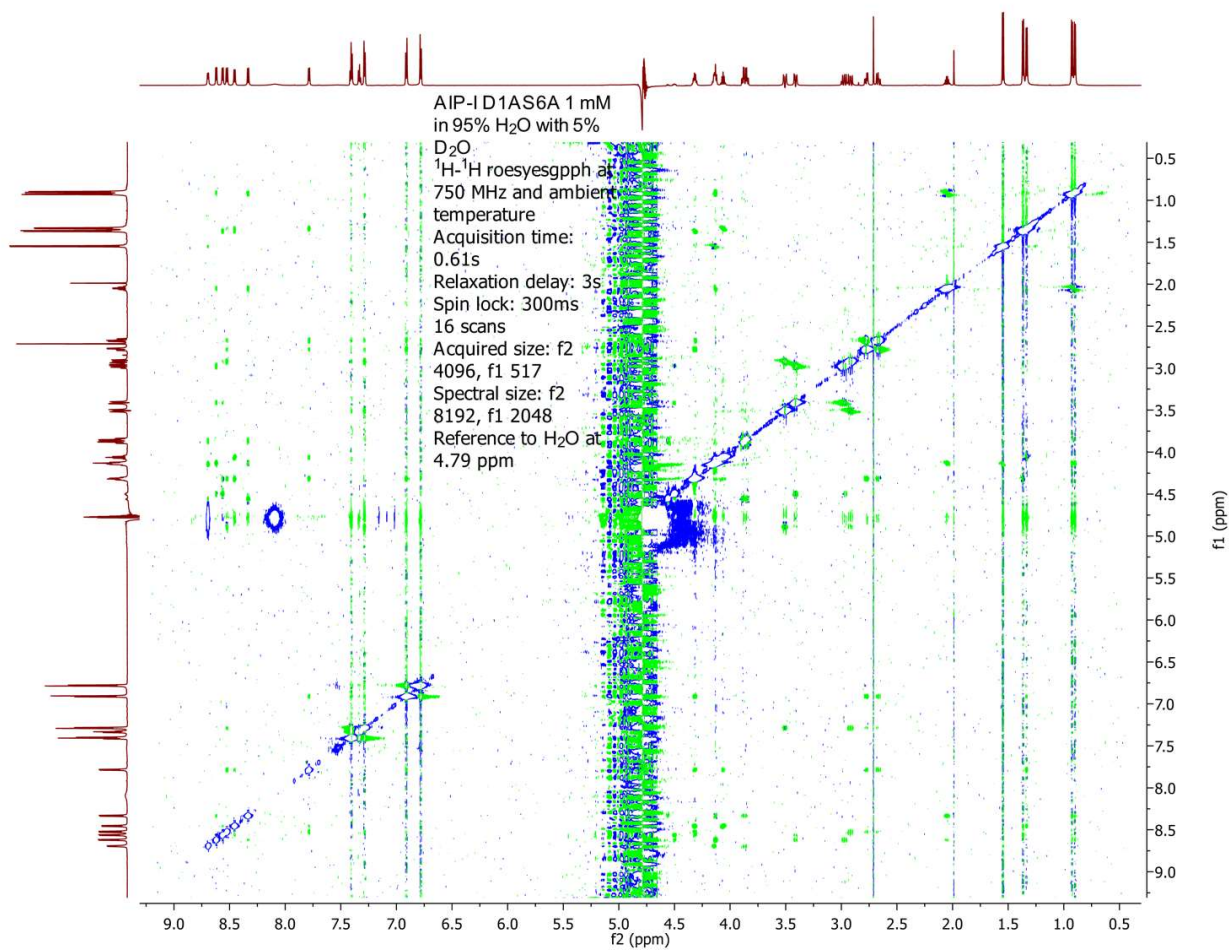
- AIP-I D1A ^1H - ^1H ROESY spectrum



- AIP-I D1AS6A ^1H - ^1H TOCSY spectrum

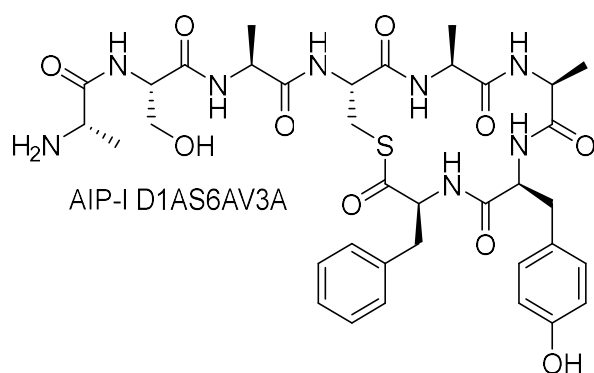
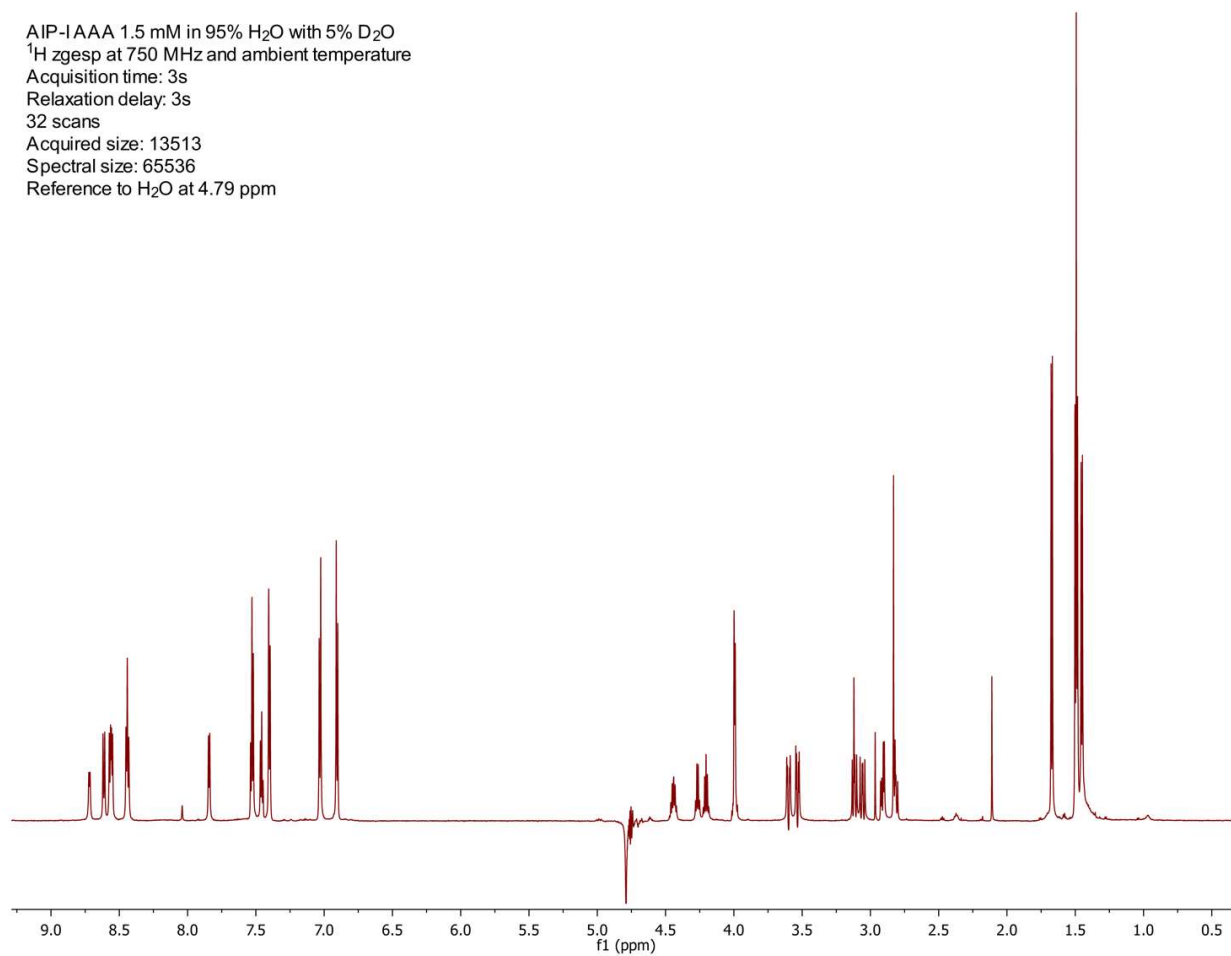


- AIP-I D1AS6A ^1H - ^1H ROESY spectrum

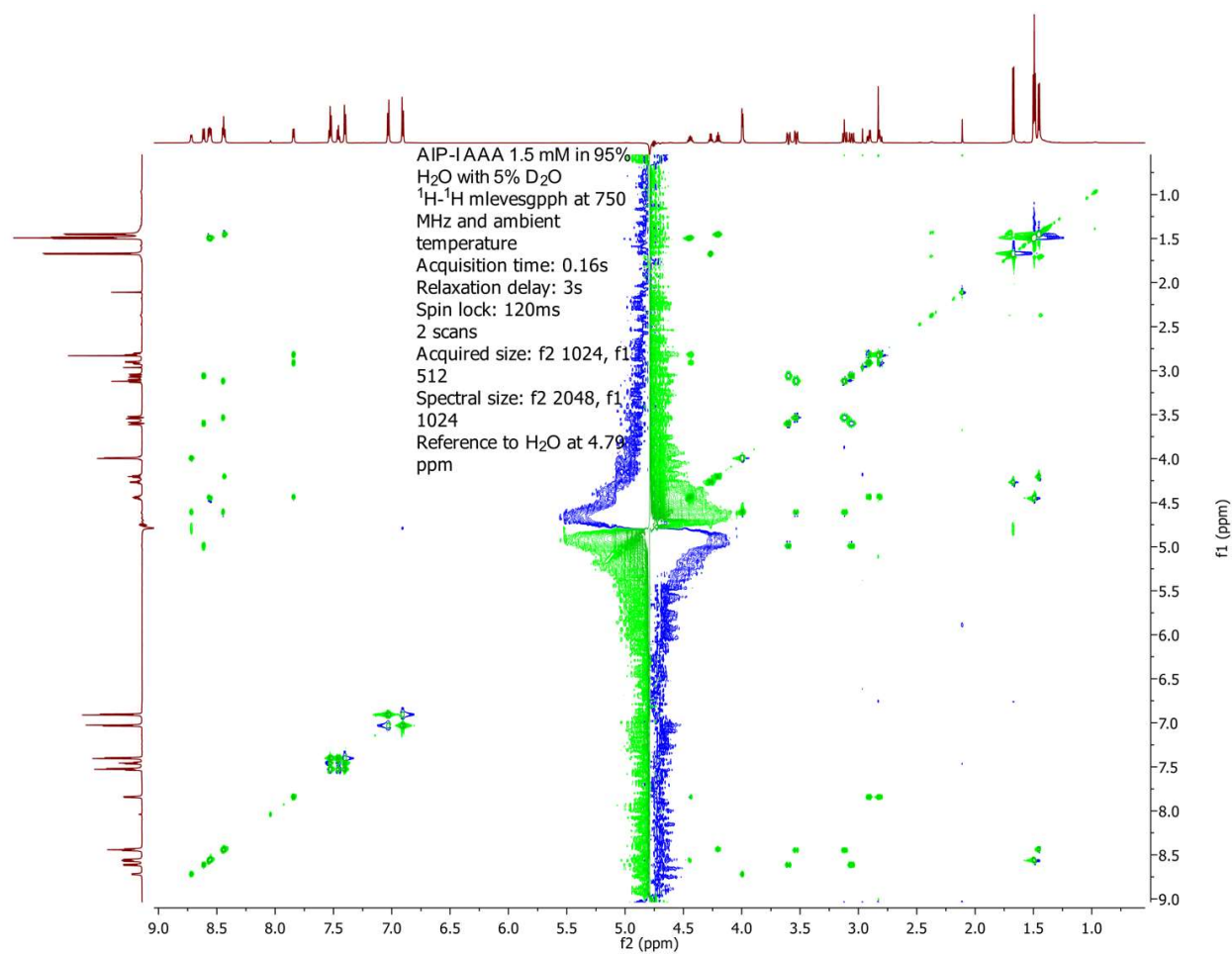


- *AIP-I D1AV3AS6A (AAA) ¹H NMR spectrum (1.5 mM dissolved in 95% H₂O with 5% D₂O, pH ~6.5)*

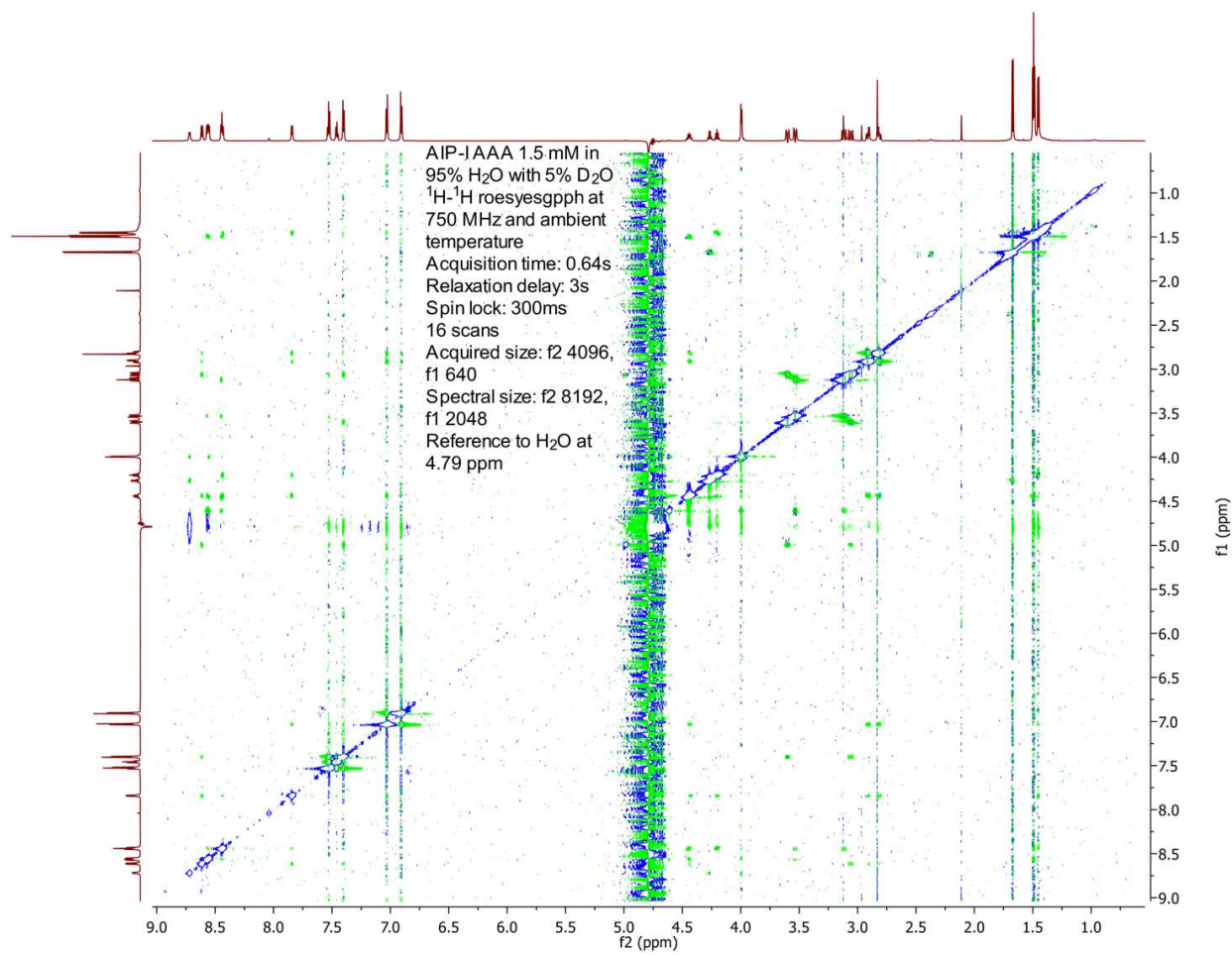
AIP-I AAA 1.5 mM in 95% H₂O with 5% D₂O
¹H zgsp at 750 MHz and ambient temperature
Acquisition time: 3s
Relaxation delay: 3s
32 scans
Acquired size: 13513
Spectral size: 65536
Reference to H₂O at 4.79 ppm



- AAA ^1H - ^1H TOCSY spectrum

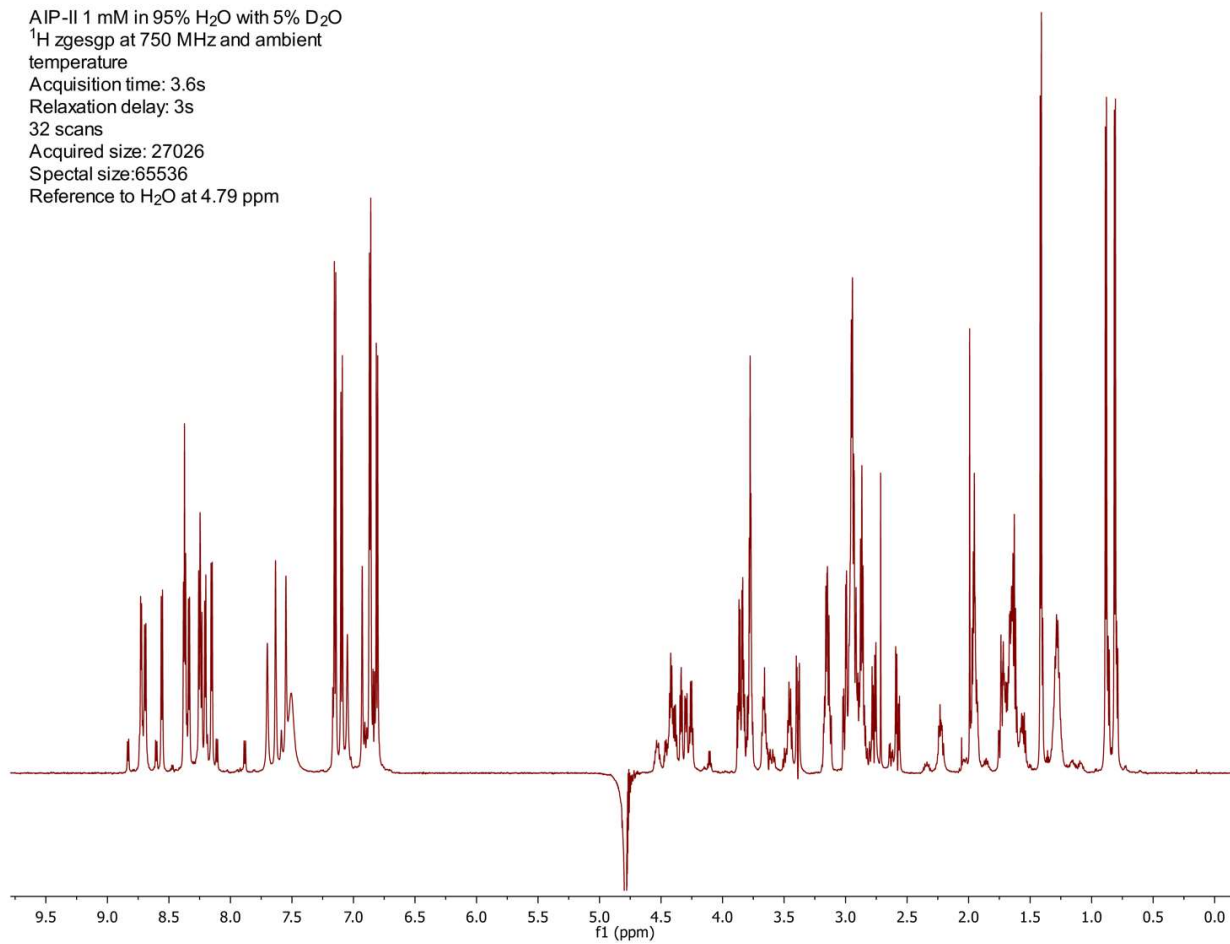


- AAA ^1H - ^1H ROESY spectrum

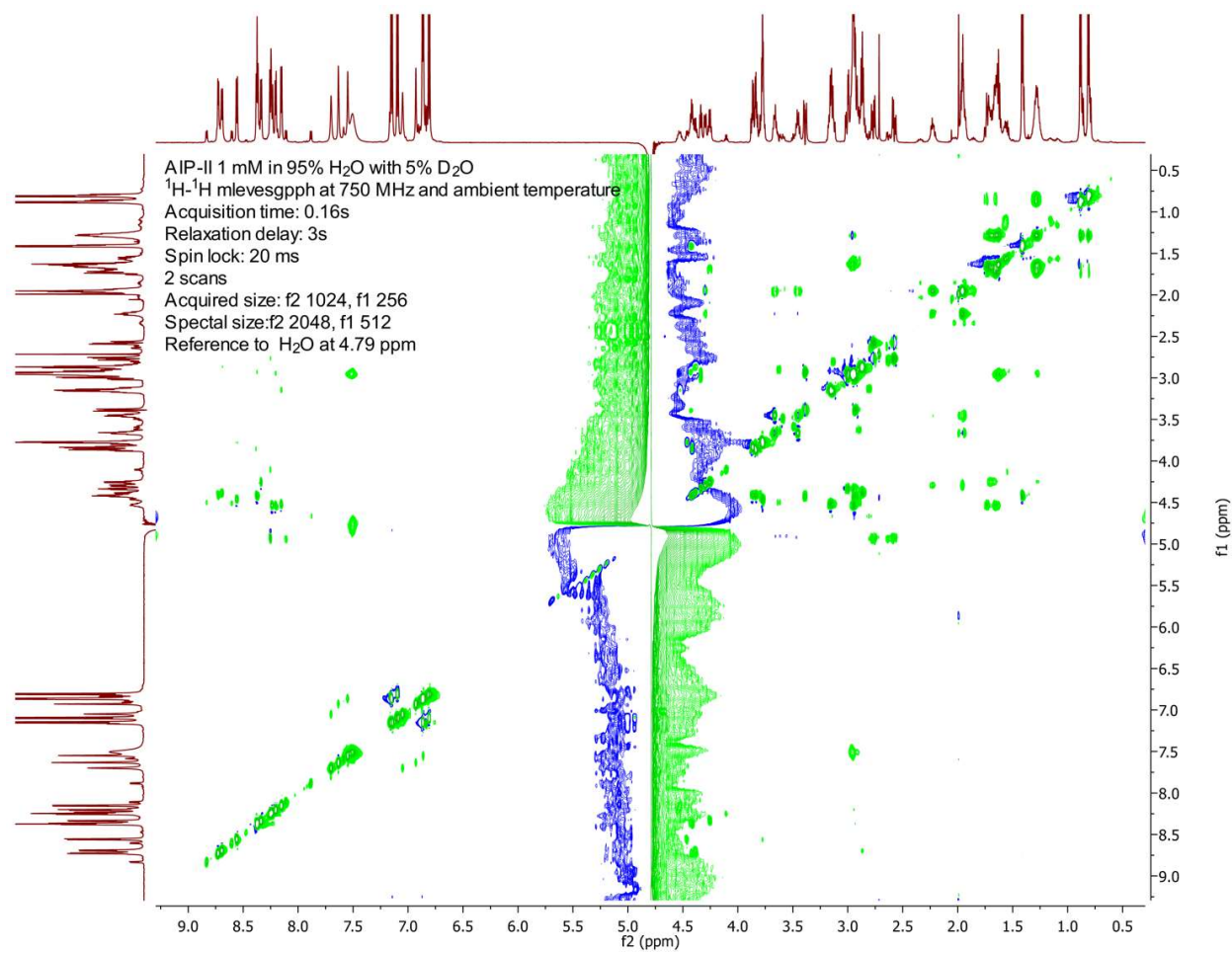


- *AIP-II* ^1H NMR spectrum (1 mM dissolved in 95% H_2O with 5% D_2O , pH ~6.5)

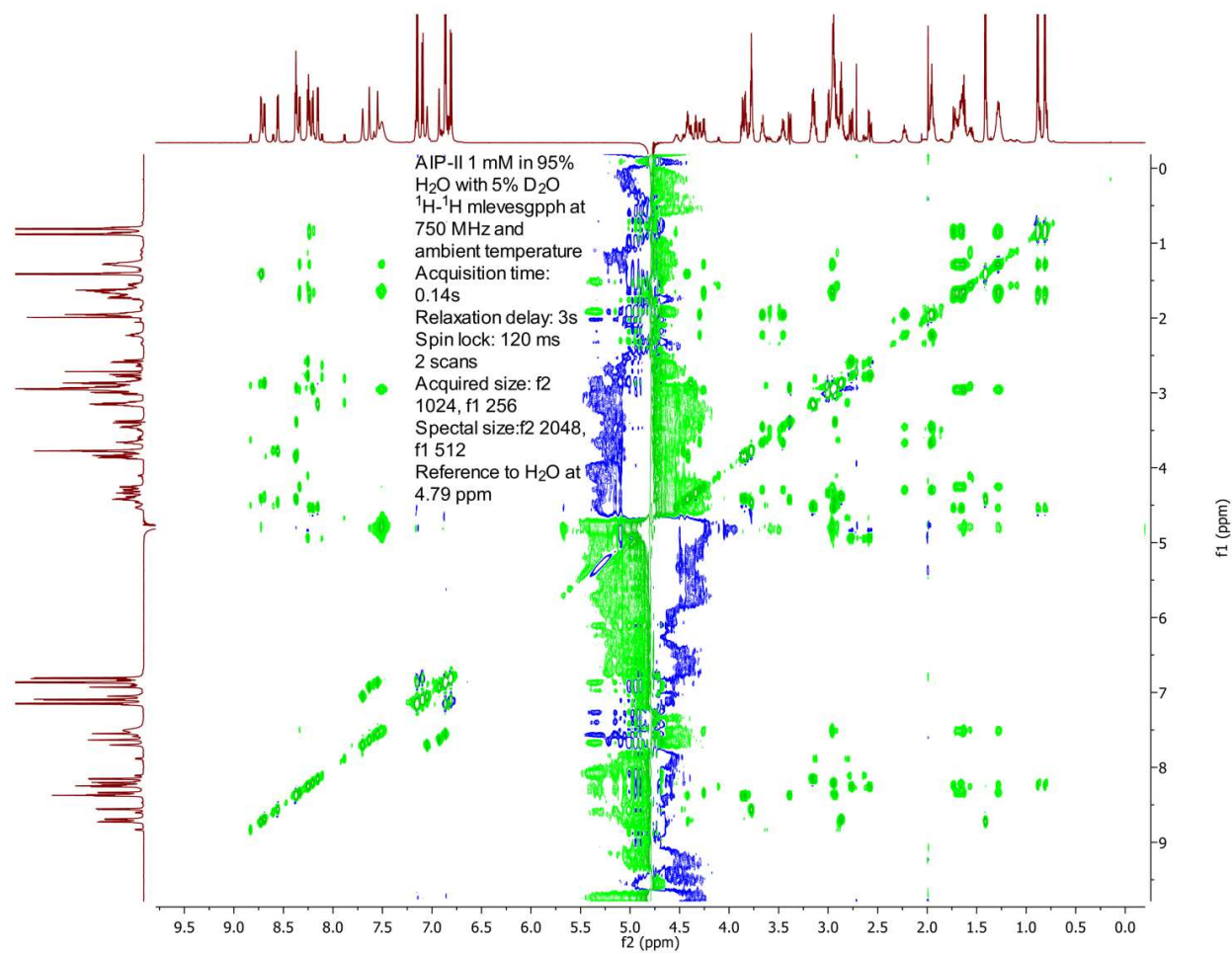
AIP-II 1 mM in 95% H_2O with 5% D_2O
 ^1H NMR at 750 MHz and ambient
temperature
Acquisition time: 3.6s
Relaxation delay: 3s
32 scans
Acquired size: 27026
Spectral size: 65536
Reference to H_2O at 4.79 ppm



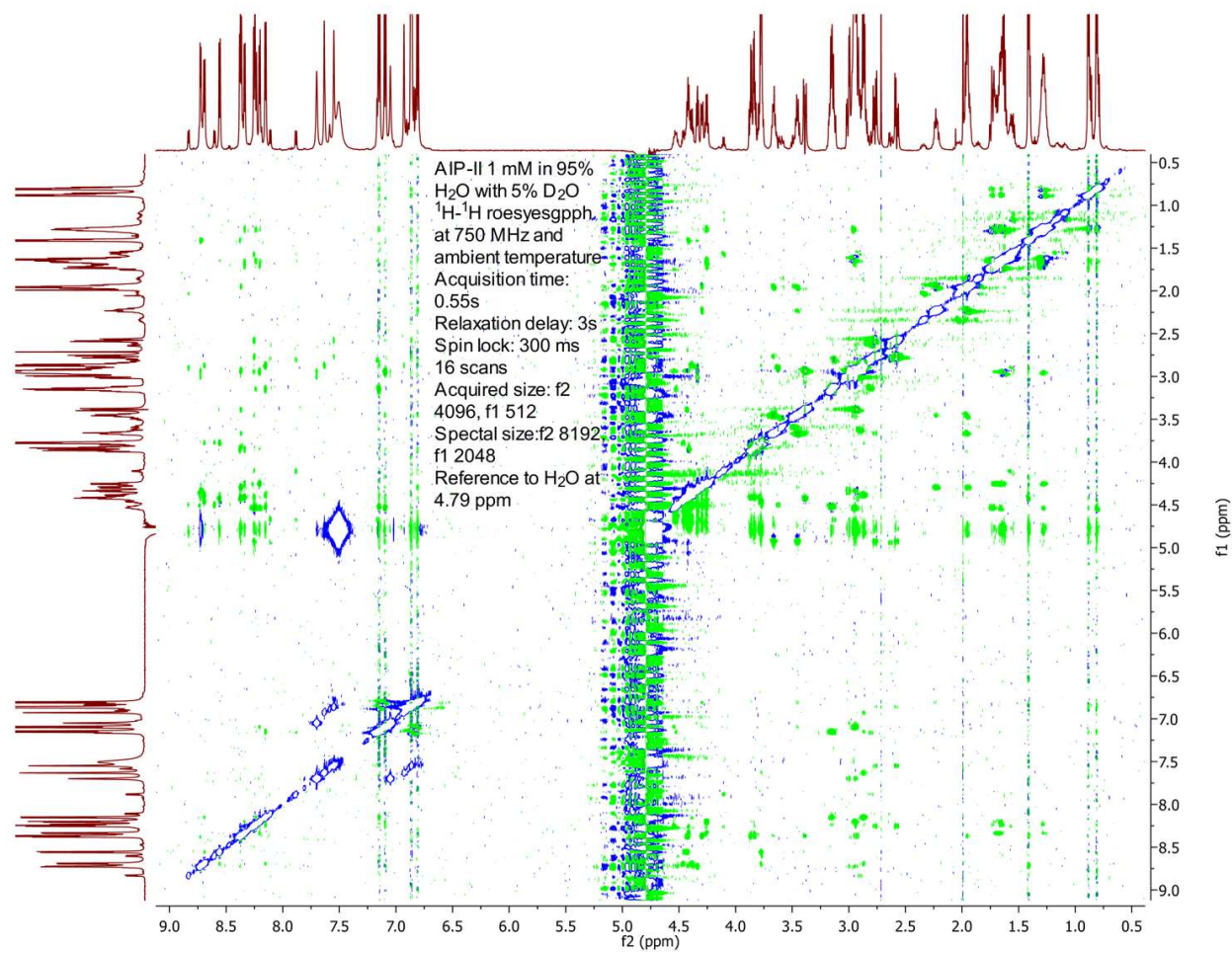
- AIP-II ^1H - ^1H TOCSY spectrum (20 ms spin lock)



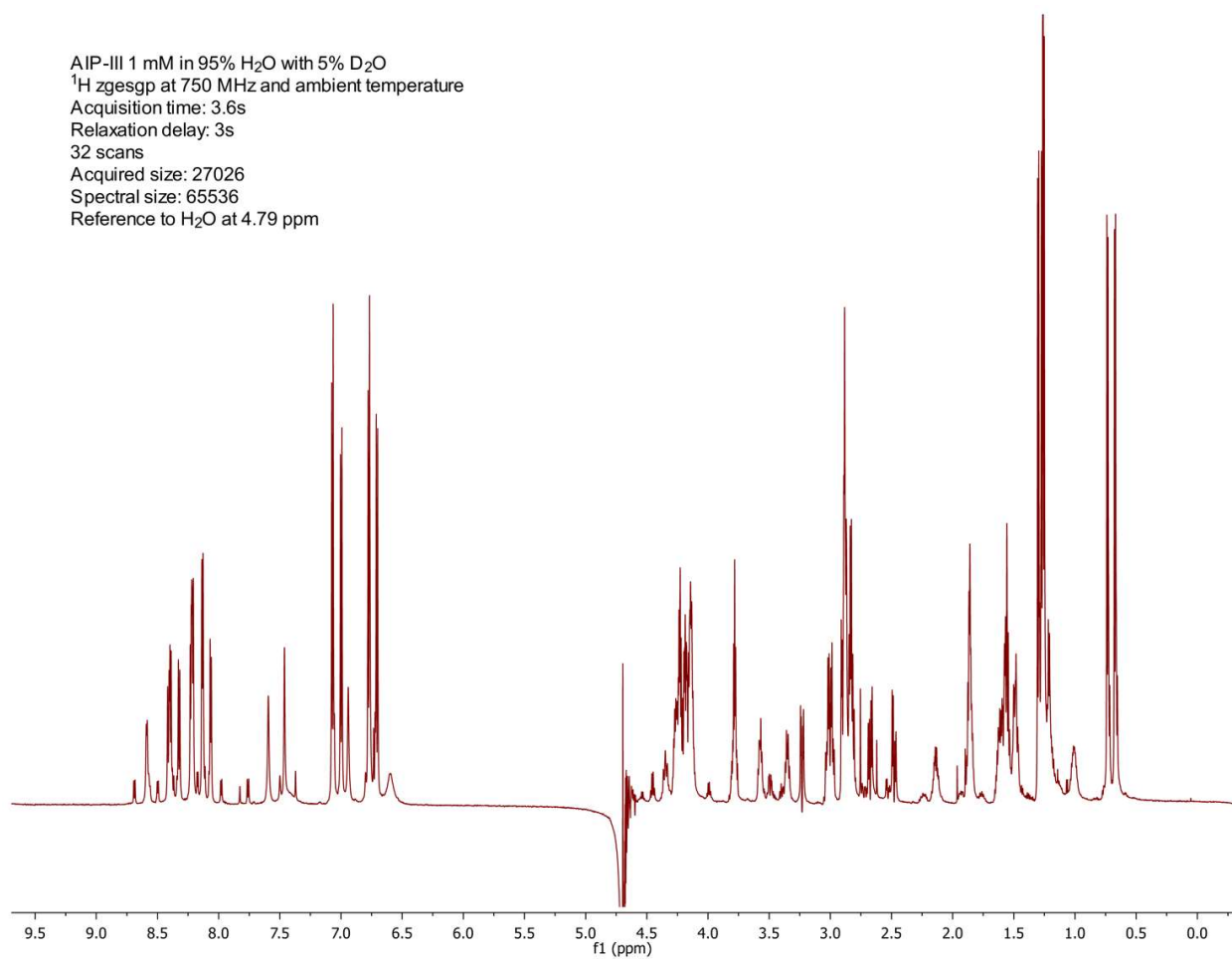
- AIP-II ^1H - ^1H TOCSY spectrum (120 ms spin lock)



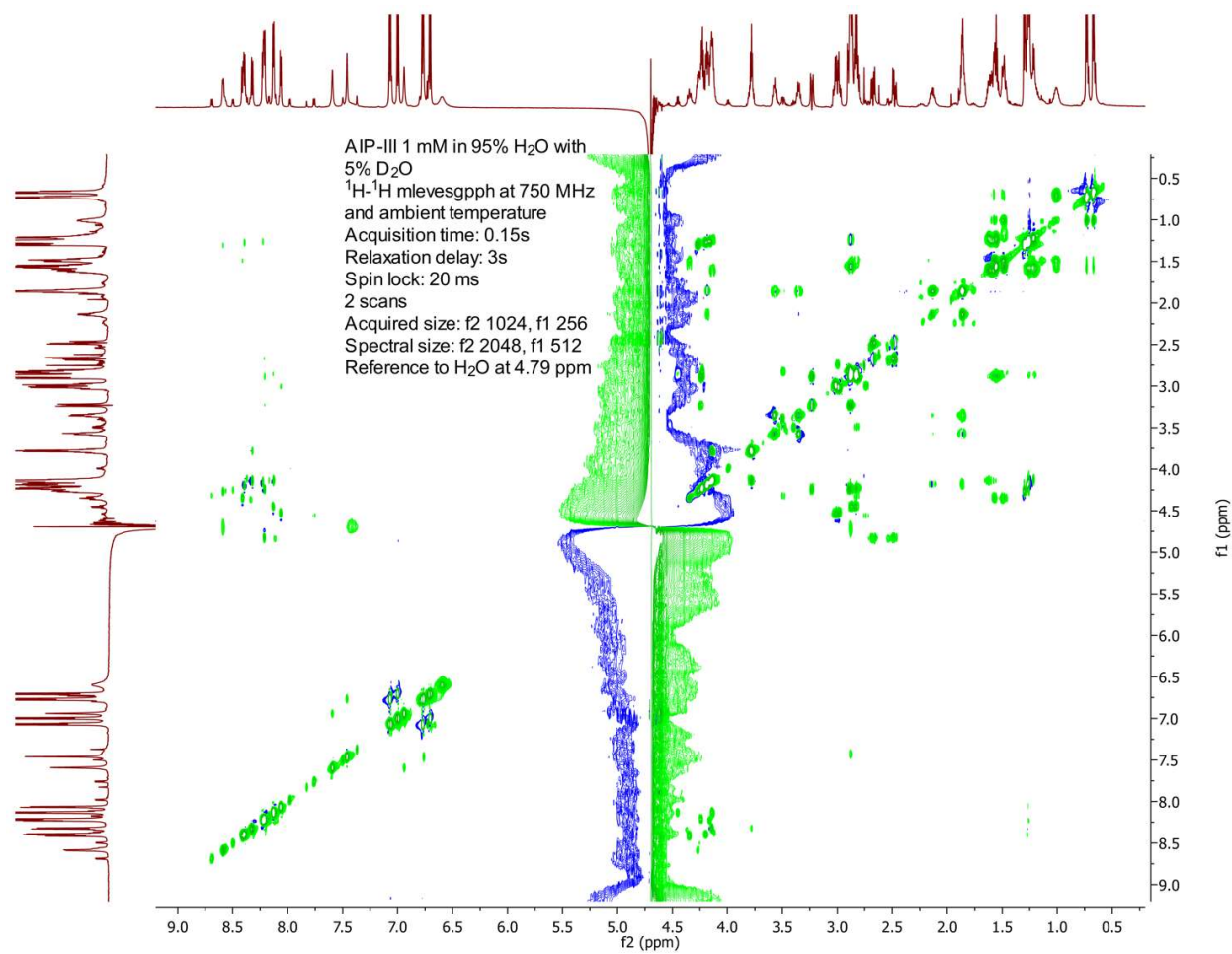
- AIP-II ^1H - ^1H ROESY spectrum



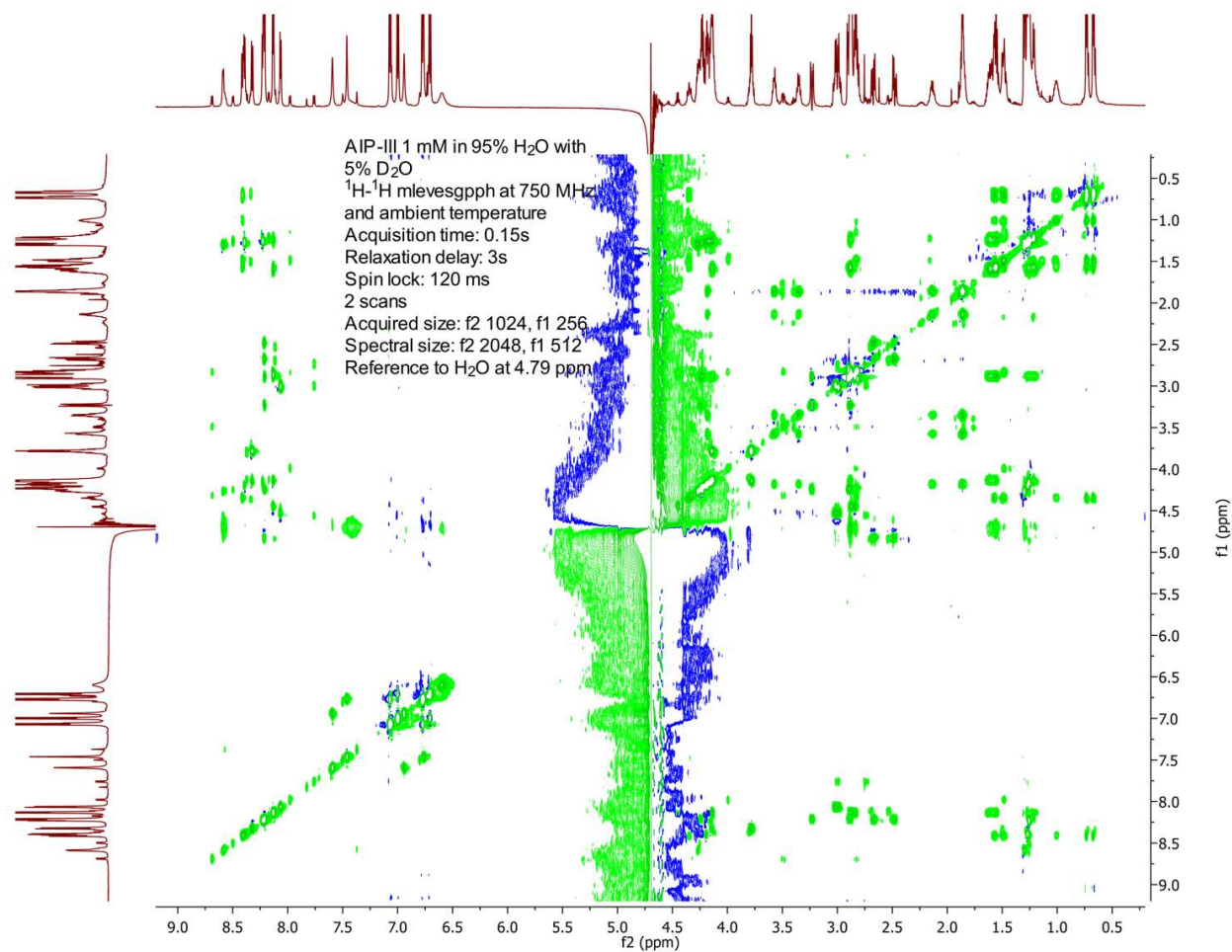
- *AIP-III* ^1H NMR spectrum (1 mM dissolved in 95% H_2O with 5% D_2O , pH ~6.5)



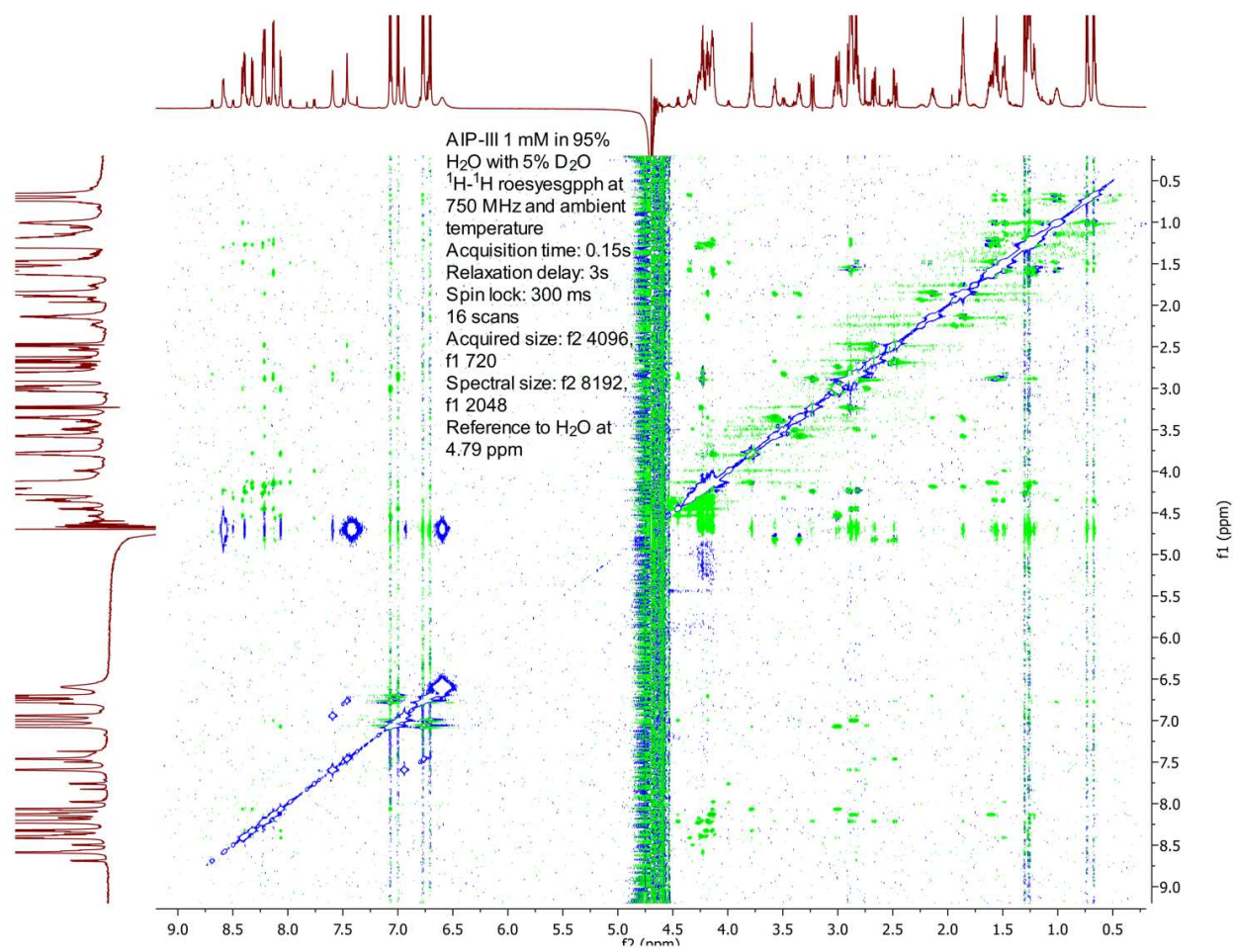
- AIP-III ^1H - ^1H TOCSY spectrum (20 ms spin lock)



- AIP-III ^1H - ^1H TOCSY spectrum (120 ms spin lock)



- AIP-III ^1H - ^1H ROESY spectrum



3.4.3 3J coupling constants for 3-D solution-phase structures

3J coupling constants are listed below (if resolved from spectra).

Table 3.S1 Important 3J coupling constants of AIP-I in Hz

Residue	H α -HN	H α -H β_1	H α -H β_2	H β_1 -H β_2	H α -H β	H β -H γ_1	H β -H γ_2
Ser2	7.1						
Val3	8.3				8.2	7.2	7.0
Cys4	7.4	11.2	4.7	14.4			
Ala5	7.0				7.5		
Ser6	8.5	4.8*	4.5*	11.6			
Tyr7	6.8	3.8	9.7	14.9			
Phe8	9.3	4.3	10.7	14.9			

* indicates stereochemistry ambiguous, not defined

Table 3.S2 Important 3J coupling constants of t-AIP-I in Hz

Residue	H α -HN	H α -H β_1	H α -H β_2	H β_1 -H β_2	H α -H β	H β -H γ_1	H β -H γ_2
Cys1	7.7	10.6	4.5	13.8			
Ala2	6.7				7.3		
Ser3	8.3	4.8*	6.5*	11.7			
Tyr4	6.5	5.7	9.5	14.8			
Phe5	9.6	4.5	11.0	14.8			

* indicates stereochemistry ambiguous, not defined

Table 3.S3 Important 3J coupling constants of AIP-I V3A in Hz

Residue	H α -HN	H α -H β_1	H α -H β_2	H β_1 -H β_2	H α -H β	H β -H γ_1	H β -H γ_2
Ser2	6.6						
Ala3	6.8				7.8		
Cys4	7.6	10.6	4.5	14.0			
Ala5	6.3				7.7		
Ser6	8.4	5.1*	6.7*	11.6			
Tyr7	6.4	6.2	9.6	14.8			
Phe8	9.4	4.3	11.0	14.9			

* indicates stereochemistry ambiguous, not defined

Table 3.S4 Important 3J coupling constants of AIP-I D1A in Hz

Residue	H α -HN	H α -H β_1	H α -H β_2	H β_1 -H β_2	H α -H β	H β -H γ_1	H β -H γ_2
Ser2	6.9	5.3*	6.9*	11.6			
Val3	8.1				7.9	7.1	7.1
Cys4	7.4	10.8	4.5	14.0			
Ala5	7.0				7.4		
Ser6	8.5	5.2*	6.8*	11.4			
Tyr7	6.7	5.9	9.6	14.9			
Phe8	9.4	4.4	11.0	14.9			

* indicates stereochemistry ambiguous, not defined

Table 3.S5 Important 3J coupling constants of AIP-I D1AS6A in Hz

Residue	H α -HN	H α -H β_1	H α -H β_2	H β_1 -H β_2	H α -H β	H β -H γ_1	H β -H γ_2
Ser2	7.0	5.3*	6.5*	11.6			
Val3	8.2				8.3	7.2	7.2
Cys4	7.3	10.9	4.6	14.2			
Ala5	7.3				7.5		
Ala6	8.2				7.6		
Tyr7	7.4	6.3	10.0	14.4			
Phe8	9.4	4.0	11.1	15.0			

* indicates stereochemistry ambiguous, not defined

Table 3.S6 Important 3J coupling constants of AIP-I D1AV3AS6S (AAA) in Hz

Residue	H α -HN	H α -H β_1	H α -H β_2	H β_1 -H β_2	H α -H β	H β -H γ_1	H β -H γ_2
Ser2	6.5						
Ala3	6.4				7.2		
Cys4	7.4	10.4	4.5	14.1			
Ala5	7.0				7.3		
Ala6	8.4				7.3		
Tyr7	7.2	6.2	9.6	14.4			
Phe8	9.3	4.2	10.9	14.9			

* indicates stereochemistry ambiguous, not defined

Table 3.S7 Important 3J coupling constants of AIP-II in Hz

Residue	H α -HN	H α -H β_1	H α -H β_2	H β_1 -H β_2	H α -H β	H γ -H δ_1	H γ -H δ_2
Ala2	5.7				7.4		
Ser3	6.6	6.1*	5.5*	11.4			
Lys4	7.0						
Tyr5	7.3	7.8*	8.3*	13.9			
Asn6	8.2	7.3*	7.2*	16.0			
Pro7							
Cys8	7.2	11.1	4.7	14.2			
Ser9	8.0	6.3*	5.6*	12.0			
Asn10	8.1	7.8*	6.4*	15.6			
Tyr11	7.4	6.1	9.1	14.1			
Leu12	9.3					7.0	7.0

* indicates stereochemistry ambiguous, not defined

Table 3.S8 Important 3J coupling constants of AIP-III in Hz

Residue	H α -HN	H α -H β_1	H α -H β_2	H β_1 -H β_2	H α -H β	H γ -H δ_1	H γ -H δ_2
Ala2	5.6				7.4		
Ala3	6.2				7.4		
Lys4	7.2						
Tyr5	7.2	8.4*	7.6*	14.2			
Asn6	7.5	7.5*	7.0*	16.1			
Pro7							
Cys8	7.6	11.3	4.4	14.0			
Ala9	6.8				7.4		
Ser10	8.6	6.5*	5.9*	11.5			
Tyr11	7.2	7.6*	6.8*	14.2			
Leu12	9.3					7.0	7.0

* indicates stereochemistry ambiguous, not defined

3.4.4 Chemical shift assignment for 3-D solution-phase structures

Table 3.S9 Assignments for AIP-I

Residue	HN (ppm)	H α (ppm)	H β (ppm)	Others (ppm)
Asp1		4.19	2.75, 2.75	
Ser2	8.57	4.43	3.76, 3.76	
Val3	8.01	4.02	1.97	H γ 0.80, 0.82
Cys4	8.41	4.37	2.89, 3.28	
Ala5	8.35	4.21	1.28	
Ser6	8.20	4.03	3.65, 3.75	
Tyr7	7.92	4.20	2.40, 2.64	H δ 6.82; H ϵ 6.68
Phe8	8.37	4.80	2.82, 3.37	H δ 7.15; H ϵ 7.30; H ζ 7.23

Table 3.S10 Assignments for t-AIP-I

Residue	HN (ppm)	H α (ppm)	H β (ppm)	Others (ppm)
Ac		1.89		
Cys1	8.15	4.34	2.89, 3.25	
Ala2	8.20	4.21	1.27	
Ser3	8.03	4.02	3.65, 3.75	
Tyr4	7.88	4.16	2.40, 2.64	H δ 6.81; H ϵ 6.66
Phe5	8.29	4.77	2.81, 3.36	H δ 7.17; H ϵ 7.29; H ζ 7.22

Table 3.S11 Assignments for AIP-I V3A

Residue	HN (ppm)	H α (ppm)	H β (ppm)	Others (ppm)
Asp1		4.32	3.97, 3.03	
Ser2	8.70	4.41	3.81, 3.81	
Ala3	8.24	4.23	1.30	
Cys4	8.23	4.40	2.93, 3.33	
Ala5	8.48	4.24	1.31	
Ser6	8.38	4.08	3.69, 3.78	
Tyr7	7.98	4.32	2.45, 2.66	H δ 6.82; H ϵ 6.70
Phe8	8.48	4.83	2.84, 3.39	H δ 7.17; H ϵ 7.31; H ζ 7.24

Table 3.S12 Assignments for AIP-I D1A

Residue	HN (ppm)	H α (ppm)	H β (ppm)	Others (ppm)
Ala1		4.06	1.46	
Ser2	8.61	4.47	3.78, 3.78	
Val3	8.25	4.04	1.97	H γ 0.81, 0.84
Cys4	8.55	4.41	2.91, 3.32	
Ala5	8.47	4.24	1.29	
Ser6	8.32	4.02	3.68, 3.77	
Tyr7	7.96	4.24	2.42, 2.67	H δ 6.83; H ϵ 6.70
Phe8	8.44	4.83	2.83, 3.38	H δ 7.15; H ϵ 7.30; H ζ 7.24

Table 3.S13 Assignments for AIP-I D1AS6A

Residue	HN (ppm)	H α (ppm)	H β (ppm)	Others (ppm)
Ala1		4.05	1.46	
Ser2	8.60	4.47	3.76, 3.79	
Val3	8.24	4.04	1.96	H γ 0.81, 0.84
Cys4	8.53	4.41	2.88, 3.32	
Ala5	8.47	4.22	1.28	
Ala6	8.36	3.97	1.24	
Tyr7	7.69	4.22	2.58, 2.69	H δ 6.82; H ϵ 6.69
Phe8	8.43	4.80	2.83, 3.42	H δ 7.20; H ϵ 7.32; H ζ 7.24

Table 3.S14 Assignments for AIP-I D1AV3AS6A (AAA)

Residue	HN (ppm)	H α (ppm)	H β (ppm)	Others (ppm)
Ala1		4.18	1.58	
Ser2	8.63	4.52	3.91, 3.91	
Ala3	8.46	4.36	1.41	
Cys4	8.36	4.41	3.03, 3.45	
Ala5	8.48	4.35	1.40	
Ala6	8.35	4.12	1.36	
Tyr7	7.75	4.35	2.73, 2.82	H δ 6.94; H ϵ 6.82
Phe8	8.52	4.90	2.97, 3.51	H δ 7.31; H ϵ 7.44; H ζ 7.37

Table 3.S15 Assignments for AIP-II

Residue	HN (ppm)	Hα (ppm)	Hβ (ppm)	Others (ppm)
Asn1		4.34	2.94, 3.01	H δ 7.05, 7.50
Ala2	8.73	4.42	1.41	
Ser3	8.38	4.41	3.83, 3.87	
Lys4	8.34	4.26	1.65, 1.70	H γ 1.28; H δ 1.60, 1.66; H ϵ 2.96
Tyr5	8.20	4.54	2.93, 2.96	H δ 7.10; H ϵ 6.81
Asn6	8.25	4.93	2.58, 2.77	H δ 6.86, 7.55
Pro7		4.30	1.96, 2.23	H γ 1.94, 1.98; H δ 3.49, 3.63
Cys8	8.37	4.43	2.93, 3.39	
Ser9	8.56	4.46	3.77, 3.79	
Asn10	8.69	4.39	2.85, 2.89	H δ 6.93, 7.63
Tyr11	8.15	4.52	3.12, 3.17	H δ 7.15; H ϵ 6.87
Leu12	8.24	4.54	1.64, 1.74	H γ 1.29; H δ 0.81, 0.88

Table 3.S16 Assignments for AIP-III

Residue	HN (ppm)	Hα (ppm)	Hβ (ppm)	Others (ppm)
Asn1		4.23	2.83, 2.89	H δ 6.94, 7.59
Ala2	8.59	4.27	1.30	
Ala3	8.23	4.16	1.26	
Lys4	8.13	4.13	1.59, 1.63	H γ 1.22, 1.26; H δ 1.54, 1.57; H ϵ 2.88
Tyr5	8.13	4.45	2.84, 2.88	H δ 7.00; H ϵ 6.70
Asn6	8.21	4.82	2.48, 2.67	H δ 6.76, 7.46
Pro7		4.18	1.87, 2.14	H γ 1.85, 1.88; H δ 3.35, 3.57
Cys8	8.21	4.24	2.89, 3.23	
Ala9	8.39	4.20	1.27	
Ser10	8.32	4.14	3.78	
Tyr11	8.06	4.53	2.98, 3.02	H δ 7.07; H ϵ 6.77
Leu12	8.41	4.35	1.49, 1.57	H γ 1.01; H δ 0.67, 0.74

3.4.5 ROE constraint statistics

AIP-I

```
=====
total NOEs in noe-sq.tbl residue 1 to residue 8: 66
=====
```

```
intra_residual (j-i = 0): 46
sequential (j-i = 1): 20
medium range (j-i = 2 ): 0
medium range (j-i = 3 ): 0
medium range (j-i = 4 ): 0
long range (j-i >= 5 ): 0
```

```
residue 1 has 2 NOEs
residue 2 has 5 NOEs
residue 3 has 9 NOEs
residue 4 has 7 NOEs
residue 5 has 6 NOEs
residue 6 has 8 NOEs
residue 7 has 19 NOEs
residue 8 has 10 NOEs
```

t-AIP-I

```
=====
total NOEs in noe-sq.tbl residue 0 to residue 5: 63
=====
```

```
intra_residual (j-i = 0): 33
sequential (j-i = 1): 25
medium range (j-i = 2 ): 2
medium range (j-i = 3 ): 1
medium range (j-i = 4 ): 2
long range (j-i >= 5 ): 0
```

```
residue 0 has 1 NOEs
residue 1 has 9 NOEs
residue 2 has 10 NOEs
residue 3 has 12 NOEs
residue 4 has 21 NOEs
residue 5 has 10 NOEs
```

AIP-I V3A

```
=====
total NOEs in noe-sq.tbl residue 1 to residue 8: 78
=====
```

```
intra_residual (j-i = 0):  41
sequential   (j-i = 1):   34
medium range (j-i = 2 ):   1
medium range (j-i = 3 ):   0
medium range (j-i = 4 ):   2
long range  (j-i >= 5 ):   0
```

```
residue 1 has 7 NOEs
residue 2 has 9 NOEs
residue 3 has 5 NOEs
residue 4 has 9 NOEs
residue 5 has 6 NOEs
residue 6 has 10 NOEs
residue 7 has 20 NOEs
residue 8 has 12 NOEs
```

AIP-I D1A

```
=====
total NOEs in noe-sq.tbl residue 1 to residue 8: 88
=====
```

```
intra_residual (j-i = 0):  39
sequential   (j-i = 1):   39
medium range (j-i = 2 ):   6
medium range (j-i = 3 ):   0
medium range (j-i = 4 ):   4
long range  (j-i >= 5 ):   0
```

```
residue 1 has 6 NOEs
residue 2 has 9 NOEs
residue 3 has 13 NOEs
residue 4 has 12 NOEs
residue 5 has 6 NOEs
residue 6 has 15 NOEs
residue 7 has 18 NOEs
residue 8 has 9 NOEs
```

AIP-I D1AS6A

```
=====
total NOEs in noe-sq.tbl residue 1 to residue 8: 74
=====
```

```
intra_residual (j-i = 0):  37
sequential   (j-i = 1):   30
medium range (j-i = 2 ):   2
medium range (j-i = 3 ):   1
medium range (j-i = 4 ):   4
long range  (j-i >= 5 ):   0
```

```
residue 1 has 2 NOEs
residue 2 has 7 NOEs
residue 3 has 12 NOEs
residue 4 has 11 NOEs
residue 5 has 6 NOEs
residue 6 has 8 NOEs
residue 7 has 20 NOEs
residue 8 has 8 NOEs
```

AIP-I D1AV3AS6A (AAA)

```
=====
total NOEs in noe-sq.tbl residue 1 to residue 8: 72
=====
```

```
intra_residual (j-i = 0):  32
sequential   (j-i = 1):   31
medium range (j-i = 2 ):   1
medium range (j-i = 3 ):   1
medium range (j-i = 4 ):   7
long range  (j-i >= 5 ):   0
```

```
residue 1 has 3 NOEs
residue 2 has 6 NOEs
residue 3 has 5 NOEs
residue 4 has 15 NOEs
residue 5 has 7 NOEs
residue 6 has 7 NOEs
residue 7 has 20 NOEs
residue 8 has 9 NOEs
```


AIP-II

```
=====
total NOEs in noe-sq.tbl residue 1 to residue 12: 158
=====
```

```
intra_residual (j-i = 0): 82
sequential (j-i = 1): 56
medium range (j-i = 2 ): 14
medium range (j-i = 3 ): 5
medium range (j-i = 4 ): 0
long range (j-i >= 5 ): 1
```

```
residue 1 has 11 NOEs
residue 2 has 6 NOEs
residue 3 has 16 NOEs
residue 4 has 16 NOEs
residue 5 has 19 NOEs
residue 6 has 16 NOEs
residue 7 has 13 NOEs
residue 8 has 8 NOEs
residue 9 has 9 NOEs
residue 10 has 11 NOEs
residue 11 has 20 NOEs
residue 12 has 13 NOEs
```

AIP-III

```
=====
total NOEs in noe-sq.tbl residue 1 to residue 12: 137
=====
```

```
intra_residual (j-i = 0): 75
sequential (j-i = 1): 52
medium range (j-i = 2 ): 8
medium range (j-i = 3 ): 0
medium range (j-i = 4 ): 2
long range (j-i >= 5 ): 0
```

```
residue 1 has 11 NOEs
residue 2 has 8 NOEs
residue 3 has 6 NOEs
residue 4 has 12 NOEs
residue 5 has 17 NOEs
residue 6 has 13 NOEs
residue 7 has 13 NOEs
residue 8 has 11 NOEs
residue 9 has 6 NOEs
residue 10 has 8 NOEs
residue 11 has 21 NOEs
residue 12 has 11 NOEs
```

3.4.6 Additional images of structure ensembles

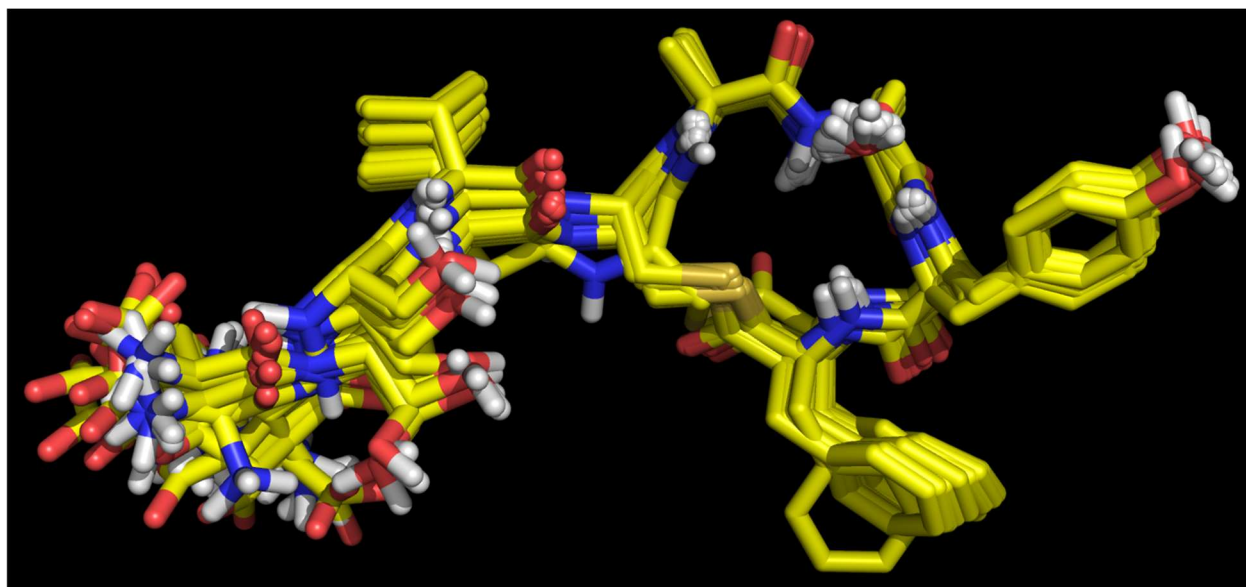


Figure 3.S1 Heavy atom ensemble of the 20 lowest-energy structures for AIP-I. Backbone RMSD from average = 0.4 Å, heavy atom RMSD from average = 1.2 Å.

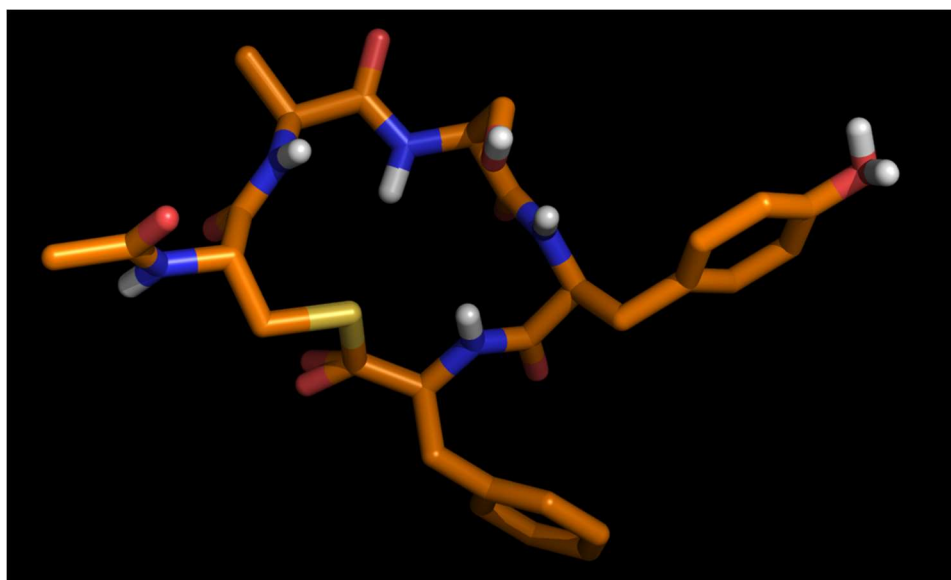


Figure 3.S2 Heavy atom ensemble of the 20 lowest-energy structures for t-AIP-I. Backbone RMSD from average = 0.1 Å, heavy atom RMSD from average = 0.5 Å.

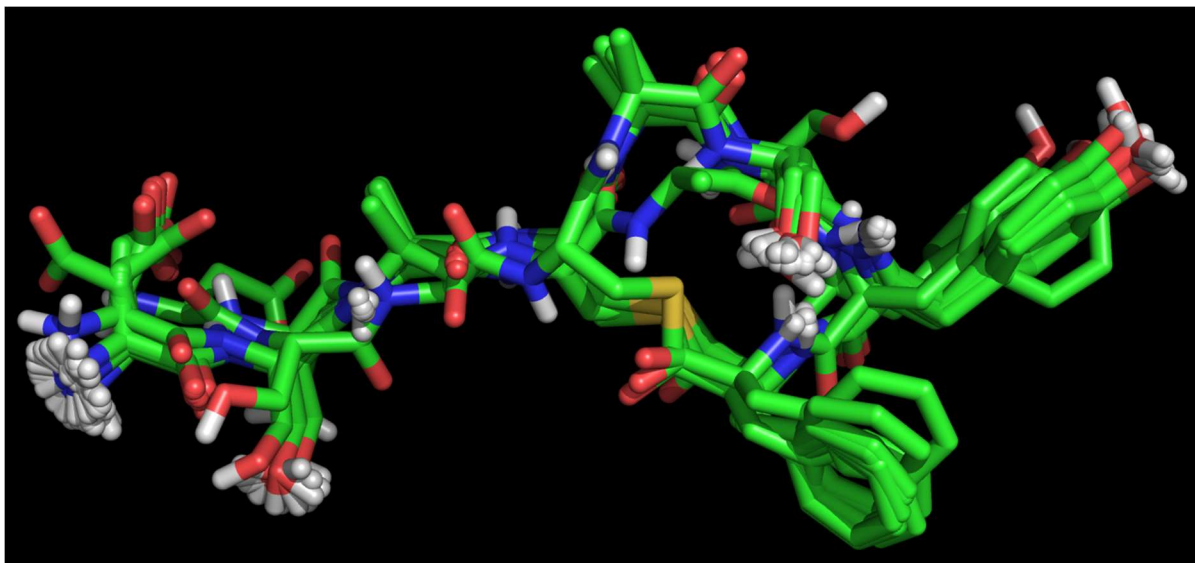


Figure 3.S3 Heavy atom ensemble of the 20 lowest-energy structures for AIP-I V3A. Backbone RMSD from average = 0.3 Å, heavy atom RMSD from average = 1.0 Å.

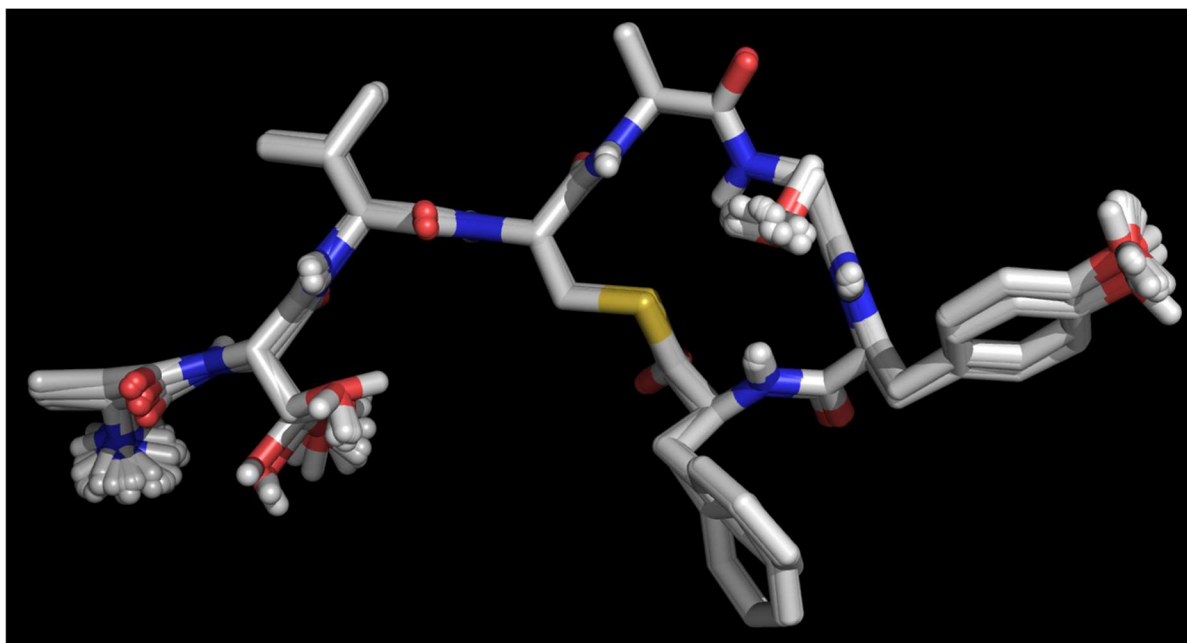


Figure 3.S4 Heavy atom ensemble of the 20 lowest-energy structures for AIP-I D1A. Backbone RMSD from average = 0.1 Å, heavy atom RMSD from average = 0.7 Å.

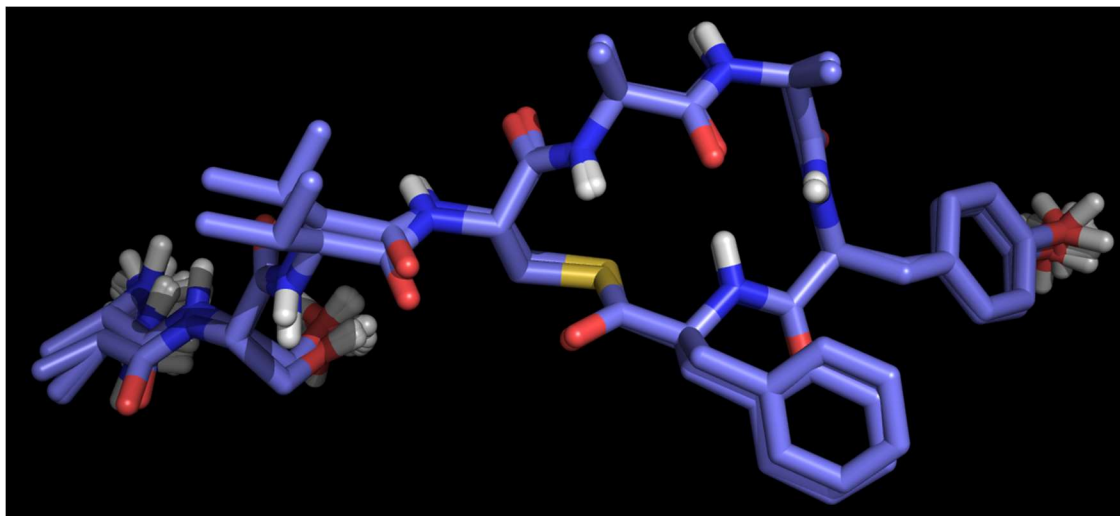


Figure 3.S5 Heavy atom ensemble of the 20 lowest-energy structures for AIP-I D1AS6A. Backbone RMSD from average = 0.1 Å, heavy atom RMSD from average = 0.5 Å.

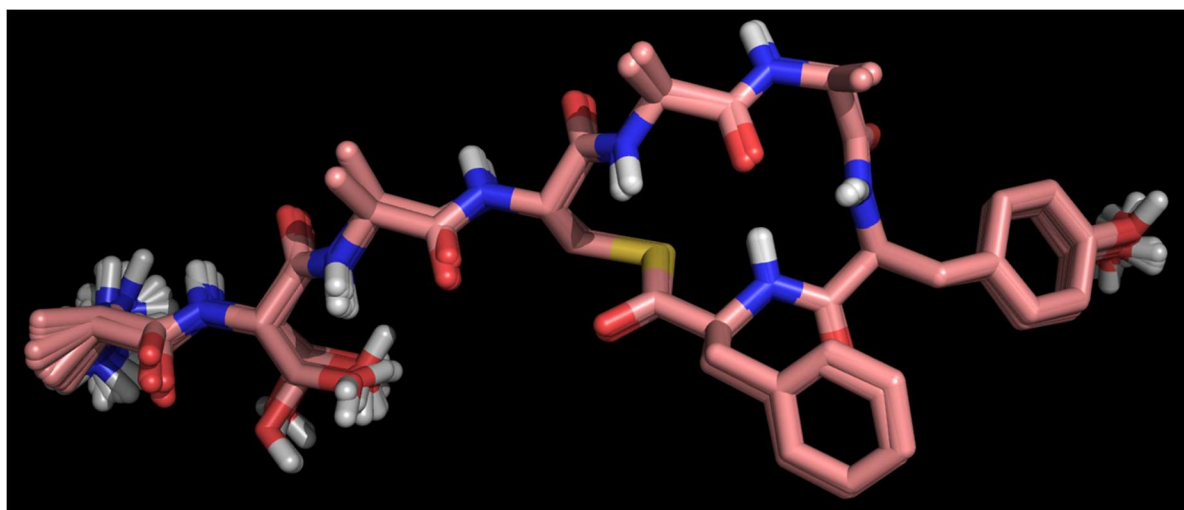


Figure 3.S6 Heavy atom ensemble of the 20 lowest-energy structures for AIP-I D1AV3AS6A (AAA). Backbone RMSD from average = 0.2 Å, heavy atom RMSD from average = 0.6 Å.

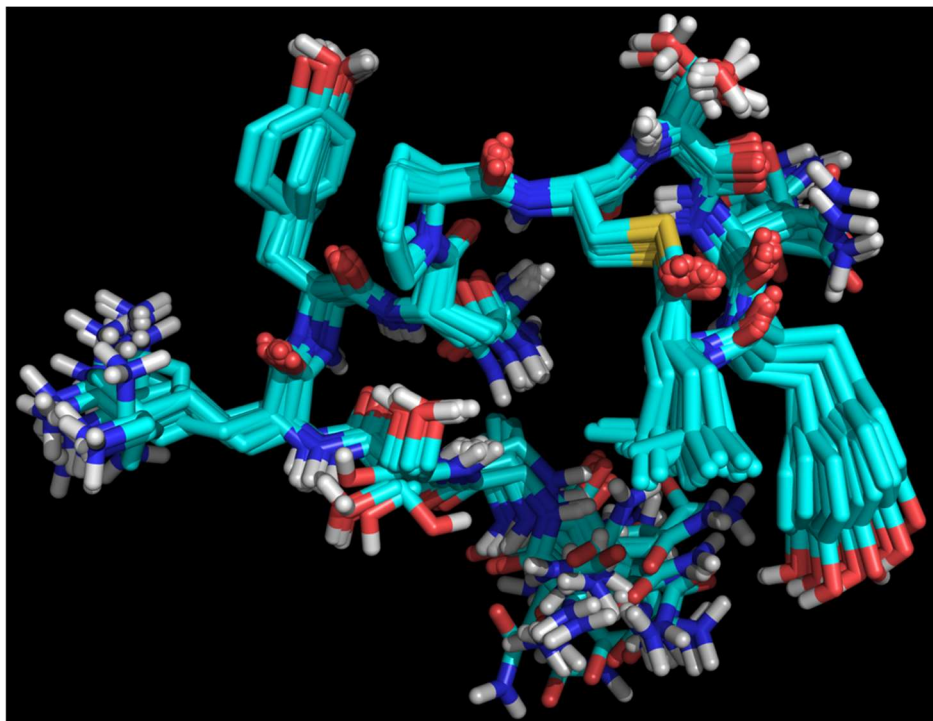


Figure 3.S7 Heavy atom ensemble of the 20 lowest-energy structures for AIP-II. Backbone RMSD from average = 0.4 Å, heavy atom RMSD from average = 1.1 Å.

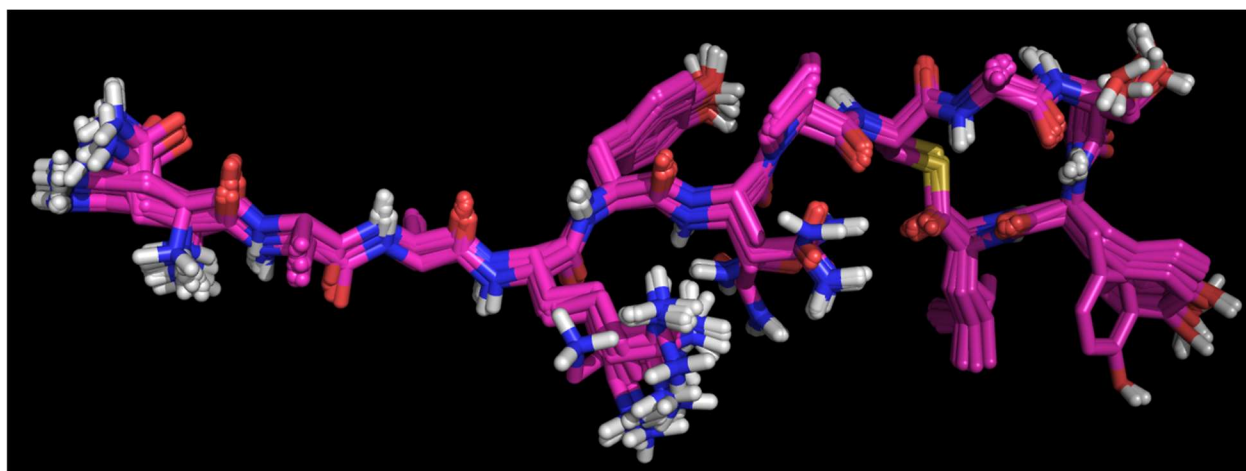


Figure 3.S8 Heavy atom ensemble of the 20 lowest-energy structures for AIP-III. Backbone RMSD from average = 0.3 Å, heavy atom RMSD from average = 0.9 Å.

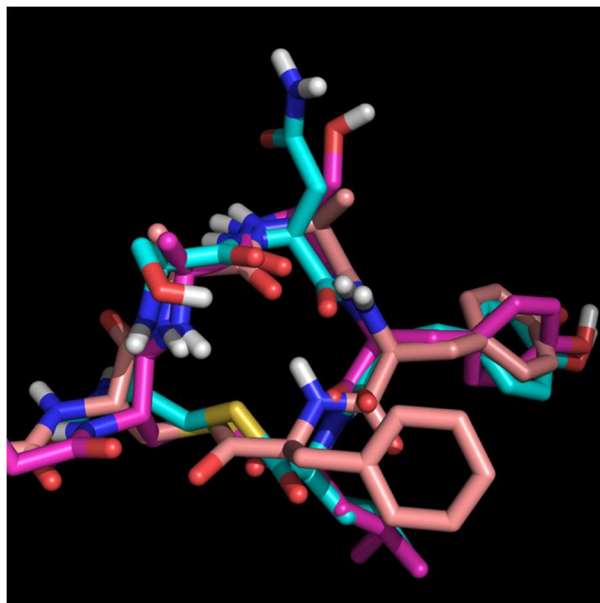


Figure 3.S9 Overlay of the macrocycles from AAA, AIP-II, and AIP-III. The tails are removed for clarity. All-atom RMS difference of AIP-II to AAA = 1.9 Å, and all-atom RMS difference of AIP-III to AAA = 1.2 Å.

3.4.7 Validation using MolProbity

- Analysis of AIP-I representative structure

5/8/2019

Viewing AIP-I-multi.table - MolProbity



Viewing AIP-I-multi.table

Duke Biochemistry
Duke University School of MedicineWhen finished, you should [close this window](#).*Hint: Use File | Save As... to save a copy of this page.*

All-Atom Contacts	Clashscore, all atoms:	0	100 th percentile* (N=1784, all resolutions)
	Clashscore is the number of serious steric overlaps (> 0.4 Å) per 1000 atoms.		
Protein Geometry	Poor rotamers	0	0.00% Goal: <0.3%
	Favored rotamers	7	100.00% Goal: >98%
	Ramachandran outliers	1	16.67% Goal: <0.05%
	Ramachandran favored	4	66.67% Goal: >98%
	MolProbity score [^]	1.37	98 th percentile* (N=27675, 0Å - 99Å)
	Cβ deviations >0.25Å	0	0.00% Goal: 0
	Bad bonds:	0 / 62	0.00% Goal: 0%
Bad angles:	1 / 83	1.20% Goal: <0.1%	
Peptide Omegas	Cis Prolines:	0 / 0	0.00% Expected: ≤1 per chain, or ≤5%

In the two column results, the left column gives the raw count, right column gives the percentage.

* 100th percentile is the best among structures of comparable resolution; 0th percentile is the worst. For clashscore the comparative set of structures was selected in 2004, for MolProbity score in 2006.[^]MolProbity score combines the clashscore, rotamer, and Ramachandran evaluations into a single score, normalized to be on the same scale as X-ray resolution.

#	Alt Res	High B	Clash > 0.4Å	Ramachandran	Rotamer	Cβ deviation	Bond lengths	Bond angles	Cis Peptides
		Avg: 0.00	Clashscore: 0	Outliers: 1 of 6	Poor rotamers: 0 of 7 Favored (98.1%) <i>m</i> -30 chi angles: 286.9,167.7	Outliers: 0 of 8 0.06Å	Outliers: 0 of 8	Outliers: 1 of 8	Non-Trans: 0 of 7
1	ASP	0	-	-			-	-	-
2	SER	0	-	Favored (24.33%) General / -153.6,146.4	Favored (46.9%) <i>t</i> chi angles: 180.2	0.03Å	-	-	-
3	VAL	0	-	Favored (70.89%) Ile or Val /	Favored (83.5%) <i>t</i> chi angles: 177	0.03Å	-	-	-
				-127.0,128.6					
4	CYS	0	-	Favored (33%) General / -125.3,121.1	Favored (52.5%) <i>t</i> chi angles: 180.6	0.05Å	-	-	-
5	ALA	0	-	Allowed (1.67%) General / -135.0,61.5	-	0.04Å	-	-	-
6	SER	0	-	OUTLIER (0%) General / -174.5,-97.4	Favored (69.9%) <i>p</i> chi angles: 58.9	0.02Å	-	-	-
7	TYR	0	-	Favored (81.51%) General / -68.0,-37.6	Favored (67%) <i>m</i> -80 chi angles: 286.9,99.5	0.02Å	-	-	-
8	PHE	0	-	-	Favored (70.2%) <i>m</i> -80 chi angles: 288.5,102.5	0.04Å	-	OUTLIER(S) worst is CA-CB-CG: 4.1 6	-

- Analysis of AIP-II representative structure

5/8/2019

Viewing AIP-II-multi.table - MolProbity



Viewing AIP-II-multi.table



Duke Biochemistry
Duke University School of Medicine

When finished, you should [close this window](#).

Hint: Use File | Save As... to save a copy of this page.

All-Atom Contacts	Clashscore, all atoms:	5.46	92 nd percentile* (N=1784, all resolutions)
	Clashscore is the number of serious steric overlaps (> 0.4 Å) per 1000 atoms.		
Protein Geometry	Poor rotamers	1	9.09% Goal: <0.3%
	Favored rotamers	9	81.82% Goal: >98%
	Ramachandran outliers	3	30.00% Goal: <0.05%
	Ramachandran favored	5	50.00% Goal: >98%
	MolProbity score [^]	2.99	23 rd percentile* (N=27675, 0Å - 99Å)
	Cβ deviations >0.25Å	0	0.00% Goal: 0
	Bad bonds:	0 / 97	0.00% Goal: 0%
Bad angles:	0 / 131	0.00% Goal: <0.1%	
Peptide Omegas	Cis Prolines:	0 / 1	0.00% Expected: ≤1 per chain, or ≤5%

In the two column results, the left column gives the raw count, right column gives the percentage.

* 100th percentile is the best among structures of comparable resolution; 0th percentile is the worst. For clashscore the comparative set of structures was selected in 2004, for MolProbity score in 2006.[^]MolProbity score combines the clashscore, rotamer, and Ramachandran evaluations into a single score, normalized to be on the same scale as X-ray resolution.

#	Alt Res	High B	Clash > 0.4Å	Ramachandran	Rotamer	Cβ deviation	Bond lengths	Bond angles	Cis Peptides
		Avg:	Clashscore:	Outliers: 3 of 10	Poor rotamers: 1 of 11	Outliers: 0 of 12	Outliers: 0 of 12	Outliers: 0 of 12	Non-Trans: 0 of 11
		0.00	5.46						
1	ASN	0	-	-	Favored (2.4%) <i>m-40</i> chi angles: 263.1,17.6	0.06Å	-	-	-
2	ALA	0	-	Favored (2.63%) General / -160.8,120.1	-	0.03Å	-	-	-
3	SER	0	0.40Å O with 5 TYR N	Favored (36.09%) General / -71.8,158.4	Favored (86.9%) <i>p</i> chi angles: 67.1	0.03Å	-	-	-
4	LYS	0	-	OUTLIER (0.01%)	Favored (50.7%) <i>tttp</i> chi angles:	0.06Å	-	-	-
5	TYR	0	0.40Å N with 3 SER O	General / -51.0,94.6 Favored (2.17%) General / 60.6,59.4	179.1,179.7,177.4,62.7 Favored (37.7%) <i>t80</i> chi angles: 193.4,258.6	0.03Å	-	-	-
6	ASN	0	-	Allowed (1.66%) Pre-Pro / -49.1,110.9	Allowed (1.2%) <i>p0</i> chi angles: 40.5,21.7	0.07Å	-	-	-
7	PRO	0	-	Favored (3.38%) Trans-Pro / -81.8,50.1	Favored (82.3%) <i>Cg_endo</i> chi angles: 30.5,330.4,16.7	0.05Å	-	-	-
8	CYS	0	-	Favored (35.81%) General / -136.7,133.1	Favored (23.4%) <i>t</i> chi angles: 173.3	0.04Å	-	-	-
9	SER	0	-	Allowed (0.48%) General / -69.9,84.3	Favored (7.3%) <i>p</i> chi angles: 49.1	0.04Å	-	-	-
10	ASN	0	-	OUTLIER (0.01%) General / 62.9,127.7	Favored (98.9%) <i>m-40</i> chi angles: 289.4,342	0.02Å	-	-	-
11	TYR	0	-	OUTLIER (0.01%) General / 44.6,90.9	OUTLIER (0.2%) chi angles: 239.9,256.5	0.01Å	-	-	-
12	LEU	0	-	-	Favored (5.8%) <i>mt</i> chi angles: 315,189.5	0.04Å	-	-	-

- Analysis of AIP-III representative structure

5/8/2019

Viewing AIP-III-multi.table - MolProbity



Viewing AIP-III-multi.table



Duke Biochemistry
Duke University School of Medicine

When finished, you should [close this window](#).

Hint: Use File | Save As... to save a copy of this page.

All-Atom Contacts	Clashscore, all atoms:	0	100 th percentile* (N=1784, all resolutions)	
	Clashscore is the number of serious steric overlaps (> 0.4 Å) per 1000 atoms.			
Protein Geometry	Poor rotamers	3	33.33%	Goal: <0.3%
	Favored rotamers	6	66.67%	Goal: >98%
	Ramachandran outliers	0	0.00%	Goal: <0.05%
	Ramachandran favored	9	90.00%	Goal: >98%
	MolProbity score [^]	2.21	64 th percentile* (N=27675, 0Å - 99Å)	
	Cβ deviations >0.25Å	0	0.00%	Goal: 0
	Bad bonds:	0 / 93	0.00%	Goal: 0%
Bad angles:	0 / 126	0.00%	Goal: <0.1%	
Peptide Omegas	Cis Prolines:	0 / 1	0.00%	Expected: ≤1 per chain, or ≤5%

In the two column results, the left column gives the raw count, right column gives the percentage.

* 100th percentile is the best among structures of comparable resolution; 0th percentile is the worst. For clashscore the comparative set of structures was selected in 2004, for MolProbity score in 2006.

[^]MolProbity score combines the clashscore, rotamer, and Ramachandran evaluations into a single score, normalized to be on the same scale as X-ray resolution.

#	Alt Res	High B	Clash > 0.4Å	Ramachandran	Rotamer	Cβ deviation	Bond lengths	Bond angles	Cis Peptides
		Avg: 0.00	Clashscore: 0	Outliers: 0 of 10	Poor rotamers: 3 of 9	Outliers: 0 of 12	Outliers: 0 of 12	Outliers: 0 of 12	Non-Trans: 0 of 11
1	ASN	0	-	-	Favored (43.5%) <i>t0</i> chi angles: 189.1,359.7	0.06Å	-	-	-
2	ALA	0	-	Favored (17.96%) General / -156.1,141.9	-	0.04Å	-	-	-
3	ALA	0	-	Favored (33.97%) General / -149.2,151.2	-	0.04Å	-	-	-
4	LYS	0	-	Favored (39.71%) General / -106.7,119.6	Favored (51.5%) <i>ttp</i> chi angles: 181,178.6,177.5,62.4	0.04Å	-	-	-
5	TYR	0	-	Favored (47.11%) General / -118.8,124.4	Favored (89.2%) <i>t80</i> chi angles: 180,78.9	0.05Å	-	-	-
6	ASN	0	-	Favored (54.95%) Pre-Pro / -107.4,117.8	OUTLIER (0.2%) chi angles: 180.5,109.7	0.02Å	-	-	-
7	PRO	0	-	Favored (73.4%) Trans-Pro / -68.9,150.6	Favored (56.6%) <i>Cg_endo</i> chi angles: 26,326.1,28.2	0.04Å	-	-	-
8	CYS	0	-	Favored (25.3%) General / -99.1,113.2	Favored (45%) <i>t</i> chi angles: 177.4	0.04Å	-	-	-
9	ALA	0	-	Favored (29.37%) General / -119.8,117.9	-	0.04Å	-	-	-
10	SER	0	-	Allowed (0.15%) General / 69.8,-70.1	OUTLIER (0%) chi angles: 250.7	0.02Å	-	-	-
11	TYR	0	-	Favored (46.11%) General / -111.1,121.7	OUTLIER (0.2%) chi angles: 237.8,128.2	0.05Å	-	-	-
12	LEU	0	-	-	Favored (50.9%) <i>mt</i> chi angles: 285.9,174	0.04Å	-	-	-

- Analysis of *t*-AIP-I representative structure

5/8/2019

Viewing t-AIP-I-multi.table - MolProbity



Viewing t-AIP-I-multi.table



Duke Biochemistry
Duke University School of Medicine

When finished, you should

Hint: Use File | Save As... to save a copy of this page.

All-Atom Contacts	Clashscore, all atoms:	0		100 th percentile* (N=1784, all resolutions)
	Clashscore is the number of serious steric overlaps (> 0.4 Å) per 1000 atoms.			
Protein Geometry	Poor rotamers	0	0.00%	Goal: <0.3%
	Favored rotamers	4	100.00%	Goal: >98%
	Ramachandran outliers	1	33.33%	Goal: <0.05%
	Ramachandran favored	1	33.33%	Goal: >98%
	MolProbity score [^]	1.55		94 th percentile* (N=27675, 0Å - 99Å)
	Cβ deviations >0.25Å	0	0.00%	Goal: 0
	Bad bonds:	0 / 43	0.00%	Goal: 0%
Bad angles:	1 / 56	1.79%	Goal: <0.1%	
Peptide Omegas	Cis Prolines:	0 / 0	0.00%	Expected: ≤1 per chain, or ≤5%

In the two column results, the left column gives the raw count, right column gives the percentage.

* 100th percentile is the best among structures of comparable resolution; 0th percentile is the worst. For clashscore the comparative set of structures was selected in 2004, for MolProbity score in 2006.

[^]MolProbity score combines the clashscore, rotamer, and Ramachandran evaluations into a single score, normalized to be on the same scale as X-ray resolution.

#	Alt Res	High B	Clash > 0.4Å	Ramachandran	Rotamer	Cβ deviation	Bond lengths	Bond angles	Cis Peptides
		Avg: 0.00	Clashscore: 0	Outliers: 1 of 3	Poor rotamers: 0 of 4	Outliers: 0 of 5	Outliers: 0 of 6	Outliers: 1 of 6	Non-Trans: 0 of 5
0	ACE	0	-	-	-	-	-	-	-
1	CYS	0	-	-	Favored (44.8%) <i>t</i> chi angles: 177.4	0.04Å	-	-	-
2	ALA	0	-	Allowed (1.8%) General / -138.5,52.8	-	0.02Å	-	-	-
3	SER	0	-	OUTLIER (0.02%) General / -159.3,-103.5	Favored (80.1%) <i>p</i> chi angles: 61.4	0.03Å	-	-	-
4	TYR	0	-	Favored (89.52%) General / -65.9,-38.8	Favored (38.8%) <i>m</i> - 80 chi angles: 282.5,111	0.03Å	-	-	-
5	PHE	0	-	-	Favored (41.7%) <i>m</i> - 80 chi angles: 285.4,114.7	0.03Å	-	OUTLIER(S) worst is CA-CB-CG: 4.1 σ	-

About MolProbity | Website for the Richardson Lab | Using nuclear x-H | Internal reference 4.4

- Analysis of AIP-I D1A representative structure

5/8/2019

Viewing D1A-multi.table - MolProbity



Viewing D1A-multi.table



Duke Biochemistry
Duke University School of Medicine

When finished, you should [close this window](#).

Hint: Use File | Save As... to save a copy of this page.

All-Atom Contacts	Clashscore, all atoms:	0	100 th percentile* (N=1784, all resolutions)	
	Clashscore is the number of serious steric overlaps (> 0.4 Å) per 1000 atoms.			
Protein Geometry	Poor rotamers	0	0.00%	Goal: <0.3%
	Favored rotamers	6	100.00%	Goal: >98%
	Ramachandran outliers	1	16.67%	Goal: <0.05%
	Ramachandran favored	5	83.33%	Goal: >98%
	MolProbity score [^]	1.19		99 th percentile* (N=27675, 0Å - 99Å)
	Cβ deviations >0.25Å	0	0.00%	Goal: 0
	Bad bonds:	0 / 59	0.00%	Goal: 0%
Bad angles:	1 / 79	1.27%	Goal: <0.1%	
Peptide Omegas	Cis Prolines:	0 / 0	0.00%	Expected: ≤1 per chain, or ≤5%

In the two column results, the left column gives the raw count, right column gives the percentage.

* 100th percentile is the best among structures of comparable resolution; 0th percentile is the worst. For clashscore the comparative set of structures was selected in 2004, for MolProbity score in 2006.[^]MolProbity score combines the clashscore, rotamer, and Ramachandran evaluations into a single score, normalized to be on the same scale as X-ray resolution.

#	Alt Res	High B	Clash > 0.4Å	Ramachandran	Rotamer	Cβ deviation	Bond lengths	Bond angles	Cis Peptides
		Avg: 0.00	Clashscore: 0	Outliers: 1 of 6	Poor rotamers: 0 of 6	Outliers: 0 of 8	Outliers: 0 of 8	Outliers: 1 of 8	Non-Trans: 0 of 7
1	ALA	0	-	-	-	0.06Å	-	-	-
2	SER	0	-	Favored (21.9%) General / -157.1,148.3	Favored (33.9%) <i>t</i> chi angles: 181.8	0.02Å	-	-	-
3	VAL	0	-	Favored (51.59%) Ile or Val / -123.9,117.6	Favored (57.3%) <i>t</i> chi angles: 180.3	0.08Å	-	-	-
4	CYS	0	-	Favored (53.46%) General / -119.9,128.2	Favored (48.3%) <i>t</i> chi angles: 178.8	0.04Å	-	-	-
5	ALA	0	-	Favored (2.07%) General / -130.0,51.6	-	0.04Å	-	-	-
6	SER	0	-	OUTLIER (0.01%) General / -171.0,-121.9	Favored (58.9%) <i>p</i> chi angles: 73.3	0.06Å	-	-	-
7	TYR	0	-	Favored (93.86%) General / -64.7,-39.5	Favored (93.6%) <i>m-80</i> chi angles: 296.8,102.1	0.03Å	-	-	-
8	PHE	0	-	-	Favored (89%) <i>m-80</i> chi angles: 292,99.6	0.04Å	-	OUTLIER(S) worst is CA-CB-CG: 4.2 σ	-

- Analysis of AIP-I V3A representative structure

5/8/2019

Viewing V3A-multi.table - MolProbity



Viewing V3A-multi.table



Duke Biochemistry
Duke University School of Medicine

When finished, you should [close this window](#).

Hint: Use File | Save As... to save a copy of this page.

All-Atom Contacts	Clashscore, all atoms:	0	100 th percentile* (N=1784, all resolutions)	
	Clashscore is the number of serious steric overlaps (> 0.4 Å) per 1000 atoms.			
Protein Geometry	Poor rotamers	0	0.00%	Goal: <0.3%
	Favored rotamers	5	83.33%	Goal: >98%
	Ramachandran outliers	0	0.00%	Goal: <0.05%
	Ramachandran favored	4	66.67%	Goal: >98%
	MolProbity score [^]	1.37		98 th percentile* (N=27675, 0Å - 99Å)
	Cβ deviations >0.25Å	0	0.00%	Goal: 0
	Bad bonds:	0 / 60	0.00%	Goal: 0%
Bad angles:	1 / 80	1.25%	Goal: <0.1%	
Peptide Omegas	Cis Prolines:	0 / 0	0.00%	Expected: ≤1 per chain, or ≤5%

In the two column results, the left column gives the raw count, right column gives the percentage.

* 100th percentile is the best among structures of comparable resolution; 0th percentile is the worst. For clashscore the comparative set of structures was selected in 2004, for MolProbity score in 2006.[^]MolProbity score combines the clashscore, rotamer, and Ramachandran evaluations into a single score, normalized to be on the same scale as X-ray resolution.

#	Alt Res	High B	Clash > 0.4Å	Ramachandran	Rotamer	Cβ deviation	Bond lengths	Bond angles	Cis Peptides
		Avg: 0.00	Clashscore: 0	Outliers: 0 of 6	Poor rotamers: 0 of 6	Outliers: 0 of 8	Outliers: 0 of 8	Outliers: 1 of 8	Non-Trans: 0 of 7
1	ASP	0	-	-	Favored (27.1%) <i>t</i> chi angles: 200.1,8	0.06Å	-	-	-
2	SER	0	-	Favored (8.37%) General / -144.7,116.8	Allowed (1.8%) <i>m</i> chi angles: 275.9	0.07Å	-	-	-
3	ALA	0	-	Favored (22.4%) General / -149.9,140.4	-	0.03Å	-	-	-
4	CYS	0	-	Favored (26.67%)	Favored (53%) <i>t</i>	0.05Å	-	-	-
5	ALA	0	-	General / -125.5,118.8 Allowed (0.75%) General / -111.0,52.1	chi angles: 180.8	0.03Å	-	-	-
6	SER	0	-	Allowed (0.25%) General / -165.8,-155.8	Favored (2.8%) <i>p</i> chi angles: 87.5	0.05Å	-	-	-
7	TYR	0	-	Favored (68.91%) General / -60.4,-29.4	Favored (70%) <i>m-80</i> chi angles: 290.5,107.6	0.03Å	-	-	-
8	PHE	0	-	-	Favored (36.5%) <i>m-80</i> chi angles: 309.5,114.6	0.03Å	-	OUTLIER(S) worst is CA-CB-CG: 4.3 σ	-

- Analysis of AIP-I D1AS6A representative structure

5/8/2019

Viewing AA-multi.table - MolProbity



Viewing AA-multi.table



Duke Biochemistry
Duke University School of Medicine

When finished, you should [close this window](#).

Hint: Use File | Save As... to save a copy of this page.

All-Atom Contacts	Clashscore, all atoms:	0	100 th percentile* (N=1784, all resolutions)	
	Clashscore is the number of serious steric overlaps (> 0.4 Å) per 1000 atoms.			
Protein Geometry	Poor rotamers	0	0.00%	Goal: <0.3%
	Favored rotamers	4	80.00%	Goal: >98%
	Ramachandran outliers	1	16.67%	Goal: <0.05%
	Ramachandran favored	5	83.33%	Goal: >98%
	MolProbity score [^]	1.19	99 th percentile* (N=27675, 0Å - 99Å)	
	Cβ deviations >0.25Å	0	0.00%	Goal: 0
	Bad bonds:	0 / 58	0.00%	Goal: 0%
Bad angles:	1 / 78	1.28%	Goal: <0.1%	
Peptide Omegas	Cis Prolines:	0 / 0	0.00%	Expected: ≤1 per chain, or ≤5%

In the two column results, the left column gives the raw count, right column gives the percentage.

* 100th percentile is the best among structures of comparable resolution; 0th percentile is the worst. For clashscore the comparative set of structures was selected in 2004, for MolProbity score in 2006.[^]MolProbity score combines the clashscore, rotamer, and Ramachandran evaluations into a single score, normalized to be on the same scale as X-ray resolution.

#	Alt Res	High B	Clash > 0.4Å	Ramachandran	Rotamer	Cβ deviation	Bond lengths	Bond angles	Cis Peptides
		Avg: 0.00	Clashscore: 0	Outliers: 1 of 6	Poor rotamers: 0 of 5	Outliers: 0 of 8	Outliers: 0 of 8	Outliers: 1 of 8	Non-Trans: 0 of 7
1	ALA	0	-	-	-	0.06Å	-	-	-
2	SER	0	-	Favored (43.41%) General / -149.9,157.7	Favored (93.8%) <i>p</i> chi angles: 66.3	0.06Å	-	-	-
3	VAL	0	-	Favored (18.58%) Ile or Val / -117.6,105.7	Favored (63.1%) <i>t</i> chi angles: 179.6	0.07Å	-	-	-
4	CYS	0	-	Favored (26.43%) General / -144.2,136.4	Favored (46.7%) <i>t</i> chi angles: 177.9	0.02Å	-	-	-
5	ALA	0	-	Favored (48.34%) General / -133.1,141.7	-	0.04Å	-	-	-
6	ALA	0	-	OUTLIER (0.03%) General / 62.7,-88.2	-	0.02Å	-	-	-
7	TYR	0	-	Favored (8.47%) General / -125.1,16.0	Allowed (0.4%) <i>m-80</i> chi angles: 253.9,52.8	0.03Å	-	-	-
8	PHE	0	-	-	Favored (94.7%) <i>m-80</i> chi angles: 298,100.7	0.02Å	-	OUTLIER(S) worst is CA-CB-CG: 4.2 σ	-

- Analysis of AIP-I AAA representative structure

5/8/2019

Viewing AAA-multi.table - MolProbity



Viewing AAA-multi.table



Duke Biochemistry
Duke University School of Medicine

When finished, you should [close this window](#).

Hint: Use File | Save As... to save a copy of this page.

All-Atom Contacts	Clashscore, all atoms:	0	100 th percentile* (N=1784, all resolutions)	
	Clashscore is the number of serious steric overlaps (> 0.4 Å) per 1000 atoms.			
Protein Geometry	Poor rotamers	0	0.00%	Goal: <0.3%
	Favored rotamers	3	75.00%	Goal: >98%
	Ramachandran outliers	1	16.67%	Goal: <0.05%
	Ramachandran favored	5	83.33%	Goal: >98%
	MolProbity score [^]	1.19	99 th percentile* (N=27675, 0Å - 99Å)	
	Cβ deviations >0.25Å	0	0.00%	Goal: 0
	Bad bonds:	0 / 56	0.00%	Goal: 0%
Bad angles:	1 / 75	1.33%	Goal: <0.1%	
Peptide Omegas	Cis Prolines:	0 / 0	0.00%	Expected: ≤1 per chain, or ≤5%

In the two column results, the left column gives the raw count, right column gives the percentage.

* 100th percentile is the best among structures of comparable resolution; 0th percentile is the worst. For clashscore the comparative set of structures was selected in 2004, for MolProbity score in 2006.

[^]MolProbity score combines the clashscore, rotamer, and Ramachandran evaluations into a single score, normalized to be on the same scale as X-ray resolution.

#	Alt Res	High B	Clash > 0.4Å	Ramachandran	Rotamer	Cβ deviation	Bond lengths	Bond angles	Cis Peptides
		Avg: 0.00	Clashscore: 0	Outliers: 1 of 6	Poor rotamers: 0 of 4	Outliers: 0 of 8	Outliers: 0 of 8	Outliers: 1 of 8	Non-Trans: 0 of 7
1	ALA	0	-	-	-	0.07Å	-	-	-
2	SER	0	-	Favored (28.91%) General / -149.1,147.8	Favored (46.7%) <i>t</i> chi angles: 180	0.03Å	-	-	-
3	ALA	0	-	Favored (40.65%) General / -136.7,138.1	-	0.05Å	-	-	-
4	CYS	0	-	Favored (27.58%) General / -143.8,136.8	Favored (48.4%) <i>t</i> chi angles: 178.4	0.03Å	-	-	-
5	ALA	0	-	Favored (50.03%) General / -130.3,137.6	-	0.03Å	-	-	-
6	ALA	0	-	OUTLIER (0.03%) General / 62.2,-89.2	-	0.03Å	-	-	-
7	TYR	0	-	Favored (10.43%) General / -122.6,18.4	Allowed (0.4%) <i>m-80</i> chi angles: 253.5,52.4	0.04Å	-	-	-
8	PHE	0	-	-	Favored (93%) <i>m-80</i> chi angles: 299.9,95.6	0.03Å	-	OUTLIER(S) worst is CA-CB-CG: 4.4 σ	-

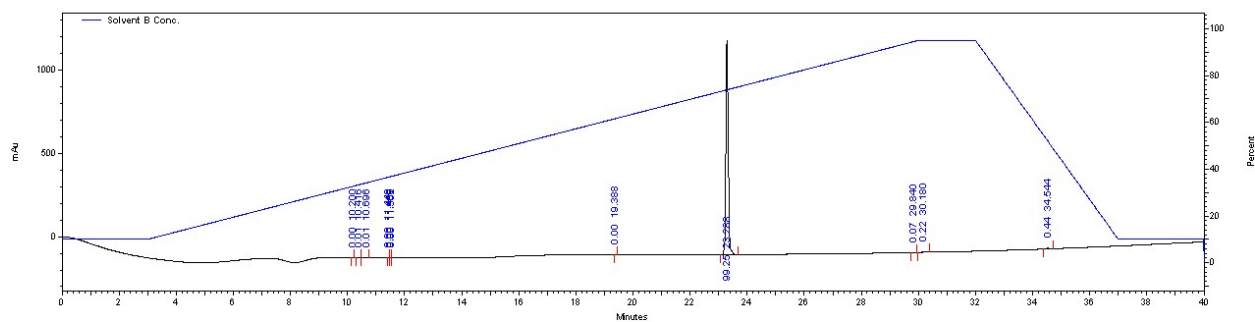
About MolProbity | Website for the Richardson Lab | Using nuclear x-H | Internal reference 4.4

3.4.8 MS and analytical HPLC data for β -turn modifying analogs**Table 3.S17 MS spectral data, HPLC retention times, and purity data for the β -turn modifying analogs.** The m/z of each peptide is given as $[M+H]^+$.

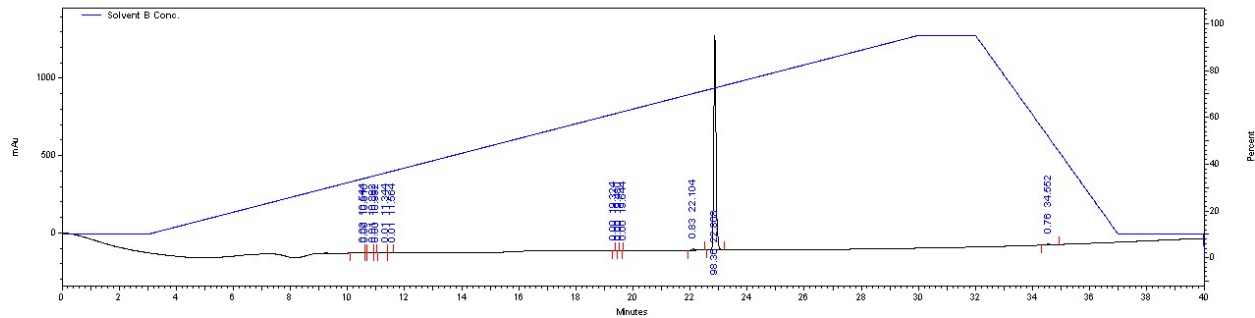
peptide	calculated m/z (Da)	observed m/z (Da)	Δm (ppm)	retention time (min)	HPLC trace purity (% , 220 nm)
AIP-I D1AS6dA	813.3600	813.3597	0.4	23.29	>99
AIP-I D1AS6G	799.3443	799.3442	0.1	22.87	98.3
AIP-I D1AS6A [N-MeF8]	827.3756	827.3750	0.7	23.71	98.7
AIP-I D1AS6A [F8PLA]	814.3440	814.3444	0.5	24.09	95.4
AAdA	785.3287	785.3287	<0.1	22.62	99.0
AAG	771.3130	771.3129	0.1	22.72	96.1
AAA [N-MeF8]	799.3443	799.3438	0.6	23.10	96.6
AAA [F8PLA]	786.3127	786.3130	0.4	23.45	95.6

Analytical HPLC traces for β -turn modifying analogs

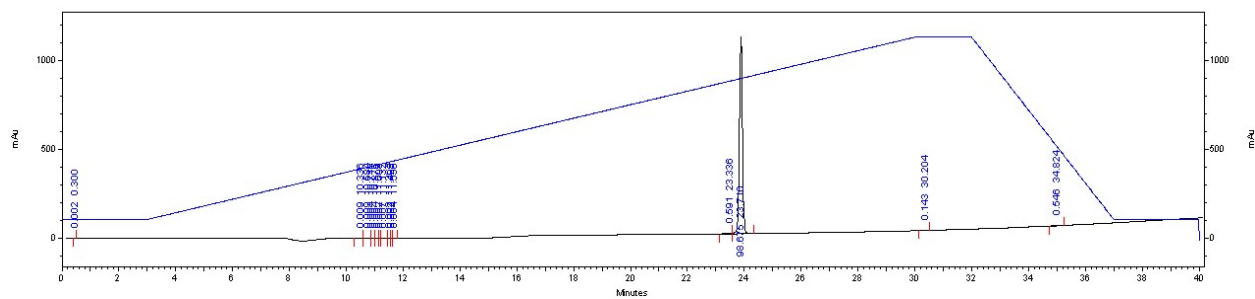
AIP-I D1AS6dA



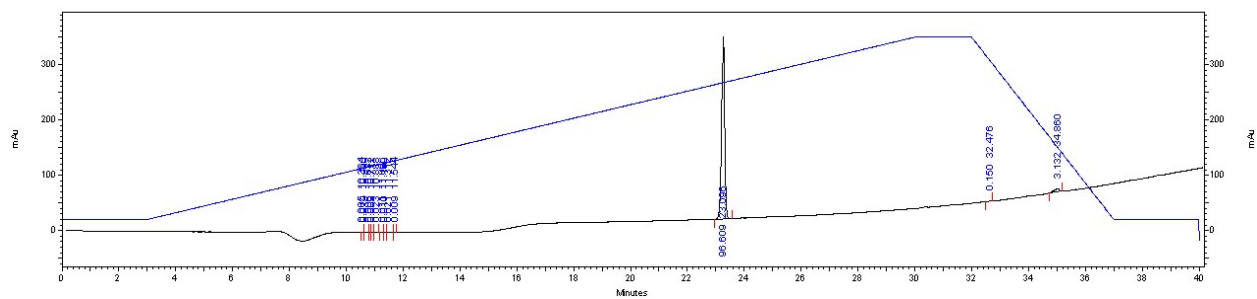
AIP-I D1AS6G



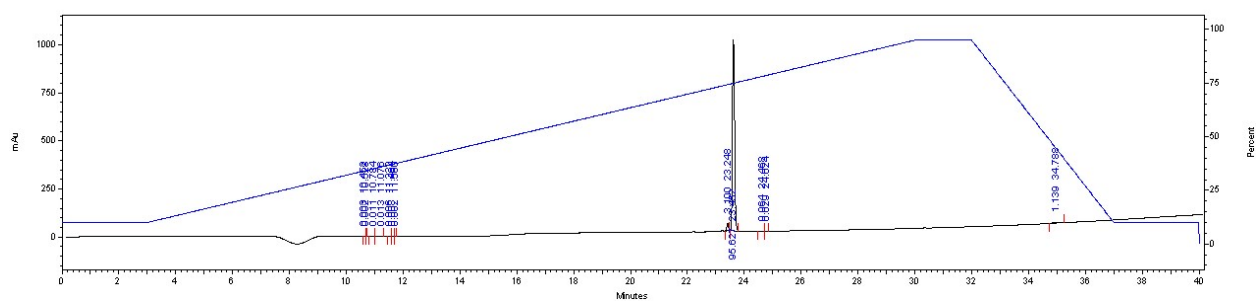
AIP-I D1AS6A [N-MeF8]



AAA [N-MeF8]



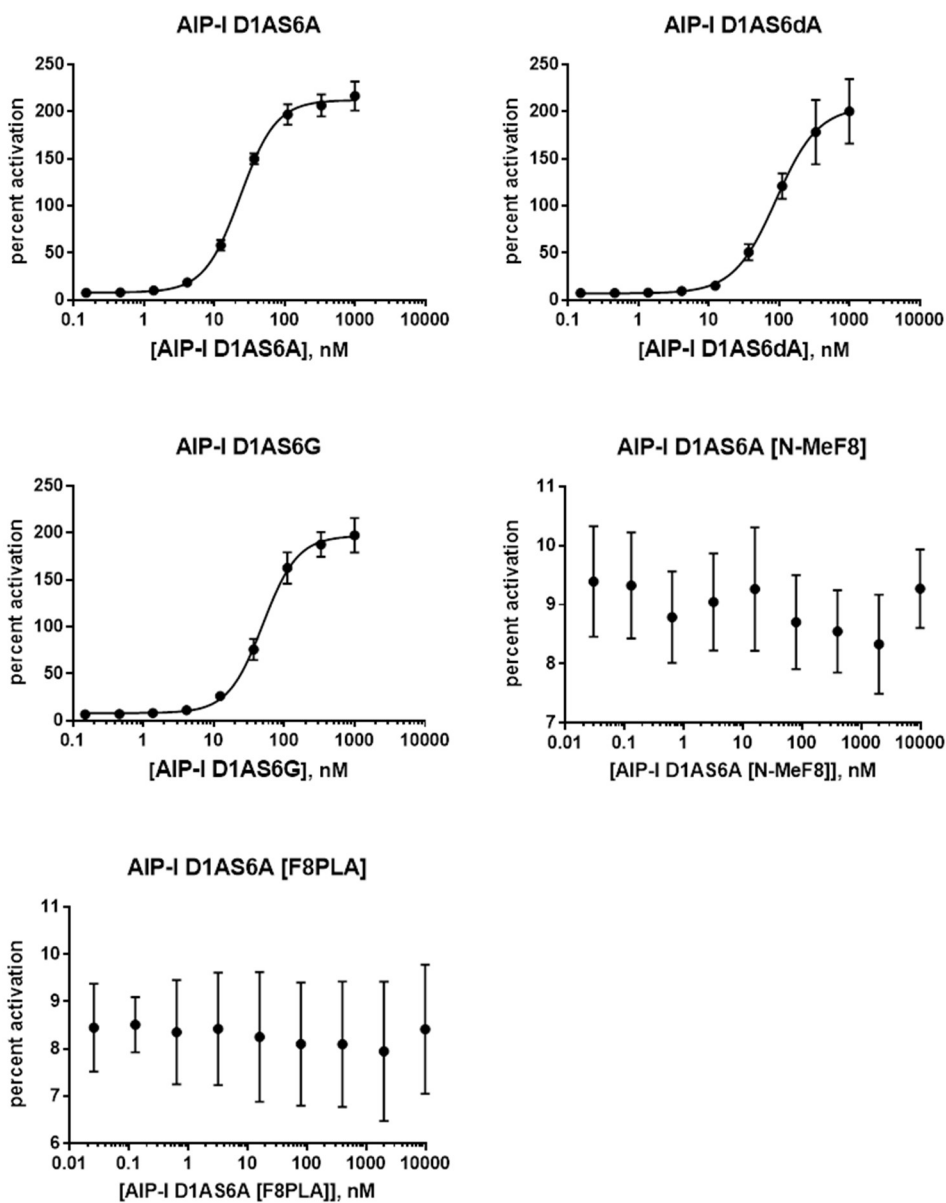
AAA [F8PLA]



3.4.9 *AgrC-I* dose-response assay data for new analogs

Error bars indicate standard deviation (SD). Three biological replicates were used to generate each curve. Curves for the parent agonist (AIP-I D1AS6A) and antagonist (AAA) are also provided. See assay protocol in the experimental procedures section of the SI for details of method.

Agonists



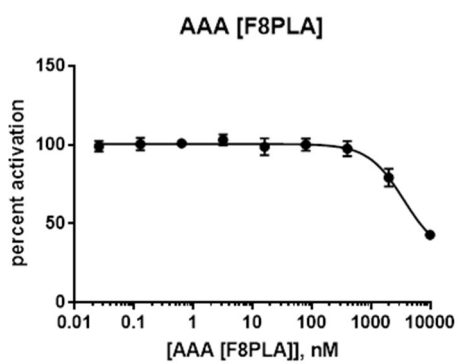
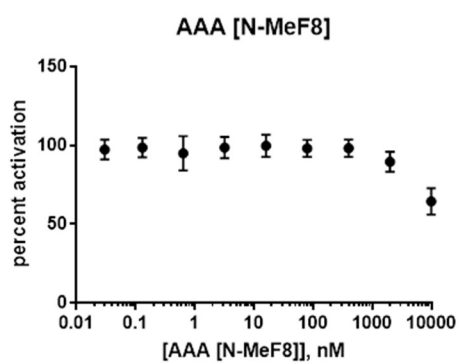
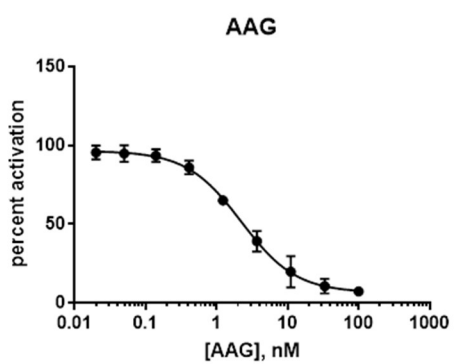
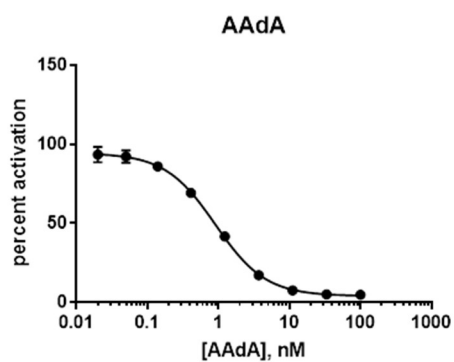
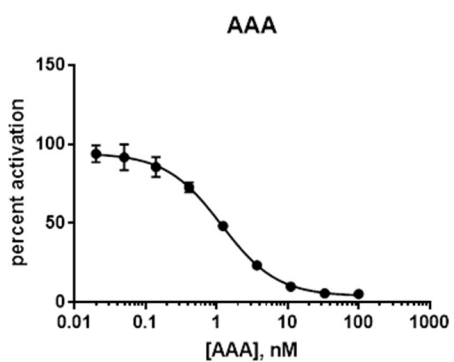
Antagonists

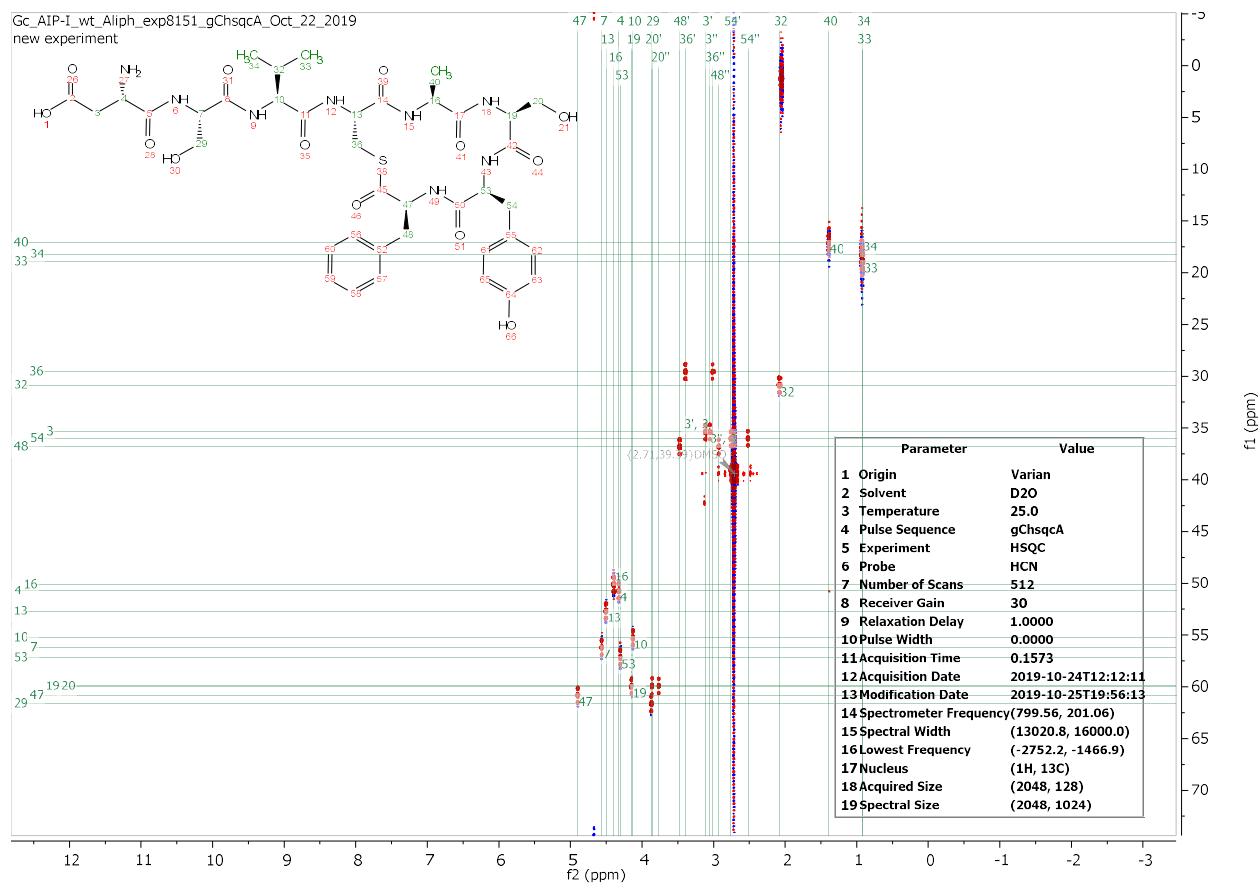
Table 3.S18 Cell-based reporter activities in AgrC-I of agonist AIP-I D1AS6A, antagonist AAA, and the β -turn modifying peptide analogs. CI = 95% confidence interval.

peptide name	sequence	EC ₅₀ in nM, (95% CI)	IC ₅₀ in nM, (95% CI)
AIP-I D1AS6A	A-S-V-(C-A-A-Y-F)	23.4 (21.9-25.0)	---
AIP-I D1AS6dA	A-S-V-(C-A-dA-Y-F)	90.6 (75.7-111)	---
AIP-I D1AS6G	A-S-V-(C-A-G-Y-F)	49.9 (45.7-54.6)	---
AIP-I D1AS6A [N-MeF8]	A-S-V-(C-A-A-Y-[N-MeF])	---	---
AIP-I D1AS6A [F8PLA]	A-S-V-(C-A-A-Y-PLA)	---	---
AAA	A-S-A-(C-A-A-Y-F)	---	1.16 (1.04-1.30)
AAdA	A-S-A-(C-A-dA-Y-F)	---	0.908 (0.852-0.967)
AAG	A-S-A-(C-A-G-Y-F)	---	2.23 (1.94-2.58)
AAA [N-MeF8]	A-S-A-(C-A-A-Y-[N-MeF])	---	>1000
AAA [F8PLA]	A-S-A-(C-A-A-Y-PLA)	---	>1000

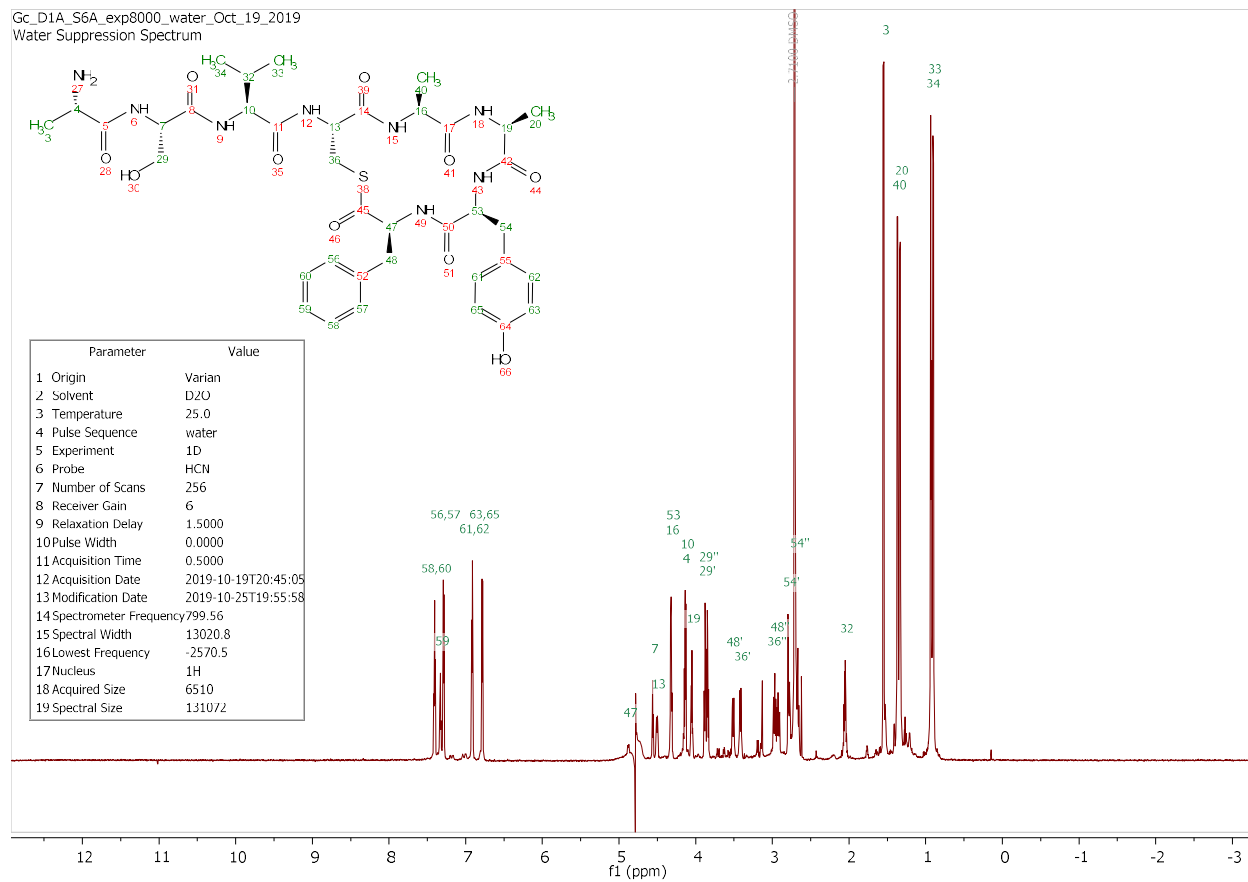
3.4.10 NMR spectra for select β -turn modifying analogs

Two-dimensional ^1H - ^{13}C HSQC NMR experiments were performed for each peptide as described in the experimental procedures above, along with 1-D proton and 2-D TOCSY NMR experiments for select peptides. Selected parameters for each experiment are included in each spectrum. For the 2-D experiments, blue indicates negative peak intensity and red indicates positive peak intensity.

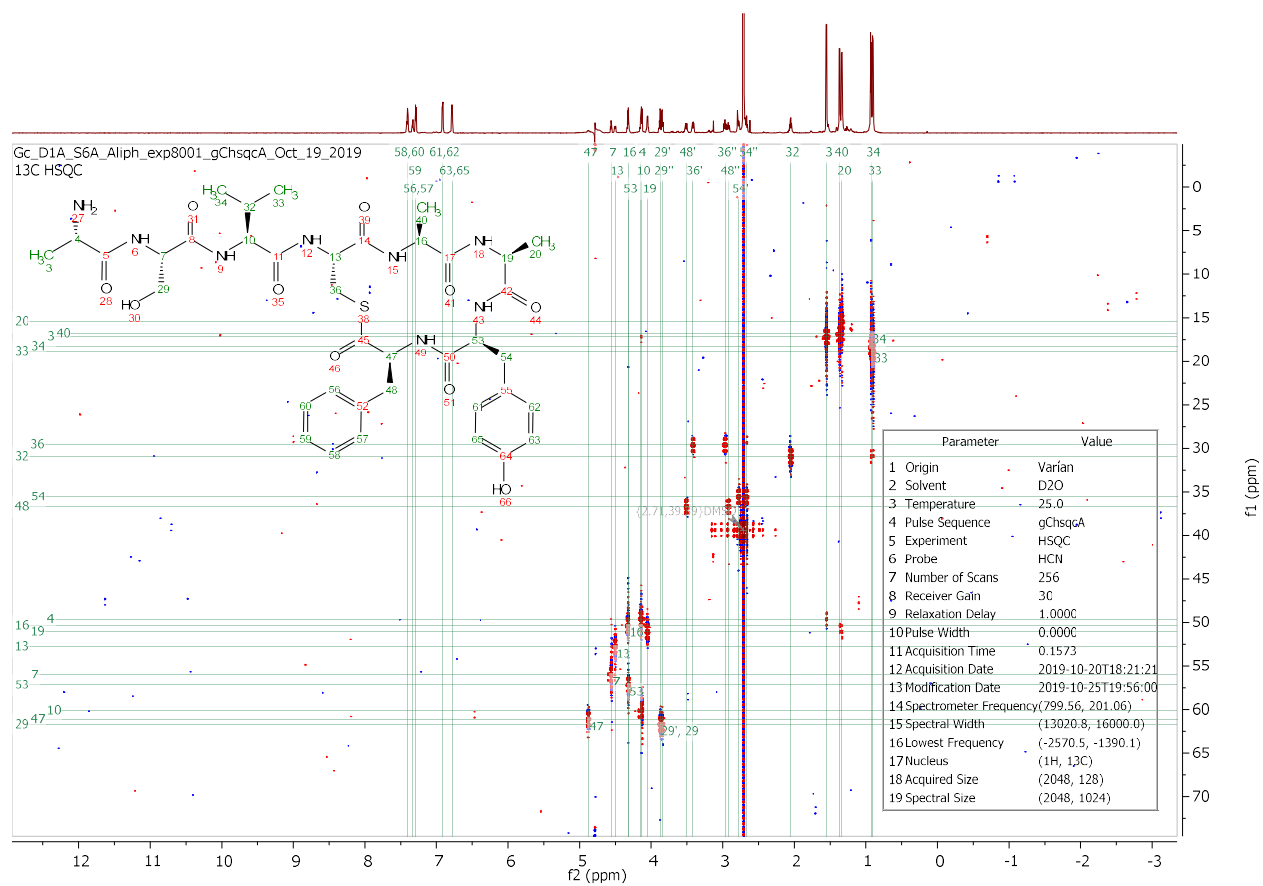
- *AIP-I* ^1H - ^{13}C HSQC NMR spectrum (700 μM dissolved in 12.5% CD_3CN in D_2O , pH ~5)



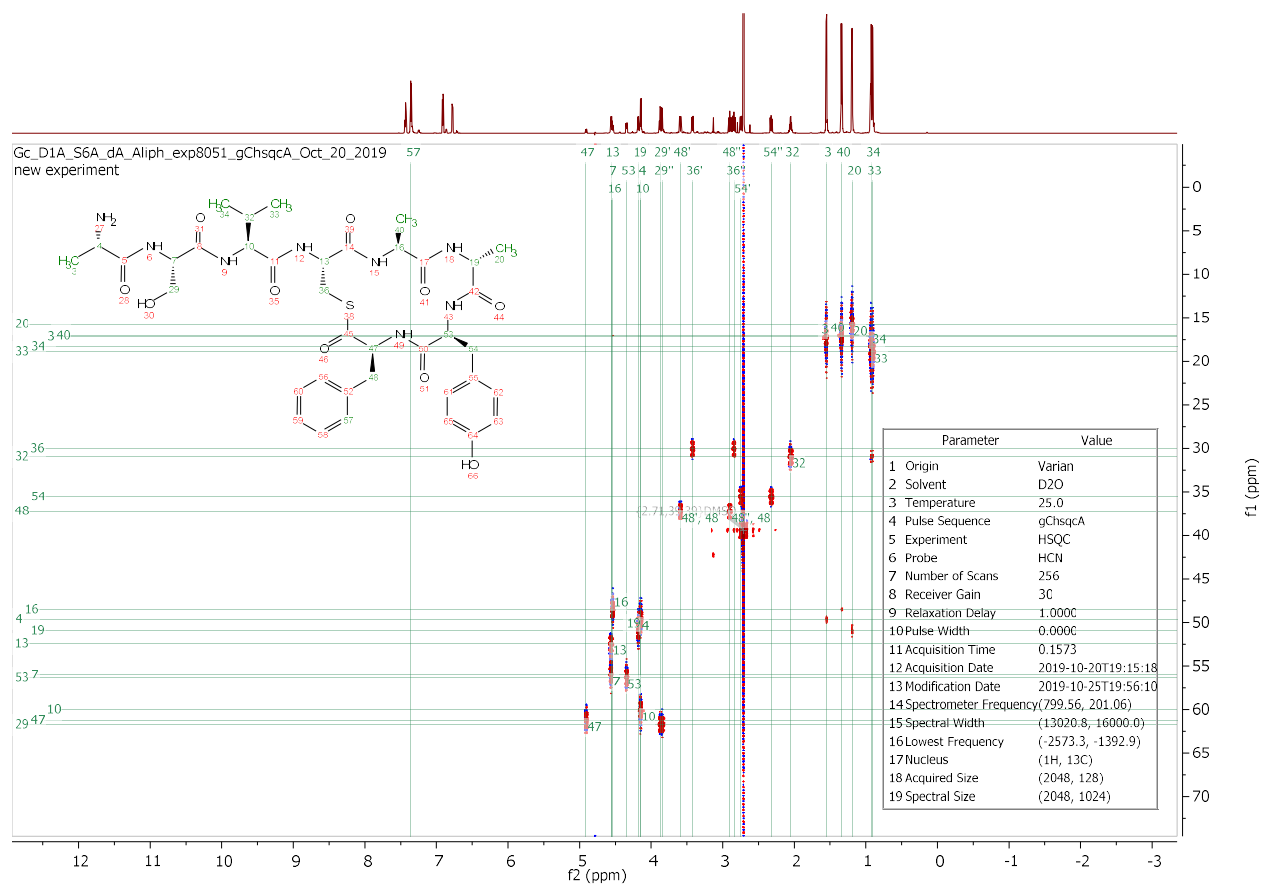
- AIP-I D1AS6A ^1H NMR spectrum (1.43 mM dissolved in D_2O , pH ~5)



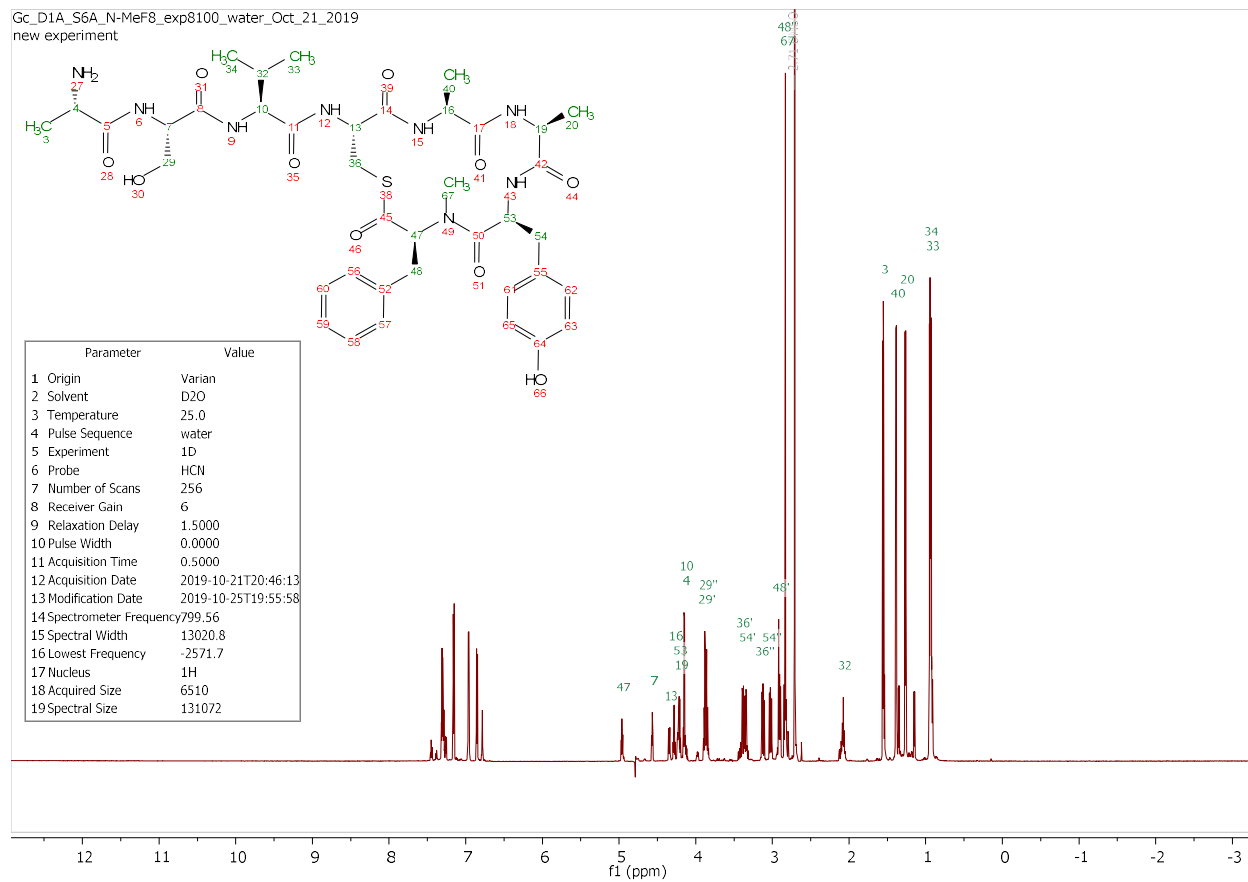
- AIP-I D1AS6A ^1H - ^{13}C HSQC NMR spectrum



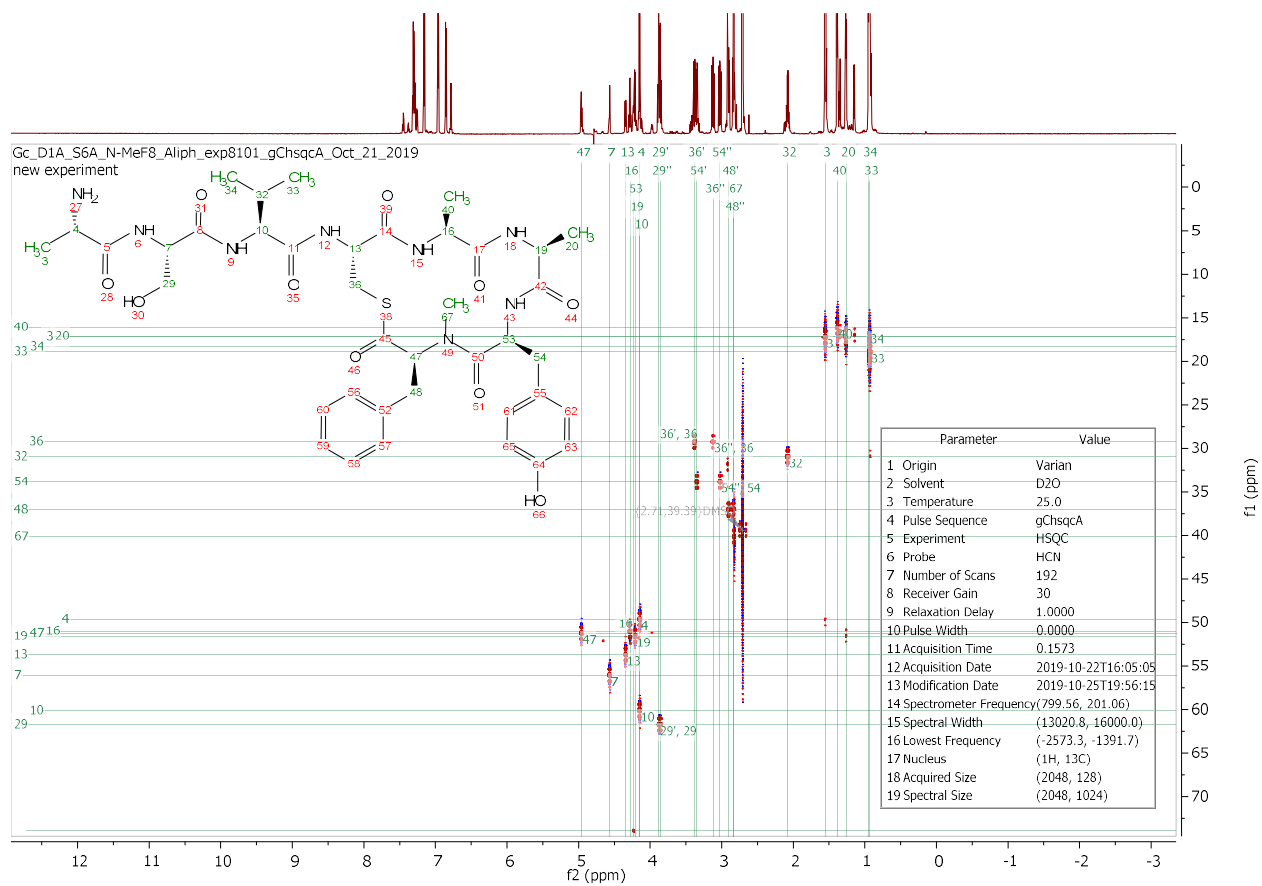
- AIP-I D1AS6dA ^1H - ^{13}C HSQC NMR spectrum



- *AIP-I D1AS6A [N-MeF8]* ^1H NMR spectrum (1.43 mM dissolved in D_2O , pH ~5)



• AIP-I D1AS6A [N-MeF8] ^1H - ^{13}C HSQC NMR spectrum



3.4.11 Chemical shift assignments for select β -turn modifying analogs**Table 3.S19 Assignments for AIP-I**

Residue	Hα (ppm)	Cα (ppm)	Hβ (ppm)	Cβ (ppm)	Others (ppm)
Asp1	4.32	50.73	3.06, 3.11	35.37	
Ser2	4.56	56.20	3.87	61.61	
Val3	4.13	55.26	2.08	30.87	Hy 0.92, 0.93 and Cy 18.92, 18.23
Cys4	4.50	52.67	3.01, 3.39	29.56	
Ala5	4.40	50.11	1.39	17.09	
Ser6	4.15	59.94	3.77, 3.86	59.91	
Tyr7	4.30	57.16	2.52, 2.76	36.00	
Phe8	4.90	60.81	2.93, 3.48	36.81	

Table 3.S20 Assignments for AIP-I D1AS6A

Residue	Hα (ppm)	Cα (ppm)	Hβ (ppm)	Cβ (ppm)	Others (ppm)
Ala1	4.14	49.62	1.55	17.20	
Ser2	4.56	56.01	3.85, 3.87	61.69	
Val3	4.13	60.07	2.05	30.96	Hy 0.90, 0.93 and Cy 18.88, 18.34
Cys4	4.50	52.78	2.97, 3.42	29.60	
Ala5	4.32	50.36	1.37	16.83	
Ala6	4.05	51.08	1.33	15.46	
Tyr7	4.32	57.17	2.67, 2.78	35.57	
Phe8	4.88	61.14	2.92, 3.51	36.69	

Table 3.S21 Assignments for AIP-I D1AS6dA

Residue	Hα (ppm)	Cα (ppm)	Hβ (ppm)	Cβ (ppm)	Others (ppm)
Ala1	4.15	49.63	1.55	17.21	
Ser2	4.56	56.00	3.85, 3.87	61.71	
Val3	4.15	60.02	2.05	30.98	Hy 0.90, 0.93 and Cy 18.91, 18.32
Cys4	4.56	52.44	2.84, 3.42	30.05	
Ala5	4.54	48.50	1.34	17.04	
dAla6	4.18	50.93	1.19	15.74	
Tyr7	4.35	56.32	2.32, 2.75	35.56	
Phe8	4.91	61.20	2.90, 3.59	37.24	

Table 3.S22 Assignments for AIP-I D1AS6A [N-MeF8]

Residue	Hα (ppm)	Cα (ppm)	Hβ (ppm)	Cβ (ppm)	Others (ppm)
Ala1	4.14	49.63	1.55	17.22	
Ser2	4.57	56.03	3.86, 3.88	61.71	
Val3	4.15	60.08	2.08	30.95	Hy 0.93, 0.95 and Cy 18.92, 18.34
Cys4	4.35	53.67	3.12, 3.38	29.24	
Ala5	4.28	51.01	1.39	16.11	
Ala6	4.21	51.55	1.26	17.13	
Tyr7	4.23	73.91	3.03, 3.35	33.84	
N-MePhe8	4.96	51.22	2.83, 2.91	37.02	N-Me H 2.83, C 40.12

3.4.12 TALOS-N predictions for AIP-I and AIP-I D1AS6A

Table 3.S23 Torsion angle analysis for AIP-I

Residue	Predicted			Observed*		Ramachandran
	Phi	Psi	CLASS	Phi	Psi	
Asp1	none	none	none	none	45.393	N/A
Ser2	-103.427 ± 26.247	101.222 ± 63.095	warn	-153.616	146.409	MATCH
Val3	-103.571 ± 14.362	126.446 ± 5.802	strong	-126.956	128.62	MATCH
Cys4	-104.668 ± 14.482	130.147 ± 12.928	strong	-125.294	121.087	MATCH
Ala5	-104.113 ± 26.363	135.859 ± 24.183	generous	-135.013	61.471	MISMATCH
Ser6	-68.757 ± 15.126	-17.975 ± 17.111	warn	-174.485	-97.422	MISMATCH
Tyr7	-90.578 ± 11.683	0.962 ± 11.899	strong	-68.035	-37.567	MATCH
Phe8	none	none	none	-135.013	none	N/A

*As determined from the solution-phase NMR structure in this study.

Table 3.S24 Torsion angle analysis for AIP-I D1AS6A

Residue	Predicted			Observed*		Ramachandran
	Phi	Psi	CLASS	Phi	Psi	
Ala1	none	none	none	none	63.436	N/A
Ser2	-90.000 ± 13.261	129.065 ± 12.271	strong	-149.893	157.675	MATCH
Val3	-100.836 ± 14.319	122.150 ± 8.839	strong	-117.633	105.724	MATCH
Cys4	-111.628 ± 9.710	134.821 ± 10.895	strong	-144.247	136.439	MATCH
Ala5	-102.063 ± 28.363	133.140 ± 22.407	warn	-133.073	141.684	MATCH
Ala6	-87.544 ± 22.952	128.997 ± 32.590	warn	62.737	-88.195	MISMATCH
Tyr7	-104.505 ± 28.071	139.797 ± 14.313	warn	-125.077	15.963	MISMATCH
Phe8	none	none	none	-133.073	none	N/A

*As determined from the solution-phase NMR structure in this study.

Discussion of TALOS-N usage with AIPs and AIP analogs

The TALOS-N program (<https://spin.niddk.nih.gov/bax/software/TALOS-N/>) is an artificial neural network based system for the prediction of protein backbone ϕ/ψ torsion angles, sidechain χ_1 torsion angles, and secondary structure using NMR chemical shift assignments. Along with angle predictions for specific residues, TALOS-N assigns a level of confidence to each prediction (indicated in the “CLASS” columns of Tables 3.S23 and 3.S24 above).^{68, 78} Predictions classified as “strong” indicate that the 25 best database matches to the residue are well-clustered on the Ramachandran map. If instead only the top 10 best database matches are well-clustered, the prediction is classified as “generous”. All other cases are considered ambiguous and are designated as “warn.” However, even with the “warn” status, the ϕ/ψ angle predictions can still be useful if clustered.

Although some predictions of the AIP-I and AIP-I D1AS6A residue torsion angles are “strong,” just as many are classified as “generous” or “warn,” and these do not always match the region of the Ramachandran map in which these angles were determined experimentally to reside (via their solution-phase NMR structures; Tables 3.S23 and 3.S24). As these peptides look different from the natural proteins the TALOS-N database utilizes, especially in regard to the constrained thiolactone macrocycle, the lack of consistent, high quality predictions is perhaps not surprising. That said, the TALOS-N predictions appear consistent within the exocyclic tail regions (residues 1-3 in the peptides tested herein), most likely because being outside the macrocycle allows these residues to adopt conformations commonly found in proteins within the database that TALOS-N queries.

3.4.13 Comparative chemical shift analysis for select β -turn modifying analogs

Table 3.S25 Calculated NMR chemical shift differences between AIP-I D1AS6A and either AIP-I D1AS6dA or AIP-I D1AS6A [N-MeF8]. Positive values indicate the shift of the analog's atom is further downfield than the corresponding shift in AIP-I D1AS6A, while negative values indicate the shift is further upfield. A standard method was used to determine the threshold for which chemical shift differences were deemed significant, and these shifts are indicated in yellow (see calculations below).⁶⁹ Briefly, the mean and standard deviation of the chemical shift difference magnitudes were calculated for each nucleus, and the significance threshold was set at any shift with a magnitude greater than two standard deviations above the mean.

Residue	AIP-I D1AS6A vs. AIP-I D1AS6dA					AIP-I D1AS6A vs. AIP-I D1AS6A [N-MeF8]				
	H α (ppm)	C α (ppm)	H β 1 (ppm)	H β 2 (ppm)	C β (ppm)	H α (ppm)	C α (ppm)	H β 1 (ppm)	H β 2 (ppm)	C β (ppm)
1	+0.01	+0.01	+0.00	-----	+0.01	+0.00	+0.01	+0.00	-----	+0.02
2	+0.00	-0.01	+0.00	+0.00	+0.02	+0.01	+0.02	+0.01	+0.01	+0.02
3	+0.02	-0.05	+0.00	-----	+0.02	+0.02	+0.01	+0.03	-----	-0.01
4	+0.06	-0.34	-0.13	+0.00	+0.45	-0.15	+0.89	+0.15	-0.04	-0.36
5	+0.22	-1.86	-0.03	-----	+0.21	-0.04	+0.65	+0.02	-----	-0.72
6	+0.13	-0.15	-0.14	-----	+0.28	0.16	+0.47	-0.07	-----	+1.67
7	+0.03	-0.85	-0.35	-0.03	-0.01	-0.09	+16.74	+0.36	+0.57	-1.73
8	+0.03	+0.06	-0.02	+0.08	+0.55	+0.08	-9.92	-0.09	-0.60	+0.33

Equation 3.S1 **Calculation of the mean for proton chemical shift differences.**

$$\mu_{\text{H}} = \frac{\sum^N |\delta_{\text{H[AIP-I D1AS6A]}} - \delta_{\text{H[analogs]}}|}{N} = 0.09 \text{ ppm}$$

Equation 3.S2 **Standard deviation calculation for proton chemical shift differences.**

$$\sigma_{\text{H}} = \sqrt{\frac{\sum^N (\delta_{\text{H[analog]}} - \mu_{\text{H}})^2}{N - 1}} = 0.14 \text{ ppm}$$

Equation 3.S3 **Determination of the cutoff value for significant proton shifts differences.**

$$\text{Proton Cutoff} \geq \mu_{\text{H}} + 2\sigma_{\text{H}} = 0.37 \text{ ppm}$$

Equation 3.S4 **Calculation of the mean for carbon chemical shift differences.**

$$\mu_{\text{C}} = \frac{\sum^N |\delta_{\text{C[AIP-I D1AS6A]}} - \delta_{\text{C[analogs]}}|}{N} = 1.20 \text{ ppm}$$

Equation 3.S5 **Standard deviation calculation for carbon chemical shift differences.**

$$\sigma_{\text{C}} = \sqrt{\frac{\sum^N (\delta_{\text{C[analog]}} - \mu_{\text{C}})^2}{N - 1}} = 3.34 \text{ ppm}$$

Equation 3.S6 **Determination of the cutoff value for significant carbon shifts differences.**

$$\text{Carbon Cutoff} \geq \mu_{\text{C}} + 2\sigma_{\text{C}} = 7.88 \text{ ppm}$$

Discussion of chemical shift differences for select β -turn modifying analogs

When comparing the ^1H and ^{13}C chemical shifts for analogous residues between AIP-I D1AS6A and either AIP-I D1AS6dA or AIP-I D1AS6A [N-MeF8], the ^1H and ^{13}C shifts of the exocyclic residues were nearly identical. The chemical shift differences were within 0.03 ppm for ^1H chemical shifts and 0.06 ppm for ^{13}C chemical shifts (see Table 3.S25 above).

For the endocyclic residues, the differences were slightly larger than those in the exocyclic tail for similar residues (<0.25 or <1 ppm for most ^1H or ^{13}C shifts, respectively; see Table 3.S25) unless a large difference in conformation was suspected. The most significant differences are commented on here. The first macrocyclic residue, Cys4, exhibits little variation in chemical shifts in most of the peptides, but there is a noticeable 0.2 ppm change in the $\text{H}\alpha$ shift and a 1 ppm difference in the $\text{C}\alpha$ shift of AIP-I D1AS6A [N-MeF8]. With Ala5, all three peptides exhibit small changes in $\text{H}\alpha$, $\text{C}\alpha$, and $\text{C}\beta$ shifts relative to each other. For the sixth residue, either L-Ala or D-Ala fills this position, and the ^1H and ^{13}C shifts all differ between the peptides. Interestingly, AIP-I D1AS6A and AIP-I D1AS6A [N-MeF8] share the same amino acid at this residue (L-Ala) and at the flanking positions, yet there are ^1H and ^{13}C shift differences at Ala6 between the two peptides, suggestive of a conformational difference between these two peptides and that the β -turn structure could be perturbed in AIP-I D1AS6A [N-MeF8]. Of all the changes in chemical shifts between the three peptides, the largest deviation occurs in Tyr7. While the shifts of Tyr7 in AIP-I D1AS6A and AIP-I D1AS6dA are very close, and almost indistinguishable in some cases (differences of <0.05, <0.9, <0.4, <0.05, and

<0.05 ppm for H α , C α , H β 1, H β 2, and C β respectively), there are large shift differences for AIP-I D1AS6A [N-MeF8]. Most notable are those that surpass two standard deviations above the average shift displacement, namely the C α with a shift difference >15 ppm and H β 2 with a shift difference of >0.5 ppm. These large changes in chemical shift for AIP-I D1AS6A [N-MeF8], alongside a smaller but still noticeable C β shift of 1.7 ppm, suggests a perturbation in the local conformation around this residue, presumably as a result of the *N*-methylation of Phe8. Lastly, while the final residues' shifts are fairly consistent between AIP-I D1AS6A and AIP-I D1AS6dA, there are significant shift differences in H β and C α of AIP-I D1AS6A [N-MeF8] (0.6 and 10 ppm, respectively), again, presumably due to the *N*-methylation of Phe8 in this analog.

3.5 Acknowledgements

Financial support for this work was provided by the Office of Naval Research (N00014-16-1-2185), the NSF (CHE-1708714), and the Wisconsin Alumni Research Foundation (UW 2020 Program). J.K.V. was supported in part by an NSF Graduate Research Fellowship (DGE-1747503). J.K.V., K.H.J.W., and T.J.P. were supported in part by the UW–Madison NIH Chemistry–Biology Interface Training Program (T32 GM008505), the UW–Madison Office of the Vice Chancellor for Research and Graduate Education (with funding from the Wisconsin Alumni Research Foundation). T.Y. was supported in part by the UW–Madison NIH Biotechnology Training Program (T32 GM008349). G.C. and M.T. were supported by NIH grant P41 GM103399. This study made use of the National Magnetic Resonance Facility at Madison, which is supported by NIH grants P41 GM103399 and P41 GM66326. Additional equipment was purchased with funds from the University of Wisconsin, the NIH (RR02781, RR08438), the NSF (DMB-8415048, OIA-9977486, BIR-9214394), and the USDA.

3.6 References

1. Vuong, C.; Otto, M., *Staphylococcus epidermidis* infections. *Microb. Infect.* **2002**, 4 (4), 481-489.
2. von Eiff, C.; Peters, G.; Heilmann, C., Pathogenesis of infections due to coagulase-negative staphylococci. *The Lancet Infectious Diseases* **2002**, 2 (11), 677-685.
3. Otto, M., *Staphylococcus epidermidis* — the 'accidental' pathogen. *Nature Reviews Microbiology* **2009**, 7, 555-567.
4. Mack, D.; Davies, A. P.; Harris, L. G.; Rohde, H.; Horstkotte, M. A.; Knobloch, J. K.-M., Microbial interactions in *Staphylococcus epidermidis* biofilms. *Anal. Bioanal. Chem.* **2007**, 387 (2), 399-408.
5. McCann, M. T.; Gilmore, B. F.; Gorman, S. P., *Staphylococcus epidermidis* device-related infections: pathogenesis and clinical management. *J. Pharm. Pharmacol.* **2008**, 60 (12), 1551-1571.
6. Rogers, K. L.; Fey, P. D.; Rupp, M. E., Coagulase-Negative Staphylococcal Infections. *Infect. Dis. Clin. North Am.* **2009**, 23 (1), 73-98.
7. Mertens, A.; Ghebremedhin, B., Genetic determinants and biofilm formation of clinical *Staphylococcus epidermidis* isolates from blood cultures and indwelling devices. *Eur. J. Microbiol. Immunol. (Bp)* **2013**, 3 (2), 111-119.
8. Harris, L. G.; Dudley, E.; Rohde, H.; Frommelt, L.; Siemssen, N.; Wilkinson, T. S.; Mack, D., Limitations in the use of PSM γ , agr, RNAlII, and biofilm formation as biomarkers to define invasive *Staphylococcus epidermidis* from chronic biomedical device-associated infections. *Int. J. Med. Microbiol.* **2017**, 307 (7), 382-387.
9. Costerton, J. W.; Stewart, P. S.; Greenberg, E. P., Bacterial Biofilms: A Common Cause of Persistent Infections. *Science* **1999**, 284 (5418), 1318-1322.
10. Claessens, J.; Roriz, M.; Merckx, R.; Baatsen, P.; Van Mellaert, L.; Van Eldere, J., Inefficacy of vancomycin and teicoplanin in eradicating and killing *Staphylococcus epidermidis* biofilms in vitro. *Int. J. Antimicrob. Agents* **2015**, 45 (4), 368-375.
11. Sabaté Brescó, M.; Harris, L. G.; Thompson, K.; Stanic, B.; Morgenstern, M.; O'Mahony, L.; Richards, R. G.; Moriarty, T. F., Pathogenic Mechanisms and Host Interactions in *Staphylococcus epidermidis* Device-Related Infection. *Front. Microbiol.* **2017**, 8 (1401).

12. Vuong, C.; Dürr, M.; Carmody, A. B.; Peschel, A.; Klebanoff, S. J.; Otto, M., Regulated expression of pathogen-associated molecular pattern molecules in *Staphylococcus epidermidis*: quorum-sensing determines pro-inflammatory capacity and production of phenol-soluble modulins. *Cell. Microbiol.* **2004**, *6* (8), 753-759.
13. Kong, K.-F.; Vuong, C.; Otto, M., *Staphylococcus* quorum sensing in biofilm formation and infection. *Int. J. Med. Microbiol.* **2006**, *296* (2), 133-139.
14. Yao, Y.; Vuong, C.; Kocianova, S.; Villaruz, A. E.; Lai, Y.; Sturdevant, D. E.; Otto, M., Characterization of the *Staphylococcus epidermidis* Accessory-Gene Regulator Response: Quorum-Sensing Regulation of Resistance to Human Innate Host Defense. *J. Infect. Dis.* **2006**, *193* (6), 841-848.
15. Wang, C.; Li, M.; Dong, D.; Wang, J.; Ren, J.; Otto, M.; Gao, Q., Role of ClpP in biofilm formation and virulence of *Staphylococcus epidermidis*. *Microb. Infect.* **2007**, *9* (11), 1376-1383.
16. Cheung, G. Y. C.; Joo, H.-S.; Chatterjee, S. S.; Otto, M., Phenol-soluble modulins – critical determinants of staphylococcal virulence. *FEMS Microbiol. Rev.* **2014**, *38* (4), 698-719.
17. Otto, M., Phenol-soluble modulins. *Int. J. Med. Microbiol.* **2014**, *304* (2), 164-169.
18. Camilli, A.; Bassler, B. L., Bacterial Small-Molecule Signaling Pathways. *Science* **2006**, *311* (5764), 1113-1116.
19. Rutherford, S. T.; Bassler, B. L., Bacterial Quorum Sensing: Its Role in Virulence and Possibilities for Its Control. *Cold Spring Harb. Perspect. Med.* **2012**, *2*:a012427 (11).
20. Lyon, G. J.; Novick, R. P., Peptide signaling in *Staphylococcus aureus* and other Gram-positive bacteria. *Peptides* **2004**, *25* (9), 1389-1403.
21. George, E. A.; Muir, T. W., Molecular Mechanisms of agr Quorum Sensing in Virulent Staphylococci. *ChemBioChem* **2007**, *8* (8), 847-855.
22. Novick, R. P.; Geisinger, E., Quorum Sensing in Staphylococci. *Annu. Rev. Genet.* **2008**, *42*, 541-64.
23. Thoendel, M.; Kavanaugh, J. S.; Flack, C. E.; Horswill, A. R., Peptide Signaling in the Staphylococci. *Chem. Rev.* **2011**, *111* (1), 117-151.
24. Otto, M., Virulence factors of the coagulase-negative staphylococci. *Front. Biosci.* **2004**, *9*, 841-863.

25. Wang, R.; Khan, B. A.; Cheung, G. Y. C.; Bach, T.-H. L.; Jameson-Lee, M.; Kong, K.-F.; Queck, S. Y.; Otto, M., *Staphylococcus epidermidis* surfactant peptides promote biofilm maturation and dissemination of biofilm-associated infection in mice. *The Journal of Clinical Investigation* **2011**, *121* (1), 238-248.
26. Otto, M., Staphylococcal Infections: Mechanisms of Biofilm Maturation and Detachment as Critical Determinants of Pathogenicity. *Annu. Rev. Med.* **2013**, *64* (1), 175-188.
27. Le, K. Y.; Dastgheyb, S.; Ho, T. V.; Otto, M., Molecular determinants of staphylococcal biofilm dispersal and structuring. *Frontiers in Cellular and Infection Microbiology* **2014**, *4*, 167.
28. Cheung, G. Y. C.; Rigby, K.; Wang, R.; Queck, S. Y.; Braughton, K. R.; Whitney, A. R.; Teintze, M.; DeLeo, F. R.; Otto, M., *Staphylococcus epidermidis* Strategies to Avoid Killing by Human Neutrophils. *PLoS Path.* **2010**, *6* (10), e1001133.
29. Boles, B. R.; Horswill, A. R., agr-Mediated Dispersal of *Staphylococcus aureus* Biofilms. *PLoS Path.* **2008**, *4* (4), e1000052.
30. Olson, M. E.; Todd, D. A.; Schaeffer, C. R.; Paharik, A. E.; Van Dyke, M. J.; Büttner, H.; Dunman, P. M.; Rohde, H.; Cech, N. B.; Fey, P. D.; Horswill, A. R., *Staphylococcus epidermidis* agr Quorum-Sensing System: Signal Identification, Cross Talk, and Importance in Colonization. *J. Bacteriol.* **2014**, *196* (19), 3482-3493.
31. Qin, L.; Da, F.; Fisher, E. L.; Tan, D. C. S.; Nguyen, T. H.; Fu, C.-L.; Tan, V. Y.; McCausland, J. W.; Sturdevant, D. E.; Joo, H.-S.; Queck, S. Y.; Cheung, G. Y. C.; Otto, M., Toxin Mediates Sepsis Caused by Methicillin-Resistant *Staphylococcus epidermidis*. *PLoS Path.* **2017**, *13* (2), e1006153.
32. Le, K. Y.; Otto, M., Quorum-sensing regulation in staphylococci-an overview. *Front. Microbiol.* **2015**, *6*, 1174.
33. Mayville, P.; Ji, G.; Beavis, R.; Yang, H.; Goger, M.; Novick, R. P.; Muir, T. W., Structure-activity analysis of synthetic autoinducing thiolactone peptides from *Staphylococcus aureus* responsible for virulence. *Proc. Natl. Acad. Sci. USA* **1999**, *96* (4), 1218-1223.
34. Lyon, G. J.; Mayville, P.; Muir, T. W.; Novick, R. P., Rational design of a global inhibitor of the virulence response in *Staphylococcus aureus*, based in part on localization of the site of inhibition to the receptor-histidine kinase, AgrC. *Proc. Natl. Acad. Sci. U. S. A.* **2000**, *97* (24), 13330-13335.
35. McDowell, P.; Affas, Z.; Reynolds, C.; Holden, M. T.; Wood, S. J.; Saint, S.; Cockayne, A.; Hill, P. J.; Dodd, C. E.; Bycroft, B. W.; Chan, W. C.; Williams, P.,

- Structure, activity and evolution of the group I thiolactone peptide quorum-sensing system of *Staphylococcus aureus*. *Mol. Microbiol.* **2001**, *41* (2), 503-12.
36. Lyon, G. J.; Wright, J. S.; Muir, T. W.; Novick, R. P., Key Determinants of Receptor Activation in the agr Autoinducing Peptides of *Staphylococcus aureus*. *Biochemistry* **2002**, *41* (31), 10095-10104.
 37. Scott, R. J.; Lian, L.-Y.; Muharram, S. H.; Cockayne, A.; Wood, S. J.; Bycroft, B. W.; Williams, P.; Chan, W. C., Side-chain-to-tail thiolactone peptide inhibitors of the staphylococcal quorum-sensing system. *Bioorg. Med. Chem. Lett.* **2003**, *13* (15), 2449-2453.
 38. Fowler, S. A.; Stacy, D. M.; Blackwell, H. E., Design and Synthesis of Macrocyclic Peptomers as Mimics of a Quorum Sensing Signal from *Staphylococcus aureus*. *Org. Lett.* **2008**, *10* (12), 2329-2332.
 39. George, E. A.; Novick, R. P.; Muir, T. W., Cyclic Peptide Inhibitors of Staphylococcal Virulence Prepared by Fmoc-Based Thiolactone Peptide Synthesis. *J. Am. Chem. Soc.* **2008**, *130* (14), 4914-4924.
 40. Tal-Gan, Y.; Stacy, D. M.; Foegen, M. K.; Koenig, D. W.; Blackwell, H. E., Highly Potent Inhibitors of Quorum Sensing in *Staphylococcus aureus* Revealed Through a Systematic Synthetic Study of the Group-III Autoinducing Peptide. *J. Am. Chem. Soc.* **2013**, *135* (21), 7869-7882.
 41. Tal-Gan, Y.; Stacy, D. M.; Blackwell, H. E., *N*-Methyl and peptoid scans of an autoinducing peptide reveal new structural features required for inhibition and activation of AgrC quorum sensing receptors in *Staphylococcus aureus*. *Chem. Commun.* **2014**, *50* (23), 3000-3003.
 42. Johnson, J. G.; Wang, B.; Debelouchina, G. T.; Novick, R. P.; Muir, T. W., Increasing AIP Macrocycle Size Reveals Key Features of agr Activation in *Staphylococcus aureus*. *ChemBioChem* **2015**, *16* (7), 1093-100.
 43. Vasquez, J. K.; Tal-Gan, Y.; Cornilescu, G.; Tyler, K. A.; Blackwell, H. E., Simplified AIP-II Peptidomimetics Are Potent Inhibitors of *Staphylococcus aureus* AgrC Quorum Sensing Receptors. *ChemBioChem* **2017**, *18* (4), 413-423.
 44. Kirchdoerfer, R. N.; Garner, A. L.; Flack, C. E.; Mee, J. M.; Horswill, A. R.; Janda, K. D.; Kaufmann, G. F.; Wilson, I. A., Structural Basis for Ligand Recognition and Discrimination of a Quorum-quenching Antibody. *J. Biol. Chem.* **2011**, *286* (19), 17351-17358.
 45. Nielsen, A.; Mansson, M.; Bojer, M. S.; Gram, L.; Larsen, T. O.; Novick, R. P.; Frees, D.; Frokiaer, H.; Ingmer, H., Solonamide B inhibits quorum sensing and

- reduces *Staphylococcus aureus* mediated killing of human neutrophils. *PLoS One* **2014**, *9* (1), e84992.
46. Sully, E. K.; Malachowa, N.; Elmore, B. O.; Alexander, S. M.; Femling, J. K.; Gray, B. M.; DeLeo, F. R.; Otto, M.; Cheung, A. L.; Edwards, B. S.; Sklar, L. A.; Horswill, A. R.; Hall, P. R.; Gresham, H. D., Selective Chemical Inhibition of *agr* Quorum Sensing in *Staphylococcus aureus* Promotes Host Defense with Minimal Impact on Resistance. *PLoS Path.* **2014**, *10* (6), e1004174.
 47. Tal-Gan, Y.; Ivancic, M.; Cornilescu, G.; Yang, T.; Blackwell, H. E., Highly Stable, Amide-Bridged Autoinducing Peptide Analogues that Strongly Inhibit the AgrC Quorum Sensing Receptor in *Staphylococcus aureus*. *Angew. Chem. Int. Ed.* **2016**, *55* (31), 8913-8917.
 48. Vasquez, J. K.; Blackwell, H. E., Simplified Autoinducing Peptide Mimetics with Single-Nanomolar Activity Against the *Staphylococcus aureus* AgrC Quorum Sensing Receptor. *ACS Infectious Diseases* **2019**, *5* (4), 484-492.
 49. Dufour, P.; Jarraud, S.; Vandenesch, F.; Greenland, T.; Novick, R. P.; Bes, M.; Etienne, J.; Lina, G., High Genetic Variability of the *agr* Locus in *Staphylococcus* Species. *J. Bacteriol.* **2002**, *184* (4), 1180-1186.
 50. Yang, T.; Tal-Gan, Y.; Paharik, A. E.; Horswill, A. R.; Blackwell, H. E., Structure–Function Analyses of a *Staphylococcus epidermidis* Autoinducing Peptide Reveals Motifs Critical for AgrC-type Receptor Modulation. *ACS Chem. Biol.* **2016**, *11* (7), 1982-1991.
 51. Tal-Gan, Y.; Ivancic, M.; Cornilescu, G.; Blackwell, H. E., Characterization of structural elements in native autoinducing peptides and non-native analogues that permit the differential modulation of AgrC-type quorum sensing receptors in *Staphylococcus aureus*. *Org. Biomol. Chem.* **2016**, *14* (1), 113-121.
 52. Tal-Gan, Y.; Ivancic, M.; Cornilescu, G.; Cornilescu, C. C.; Blackwell, H. E., Structural Characterization of Native Autoinducing Peptides and Abiotic Analogues Reveals Key Features Essential for Activation and Inhibition of an AgrC Quorum Sensing Receptor in *Staphylococcus aureus*. *J. Am. Chem. Soc.* **2013**, *135* (49), 18436-18444.
 53. Schwieters, C. D.; Kuszewski, J. J.; Tjandra, N.; Clore, G. M., The Xplor-NIH NMR Molecular Structure Determination Package. *J. Magn. Reson.* **2003**, *160*, 66-74.
 54. Schwieters, C.; Kuszewski, J.; Mariusclore, G., Using Xplor–NIH for NMR molecular structure determination. *Prog. Nucl. Magn. Reson. Spectrosc.* **2006**, *48* (1), 47-62.

55. The PyMOL Molecular Graphics System, Version 1.7, Schrödinger, LLC.: 2015.
56. Vijayakumar, M.; Qian, H.; Zhou, H. X., Hydrogen bonds between short polar side chains and peptide backbone: Prevalence in proteins and effects on helix-forming propensities. *Proteins: Structure, Function, and Bioinformatics* **1999**, *34* (4), 497-507.
57. Flöckner, H.; Braxenthaler, M.; Lackner, P.; Jaritz, M.; Ortner, M.; Sippl, M. J., Progress in fold recognition. *Proteins: Structure, Function, and Bioinformatics* **1995**, *23* (3), 376-386.
58. Khan, B. A.; Yeh, A. J.; Cheung, G. Y.; Otto, M., Investigational therapies targeting quorum-sensing for the treatment of *Staphylococcus aureus* infections. *Expert Opinion on Investigational Drugs* **2015**, *24* (5), 689-704.
59. Wilmot, C. M.; Thornton, J. M., β -Turns and their distortions: a proposed new nomenclature. *Protein Eng.* **1990**, *3* (6), 479-493.
60. Davis, I. W.; Leaver-Fay, A.; Chen, V. B.; Block, J. N.; Kapral, G. J.; Wang, X.; Murray, L. W.; Arendall, W. B., 3rd; Snoeyink, J.; Richardson, J. S.; Richardson, D. C., MolProbity: all-atom contacts and structure validation for proteins and nucleic acids. *Nucleic Acids Research* **2007**, *35* (suppl_2), W375-W383.
61. Chen, V. B.; Arendall III, W. B., 3rd; Headd, J. J.; Keedy, D. A.; Immormino, R. M.; Kapral, G. J.; Murray, L. W.; Richardson, J. S.; Richardson, D. C., MolProbity: all-atom structure validation for macromolecular crystallography. *Acta Crystallographica, Section D: Structural Biology* **2010**, *66* (1), 12-21.
62. Stanger, H. E.; Gellman, S. H., Rules for Antiparallel β -Sheet Design: D -Pro-Gly Is Superior to L -Asn-Gly for β -Hairpin Nucleation. *J. Am. Chem. Soc.* **1998**, *120* (17), 4236-4237.
63. Mitchell, J. B. O.; Smith, J., D -amino acid residues in peptides and proteins. *Proteins: Structure, Function, and Bioinformatics* **2003**, *50* (4), 563-571.
64. Mielke, S. P.; Krishnan, V. V., Characterization of protein secondary structure from NMR chemical shifts. *Prog. Nucl. Magn. Reson. Spectrosc.* **2009**, *54* (3-4), 141-165.
65. Saitô, H., Conformation-dependent ^{13}C chemical shifts: A new means of conformational characterization as obtained by high-resolution solid-state ^{13}C NMR. *Magn. Reson. Chem.* **1986**, *24* (10), 835-852.
66. Szilagyi, L., Chemical shifts in proteins come of age. *Prog. Nucl. Magn. Reson. Spectrosc.* **1995**, *27*, 325-443.

67. Wishart, D. S.; Sykes, B. D., The ^{13}C chemical-shift index: a simple method for the identification of protein secondary structure using ^{13}C chemical-shift data. *J. Biomol. NMR* **1994**, *4* (2), 171-80.
68. Shen, Y.; Bax, A., Protein backbone and sidechain torsion angles predicted from NMR chemical shifts using artificial neural networks. *J. Biomol. NMR* **2013**, *56* (3), 227-41.
69. Williamson, M. P., Using chemical shift perturbation to characterise ligand binding. *Prog. Nucl. Magn. Reson. Spectrosc.* **2013**, *73*, 1-16.
70. Cavanagh, J.; Fairbrother, W. J.; Palmer, A. G.; Rance, M.; Skelton, N. J., *Protein NMR Spectroscopy: Principles and Practice*. Academic Press, Elsevier Science: 1995.
71. Wüthrich, K., *NMR of Proteins and Nucleic Acids*. John Wiley and Sons: New York, 1986.
72. Evans, J. N. S., *Biomolecular NMR Spectroscopy*. Oxford University Press: New York, 1995.
73. Nilges, M.; Clore, G. M.; Gronenborn, A. M., Determination of three-dimensional structures of proteins from interproton distance data by hybrid distance geometry-dynamical simulated annealing calculations. *FEBS Lett.* **1988**, *229* (2), 317-324.
74. Schwieters, C. D.; Clore, G. M., Internal coordinates for molecular dynamics and minimization in structure determination and refinement. *J. Magn. Reson.* **2001**, *152* (2), 288-302.
75. Clore, G. M.; Kuszewski, J., Chi(1) rotamer populations and angles of mobile surface side chains are accurately predicted by a torsion angle database potential of mean force. *J. Am. Chem. Soc.* **2002**, *124* (12), 2866-7.
76. Schwieters, C. D.; Clore, G. M., A pseudopotential for improving the packing of ellipsoidal protein structures determined from NMR data. *J. Phys. Chem. B* **2008**, *112* (19), 6070-3.
77. Schwieters, C. D.; Bermejo, G. A.; Clore, G. M., Xplor-NIH for molecular structure determination from NMR and other data sources. *Protein Sci.* **2018**, *27* (1), 26-40.
78. Shen, Y.; Bax, A., Protein structural information derived from NMR chemical shift with the neural network program TALOS-N. *Methods Mol. Biol.* **2015**, *1260*, 17-32.

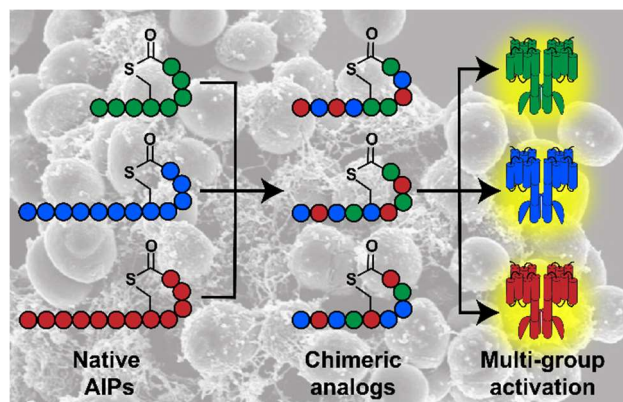
Chapter 4:
**Non-Native Peptides Capable of Pan-Activating the *agr* Quorum
Sensing System across Multiple Specificity Groups of
*Staphylococcus epidermidis***

Contributions: K. H. J. West designed experiments, synthesized peptides, performed fluorescence reporter assays, and wrote the chapter. W. Shen and T. Yang assisted in experimental design, peptide preparation, fluorescence reporter assays, and writing. E. L. Eisenbraun assisted in PSM quantification and writing. J. K. Vasquez assisted in experimental design. A. R. Horswill assisted in reporter strain construction. H. E. Blackwell guided research and assisted in writing.

*This chapter is published under the same title:

West, K. H. J.; Shen, W.; Eisenbraun, E. L.; Yang, T.; Vasquez, J. K.; Horswill, A. R.; Blackwell, H. E. Non-native peptides capable of pan-activating the *agr* quorum sensing system across multiple specificity groups of *Staphylococcus epidermidis*. *ACS Chem. Biol.* **2021**, *in press*.

Abstract



Staphylococcus epidermidis is a leading cause of hospital-acquired infections. Traditional antibiotics have significantly reduced efficacy against this pathogen due to its ability to form biofilms on abiotic surfaces and drug resistance. The accessory gene regulator (*agr*) quorum sensing system is directly involved in *S. epidermidis* pathogenesis. Activation of *agr* is achieved via binding of the autoinducing peptide (AIP) signal to the extracellular sensor domain of its cognate receptor, AgrC. Divergent evolution has given rise to four *agr* specificity groups in *S. epidermidis* defined by the unique AIP sequence used by each group (AIPs-I–IV), with observed cross-group activities. As *agr* agonism has been shown to reduce biofilm growth in *S. epidermidis*, the development of pan-group activators of the *agr* system is of interest as a potential anti-virulence strategy. To date, no synthetic compounds have been identified that are capable of appreciably activating the *agr* system of more than one specificity group of *S. epidermidis* or, to our knowledge, of any other of the Staphylococci. Here, we report the characterization of the structure-activity relationships (SARs) for *agr* agonism by *S. epidermidis* AIP-II and AIP-III, and the application of these new SAR data and those previously reported for AIP-I for the design and synthesis of the first multi-group *agr* agonists. These non-native peptides were capable of inducing the expression of critical

biofilm dispersal agents (i.e., phenol soluble modulins) in cell-culture and represent new tools to study the role of quorum sensing in *S. epidermidis* infections.

4.1 Introduction

The bacterium *Staphylococcus epidermidis*, previously thought to be an innocuous commensal that colonizes the skin and mucosal tissues, has been recognized recently as a leading cause of hospital-acquired, or nosocomial, infections.¹⁻³ Coagulase-negative Staphylococci account for over a third of all hospital-acquired bloodstream infections in the US,⁴⁻⁵ and *S. epidermidis* represents the dominant pathogen within this group due to its propensity to form robust biofilms on abiotic surfaces and its prevalence in the human microbiome.⁵⁻⁶ These traits, in combination with the rise of antibiotic resistance, make treating *S. epidermidis* infections increasingly difficult.⁷⁻⁸ Alternative approaches to combat the virulence of this pathogen would be advantageous to public health.

Pathogenesis in *S. epidermidis* is largely under the regulation of quorum sensing (QS), a chemical-based cell-cell communication system, which makes QS an attractive target to potentially attenuate virulence phenotypes in this bacterium.⁹⁻¹³ QS activation can increase *S. epidermidis*' capability for skin colonization,⁶ evasion of the host immune system,¹⁴ and tissue infiltration.¹⁵⁻¹⁶ In contrast, QS inhibition in *S. epidermidis* has been shown to allow for more resilient biofilm formation, shielding *S. epidermidis* from antibiotics and the immune system.^{6, 15, 17} Non-native small molecules and peptides capable of either inhibiting or activating QS have been developed in other bacteria, and have shown significant value as research tools and as potential anti-virulence agents.¹⁸⁻²¹ While there are merits to either intentionally activating or inhibiting QS in order to curb *S. epidermidis* infections, given that the primary mechanism by which *S. epidermidis* causes device-associated infections is through biofilm formation,^{1,}

^{3, 22} this connection suggests that the development of chemical tools to *agonize* QS and thereby promote biofilm dispersion may provide the most benefit in reducing *S. epidermidis* growth on surfaces and rendering them more vulnerable to treatment with antibiotics or clearance via the host immune system.^{15, 23} Studies in *S. aureus*, which utilizes a similar QS system to regulate biofilm formation, have demonstrated that activation of QS through addition of agonists dispersed biofilms, significantly increasing their susceptibility to antibiotics relative to untreated *S. aureus* biofilms.²⁴ Identifying such QS agonists to combat *S. epidermidis* biofilms was a motivation for the current study.

Like other Staphylococci, *S. epidermidis* uses the accessory gene regulator (*agr*) system for QS (Figure 4.1), which consists of four protein components (AgrA–D) and a signaling molecule known as the autoinducing peptide (AIP).^{12, 25} The AIP sequence is contained within the propeptide AgrD that is processed in part by the membrane peptidase AgrB.²⁶ In a manner still not well-understood, the processed AgrD is further modified and exported out of the cell as the mature AIP signal.^{11, 27} The AIP concentration in the local extracellular matrix increases with cell density; upon reaching a threshold concentration, the AIP effectively binds to its receptor, the transmembrane histidine kinase AgrC, and induces *trans*-autophosphorylation.²⁸ Phosphorylated AgrC next activates the intracellular response regulator AgrA through phosphorelay. Thereafter, the activated AgrA dimerizes and binds to various promoters to regulate QS gene expression.²⁸⁻²⁹ Binding to the P2 promoter upregulates the *agr* operon and completes the auto-induction circuit;³⁰ binding to the P3 promoter upregulates RNAlII, which is the main effector molecule of *agr*;³¹ and binding to the PSM promoters

upregulates genes for phenol-soluble modulins (PSMs), peptides that promote biofilm dispersal among other functions.³²⁻³³

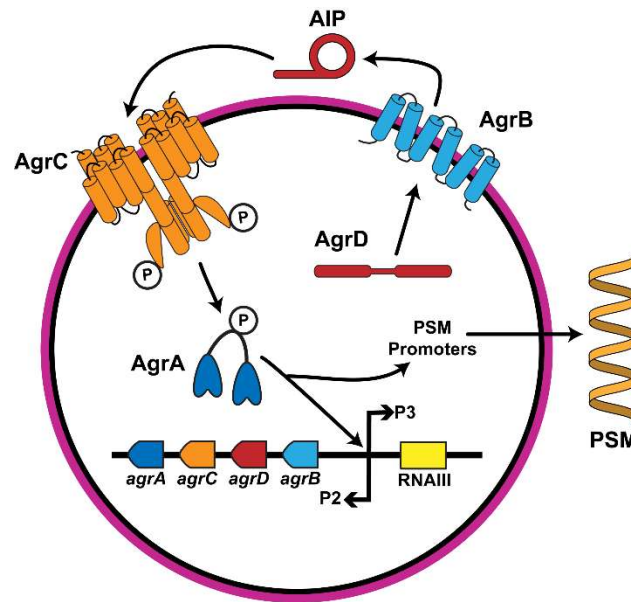


Figure 4.1 A simplified diagram of the *agr* QS system in *S. epidermidis*. AIP is produced through processing of AgrD polypeptide in part by AgrB and exported out of cell. AIPs bind to AgrC receptor and induce phosphorylation and activation of AgrA response regulator, upregulating expression of the *agr* operon, the RNAIII effector molecule, and PSM proteins that lead to biofilm dispersal upon secretion. Divergent evolution has led to four *agr* specificity groups with unique AIPs and *agr* machinery.

Similar to *S. aureus*,³⁴ *S. epidermidis* has evolved into divergent *agr* specificity groups, where allelic variations of the *agr* machinery are tuned to respond to their own unique AIP signals. Despite attempts by multiple laboratories to quantify the abundance of different *agr* groups in human infections, consensus has not yet been reached because the distribution of groups varies substantially in these studies.^{2, 35-39} The *S. epidermidis* *agr* groups-I–III were identified over a decade ago,³⁵ and very recently a new *agr* group (group-IV) was reported.³⁸ As the latter group still awaits significant

further characterization (such as confirmation of its native AIP structure) and appears to be rare, the work presented herein focuses on *agr* groups-I–III.

Interestingly, and again similar to *S. aureus*, the AIP signal from one *S. epidermidis* *agr* group can have cross-activity in another, “non-self” *agr* group, resulting in a network of possible *agr* interference (e.g., AIP-I activates its cognate receptor, AgrC-I, but inhibits both AgrC-II and -III).^{6, 35, 38} These cross-activity profiles raise interesting questions about the role of *agr* QS in mixed microbial environments, allowing one group to potentially outcompete another by blocking the non-self group QS system while simultaneously activating its own.⁴⁰ However, in the development of chemical tools to combat *S. epidermidis* biofilms in native environments, the cross-activity among *agr* specificity groups complicates the use of any single native AIP or even a cocktail of the native AIPs to block biofilms without *a priori* knowledge of the *agr* specificity groups present in the sample/isolate.²¹ This challenge could be overcome with a “pan-group” agonist capable of activating all *S. epidermidis* *agr* groups. To our knowledge, no such pan-group agonist has been reported in the Staphylococci.^{11, 41}

Our laboratory performed the first study of the structure-activity relationships (SARs) for *agr* agonism by *S. epidermidis* AIP-I,⁴² as well as a NMR structural study of key agonists and antagonists that we identified side-by-side with the native AIPs-I–III.⁴³ These past studies suggested that a multi-group agonist could be designed based on two observations. First, *agr* activation in group-I *S. epidermidis* was found to be largely dependent on a single exocyclic residue in AIP-I that likely could be incorporated into new scaffolds.⁴³ Second, AIP-II and AIP-III do not exhibit cross-group inhibition.⁶ In order to design multi-group agonists, however, we require further information beyond

these observations; namely, we need to identify the key agonizing features for each cognate AIP–AgrC interaction in groups-I–III so we can attempt to combine these features to target all three major *S. epidermidis* groups effectively using one peptide scaffold.

Herein, we report the characterization of SARs for *agr* agonism by the native AIP-II and AIP-III signals and the combination of these SARs with those for AIP-I to design, synthesize, and identify the first multi-group *agr* agonists in *S. epidermidis*. These new peptides were active in cell-based reporters of *agr* activity and capable of modulating a key phenotype associated with biofilms, PSM production. This study provides powerful chemical tools to investigate the role of QS in *S. epidermidis* infections, examine interference between groups, and assess pan-group *agr* activation as a possible approach to prevent or clear biofilm.

4.2 Results and Discussion

4.2.1 Overview of methods and analysis of reported SARs for *agr* agonism by group-I *S. epidermidis* AIP

In our prior study, we determined key SARs for group-I *agr* agonism by AIP-I through synthesizing a set of analogs and assaying their agonism and antagonism profiles in a group-I *S. epidermidis* reporter strain (assumed to act via competitively binding AgrC-I due to their very close structural similarity to AIP-I).⁴²⁻⁴³ The experimental methods and AIP-I features most pertinent to the current study are highlighted here (shown in Figure 4.2A; select assay data in Table 4.1). Briefly, we performed systematic alanine and D-amino acid scans of the AIP-I structure to ascertain the importance of

each residue to agonistic activity (Cys4 was not mutated to Ala as it is required for macrocycle formation). We also examined truncated analogs that lacked the exocyclic tail. Peptide activity was measured using a previously reported group-I *S. epidermidis* strain (AH3408) harboring a reporter plasmid encoding a *gfp* gene fused to the P3 promoter.⁶ Activation of the AgrC-I receptor in this strain leads to GFP production, which can be quantitated by fluorescence. AgrC-I agonism by AIP-I analogs was measured in the presence of a known AgrC-I inhibitor, the native *S. epidermidis* AIP-II. AgrC-I antagonism was measured by testing AIP-I analogs alone.

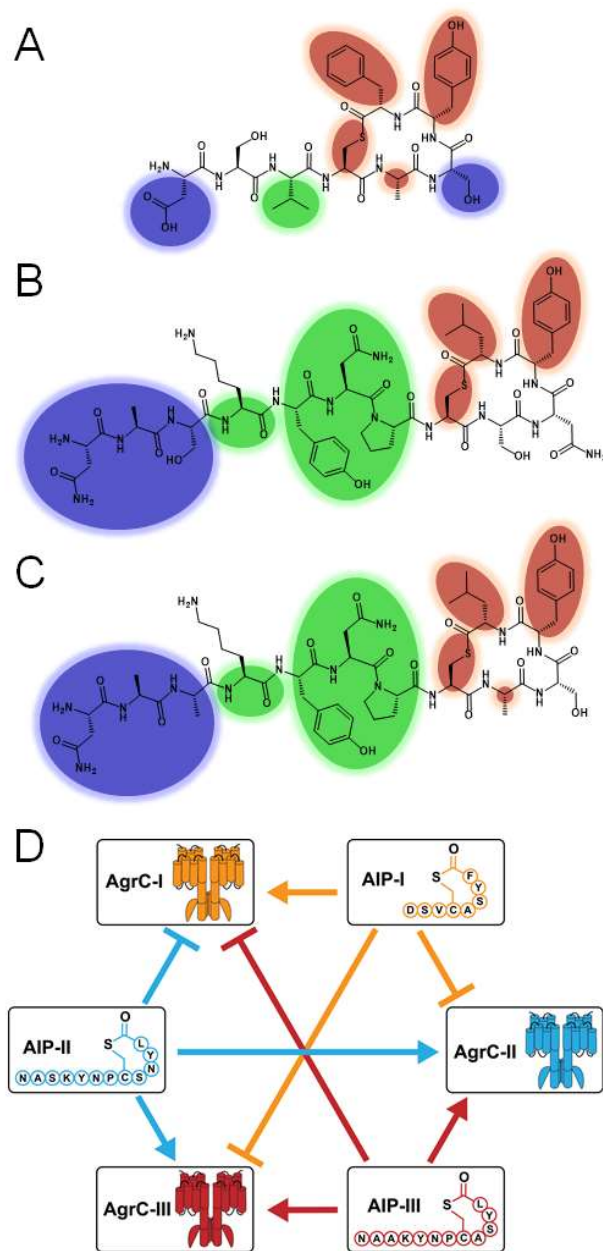


Figure 4.2 Summary of SAR trends for activation of the three *S. epidermidis* AgrC receptors by their cognate AIPs. SAR trends for (A) AIP-I as determined in our previous report.⁴² SAR trends for (B) AIP-II and (C) AIP-III determined in the current study. Red: essential for receptor binding. Green: crucial for receptor activation. Blue: either inconsequential or detrimental to receptor binding and activation. Unshaded residues/motifs contribute to receptor activation but are tolerant to changes. (D) Cross-activity network of AIPs-I–III for three *S. epidermidis* agr specificity groups (groups-I–III) as determined in the current study; \rightarrow indicates inhibition and \longrightarrow indicates activation.

Using these assays, we identified the first exocyclic residue of AIP-I (Val3) to be absolutely critical to agonizing AgrC-I because any substitutions at this position eliminated all agonistic activity (Figure 4.2A, Table 4.1). Interestingly, an alanine substitution at this position did not affect the overall 3D conformation of the peptide relative to AIP-I, as determined by solution-phase NMR;⁴³ however, this substitution converted the peptide into a potent antagonist, which implicated the branched side chain of Val3 as the principal structural element required for AgrC-I activation. Similarly, removal of the entire exocyclic tail yielded an analog with antagonistic activity. Analogous to the SARs ascertained for AIPs in *S. aureus*,⁴⁴ AIP-I binding to AgrC-I appears to be mediated largely by endocyclic hydrophobic residues (i.e., Tyr7 and Phe8). The solution-phase NMR structures of AIP-I reveal a hydrophobic face formed by these residues that is oriented in the opposite direction of Val3, suggestive that the initial binding/recognition site on AgrC-I is relatively distanced from the contact site that engenders receptor activation. Finally, replacing either of the hydrophilic residues Asp1 and Ser6 with alanine increased the agonistic potency of the resulting peptides. Replacement of Ser6 with alanine enforced a β -turn conformation in the macrocycle not present in the native AIP (as revealed by NMR),⁴³ which appears to play a key role in the observed increase in agonism potency. Using these SARs, we developed a second-generation agonist containing two non-native alanine residues (AIP-I D1AS6A) that displayed a ten-fold improvement in potency in AgrC-I relative to AIP-I (Table 4.1), as well as a potent multi-group antagonist containing three non-native alanine residues (AIP-I D1AV3AS6A, hereby referred to as AAA; Table 4.1).

Table 4.1 Selected activity data for native *S. epidermidis* AIPs and key analogs from SAR studies in corresponding reporter strains.

<i>agr</i> group tested	Compound	EC ₅₀ [nM] ^a	IC ₅₀ [nM] ^b
<i>agr</i> -I	AIP-I	170	
	AIP-II		9.64 ^c
	AIP-III		34.3 ^c
	AIP-I V3A		51.9 ^c
	AIP-I D1AS6A	10.3 ^c	
	AAA		2.84 ^c
<i>agr</i> -II	AIP-I		13.9
	AIP-II	226	
	AIP-III	648	
	AAA		0.36 ^c
	AIP-II K4A	>2000	
	AIP-II D-K4	>2000	
	AIP-II S9A	>2000	
	AIP-II D-S9	Inactive ^d	
	AIP-II N10A	>2000	
	AIP-II D-N10	Inactive ^d	
AIP-II 9aa	83.5		
<i>agr</i> -III	AIP-I		2.13
	AIP-II	n/c ^e	
	AIP-III	71.8	
	AAA		0.87 ^c
	AIP-III K4A	>2000	
	AIP-III D-K4		26.1
	AIP-III D-A9	Inactive ^d	
	AIP-III S10A	Inactive ^d	
	AIP-III D-S10	145	
AIP-III 9aa	28.9		

^aAgonism and ^bantagonism assay data obtained in *S. epidermidis* group-I–III reporter strains. See SI for full data sets. ^cData reproduced from reference.⁴² ^dDose-response assays revealed no substantial agonism nor antagonism activity over concentration range tested. ^eAgonism dose-response curve did not converge over concentration range tested.

4.2.2 SARs for agr agonism by group-II and group-III *S. epidermidis* AIPs

We next gathered corresponding SAR data for AIP-II and AIP-III using similar residue scanning methods as for AIP-I. These sets of AIP-II and AIP-III analogs were synthesized using solid-phase peptide chemistry and purified by HPLC using procedures based on our established protocols (see SI).^{42, 45-46} Each analog was then tested for its effects on the cognate AgrC receptors using previously reported *S. epidermidis* group-II and group-III fluorescence reporter strains (AH2673 and AH3409, respectively)⁶ and methods analogous to those for group-I introduced above. To measure AgrC agonism, we used our multi-group antagonist AAA to block the activation of AgrC-II and AgrC-III by the endogenously produced AIPs.

To start, we first evaluated the activities of the native *S. epidermidis* AIPs (AIP-I–III) in the group-II and group-III reporters (Table 4.1, Tables 4.S1–4.S2), to compare our methods to a prior report by Olson *et al.*⁶ While the inhibitory activity of AIP-I against AgrC-II and AgrC-III (~70% and 90% inhibition at 10 μ M, respectively) was in agreement with that past study, the group-II and group-III cross-activity differed (trends summarized in Figure 4.2D). Instead of showing inactivity,⁶ cross-group *activation* was observed by AIP-II in AgrC-III and AIP-III in AgrC-II (~40% and 180% activation at 10 μ M, respectively). This difference is most likely the result of variances in the agonism assay protocol used in each study. The original report examined whether spent media from one *S. epidermidis agr* specificity group would affect *agr* activity in another *agr* specificity group using a fluorescent reporter as compared to controls without spent media.⁶ While compounds with strong agonistic or antagonistic activity could be characterized with this assay, compounds with partial agonism activity could be

misinterpreted as inactive. Our agonism assay assesses the ability of compounds to agonize *agr* activity in the presence of a strong antagonist. Inactive or inhibitory compounds will result in no observable activity, while partial or full agonists will restore *agr* activity. As our assay can more clearly distinguish between inactive compounds and partial agonists relative to the prior study, we believe the observed cross-group activation more accurately defines the interactions between group-II and group-III. This cross-group activation is intriguing, as it suggests the possibility of QS cooperativity between group-II and group-III in a mixed environment; further studies are needed to better understand the mechanisms and extent by which *agr* cross-group activity could shape native *S. epidermidis* communities.

Although the sequences of AIP-II and AIP-III differ at only three residues, our previous NMR studies showed substantial differences in their solution-phase conformations.⁴³ While the macrocycle conformations were modestly similar despite differences at positions 9 and 10, the seven residue exocyclic tails exhibited remarkably different conformations in solution (presumably due to the single residue difference at position 3).⁴³ However, in the current study we observed largely comparable trends in the SARs for agonism by these two signals in the reporter assays (Figure 4.2B–C; see Tables 4.S1–4.S2 for full efficacy and potency data), which suggests that the exocyclic tails may reorganize to more similar conformations upon binding to their cognate AgrC receptors. We summarize key trends here.

Beginning at the C-terminus of the peptides, we found that substitutions at the endocyclic hydrophobic residues (Tyr11 and Leu12) of AIP-II and AIP-III drastically impaired activity. These observations align well with our findings in AIP-I (*vide supra*),⁴²⁻

⁴³ suggesting that these endocyclic hydrophobic residues likely share a common role in initial binding to their respective AgrC receptors. The residues at positions 9 and 10 differ between AIP-II and AIP-III (Figure 4.2B–C), and we hypothesized that these two positions could dictate receptor specificity. This reasoning was supported by the consequences of substitution at position 10 differing between AIP-II and AIP-III (Table 4.1). The alanine substitution at position 10 in AIP-II reduced potency but the same substitution in AIP-III completely inactivated the analog; meanwhile, stereochemical inversion of position 10 in AIP-II obliterated activity, while the corresponding inversion in AIP-III had almost no effect on activity (Table 4.1). Position 9 was more similar between the two AIPs, with substitutions generally being poorly tolerated in terms of agonism efficacy and potency. Taken together, the activity profiles of the AIP-II and AIP-III analogs exploring positions 9 and 10 suggest that these two positions each make significant and distinct contributions to agonistic activity, likely driving receptor specificity.

The final endocyclic residue in AIP-II and AIP-III is Cys8, which forms the thioester linkage with Leu12 to generate the macrocycle. The incorporation of D-cysteine fully inactivated both AIP-II and AIP-III, similar to our result for D-cysteine replacement in AIP-I.⁴² This loss of activity could be attributed to a stringent requirement for the local orientation of the thioester bridge for binding, or perhaps this inversion has more global ramifications on peptide conformation. Further structural studies are needed to distinguish these effects and are ongoing in our laboratory.

Turning to the exocyclic tail, we found that both AIP-II and AIP-III, analogous to AIP-I,⁴² require specific exocyclic residues for AgrC activation. Alanine and D-amino

acid substitutions of Tyr5, Asn6, or Pro7 converted the peptides into antagonists or removed any observable activity. These findings are interesting because while AIP-I depends on Val3 alone for nearly all agonistic activity,⁴² AIP-II and AIP-III appear to depend on the simultaneous presence of multiple residues in this region of the exocyclic tail to activate their cognate receptors. The subsequent residue Lys4 also appears essential for AgrC agonism, but its role differs between AIP-II and AIP-III. In AIP-II, altering Lys4 appears to mainly affect potency without affecting agonism efficacy, while the same changes to AIP-III at Lys4 affect both potency and efficacy (Table 4.1). These divergent outcomes for substitution at an identical residue and position suggests Lys4 may play unique roles when these AIP analogs interact with AgrC-II versus AgrC-III.

Substitutions at the remaining three N-terminal residues of AIP-II and AIP-III had little impact on their activities. Again, this result contrasts with their NMR solution structures that show the end of the exocyclic tails of AIP-II and AIP-III to be in drastically different conformations.⁴³ In fact, removal of these residues through tail truncation actually *increased* the potency of the peptides, as the AIP analogs with all three N-terminal residues removed (AIP-II 9aa and AIP-III 9aa) were two-fold more potent than their parent AIPs (Table 4.1). These data suggest that the final three N-terminal residues of AIP-II and AIP-III fail to engage in meaningful contacts with AgrC and may possibly hamper optimal contacts. Continued removal of additional residues, however, turned the AIP analogs into potent antagonists (Tables 4.S1–4.S2). We also explored extending the exocyclic tail by one residue (i.e., AIP-II 13aa and AIP-III 13aa, each containing an N-terminal glycine in accordance with the next residue in the AgrD sequence), but this had no effect on efficacy or potency. These results underscore the

minor role of the N-terminal residues in AIP-II and AIP-III for AgrC agonism. These surprising data suggest the possibility that AIP-II and AIP-III could be further tailored to 9-mers outside of the cell (i.e., by some extracellular peptidase), and these shorter and more potent agonists may represent the native forms of AIP-II and AIP-III. Additional studies are warranted to probe this hypothesis.

4.2.3 Design and biological characterization of multi-group agonist scaffolds

With SARs in hand for agonism of AIPs-I–III in their cognate AgrCs, we used these collected data to design peptides that united various motifs critical for activity in an attempt to generate scaffolds with multi-group agonistic activity. We designed the scaffolds with the following features in mind: 1) the endocyclic, hydrophobic residues of all three AIPs are essential and likely adopt similar orientations for receptor binding; 2) a length of nine amino acids appears optimal for agonistic activity in AgrC-II and AgrC-III; 3) the exocyclic residues immediately neighboring the cysteine (Val3 in AIP-I, and Tyr5, Asn6, and Pro7 in AIP-II and AIP-III) largely control agonism in all three AgrC receptors; and 4) the endocyclic residues neighboring the cysteine likely dictate specificity between AgrC-II and AgrC-III. From these features, we designed and synthesized a series of chimeric peptide scaffolds blending the three native AIPs together (see SI for discussion of all scaffolds explored) and identified three peptides for further study: Chimeras 1, 2, and 3 (Cmr1, Cmr2, and Cmr3; Figure 4.3).

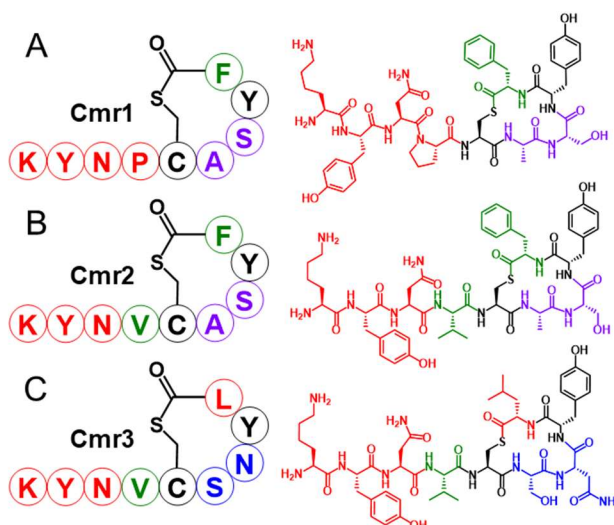


Figure 4.3 Structures of the three AIP chimeric scaffolds (Cmr 1–3). Each scaffold represented with single-letter amino acid abbreviation (*left*) and chemical structure (*right*). Black signifies residues shared by AIPs-I–III, green signifies residues solely from AIP-I, blue signifies residues from AIP-II, purple signifies residues shared by AIP-I and AIP-III, and red signifies residues of the shared by AIP-II and AIP-III.

Cmr1 combined the macrocycle of AIP-I with the shared exocyclic tail of AIP-II 9aa and AIP-III 9aa (Figure 4.3). Given that Cmr1 lacks the exocyclic valine deemed critical for agonism of AgrC-I, we initially expected this scaffold to be an antagonist of AgrC-I, while functioning as an agonist in AgrC-II and AgrC-III. To our surprise, Cmr1 exhibited agonistic activity in all three AgrC receptors, albeit with varying efficacies and potencies (Table 4.2). Cmr1 was capable of agonizing AgrC-I to approximately 50%, yet displayed low potency. We hypothesize that this reduced activity for Cmr1 is due to the inability of the exocyclic Pro4 to fully replace the agonizing, hydrophobic interactions of the native valine residue in AIP-I with AgrC-I. Cmr1 was similarly able to activate AgrC-II to 60%. In AgrC-III, Cmr1 had an exceptional agonism profile, displaying full activation and sub-nanomolar potency and signifying the most potent AgrC-III agonist we have discovered thus far. Indeed, with activity in all three groups, Cmr1 represents to our

knowledge the first known multi-group agonist for the *agr* systems in *S. epidermidis*, and in any other related Staphylococci.

Table 4.2 Agonism activity data for native AIPs, chimera scaffolds, and identified multi-group agonists (indicated in bold).

Peptide Name	AgrC-I		AgrC-II		AgrC-III	
	Max. Activation (%) ^b	EC ₅₀ (nM) ^c	Max. Activation (%) ^b	EC ₅₀ (nM) ^c	Max. Activation (%) ^b	EC ₅₀ (nM) ^c
AIP-I	147	170	--- ^d	--- ^d	--- ^d	--- ^d
AIP-II	--- ^d	--- ^d	421	226	39.1	n/c ^e
AIP-III	--- ^d	--- ^d	182	648	220	71.8
Cmr1	51.1	>2000	60.4	61.3	223	0.929
Cmr2	146	71.8	--- ^d	--- ^d	46.8	40.6
Cmr3	--- ^d	--- ^d	290	>2000	--- ^d	--- ^d
Cmr1 S7A	38.4	844	136	63.7	398	1.47

^aAgonism assay data obtained in *S. epidermidis* group-I–III reporter strains. See text.

^b100% activity corresponds to level of activity produced by endogenously-produced AIP from vehicle controls in absence of 25 nM AAA, 0% activity corresponds to media controls. ^cAs determined by dose-response curves with compound competing against 25 nM AAA. ^dOnly antagonism activity observed. ^eDose-response analysis did not converge over concentration range tested.

While Cmr2 also incorporates the macrocycle of AIP-I, Cmr2 differs from Cmr1 in its tail sequence that unites the critical valine residue of AIP-I with the remaining tail residues of AIP-II 9aa and AIP-III 9aa (Figure 4.3). With the valine residue in place, Cmr2 performed substantially better as an AgrC-I agonist, with mid-nanomolar potency and full efficacy (Table 4.2). However, the presence of this valine reduced its activity in AgrC-II and AgrC-III; Cmr2 had no observable agonism activity in AgrC-II and had greatly reduced agonistic activity in AgrC-III relative to Cmr1. Lastly, Cmr3 incorporates

the hybrid tail of Cmr2 but instead trades the AIP-I macrocycle for the AIP-II macrocycle. While Cmr3 could strongly agonize AgrC-II (Table 4.2), it showed no agonism activity in either AgrC-I or AgrC-III. Although Cmr3 does not demonstrate multi-group agonism, it did provide new insights into the importance of the macrocycle on AgrC agonism. The inability of Cmr3 to agonize AgrC-I—even with the critical exocyclic valine present—suggests that the macrocycle likely aids in presenting this side chain properly to AgrC-I for activation and that improper orientation by the AIP-II macrocycle thereby hinders agonism. Conversely, Cmr3 was able to strongly agonize AgrC-II, which suggests the AIP-II macrocycle orients the valine to contact and agonize AgrC-II in a functionally similar fashion to the native proline in AIP-II. These new SARs and the differential activities of the three chimeras in the AgrC receptors guided our design of second-generation chimeras; we return to those below.

4.2.4 Multi-group agonists promote PSM production in *S. epidermidis*

We sought to demonstrate that the multi-group *agr* agonist Cmr1 was capable of modulating a phenotype in *S. epidermidis* relevant to virulence. We selected to investigate PSM production, as PSMs have been shown to facilitate biofilm dispersal and are positively regulated by the *agr* system in *S. epidermidis*.^{15-16, 23, 47-49} PSMs also can be readily isolated from bacterial culture and quantitated using RP-HPLC.^{48, 50-51} As wild-type *S. epidermidis* cultures can produce a substantial amount of PSMs without exogenous *agr* agonists added (Figure 4.4A-C, black trace; see SI for details), we first inhibited PSM production in group I–III strains by adding one of our in-house *agr* antagonists. When added alone, the antagonists either eliminated or substantially

reduced the production of PSMs for each of the three *agr* groups (Figure 4.4A–C, red trace); however, addition of both an antagonist and the multi-group agonist Cmr1 was observed to fully or partially restore the production of PSMs for the three *agr* groups (as determined by comparison to an internal standard; Figure 4.4A–C, blue trace). PSM peaks were restored to 47% of the baseline value in group-I, and to 11% and 263% in group-II and group-III, respectively. MALDI-MS and ESI-MS confirmed the peak with a RT of 46 minutes contained PSM α , PSM β , and PSM γ (see SI Table 4.D). The restoration of PSM production by Cmr1 signifies activation of *agr* within each group and serves to validate the use of reporter strains to identify compounds capable of modulating *agr* controlled phenotypes in *S. epidermidis*. Moreover, the ability of Cmr1 to activate PSM production in all three groups underscore the potential of this chemical approach to combat virulence via the pan-group or “global” targeting of the *agr* system.

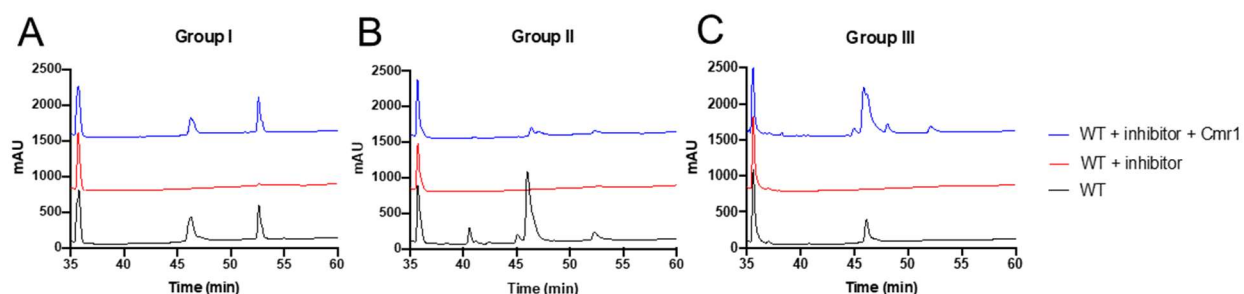


Figure 4.4 Representative portions of HPLC traces of samples of *S. epidermidis* cultures showing the PSM peaks. (A) Group-I PSM production inhibited with 1 μ M AIP-II 9aa and restored with 9 μ M Cmr1. (B) Group-II PSM production inhibited with 250 nM AAA and restored with 9 μ M Cmr1. (C) Group-III PSM production inhibited with 1 μ M AAA and restored with 9 μ M Cmr1. See SI for strain and assays details.

4.2.5 Design and characterization of second-generation multi-group agonist scaffolds

From the assay data accrued for the three chimera scaffolds above, we designed and synthesized a set of second-generation analogs in an attempt to identify peptide

scaffolds with improved agonistic activity in the three *S. epidermidis agr* groups (see Figures 4.S1–4.S6, Tables 4.S3–4.S10 for full list of compounds and activity data). We largely focused on altering the macrocycle of our chimera scaffolds, guided by the hypothesis that we could improve activity in specific groups by tailoring the macrocycle to be more similar to that of the native AIP of the desired group. For example, starting with Cmr1, we aimed to enhance its activity towards AgrC-II by making substitutions at positions 6 and 7 to more resemble AIP-II. As expected, the more closely these analogs resembled the AIP-II macrocycle, the more active they were at agonizing AgrC-II, but unfortunately often at the cost of losing activity toward AgrC-I (Figure 4.S7).

Corresponding strategies in Cmr2 and Cmr3 met with similar results (see SI for further discussion). The only analog resulting from these follow-up studies that displayed multi-group agonism activity was Cmr1 S7A, which maintained activity in group-I and group-III while substantially improving group-II activity when compared to Cmr1 (Table 4.2, Figure 4.S7). This compound was also active in the *S. epidermidis agr* phenotypic assay, stimulating PSM production levels comparable to or surpassing Cmr1 in the three *agr* groups (Figure 4.S8).

Beyond the discovery of Cmr1 S7A, the activity survey of the second-generation analogs had an additional positive outcome as it revealed a new SAR for high potency in the three AgrC receptors; namely, the preferred C-terminal residue for high multi-group potency by AIP analogs appears to be a phenylalanine (native to AIP-I) over leucine (native to AIP-II and AIP-III). In most cases where two peptide analogs differ only at the C-terminal residue, the C-terminal phenylalanine analog is at least as potent as the corresponding C-terminal leucine analog and often substantially more potent

across the three *agr* groups, with few exceptions, namely AIP-II 9aa and AIP-II 9aa L9F in group-II (Table 4.3). This activity trend holds regardless of whether the peptide is an agonist or antagonist. This result is intriguing and strongly supports the installation of phenylalanine as the C-terminal residue in design of future pan-group modulators of *S. epidermidis* AgrC receptors.

Table 4.3 Potency data for pairs of AIP analogs where the only sequence difference is a C-terminal phenylalanine or leucine.

<i>agr</i> group tested	Peptide containing Phe	EC ₅₀ [nM] ^a	IC ₅₀ [nM] ^b	Peptide containing Leu	EC ₅₀ [nM] ^a	IC ₅₀ [nM] ^b	Fold change
<i>agr-I</i>	AIP-I	170		I-tail, III-ring	1870		11.0
	AIP-II 9aa L9F		0.470	AIP-II 9aa		2.84	6.04
	Cmr2	71.8		Cmr2 F9L	1020		14.2
	Cmr3 L9F		2.15	Cmr3		75.8	35.2
<i>agr-II</i>	AIP-I		13.9	I-tail, III-ring		50.9	3.66
	AIP-II 9aa L9F	203		AIP-II 9aa	83.5		0.41
	Cmr3 L9F	210		Cmr3	>2000		--- ^c
<i>agr-III</i>	AIP-I		2.13	I-tail, III-ring		31.8	14.9
	AIP-II 9aa L9F	>2000		AIP-II 9aa	>2000		--- ^c
	Cmr1	0.929		AIP-III 9aa	28.9		31.1
	Cmr2	40.6		Cmr2 F9L	>2000		--- ^c
	Cmr3 L9F		34.9	Cmr3		>2000	--- ^c

Collected from ^aagonism or ^bantagonism assay data obtained in *S. epidermidis* group-I–III reporter strains. See Si for methods. ^cNot calculated due to low potency.

4.3 Summary and Conclusions

The *agr* system plays a critical role in the biofilm life cycle and virulence of *S. epidermidis*, making chemical or biological agents capable of *agr* modulation valuable

tools to probe and potentially limit infectivity.^{2, 15-16, 22, 47} The intentional activation of *agr* could reduce biofilm accumulation and thereby render the dispersed bacteria more susceptible to antimicrobial agents.⁸ In this study, we report the design, synthesis, and biological characterization of AIP signal analogs capable of agonizing three specificity groups of *S. epidermidis* (I–III). Through systematic amino acid scans, we determined the key SARs that engendered AgrC agonism by AIP-II and AIP-III, and combined these SARs strategically with those we previously reported for AIP-I⁴²⁻⁴³ to design chimeric peptide scaffolds. These investigations revealed two chimeric peptides (Cmr1 and Cmr1 S7A) that were capable of activating the *agr* systems in groups-I–III of *S. epidermidis*. In addition, we demonstrated that these multi-group agonists could stimulate production of PSMs, which plays a key role in the dispersal of biofilms, serving to validate their use as probes to study infection relevant phenotypes in *S. epidermidis*.

The results of this study are significant as they provide peptide chimeras that represent, to our knowledge, the first reported non-native multi-group activators of the *agr* QS system in any bacterium. This study also provided a deeper understanding of the signal–receptor interactions for the *S. epidermidis agr* systems. For example, we discovered that the two endocyclic residues adjacent to the conserved cysteine likely contribute towards group specificity and facilitate AIP recognition by the *S. epidermidis* AgrC receptors. In addition, we observed that the inclusion of a C-terminal phenylalanine can enhance potency of AIP analogs in all three AgrC receptors. Lastly, and perhaps with the most implications for future ligand design, we identified that the exocyclic residue adjacent to the conserved cysteine is likely the critical residue to explore in future work aimed at increasing the multi-group agonistic activity of AIP

analogs. While the current study only examined two amino acids at that position (valine and proline), introducing other natural and non-canonical amino acids (e.g., leucine, pipecolic acid, or thioproline) at this position could reveal side chains with optimal sterics and/or hydrophobicity for agonizing the three AgrC receptors. Ongoing studies focus on exploring these motifs in new peptides to target not only groups-I–III *S. epidermidis*, but also the newly reported group-IV.³⁸

4.4 Supplemental Information

4.4.1 Experimental procedures and methods

Reagents, strains, and general methods

All biological and chemical reagents, solvents, and resins were purchased from commercial sources and used according to instructions. All *S. epidermidis* strains were grown in Tryptic Soy Broth (TSB, Sigma), incubated at 37 °C with shaking at 200 rpm unless otherwise noted. Cultures of *S. epidermidis* fluorescence reporter strains AH3408 (group-I), AH2673 (group-II), and AH3409 (group-III) were supplemented with 10 µg/mL of erythromycin, while the *S. epidermidis* wild-type strains RP62A (group-I) and 1457 (group-II) were not supplemented with erythromycin. Water (18 MΩ) was purified using an arium® pro ultrapure water system (Sartorius). Samples of native *S. epidermidis* AIPs and analogs previously reported by our laboratory⁴² were acquired from in-house stocks.

Instrumentation

Reverse-phase high performance liquid chromatography (RP-HPLC) was carried out on a Shimadzu system equipped with a SLC-10Avp controller, a LC-10AT pump, a

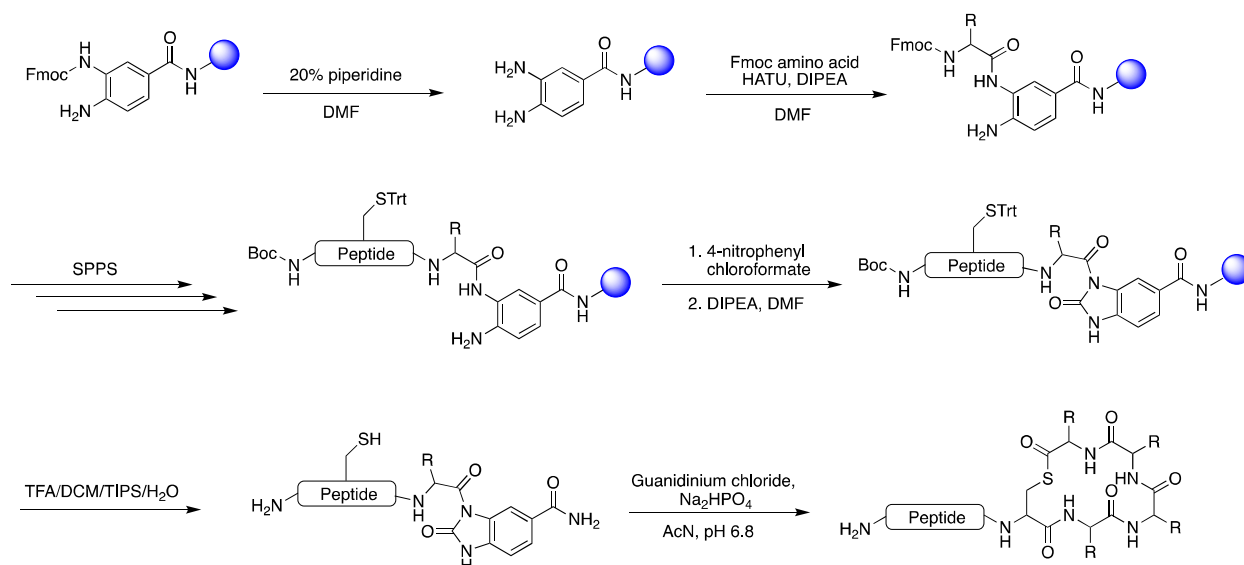
FCV-ALvp solvent mixer, and a SPC-10MAvp UV/Vis diode array detector. Peptides were purified using a semi-preparative Kromasil Eternity C18 column (10 mm x 250 mm, 5 μ m particle size with 100 Å pore size) with a 5 mL/min flow rate. Peptide purity was assessed on an analytical Kromasil Eternity C18 column (4.6 mm x 250 mm, 5 μ m particle size with 100 Å pore size) with a 1 mL/min flow rate. Solvent A = 18 M Ω water + 0.1% trifluoroacetic acid (TFA); solvent B = acetonitrile + 0.1% TFA. Peptide identity was determined using mass spectrometry (MS). MALDI-TOF MS data were obtained using a Bruker microflex LRF spectrometer equipped with a 337 nm laser and a reflectron. Exact mass (EM) MS data were obtained using a Thermo Q Exactive Plus ESI-Q-IT (orbitrap) mass spectrometer.

Peptide synthesis and characterization

Linear versions of the *S. epidermidis* AIP analogs reported in this study were synthesized using a modified protocol of the Fmoc/tBu based solid-phase peptide synthesis (SPPS) approach developed by Blanco-Canosa and Dawson (Scheme 4.S1).^{42, 45} All SPPS reactions were mixed by agitation on a benchtop shaker. Briefly, Dawson 3-(Fmoc-amino)-4-aminobenzoyl (Dbz) AM resin (100-200 mesh) was swelled in CH₂Cl₂ for 40 min, and the solvent was exchanged for dimethylformamide (DMF). Fmoc-group deprotections were achieved using piperidine solution (20% in DMF, 2 mL, 5 min x 3). For each amino acid coupling, except for the final coupling, *N*-Fmoc-protected amino acid (4 mole equiv. relative to the resin), *N*-[(dimethylamino)-1H-1,2,3-triazolo-[4,5-b]pyridin-1-ylmethylene]-*N*-methylmethanaminium hexafluorophosphate *N*-oxide (HATU, 4 mole equiv.), and diisopropylethylamine (DIPEA, 8 mole equiv.) were

dissolved in 2 mL of DMF, preactivated for 1 min, and added to the resin for 30 min. For the final coupling, *N*-Boc-protected amino acids were used instead. Following the final amino acid coupling, the Dbz group was activated by the addition of 4-nitrophenylchloroformate in CH₂Cl₂ (4 mole equiv., 30 min x 2), and then treated with DIPEA (0.5 M in DMF, 10 min x 3). The resin was washed sequentially with DMF, CH₂Cl₂, and diethyl ether, dried under N₂, and under vacuum for 18 hr. To cleave the linear peptide, the resin was resuspended in a cleavage cocktail of TFA/CH₂Cl₂/H₂O/triisopropylsilane (90:5:2.5:2.5) for 2 hr (Scheme 1). The resulting mixture was syringe-filtered, rinsed with the cleavage cocktail once, and precipitated in diethyl ether at -20 °C for at least 1 hr. The precipitate was dissolved in acetonitrile/H₂O (1:1) and lyophilized.

The linear AIP analogs were purified by semi-preparative RP-HPLC as described below, and the fractions with the desired product, as confirmed by MALDI-MS, were collected, lyophilized, and then cyclized according our previously reported solution-phase macrocyclization protocol (Scheme 4.S1).⁴² The resulting cyclic peptides products were purified by RP-HPLC as described below, and their purities and identities were confirmed by analytical RP-HPLC and EM MS, respectively. The purified AIP analogs were lyophilized, weighed, and stored as 1 mM stock solutions in DMSO at 4 °C. The native *S. epidermidis* AIPs (I-III), as well as AIP-I D1AV3AS6A, AIP-II 11aa, 10aa, 9aa, 8aa, and tAIP-II were all previously prepared in our laboratory,⁴² and therefore were not re-synthesized for the present study.



Scheme 4.S1 Solid-phase synthesis of standard thioester AIP analogs.

Peptide purification

Linear peptides were purified by RP-HPLC over a linear gradient of 20% → 50% solvent B over 30 min, and cyclic peptides were purified over a linear gradient of 23% → 38% solvent B over 36 min. Peptide purity was determined using a linear gradient of 10% → 95% solvent B over 27 min, with integration of peaks detected at 220 nm.

Fluorescence reporter assay protocol

Agonism and antagonism assays in the *S. epidermidis* reporter strains were performed using a previously established protocol with two modifications.⁴² First, to block AgrC activation by endogenously produced AIP, the multi-group antagonist AAA uncovered in our prior study⁴² was used for the agonism assay at a final concentration of 25 nM. Second, in the assessment of AIP-II SARs and potential multi-group agonists, group-II cultures were grown for 8 hours with 500 nM of AIP-II 9aa, an agonist of AgrC-

II, to ensure consistent activation of the agr system, prior to dilution for plating (AIP-II 9aa was used instead of native AIP-II due to compound availability and enhanced potency). A Biotek Synergy 2 microplate reader was used to record absorbance and fluorescence measurements in reporter assays. Data was normalized to vehicle (100%) and media (0%) controls, and then analyzed with GraphPad Prism (v. 8.0.1) to determine sigmoidal curve fits ([compound] vs. response, 4-parameters), calculate IC50/EC50 values and corresponding 95% confidence intervals, as well as determine maximal percent activation and inhibition values.

PSM quantification protocol

The quantity of PSMs produced by *S. epidermidis* cultures was measured using previously reported methods, with some minor adaptations.⁴⁹⁻⁵¹ *S. epidermidis* overnight cultures were prepared of strains RP62A (group-I), 1457 (group-II), and AH3409 (group-III) in TSB. Antagonists were added to the overnight liquid cultures prior to incubation to block PSM production, and the multi-group agonists were added prior to incubation to outcompete the antagonist and turn on PSM production. For group-I, 1 μ M of the antagonist AIP-II 9aa was used. For group-II, 250 nM of the antagonist AIP-I D1AS6AV3A was used. For group-III, 1 μ M of the antagonist AIP-I D1AS6AV3A was used. In the three groups, 9 μ M of the multi-group agonist Cmr1 or Cmr1S7A was added. The cultures were incubated for 24 hours on a 37 °C shaker.

After incubation, cultures were centrifuged for 5 minutes at 16.1 rcf. The supernatant was filtered using 0.45 μ M Perkin Elmer PTFE syringe filters and 10% v/v LM F3L (sequence A-CLMFV, a peptide synthesized for unrelated species *Listeria*

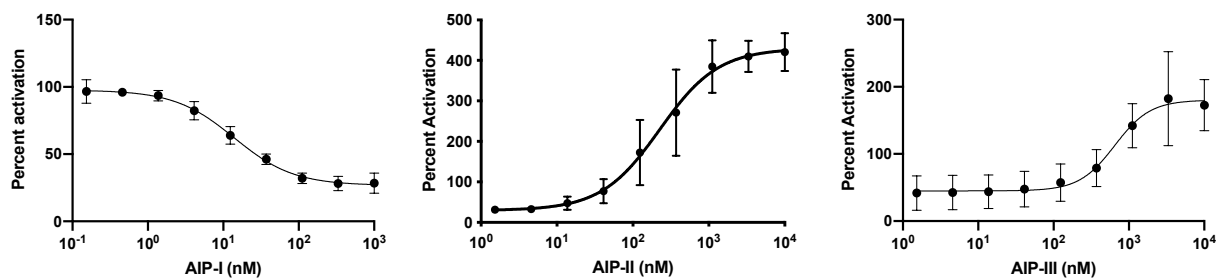
monocytogenes that was chosen because of its separation on RP-HPLC) was added as an internal standard to a final concentration of 100 μ M. Samples were analyzed using analytical RP-HPLC, where 500 μ L of supernatant was injected onto a Kromasil Eternity C18 column (4.6 mm x 250 mm, 5 μ m particle size with 100 Å pore size) with a 1 mL/min flow rate. Solvent A = 18.2 M Ω water + 0.1% trifluoroacetic acid (TFA); solvent B = acetonitrile (ACN) + 0.1% TFA. The method used involved a 40 min ramp up from 0% solvent B to 100% solvent B, followed by a 10 min hold at 100% solvent B. PSMs were identified using MALDI-MS (Bruker microflex LRF™) and ESI/EMM MS (Thermo Q Exactive Plus™). Relative PSM quantification was achieved by analyzing the area under the internal standard and PSM curves using GraphPad Prism (v. 8.0.1). Because the ratio of peak area: concentration is proportional between the internal standard and the PSMs, and the internal standard concentration is known, the relative amounts of PSMs could be quantified.

4.4.2 Activity data for AIP-II analogs in group-II and group-III reporters

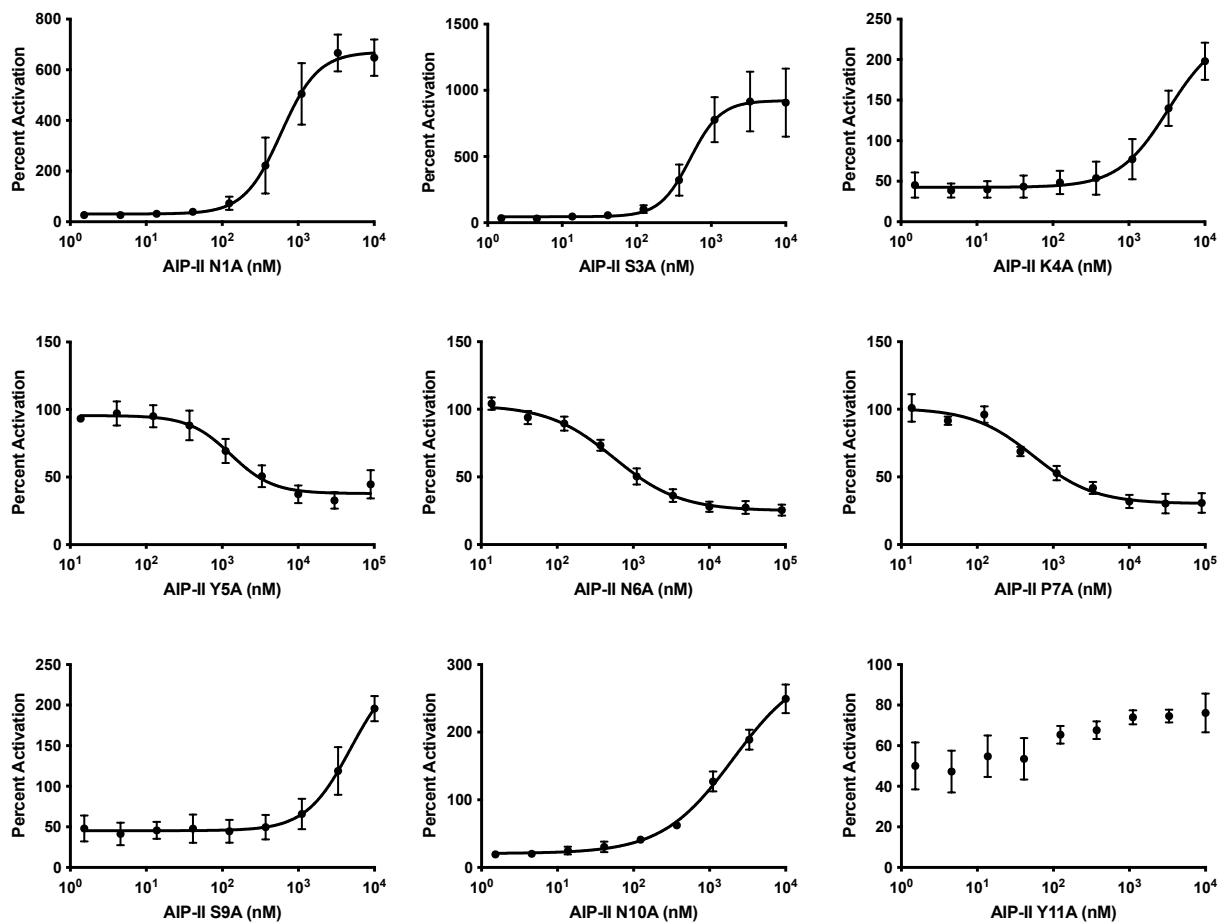
Dose-response curves for AIP-II based alanine, D-amino acid, and varied tail length analogs

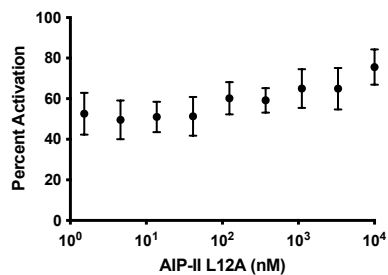
All compounds assayed in *S. epidermidis* AH2673 (group-II). Compound names are indicated on the X-axis on each curve plot. Error bars represent SEM of three biological replicates. Percent activation was normalized to a DMSO control.

- Control peptides (native AIPs I-III)

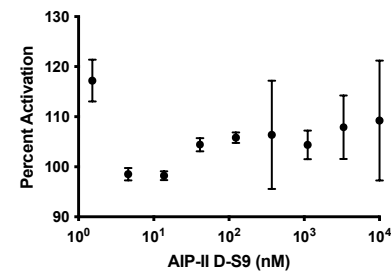
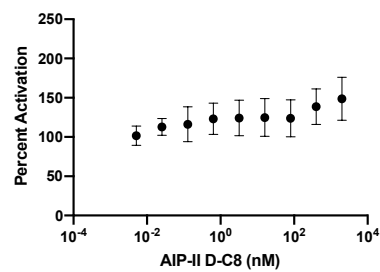
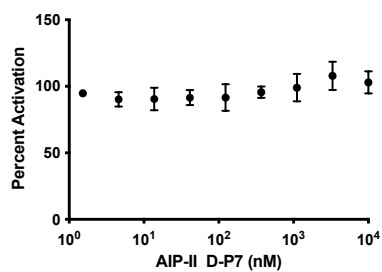
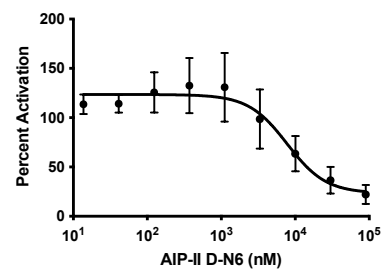
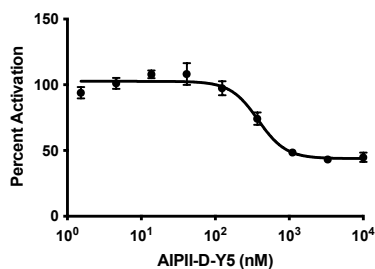
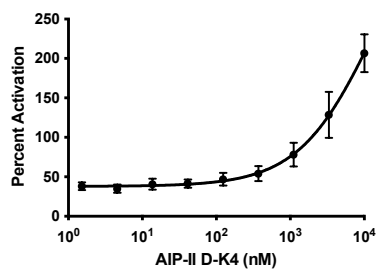
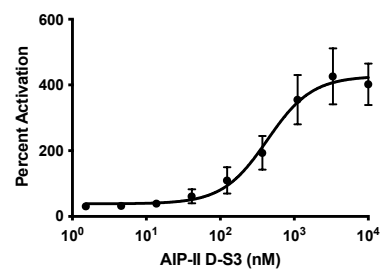
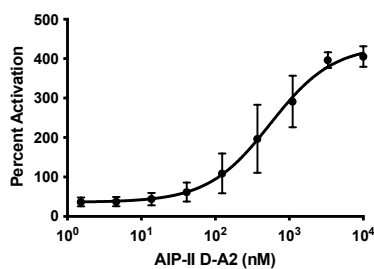
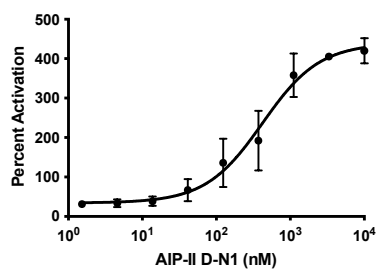


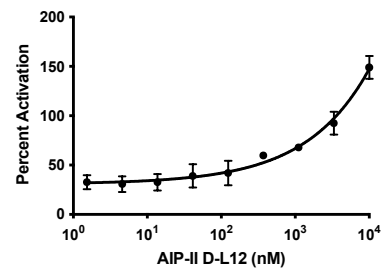
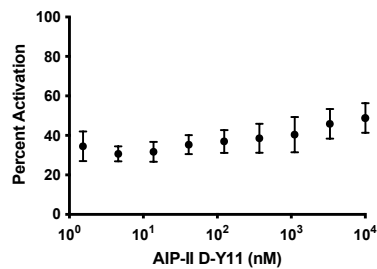
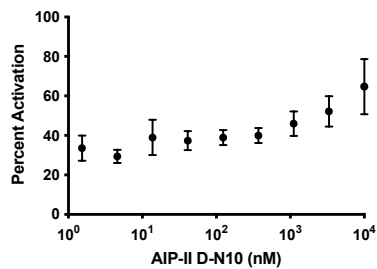
- Alanine analogs





- D-Amino acid analogs





• Tail truncated analogs

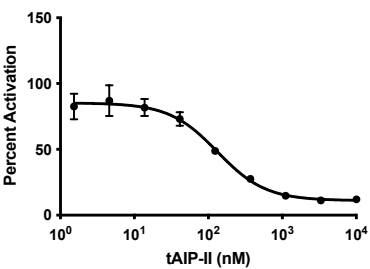
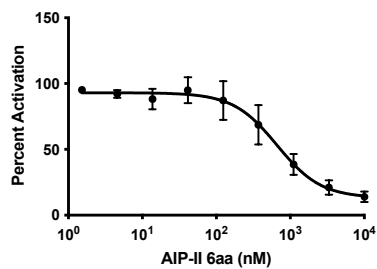
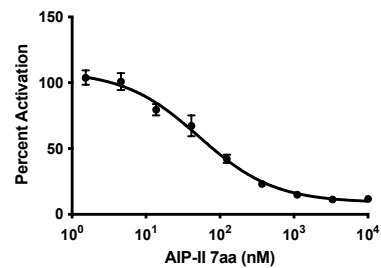
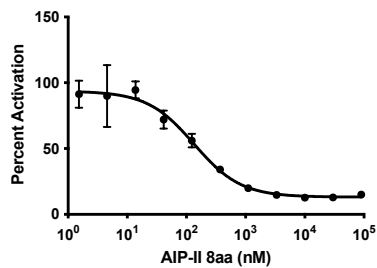
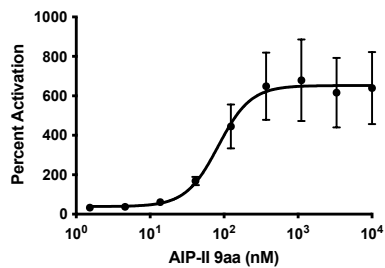
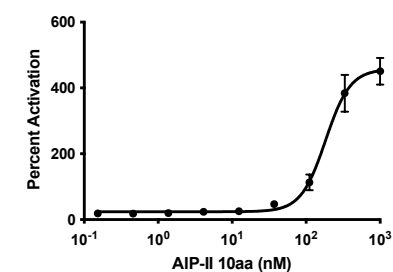
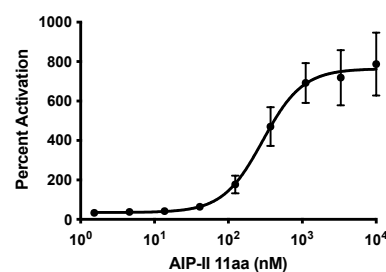
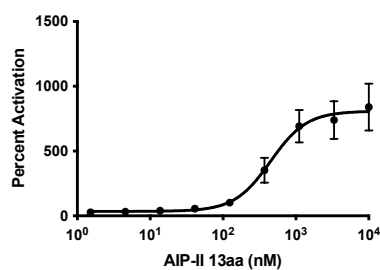


Table 4.S1 Summary of agonism and antagonism dose-response data for AIP-II based analogs in *S. epidermidis* AH2673 (group-II). Potency values in nanomolar, CI = confidence interval.

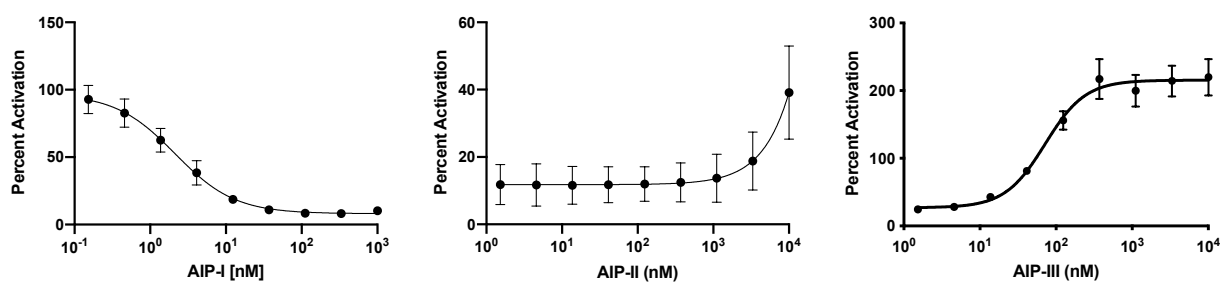
Peptide	Sequence	IC ₅₀	EC ₅₀	95% CI	Min Activity [%]	Max Activity [%]
AIP-I	D-S-V-(C-A-S-Y-F)	13.9	-	10.1 - 19.2	28.1	-
AIP-II	N-A-S-K-Y-N-P-(C-S-N-Y-L)	-	226	81.5 - 2360	-	421
AIP-III	N-A-A-K-Y-N-P-(C-A-S-Y-L)	-	648	303 - 2410	-	182
AIP-II N1A	A-A-S-K-Y-N-P-(C-S-N-Y-L)	-	597	372 - 1020	-	666
AIP-II S3A	N-A-A-K-Y-N-P-(C-S-N-Y-L)	-	523	276 - 1220	-	916
AIP-II K4A	N-A-S-A-Y-N-P-(C-S-N-Y-L)	-	>2000	-	-	198
AIP-II Y5A	N-A-S-K-A-N-P-(C-S-N-Y-L)	1300	-	605 - 2760	32.7	-
AIP-II N6A	N-A-S-K-Y-A-P-(C-S-N-Y-L)	557	-	302 - 887	25.5	-
AIP-II P7A	N-A-S-K-Y-N-A-(C-S-N-Y-L)	547	-	232 - 1070	30.4	-
AIP-II S9A	N-A-S-K-Y-N-P-(C-A-N-Y-L)	-	>2000	-	-	196
AIP-II N10A	N-A-S-K-Y-N-P-(C-S-A-Y-L)	-	>2000	-	-	249
AIP-II Y11A	N-A-S-K-Y-N-P-(C-S-N-A-L)	Inactive ^a		-	-	-
AIP-II L12A	N-A-S-K-Y-N-P-(C-S-N-Y-A)	Inactive ^a		-	-	-
AIP-II D-N1	DN-A-S-K-Y-N-P-(C-S-N-Y-L)	-	422	202 - 1710	-	420
AIP-II D-A2	N-DA-S-K-Y-N-P-(C-S-N-Y-L)	-	554	232 - 44000	-	405
AIP-II D-S3	N-A-dS-K-Y-N-P-(C-S-N-Y-L)	-	433	200 - 1290	-	427
AIP-II D-K4	N-A-S-dK-Y-N-P-(C-S-N-Y-L)	-	>2000	-	-	207
AIP-II D-Y5	N-A-S-K-dY-N-P-(C-S-N-Y-L)	379	-	271 - 543	43.3	-
AIP-II D-N6	N-A-S-K-Y-dN-P-(C-S-N-Y-L)	>2000	-	-	22.1	-
AIP-II D-P7	N-A-S-K-Y-N-dP-(C-S-N-Y-L)	Inactive ^a		-	-	-
AIP-II D-C8	N-A-S-K-Y-N-P-(dC-S-N-Y-L)	Inactive ^a		-	-	-
AIP-II D-S9	N-A-S-K-Y-N-P-(C-dS-N-Y-L)	Inactive ^a		-	-	-
AIP-II D-N10	N-A-S-K-Y-N-P-(C-S-dN-Y-L)	Inactive ^a		-	-	-
AIP-II D-Y11	N-A-S-K-Y-N-P-(C-S-N-dY-L)	Inactive ^a		-	-	-
AIP-II D-L12	N-A-S-K-Y-N-P-(C-S-N-Y-dL)	-	n/c ^b	-	-	149
AIP-II 13aa	G-N-A-S-K-Y-N-P-(C-S-N-Y-L)	-	451	257 - 1090	-	840
AIP-II 11aa	A-S-K-Y-N-P-(C-S-N-Y-L)	-	292	163 - 605	-	787
AIP-II 10aa	S-K-Y-N-P-(C-S-N-Y-L)	-	183	141 - 235	-	451
AIP-II 9aa	K-Y-N-P-(C-S-N-Y-L)	-	83.5	23.3 - 206	-	679
AIP-II 8aa	Y-N-P-(C-S-N-Y-L)	135	-	66.0 - 260	12.6	-
AIP-II 7aa	N-P-(C-S-N-Y-L)	52.4	-	29.0 - 81.5	11.3	-
AIP-II 6aa	P-(C-S-N-Y-L)	664	-	354 - 2480	13.9	-
tAIP-II	Ac-(C-S-N-Y-L)	133	-	84.4 - 212	11.2	-

^aNo activity observed over concentration range. ^bDose-response analysis did not converge.

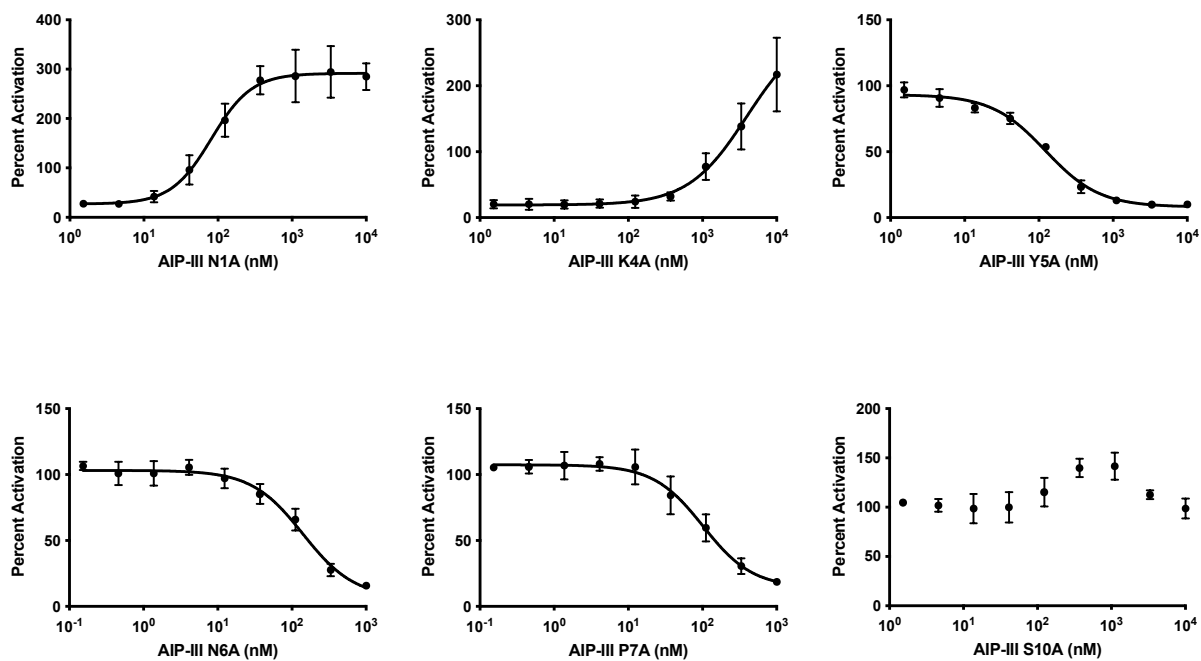
Dose-response curves for AIP-III based alanine, D-amino acid, and varied tail length analogs

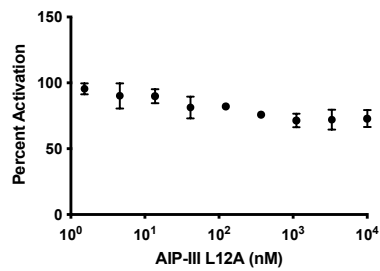
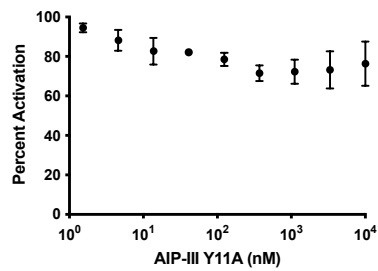
All compounds assayed in *S. epidermidis* AH3409 (group-III). Compound names are indicated on the X-axis on each curve plot. Error bars represent SEM of three biological replicates. Percent activation was normalized to a DMSO control.

- **Control peptides (native AIPs I-III)**

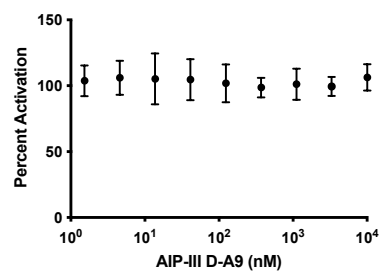
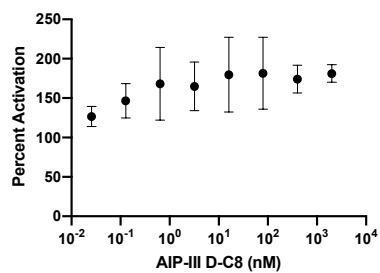
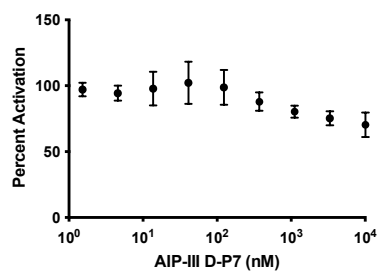
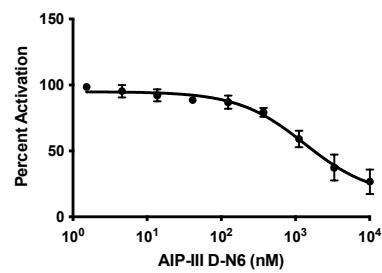
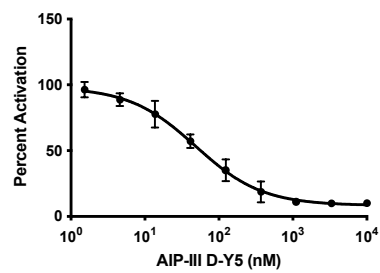
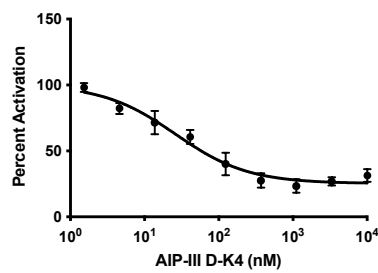
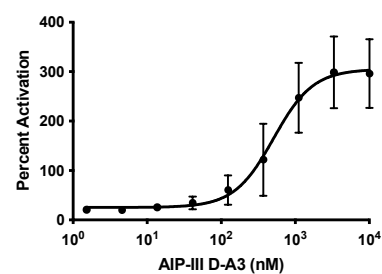
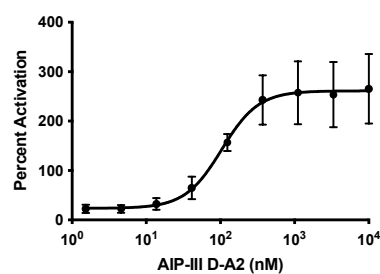
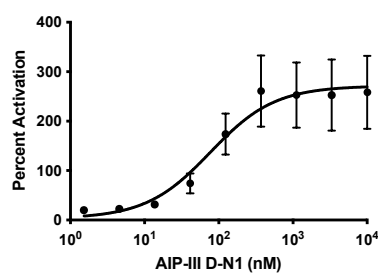


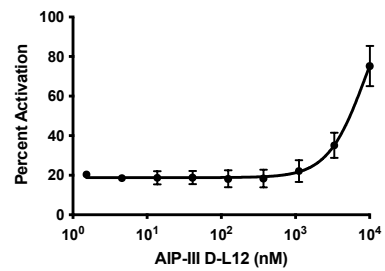
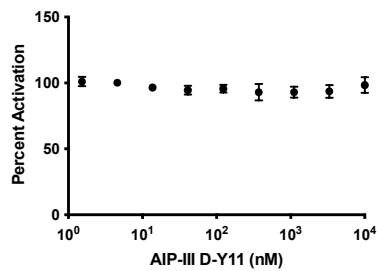
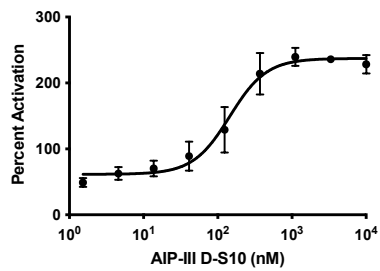
- **Alanine analogs**





• D-Amino acid analogs





- Tail truncated analogs

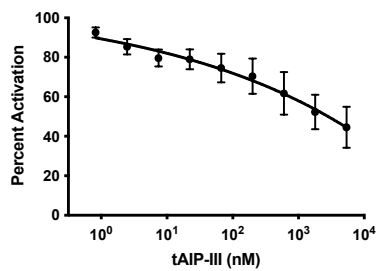
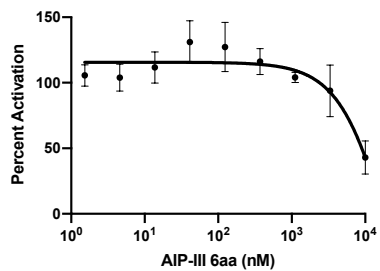
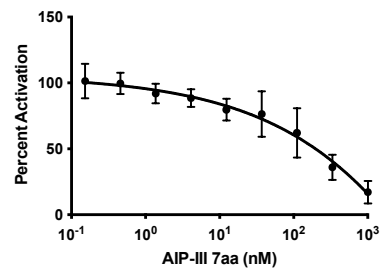
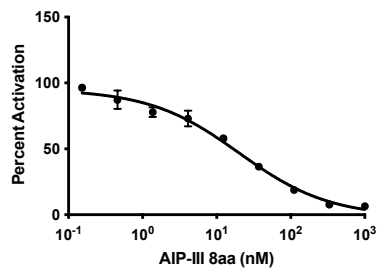
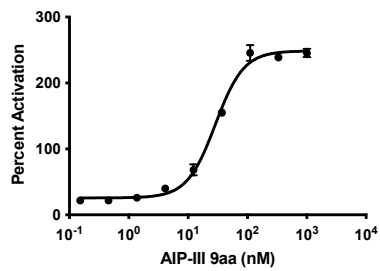
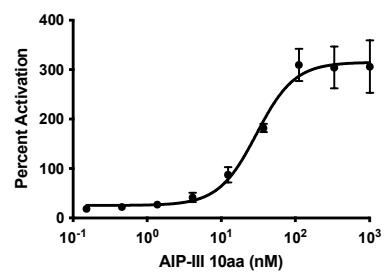
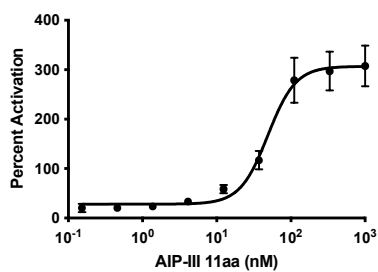
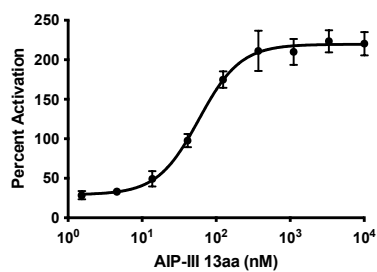


Table 4.S2 Summary of agonism and antagonism dose-response data for AIP-III based analogs in *S. epidermidis* AH3409 (group-III). Potency values in nanomolar, CI = confidence interval.

Peptide Name	Sequence	IC ₅₀ [nM]	EC ₅₀ [nM]	95% CI [nM]	Minimum Activity [%]	Maximum Activity [%]
AIP-I	D-S-V-(C-A-S-Y-F)	2.13	-	1.33 - 2.99	8.11	-
AIP-II	N-A-S-K-Y-N-P-(C-S-N-Y-L)	-	n/c ^b	-	-	39.1
AIP-III	N-A-A-K-Y-N-P-(C-A-S-Y-L)	-	71.8	53.1 - 95.4	-	220
AIP-III N1A	A-A-A-K-Y-N-P-(C-A-S-Y-L)	-	81.5	57.2 - 114	-	294
AIP-III K4A	N-A-A-A-Y-N-P-(C-A-S-Y-L)	-	>2000	-	-	217
AIP-III Y5A	N-A-A-K-A-N-P-(C-A-S-Y-L)	123	-	99.0 - 151	9.92	-
AIP-III N6A	N-A-A-K-Y-A-P-(C-A-S-Y-L)	141	-	101 - 250	15.8	-
AIP-III P7A	N-A-A-K-Y-N-A-(C-A-S-Y-L)	102	-	69.3 - 180	18.7	-
AIP-III S10A	N-A-A-K-Y-N-P-(C-A-A-Y-L)	Inactive ^a		-	-	-
AIP-III Y11A	N-A-A-K-Y-N-P-(C-A-S-A-L)	Inactive ^a		-	-	-
AIP-III L12A	N-A-A-K-Y-N-P-(C-A-S-Y-A)	Inactive ^a		-	-	-
AIP-III D-N1	DN-A-A-K-Y-N-P-(C-A-S-Y-L)	-	77.1	36.8 - 160	-	261
AIP-III D-A2	N-DA-A-K-Y-N-P-(C-A-S-Y-L)	-	104	62.8 - 167	-	265
AIP-III D-A3	N-A-DA-K-Y-N-P-(C-A-S-Y-L)	-	510	306 - 926	-	299
AIP-III D-K4	N-A-A-DK-Y-N-P-(C-A-S-Y-L)	26.1	-	7.05 - 48.5	23.3	-
AIP-III D-Y5	N-A-A-K-DY-N-P-(C-A-S-Y-L)	48.6	-	33.3 - 66.7	9.97	-
AIP-III D-N6	N-A-A-K-Y-DN-P-(C-A-S-Y-L)	1330	-	808 - 7790	26.7	-
AIP-III D-P7	N-A-A-K-Y-N-DP-(C-A-S-Y-L)	Inactive ^a		-	-	-
AIP-III D-C8	N-A-A-K-Y-N-P-(DC-A-S-Y-L)	Inactive ^a		-	-	-
AIP-III D-A9	N-A-A-K-Y-N-P-(C-DA-S-Y-L)	Inactive ^a		-	-	-
AIP-III D-S10	N-A-A-K-Y-N-P-(C-A-DS-Y-L)	-	145	103 - 197	-	240
AIP-III D-Y11	N-A-A-K-Y-N-P-(C-A-S-DY-L)	Inactive ^a		-	-	-
AIP-III D-L12	N-A-A-K-Y-N-P-(C-A-S-Y-DL)	-	>2000	-	-	75.3
AIP-III 13aa	G-N-A-A-K-Y-N-P-(C-A-S-Y-L)	-	58.4	47.1 - 72.0	-	224
AIP-III 11aa	A-A-K-Y-N-P-(C-A-S-Y-L)	-	49.0	39.8 - 61.0	-	308
AIP-III 10aa	A-K-Y-N-P-(C-A-S-Y-L)	-	29.9	22.5 - 38.9	-	310
AIP-III 9aa	K-Y-N-P-(C-A-S-Y-L)	-	28.9	25.7 - 32.3	-	246
AIP-III 8aa	Y-N-P-(C-A-S-Y-L)	20.2	-	14.3 - 29.2	6.48	-
AIP-III 7aa	N-P-(C-A-S-Y-L)	n/c ^b	-	-	17.2	-
AIP-III 6aa	P-(C-A-S-Y-L)	>2000	-	-	43.0	-
tAIP-III	Ac-(C-A-S-Y-L)	n/c ^b	-	-	44.5	-

^aNo activity observed over concentration range. ^bDose-response analysis did not converge.

4.4.3 Chimeric peptide scaffolds and activity data

Discussion of additional peptide scaffolds explored for multi-group agr agonism

In addition to the three chimeric peptide scaffolds we discuss in the main text (Cmr1, Cmr2, and Cmr3), we also explored the multi-group agonistic activity of a few other scaffolds in the *S. epidermidis* reporter strains. As the reverse of Cmr1, which incorporates the macrocycle of AIP-I and the four tail residues of both AIP-II and AIP-III, we made peptides that incorporate the macrocycles of either AIP-II or AIP-III with the three tail residues of AIP-I (aptly named “I tail, II ring” and “I tail, III ring”, respectively). However, it was clear that scaffolds based on the AIP-I tail would not be suitable for multi-group activity, as neither of these analogs had any observable agonism activity in the group-II or group-III reporter assays. This result does reinforce the SARs noted in the main text about multiple residues in the AIP-II and AIP-III tail contributing to activation, and since no residues are shared between AIP-I and AIP-II/AIP-III in the exocyclic tail, it follows that no activation occurs. In fact, these two scaffolds either partially or fully inhibited the two groups, and thus both “I tail, II ring” and “I tail, III ring” scaffolds were not further investigated.

The remaining scaffold that we examined was the AIP-II 9aa scaffold. Given that this compound was already known to be a potent inhibitor of group-I, a potent group-II activator, and also had small but significant agonism activity in group-III reporters,⁴² we were curious if substitution of certain residues to make the scaffold more similar to AIP-I could mode-switch the peptide into an agonist of group-I, thereby producing a multi-group agonist. However, substitutions to mimic the critical valine residue in AIP-I were unsuccessful in producing strong agonists against the three *agr* groups. That said,

substitution of the final endocyclic residue Leu9 to a phenylalanine improved efficacy against group-III substantially. In light of heightened activities observed in our other scaffolds, we decided to pursue those over the AIP-II 9aa scaffold.

Single-point screening data for chimeric peptides.

We screened each of the chimeric compounds at 10 μ M in the *S. epidermidis* group-I–III reporter strains for both agonism and antagonism activity. For the agonism screens, a 25 nM AAA antagonist control was used to ensure normal inhibition for each replicate. Error bars represent SEM of three biological replicates. See main text for details of strains and assay protocols.

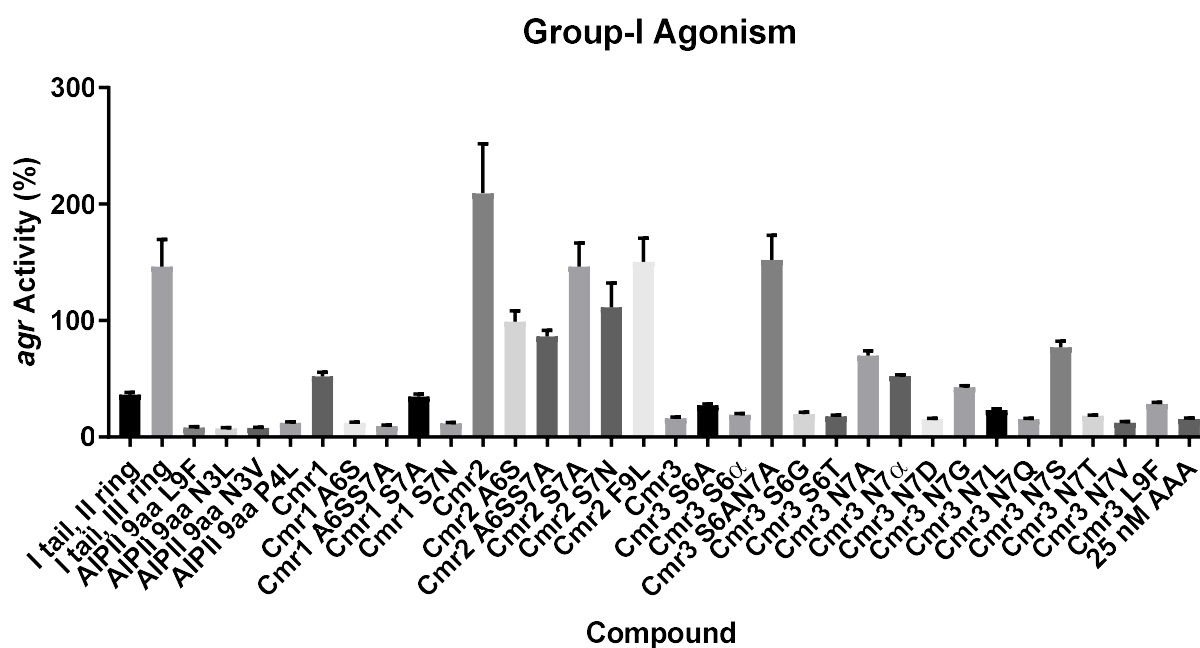


Figure 4.S1 *S. epidermidis* group-I agonism screen of chimeric peptides.

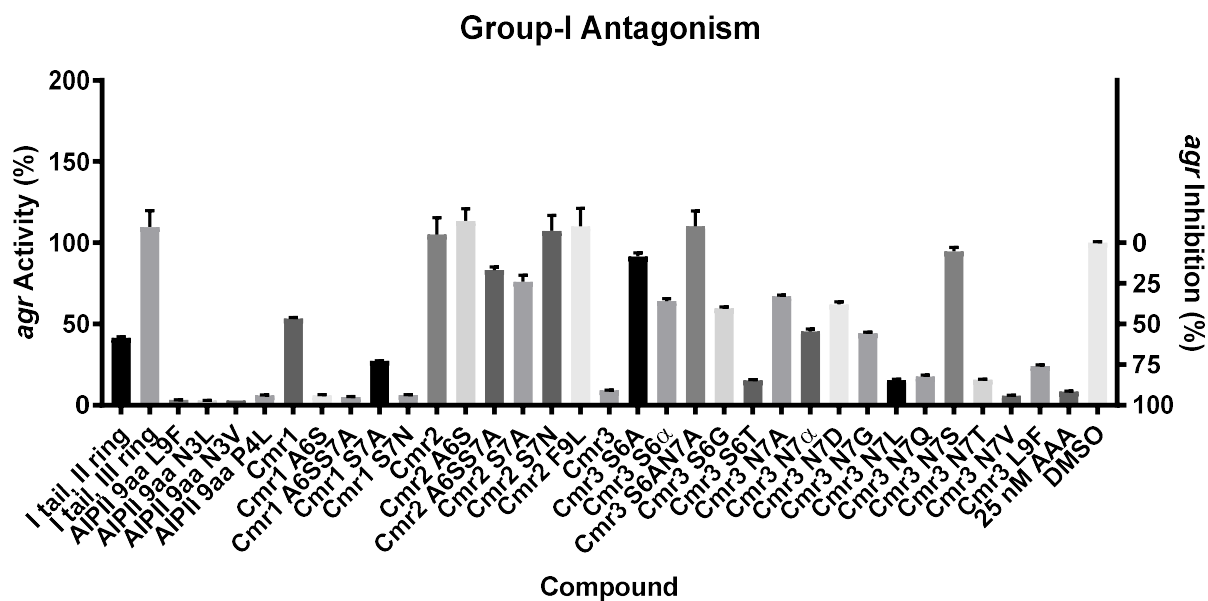


Figure 4.S2 *S. epidermidis* group-I antagonism screen of chimeric peptides.

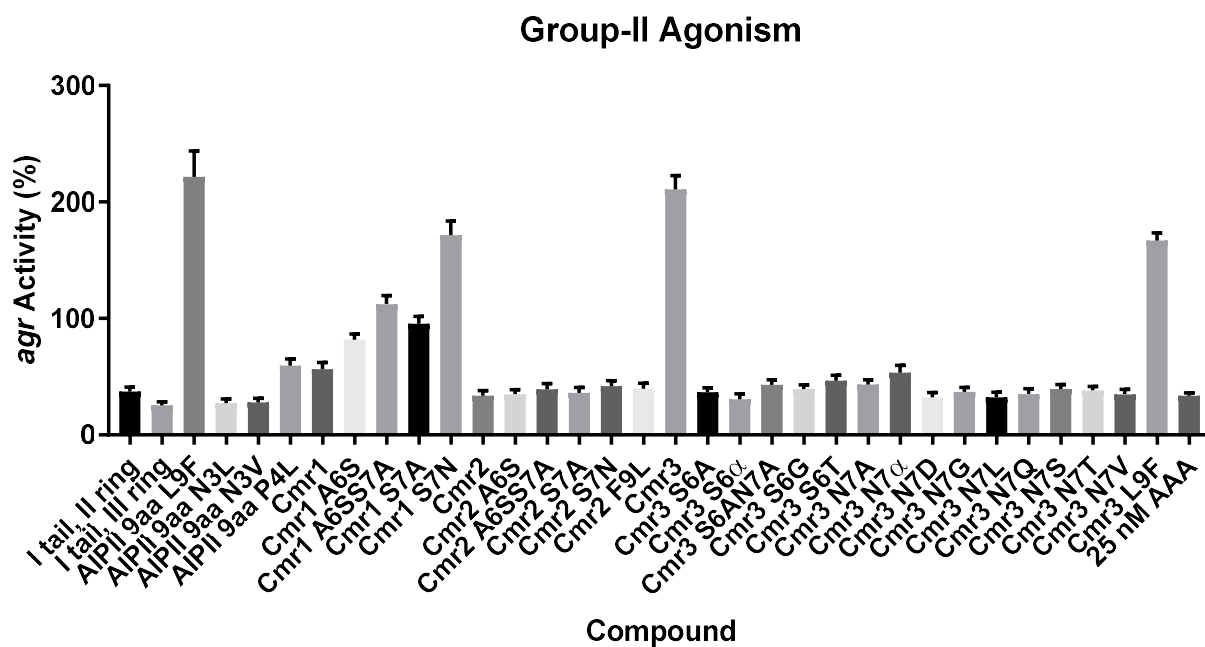


Figure 4.S3 *S. epidermidis* group-II agonism screen of chimeric peptides.

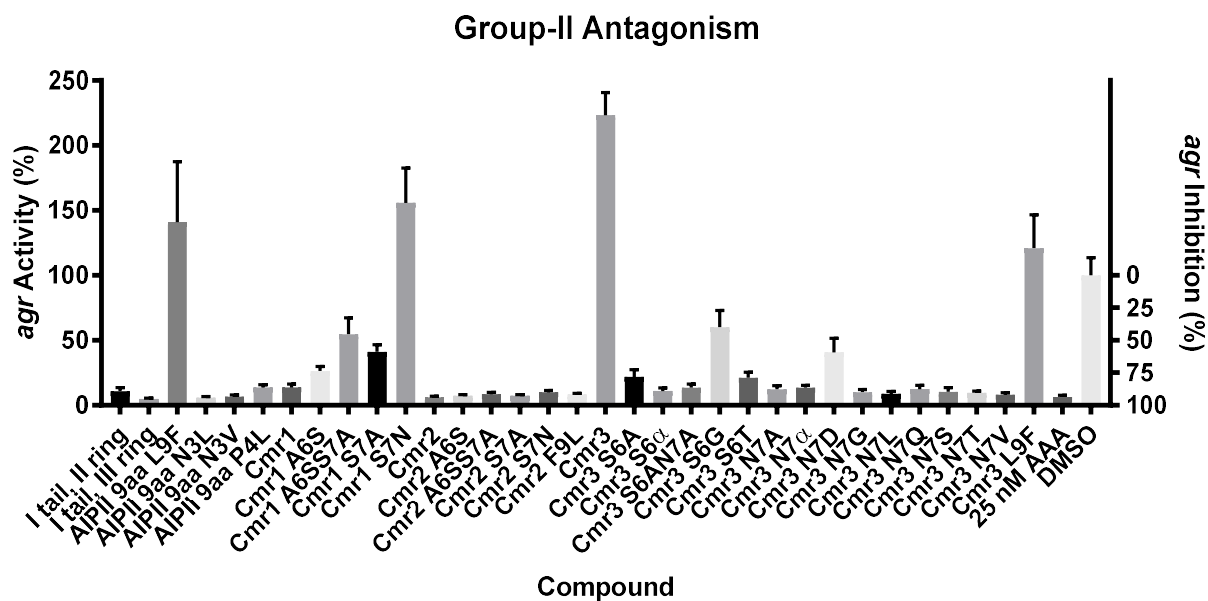


Figure 4.S4 *S. epidermidis* group-II antagonism screen of chimeric peptides.

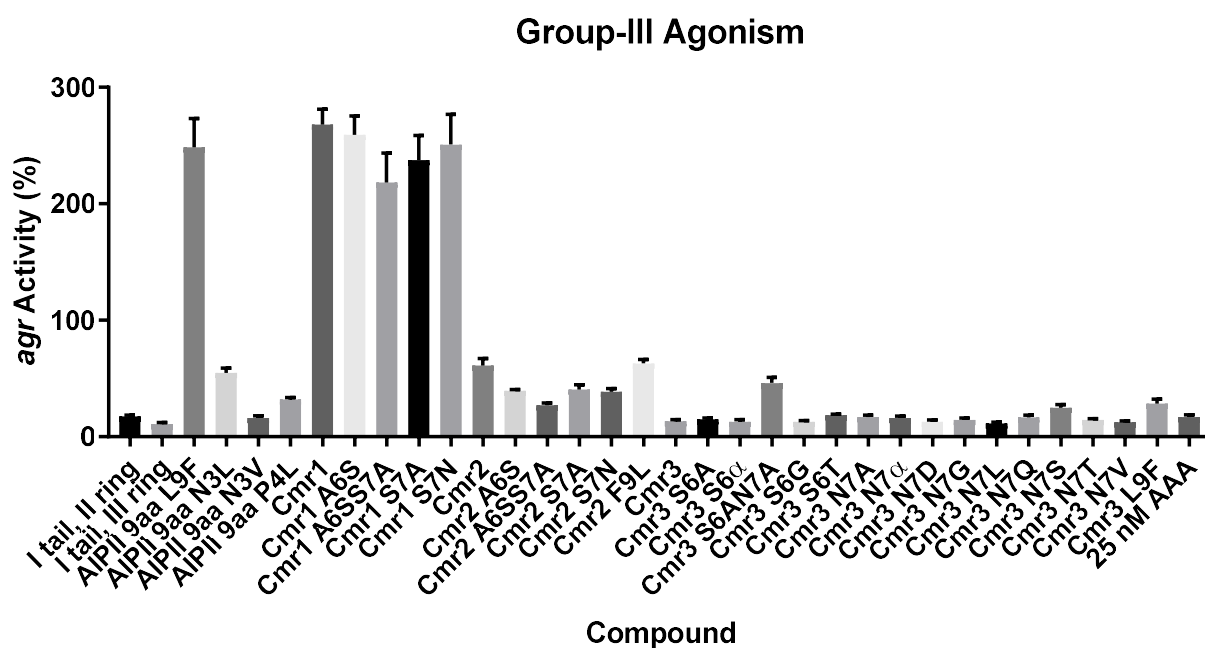


Figure 4.S5 *S. epidermidis* group-III agonism screen of chimeric peptides.

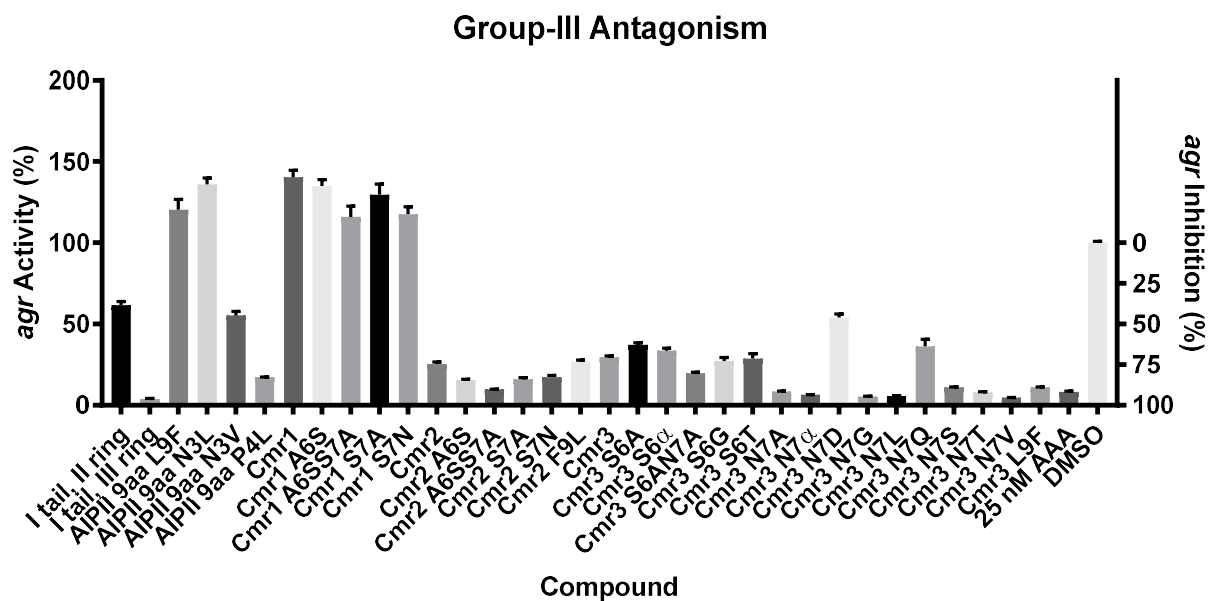


Figure 4.S6 *S. epidermidis* group-III antagonism screen of chimeric peptides.

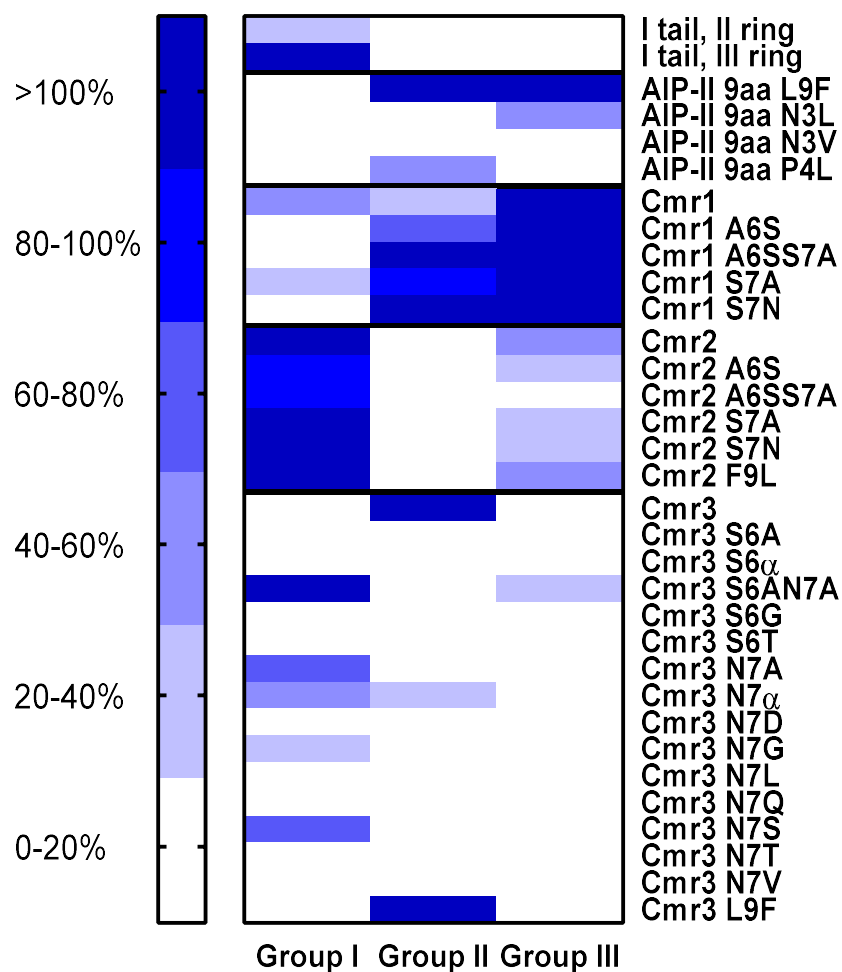


Figure 4.S7 Summary heatmap of single-point agonism activity of chimeric analogs in groups-I-III. Each chimeric analog was screened for agonism in each of the three AgrC receptors at 10 μ M. Data was normalized to the vehicle control (100% activity) and AAA inhibition control (0% activity).

Table 4.S3 Summary of agonism dose-response data for select non-chimera peptides. Bolded peptides are the native AIPs. CI = confidence interval for EC₅₀ value. See main text for details of strains and assay protocols.

Compound	Activation				Group-I		Group-II		Group-III		
	Maximum activity [%]	EC ₅₀ [nM]	95% CI [nM]	Maximum activity [%]	EC ₅₀ [nM]	95% CI [nM]	Maximum activity [%]	EC ₅₀ [nM]	95% CI [nM]		
AIP-I	147	170	89.4 - 400.	-	-	-	-	-	-	-	
AIP-II	-	-	-	421	226	81.5 - 2360	39.1	n/c ^b	-	-	
AIP-III	-	-	-	182	648	303 - 2410	220	71.8	53.1 - 95.4	-	
AIP-I tail: AIP-II ring	-	-	-	-	-	-	-	Inactive ^a	-	-	
AIP-I tail: AIP-III ring	129	1870	1070 - 10700	-	-	-	-	-	-	-	
AIP-II 9aa	-	-	-	679	83.5	23.3-206	25.2	>2000	-	-	
AIP-II 9aa N3L	-	-	-	-	-	-	-	Inactive ^a	-	-	
AIP-II 9aa N3V	-	-	-	-	-	-	-	Inactive ^a	-	-	
AIP-II 9aa P4L	-	-	-	72.6	630	NA	-	-	-	-	
AIP-II 9aa L9F	-	-	-	889	203	100 - 469	469	>2000	-	-	

^aDose-response curves revealed neither agonism nor antagonism activities over the concentration range tested. ^bDose-response analysis did not converge over concentration range tested. NA: Curve did not plateau on one side and Prism did not calculate the 95% CI.

Table 4.S4 Summary of agonism dose-response data for select Cmr1 peptides. Bolded peptides are the native ALPs. CI = confidence interval for EC₅₀ value. See main text for details of strains and assay protocols.

Compound	Activation								
	Group-I		Group-II		Group-III				
	Maximum activity [%]	EC ₅₀ [nM]	95% CI [nM]	Maximum activity [%]	EC ₅₀ [nM]	95% CI [nM]			
Cmr1	51.1	>2000	-	60.4	61.3	NA	223	0.929	0.732 - 1.16
Cmr1 A6S	-	-	-	86.8	>2000	-	201	13.6	8.21 - 18.5
Cmr1 A6SS7A	-	-	-	185	245	147 - 495	215	13.4	7.97 - 18.3
Cmr1 S7A	38.4	844	677 - 1260	136	63.7	16.0 - 150.	398	1.47	1.21 - 1.83
Cmr1 S7N	-	-	-	378	>2000	-	484	>2000	-

^aDose-response curves revealed neither agonism nor antagonism activities over the concentration range tested. ^bDose-response analysis did not converge over concentration range tested. NA: Curve did not plateau on one side and Prism did not calculate the 95% CI.

Table 4.S5 Summary of agonism dose-response data for select Cmr2 peptides. Bolded peptides are the native ALPs. CI = confidence interval for EC₅₀ value. See main text for details of strains and assay protocols.

Compound	Activation								
	Group-I		Group-II		Group-III				
	Maximum activity [%]	EC ₅₀ [nM]	95% CI [nM]	Maximum activity [%]	EC ₅₀ [nM]	95% CI [nM]	Maximum activity [%]	EC ₅₀ [nM]	95% CI [nM]
Cmr2	146	71.8	40.1 - 121	-	-	-	46.8	40.6	NA
Cmr2 A6S	116	796	508 - 1810	-	-	-	-	-	-
Cmr2 A6SS7A	92.6	169	119 - 252	-	-	-	-	-	-
Cmr2 57A	157	12.4	NA	-	-	-	40.8	n/c ^b	-
Cmr2 57N	156	656	464 - 1070	-	-	-	-	-	-
Cmr2 F9L	140	1020	658 - 2400	-	-	-	54.1	>2000	-

^aDose-response curves revealed neither agonism nor antagonism activities over the concentration range tested. ^bDose-response analysis did not converge over concentration range tested. NA: Curve did not plateau on one side and Prism did not calculate the 95% CI.

Table 4.S6 Summary of agonism dose-response data for select Cmr3 peptides. Bolded peptides are the native AIPs. CI = confidence interval for EC₅₀ value. See main text for details of strains and assay protocols.

Compound	Activation			Group-II			Group-III		
	Group-I	Group-II	Group-III	Maximum activity [%]	EC ₅₀ [nM]	95% CI [nM]	Maximum activity [%]	EC ₅₀ [nM]	95% CI [nM]
Cmr3	-	-	-	290	>2000	-	-	-	-
Cmr3 S6A	-	Inactive ^a	-	63.3	>2000	-	-	-	-
Cmr3 S6AN7A	135	134	85.3 - 216	52.1	192	NA	43.33	1212	575 - 23700
Cmr3 S6G	-	-	-	43.8	n/c ^b	-	-	-	-
Cmr3 S6T	-	-	-	-	Inactive ^a	-	-	-	-
Cmr3 N7α	58.1	1640	1040 - 4310	-	-	-	-	-	-
Cmr3 N7A	66.2	1940	1080 - 9700	-	Inactive ^a	-	-	-	-
Cmr3 N7D	-	Inactive ^a	-	-	Inactive ^a	-	-	Inactive ^a	-
Cmr3 N7S	73.4	>2000	-	-	-	-	-	-	-
Cmr3 L9F	-	-	-	211	210	120 - 473	-	-	-

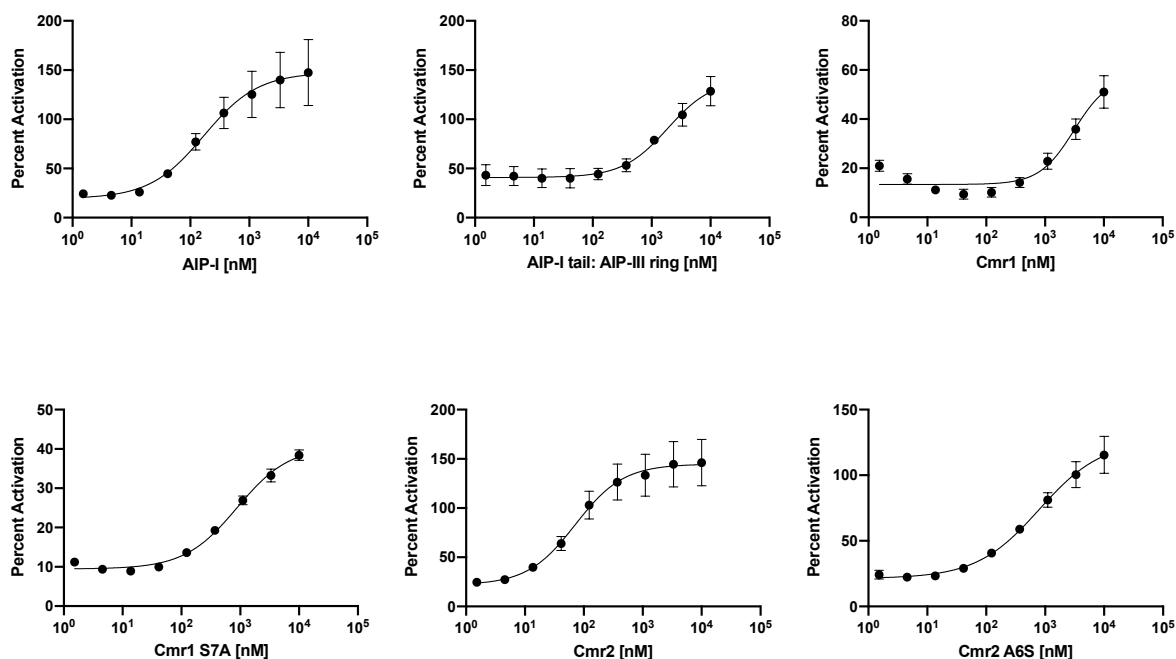
^aDose-response curves revealed neither agonism nor antagonism activities over the concentration range tested.

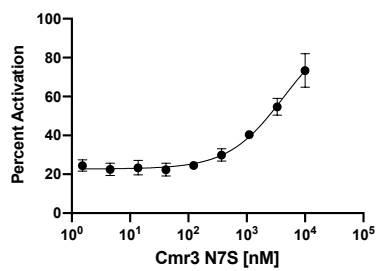
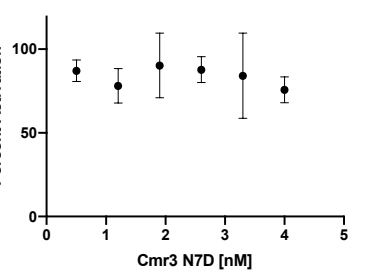
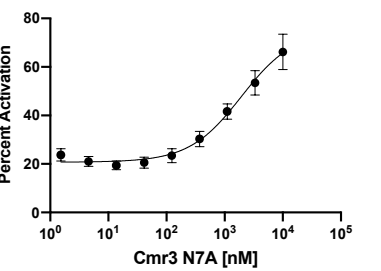
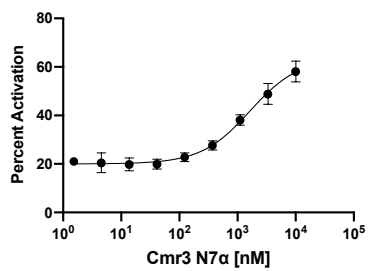
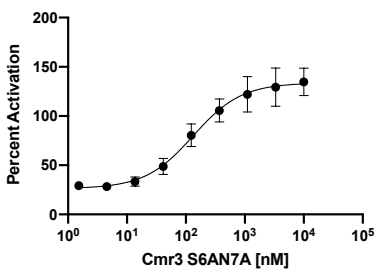
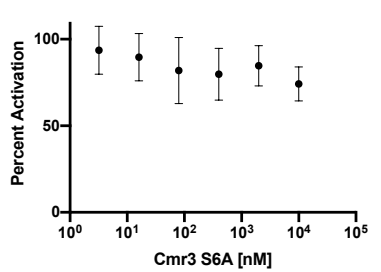
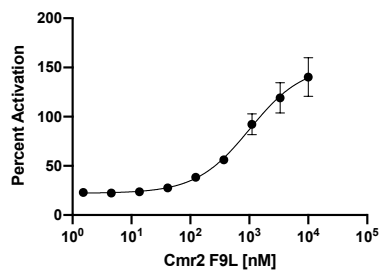
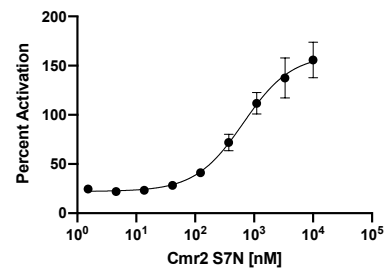
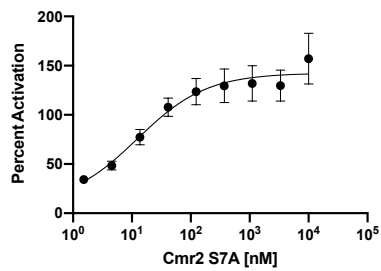
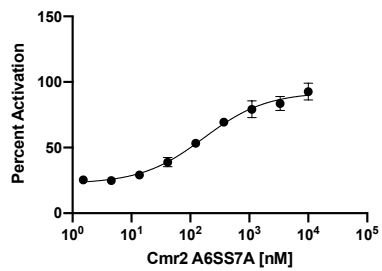
^bDose-response analysis did not converge over concentration range tested. NA: Curve did not plateau on one side and Prism did not calculate the 95% CI.

Agonism dose-response curves for select chimeric peptides.

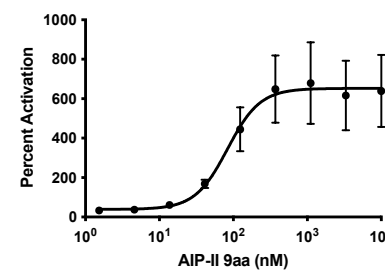
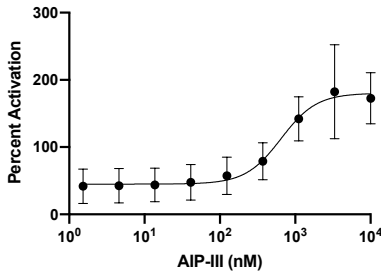
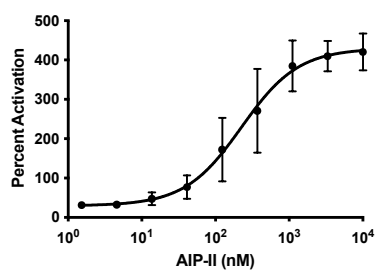
The analogs were assayed over increasing concentrations in the appropriate *S. epidermidis* fluorescence reporter strains for AgrC receptor agonism. Compound names are indicated on the X-axis on each curve plot. Error bars represent SEM of three biological replicates, except for compound Cmr3 S6A and Cmr3 N7D in AH3408, Cmr3 S6T and Cmr3 N7D in AH2673, and AIP-I tail: AIP-II ring, AIP-II 9aa N3L, AIP-II 9aa N3V, and Cmr3 N7D in AH3409, in which only biological duplicates were used. See main text for details of strains and assay protocols.

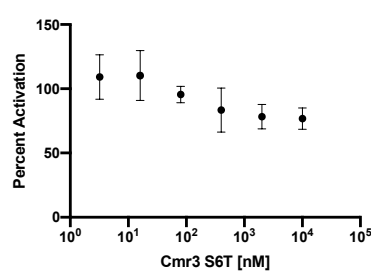
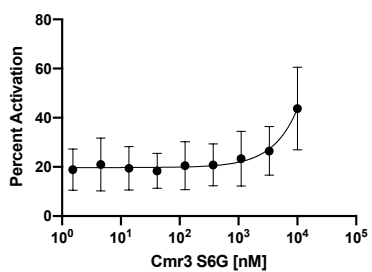
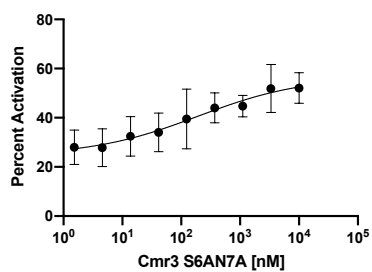
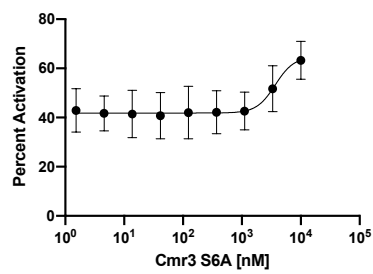
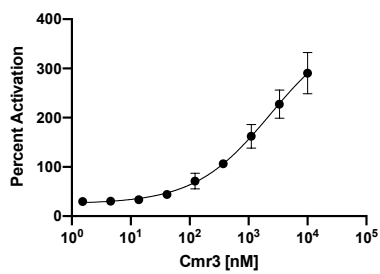
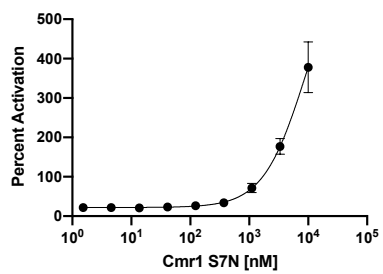
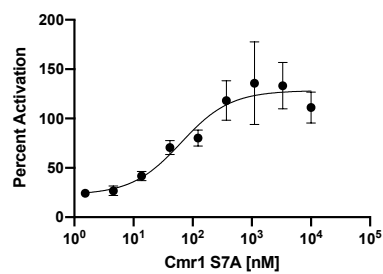
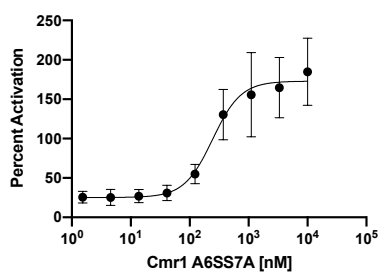
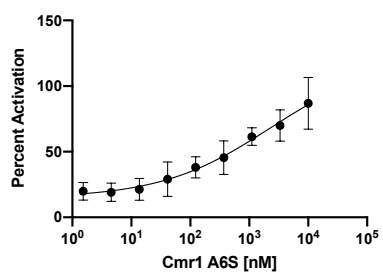
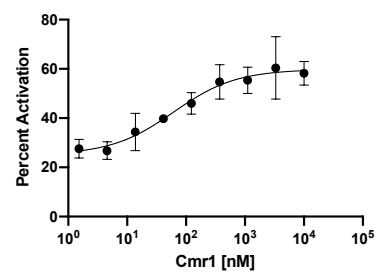
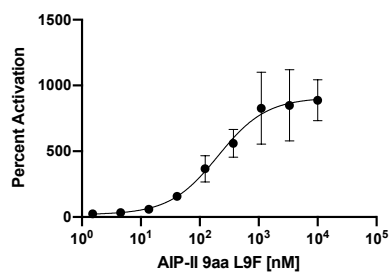
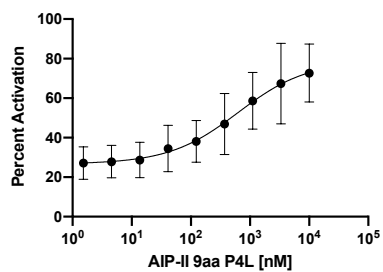
• **AH3408 (group-I)**

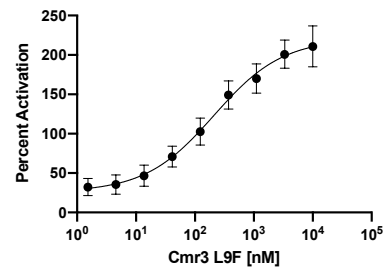
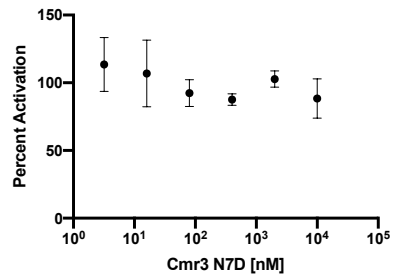
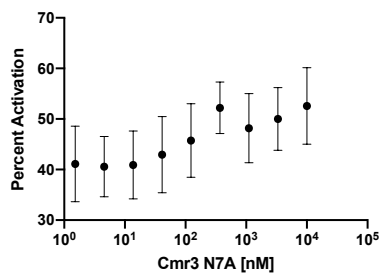




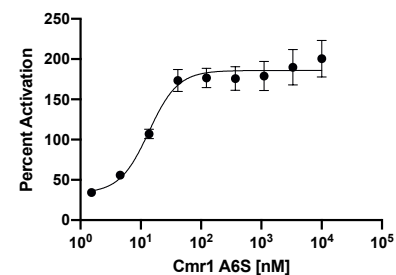
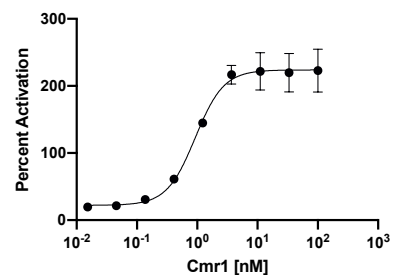
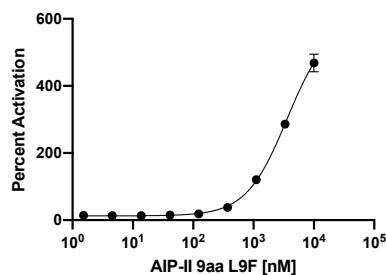
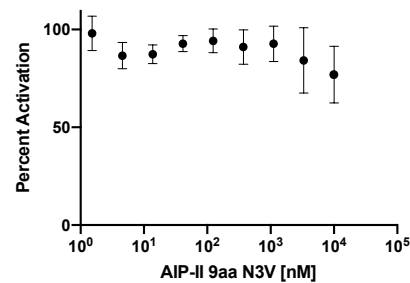
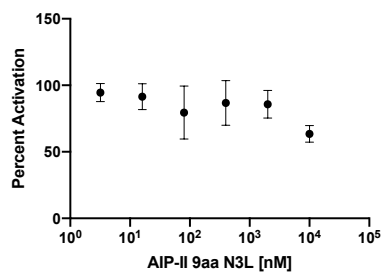
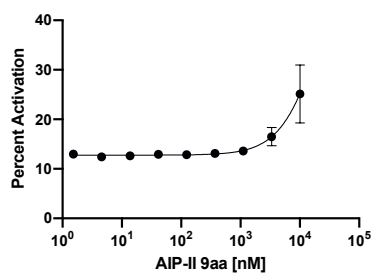
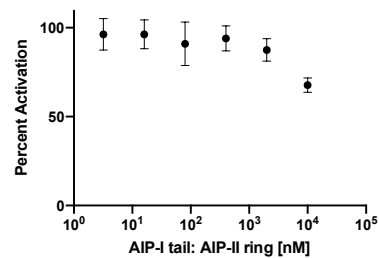
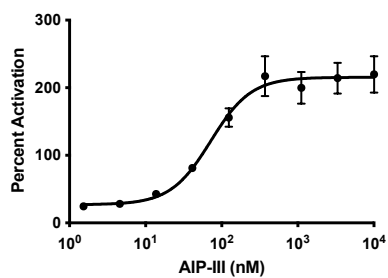
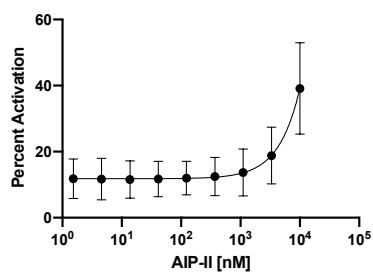
• **AH2673 (group-II)**







• **AH3409 (group-III)**



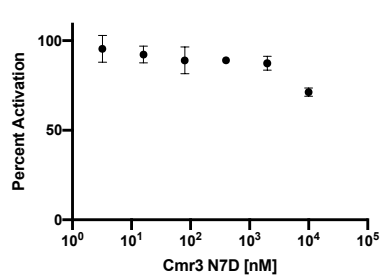
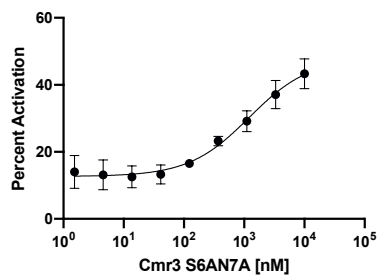
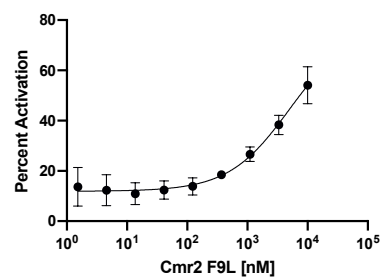
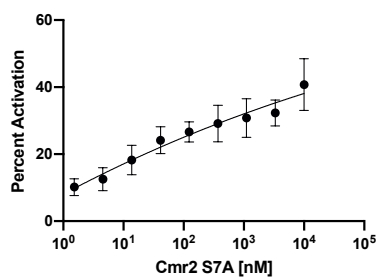
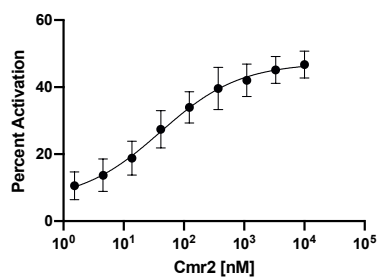
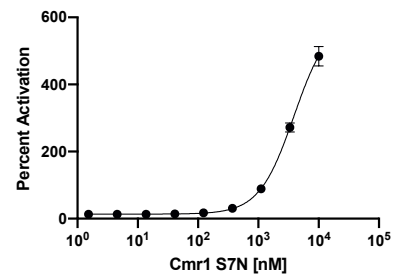
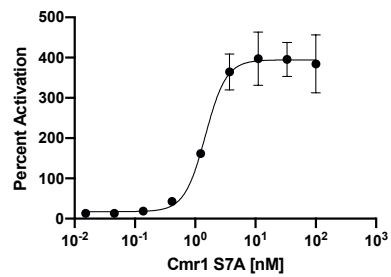
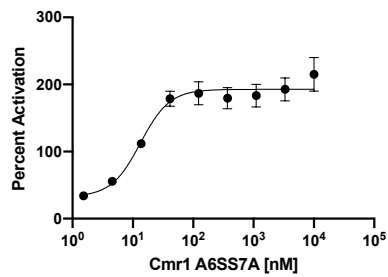


Table 4.S7 Summary of antagonism dose-response data for select non-chimera peptides. Bolded peptides are the native AIPs. CI = confidence interval for IC₅₀ values See main text for details of strains and assay protocols.

Compound	Inhibition				Group-II				Group-III			
	Group-I		Group-II		Group-III		Group-IV		Group-V		Group-VI	
	Minimum activity [%]	IC ₅₀ [nM]	95% CI [nM]	Minimum activity [%]	IC ₅₀ [nM]	95% CI [nM]	Minimum activity [%]	IC ₅₀ [nM]	95% CI [nM]	Minimum activity [%]	IC ₅₀ [nM]	95% CI [nM]
AIP-I	-	-	-	28.1	13.9	10.1 - 19.2	8.11	2.13	1.33 - 2.99	-	-	-
AIP-II	3.47	9.67	8.88 - 10.5	-	-	-	-	-	-	-	-	-
AIP-III	4.59	225	184 - 274	-	-	-	-	-	-	-	-	-
AIP-I tail: AIP-II ring	35.4	203	127 - 322	-	-	-	-	-	-	-	-	-
AIP-I tail: AIP-III ring	-	-	-	10.6	50.9	35.0 - 71.6	6.81	31.8	7.91 - 72.2	-	-	-
AIP-II 9aa	3.41	2.84	2.61 – 3.09	-	-	-	-	-	-	-	-	-
AIP-II 9aa N3L	6.46	11.3	8.66 - 14.9	21.6	219	NA	-	-	-	-	-	-
AIP-II 9aa N3V	6.14	8.49	6.51 - 11.1	25.6	320	180 - 607	-	-	-	-	-	-
AIP-II 9aa P4L	8.51	6.45	5.32 - 7.78	-	-	-	15.4	105	74.4 - 145	-	-	-
AIP-II 9aa L9F	6.28	0.470	0.419 - 0.524	-	-	-	-	-	-	-	-	-

^aDose-response curves revealed neither agonism nor antagonism activities over the concentration range tested. ^bDose-response analysis did not converge over concentration range tested. NA: Curve did not plateau on one side and Prism did not calculate the 95% CI.

Table 4.S8 Summary of antagonism dose-response data for select Cmr1 peptides. Bolded peptides are the native AIPs. CI = confidence interval for IC₅₀ value. See main text for details of strains and assay protocols.

Compound	Inhibition								
	Group-I			Group-II		Group-III			
	Minimum activity [%]	IC ₅₀ [nM]	95% CI [nM]	Minimum activity [%]	IC ₅₀ [nM]	95% CI [nM]	Minimum activity [%]	IC ₅₀ [nM]	95% CI [nM]
Cmr1 A6S	7.09	0.829	0.484 - 1.19	-	-	-	-	-	-
Cmr1 A6SS7A	6.58	0.298	0.211 - 0.389	-	-	-	-	-	-
Cmr1 S7N	9.61	16.8	10.4 - 36.7	-	-	-	-	-	-

^aDose-response curves revealed neither agonism nor antagonism activities over the concentration range tested. ^bDose-response analysis did not converge over concentration range tested. NA: Curve did not plateau on one side and Prism did not calculate the 95% CI.

Table 4.S9 Summary of antagonism dose-response data for select Cmr2 peptides. Bolded peptides are the native ALPs. CI = confidence interval for IC₅₀ value. See main text for details of strains and assay protocols.

Compound	Inhibition			Group-II			Group-III		
	Group-I	Group-II	Group-III	Minimum activity [%]	IC ₅₀ [nM]	95% CI [nM]	Minimum activity [%]	IC ₅₀ [nM]	95% CI [nM]
Cmr2	-	-	-	22.4	0.650	NA	-	-	-
Cmr2 A6S	-	-	-	11.8	3.82	2.55 - 5.75	11.2	0.763	0.593 - 0.938
Cmr2 A6SS7A	-	-	-	13.4	1.07	0.000275 - 2.25	11.9	0.495	0.411 - 0.579
Cmr2 S7A	-	-	-	25.5	0.598	NA	-	-	-
Cmr2 S7N	-	-	-	19.0	127	73.8 - 211	31.5	84.0	61.2 - 113
Cmr2 F9L	-	-	-	13.4	0.808	NA	-	-	-

^aDose-response curves revealed neither agonism nor antagonism activities over the concentration range tested. ^bDose-response analysis did not converge over concentration range tested. NA: Curve did not plateau on one side and Prism did not calculate the 95% CI.

Table 4.S10 Summary of antagonism dose-response data for select Cmr3 peptides. Bolded peptides are the native AIPs. CI = confidence interval for IC₅₀ value. See main text for details of strains and assay protocols.

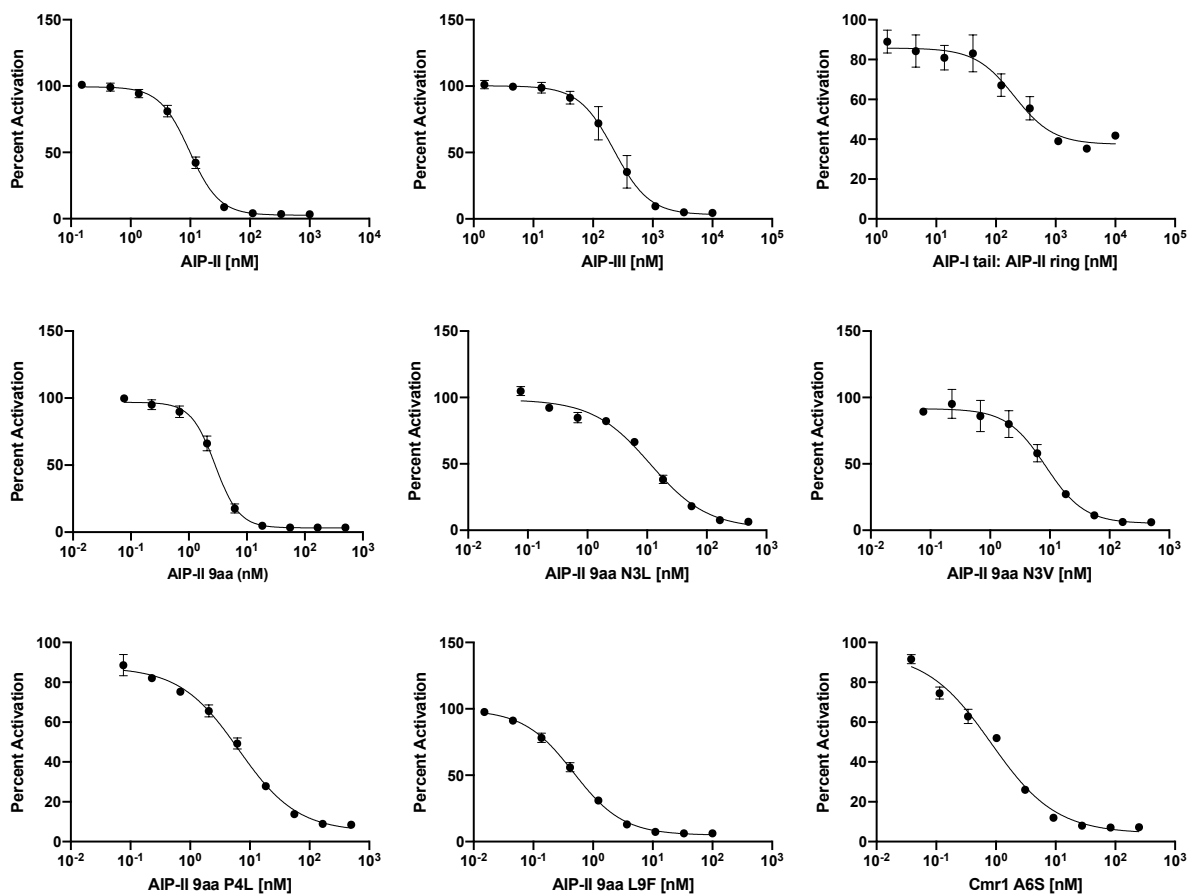
Compound	Inhibition			Group-II			Group-III		
	Group-I	Group-II	Group-III	Minimum activity [%]	IC ₅₀ [nM]	95% CI [nM]	Minimum activity [%]	IC ₅₀ [nM]	95% CI [nM]
Cmr3	13.2	75.8	55.9 - 113	-	-	-	47.4	>2000	-
Cmr3 S6α	63.5	n/c ^b	-	26.1	1420	NA	-	-	-
Cmr3 S6A	-	-	-	-	-	-	-	-	-
Cmr3 S6AN7A	-	-	-	-	-	-	-	-	-
Cmr3 S6G	-	Inactive ^a	-	-	-	-	-	-	-
Cmr3 S6T	25.8	1340	903 - 2650	-	-	-	45.8	>2000	-
Cmr3 N7α	-	-	-	40.4	11.5	0.00130 - 27.7	12.1	57.6	44.2 - 73.5
Cmr3 N7A	-	-	-	-	-	-	10.5	11.3	8.31 - 15.6
Cm3 N7D	-	-	-	-	-	-	-	-	-
Cmr3 N7G	36.6	97.1	70.0 - 131	26.9	32.3	6.63 - 64.4	9.45	45.4	34.1 - 64.6
Cmr3 N7L	16.9	24.9	19.0 - 33.1	22.3	73.8	31.8 - 139	8.27	398	318 - 512
Cmr3 N7Q	29.7	>2000	-	25.2	4870	NA	-	-	-
Cmr3 N7S	-	-	-	37.0	11.7	6.26 - 20.6	11.6	17.7	13.9 - 23.0
Cmr3 N7T	26.3	766	517 - 1570	15.8	194	109 - 363	11.6	991	803 - 1300
Cmr3 N7V	10.3	157	122 - 202	29.8	26.4	NA	8.18	323	235- 467
Cmr3 L9F	21.1	2.15	1.02 - 3.54	-	-	-	13.0	34.9	24.8 - 51.9

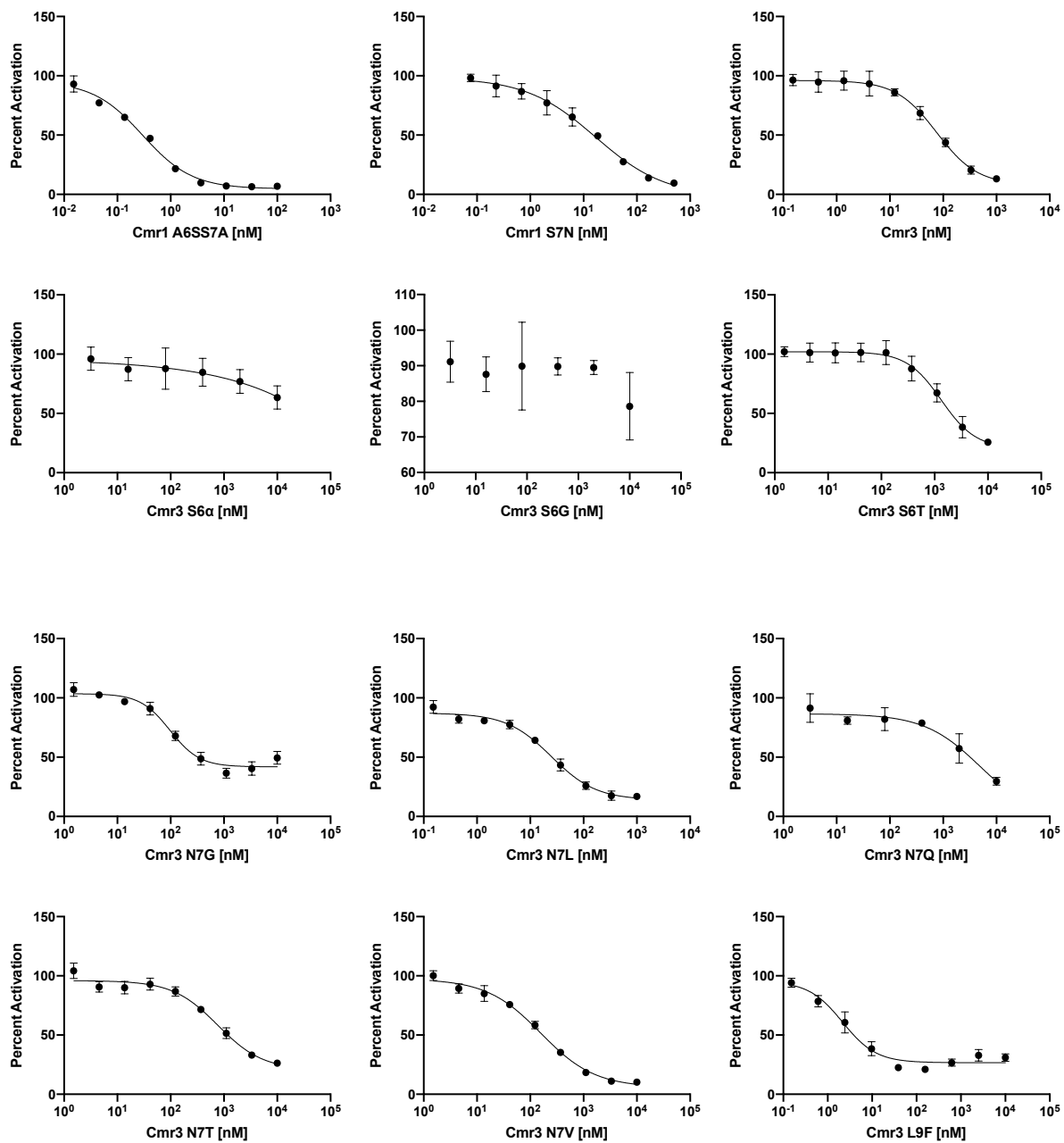
^aDose-response curves revealed neither agonism nor antagonism activities over the concentration range tested. ^bDose-response analysis did not converge over concentration range tested. NA: Curve did not plateau on one side and Prism did not calculate the 95% CI.

Antagonism dose-response curves for select chimeric peptides

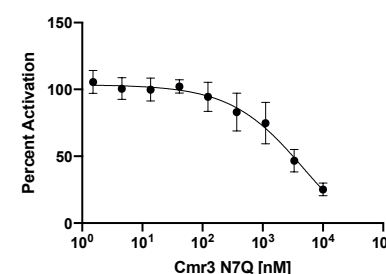
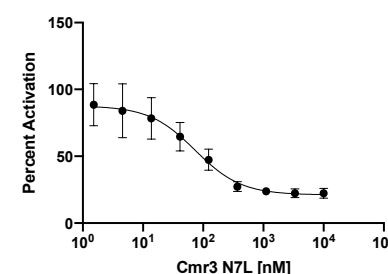
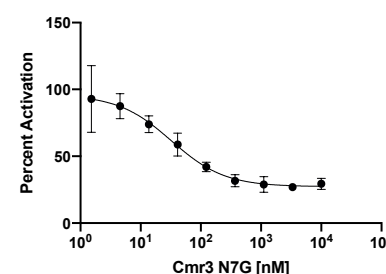
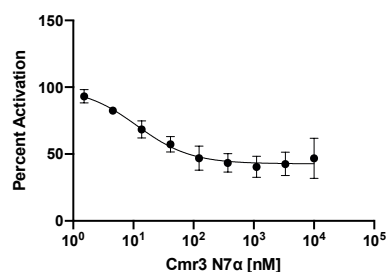
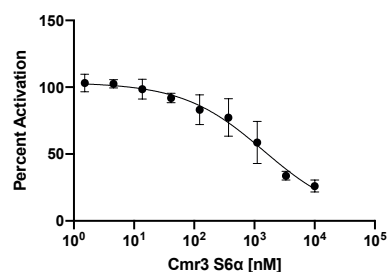
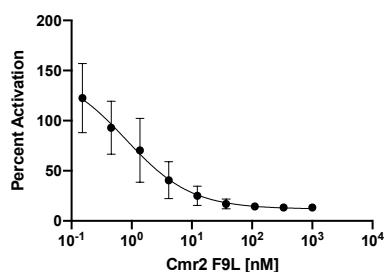
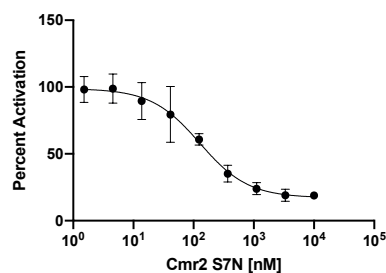
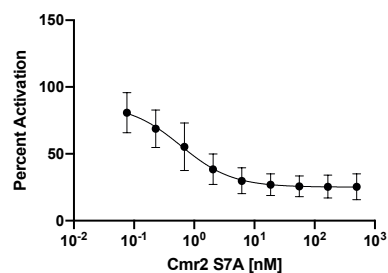
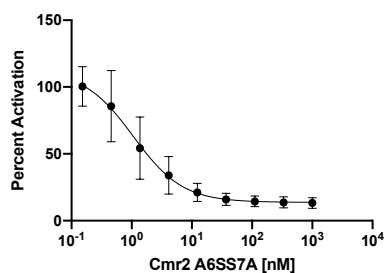
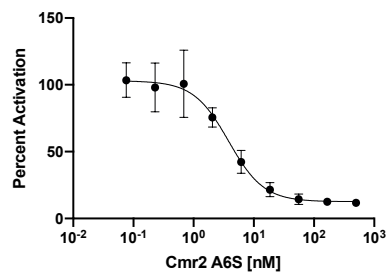
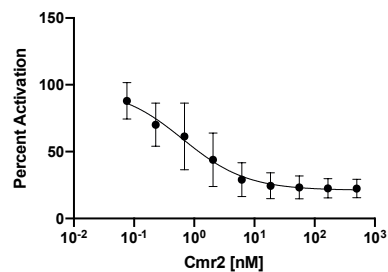
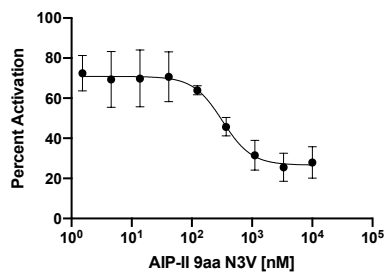
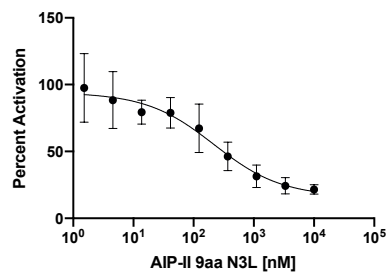
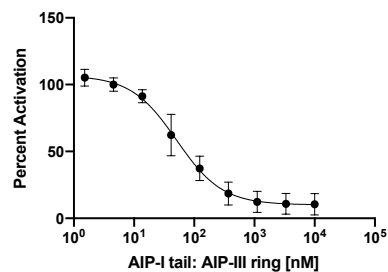
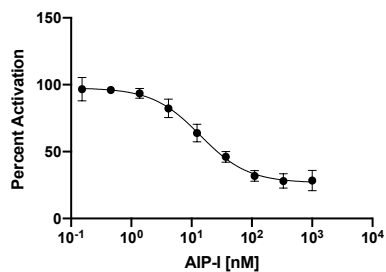
The analogs were assayed over increasing concentrations in the appropriate *S. epidermidis* fluorescence reporter strains for AgrC receptor antagonism. Compound names are indicated on the X-axis on each curve plot. Error bars represent SEM of three biological replicates, except for Cmr3 in AH3409, which uses two biological replicates. See main text for details of strains and assay protocols.

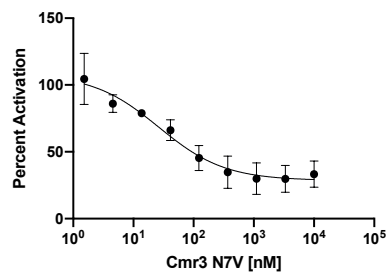
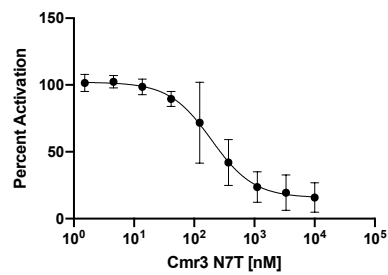
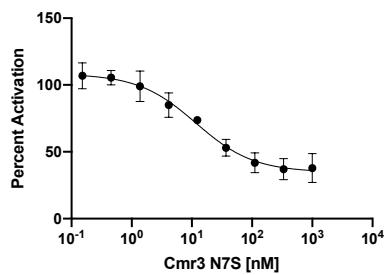
- **AH3408 (group-I)**



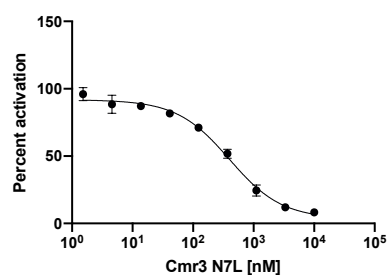
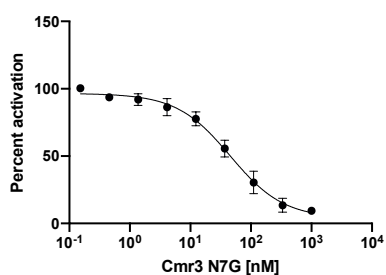
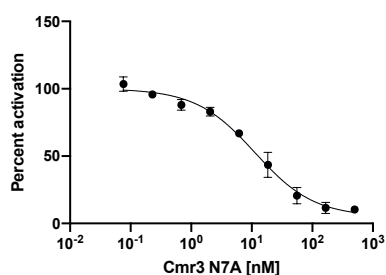
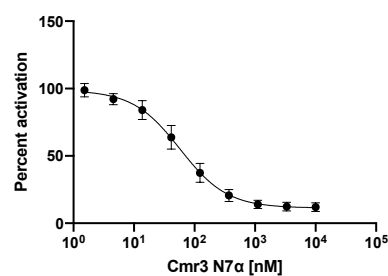
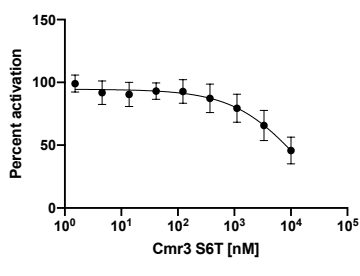
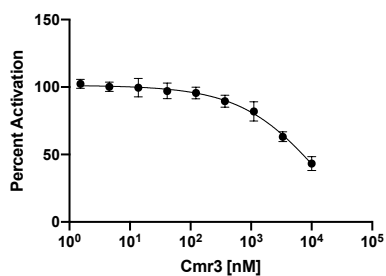
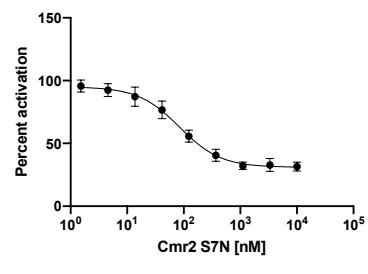
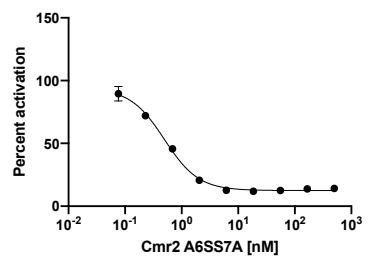
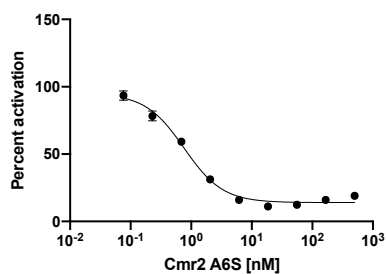
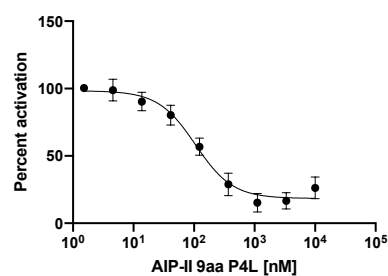
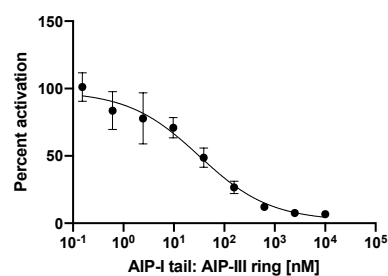
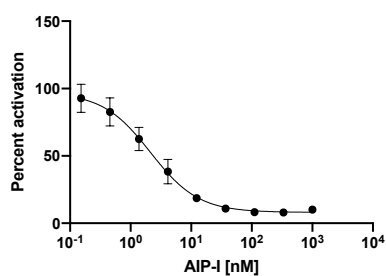


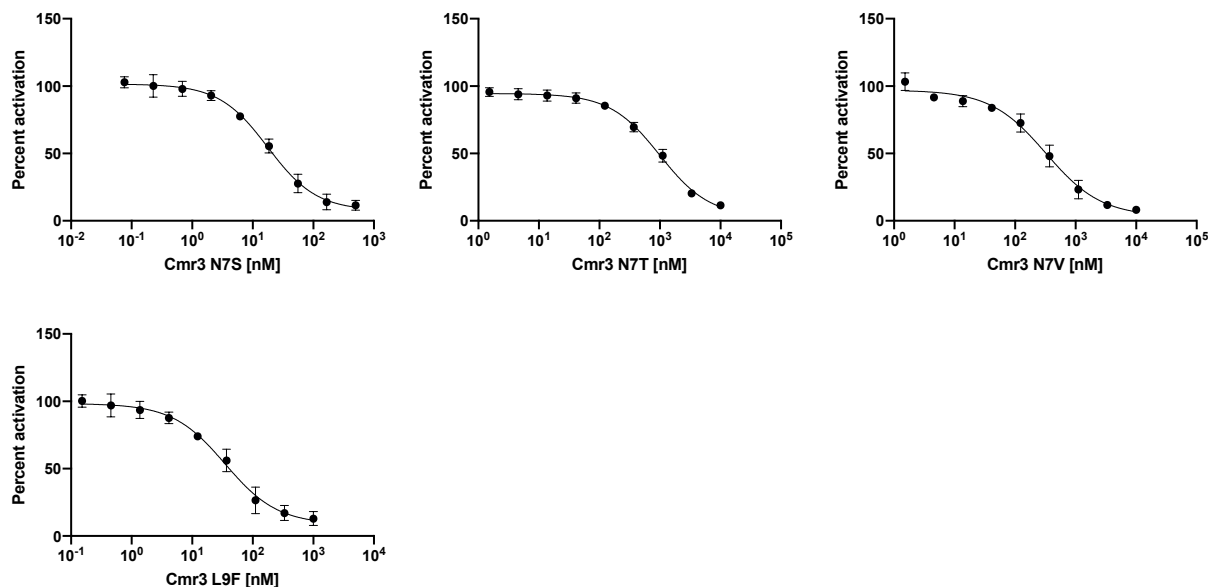
- AH2673 (group-II)





- AH3409 (group-III)**





Discussion of additional optimization of multi-group agonist scaffolds

Beginning with our first multi-group agonist Cmr1, we aimed to improve activity towards AgrC-II by focusing on substitutions at residues 6 and 7 within the macrocycle to have more “AIP-II-like” character. As expected, the more similar these analogs resembled the AIP-II macrocycle, the more active they were as AgrC-II agonists. While these analogs all maintained their agonism efficacy against AgrC-III, unfortunately many analogs lost what little activity they had towards AgrC-I. In fact, the only analog that maintained the multi-group agonism activity of Cmr1 was the analog Cmr1 S7A; while this analog had substantial gains in activity in AgrC-II and maintained AgrC-III activity, it had slightly reduced activity in AgrC-I. Given that the most active AgrC-I agonists contain an exocyclic valine and not a proline, future work should explore other substitutions at the proline position of Cmr1 to survey which side chains may better improve agonism efficacy in AgrC-I.

Turning towards the Cmr2 scaffold with strong agonistic activity in AgrC-I and low activity in AgrC-III, we sought to broaden agonism activity to include AgrC-II. As we had seen improved AgrC-II activity in Cmr1 when substituting the macrocycle to be more like AIP-II, we tried a similar approach with Cmr2. Despite the success in the Cmr1 scaffold, substitutions to the Cmr2 macrocycle failed to produce any agonists in AgrC-II . Moreover, these substitutions negatively affected agonism towards AgrC-III relative to their parent Cmr2. Lastly, all the Cmr2 analogs maintain activity in AgrC-I, which is unsurprising given that the macrocycle was originally based on AIP-I (which should optimally orient the exocyclic valine for AgrC-I activation). One interesting observation gathered from the AgrC-I screening data for the Cmr2 analogs was that substitution of the final endocyclic residue Phe9 to leucine decreased potency ten-fold. This indicates AgrC-I is not completely tolerant of any hydrophobic residue in this position for binding and could be useful for future analog design.

While Cmr3 had agonist activity in AgrC-II, we next set out to increase its activity in AgrC-I and AgrC-III by modifying the macrocycle to be either more like AIP-I or AIP-III. As we observed in our studies with Cmr2, however, the process of making substitutions to more closely resemble the macrocycle of one AIP or another did not often produce the desired results, and many were inactive against the three receptors. We also tried a series of other substitutions to more broadly explore chemical space in the macrocycle, but this strategy proved ineffective at improving multi-group activity of Cmr3 analogs as well. The most promising analog from the Cmr3 scaffold was Cmr3 S6AN7A, which gained agonism activity in AgrC-I and AgrC-III at the cost of eliminating AgrC-II activity.

4.4.4 *S. epidermidis* PSM production with multi-group agonist Cmr1 S7A

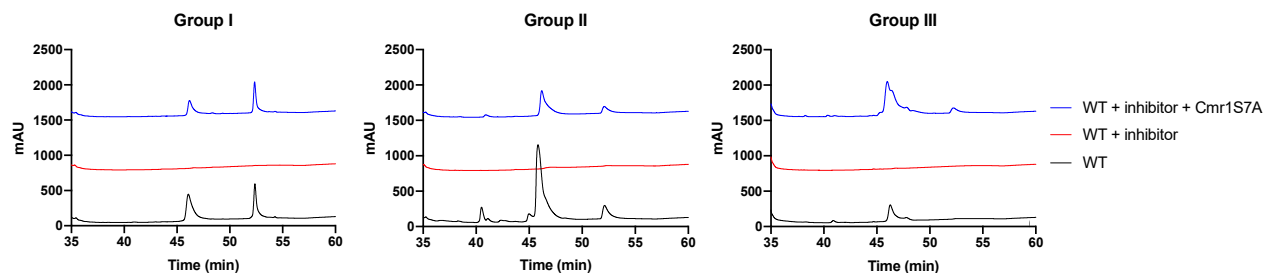


Figure 4.S8 HPLC traces of PSM production restoration by Cmr1 S7A in groups I–III. Triplicate HPLC runs were conducted for multi-group agonist Cmr1 S7A following the same procedure used for Cmr1. Representative HPLC traces in all three *S. epidermidis* groups are shown below.

4.4.5 HPLC and MS characterization of AIP-II analogs, AIP-III analogs, chimera analogs, and PSMs

Table 4.A MS and HPLC data for the *S. epidermidis* AIP-II analogs synthesized in this study. EM = exact mass for $[M+H]^+$ unless otherwise noted. Rt = retention time.
* = $[M+2H]^{2+}$

Peptide Name	Sequence	Calc. EM	Obs. EM	Rt (min)	Purity (%)
AIP-II N1A	A-A-S-K-Y-N-P-(C-S-N-Y-L)	1312.5991	1312.6010	18.5	>99
AIP-II S3A	N-A-A-K-Y-N-P-(C-S-N-Y-L)	1339.6100	1339.6121	16.0	>99
AIP-II K4A	N-A-S-A-Y-N-P-(C-S-N-Y-L)	1298.5471	1298.5459	16.7	>99
AIP-II Y5A	N-A-S-K-A-N-P-(C-S-N-Y-L)	1263.5787	1263.5764	17.1	>97
AIP-II N6A	N-A-S-K-Y-A-P-(C-S-N-Y-L)	1312.5991	1312.6021	17.6	>99
AIP-II P7A	N-A-S-K-Y-N-A-(C-S-N-Y-L)	1329.5893	1329.5895	17.3	>99
AIP-II S9A	N-A-S-K-Y-N-P-(C-A-N-Y-L)	1339.1600	1339.1606	17.3	>99
AIP-II N10A	N-A-S-K-Y-N-P-(C-S-A-Y-L)	1312.5991	1312.6014	17.7	>99
AIP-II Y11A	N-A-S-K-Y-N-P-(C-S-N-A-L)	1263.5787	1263.5811	16.3	>99
AIP-II L12A	N-A-S-K-Y-N-P-(C-S-N-Y-A)	1313.5580	1313.5575	15.3	>99
AIP-II D-N1	DN-A-S-K-Y-N-P-(C-S-N-Y-L)	678.3056*	678.3054*	16.0	>97
AIP-II D-A2	N-DA-S-K-Y-N-P-(C-S-N-Y-L)	678.3056*	678.3065*	16.7	>98
AIP-II D-S3	N-A-DS-K-Y-N-P-(C-S-N-Y-L)	678.3056*	678.3051*	15.9	>97
AIP-II D-K4	N-A-S-DK-Y-N-P-(C-S-N-Y-L)	678.3056*	678.3063*	16.0	>96
AIP-II D-Y5	N-A-S-K-DY-N-P-(C-S-N-Y-L)	678.3056*	678.3061*	16.1	>95
AIP-II D-N6	N-A-S-K-Y-DN-P-(C-S-N-Y-L)	678.3056*	678.3049*	15.9	>94
AIP-II D-P7	N-A-S-K-Y-N-DP-(C-S-N-Y-L)	678.3056*	678.3065*	16.0	>97
AIP-II D-C8	N-A-S-K-Y-N-P-(DC-S-N-Y-L)	678.3056*	678.3066*	16.8	>97
AIP-II D-S9	N-A-S-K-Y-N-P-(C-DS-N-Y-L)	678.3056*	678.3041*	16.2	>97
AIP-II D-N10	N-A-S-K-Y-N-P-(C-S-DN-Y-L)	678.3056*	678.3040*	15.8	>98
AIP-II D-Y11	N-A-S-K-Y-N-P-(C-S-N-DY-L)	678.3056*	678.3044*	15.5	>95
AIP-II D-L12	N-A-S-K-Y-N-P-(C-S-N-Y-DL)	678.3056*	678.3047*	15.6	>99
AIP-II 13aa	G-N-A-S-K-Y-N-P-(C-S-N-Y-L)	1412.6264	1412.6256	21.4	>98
AIP-II 6aa	P-(C-S-N-Y-L)	678.2916	678.2913	16.5	>99

Table 4.B MS and HPLC data for the *S. epidermidis* AIP-III analogs synthesized in this study. EM = exact mass for $[M+H]^+$ unless otherwise noted. Rt = retention time.

* = $[M+2H]^{2+}$

Peptide Name	Sequence	Calc. EM	Obs. EM	Rt (min)	Purity (%)
AIP-III N1A	A-A-A-K-Y-N-P-(C-A-S-Y-L)	627.3028*	627.3029*	18.4	>96
AIP-III K4A	N-A-A-A-Y-N-P-(C-A-S-Y-L)	620.2768*	620.2776*	18.8	>99
AIP-III Y5A	N-A-A-K-A-N-P-(C-A-S-Y-L)	602.7926*	602.7935*	17.8	>97
AIP-III N6A	N-A-A-K-Y-A-P-(C-A-S-Y-L)	627.3028*	627.3038*	18.4	>99
AIP-III P7A	N-A-A-K-Y-N-A-(C-A-S-Y-L)	635.7979*	635.7994*	18.1	>99
AIP-III S10A	N-A-A-K-Y-N-P-(C-A-A-Y-L)	640.8082*	640.8109*	19.4	>99
AIP-III Y11A	N-A-A-K-Y-N-P-(C-A-S-A-L)	602.7926*	602.7922*	17.7	>96
AIP-III L12A	N-A-A-K-Y-N-P-(C-A-S-Y-A)	627.7822*	627.7824*	16.8	>97
AIP-III D-N1	DN-A-A-K-Y-N-P-(C-A-S-Y-L)	648.8057*	648.8054*	16.7	>99
AIP-III D-A2	N-DA-A-K-Y-N-P-(C-A-S-Y-L)	648.8057*	648.8050*	16.8	>99
AIP-III D-A3	N-A-DA-K-Y-N-P-(C-A-S-Y-L)	648.8057*	648.8056*	16.7	>99
AIP-III D-K4	N-A-A-DK-Y-N-P-(C-A-S-Y-L)	648.8057*	648.8052*	16.7	>98
AIP-III D-Y5	N-A-A-K-DY-N-P-(C-A-S-Y-L)	648.8057*	648.8055*	16.7	>99
AIP-III D-N6	N-A-A-K-Y-DN-P-(C-A-S-Y-L)	648.8057*	648.8052*	16.5	>99
AIP-III D-P7	N-A-A-K-Y-N-DP-(C-A-S-Y-L)	648.8057*	648.8061*	16.6	>99
AIP-III D-C8	N-A-A-K-Y-N-P-(DC-A-S-Y-L)	648.8057*	648.8058*	17.4	>99
AIP-III D-A9	N-A-A-K-Y-N-P-(C-DA-S-Y-L)	648.8057*	648.8063*	16.9	>99
AIP-III D-S10	N-A-A-K-Y-N-P-(C-A-DS-Y-L)	648.8057*	648.8063*	16.5	>97
AIP-III D-Y11	N-A-A-K-Y-N-P-(C-A-S-DY-L)	648.8057*	648.8062*	15.9	>99
AIP-III D-L12	N-A-A-K-Y-N-P-(C-A-S-Y-DL)	648.8057*	648.8060*	16.2	>99
AIP-III 13aa	G-N-A-A-K-Y-N-P-(C-A-S-Y-L)	1353.6267	1353.6256	17.8	>96
AIP-III 11aa	A-A-K-Y-N-P-(C-A-S-Y-L)	1182.5612	1182.5618	17.9	>98
AIP-III 10aa	A-K-Y-N-P-(C-A-S-Y-L)	1111.5241	1111.5226	18.0	>96
AIP-III 9aa	K-Y-N-P-(C-A-S-Y-L)	1040.4870	1040.4851	18.0	>97
AIP-III 8aa	Y-N-P-(C-A-S-Y-L)	912.3920	912.3917	19.4	>97
AIP-III 7aa	N-P-(C-A-S-Y-L)	729.3287	749.3289	18.7	>96
AIP-III 6aa	P-(C-A-S-Y-L)	635.2858	635.2856	17.1	>98
tAIP-III	Ac-(C-A-S-Y-L)	580.2436	580.2436	17.8	>98

Table 4.C MS and HPLC data for the *S. epidermidis* chimera analogs synthesized in this study. EM = exact mass for $[M+H]^+$ unless otherwise noted. Rt = retention time. * = $[M+2H]^{2+}$

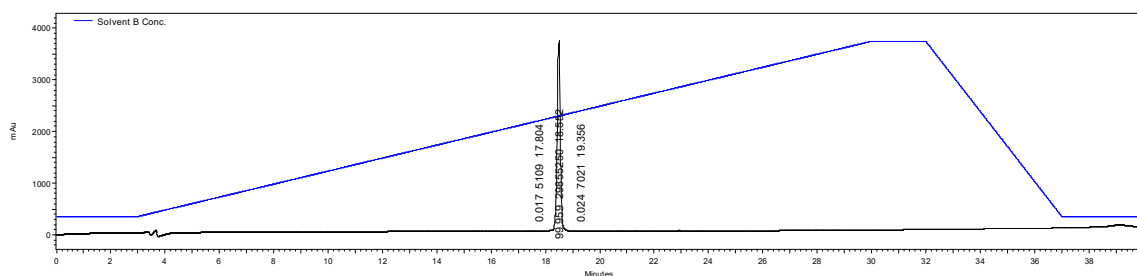
Peptide Name	Sequence	Calc. EM	Obs. EM	Rt (min)	Purity (%)
AIP-I tail: AIP-II ring	D-S-V-(C-S-N-Y-L)	882.3662	882.3660	17.0	>94
AIP-I tail: AIP-III ring	D-S-V-(C-A-S-Y-L)	839.3604	839.3613	18.8	>96
AIP-II 9aa N3L	K-Y-L-P-(C-S-N-Y-L)	541.7706*	541.7706*	17.7	>92
AIP-II 9aa N3V	K-Y-V-P-(C-S-N-Y-L)	534.7628*	534.7624*	17.0	>97
AIP-II 9aa P4L	K-Y-N-L-(C-S-N-Y-L)	1099.5241	1099.5240	17.7	>97
Cmr1	K-Y-N-P-(C-A-S-Y-F)	1074.4713	1074.4710	17.6	>95
Cmr1 A6S	K-Y-N-P-(C-S-S-Y-F)	1090.4662	1090.4663	19.1	>97
Cmr1 A6SS7A	K-Y-N-P-(C-S-A-Y-F)	1074.4713	1074.4692	19.5	>95
Cmr1 A6SS7N	K-Y-N-P-(C-S-N-Y-F)	1117.4771	1117.4780	16.8	>98
Cmr1 S7A	K-Y-N-P-(C-A-A-Y-F)	1058.4764	1058.4752	17.9	>97
Cmr1 S7N	K-Y-N-P-(C-A-N-Y-F)	1101.4822	1101.4825	16.9	>98
Cmr2	K-Y-N-V-(C-A-S-Y-F)	538.7471*	538.7466*	17.8	>96
Cmr2 A6S	K-Y-N-V-(C-S-S-Y-F)	1092.4819	1092.4828	18.1	>92
Cmr2 A6SS7A	K-Y-N-V-(C-S-A-Y-F)	1076.4870	1076.4878	19.0	>91
Cmr2 S7A	K-Y-N-V-(C-A-A-Y-F)	1060.4921	1060.4928	19.4	>93
Cmr2 S7N	K-Y-N-V-(C-A-N-Y-F)	1103.4979	1103.4988	18.4	>98
Cmr2 F9L	K-Y-N-V-(C-A-S-Y-L)	1042.5026	1042.5037	17.9	>97
Cmr3	K-Y-N-V-(C-S-N-Y-L)	543.2579*	543.2575*	17.0	>95
Cmr3 S6 α	K-Y-N-V-(C- α -N-Y-L)	542.2682*	542.2680*	18.5	>96
Cmr3 S6A	K-Y-N-V-(C-A-N-Y-L)	535.2604*	535.2603*	17.6	>98
Cmr3 S6AN7A	K-Y-N-V-(C-A-A-Y-L)	513.7575*	513.7578*	18.6	>94
Cmr3 S6G	K-Y-N-V-(C-G-N-Y-L)	1055.4979	1055.4988	17.9	>95
Cmr3 S6T	K-Y-N-V-(C-T-N-Y-L)	1099.5241	1099.5251	18.3	>93
Cmr3 N7 α	K-Y-N-V-(C-S- α -Y-L)	528.7623*	528.7626*	19.4	>97
Cmr3 N7A	K-Y-N-V-(C-S-A-Y-L)	521.7550*	521.7549*	18.0	>97
Cmr3 N7D	K-Y-N-V-(C-S-D-Y-L)	1086.4925	1086.4920	18.2	>93
Cmr3 N7G	K-Y-N-V-(C-S-G-Y-L)	1028.4870	1028.4875	18.0	>96
Cmr3 N7L	K-Y-N-V-(C-S-L-Y-L)	1084.5496	1084.5497	19.9	>96
Cmr3 N7Q	K-Y-N-V-(C-S-Q-Y-L)	550.2657*	550.2654*	18.5	>96
Cmr3 N7S	K-Y-N-V-(C-S-S-Y-L)	1058.4975	1058.4988	17.7	>95
Cmr3 N7T	K-Y-N-V-(C-S-T-Y-L)	1072.5132	1072.5137	18.7	>95
Cmr3 N7V	K-Y-N-V-(C-S-V-Y-L)	535.7706*	535.7705*	19.8	>93
Cmr3 L9F	K-Y-N-V-(C-S-N-Y-F)	560.2500*	560.2503*	17.8	>99

Table 4.D MS and HPLC data for the *S. epidermidis* PSM α , PSM β , and PSM γ isolated from group-I (RP62A) cellular supernatant. The PSMs were not separated from one other using this HPLC method. All PSMs are formylated. EM = exact mass for [M+3H]⁺ unless otherwise noted. Rt = retention time. * = [M+2H]⁺

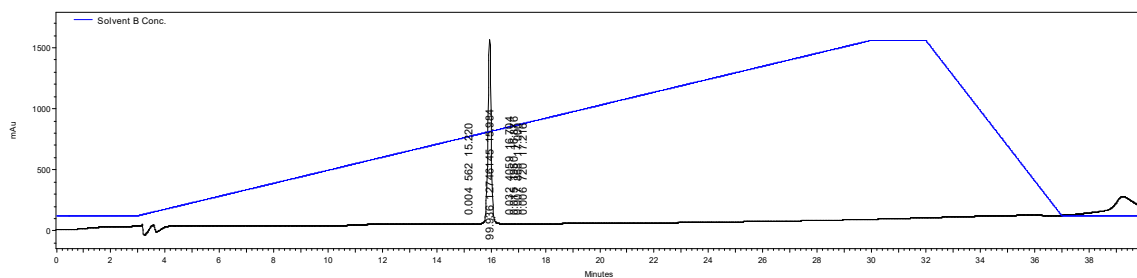
PSM	Sequence	Calc. EM	Obs. EM	Rt (min)
PSM α	fMADVIAKIVEIVKGLIDQFTQK	1244.198*	1244.6946*	41.5
PSM β	fMSKLAEAIANTVCAAQDQDWTKLGTIV DIVESGVSVLGKIFGF	1555.821	1556.8161	41.5
PSM γ	fMAADIISTIGDLVKWIIDTVNKFVK	949.861	949.8561	41.5

HPLC traces for AIP-II analogs

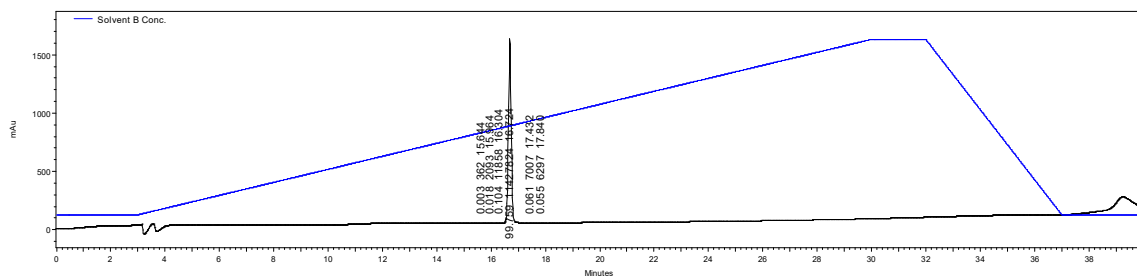
AIP-II N1A



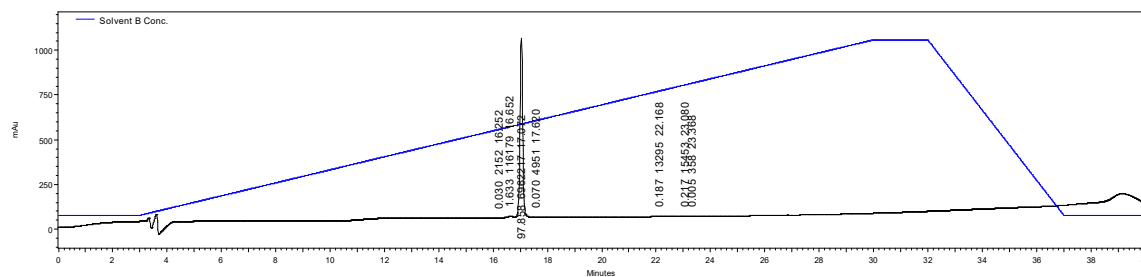
AIP-II S3A



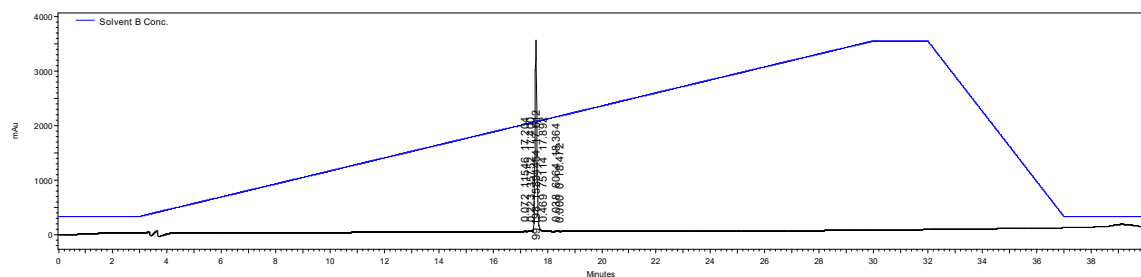
AIP-II K4A



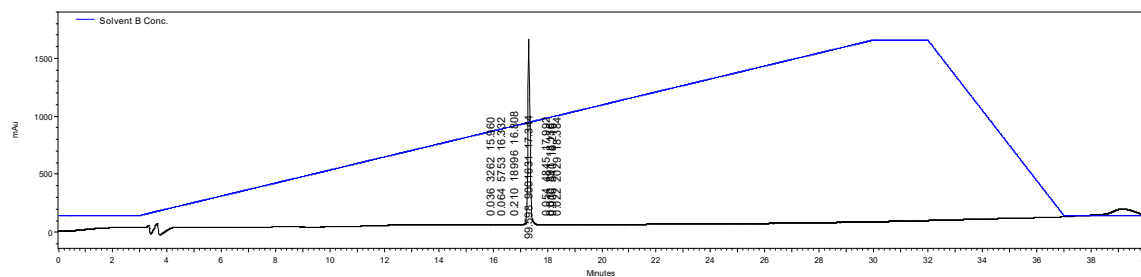
AIP-II Y5A



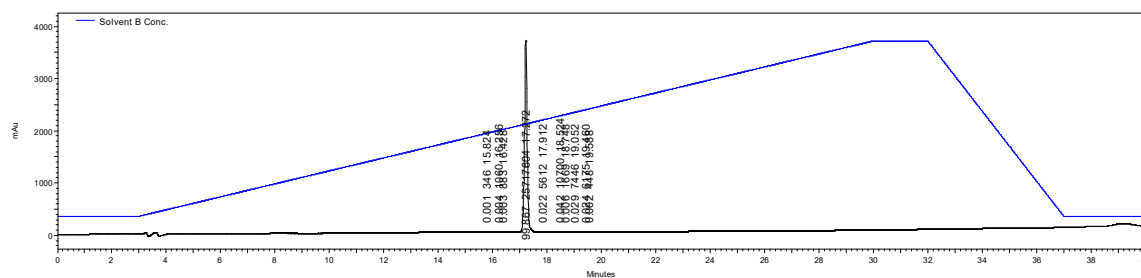
AIP-II N6A



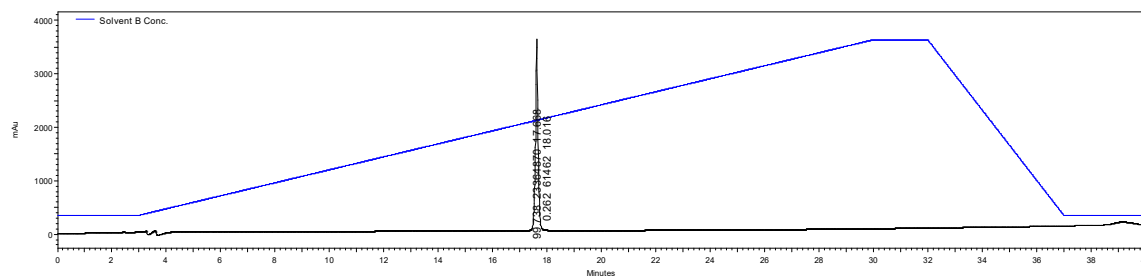
AIP-II P7A



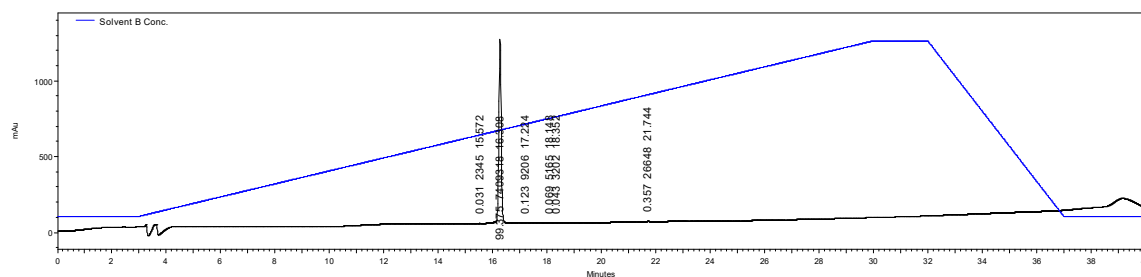
AIP-II S9A



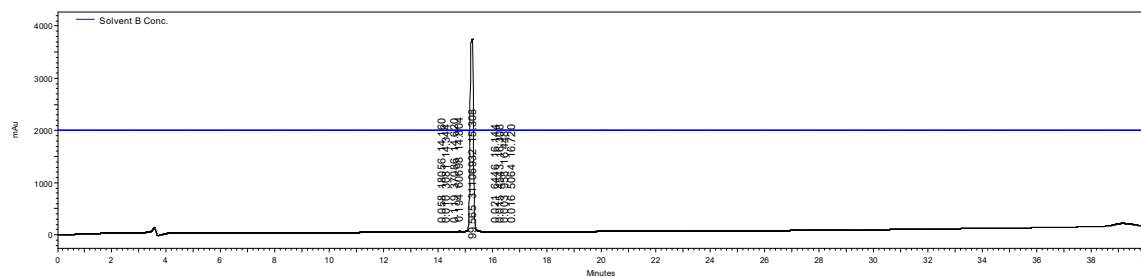
AIP-II N10A



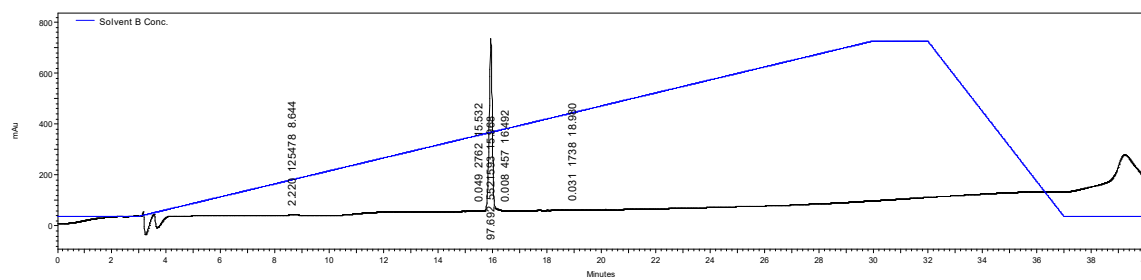
AIP-II Y11A



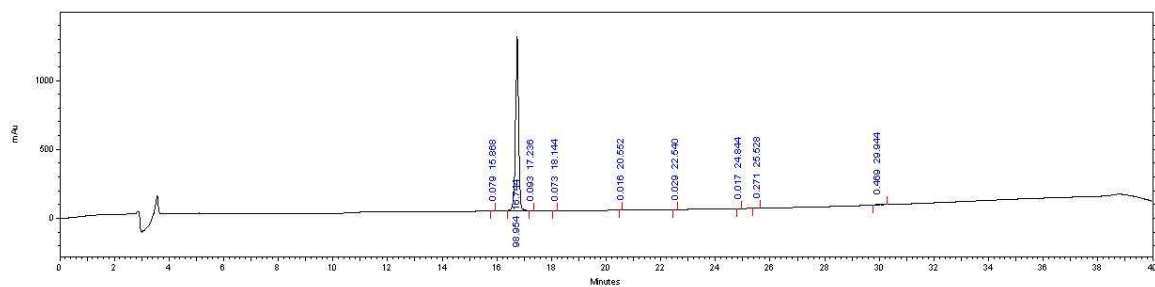
AIP-II L12A



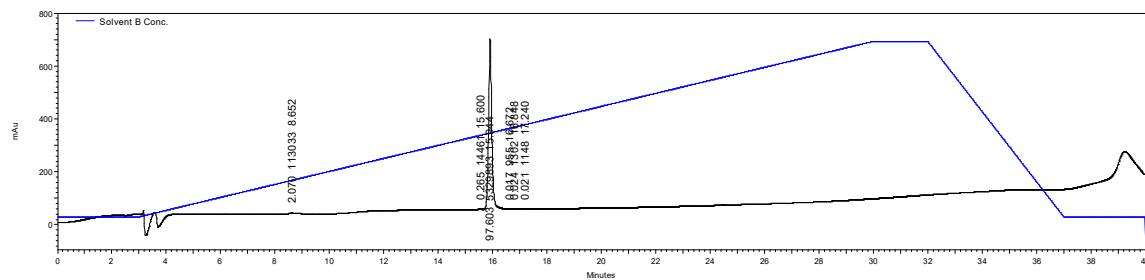
AIP-II D-N1



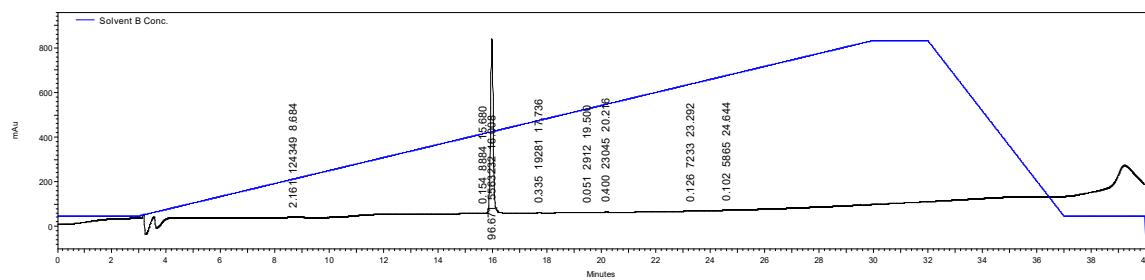
AIP-II D-A2



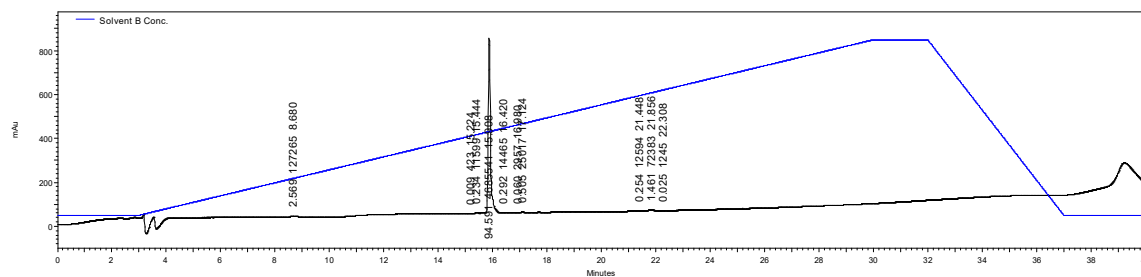
AIP-II D-S3



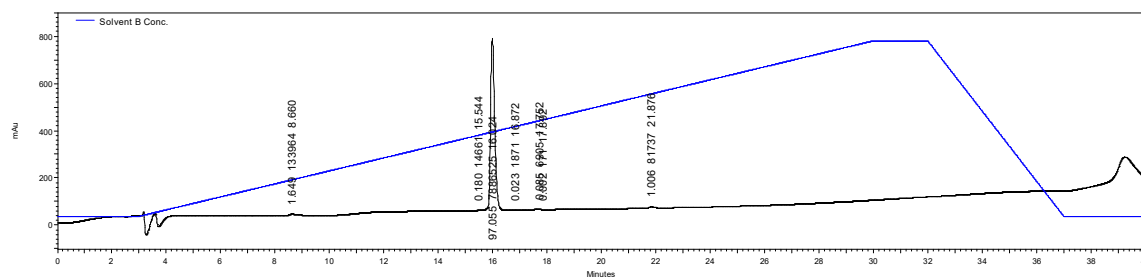
AIP-II D-K4



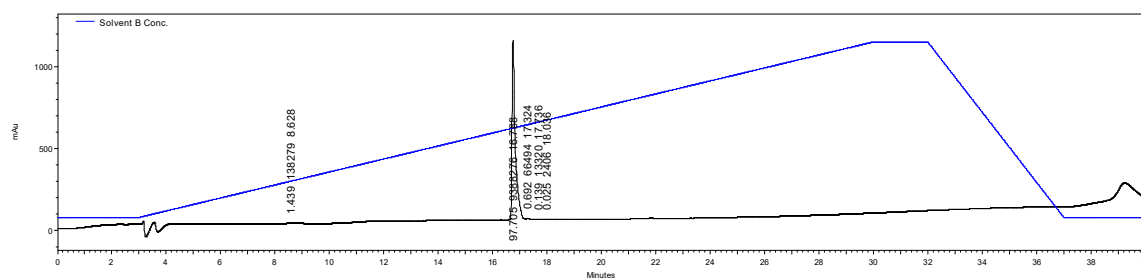
AIP-II D-N6



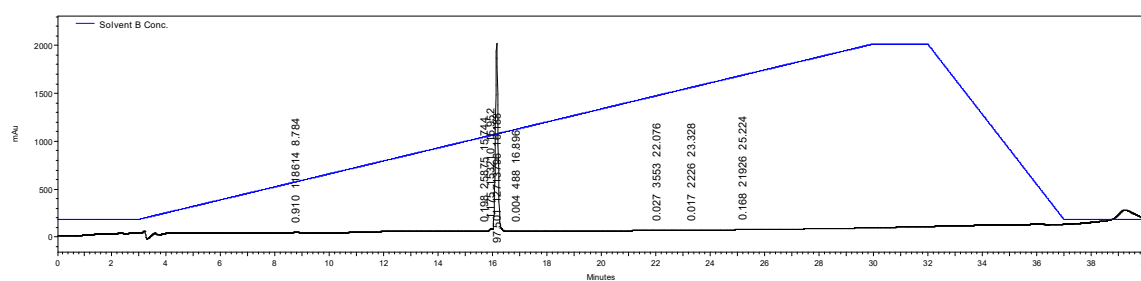
AIP-II D-P7



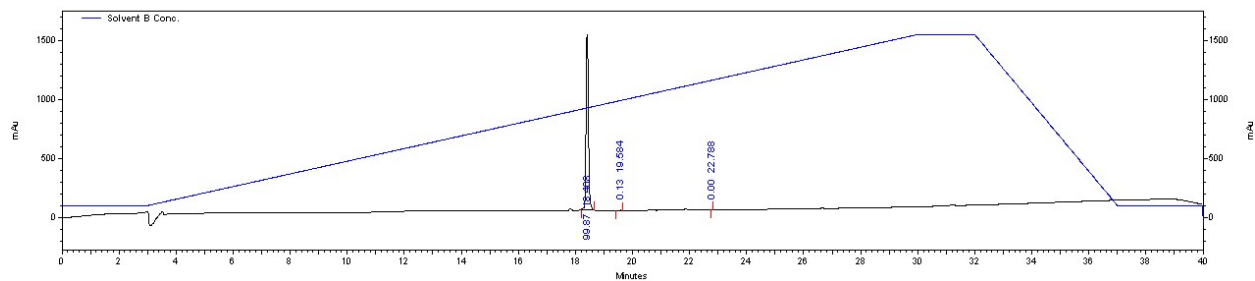
AIP-II D-C8



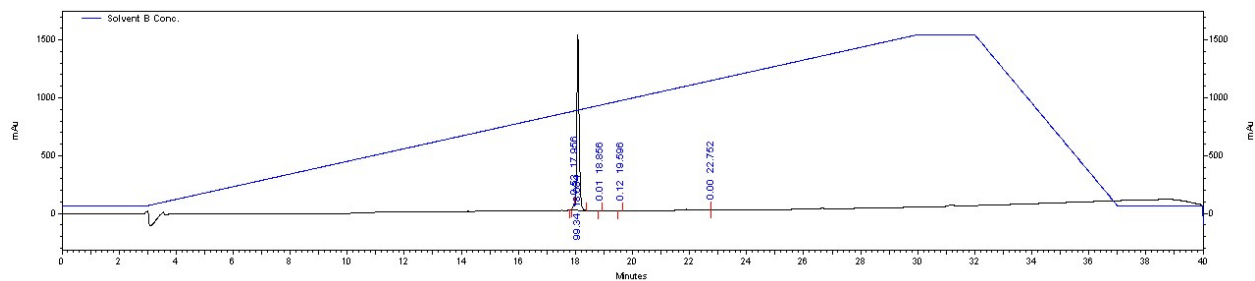
AIP-II D-S9



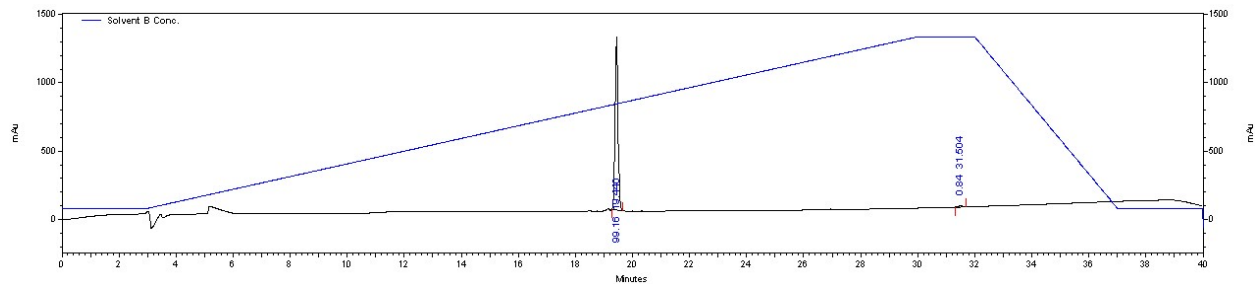
AIP-III N6A



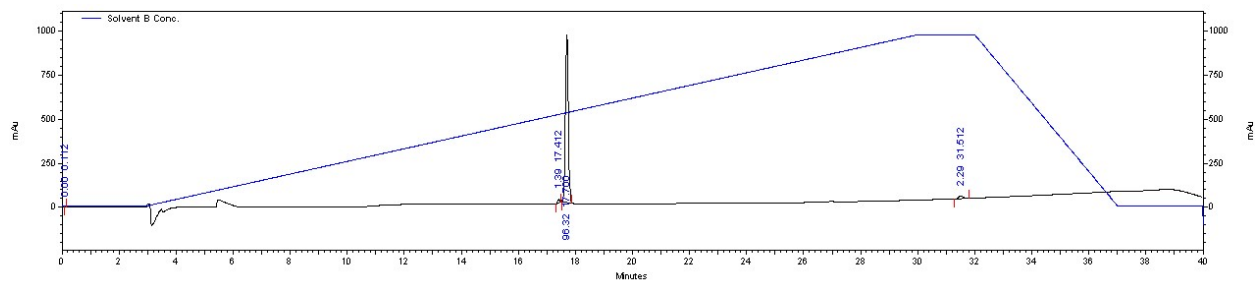
AIP-III P7A



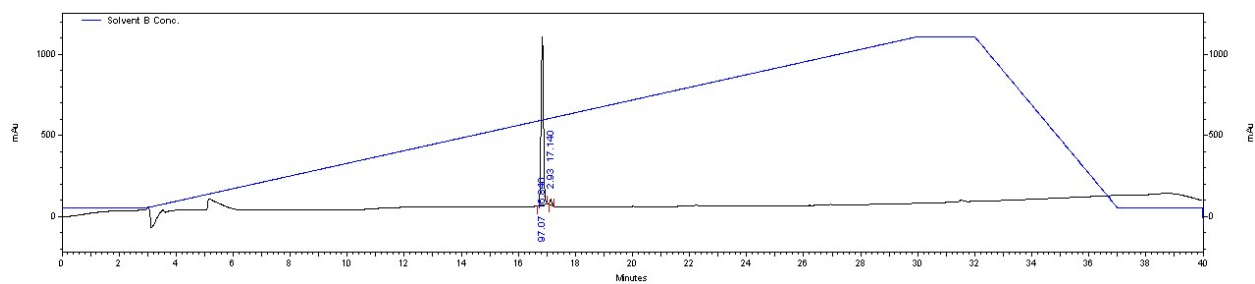
AIP-III S10A



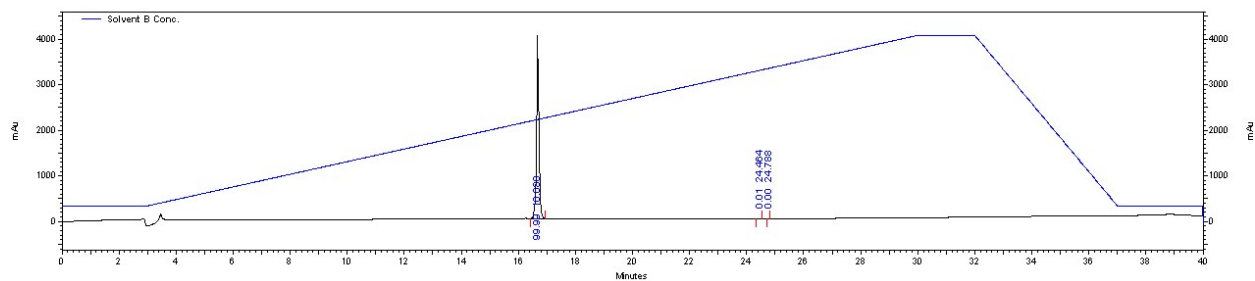
AIP-III Y11A



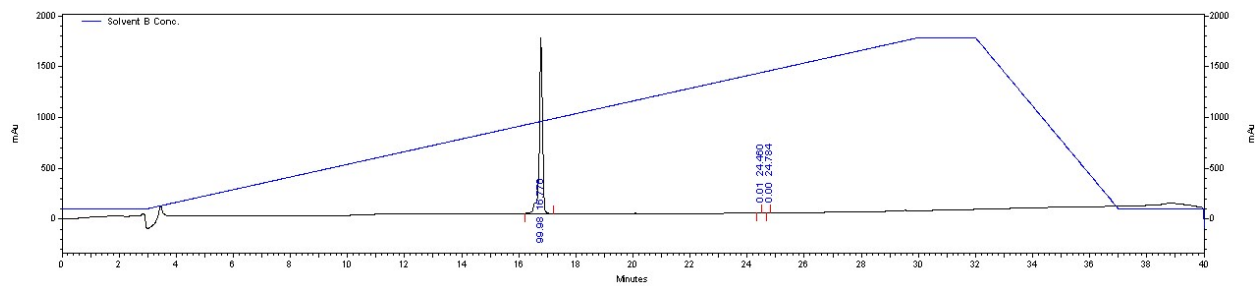
AIP-III L12A



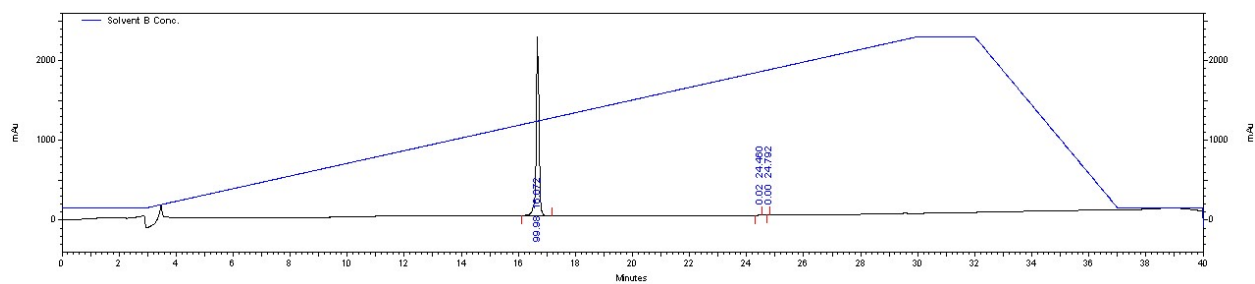
AIP-III D-N1



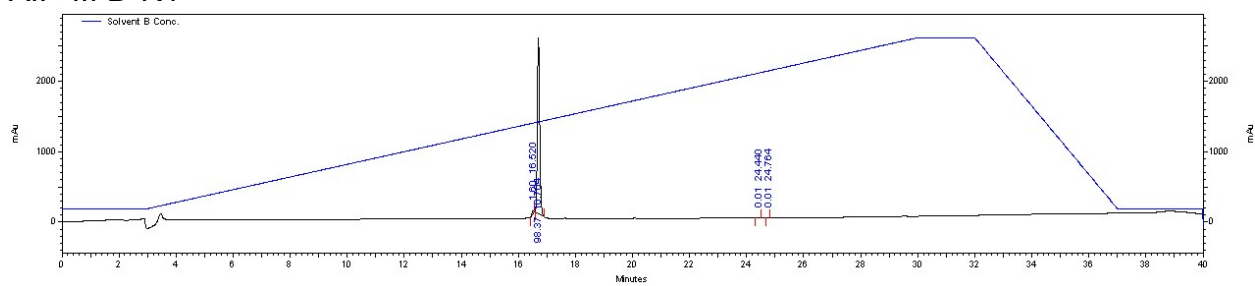
AIP-III D-A2



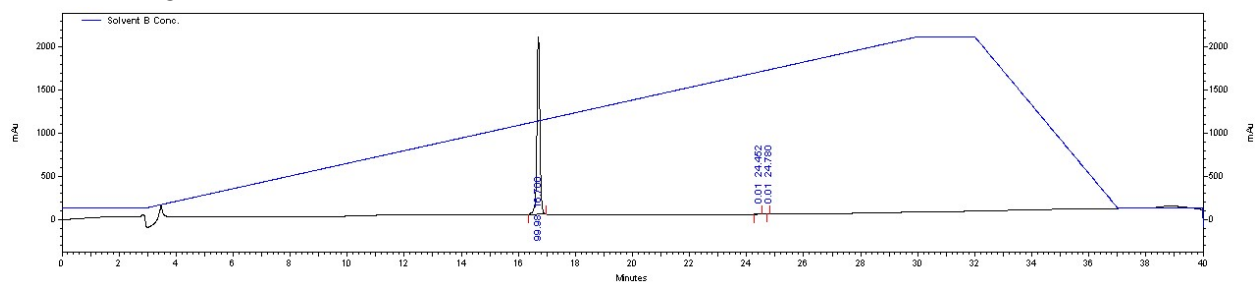
AIP-III D-A3



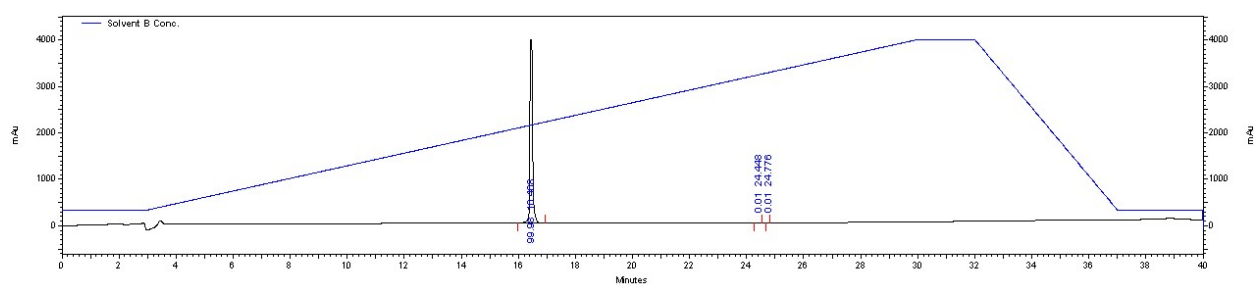
AIP-III D-K4



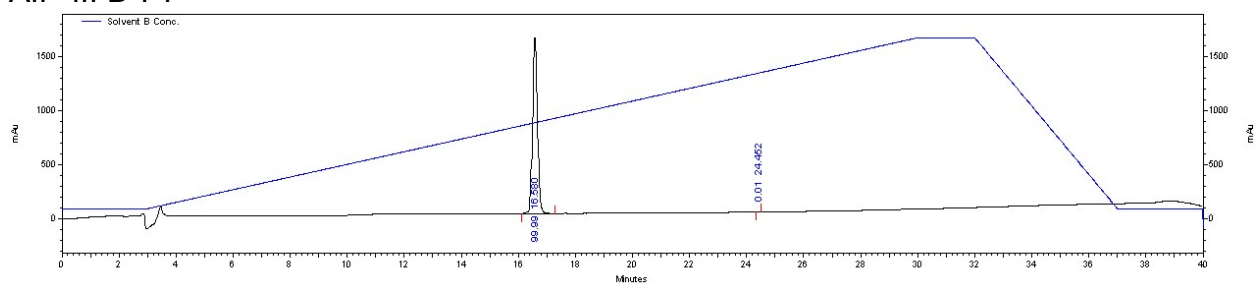
AIP-III D-Y5



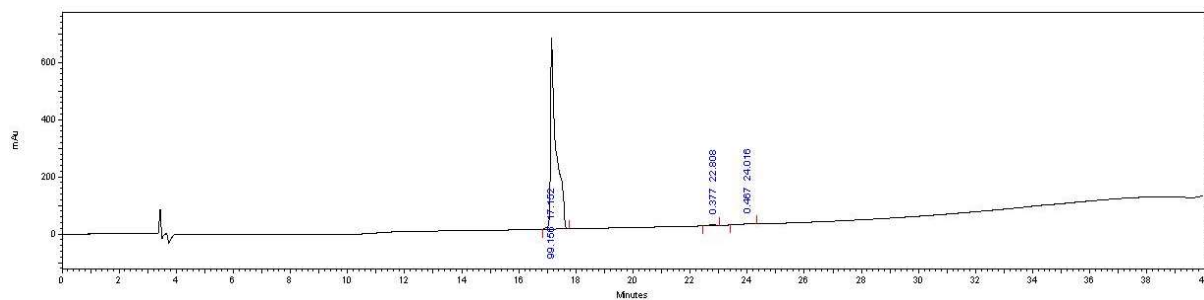
AIP-III D-N6



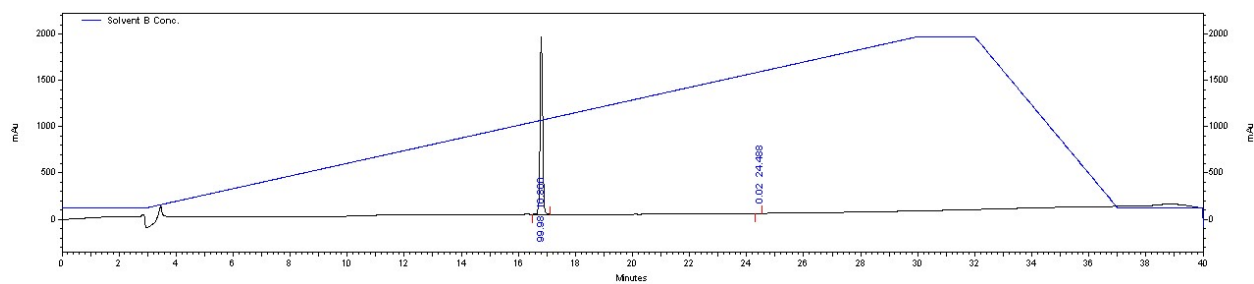
AIP-III D-P7



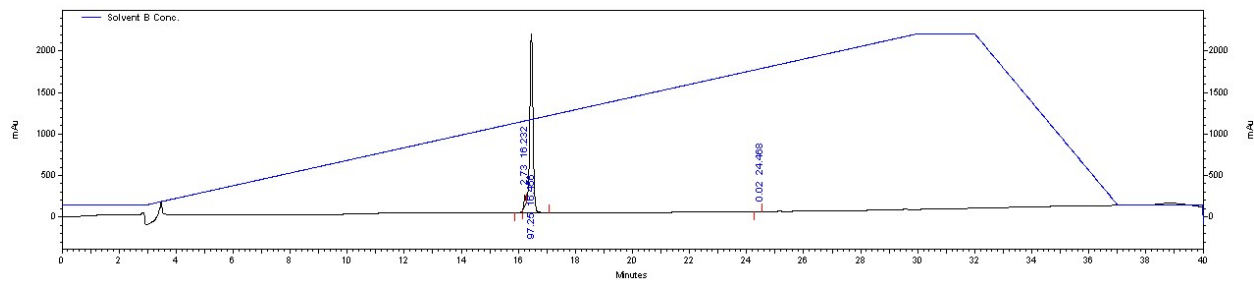
AIP-III D-C8



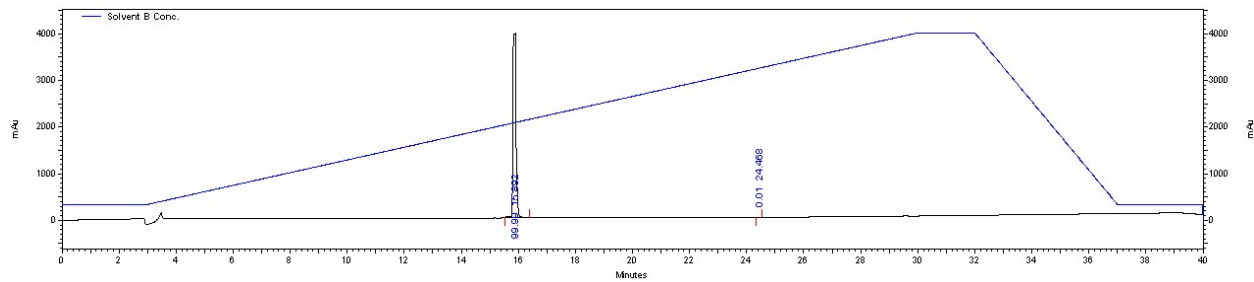
AIP-III D-A9



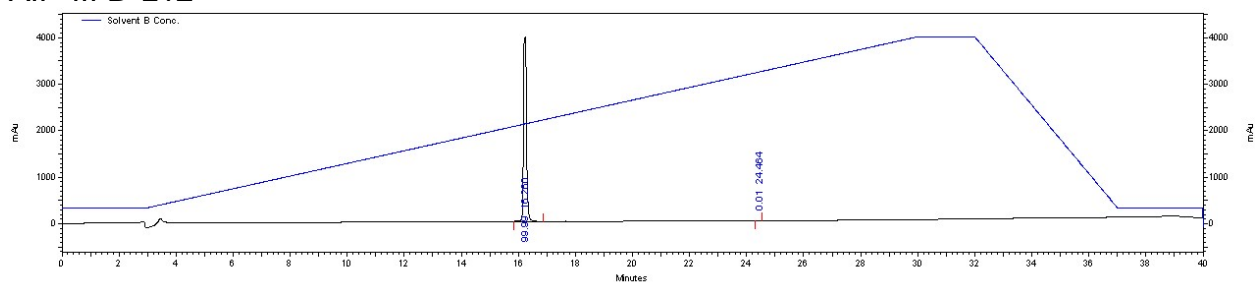
AIP-III D-S10



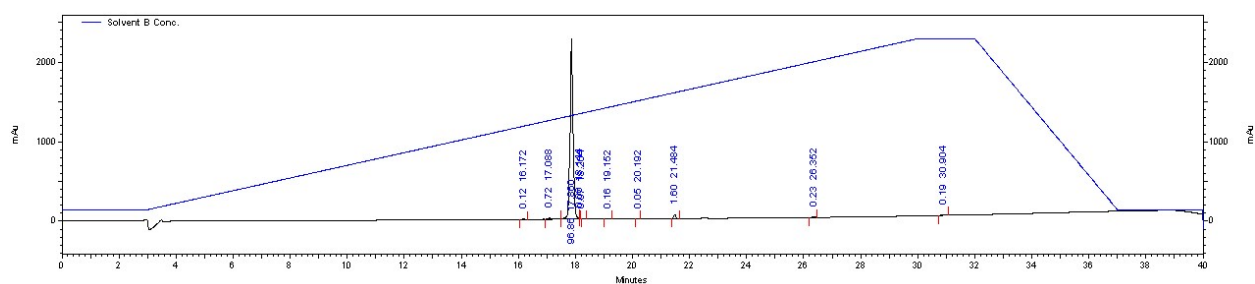
AIP-III D-Y11



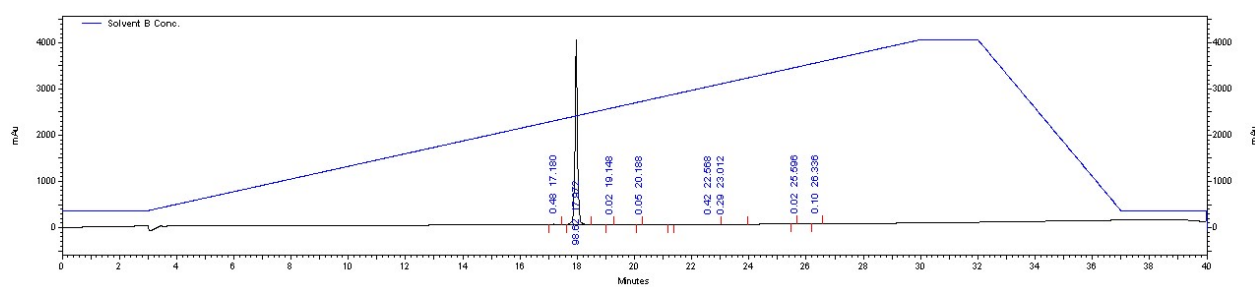
AIP-III D-L12



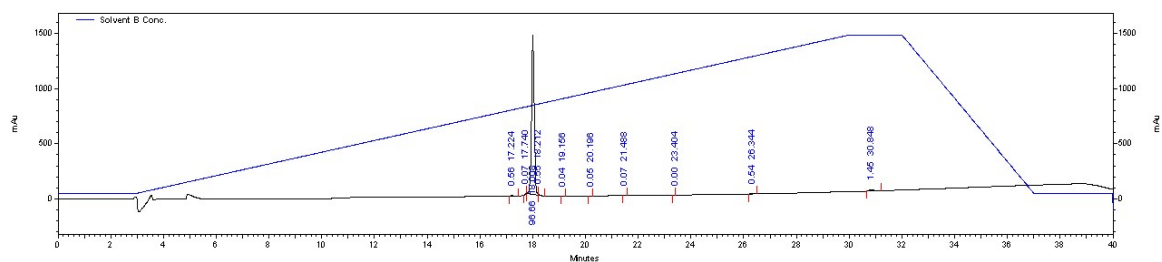
AIP-III 13aa



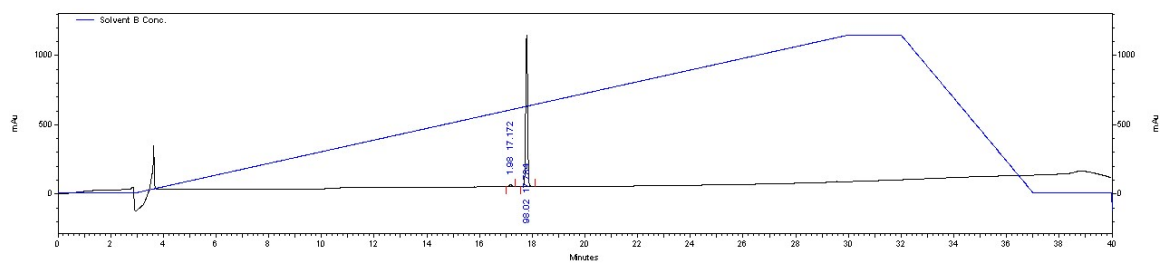
AIP-III 11aa



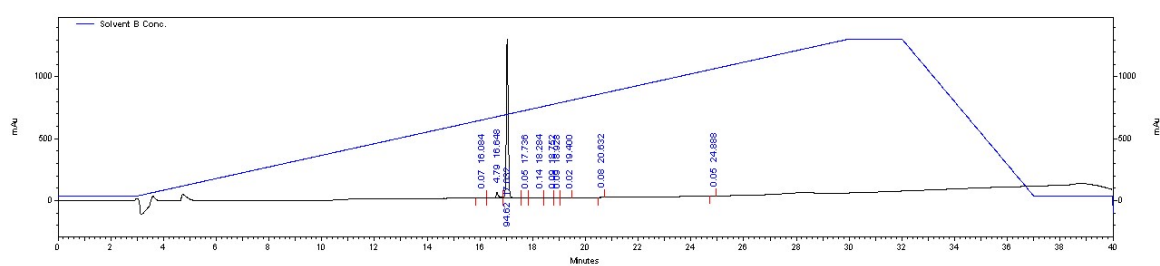
AIP-III 10aa



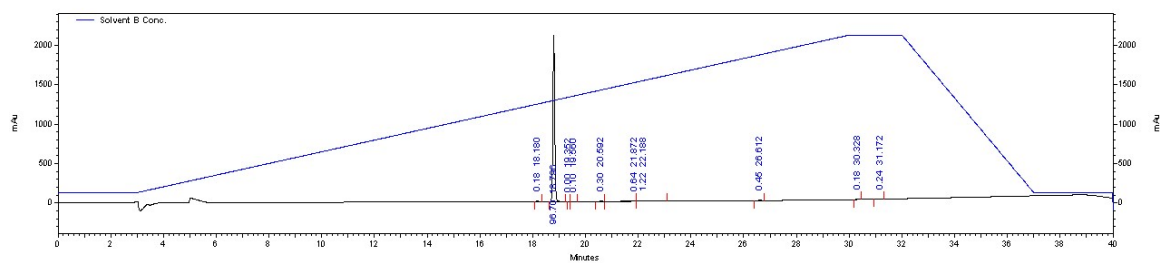
tAIP-III

HPLC traces for chimera analogs

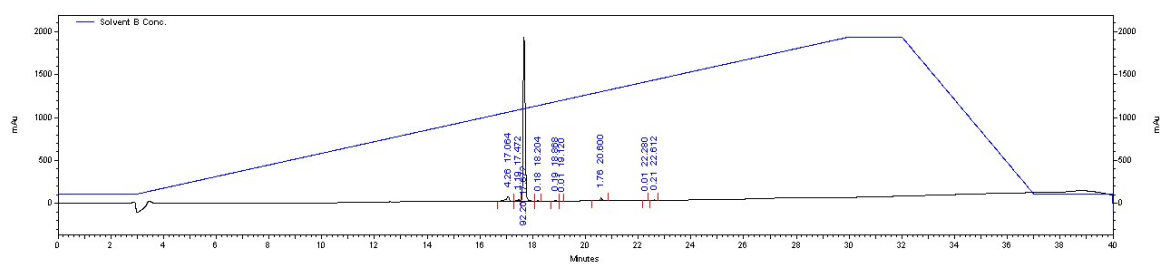
AIP-I tail: AIP-II ring



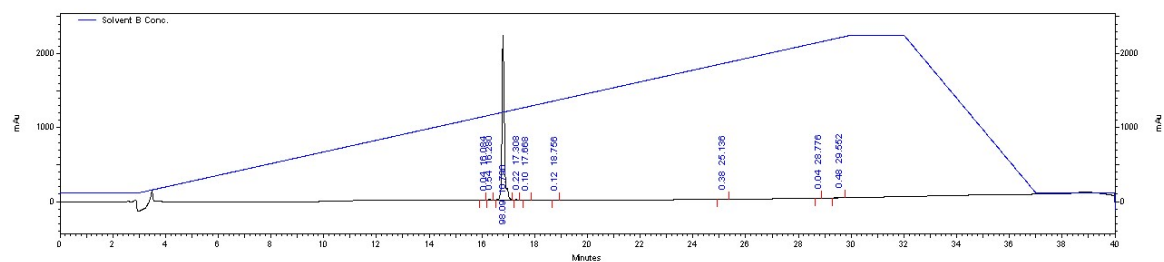
AIP-I tail: AIP-III ring



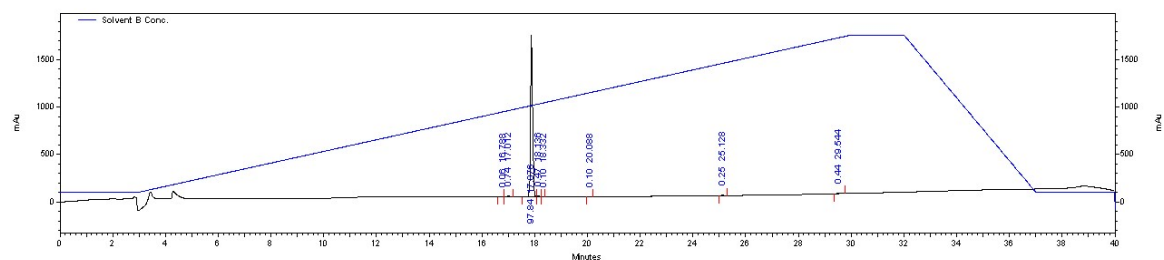
AIP-II 9aa N3L



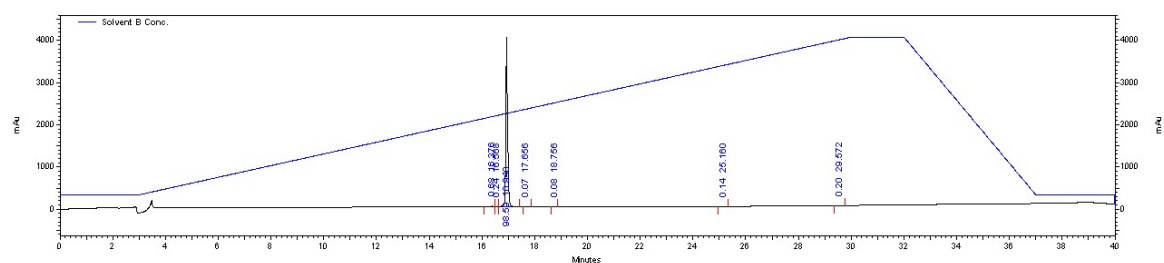
Cmr1 A6SS7N



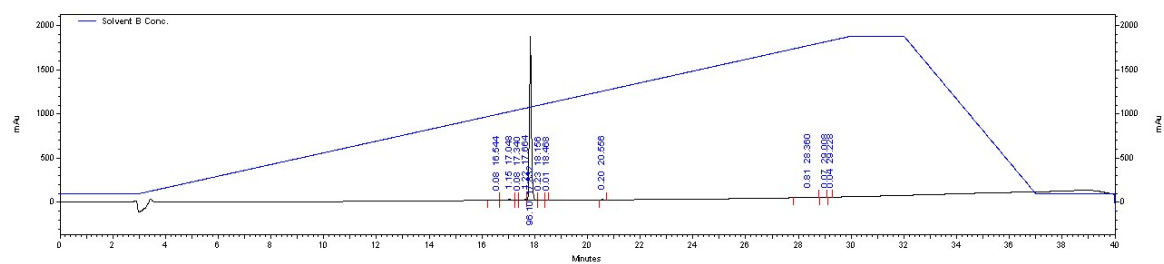
Cmr1 S7A



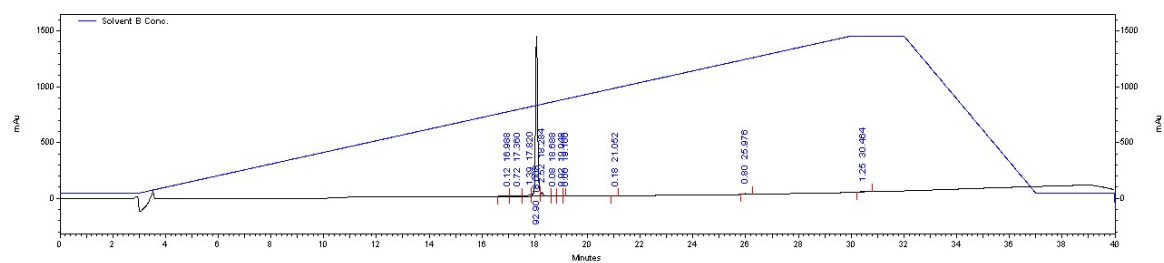
Cmr1 S7N



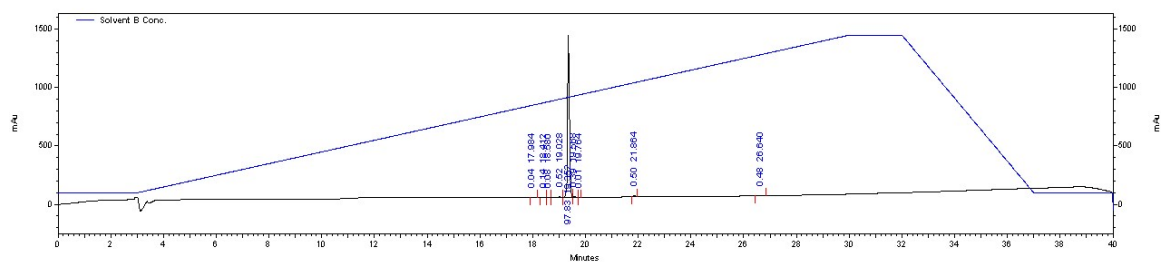
Cmr2



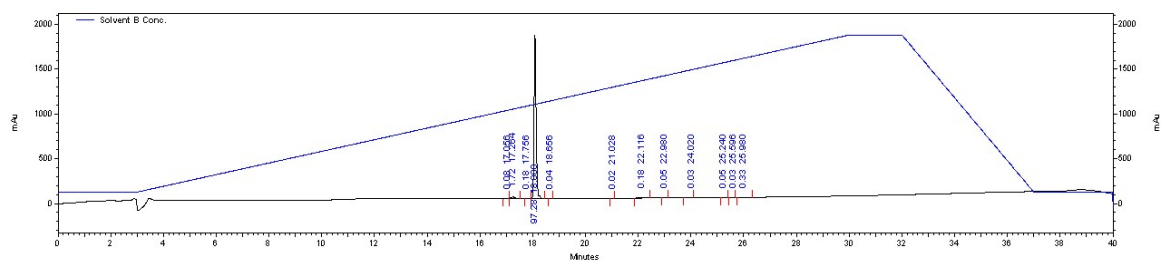
Cmr2 A6S



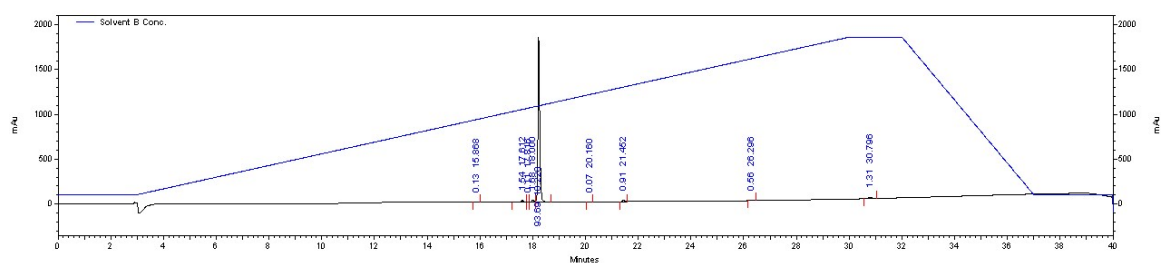
Cmr3 N7α



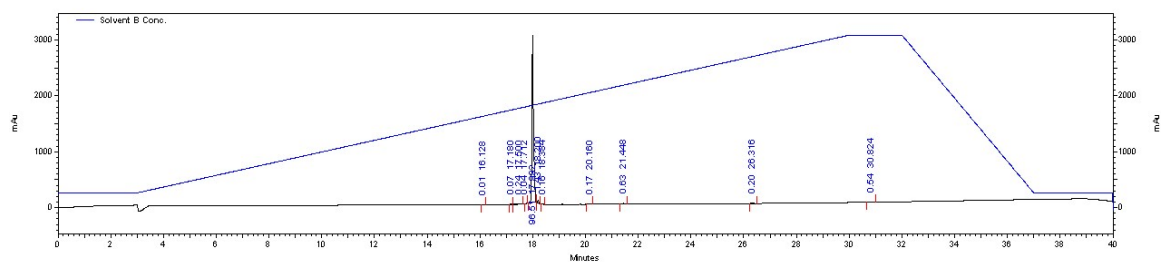
Cmr3 N7A



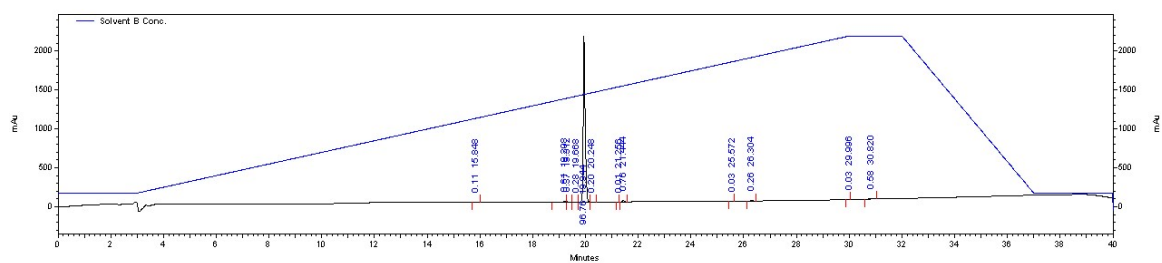
Cmr3 N7D



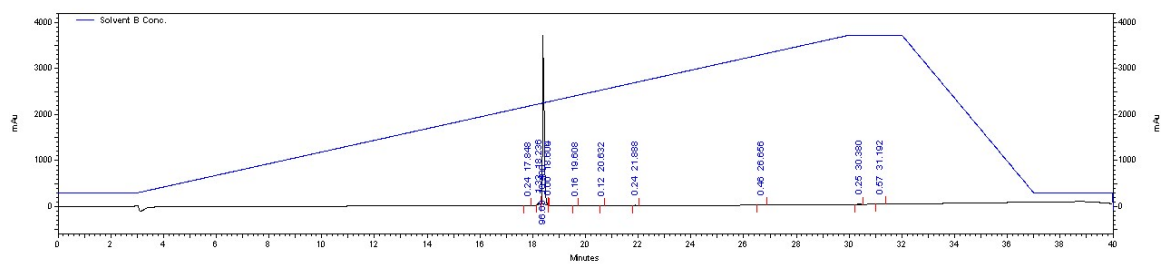
Cmr3 N7G



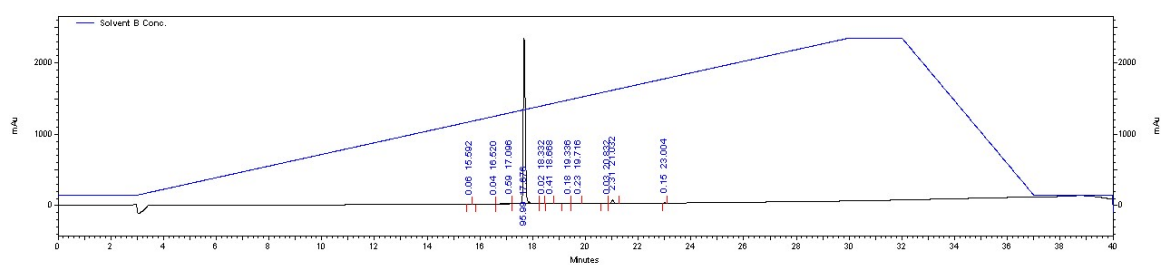
Cmr3 N7L



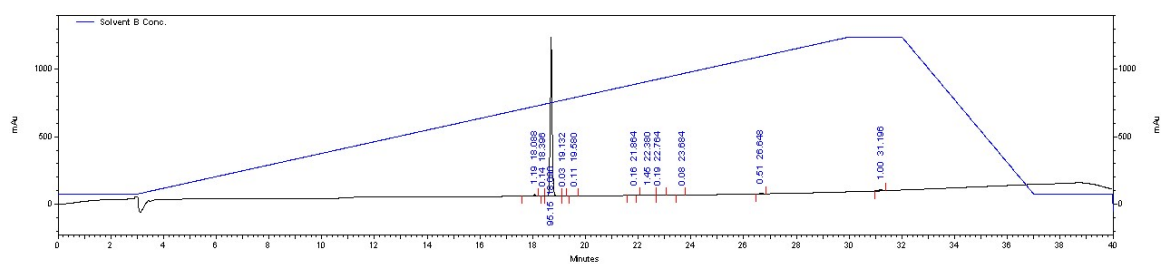
Cmr3 N7Q



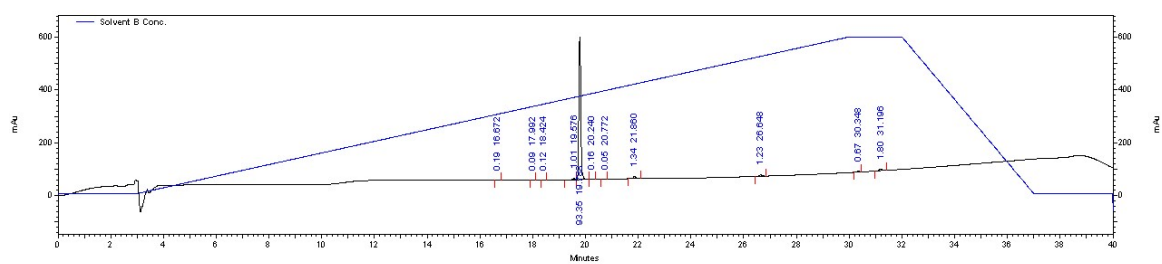
Cmr3 N7S



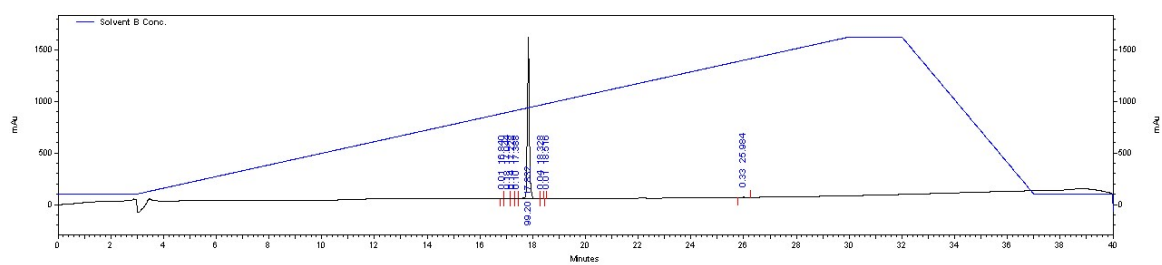
Cmr3 N7T



Cmr3 N7V

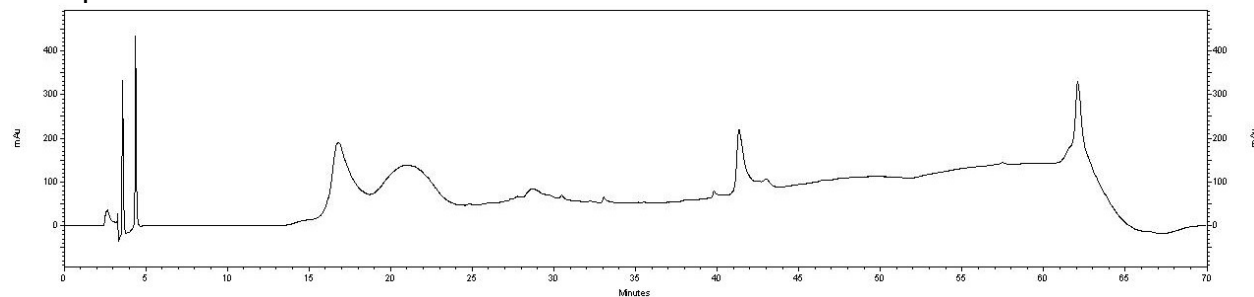


Cmr3 L9F

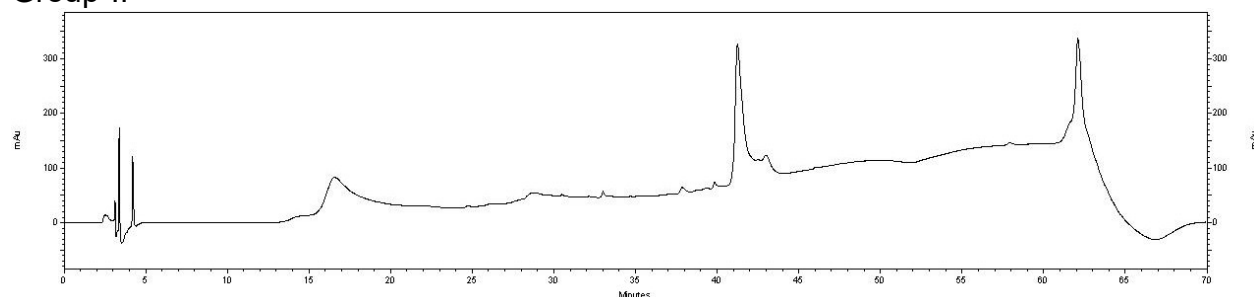


HPLC traces for PSM α , PSM β , and PSM γ

Group-I



Group-II



4.5 Acknowledgements

This work was supported by the NSF (CHE-1708714 to H.E.B.), the NIH (AI153185 to A.R.H.), and by a Merit Award from the Department of Veteran Affairs (I01 BX002711 to A.R.H.). K.H.J.W. and J.K.V. were supported in part by the UW–Madison NIH Chemistry–Biology Interface Training Program (T32 GM008505). T.Y. was supported in part by the UW–Madison NIH Biotechnology Training Program (T32 GM008349). J.K.V. was supported in part by an NSF Graduate Research Fellowship (DGE-1747503). MS facilities in the Department of Chemistry were supported by the NIH (1S10 OD020022-1) and a gift from P. Bender. We thank Sally R. Ruderman for her early experimental contributions to this project.

4.6 References

1. Otto, M., *Staphylococcus epidermidis*--the 'accidental' pathogen. *Nat. Rev. Microbiol.* **2009**, 7 (8), 555-67.
2. Mertens, A.; Ghebremedhin, B., Genetic determinants and biofilm formation of clinical *Staphylococcus epidermidis* isolates from blood cultures and indwelling devices. *Eur. J. Microbiol. Immunol. (Bp)* **2013**, 3 (2), 111-9.
3. Sabate Bresco, M.; Harris, L. G.; Thompson, K.; Stanic, B.; Morgenstern, M.; O'Mahony, L.; Richards, R. G.; Moriarty, T. F., Pathogenic Mechanisms and Host Interactions in *Staphylococcus epidermidis* Device-Related Infection. *Front. Microbiol.* **2017**, 8, 1401.
4. Rogers, K. L.; Fey, P. D.; Rupp, M. E., Coagulase-negative staphylococcal infections. *Infect. Dis. Clin. North Am.* **2009**, 23 (1), 73-98.
5. Uckay, I.; Pittet, D.; Vaudaux, P.; Sax, H.; Lew, D.; Waldvogel, F., Foreign body infections due to *Staphylococcus epidermidis*. *Ann. Med.* **2009**, 41 (2), 109-19.
6. Olson, M. E.; Todd, D. A.; Schaeffer, C. R.; Paharik, A. E.; Van Dyke, M. J.; Buttner, H.; Dunman, P. M.; Rohde, H.; Cech, N. B.; Fey, P. D.; Horswill, A. R., *Staphylococcus epidermidis* agr quorum-sensing system: signal identification, cross talk, and importance in colonization. *J. Bacteriol.* **2014**, 196 (19), 3482-93.
7. Qin, L.; Da, F.; Fisher, E. L.; Tan, D. C.; Nguyen, T. H.; Fu, C. L.; Tan, V. Y.; McCausland, J. W.; Sturdevant, D. E.; Joo, H. S.; Queck, S. Y.; Cheung, G. Y.; Otto, M., Toxin Mediates Sepsis Caused by Methicillin-Resistant *Staphylococcus epidermidis*. *PLoS Pathog.* **2017**, 13 (2), e1006153.
8. Davies, D., Understanding biofilm resistance to antibacterial agents. *Nat. Rev. Drug Discov.* **2003**, 2 (2), 114-22.
9. Fuqua, C.; Greenberg, E. P., Listening in on bacteria: acyl-homoserine lactone signalling. *Nat. Rev. Mol. Cell Biol.* **2002**, 3 (9), 685-95.
10. Rutherford, S. T.; Bassler, B. L., Bacterial quorum sensing: its role in virulence and possibilities for its control. *Cold Spring Harb. Perspect. Med.* **2012**, 2 (11), a012427.
11. Wang, B.; Muir, T. W., Regulation of Virulence in *Staphylococcus aureus*: Molecular Mechanisms and Remaining Puzzles. *Cell Chem. Biol.* **2016**, 23 (2), 214-224.
12. Novick, R. P.; Geisinger, E., Quorum Sensing in Staphylococci. *Annu. Rev. Genet.* **2008**, 42, 541-64.

13. Amara, N.; Mashiach, R.; Amar, D.; Krief, P.; Spieser, S. A.; Bottomley, M. J.; Aharoni, A.; Meijler, M. M., Covalent inhibition of bacterial quorum sensing. *J. Am. Chem. Soc.* **2009**, *131* (30), 10610-9.
14. Yao, Y.; Vuong, C.; Kocianova, S.; Villaruz, A. E.; Lai, Y.; Sturdevant, D. E.; Otto, M., Characterization of the *Staphylococcus epidermidis* accessory-gene regulator response: quorum-sensing regulation of resistance to human innate host defense. *J. Infect. Dis.* **2006**, *193* (6), 841-8.
15. Wang, R.; Khan, B. A.; Cheung, G. Y.; Bach, T. H.; Jameson-Lee, M.; Kong, K. F.; Queck, S. Y.; Otto, M., *Staphylococcus epidermidis* surfactant peptides promote biofilm maturation and dissemination of biofilm-associated infection in mice. *J. Clin. Invest.* **2011**, *121* (1), 238-48.
16. Otto, M., Staphylococcal infections: mechanisms of biofilm maturation and detachment as critical determinants of pathogenicity. *Annu. Rev. Med.* **2013**, *64*, 175-88.
17. Mah, T.-F. C.; O'Toole, G. A., Mechanisms of biofilm resistance to antimicrobial agents. *Trends Microbiol.* **2001**, *9* (1), 34-39.
18. Tal-Gan, Y.; Stacy, D. M.; Foegen, M. K.; Koenig, D. W.; Blackwell, H. E., Highly potent inhibitors of quorum sensing in *Staphylococcus aureus* revealed through a systematic synthetic study of the group-III autoinducing peptide. *J. Am. Chem. Soc.* **2013**, *135* (21), 7869-82.
19. Khan, B. A.; Yeh, A. J.; Cheung, G. Y.; Otto, M., Investigational therapies targeting quorum-sensing for the treatment of *Staphylococcus aureus* infections. *Expert Opin. Investig. Drugs* **2015**, *24* (5), 689-704.
20. Sully, E. K.; Malachowa, N.; Elmore, B. O.; Alexander, S. M.; Femling, J. K.; Gray, B. M.; DeLeo, F. R.; Otto, M.; Cheung, A. L.; Edwards, B. S.; Sklar, L. A.; Horswill, A. R.; Hall, P. R.; Gresham, H. D., Selective chemical inhibition of agr quorum sensing in *Staphylococcus aureus* promotes host defense with minimal impact on resistance. *PLoS Pathog.* **2014**, *10* (6), e1004174.
21. Kim, M. K.; Zhao, A.; Wang, A.; Brown, Z. Z.; Muir, T. W.; Stone, H. A.; Bassler, B. L., Surface-attached molecules control *Staphylococcus aureus* quorum sensing and biofilm development. *Nat. Microbiol.* **2017**, *2*, 17080.
22. Harris, L. G.; Dudley, E.; Rohde, H.; Frommelt, L.; Siemssen, N.; Wilkinson, T. S.; Mack, D., Limitations in the use of PSMgamma, agr, RNAlII, and biofilm formation as biomarkers to define invasive *Staphylococcus epidermidis* from chronic biomedical device-associated infections. *Int. J. Med. Microbiol.* **2017**, *307* (7), 382-387.

23. Vuong, C.; Durr, M.; Carmody, A. B.; Peschel, A.; Klebanoff, S. J.; Otto, M., Regulated expression of pathogen-associated molecular pattern molecules in *Staphylococcus epidermidis*: quorum-sensing determines pro-inflammatory capacity and production of phenol-soluble modulins. *Cell. Microbiol.* **2004**, *6* (8), 753-9.
24. Boles, B. R.; Horswill, A. R., Agr-mediated dispersal of *Staphylococcus aureus* biofilms. *PLoS Pathog.* **2008**, *4* (4), e1000052.
25. Thoendel, M.; Kavanaugh, J. S.; Flack, C. E.; Horswill, A. R., Peptide Signaling in the Staphylococci. *Chem. Rev.* **2011**, *111* (1), 117-51.
26. Zhang, L.; Gray, L.; Novick, R. P.; Ji, G., Transmembrane topology of AgrB, the protein involved in the post-translational modification of AgrD in *Staphylococcus aureus*. *J. Biol. Chem.* **2002**, *277* (38), 34736-42.
27. Kavanaugh, J. S.; Thoendel, M.; Horswill, A. R., A role for type I signal peptidase in *Staphylococcus aureus* quorum sensing. *Mol. Microbiol.* **2007**, *65* (3), 780-98.
28. Wang, B.; Zhao, A.; Novick, R. P.; Muir, T. W., Activation and inhibition of the receptor histidine kinase AgrC occurs through opposite helical transduction motions. *Mol. Cell* **2014**, *53* (6), 929-40.
29. Koenig, R. L.; Ray, J. L.; Maleki, S. J.; Smeltzer, M. S.; Hurlburt, B. K., *Staphylococcus aureus* AgrA binding to the RNAIII-agr regulatory region. *J. Bacteriol.* **2004**, *186* (22), 7549-55.
30. Novick, R. P.; Projan, S. J.; Kornblum, J.; Ross, H. F.; Ji, G.; Kreiswirth, B.; Vandenesch, F.; Moghazeh, S., The agr P2 operon: an autocatalytic sensory transduction system in *Staphylococcus aureus*. *Mol. Gen. Genet.* **1995**, *248*, 446-458.
31. Novick, R. P.; Ross, H. F.; Projan, S. J.; Kornblum, J.; Kreiswirth, B.; Moghazeh, S., Synthesis of staphylococcal virulence factors is controlled by a regulatory RNA molecule. *EMBO J.* **1993**, *12* (10), 3967-3975.
32. Queck, S. Y.; Jameson-Lee, M.; Villaruz, A. E.; Bach, T. H.; Khan, B. A.; Sturdevant, D. E.; Ricklefs, S. M.; Li, M.; Otto, M., RNAIII-independent target gene control by the agr quorum-sensing system: insight into the evolution of virulence regulation in *Staphylococcus aureus*. *Mol. Cell* **2008**, *32* (1), 150-8.
33. Otto, M., Phenol-soluble modulins. *Int. J. Med. Microbiol.* **2014**, *304* (2), 164-9.
34. Ji, G.; Beavis, R.; Novick, R. P., Bacterial interference caused by autoinducing peptide variants. *Science* **1997**, *276* (5321), 2027-30.

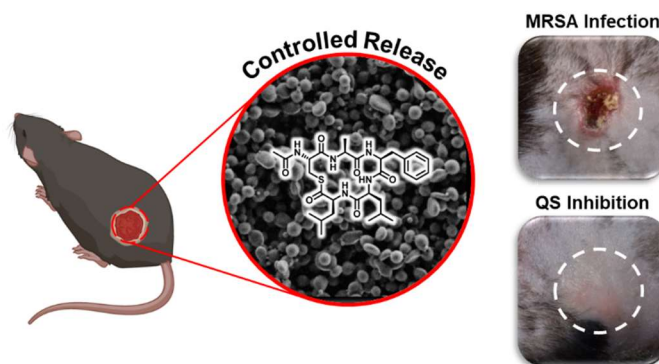
35. Carmody, A. B.; Otto, M., Specificity grouping of the accessory gene regulator quorum-sensing system of *Staphylococcus epidermidis* is linked to infection. *Arch. Microbiol.* **2004**, *181* (3), 250-3.
36. Li, M.; Guan, M.; Jiang, X. F.; Yuan, F. Y.; Xu, M.; Zhang, W. Z.; Lu, Y., Genetic polymorphism of the accessory gene regulator (*agr*) locus in *Staphylococcus epidermidis* and its association with pathogenicity. *J. Med. Microbiol.* **2004**, *53* (Pt 6), 545-549.
37. Hellmark, B.; Soderquist, B.; Unemo, M.; Nilsson-Augustinsson, A., Comparison of *Staphylococcus epidermidis* isolated from prosthetic joint infections and commensal isolates in regard to antibiotic susceptibility, *agr* type, biofilm production, and epidemiology. *Int. J. Med. Microbiol.* **2013**, *303* (1), 32-9.
38. Zhou, W.; Spoto, M.; Hardy, R.; Guan, C.; Fleming, E.; Larson, P. J.; Brown, J. S.; Oh, J., Host-Specific Evolutionary and Transmission Dynamics Shape the Functional Diversification of *Staphylococcus epidermidis* in Human Skin. *Cell* **2020**, *180* (3), 454-470 e18.
39. Martinez-Garcia, S.; Ortiz-Garcia, C. I.; Cruz-Aguilar, M.; Zenteno, J. C.; Murrieta-Coxca, J. M.; Perez-Tapia, S. M.; Rodriguez-Martinez, S.; Cancino-Diaz, M. E.; Cancino-Diaz, J. C., Competition/antagonism associations of biofilm formation among *Staphylococcus epidermidis* Agr groups I, II, and III. *J. Microbiol.* **2019**, *57* (2), 143-153.
40. Brown, M. M.; Kwiecinski, J. M.; Cruz, L. M.; Shahbandi, A.; Todd, D. A.; Cech, N. B.; Horswill, A. R., Novel Peptide from Commensal *Staphylococcus simulans* Blocks Methicillin-Resistant *Staphylococcus aureus* Quorum Sensing and Protects Host Skin from Damage. *Antimicrob. Agents Chemother.* **2020**, *64* (6), e00172-20.
41. Horswill, A. R.; Gordon, C. P., Structure-Activity Relationship Studies of Small Molecule Modulators of the Staphylococcal Accessory Gene Regulator. *J. Med. Chem.* **2020**, *63* (6), 2705-2730.
42. Yang, T.; Tal-Gan, Y.; Paharik, A. E.; Horswill, A. R.; Blackwell, H. E., Structure-Function Analyses of a *Staphylococcus epidermidis* Autoinducing Peptide Reveals Motifs Critical for AgrC-type Receptor Modulation. *ACS Chem. Biol.* **2016**, *11* (7), 1982-91.
43. Vasquez, J. K.; West, K. H. J.; Yang, T.; Polaske, T. J.; Cornilescu, G.; Tonelli, M.; Blackwell, H. E., Conformational Switch to a beta-Turn in a Staphylococcal Quorum Sensing Signal Peptide Causes a Dramatic Increase in Potency. *J. Am. Chem. Soc.* **2020**, *142* (2), 750-761.

44. Wright, J. S., 3rd; Lyon, G. J.; George, E. A.; Muir, T. W.; Novick, R. P., Hydrophobic interactions drive ligand-receptor recognition for activation and inhibition of staphylococcal quorum sensing. *Proc. Natl. Acad. Sci. U. S. A.* **2004**, *101* (46), 16168-73.
45. Blanco-Canosa, J. B.; Dawson, P. E., An efficient Fmoc-SPPS approach for the generation of thioester peptide precursors for use in native chemical ligation. *Angew. Chem. Int. Ed. Engl.* **2008**, *47* (36), 6851-5.
46. Tal-Gan, Y.; Ivancic, M.; Cornilescu, G.; Blackwell, H. E., Characterization of structural elements in native autoinducing peptides and non-native analogues that permit the differential modulation of AgrC-type quorum sensing receptors in *Staphylococcus aureus*. *Org. Biomol. Chem.* **2016**, *14* (1), 113-21.
47. Kong, K. F.; Vuong, C.; Otto, M., Staphylococcus quorum sensing in biofilm formation and infection. *Int. J. Med. Microbiol.* **2006**, *296* (2-3), 133-9.
48. Cheung, G. Y.; Joo, H. S.; Chatterjee, S. S.; Otto, M., Phenol-soluble modulins--critical determinants of staphylococcal virulence. *FEMS Microbiol. Rev.* **2014**, *38* (4), 698-719.
49. Le, K. Y.; Villaruz, A. E.; Zheng, Y.; He, L.; Fisher, E. L.; Nguyen, T. H.; Ho, T. V.; Yeh, A. J.; Joo, H. S.; Cheung, G. Y. C.; Otto, M., Role of Phenol-Soluble Modulins in *Staphylococcus epidermidis* Biofilm Formation and Infection of Indwelling Medical Devices. *J. Mol. Biol.* **2019**, *431* (16), 3015-3027.
50. Yao, Y.; Sturdevant, D. E.; Otto, M., Genomewide analysis of gene expression in *Staphylococcus epidermidis* biofilms: insights into the pathophysiology of *S. epidermidis* biofilms and the role of phenol-soluble modulins in formation of biofilms. *J. Infect. Dis.* **2005**, *191* (2), 289-98.
51. Mehlin, C.; Headley, C. M.; Klebanoff, S. J., An inflammatory polypeptide complex from *Staphylococcus epidermidis*: isolation and characterization. *J. Exp. Med.* **1999**, *189* (6), 907-18.

Chapter 5:
Sustained Release of a Synthetic Autoinducing Peptide Mimetic
Strongly Attenuates MRSA Infections *In Vivo*

Contributions: K. H. J. West designed and conducted the experiments. C. G. Gahan fabricated PLG microparticles and assisted with experimental design, compound sequestration with ApoB, and materials characterization. K. H. J. West and C. G. Gahan wrote the chapter together. D. F. Calderon and P. R. Kierski assisted with murine infection models. C. J. Czuprynski and J. F. McNulty assisted with experimental design of murine infection models. D. M. Lynn and H. E. Blackwell guided research and assisted in writing.

Abstract



There is significant and growing interest in the development of approaches to the treatment of bacterial infections that have the potential to block virulence without creating selective pressures that lead to antimicrobial resistance. Quorum sensing (QS) regulates key virulence behaviors in many common bacterial pathogens. Here, we report the development of an 'anti-virulence' strategy that exploits the activity of potent synthetic inhibitors of *S. aureus agr*-type QS. We identify peptide-based inhibitors of QS that are resistant to sequestration or degradation by components of murine tissue, and demonstrate that encapsulation of a lead inhibitor in degradable polymer microparticles substantially inhibits *agr*-based QS *in vitro* over at least seven days. Using a murine dermonecrosis abscess model, we demonstrate that this synthetic inhibitor attenuates methicillin-resistant *S. aureus* (MRSA) infections *in vivo*, and that our controlled release strategy significantly improved outcomes compared to mice that received a single-dose bolus administration of the inhibitor. Our results present an effective and potentially modular approach to controlling bacterial virulence *in vivo* by providing new tools for addressing connections between bacterial QS and infection, and could help guide the development of new approaches to target QS inhibition as a therapeutic strategy.

5.1 Introduction

Hospital-acquired infections present a sustained and increasingly critical health threat. *Staphylococcus aureus*, an opportunistic Gram-positive pathogen, currently causes over 100,000 hospital-acquired infections per year in the US alone, with nearly 20,000 of those infections becoming fatal.¹ A major barrier to combating *S. aureus* infections is the emergence of widespread resistance to conventional antibiotics, with strains such as the persistent and hardy methicillin-resistant *S. aureus* (MRSA) plaguing healthcare systems worldwide.²⁻⁴ This emerging antibiotic crisis has motivated researchers to explore alternative, non-biocidal approaches to treat and clear bacterial infections. So-called 'anti-virulence' strategies are of particular interest in this context, as they aim to reduce the severity of an infection without killing the infective organism. By doing so, they reduce selective pressures that ultimately lead to resistance and potentially allow a host's immune response to naturally clear the infection.⁵⁻⁷

Quorum sensing (QS) is a cell-cell communication system used by bacteria that relies on the production and reception of chemical signals.⁸ Because many human pathogens use QS to regulate the production of virulence factors that lead to or further sustain infections, QS presents an attractive target for the development of new anti-virulence approaches.⁸⁻¹⁰ QS in *S. aureus* and other related Gram-positive bacteria is governed by the accessory gene regulator (*agr*) QS system, which utilizes an autoinducing peptide (AIP) as its signaling molecule. The *agr* system is now widely understood to be a major regulator of virulence in *S. aureus*, controlling biofilm formation and the production of hemolysins and toxic shock syndrome toxin, among many other virulence factors.¹¹⁻¹³ In recent years, chemical inhibition of the *agr* system

has proven effective in attenuating *S. aureus* virulence phenotypes in bacterial cultures.¹⁴⁻¹⁸ Several reports have demonstrated that *agr*-based QS can be strongly antagonized by a range of synthetic small-molecules,^{15, 17, 19} natural products (or their derivatives),²⁰⁻²⁵ and macromolecular agents.²⁶⁻²⁸ To date, peptide-based *agr* inhibitors represent the most potent and efficacious QS blockers known in *S. aureus*.^{12, 14, 18, 29-30}

The ability of certain *agr* inhibitors to attenuate *S. aureus* infections *in vivo* has been investigated in past studies using murine models. As an example, co-injection of non-cognate native AIPs with *S. aureus* has been reported to inhibit *agr* activity in an abscess model by competing with the cognate AIP during infection, preventing *agr* activation and thereby reducing abscess formation.³¹⁻³² These results are exciting in view of the well characterized cross-activity between many *agr* systems and non-cognate AIPs.^{13, 18, 33} However, native AIPs have short half-lives *in vivo* (~ 4 hours)³¹ and are susceptible to interference with or sequestration by host proteins.^{26-27, 34} Small-molecule^{15, 19} and natural product-based²⁰⁻²² *agr* inhibitors can also attenuate *S. aureus* infection *in vivo*; however, the lower potencies of these agents often requires larger quantities of compound to be administered (e.g., on the order of micrograms per animal), and the mechanisms by which some of these inhibitors function is not yet well understood.²⁰⁻²¹ Many important questions remain to be answered before inhibition of the *agr* system can be deployed *in vivo* as an effective anti-virulence strategy. For example, while inhibition of *agr* blocks the production of toxins and exoproducts that are part of acute *S. aureus* infections,^{14, 35} inhibition of *agr* has also been shown to induce biofilm formation (a growth state common in chronic infections) in a limited set of *in vivo* studies.³⁶⁻³⁷ In addition, many of the most potent synthetic QS modulators are thioester-

linked peptide macrocycles^{14, 18, 29} that, like their native AIP counterparts, have short half-lives, low solubilities in biologically-relevant media, and are prone to sequestration or degradation by serum proteins.^{26-27, 34}

In this study, we report the identification of a stable and exceptionally potent synthetic peptide-based inhibitor of the *agr* system that attenuates *S. aureus* infections in a murine dermonecrosis abscess model. We first identified synthetic QS inhibitors that are resistant to interference by host tissue sequestration and degradation using an initial *ex vivo* screen, and then investigated the ability of a lead compound to attenuate *S. aureus* infection *in vivo*. Our results demonstrate that this inhibitor can substantially reduce the severity of infection, and that delivery of this inhibitor using degradable polymers can prolong release and significantly improve infection outcomes relative to mice receiving a single bolus administration of the inhibitor. The results of this proof-of-concept study present an effective and potentially modular anti-virulence approach to controlling bacterial infections *in vivo* in a well-studied wound model. In a broader context, this work also provides new and useful chemical/material tools that could be used to address fundamental connections between QS and *S. aureus* infection. With further development, this effort could provide a pathway toward new approaches that target QS as a therapeutic strategy.

5.2 Results and Discussion

5.2.1 *Ex vivo* screening reveals two stable and highly potent synthetic inhibitors of *agr*

We began our studies by focusing on a set of six synthetic peptide-based inhibitors of the *S. aureus agr* system on which we reported previously (Figure 5.1).^{14, 38-}

³⁹ This family of inhibitors comprises thioester- and amide-containing full or tail-truncated (tr) structural mimics of native AIP signals used by *S. aureus*, all of which are highly potent and efficacious at blocking *agr* activity, as measured in cell-based reporter gene assays and QS phenotypic assays (i.e., hemolysin and other toxin production). None of the compounds investigated in this study affect *S. aureus* growth at concentrations up to 10 μM .

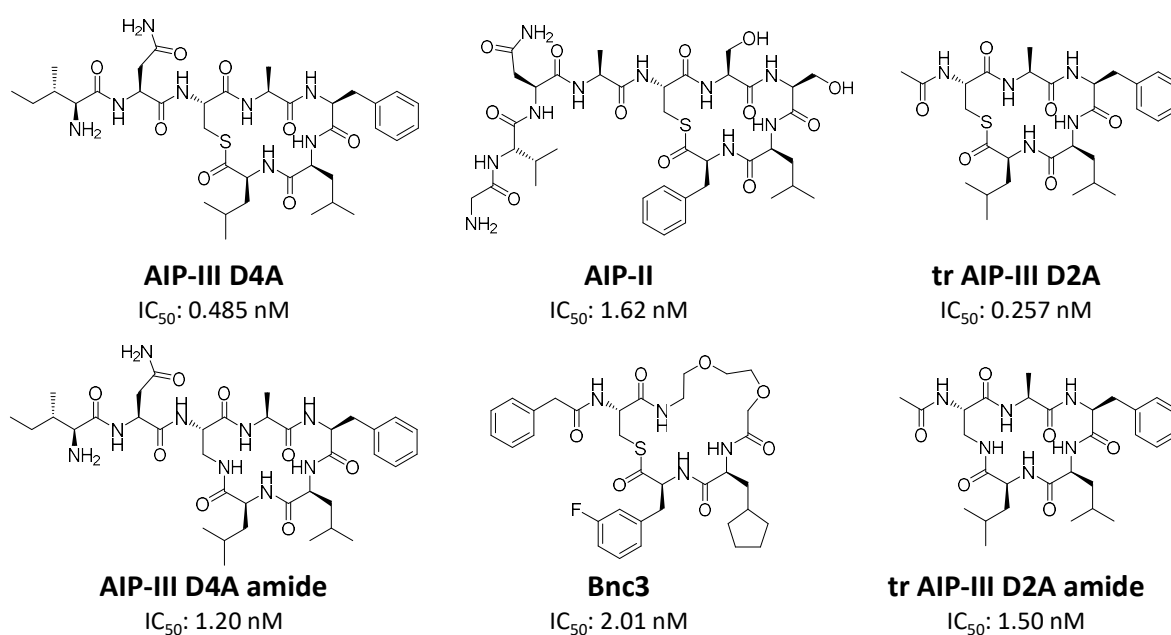


Figure 5.1 Chemical structures and potency values for QS inhibitors evaluated in this study. Potency values are from previous reports (see references 14 and 38-39) and were determined by dose-dependent inhibition of compounds in cell-based reporter assays in wild-type *S. aureus* (group-I).

A series of exploratory experiments with one of our most potent inhibitors (AIP-III D4A; Figure 5.1) showed only a limited benefit on wound healing in a murine open-wound model of *S. aureus* infection, even at relatively high concentrations (e.g., at 10 μM ; >20,000-fold above the IC₅₀ of this compound in culture).¹⁴ We considered the

possibility that this disappointing outcome could result from inactivation of this inhibitor *in vivo*. Prior reports revealed native AIPs to be relatively short-lived *in vivo* (as highlighted above),³¹ likely due to sequestration by proteins in serum (e.g., apolipoprotein B; ApoB)^{26-27, 34} or other proteins that can degrade native AIP signals. We therefore developed an *ex vivo* assay (Figure 5.S1) to evaluate this inhibitor in the presence of murine tissue samples (~6 mm in diameter; 1 mm thick; acquired via a tissue punch of C57BL/6-type mouse epidermis; see Methods). AIP-III D4A was incubated in the presence of tissue punches at 4.85 μ M in PBS for 24 hours. Portions of the supernatant were removed over time, diluted 100-fold, and added to a *S. aureus agr* fluorescence reporter strain to measure inhibitor activity (see Methods). This reporter strain produces native AIP at wild-type levels, activating the *agr* system at quorate cell densities and inducing expression of yellow fluorescent protein (YFP). The level of YFP fluorescence thus serves as a proxy for *agr* activity, and the efficacy of added inhibitors can be measured by reductions in fluorescence.

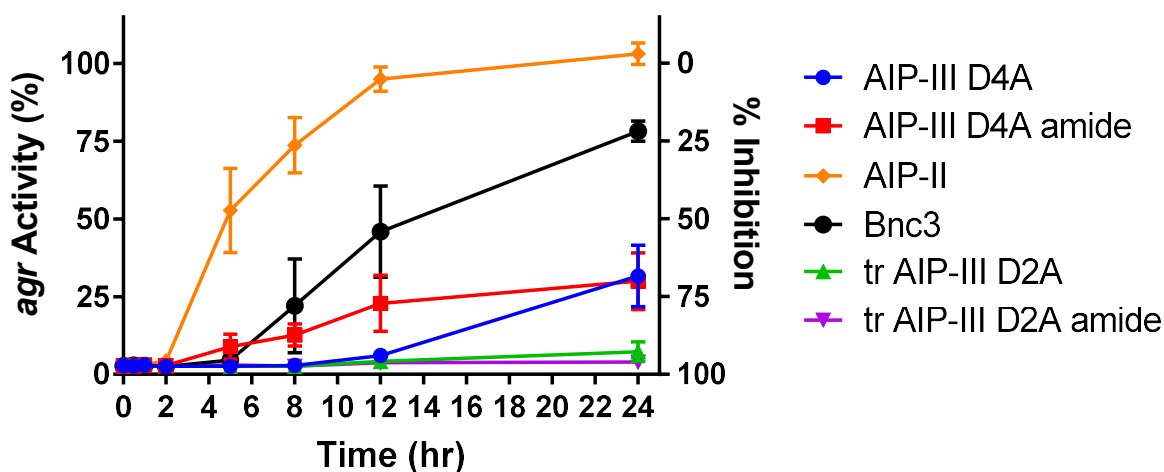


Figure 5.2 Time course of *S. aureus agr* activity for compounds incubated with mouse tissue. *agr* activity measured using a fluorescent reporter assay. The values shown are the average and SEM of three (n=3) independent *ex vivo* experiments. Some error bars are obscured due to the size of the data point.

We found that AIP-III D4A was no longer capable of fully inhibiting *S. aureus agr* activity (Figure 5.2, blue line) after 24 hours of *ex vivo* incubation with mouse tissue, even at the relatively high concentration used in this experiment (~10,000-fold its IC_{50}). The roughly 25% loss of *agr* inhibition at 24 hours corresponds to approximately 150 nM of free and active compound remaining in solution (as determined from a previous dose-response assay).¹⁴ This substantial reduction represents an ~95% loss of active compound. We have previously shown that AIPs in general are modestly stable to thioester hydrolysis in PBS (~20% hydrolysis after 24 hours).³⁸ A control study performed with AIP-III D4A in the absence of mouse tissue revealed no loss of inhibitory activity in 24 hr (Figure 5.S2). Taken together, these results suggest that AIP-III D4A is degraded or sequestered by components of mouse tissue. Subsequent experiments demonstrated that this loss of activity could be prevented by heat treating the tissue sample at 80 °C for 15 min prior to the addition of AIP-III D4A (Figure 5.S3; see

Methods), suggesting that loss of activity likely involves a tissue protein or other component that is rendered irreversibly non-functional by heat.

We used this *ex vivo* assay to identify synthetic inhibitors that were stable to components of murine skin tissue. The results of a screen of all six inhibitors shown in Figure 5.1 at concentrations 10,000-fold above their respective IC_{50} values is illustrated in Figure 5.2. Inspection of these results reveals several useful structure-function relationships. AIP-II (a native *S. aureus* AIP; orange curve) and Bnc3 (a synthetic peptidomimetic based on AIP-II; black curve)³⁹ lost nearly all antagonistic activity within 24 hours, far exceeding the 25% loss in inhibitory activity observed for the synthetic AIP-III mimic, AIP-III D4A. AIP-III D4A amide (red curve),³⁸ an analog of AIP-III D4A in which the thioester is replaced with a more hydrolytically-stable amide linkage, exhibited a loss of activity that was similar in magnitude to that of AIP-III D4A (blue curve). This result suggests that the loss of activity of AIP-III D4A in the experiments above was not a result of accelerated thioester hydrolysis. In stark contrast to these results, tr AIP-III D2A¹⁴ (green curve) and tr AIP-III D2A amide (purple curve),³⁸ which are truncated (tr) versions of AIP-III D4A in which the exocyclic tail is replaced with acetyl group, retained essentially full activity after 24 hours of incubation with murine tissue.

The reason for the surprisingly high retention of activity by these truncated compounds is unclear; however, we note that the absence of the two amino acid tail and the lack of a free amine terminus alter the polarity, amphipathic nature, and solution-phase conformation of these compounds,⁴⁰ which could substantially impact interactions with proteins present in skin tissue. Additional experiments in which AIP-III D4A and tr AIP-III D2A were incubated with ApoB—an apolipoprotein commonly found

in skin and blood⁴¹⁻⁴² that was reported to bind to and sequester AIPs²⁶⁻²⁷—provided additional support for this view. When we incubated AIP-III D4A with ApoB for three hours, we observed a significant (~80%) decrease in AIP-III D4A recovered by analytical HPLC (Figure 5.S4A). In contrast, we observed essentially no loss of tr AIP-III D2A when it was incubated with ApoB under identical conditions (Figure 5.S4B). Although additional experiments will be required to more fully understand the basis for the increased stability of these truncated compounds, this *ex vivo* screen identified two surprisingly stable and potent candidates for further evaluation *in vivo*. We selected tr AIP-III D2A for use in all subsequent studies described below on the basis of its greater potency in culture (IC₅₀ = 0.257 nM; Figure 5.1).

5.2.2 *Bolus delivery of tr AIP-III D2A substantially reduces abscess formation in a murine dermonecrosis model*

We next evaluated the ability of tr AIP-III D2A to attenuate *S. aureus* infection using a murine dermonecrosis abscess model.⁴³ This model and related infection models have been used in past studies to characterize the role of *agr* activity in *S. aureus* infections using *agr* mutant strains,^{15-16, 21} non-cognate native AIPs,^{16, 31-32} and small-molecule chemical tools that inhibit *S. aureus* QS.^{15, 20-21} In this model, lesion development is evaluated over time by imaging the animals on predetermined days and measuring the areas of visible lesions. To validate this model in our hands, we first compared abscess formation in mice inoculated with a common lab *S. aureus* strain or with a mutant (Δagr) lacking a functional *agr* system (see Methods). We observed significantly larger abscesses to develop in mice inoculated with the wild-type strain

than in mice inoculated with the Δagr strain (Figure 5.S5). This result is comparable to previous reports indicating that the absence of *agr* activity attenuates infection.^{15-16, 21, 31} We then co-injected 1.5 μ g of tr AIP-III D2A or a vehicle control solution (DMSO with no inhibitor) and a culture of USA300 LAC MRSA and monitored infection over the course of a week using the murine abscess model. The total molar amount of compound injected in these experiments was either similar to or less than amounts used to evaluate other QS inhibitors *in vivo* in past studies.^{15-16, 21} Lesions were imaged 1, 3, 5, and 7 days after inoculation, and representative images of mice in treated groups and untreated vehicle control groups are shown in Figure 5.3A. Treatment with tr AIP-III D2A significantly reduced the sizes of lesions on each day relative to vehicle controls (Figure 5.3B), with only half of the inhibitor-treated mice showing visible lesions seven days after infection, as opposed to 90% of the vehicle control group (see SI for pictures of the abscesses of all mice in this study on day 7). These results indicate that bolus administration of tr AIP-III D2A can substantially diminish the severity of *S. aureus* infections in this mouse model. These results constitute the first demonstration of inhibitory activity *in vivo* using this class of synthetic *agr* inhibitors based on native AIP-III, and are consistent with *agr* inhibition as the likely cause for attenuation.

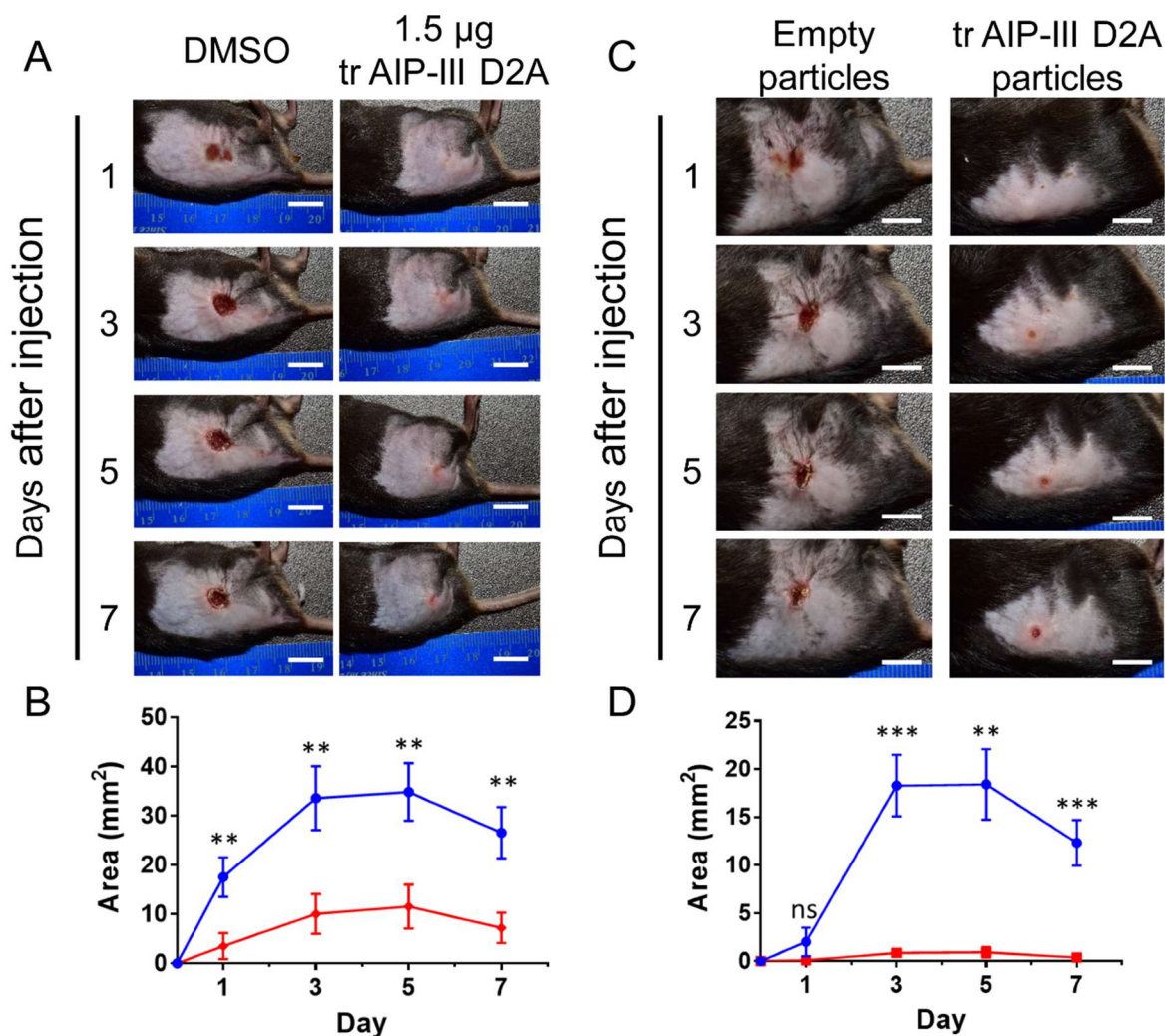


Figure 5.3 Abscess attenuation due to tr AIP-III D2A delivered as a bolus in solution (A–B) or delivered in 1 mg of PLG microparticles (C–D). (A) Representative images for the DMSO vehicle and compound-treated groups. (B) Average abscess size with SEM for vehicle group (blue line, n=10) and compound-treated group (red line, n=10). (C) Representative images for groups treated with empty, non-loaded microparticles and compound-loaded microparticles. (D) Average abscess size with SEM for empty microparticle group (blue line, n=9) and compound-loaded particle group (red line, n=10). Statistical analysis with Mann-Whitney test, **p < 0.01, ***p < 0.001.

5.2.3 tr AIP-III D2A attenuates infection when released from PLG microparticles

We conducted additional experiments to investigate the ability of tr AIP-III D2A to inhibit *S. aureus* infections in this model when loaded into degradable polymer

microparticles. For these studies, we adapted a previously reported electrospaying protocol⁴⁴ to fabricate pseudo-spherical microparticles of PLG (lactide:glycolide (50:50); 30–60 kDa; see Methods), with diameters of $1.48 (\pm 0.38) \mu\text{m}$ (as characterized by SEM; see Figure 5.4A and Figure 5.S6) that were sized appropriately to fit through the 25 gauge needles used in our *in vivo* experiments. These microparticles were measured to contain $0.71 (\pm 0.14)$ nmol of peptide/mg polymer as determined using analytical HPLC (see Methods and Figure 5.S7), or approximately 21% of the maximum theoretical loading of peptide using this fabrication approach. These particles released approximately 22 pmol of tr AIP-III D2A per mg of particle into solution over 21 days when incubated in PBS, with a large burst release over the first 24 hours (Figure 5.4B; as determined using a biological reporter assay; see Methods, Equations 5.S1–5.S2, and the SI for additional information related to these experiments). We estimate this amount to correspond to less than 1% of the total loaded peptide, suggesting that these particle formulations could be used to promote release over much longer time periods than those evaluated here.

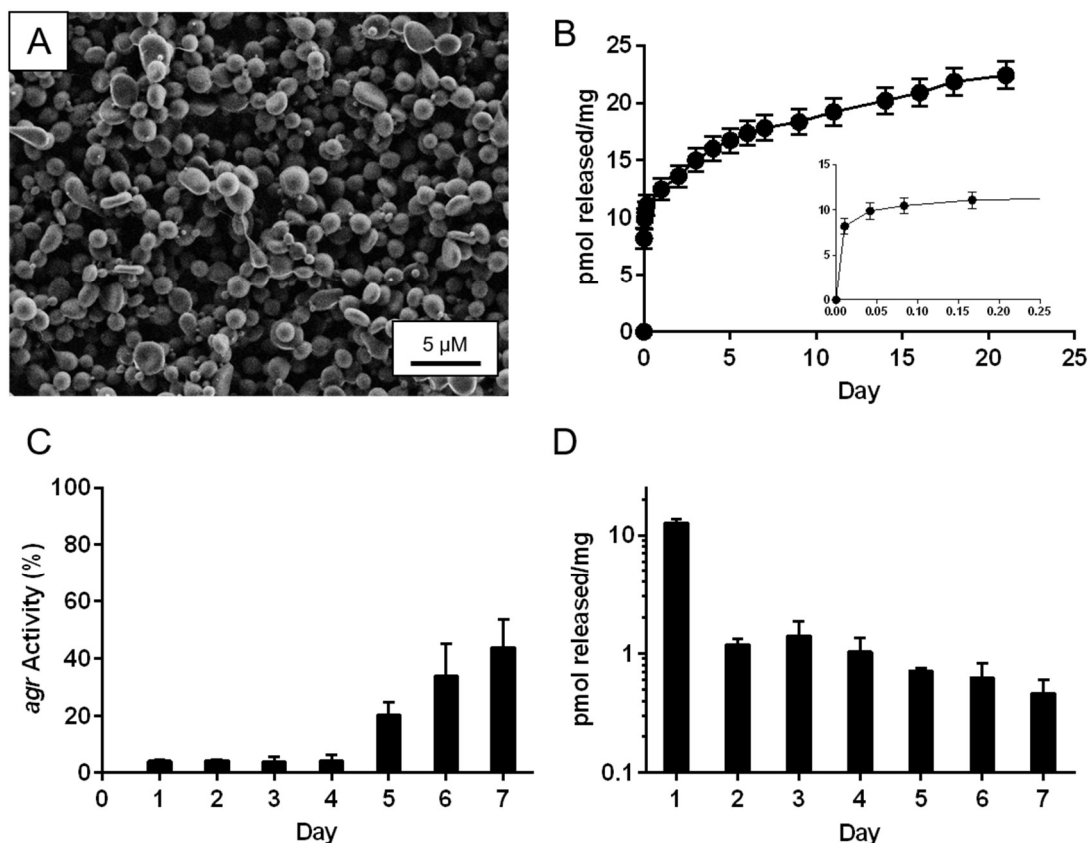


Figure 5.4 Characterization of PLG microparticles loaded with tr AIP-III D2A. (A) Top-down SEM images of tr AIP-III D2A-loaded PLG microparticles fabricated by electrospinning. (B) The normalized cumulative release of tr AIP-III D2A from the PLG microparticles over three weeks. (C) The *agr* activity of the *S. aureus* reporter incubated with undiluted aliquots acquired each day from the release experiments. (D) The normalized release of tr AIP-III D2A from the PLG microparticles each day. The values shown in (B–D) are the average and single standard deviation for three ($n=3$) independent release experiments.

Characterization of released inhibitor using our *S. aureus* fluorescent *agr* reporter strain (see Methods and Figure 5.S8) revealed that (i) tr AIP-III D2A retained its biological activity upon release from PLG and (ii) sufficient amounts were released for each of the first four days to fully inhibit *agr* activity. Amounts released in each subsequent 24-hour time period did not completely inhibit *agr* activity, but substantial inhibition was observed out to day 7 under the conditions evaluated here (Figure 5.4C–

5.4D, Figure 5.S9). We note that it should be straightforward to further modify and optimize the loading and release profiles of these particles by adjusting the chemical and physical properties of PLG and/or process parameters used to fabricate the particles.⁴⁵⁻⁴⁸ The sizes, loadings, and release profiles of the particles reported here were sufficient for all subsequent proof-of-concept experiments in mice described below.

Using the mouse abscess model, we co-injected *S. aureus* culture and either (i) 1 mg of tr AIP-III D2A-loaded microparticles (~720 ng of inhibitor total) or (ii) 1 mg of unloaded (no inhibitor) microparticles into mice. Representative images from these experiments are shown in Figure 5.3C. We observed lesions that were significantly smaller for the inhibitor-loaded particle group, as compared to the empty particle group on every day other than day 1 (Figure 5.3D). Comparing the final abscess sizes on day 7, only a single mouse out of 10 from the inhibitor-loaded particle-treated group had an observable lesion (2.89 mm²). In contrast, nearly 80% of the mice in the control group (no inhibitor) had lesions with an average size of 15.8 mm² (see SI for images of the abscesses of all mice in this study on day 7). We conclude on the basis of these results that the polymer microparticles release tr AIP-III D2A in a form that remains biologically active *in vivo*, and that this controlled release strategy yields a concentration profile at the site of infection over a seven-day period that is sufficient to inhibit bacterial virulence at levels comparable to, if not better than, those observed in the single-dose, bolus administration *in vivo* experiments described above.

The results shown in Figure 5.3 not only demonstrate that tr AIP-III D2A can provide significant protection against *S. aureus* infection, but also suggest that well

understood advantages of strategies for the localized and controlled release of active agents used in other scenarios⁴⁹⁻⁵¹ can provide additional practical benefits in this context. Specifically, we note that the amount of compound released over the course of 7 days in the microparticle-treated mice in the experiments above (Figure 5.3C) is approximately 100-fold less than the amount that was administered in the single-dose, bolus administration experiment (Figure 5.3A). This outcome is further consistent with the well-established ability of controlled release approaches to substantially improve therapeutic outcomes at reduced loadings of active agent.⁴⁹⁻⁵¹

To obtain a side-by-side comparison of the efficacies of a single-dose, bolus administration of tr AIP-III D2A to the microparticle formulation when the total amounts of inhibitor estimated to be available at the infection site were comparable, we performed a final series of *in vivo* experiments. On the basis of the release profile shown in Figure 5.4B, we estimate 18 pmol (11 ng) of tr AIP-III D2A to be released from 1 mg of particles over 7 days. We therefore compared the efficacy of our inhibitor-loaded particles directly to an approximately similar amount of inhibitor (25 pmol, or 15 ng) administered as a single-dose, bolus injection. As shown in Figure 5.5, a single bolus dose of tr AIP-III D2A did not attenuate *S. aureus* infection at any time point as compared to control mice ($p > 0.05$; Kruskal-Wallis test). In contrast, the tr AIP-III D2A-loaded microparticles substantially reduced abscess size at each time point ($p < 0.05$ for day 5, $p < 0.01$ for days 1, 3, and 7; Kruskal-Wallis test), consistent with the results of the experiments above (Figure 5.3C–5.3D). This result strongly underscores potential benefits arising from the sustained release of inhibitor in preventing abscess formation by *S. aureus*. We attribute the superior performance of the controlled release

formulation to its ability to sustain effective locally high concentrations of inhibitor in the immediate vicinity of the infection site. Conversely, the bolus administration of soluble inhibitor can rapidly drain or diffuse away from the injection site, reducing the local concentration of inhibitor below what is needed to reduce the severity of infection.

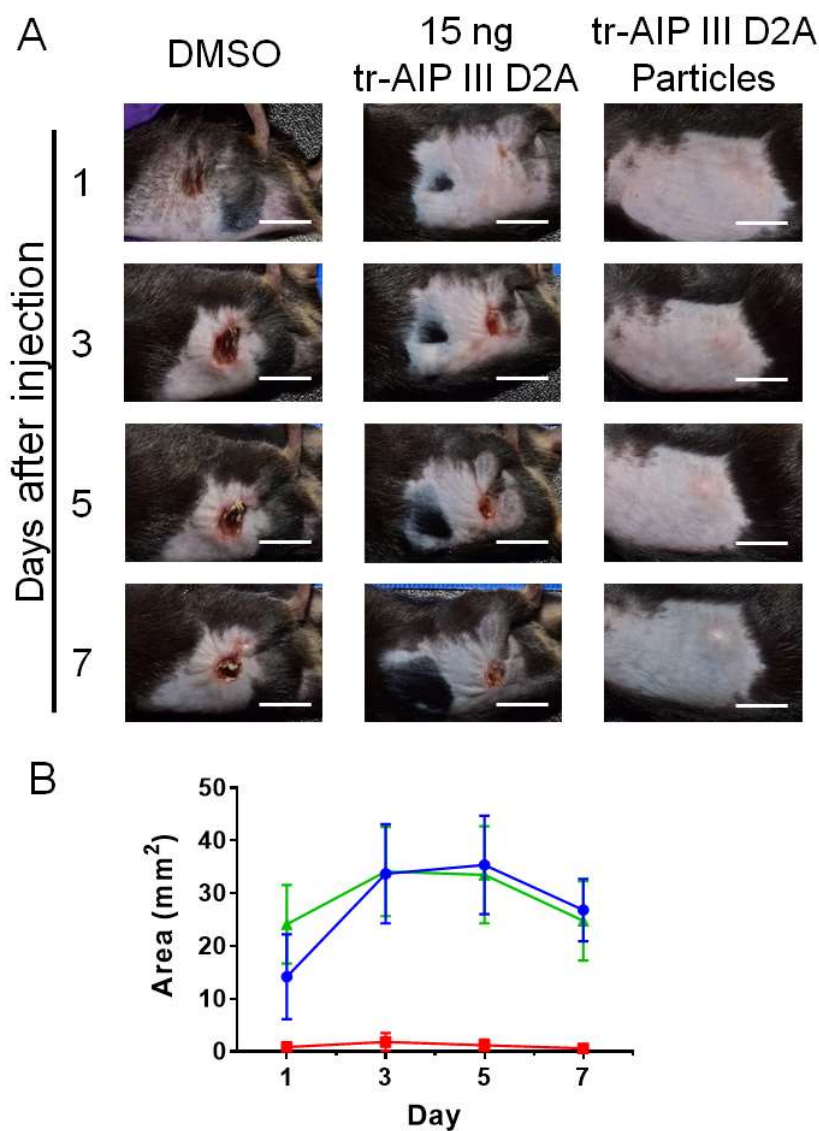


Figure 5.5 Side-by-side comparison of abscess formation after treatment with tr AIP-III D2A in solution vs PLG microparticles. (A) Representative images from mice treated with vehicle, a solution of compound, or compound loaded in microparticles. (B) Average abscess size with SEM of mice treated with vehicle (green, n=8), 15 ng of tr AIP-III D2A in solution (blue line, n=8), or with 1 mg of microparticles (red line, n=8). Data analyzed with Kruskal-Wallis test.

5.3 Summary and Conclusions

Our results demonstrate (i) the ability of a potent truncated synthetic peptide inhibitor of *S. aureus* QS to attenuate bacterial virulence *in vivo* and (ii) an efficacious controlled release strategy for reducing bacterial infection using this anti-virulence approach. These results were enabled by the *ex vivo* screening of *S. aureus agr*-inhibitors to identify compounds resistant to inactivation by components present in mouse tissue. We identified a lead compound, tr AIP-III D2A, that nearly completely blocks MRSA infection in a mouse dermonecrosis abscess model following a single-dose bolus administration of inhibitor, or by injection of polymer microparticles that sustain the local release of active inhibitor at the infection site. Our results demonstrate significantly greater efficacy using the polymer microparticle approach, underscoring the potential strategic value of using sustained-release strategies for the administration of QS inhibitors and the development of new anti-virulence approaches to combat bacterial infections *in vivo*.

The results of this study are important for several reasons. First, we demonstrate the ability of a lead *agr* inhibitor—one of the most potent known inhibitors of *S. aureus* QS in culture—to strongly block bacterial infection *in vivo*. Second, our results reveal tail truncation of two AIP-derived mimetics to be an effective strategy to eliminate interference by host tissue, in sharp contrast to inhibition of similar native AIPs and their close analogs. This observation underpins the efficacy and potency of these compounds *in vivo* and provides guidance that will prove useful for the design and discovery of new inhibitors suitable for use *in vivo*. Third, our results demonstrate that controlled release strategies can improve the therapeutic potential of these truncated

inhibitors and reduce to nanograms the total amount of compound required to attenuate infection *in vivo*. Notably, these findings represent more than an order of magnitude improvement compared to previous *in vivo* analyses that required the administration of microgram quantities of less-potent *agr* inhibitors for efficacy in similar infection models.^{15, 20-22, 31} Past studies have investigated strategies for the encapsulation of bacterial QS inhibitors into materials and the testing of these approaches *in vitro* and *ex vivo*.⁵²⁻⁵⁸ The results of this current study represent, to our knowledge, the first report of the successful application of a controlled release QS inhibition strategy to abate bacterial infection *in vivo*.

More broadly, the discovery of stable and highly potent inhibitors and the identification of strategies that enable controlled release and local availability of these agents during infection provide powerful tools, alone or in combination, to address a range of important fundamental questions. These include the role of *agr* QS in long-term chronic infections or the emergence of spontaneous QS mutants commonly isolated from patients with such infections.^{5, 35, 59} These tools also provide a foundation for the development of new types of materials (e.g., surface coatings) that could more effectively attenuate bacterial virulence in or around implantable or indwelling medical devices, or on other commercial surfaces on which *S. aureus* colonization and infections are endemic. Looking beyond *S. aureus*, the approach reported here should also be readily applicable to other combinations of QS inhibitors and polymers, significantly expanding the utility of chemical methods to explore and modulate QS pathways and outcomes, and thus has implications for new therapeutic interventions.

5.4 Materials and Methods

5.4.1 Reagents, strains, and general methods

Poly (DL-lactide-co-glycolide) (PLG; lactide:glycolide, 50:50; 30–60 kDa), *N,N*-dimethylformamide (DMF), tetrahydrofuran (THF), and dimethylsulphoxide (DMSO) were purchased from Sigma-Aldrich and used as received. Phosphate-buffered saline (PBS, 10x solution) was purchased from Dot Scientific and diluted 10x into water and titrated to pH 7.4 before use. Deionization of distilled water was performed using a Milli-Q system, yielding 18.2 M Ω water. The USA300 LAC MRSA strain AH1677⁶⁰ was used for reporter assays and general *in vivo* dermonecrosis assays. The *S. aureus* wild-type lab strain RN6390B⁶¹ and the Δagr RN9222⁶² strain were used only to examine *agr* dependence for abscess formation in the dermonecrosis model. All strains were cultured with brain heart infusion (BHI, Teknova) medium and incubated at 37 °C with shaking at 200 rpm, with AH1677 cultures supplemented with 10 μ g/mL chloramphenicol.

No unexpected or unusually high safety hazards were encountered in the course on this work.

5.4.2 Instrumentation and related considerations

Top-down scanning electron micrographs were acquired using a LEO-1550 VP field-emission SEM operated with an accelerating voltage of 1.0 kV. Microparticle diameters were measured using ImageJ version 1.52a software. Solution fluorescence and absorbance in bacterial cultures was measured using a BioTek Synergy 2 plate reader using Gen5 software. RP-HPLC was performed on a Shimadzu system with a

SCL-10Avp controller, a DGU-20A5 degasser, a LC-20AT solvent delivery unit, a SIL-10AF autosampler, a CO-20A column oven with a manual injector, a SPD-M20A UV-Vis diode array detector, and analytical Kromasil Eternity C18 column (4.6 mm by 250 mm, with a 5 mm particle size and 100 Å pore size). Solvent A was water with 0.1% trifluoroacetic acid and solvent B was acetonitrile with 0.1% trifluoroacetic acid. A linear gradient was used to analyze peptides and solutions, beginning at 10% solvent B and ramping to 95% solvent B over 27 min at a flow rate of 1 mL/min.

5.4.3 *Fluorescence-based bacterial reporter assay*

Compound activity screening was performed as previously described using *S. aureus* AH1677.³⁹ GraphPad Prism 7 was used for statistical analysis of the resulting data. Supernatants from microparticle release experiments were subjected to this reporter assay with the following modifications: supernatant was serially diluted into PBS, and 20 µL aliquots of each dilution were transferred to a black 96-well microtiter plate and incubated with 180 µL of bacterial culture. Each plate contained additional controls for data processing: a PBS control (20 µL) and a tr AIP-III D2A control (100 nM final concentration, 2 µL of 10 µM tr AIP-III D2A stock solution in DMSO and 18 µl PBS).

5.4.4 *Ex vivo tissue sequestration assay*

In 1.5 mL microcentrifuge tubes, 1 mM DMSO stock solutions of compounds were diluted in PBS to 10,000x their respective IC₅₀ values in a total volume of 500 µL, along with a PBS control without any compound. A mouse tissue sample was bath sonicated for 5 minutes (and, if appropriate, incubated at 80 °C for 15 min then cooled

in ice bath for 5 min) and transferred into each microcentrifuge tube. The tubes were vortexed, and 10 μ L aliquots were stored in a chemical resistant microtiter plate in a -20 $^{\circ}$ C freezer. The microcentrifuge tubes were incubated at 37 $^{\circ}$ C with shaking at 200 rpm until the next time point was reached, at which point the tubes were removed, vortexed, and additional 10 μ L aliquots were taken. This process was repeated for all the time points. After the final time point, 2 μ L of each aliquot, or a 1:10 dilution of each aliquot, was transferred to a black 96-well microtiter plate and tested using the fluorescence reporter assay detailed above.

5.4.5 Fabrication of tr AIP-III D2A-loaded PLG microparticles

A 0.8 mM solution of tr AIP-III D2A in DMF was diluted with THF to produce a THF:DMF solvent system (3:1, v/v) resulting in a final tr AIP-III D2A concentration of 0.2 mM. A 60 mg/mL solution of PLG in THF:DMF (3:1, v/v) was prepared and allowed to stir until the polymer was dissolved. Electro-spraying of the microparticles was conducted on a custom-built electro-spraying device with a digital syringe pump (Harvard Bioscience Co.) at a flow rate of 1.0 mL/hr. A 15 cm working distance separated a blunt 20G needle and the 10 x 10 cm grounded aluminum foil sample collector. The produced microparticles were harvested from the surface of the aluminum foil using an eyelash applicator brush, followed by immersion of the brush in water and sonicating to create a microparticle suspension. The suspension was then lyophilized to produce dry microparticles.

5.4.6 *Characterization of peptide loading of PLG microparticles*

Microparticles were dissolved in DMSO (20 mg/mL) and then precipitated into water by mixing 100 μ L of the DMSO solution into 900 μ L of water. The suspension was centrifuged at 5,000 g for 5 min, and the resulting supernatant was analyzed by analytical RP-HPLC to determine the amount of peptide in the microparticles.

5.4.7 *Characterization of peptide-loaded PLG microparticle release profiles*

PLG microparticles (10 mg) were immersed in 1 mL of PBS. The particles were sonicated to suspend them in solution and allowed to incubate while rotating at room temperature. At predetermined time points, the microparticles were centrifuged at 5,000 g for 5 min and the supernatant was removed and replaced. Each supernatant sample was immediately frozen and stored at -20 °C until analysis. At time of analysis, supernatant samples were thawed and centrifuged at 16,000 g for 5 min to remove any solid polymer debris that may have been isolated with the supernatant. The concentrations of the peptides released at each timepoint were measured using the microparticle-modified bacterial reporter assay described above. After 21 days of incubation in buffer, the remaining polymer solids were characterized to determine the amount of unreleased peptide using the dissolution and analytical RP-HPLC method described above.

5.4.8 *Murine abscess infection model*

The infection assay protocol was modified from that of Sully *et al.*¹⁵ Briefly, cultures of the appropriate *S. aureus* strain were grown overnight in BHI medium and

diluted in sterile PBS to an OD₆₀₀ corresponding to 2×10^8 CFU/mL. For experiments on peptide in solution, DMSO (1%, control) or peptide in DMSO solution (50 μ M or 500 nM) were added to 2×10^8 CFU/mL culture to reach an appropriate desired concentration. For PLG microparticle experiments, 2×10^8 CFU/mL culture was added to lyophilized microparticle tubes to reach a concentration of 20 mg/mL particles. Cultures were vortexed to mix and then 50 μ L were injected subcutaneously into the shaved flank of age- and sex-matched C57BL/6 mice. Body weight was recorded at time of injection and monitored over the course of the experiment. Images of lesions were taken on days 1, 3, 5, and 7, and analyzed using ImageJ to determine lesion area. GraphPad Prism 7 was used to obtain statistical information about the abscess sizes. All experimental protocols were approved by the Institutional Animal Care and Use Committee at UW–Madison and conformed to the NIH Guide for the Care and Use of Laboratory Animals, 8th edition (2011).

5.5 Supporting Information

5.5.1 Additional experiments and figures related to *in vitro* and *ex vivo* compound analysis

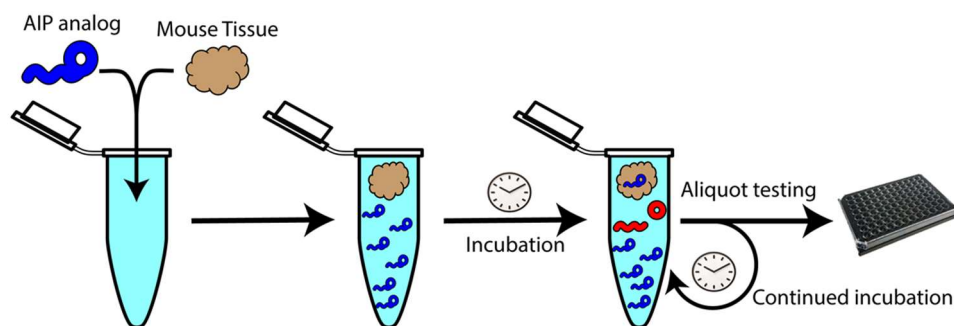


Figure 5.S1 A schematic of *ex vivo* experimental system to examine compound activity incubated at 10,000-fold IC_{50} in presence of mouse tissue.

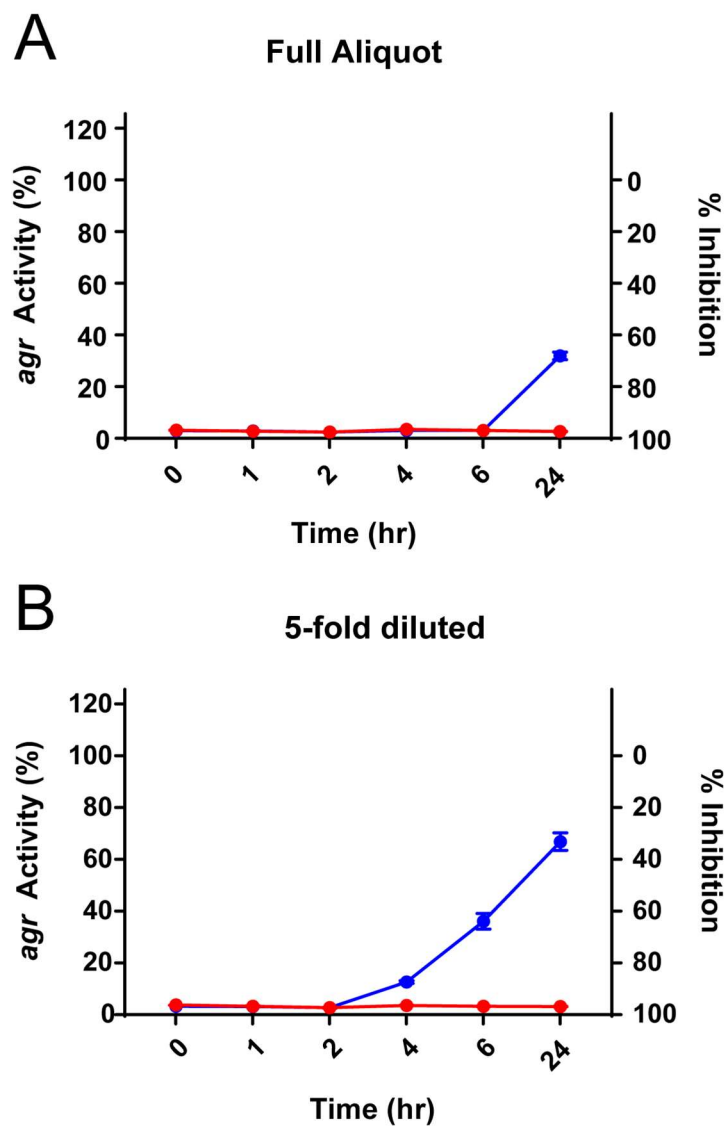


Figure 5.S2 Activity of *S. aureus agr-I* fluorescence reporter strain when exposed to supernatant of AIP-III D4A incubated in PBS in the presence (blue line) or absence (red line) of mouse tissue sample. Both a full aliquot (A) and a 5-fold dilution (B) were assayed. The values shown are the average and SEM of three (n=3) technical replicates. Some error bars are obscured due to the size of the data point.

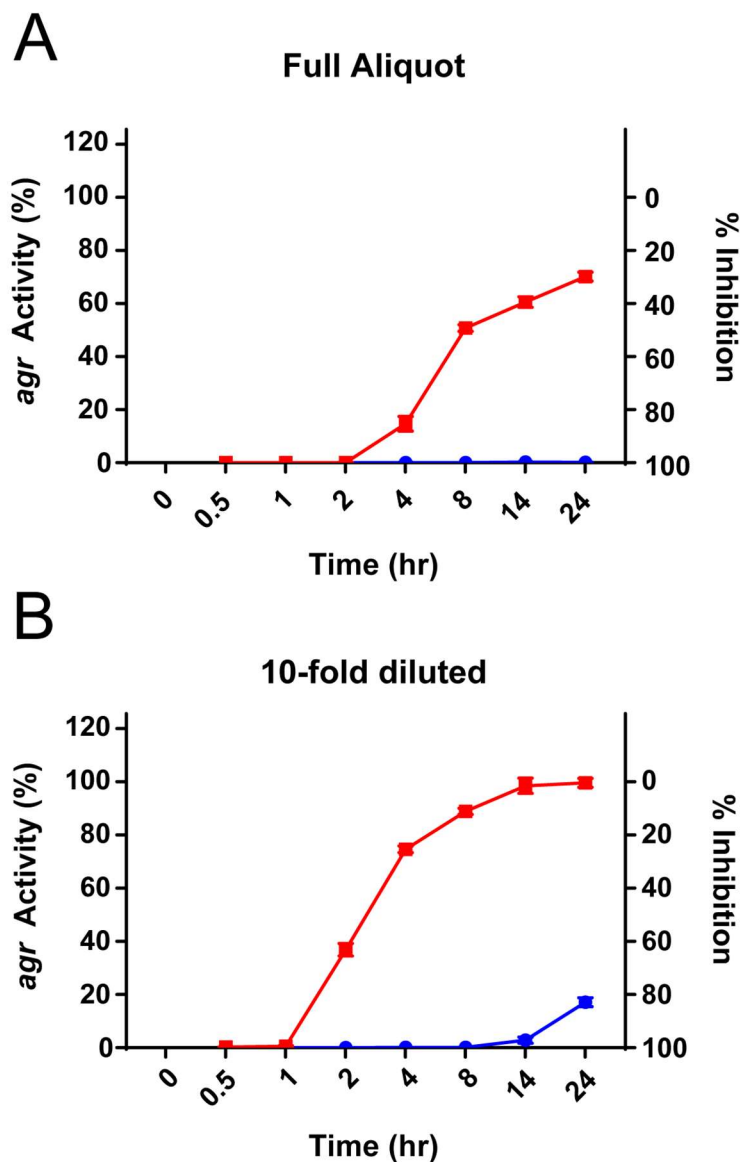


Figure 5.S3 Activity of AIP-III D4A in *S. aureus* *agr-I* fluorescent reporter strain when exposed to either heat denatured mouse tissue (blue) or a control tissue (red). Both a full aliquot (A) and a 10-fold dilution (B) were assayed. The values shown are the average and SEM of three (n=3) technical replicates. Some error bars are obscured due to the size of the data point.

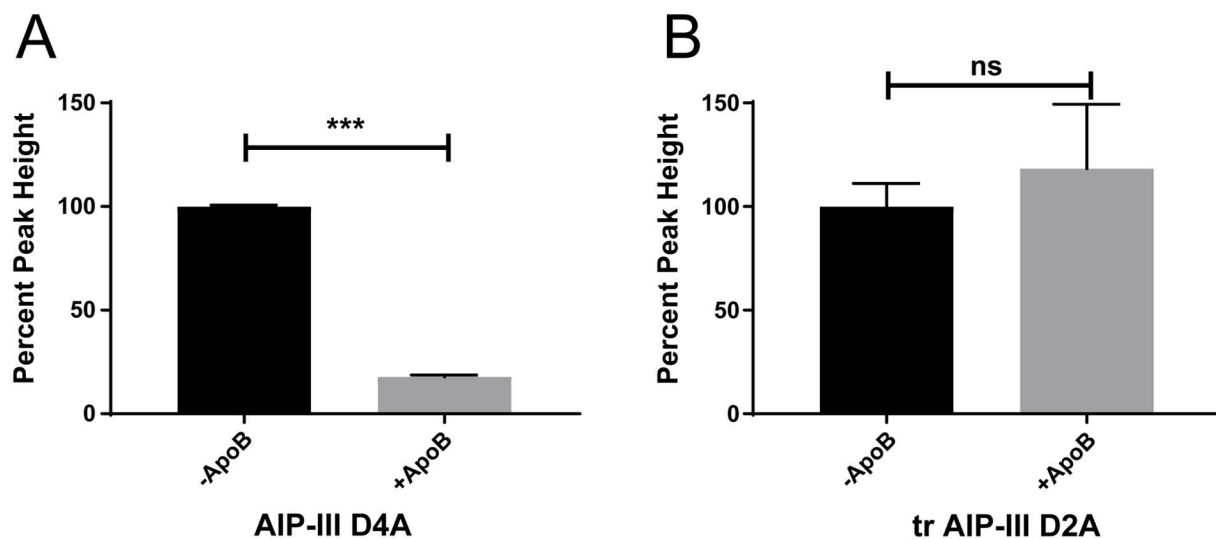


Figure 5.S4 Examination of interactions of AIP-III D4A and tr AIP-III D2A with ApoB as analyzed via analytical RP-HPLC. The peak for AIP-III D4A (A) was substantially reduced (***, $p < 0.001$, unpaired t-test) in the presence of ApoB, while there was no significant effect on the peak corresponding to tr AIP-III D2A (B) in the presence of ApoB. Peak heights were normalized to the average peak height of controls lacking ApoB. Analytical RP-HPLC analysis performed in duplicate ($n=2$). Data represented as mean and SEM.

5.5.2 Mouse abscess data for wild-type *S. aureus* lab strain and Δagr strain

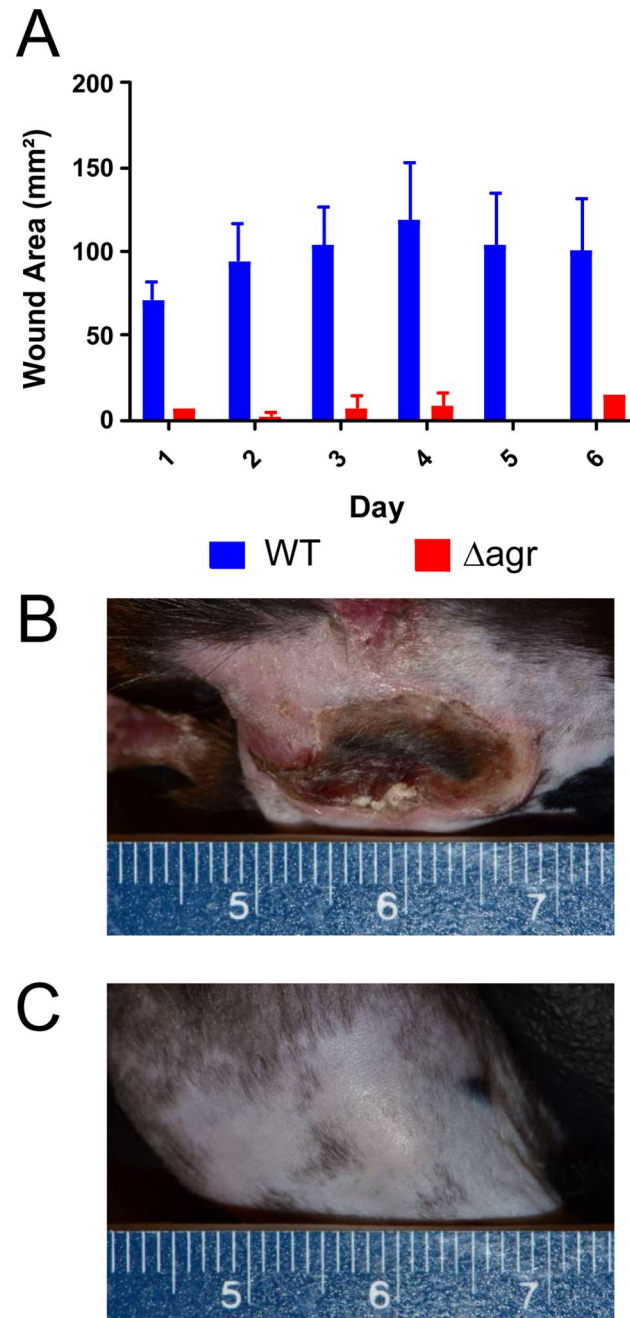


Figure 5.S5 Infection abscess analysis of mice inoculated with wild-type and Δagr *S. aureus*. (A) Observed abscess size for mice receiving either a wild-type strain of *S. aureus* (RN6390B, n=6) or an Δagr mutant of this strain (RN9222, n=6). Values shown represent averages and SEM. Representative image of mice from (B) wild-type infected group and (C) Δagr infected group. Ruler indicates centimeters.

5.5.3 Additional microparticle characterization

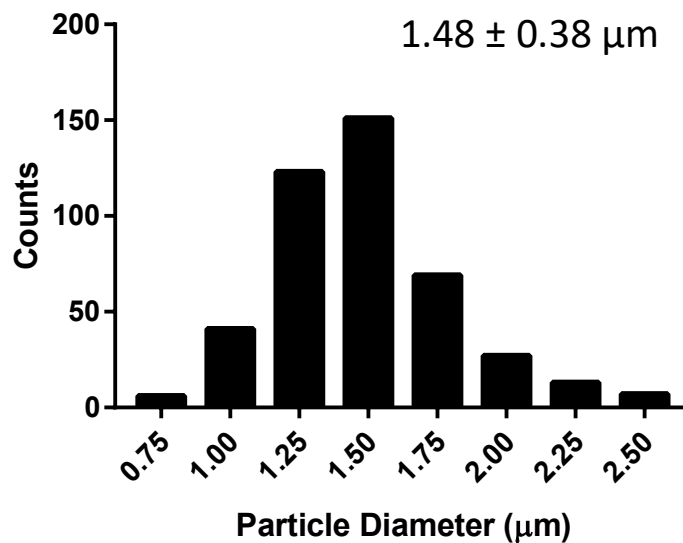


Figure 5.S6 PLG microparticle size histogram as measured by SEM. The average particle diameter was $1.48 \pm 0.38 \mu\text{m}$. Particle diameters measured by the minor axis of elliptically-shaped particles. The histogram shows measurements for (n=450) microparticles (150 particles were counted from three independent samples).

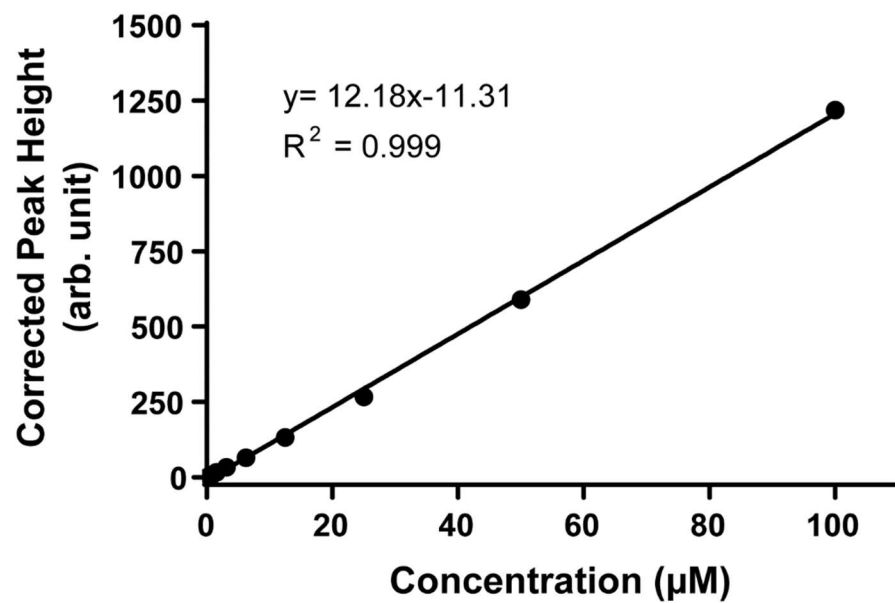


Figure 5.S7 HPLC standard curve for tr-AIP III D2A. Serially diluted tr AIP-III D2A was analyzed by RP-HPLC to determine relationship between peak height and concentration.

Discussion of peptide quantification.

We utilized Equation 5.S1, the four-parameter logistic regression model, to model the dose-response activity of our inhibitory compounds in *S. aureus agr* reporter assays. By rearranging the variables into Equation 5.S2, using the observed activity level of samples with unknown concentrations in our reporter assays we can then estimate the concentration of the compound in samples from our other assays (i.e., compound release from microparticles). Activity values between 20–80% were used to estimate compound concentration.

- Y = *agr* activity level
- X = compound concentration in nanomolar
- T = Top (upper) plateau of activity in model
- B = Bottom (lower) plateau of activity in model
- H = Hill slope
- IC₅₀ = Inhibitory Concentration at 50% activity

Equation 5.S1 Four-parameter logistic regression model

$$Y = B + \frac{T - B}{1 + \left(\frac{X}{IC_{50}}\right)^H}$$

Equation 5.S2 Equation to determine compound concentration from *agr* activity

$$X = IC_{50} \left(\frac{T - B}{Y - B} - 1 \right)^{1/H}$$

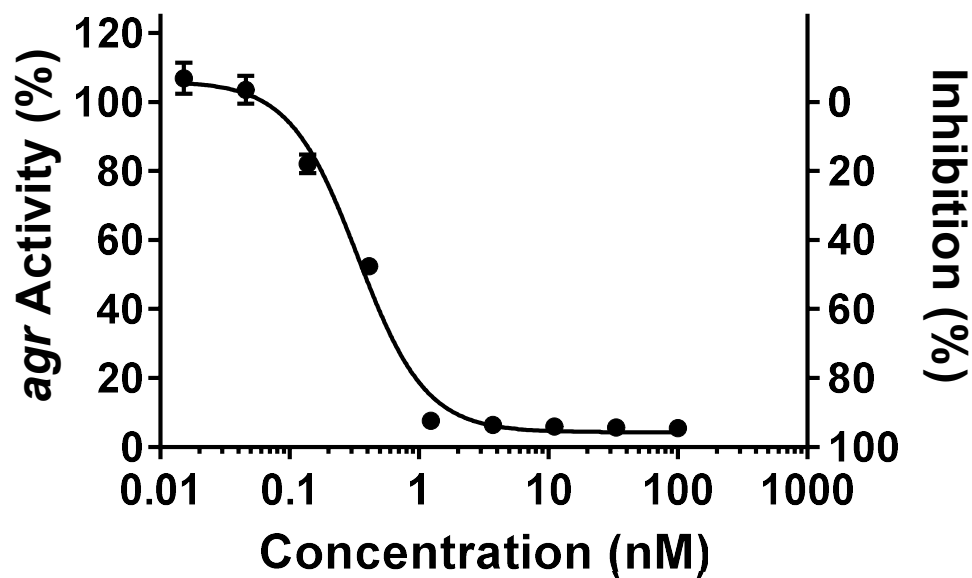


Figure 5.S8 Dose-response inhibition curve for tr AIP-III D2A. Assay performed by following the microparticle-modified *S. aureus agr* fluorescence reporter assay. The values shown are the average and SEM of three (n=3) independent technical and biological replicates. The following parameters were observed for this dose response analysis: $T=106.1$, $B=4.293$, $IC_{50}=0.3353$, $H=1.648$. These values were used in Equation 5.S2 to quantify concentration of compound released in microparticle characterization experiments.

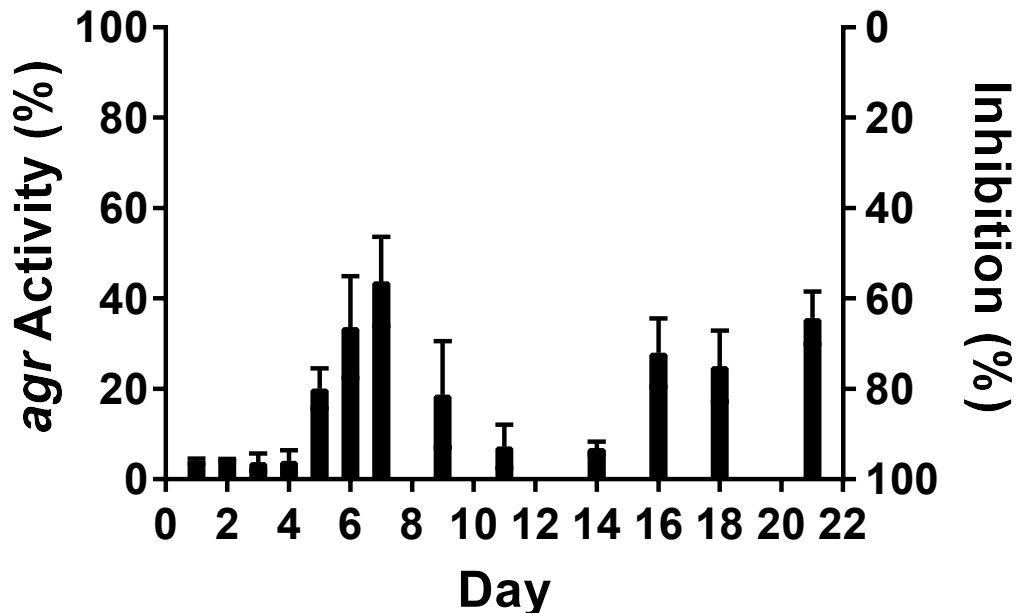
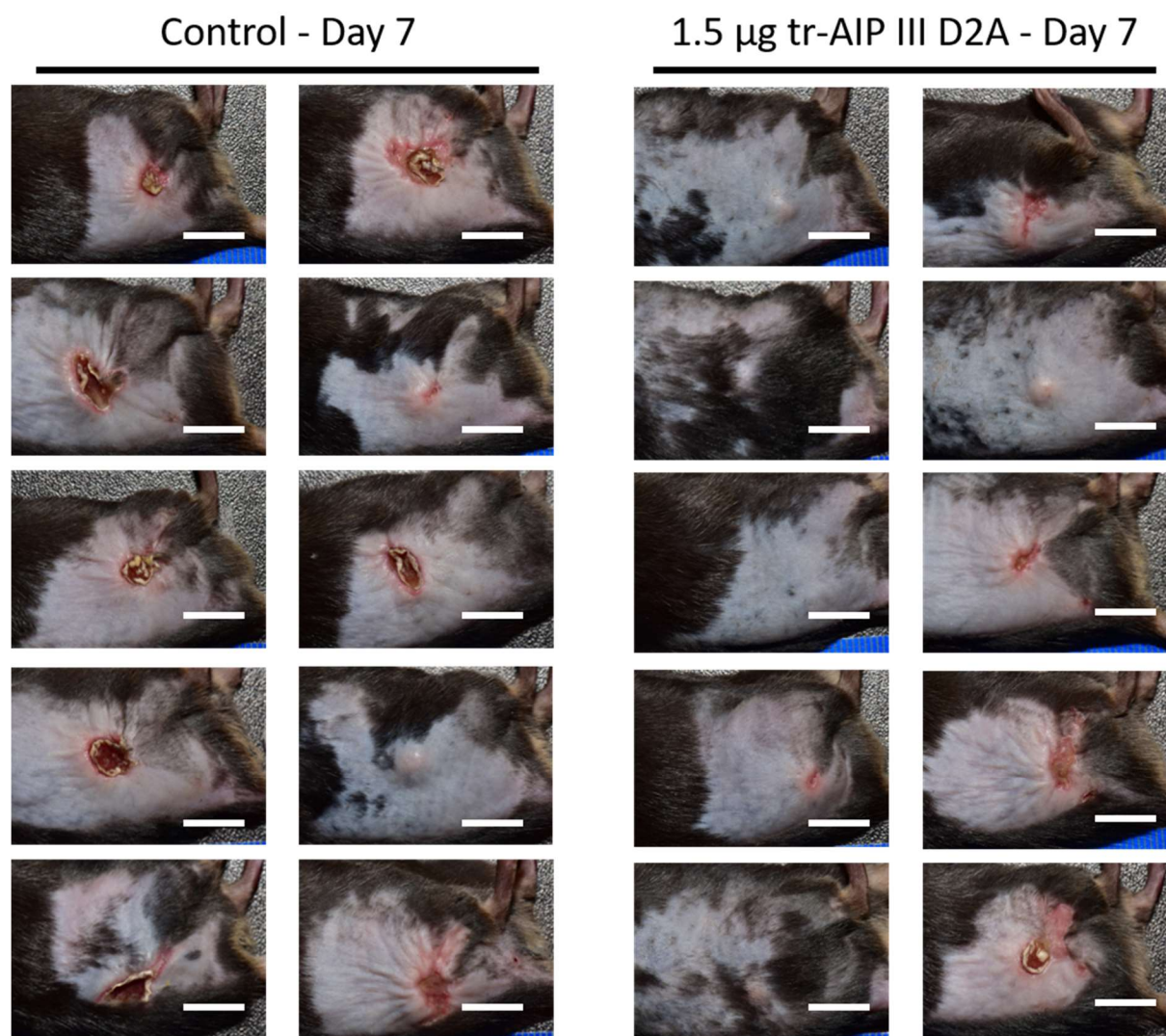


Figure 5.S9 Activity of supernatants isolated over time in release experiments from tr AIP-III D2A loaded PLG microparticles. Compound activity measured using the *S. aureus agr-I* fluorescence reporter. Supernatants were diluted 10-fold into reporter strain culture for each timepoint. The values shown are the average and single standard deviation of three (n=3) independent technical and material replicates.

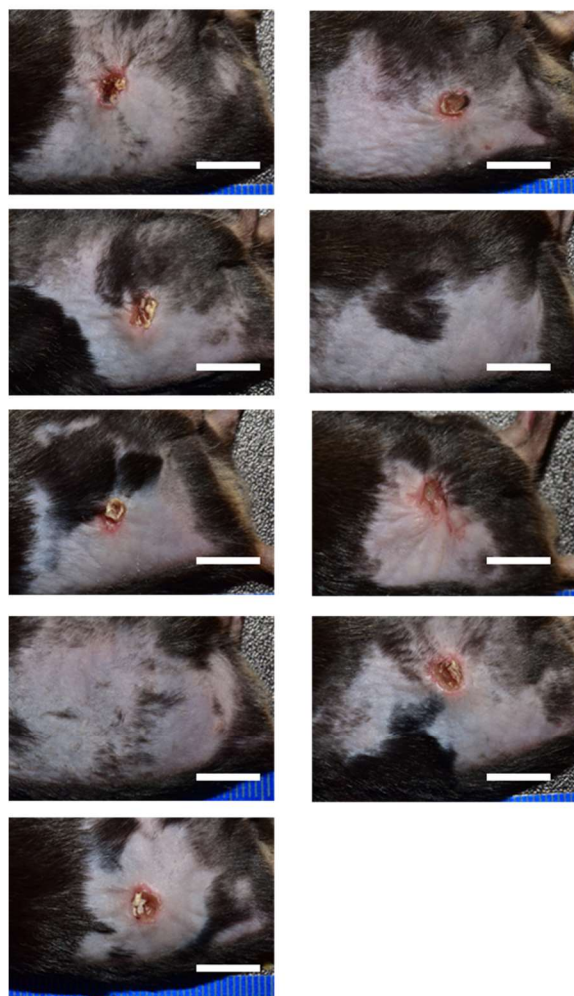
5.5.4 Images of all Day 7 lesions from mice in abscess experiments

1.5 μg tr AIP-III D2A vs. DMSO vehicle control experiment (white bar = 1 cm):

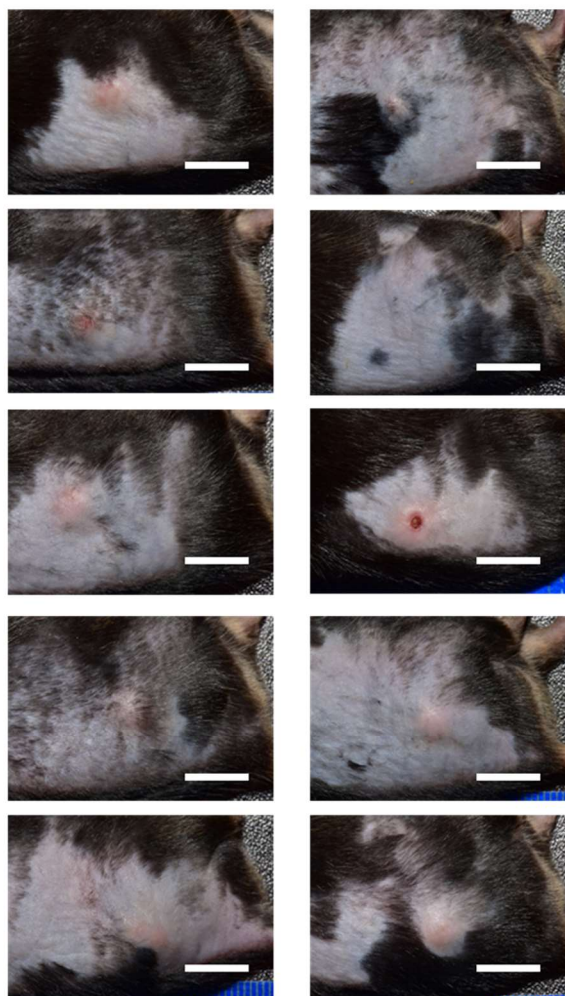


1 mg tr AIP-III D2A particles vs. empty PLG particles experiment (white bar = 1 cm):

Unloaded Microparticles - Day 7

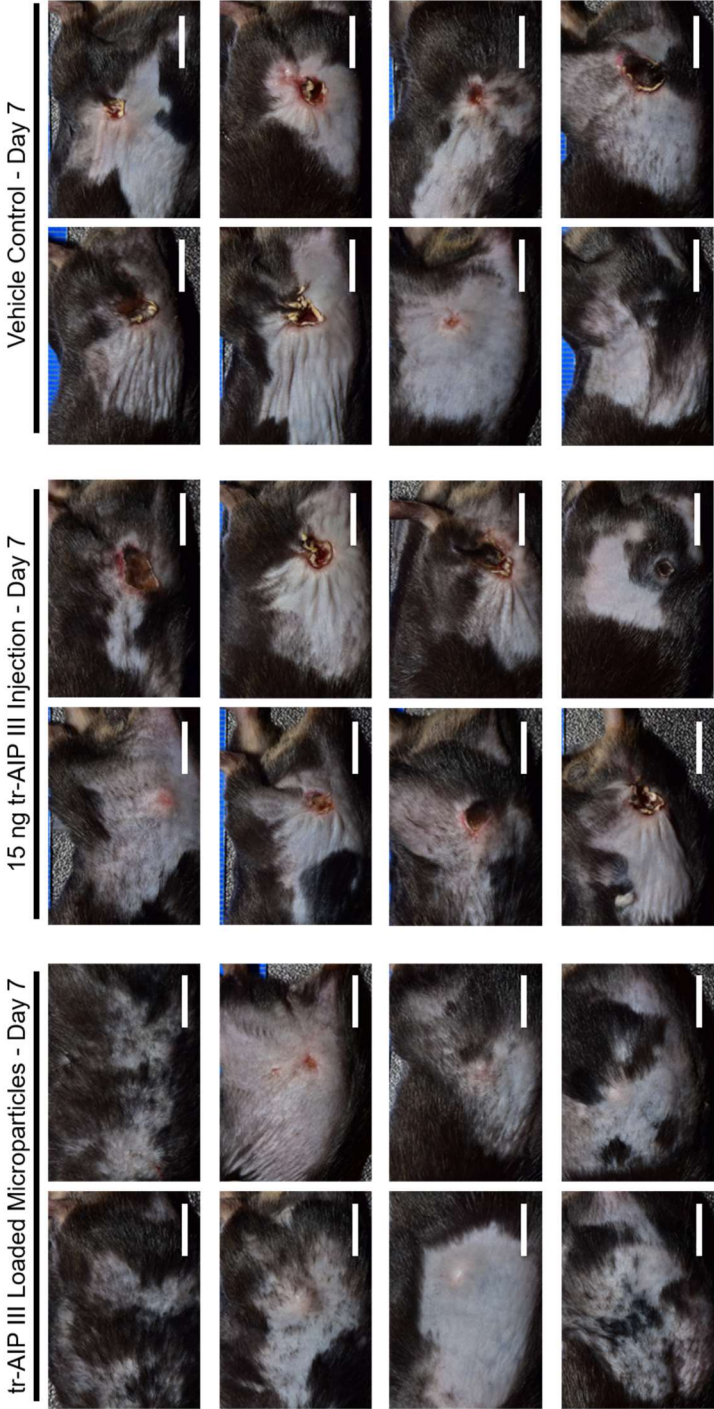


tr-AIP III Loaded Microparticles - Day 7



1 mg tr AIP-III D2A particles vs. 15 ng tr AIP-III D2A vs. DMSO vehicle experiment

(white bar = 1 cm):



5.6 Acknowledgements

Financial support for this work was provided by the NIH (R21 AI135745), the Wisconsin Alumni Research Foundation (WARF) UW2020 Program, and the NSF through a grant provided to the UW–Madison Materials Research Science and Engineering Center (MRSEC; DMR-1720415). The authors acknowledge the use of instrumentation supported by the NSF through the UW MRSEC (DMR-1720415). K. H. J. W. was supported in part by the UW–Madison NIH Chemistry–Biology Interface Training Program (T32 GM008505). C. G. G. was supported in part by a NSF Graduate Research Fellowship. J. F. M. and C. J. C. acknowledge the Walter and Martha Renk Endowed Laboratory for Food Safety and the UW–Madison Food Research Institute. We thank Prof. Alexander Horswill (University of Colorado Medical School) for *S. aureus* strains and Prof. Tom Turng (UW–Madison) for providing access to electrospraying instrumentation, and acknowledge support for those facilities provided by the Wisconsin Institutes of Discovery and the Vice Chancellor for Research and Graduate Education at UW–Madison. The table of contents graphic was created in part using BioRender.com.

5.7 References

1. Kourtis, A. P.; Hatfield, K.; Baggs, J.; Mu, Y.; See, I.; Epton, E.; Nadle, J.; Kainer, M. A.; Dumyati, G.; Petit, S.; Ray, S. M.; Emerging Infections Program, M. a. g.; Ham, D.; Capers, C.; Ewing, H.; Coffin, N.; McDonald, L. C.; Jernigan, J.; Cardo, D., Vital Signs: Epidemiology and Recent Trends in Methicillin-Resistant and in Methicillin-Susceptible *Staphylococcus aureus* Bloodstream Infections - United States. *MMWR Morb. Mortal. Wkly. Rep.* **2019**, *68* (9), 214-219.
2. Tong, S. Y.; Davis, J. S.; Eichenberger, E.; Holland, T. L.; Fowler, V. G., Jr., *Staphylococcus aureus* infections: epidemiology, pathophysiology, clinical manifestations, and management. *Clin. Microbiol. Rev.* **2015**, *28* (3), 603-61.
3. David, M. Z.; Daum, R. S., Community-associated methicillin-resistant *Staphylococcus aureus*: epidemiology and clinical consequences of an emerging epidemic. *Clin. Microbiol. Rev.* **2010**, *23* (3), 616-87.
4. Klein, E.; Smith, D. L.; Laxminarayan, R., Hospitalizations and deaths caused by methicillin-resistant *Staphylococcus aureus*, United States, 1999-2005. *Emerg. Infect. Dis.* **2007**, *13* (12), 1840-6.
5. Ford, C. A.; Hurford, I. M.; Cassat, J. E., Antivirulence Strategies for the Treatment of *Staphylococcus aureus* Infections: A Mini Review. *Front. Microbiol.* **2020**, *11*, 632706.
6. Dickey, S. W.; Cheung, G. Y. C.; Otto, M., Different drugs for bad bugs: antivirulence strategies in the age of antibiotic resistance. *Nat. Rev. Drug Discov.* **2017**, *16* (7), 457-471.
7. Allen, R. C.; Popat, R.; Diggle, S. P.; Brown, S. P., Targeting virulence: can we make evolution-proof drugs? *Nat. Rev. Microbiol.* **2014**, *12* (4), 300-8.
8. Whiteley, M.; Diggle, S. P.; Greenberg, E. P., Progress in and promise of bacterial quorum sensing research. *Nature* **2017**, *551* (7680), 313-320.
9. Azimi, S.; Klementiev, A. D.; Whiteley, M.; Diggle, S. P., Bacterial Quorum Sensing During Infection. *Annu. Rev. Microbiol.* **2020**, *74*, 201-219.
10. LaSarre, B.; Federle, M. J., Exploiting quorum sensing to confuse bacterial pathogens. *Microbiol. Mol. Biol. Rev.* **2013**, *77* (1), 73-111.
11. Novick, R. P.; Geisinger, E., Quorum Sensing in Staphylococci. *Annu. Rev. Genet.* **2008**, *42*, 541-64.

12. Wang, B.; Muir, T. W., Regulation of Virulence in *Staphylococcus aureus*: Molecular Mechanisms and Remaining Puzzles. *Cell Chem. Biol.* **2016**, *23* (2), 214-224.
13. Thoendel, M.; Kavanaugh, J. S.; Flack, C. E.; Horswill, A. R., Peptide Signaling in the Staphylococci. *Chem. Rev.* **2011**, *111* (1), 117-51.
14. Tal-Gan, Y.; Stacy, D. M.; Foegen, M. K.; Koenig, D. W.; Blackwell, H. E., Highly potent inhibitors of quorum sensing in *Staphylococcus aureus* revealed through a systematic synthetic study of the group-III autoinducing peptide. *J. Am. Chem. Soc.* **2013**, *135* (21), 7869-82.
15. Sully, E. K.; Malachowa, N.; Elmore, B. O.; Alexander, S. M.; Femling, J. K.; Gray, B. M.; DeLeo, F. R.; Otto, M.; Cheung, A. L.; Edwards, B. S.; Sklar, L. A.; Horswill, A. R.; Hall, P. R.; Gresham, H. D., Selective chemical inhibition of agr quorum sensing in *Staphylococcus aureus* promotes host defense with minimal impact on resistance. *PLoS Pathog.* **2014**, *10* (6), e1004174.
16. Mayville, P.; Ji, G.; Beavis, R.; Yang, H.; Goger, M.; Novick, R. P.; Muir, T. W., Structure-activity analysis of synthetic autoinducing thiolactone peptides from *Staphylococcus aureus* responsible for virulence. *Proc. Natl. Acad. Sci. U. S. A.* **1999**, *96* (4), 1218-23.
17. Salam, A. M.; Quave, C. L., Targeting Virulence in *Staphylococcus aureus* by Chemical Inhibition of the Accessory Gene Regulator System In Vivo. *mSphere* **2018**, *3* (1), e00500-17.
18. Horswill, A. R.; Gordon, C. P., Structure-Activity Relationship Studies of Small Molecule Modulators of the Staphylococcal Accessory Gene Regulator. *J. Med. Chem.* **2020**, *63* (6), 2705-2730.
19. Kuo, D.; Yu, G.; Hoch, W.; Gabay, D.; Long, L.; Ghannoum, M.; Nagy, N.; Harding, C. V.; Viswanathan, R.; Shoham, M., Novel quorum-quenching agents promote methicillin-resistant *Staphylococcus aureus* (MRSA) wound healing and sensitize MRSA to beta-lactam antibiotics. *Antimicrob. Agents Chemother.* **2015**, *59* (3), 1512-8.
20. Todd, D. A.; Parlet, C. P.; Crosby, H. A.; Malone, C. L.; Heilmann, K. P.; Horswill, A. R.; Cech, N. B., Signal Biosynthesis Inhibition with Ambuic Acid as a Strategy To Target Antibiotic-Resistant Infections. *Antimicrob. Agents Chemother.* **2017**, *61* (8), e00263-17.
21. Parlet, C. P.; Kavanaugh, J. S.; Crosby, H. A.; Raja, H. A.; El-Elimat, T.; Todd, D. A.; Pearce, C. J.; Cech, N. B.; Oberlies, N. H.; Horswill, A. R., Apicidin Attenuates MRSA Virulence through Quorum-Sensing Inhibition and Enhanced Host Defense. *Cell Rep.* **2019**, *27* (1), 187-198 e6.

22. Daly, S. M.; Elmore, B. O.; Kavanaugh, J. S.; Triplett, K. D.; Figueroa, M.; Raja, H. A.; El-Elmat, T.; Crosby, H. A.; Femling, J. K.; Cech, N. B.; Horswill, A. R.; Oberlies, N. H.; Hall, P. R., omega-Hydroxyemodin limits *Staphylococcus aureus* quorum sensing-mediated pathogenesis and inflammation. *Antimicrob. Agents Chemother.* **2015**, *59* (4), 2223-35.
23. Nielsen, A.; Mansson, M.; Bojer, M. S.; Gram, L.; Larsen, T. O.; Novick, R. P.; Frees, D.; Frokiaer, H.; Ingmer, H., Solonamide B inhibits quorum sensing and reduces *Staphylococcus aureus* mediated killing of human neutrophils. *PLoS One* **2014**, *9* (1), e84992.
24. Brango-Vanegas, J.; Martinho, L. A.; Bessa, L. J.; Vasconcelos, A. G.; Placido, A.; Pereira, A. L.; Leite, J.; Machado, A. H. L., Synthesis of novel sulfide-based cyclic peptidomimetic analogues to solonamides. *Beilstein J. Org. Chem.* **2019**, *15*, 2544-2551.
25. Piewngam, P.; Zheng, Y.; Nguyen, T. H.; Dickey, S. W.; Joo, H. S.; Villaruz, A. E.; Glose, K. A.; Fisher, E. L.; Hunt, R. L.; Li, B.; Chiou, J.; Pharkjaksu, S.; Khongthong, S.; Cheung, G. Y. C.; Kiratisin, P.; Otto, M., Pathogen elimination by probiotic *Bacillus* via signalling interference. *Nature* **2018**, *562* (7728), 532-537.
26. Peterson, M. M.; Mack, J. L.; Hall, P. R.; Alsup, A. A.; Alexander, S. M.; Sully, E. K.; Sawires, Y. S.; Cheung, A. L.; Otto, M.; Gresham, H. D., Apolipoprotein B Is an innate barrier against invasive *Staphylococcus aureus* infection. *Cell Host Microbe* **2008**, *4* (6), 555-66.
27. Elmore, B. O.; Triplett, K. D.; Hall, P. R., Apolipoprotein B48, the Structural Component of Chylomicrons, Is Sufficient to Antagonize *Staphylococcus aureus* Quorum-Sensing. *PLoS One* **2015**, *10* (5), e0125027.
28. Da, F.; Yao, L.; Su, Z.; Hou, Z.; Li, Z.; Xue, X.; Meng, J.; Luo, X., Antisense locked nucleic acids targeting *agrA* inhibit quorum sensing and pathogenesis of community-associated methicillin-resistant *Staphylococcus aureus*. *J. Appl. Microbiol.* **2017**, *122* (1), 257-267.
29. Lyon, G. J.; Wright, J. S.; Muir, T. W.; Novick, R. P., Key determinants of receptor activation in the *agr* autoinducing peptides of *Staphylococcus aureus*. *Biochemistry* **2002**, *41* (31), 10095-104.
30. Xie, Q.; Wiedmann, M. M.; Zhao, A.; Pagan, I. R.; Novick, R. P.; Suga, H.; Muir, T. W., Discovery of quorum quenchers targeting the membrane-embedded sensor domain of the *Staphylococcus aureus* receptor histidine kinase, AgrC. *Chem. Commun. (Camb.)* **2020**, *56* (76), 11223-11226.

31. Wright, J. S., 3rd; Jin, R.; Novick, R. P., Transient interference with staphylococcal quorum sensing blocks abscess formation. *Proc. Natl. Acad. Sci. U. S. A.* **2005**, *102* (5), 1691-6.
32. Brown, M. M.; Kwiecinski, J. M.; Cruz, L. M.; Shahbandi, A.; Todd, D. A.; Cech, N. B.; Horswill, A. R., Novel Peptide from Commensal *Staphylococcus simulans* Blocks Methicillin-Resistant *Staphylococcus aureus* Quorum Sensing and Protects Host Skin from Damage. *Antimicrob. Agents Chemother.* **2020**, *64* (6), e00172-20.
33. Ji, G.; Beavis, R.; Novick, R. P., Bacterial interference caused by autoinducing peptide variants. *Science* **1997**, *276* (5321), 2027-30.
34. Yarwood, J. M.; McCormick, J. K.; Paustian, M. L.; Kapur, V.; Schlievert, P. M., Repression of the *Staphylococcus aureus* accessory gene regulator in serum and *in vivo*. *J. Bacteriol.* **2002**, *184* (4), 1095-101.
35. Cheung, G. Y. C.; Bae, J. S.; Otto, M., Pathogenicity and virulence of *Staphylococcus aureus*. *Virulence* **2021**, *12* (1), 547-569.
36. Schilcher, K.; Horswill, A. R., Staphylococcal Biofilm Development: Structure, Regulation, and Treatment Strategies. *Microbiol. Mol. Biol. Rev.* **2020**, *84* (3).
37. Le, K. Y.; Dastgheyb, S.; Ho, T. V.; Otto, M., Molecular determinants of staphylococcal biofilm dispersal and structuring. *Front. Cell. Infect. Microbiol.* **2014**, *4*, 167.
38. Tal-Gan, Y.; Ivancic, M.; Cornilescu, G.; Yang, T.; Blackwell, H. E., Highly Stable, Amide-Bridged Autoinducing Peptide Analogues that Strongly Inhibit the AgrC Quorum Sensing Receptor in *Staphylococcus aureus*. *Angew. Chem. Int. Ed. Engl.* **2016**, *55* (31), 8913-7.
39. Vasquez, J. K.; Blackwell, H. E., Simplified Autoinducing Peptide Mimetics with Single-Nanomolar Activity Against the *Staphylococcus aureus* AgrC Quorum Sensing Receptor. *ACS Infect. Dis.* **2019**, *5* (4), 484-492.
40. Tal-Gan, Y.; Ivancic, M.; Cornilescu, G.; Cornilescu, C. C.; Blackwell, H. E., Structural characterization of native autoinducing peptides and abiotic analogues reveals key features essential for activation and inhibition of an AgrC quorum sensing receptor in *Staphylococcus aureus*. *J. Am. Chem. Soc.* **2013**, *135* (49), 18436-44.
41. Mommaas, M.; Tada, J.; Ponec, M., Distribution of low-density lipoprotein receptors and apolipoprotein B on normal and on reconstructed human epidermis. *J. Dermatol. Sci.* **1991**, *2* (2), 97-105.

42. Feingold, K. R.; Elias, P. M.; Mao-Qiang, M.; Fartasch, M.; Zhang, S. H.; Maeda, N., Apolipoprotein E deficiency leads to cutaneous foam cell formation in mice. *J. Invest. Dermatol.* **1995**, *104* (2), 246-50.
43. Bunce, C.; Wheeler, L.; Reed, G.; Musser, J.; Barg, N., Murine Model of Cutaneous Infection with Gram-Positive Cocci. *Infect. Immun.* **1992**, *60* (7), 2636-2640.
44. Almeria, B.; Deng, W.; Fahmy, T. M.; Gomez, A., Controlling the morphology of electrospray-generated PLGA microparticles for drug delivery. *J. Colloid Interface Sci.* **2010**, *343* (1), 125-33.
45. Anderson, J. M.; Shive, M. S., Biodegradation and biocompatibility of PLA and PLGA microspheres. *Adv. Drug Deliv. Rev.* **1997**, *28* (1), 5-24.
46. Tracy, M. A.; Ward, K. L.; Firouzabadian, L.; Wang, Y.; Dong, N.; Qian, R.; Zhang, Y., Factors affecting the degradation rate of poly(lactide-co-glycolide) microspheres in vivo and in vitro. *Biomaterials* **1999**, *20* (11), 1057-1062.
47. Makadia, H. K.; Siegel, S. J., Poly Lactic-co-Glycolic Acid (PLGA) as Biodegradable Controlled Drug Delivery Carrier. *Polymers* **2011**, *3* (3), 1377-1397.
48. Uhrich, K. E.; Cannizzaro, S. M.; Langer, R. S.; Shakesheff, K. M., Polymeric systems for controlled drug release. *Chem. Rev.* **1999**, *99* (11), 3181-3198.
49. Mitragotri, S.; Burke, P. A.; Langer, R., Overcoming the challenges in administering biopharmaceuticals: formulation and delivery strategies. *Nat. Rev. Drug Discov.* **2014**, *13* (9), 655-72.
50. Tibbitt, M. W.; Dahlman, J. E.; Langer, R., Emerging Frontiers in Drug Delivery. *J. Am. Chem. Soc.* **2016**, *138* (3), 704-17.
51. Fenton, O. S.; Olafson, K. N.; Pillai, P. S.; Mitchell, M. J.; Langer, R., Advances in Biomaterials for Drug Delivery. *Adv. Mater.* **2018**, e1705328.
52. Kratochvil, M. J.; Yang, T.; Blackwell, H. E.; Lynn, D. M., Nonwoven Polymer Nanofiber Coatings That Inhibit Quorum Sensing in *Staphylococcus aureus*: Toward New Nonbactericidal Approaches to Infection Control. *ACS Infect. Dis.* **2017**, *3* (4), 271-280.
53. Kratochvil, M. J.; Tal-Gan, Y.; Yang, T.; Blackwell, H. E.; Lynn, D. M., Nanoporous Superhydrophobic Coatings that Promote the Extended Release of Water-Labile Quorum Sensing Inhibitors and Enable Long-Term Modulation of Quorum Sensing in *Staphylococcus aureus*. *ACS Biomater. Sci. Eng.* **2015**, *1* (10), 1039-1049.

54. Broderick, A. H.; Stacy, D. M.; Tal-Gan, Y.; Kratochvil, M. J.; Blackwell, H. E.; Lynn, D. M., Surface coatings that promote rapid release of peptide-based AgrC inhibitors for attenuation of quorum sensing in *Staphylococcus aureus*. *Adv. Healthc. Mater.* **2014**, *3* (1), 97-105.
55. Broderick, A. H.; Breitbach, A. S.; Frei, R.; Blackwell, H. E.; Lynn, D. M., Surface-mediated release of a small-molecule modulator of bacterial biofilm formation: a non-bactericidal approach to inhibiting biofilm formation in *Pseudomonas aeruginosa*. *Adv. Healthc. Mater.* **2013**, *2* (7), 993-1000.
56. Singh, N.; Romero, M.; Travanut, A.; Monteiro, P. F.; Jordana-Lluch, E.; Hardie, K. R.; Williams, P.; Alexander, M. R.; Alexander, C., Dual bioresponsive antibiotic and quorum sensing inhibitor combination nanoparticles for treatment of *Pseudomonas aeruginosa* biofilms in vitro and ex vivo. *Biomater. Sci.* **2019**, *7* (10), 4099-4111.
57. Lu, H. D.; Spiegel, A. C.; Hurley, A.; Perez, L. J.; Maisel, K.; Ensign, L. M.; Hanes, J.; Bassler, B. L.; Semmelhack, M. F.; Prud'homme, R. K., Modulating *Vibrio cholerae* quorum-sensing-controlled communication using autoinducer-loaded nanoparticles. *Nano Lett.* **2015**, *15* (4), 2235-41.
58. Nafee, N.; Husari, A.; Maurer, C. K.; Lu, C.; de Rossi, C.; Steinbach, A.; Hartmann, R. W.; Lehr, C. M.; Schneider, M., Antibiotic-free nanotherapeutics: ultra-small, mucus-penetrating solid lipid nanoparticles enhance the pulmonary delivery and anti-virulence efficacy of novel quorum sensing inhibitors. *J. Control. Release* **2014**, *192*, 131-40.
59. Traber, K. E.; Lee, E.; Benson, S.; Corrigan, R.; Cantera, M.; Shopsin, B.; Novick, R. P., agr function in clinical *Staphylococcus aureus* isolates. *Microbiology* **2008**, *154* (Pt 8), 2265-2274.
60. Kirchdoerfer, R. N.; Garner, A. L.; Flack, C. E.; Mee, J. M.; Horswill, A. R.; Janda, K. D.; Kaufmann, G. F.; Wilson, I. A., Structural basis for ligand recognition and discrimination of a quorum-quenching antibody. *J. Biol. Chem.* **2011**, *286* (19), 17351-8.
61. Novick, R. P., Genetic systems in Staphylococci. *Methods Enzymol.* **1991**, *204*, 589-636.
62. Lyon, G. J.; Mayville, P.; Muir, T. W.; Novick, R. P., Rational design of a global inhibitor of the virulence response in *Staphylococcus aureus*, based in part on localization of the site of inhibition to the receptor-histidine kinase, AgrC. *Proc. Natl. Acad. Sci. U. S. A.* **2000**, *97* (24), 13330-5.

Chapter 6:

Future Directions

Contributions: K. H. J. West wrote the chapter. H. E. Blackwell assisted in writing.

Abstract

In this final chapter, we propose a series of future experiments for the further development of chemical tools that target *agr* and their applications *in vitro* and *in vivo*. We first outline continued SAR studies of the *L. monocytogenes* AIP to develop novel *agr* modulators and potential applications of these modulators to explore virulence phenotypes in this important food borne pathogen. Next, we highlight areas for improvement in our reported multi-group *agr* agonists in *S. epidermidis* and offer potential substitutions to explore. To continue work understanding *agr* QS *in vivo*, we suggest a broader survey of the mechanisms by which AIP-type ligands interact with tissue samples *ex vivo* to gain insight into structural features important for host interference. We also provide plans to examine the hypothesis that the sustained release of *agr* agonists may alleviate Staphylococci biofilm formation in implant infection mouse models. Finally, we offer two new projects to explore the chemistry and biology of *agr* QS using techniques not applied previously by our laboratory. The first utilizes photoreactive amino acids to identify protein partners of AgrD and to explore ligand-binding sites in AgrC, while the second incorporates intein technology to accelerate discovery of AIP-based *agr* modulators in a variety of organisms.

6.1 Introduction

In the research described in this thesis, we have uncovered and characterized new facets of *agr* QS in three species of bacteria. Although our efforts have answered many fundamental questions about the mechanisms these organisms use AIP signals and the *agr* system to dictate group behavior, our efforts have simultaneously revealed even deeper complexities of these systems worthy of additional investigation. Herein, we propose a non-exhaustive list of follow-on experiments and projects to start to pursue some of these questions.

6.2 Projects Focused on *L. monocytogenes*

6.2.1 Continued AIP SAR studies in *L. monocytogenes*

In Chapter 2, we detailed our efforts to build SARs of the native AIP in *L. monocytogenes*, resulting in the discovery of agonists with increased potency over the native AIP (i.e., AIP M4dM and AIP A1V) as well as the development of efficacious antagonists (i.e., KdCdM and 7-mer C3dC/M5dM). While the latter antagonists have good efficacy, they are poorly potent (single digit micromolar) when compared to antagonists in other *agr* systems (often single digit nanomolar). Our initial SAR study broadly surveyed many of the residues in the native AIP, but there is substantial chemical space left to explore for each position in the AIP sequence that could enhance potency of our antagonists. In terms of fundamental SARs, we could explore Val6 modifications more broadly using naturally occurring amino acids, as we had only examined an alanine and a D-valine substitution at that position. With a large number of non-canonical amino acids (ncAAs) commercially available (specifically, non-native

phenylalanine derivatives), using these ncAAs to explore Phe3 and Phe5 further could better elucidate their role in activity, as these positions poorly tolerate substitutions. The Met4 residue has been demonstrated to increase potency when in a D-configuration, so further exploration of D-amino acids at this position could reveal side chains with even greater potency. Inversion of Cys2 imparts the greatest antagonistic activity for our analogs at the cost of generally reduced potency. Exploring other linkages, such as lactone or all-carbon linkages, could imbue similar antagonistic activity without the potency loss. Finally, while Ala1 generally seems tolerant of many substitutions, we have not explored negatively charged or aromatic residues at this position. As the lysine substitution at this position offers only ~25% antagonism, it is worth further exploration to see if other chemical properties can increase efficacy. These additional SAR studies could uncover novel features on AIPs to inhibit *L. monocytogenes agr* activity, which could be used in conjunction with previous SAR data to advance more potent, next-generation antagonists.

6.2.2 Utilizing *L. monocytogenes agr* modulators to examine virulence phenotypes in culture

With our current *L. monocytogenes agr* modulators (or new ones developed from the previous section), we can begin to more thoroughly characterize the effects of altering *agr* activity on different population density dependent behaviors in *L. monocytogenes*. It is well-known that *L. monocytogenes* uses a host of virulence factors to invade eukaryotic cells, escape the phagosome, and propagate within the host cytosol before ultimately propelling themselves with host actin into neighboring cells,

enabling *L. monocytogenes* to spread to other host cells without having to re-enter the extracellular matrix.¹⁻² Many of these virulence proteins and other virulence regulators are downregulated in Δagr strains, leading to attenuated infections in cell culture and *in vivo*,³ suggesting *agr* activity can exert some controls over these behaviors. Using our modulators, we can explore if our synthetic agonists restore any of these phenotypes in *L. monocytogenes* $\Delta agrD$ strains and correspondingly if these phenotypes can be inhibited in wild-type strains with our antagonists. These questions can be pursued both in eukaryotic cells lines³ and *in vivo* with various animal models (e.g., zebrafish⁴) by examining the modes and levels by which chemically-activated or -inhibited bacteria invade host cells or activate immune responses. Adding a constitutive fluorescent reporter plasmid in addition to our *agr*-dependent plasmid in *L. monocytogenes* could also allow us to track the pathogen as it invades hosts and correlate *agr* activity with the timing of invasion.

6.2.3 Incorporating *L. monocytogenes agr* antagonists into materials to reduce biofilm on surfaces

We described in Chapter 2 that our synthetic *L. monocytogenes agr* antagonist KdCdM could reduce the formation of biofilms in microtiter plates. This is a critical first step towards creating tools to disrupt and prevent *L. monocytogenes* biofilm formation in industrial settings, environments where these biofilms can plague steel and glass equipment and are extremely challenging to remove. In an effort to make our antagonists more practical, we could utilize controlled release strategies to extend the lifetime of the antagonists on surfaces. As described in Chapter 5, controlled release

from PLG materials is well-understood and compatible with a wide variety of morphologies.⁵⁻⁶ A simple first step would be to add antagonist-loaded materials to containers with *L. monocytogenes* culture to explore if the sustained release of *agr* antagonists can limit biofilm formation. Alternatively, antagonists could be loaded into carboxymethylcellulose films that can coat simple and complex surfaces, rapidly releasing compound over time directly from surfaces and assessing initial bacterial adherence.⁷

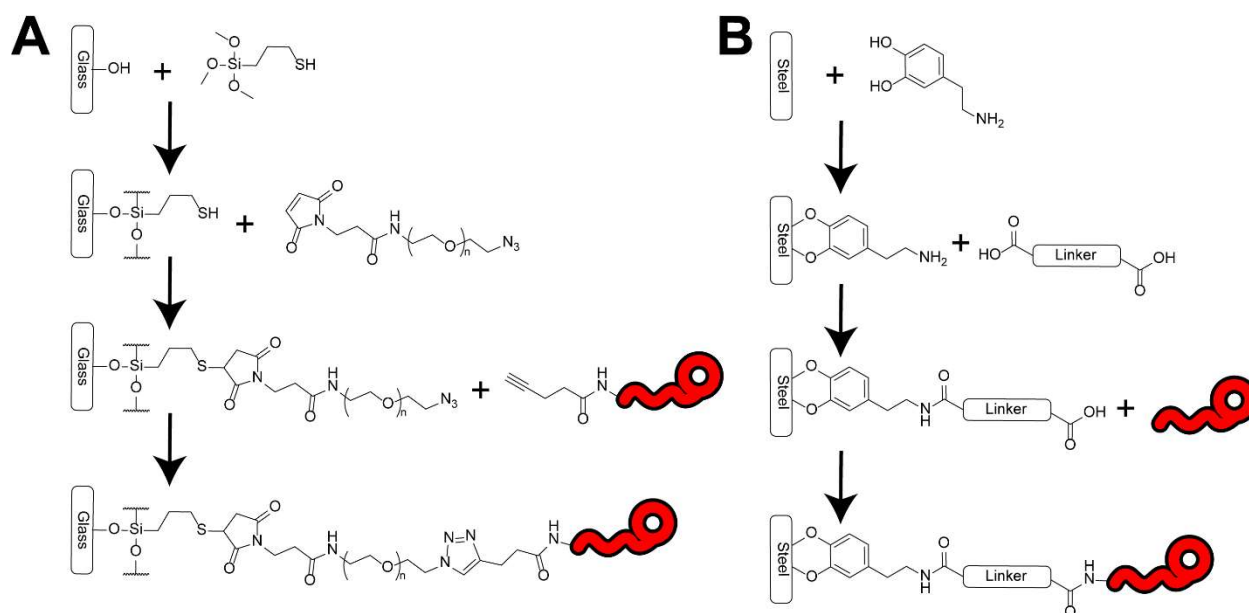


Figure 6.1 Covalent attachment of AIP analogs to surfaces. (A) After functionalizing glass with azide moieties, AIP analogs with alkyne tails can be covalently attached using click chemistry. (B) Dopamine readily coats steel and can be functionalized with various linkers and can attach AIP analogs using standard peptide coupling agents.

Covalent modifications of AIP analogs can also aid in attachment or binding to surfaces. A recent report has shown that covalently linking AIPs and AIP analogs through click chemistry to silanized glass surfaces can modulate biofilm formation in *S.*

aureus,⁸ which suggests similar methods would likely work with our *L. monocytogenes* antagonists. Dopamine is known to readily react with and coat steel,⁹ and the free amino group can be coupled to linker groups and the N-terminus of AIP analog antagonists. Recent screening efforts have identified peptides with high affinity for certain polymers such as polypropylene¹⁰⁻¹¹ or polystyrene,¹² and these peptide sequences can similarly be coupled to our antagonists. Following functionalization of the antagonists with the selective surface agent, experiments that apply these antagonists to surfaces, introduce bacterial cultures, and examine adherence and biofilm formation over time can inform which functionalization method and surface are most worthy of continued development.

6.3 Projects Focused on *S. epidermidis*

6.3.1 Approaches to improve efficacy of multi-group agonists in S. epidermidis

Unlike in *L. monocytogenes* where *agr* activation leads to increased biofilm, in many Staphylococci increased *agr* activity promotes biofilm dispersal through the production of PSMs. A pan-group *agr* agonist could activate production of PSMs and help disperse biofilms in all strains of *S. epidermidis* is highly desirable as a chemical tool to control virulence. Although we have reported some preliminary modulators in Chapter 4 with some agonistic activity in the three major *agr* groups of *S. epidermidis*, the efficacy of these modulators certainly could be improved, particularly in group-I. Our SAR studies indicate that the exocyclic residues adjacent to the macrocycle are most important for activation, and follow up studies exploring chemical space of these residues may lead to more efficacious agonists. At present, we only have detailed

activity data for proline and valine residues at that position, but there are many other hydrophobic amino acids that could be explored: leucine, isoleucine, pipecolic acid, thioprolines, or methyl prolines. As it seems that hydrophobic bulk is key for agonizing contacts, it is possible some of these substitutions can agonize the three AgrC receptors better than either valine or proline alone, leading to the development of more efficacious multi-group agonists.

6.4 Projects to Explore Modulation of *agr* Activity *In Vivo*

6.4.1 Screening *agr* modulators *ex vivo* to characterize key structural features for sequestration/degradation

In our efforts to identify lead AIP analog antagonists to use in the *in vivo* studies of *S. aureus* infection described in Chapter 5, we discovered that one of our potent antagonists, AIP-III D4A, was either sequestered or degraded by components in mouse tissue. This effect appears to be linked to compound structure, as surveying five other potent *agr* antagonists revealed a spectrum of susceptibility, with compounds based on the AIP-II scaffold being extremely sensitive to the presence of tissue while truncated analogs of AIP-III had increased resistance to tissue effects. With the small sample size examined (i.e., six compounds), it is difficult to pinpoint the source of their differences, so more compounds need to be surveyed to determine how compound structure affects sequestration and/or degradation with mouse tissue. Fortunately, over the years the Blackwell laboratory has generated a number of AIP analogs from different scaffolds. Surveying this large suite of analogs for activity loss in the presence of mouse tissue, similar to the *ex vivo* experiments in Chapter 5, could reveal structural commonalities

between compounds that are quickly sequestered/degraded and those that are highly resistant to these effects. Elucidating the structural dependence of this phenomenon, along with its biochemical mechanism, will be critical for streamlining future *in vivo* studies that utilize various chemical modulators of *agr*.

6.4.2 Sustained release of *agr* activators to reduce Staphylococcal biofilms in a murine implant infection model

While *agr* inhibition can attenuate acute *S. aureus* infection *in vivo*, such inhibition can also induce biofilm formation in many Staphylococci including *S. aureus*.¹³ Biofilms are common in chronic infections and are often associated with indwelling medical devices, suggesting chemical activation of the *agr* system to promote biofilm dispersal could be a beneficial approach in combating chronic infection.¹³⁻¹⁴ Using a similar strategy to that described in Chapter 5 for the release of *agr* antagonists from PLG materials to attenuate acute *S. aureus* infection, we could utilize PLG materials to release *agr* agonists to block or reduce the formation either *S. aureus* or *S. epidermidis* biofilms *in vivo*. Mice models examining device-associated infections have shown *S. aureus* can form biofilms on titanium implants weeks after surgery,¹⁵ so materials that keep *agr* agonists localized to the implant could act to reduce or prevent Staphylococci adherence and biofilm formation *in vivo*.

6.5 Projects to explore new approaches to probe *agr* QS

6.5.1 Incorporation of photoreactive amino acids to identify *AgrD* protein partners and ligand-binding sites of *AgrC*

Although many of the core mechanisms of the *agr* systems are fairly well-understood, there are still some gaps in our knowledge. Two particularly noteworthy knowledge gaps are (1) the mechanism by which *AgrD*, after being processed in part by *AgrB*, is further modified to produce the extracellular mature AIP, and (2) the residues on *AgrC* that directly interact with AIPs upon binding. Activity-based proteomics using photoreactive amino acid residues could be used to probe these remaining questions in *S. aureus* group-I. Many diazirine analogs of naturally-occurring amino acids (e.g., leucine, isoleucine, methionine, lysine, proline, and phenylalanine) are commercially available and readily incorporated into peptides using solid-phase peptide synthesis methods.¹⁶⁻¹⁷ Substituting these photoreactive amino acids into *AgrD* thiolactones modified with “pull-down” moieties (such as biotinylating the N-terminus or another amino acid on *AgrD*), incubating with cell lysates, cross-linking with UV light, and subsequent standard proteomic MS analyses could reveal protein partners associated with the N-terminal cleavage or transport of *AgrD*. Following a similar method, incorporation of these photoreactive amino acids into various AIP scaffolds and incubation with *AgrC* produced in nanodiscs, and subsequent protein digestion and MS analyses could reveal AIP binding sites on *AgrC*. Once examined in group-I *S. aureus*, putative *AgrD* protein partners and *AgrC* binding sites could be investigated in other *agr* systems to clarify whether these are interactions general to all *agr* systems or specific to individual systems.

6.5.2 Using AIP intein technology to rapidly generate new agr modulators

A recent report uses the Random non-standard Peptide Integrated Discovery (RaPID) system to generate macrocyclic peptides that target AgrC in *S. aureus*.¹⁸ These macrocyclic peptides are not based on native AIPs and represent novel scaffolds. While these new peptides are clearly effective AgrC antagonists, simple modifications to the native AIP scaffolds still represent the most efficacious and potent modulators of AgrC. These AIP analogs are synthesized through solid-phase peptide synthesis, which can be relatively laborious and low yielding, so new methods to rapidly generate AIP analogs could accelerate the discovery of more potent and efficacious molecules. Over a decade ago, Malone *et al.* designed an intein system to produce AIPs in *E. coli*.¹⁹ This intein system relies on oligonucleotides that code for AIPs to insert into plasmids with intein domains, which then can produce AIPs upon expression.¹⁹ Malone *et al.* only used this system to produce AIPs that mimic the native *S. aureus* AIPs, and we propose here expanding this method for AIP generation by combining it with random mutagenesis techniques (e.g., error-prone PCR) to create structurally diverse libraries of AIPs that can be screened for *agr* modulatory activity in bacteria of interest. Notably, this proposed system bypasses complications of evolving AgrD sequences to produce new AIPs, as it has been shown that AIP production is substantially affected during AgrD random mutagenesis, likely by disrupting AgrB recognition and processing of AgrD.²⁰ In addition to the known high potency and efficacy of AIP scaffolds, no other scaffolds besides AIPs have been demonstrated to effectively agonize *agr* activity, highlighting this proposed discovery-based approach as a novel approach to quickly discovering non-native *agr* agonists.

6.6 References

1. Tilney, L. G.; Portnoy, D. A., Actin filaments and the growth, movement, and spread of the intracellular bacterial parasite, *Listeria monocytogenes*. *J. Cell Biol.* **1989**, *109* (4 Pt 1), 1597-608.
2. Radoshevich, L.; Cossart, P., *Listeria monocytogenes*: towards a complete picture of its physiology and pathogenesis. *Nat. Rev. Microbiol.* **2018**, *16* (1), 32-46.
3. Riedel, C. U.; Monk, I. R.; Casey, P. G.; Waidmann, M. S.; Gahan, C. G.; Hill, C., AgrD-dependent quorum sensing affects biofilm formation, invasion, virulence and global gene expression profiles in *Listeria monocytogenes*. *Mol. Microbiol.* **2009**, *71* (5), 1177-89.
4. Vincent, W. J.; Freisinger, C. M.; Lam, P. Y.; Huttenlocher, A.; Sauer, J. D., Macrophages mediate flagellin induced inflammasome activation and host defense in zebrafish. *Cell. Microbiol.* **2016**, *18* (4), 591-604.
5. Kratochvil, M. J.; Yang, T.; Blackwell, H. E.; Lynn, D. M., Nonwoven Polymer Nanofiber Coatings That Inhibit Quorum Sensing in *Staphylococcus aureus*: Toward New Nonbactericidal Approaches to Infection Control. *ACS Infect. Dis.* **2017**, *3* (4), 271-280.
6. Kang, M.; Kim, S.; Kim, H.; Song, Y.; Jung, D.; Kang, S.; Seo, J. H.; Nam, S.; Lee, Y., Calcium-Binding Polymer-Coated Poly(lactide- co-glycolide) Microparticles for Sustained Release of Quorum Sensing Inhibitors to Prevent Biofilm Formation on Hydroxyapatite Surfaces. *ACS Appl Mater Interfaces* **2019**, *11* (8), 7686-7694.
7. Broderick, A. H.; Stacy, D. M.; Tal-Gan, Y.; Kratochvil, M. J.; Blackwell, H. E.; Lynn, D. M., Surface coatings that promote rapid release of peptide-based AgrC inhibitors for attenuation of quorum sensing in *Staphylococcus aureus*. *Adv. Healthc. Mater.* **2014**, *3* (1), 97-105.
8. Kim, M. K.; Zhao, A.; Wang, A.; Brown, Z. Z.; Muir, T. W.; Stone, H. A.; Bassler, B. L., Surface-attached molecules control *Staphylococcus aureus* quorum sensing and biofilm development. *Nat. Microbiol.* **2017**, *2*, 17080.
9. Alas, G. R.; Agarwal, R.; Collard, D. M.; Garcia, A. J., Peptide-functionalized poly[oligo(ethylene glycol) methacrylate] brushes on dopamine-coated stainless steel for controlled cell adhesion. *Acta Biomater.* **2017**, *59*, 108-116.
10. Rubsam, K.; Davari, M. D.; Jakob, F.; Schwaneberg, U., KnowVolution of the Polymer-Binding Peptide LCI for Improved Polypropylene Binding. *Polymers (Basel)* **2018**, *10* (4).

11. Rübsam, K.; Stomps, B.; Böker, A.; Jakob, F.; Schwaneberg, U., Anchor peptides: A green and versatile method for polypropylene functionalization. *Polymer* **2017**, *116*, 124-132.
12. Qiang, X.; Sun, K.; Xing, L.; Xu, Y.; Wang, H.; Zhou, Z.; Zhang, J.; Zhang, F.; Caliskan, B.; Wang, M.; Qiu, Z., Discovery of a polystyrene binding peptide isolated from phage display library and its application in peptide immobilization. *Sci. Rep.* **2017**, *7* (1), 2673.
13. Cheung, G. Y.; Joo, H. S.; Chatterjee, S. S.; Otto, M., Phenol-soluble modulins--critical determinants of staphylococcal virulence. *FEMS Microbiol. Rev.* **2014**, *38* (4), 698-719.
14. Le, K. Y.; Dastgheyb, S.; Ho, T. V.; Otto, M., Molecular determinants of staphylococcal biofilm dispersal and structuring. *Front. Cell. Infect. Microbiol.* **2014**, *4*, 167.
15. Wang, Y.; Cheng, L. I.; Helfer, D. R.; Ashbaugh, A. G.; Miller, R. J.; Tzomides, A. J.; Thompson, J. M.; Ortines, R. V.; Tsai, A. S.; Liu, H.; Dillen, C. A.; Archer, N. K.; Cohen, T. S.; Tkaczyk, C.; Stover, C. K.; Sellman, B. R.; Miller, L. S., Mouse model of hematogenous implant-related *Staphylococcus aureus* biofilm infection reveals therapeutic targets. *Proc. Natl. Acad. Sci. U. S. A.* **2017**, *114* (26), E5094-E5102.
16. Vila-Perello, M.; Pratt, M. R.; Tulin, F.; Muir, T. W., Covalent capture of phospho-dependent protein oligomerization by site-specific incorporation of a diazirine photo-cross-linker. *J. Am. Chem. Soc.* **2007**, *129* (26), 8068-9.
17. Suchanek, M.; Radzikowska, A.; Thiele, C., Photo-leucine and photo-methionine allow identification of protein-protein interactions in living cells. *Nat. Methods* **2005**, *2* (4), 261-7.
18. Xie, Q.; Wiedmann, M. M.; Zhao, A.; Pagan, I. R.; Novick, R. P.; Suga, H.; Muir, T. W., Discovery of quorum quenchers targeting the membrane-embedded sensor domain of the *Staphylococcus aureus* receptor histidine kinase, AgrC. *Chem. Commun. (Camb.)* **2020**, *56* (76), 11223-11226.
19. Malone, C. L.; Boles, B. R.; Horswill, A. R., Biosynthesis of *Staphylococcus aureus* autoinducing peptides by using the synechocystis DnaB mini-intein. *Appl. Environ. Microbiol.* **2007**, *73* (19), 6036-44.
20. Thoendel, M.; Horswill, A. R., Random mutagenesis and topology analysis of the autoinducing peptide biosynthesis proteins in *Staphylococcus aureus*. *Mol. Microbiol.* **2013**, *87* (2), 318-37.

Appendix I:

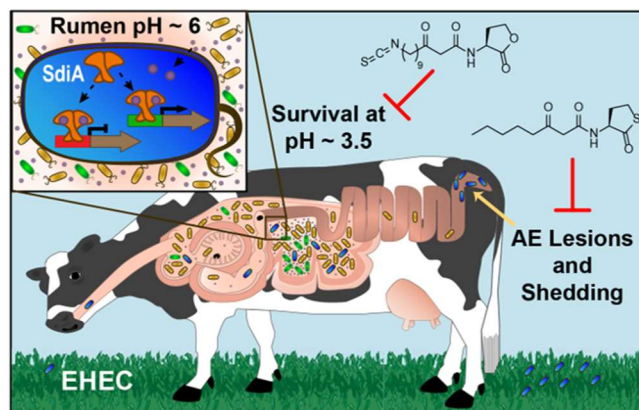
Chemical Control of Quorum Sensing in *E. coli*: Identification of Small Molecule Modulators of SdiA and Mechanistic Characterization of a Covalent Inhibitor

Contributions: M. J. Styles designed and conducted experiments and wrote the chapter. S. A. Early performed agonism and antagonism screening, constructed mutant reporter strains, and assisted in acid resistance assay development. T. Tucholski performed and analyzed mass spectrometry experiments, wrote and designed related text and figures. K. H. J. West compiled and analyzed AHL analog activity data for LuxR-type proteins and designed related figures. Y. Ge guided mass spectrometry experiments. H. E. Blackwell guided research and assisted in writing.

*This chapter is published under the same title:

Styles, M. J.; Early, S. A.; Tucholski, T; West, K. H. J.; Ge, Y.; Blackwell, H. E. Chemical control of quorum sensing in *E. coli*: characterization of small molecule modulators of SdiA and identification of a covalent inhibitor. *ACS Infect. Dis.* **2020**, *6*, 3092-3103.

Abstract



Enterohemorrhagic *Escherichia coli* (EHEC) is the causative agent of severe diarrheal disease in humans. Cattle are the natural reservoir of EHEC, and approximately 75% of EHEC infections in humans stem from bovine products. Many common bacterial pathogens, including EHEC, rely on chemical communication systems, such as quorum sensing (QS), to regulate virulence and facilitate host colonization. EHEC uses SdiA_{EHC}, an orphan LuxR-type receptor, to sense *N*-acyl *L*-homoserine lactone (AHL) QS signals produced by other members of the bovine enteric microbiome. SdiA_{EHC} regulates two phenotypes critical for colonizing cattle: acid resistance and the formation of attaching and effacing lesions. Despite the importance of SdiA_{EHC}, there is very little known about its selectivity for different AHL signals, and no chemical inhibitors that act specifically on SdiA_{EHC} have been reported. Such compounds would represent valuable tools to study the roles of QS in EHEC virulence. To identify chemical modulators of SdiA_{EHC} and delineate the structure-activity relationships (SARs) for AHL activity in this receptor, we report herein the screening of a focused library composed largely of AHLs and AHL analogues in an SdiA_{EHC} reporter assay. We describe the identity and SARs of potent modulators of SdiA_{EHC} activity, examine the

promiscuity of SdiA_{EC}, characterize the mechanism of a covalent inhibitor, and provide phenotypic assay data to support that these compounds can control SdiA_{EC} dependent acid resistance in *E. coli*. These SdiA_{EC} modulators could be used to advance the study of LuxR-type receptor:ligand interactions, the biological roles of orphan LuxR-type receptors, and potential QS-based therapeutic approaches.

I.1 Introduction

Enteric pathogens must navigate several challenges to successfully infect a host, including changes to their chemical environments (e.g., pH, salinity, and availability of resources), host innate and adaptive immune responses, competition with the existing microbiota throughout the gastrointestinal tract, and clearing the native microbial community at the site of colonization.¹⁻² To address these challenges, pathogens rely on myriad virulence traits, such as the production of toxins, adhesions, secretion/effector systems, and biofilms.³ These virulence products are energetically costly and often only effective in specific environmental contexts; therefore, virulence factor expression is tightly regulated by bacteria.³⁻⁴ Because pathogens often require virulence factors to colonize their host and cause disease, targeting the regulation or function of virulence factors represents a potential therapeutic strategy to prevent or treat infection, and has attracted considerable attention as an “anti-virulence” approach.^{3, 5}

Many common bacteria,^{3, 6} including enteric pathogens,⁷ regulate their behavior in a population dependent manner through a cell-to-cell signaling mechanism called quorum sensing (QS).⁸ To quorum sense, a bacterium produces an exoproduct, a small molecule or short peptide, that is only sensed by that individual bacterium when there is a high population density of other bacteria making this chemical signal in its environment.⁸ *N*-acyl L-homoserine lactones (AHLs) are the primary QS signaling molecules used by Gram-negative bacteria, including *Pseudomonas aeruginosa*, *Acinetobacter baumannii*, and *Burkholderia cepacia*.⁹ AHL-type QS is mediated by the canonical LuxI/LuxR system, first described in the bioluminescent symbiont *Vibrio fischeri* (Figure I.1A).⁸ In many Gram-negative bacterial pathogens, LuxI/LuxR-based

QS regulates phenotypes necessary for virulence.⁹ Accordingly, inhibition of this QS pathway could represent an approach to attenuate infection by these bacteria.⁶ Significant research has been directed toward this end, with a specific focus on the development of chemical tools to modulate LuxR-type receptor activity.^{6, 10-16}

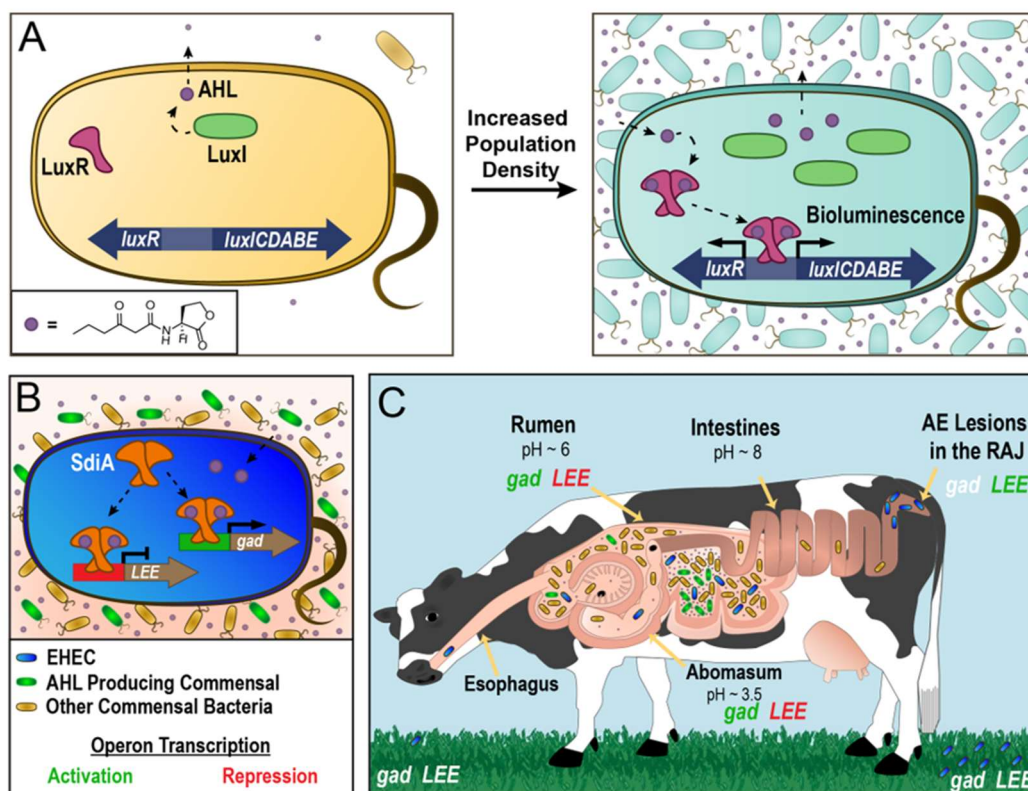


Figure I.1 AHL-mediated LuxI/LuxR-type QS overview. (A) The AHL-mediated LuxI/LuxR-type QS system from *V. fischeri*. LuxI produces *N*-(3-oxo)-hexanoyl L-homoserine lactone (OHHL), which diffuses away from the cell and into others. At high population density, the concentration of intracellular OHHL is high enough to bind to and stabilize LuxR. The OHHL:LuxR complex dimerizes, binds to DNA, and promotes transcription of the *lux* operon, which produces bioluminescence. (B) In EHEC, the LuxR homolog, SdiA, binds to exogenously produced AHLs to repress (red) the *LEE* operon and to activate (green) the *gad* operon. (C) EHEC colonization of cattle. EHEC (blue) is first eaten by the cow. When EHEC reaches the rumen, SdiA_{EHC} becomes activated by AHLs produced by other commensal bacteria (green). SdiA_{EHC} is active in the rumen and abomasum. After passage through the gastrointestinal tract, EHEC colonize the recto-anal junction (RAJ); here, no AHLs are present and the *LEE* operon is not repressed by SdiA_{EHC}.

Historically, LuxI/LuxR-type QS has been considered an intra-species cell-to-cell communication system.^{9, 17-18} LuxI-type synthases primarily produce a specific AHL, and the cognate intracellular LuxR-type receptors bind selectively to that AHL.⁸ The AHL:LuxR complex then typically dimerizes, binds to DNA, and activates transcription of QS-controlled genes. Differences in the chemical structure of the AHL allows a LuxR-type receptor to discriminate between signals (Figure I.1A inset): variations in native AHL structure include the length of the acyl tail (4-20 carbons), oxidation at the third carbon in the acyl tail (carbonyl, alcohol, or methylene), units of unsaturation, and, in some rare instances, aryl as opposed to aliphatic tails.⁸ Interestingly, many LuxR-type receptors have been identified in bacteria for which a corresponding LuxI-type synthase is not present in the genome; these receptors lack a self-produced, cognate AHL signal and are known as orphan or “solo” LuxR-type receptors.¹⁸ Bacteria with these orphan receptors are presumed to use them to respond to AHLs produced by other bacterial species in their environment. SdiA is one such orphan LuxR-type receptor (Figure I.1B), and it is highly conserved (67–84% sequence identity)¹⁹ across many enteric pathogen genera, including *Escherichia*, *Enterobacter*, *Citrobacter*, *Cronobacter*, *Klebsiella*, *Salmonella*, and *Shigella*.²⁰ Additionally, SdiA from *E. coli* (SdiA_{EC}), is remarkably stable *in vitro* in its *apo* form relative to other LuxR-type receptors. Consequently, it is the only LuxR-type receptor that has been purified and crystalized both in the presence and absence of an AHL.²¹⁻²² These prior biophysical studies, when contrasted with the current dearth of structural and mechanistic data for most other LuxR-type receptors, demonstrate the potentially unique opportunity provided by SdiA for studying LuxR-type receptor:AHL interactions.

Cattle are a natural reservoir of the enteric pathogen, enterohemorrhagic *Escherichia coli* (EHEC), which possesses SdiA_{EHC}.²³ EHEC $\Delta sdiA$ mutants have been shown to less effectively colonize cattle, suggestive of SdiA_{EHC}, and consequently AHL-based QS, playing a role in this process.²⁴⁻²⁸ The current understanding of SdiA_{EHC} in bovine EHEC colonization is outlined in Figure I.1C. EHEC are first ingested by cows; once in the rumen, commensal and/or pathogenic Gram-negative bacteria (e.g., *P. aeruginosa* and *Aeromonas hydrophila*)²⁹ produce several AHLs that can activate SdiA_{EHC}.^{24, 28, 30-31} The SdiA_{EHC}:AHL complex then increases transcription of four genes in the *gad* operon (*gadW*, *gadE*, *yhiD*, and *hdeA*).³² The *gad* operon encodes an acid resistance system that is critical to survival of EHEC in the low pH environment of the cow's final stomach (abomasum);²⁵ congruent with this observation, EHEC $\Delta sdiA$ mutant strains have decreased survival *in vitro* at low pH.^{24, 32} SdiA_{EHC} also represses the *LEE* operon via binding to the *ler* promoter region.²⁴ This repression is useful until EHEC reaches the cow intestines. Once there, expression of the *LEE* operon is necessary for the formation of attaching and effacing (AE) lesions by EHEC;^{23-24, 26} these lesions facilitate shedding of EHEC from the cattle into the environment. In humans, EHEC forms these AE lesions, which lead to bloody diarrhea and other serious conditions.²³ AHLs have not been found (and are hydrolytically unstable) in the alkaline environment of bovine intestines, and thus, SdiA_{EHC} repression of the *LEE* operon is blocked in the intestines.²⁴ This process has been demonstrated in *in vitro* experiments, in which exogenous AHLs were found to repress the *LEE* operon in an SdiA_{EHC} dependent manner.^{24, 33} In addition to these two phenotypes critical for EHEC colonization and spread, exogenous AHLs have been shown, in an SdiA_{EHC} dependent

manner, to repress the expression of genes required for motility,^{32, 34} reduce the susceptibility of *E. coli* to λ -phage,³⁵ and suppress conjugation between *E. coli* strains and between *E. coli* and *P. aeruginosa*.³⁶⁻³⁷

The importance of SdiA_{EC} to colonization by and virulence in EHEC suggests an approach to attenuate EHEC infection, and more fundamentally, provides entry into the study of the role of QS in infection by an important human pathogen. Chemical strategies to either inhibit or activate SdiA_{EC} could be particularly useful in this context. Because SdiA_{EC} must be both active and inactive during different phases of host colonization, chemical tools could provide valuable spatial and temporal control when modulating SdiA_{EC} activity during investigation of host-pathogen interactions. However, few small molecule modulators of SdiA_{EC} activity are known; to our knowledge, no antagonists have been reported, and the known agonists only include several naturally occurring AHLs³² and three weakly potent synthetic AHL analogues.³⁸ Furthermore, there is a lack of an understanding of the structural features of AHLs (i.e., structure-activity relationship (SAR) data) that are required for SdiA_{EC} activation, which limits the design of new ligands, AHL-based or not. Recently, we investigated related questions for a different SdiA receptor—SdiA_{SE} from *Salmonella*;¹⁹ we found SdiA_{SE} to be highly promiscuous, being activated by a broad range of AHLs, and we also identified several AHL-type SdiA_{SE} inhibitors. The sequence of *sdiA* is highly conserved across genera, and *sdiA*_{EC} and *sdiA*_{SE} are 72% identical.¹⁹ Therefore, we expect that similar trends in SAR could hold for SdiA from *E. coli* and other genera, but this has yet to be confirmed. The lack of small molecule modulators and SAR information for SdiA_{EC} was the primary motivation for the present study.

Herein, we report the systematic screening of a focused small molecule library, composed largely of AHLs and AHL analogues, for chemical modulators of SdiA_{EC}. We discovered that SdiA_{EC}, like SdiA_{SE}, is highly promiscuous; it is activated both by a wide array of native AHLs and by compounds with significant alterations to the AHL structure. We also report the identity and SARs of the first highly potent, synthetic AHL analogues that can either strongly agonize or antagonize SdiA_{EC}. The antagonists were shown to directly modulate a QS-controlled phenotype in *E. coli*—i.e., acid tolerance. Biochemical studies enabled by mass spectrometry (MS) support one of the SdiA_{EC} antagonists acts via a potential covalent inhibition mechanism. These compounds and insights should advance chemical approaches to study SdiA_{EC} and its role in QS.

I.2 Results and Discussion

I.2.1 Selection of a small molecule library for screening in SdiA_{EC}

We compiled a focused library of 153 AHLs and related analogs (full structures in Figure I.S1) to screen in a cell-based reporter of SdiA_{EC} activity. For this primary screen, we selected a series of sub-libraries from our in-house collection of AHL derivatives and other small molecules with demonstrated activities in other LuxR-type receptors.^{12, 19, 39-49} These compounds fall into seven categories: naturally occurring AHLs with aliphatic tails (Figure I.2i), *N*-benzoyl HLs (BnHLs, Figure I.2ii), *N*-phenylacetanoyl HLs (PHLs, Figure I.2iii), *N*-phenylpropionyl HLs (PPHLs, Figure I.2iv), other AHLs (Figure I.2v), *N*-acyl homocysteine thiolactones (AHTs, Figure I.2vi), and non-AHLs (Figure I.2vii). This focused library was a good starting point to explore the SARs for AHL:SdiA_{EC} interactions as it contains a broad sampling of changes to the aliphatic tail, amide linker,

and lactone head group of the native AHL structure. Further, we recently screened a similar subset of compounds for activity in SdiA_{SE} from *Salmonella*, allowing us to make direct comparisons among the screening data.¹⁹

1.2.2 Development of a cell-based reporter assay of SdiA_{EC} transcriptional activity

To test the library for activity in SdiA_{EC}, we built on the prior work by Dyszel *et al.*³² and generated a reporter system in *E. coli* JLD271 (Δ *sdiA*), in which SdiA_{EC} is expressed from a plasmid under the control of the L-arabinose inducible *pBAD* promoter, and on a separate reporter plasmid, the *gadW* promoter (from which activated SdiA_{EC} induces expression) is fused to *lacZ* (see Table I.S2 for strain and plasmid details). SdiA_{EC} activity in this strain is then measured using a standard β -galactosidase assay.⁵⁰ The signal was normalized to both the positive control (10 μ M *N*-(3-oxo)-octanoyl L-homoserine lactone, OOHL (**2**)) and the negative control (DMSO, vehicle). OOHL (**2**) was chosen as the positive control because it is the most potent naturally occurring agonist of SdiA_{SE} and has been crystalized with SdiA_{EC}.^{19, 22, 51} We note that, due presumably to the enhanced stability of apo-SdiA_{EC} relative to other LuxR-type receptors, this reporter assay gave a higher background signal in the absence of ligand relative to similar reporter assays for related receptors.^{12, 39} Assay conditions were carefully optimized to maximize the difference between the positive and negative controls (Figure I.S2).

I.2.3 *SdiA_{EC}* can be activated by a broad range of AHLs but is inhibited by few

All 153 compounds were screened (see Table I.S3) for agonism at 100 nM and for antagonism at 100 μ M against the EC₉₀ of **2** (10 nM). The agonism screen revealed SdiA_{EC} to display a remarkably high level of promiscuity relative to other LuxR-type receptors (except for SdiA_{SE}; see below). These differences in promiscuity are obvious in the heatmap representation in Figure I.2. Receptors such as LasR (from *P. aeruginosa*) and TraR (from *Agrobacterium tumefaciens*) are modulated by only a small subset of these AHLs. Other receptors such as LuxR (from *V. fischeri*) and QscR (from *P. aeruginosa*) bind a larger subset, but most compounds antagonize these receptors. In contrast, SdiA_{EC} is activated by nearly every compound in the tested library containing a homoserine lactone (Figure I.2i-v), except for the BnHLs (Figure I.2ii). Remarkably, more than one-third of the library (54 out of 153) had at least 85% activity at 100 nM. A secondary agonism screen with 10 nM compound was performed to narrow this list to only the most potent compounds (Table I.S4). At this lower concentration, 28 compounds had at least 50% activity. In stark contrast to the agonism screen, the antagonism screen of this library at 100 μ M yielded only two compounds displaying at least 40% inhibition of SdiA_{EC}. Given that most of the compounds containing a homoserine lactone were agonists, regardless of the structure of the acyl tail, and that this collection of compounds is heavily biased towards compounds containing a homoserine lactone, our discovery of so few antagonists is perhaps unsurprising.

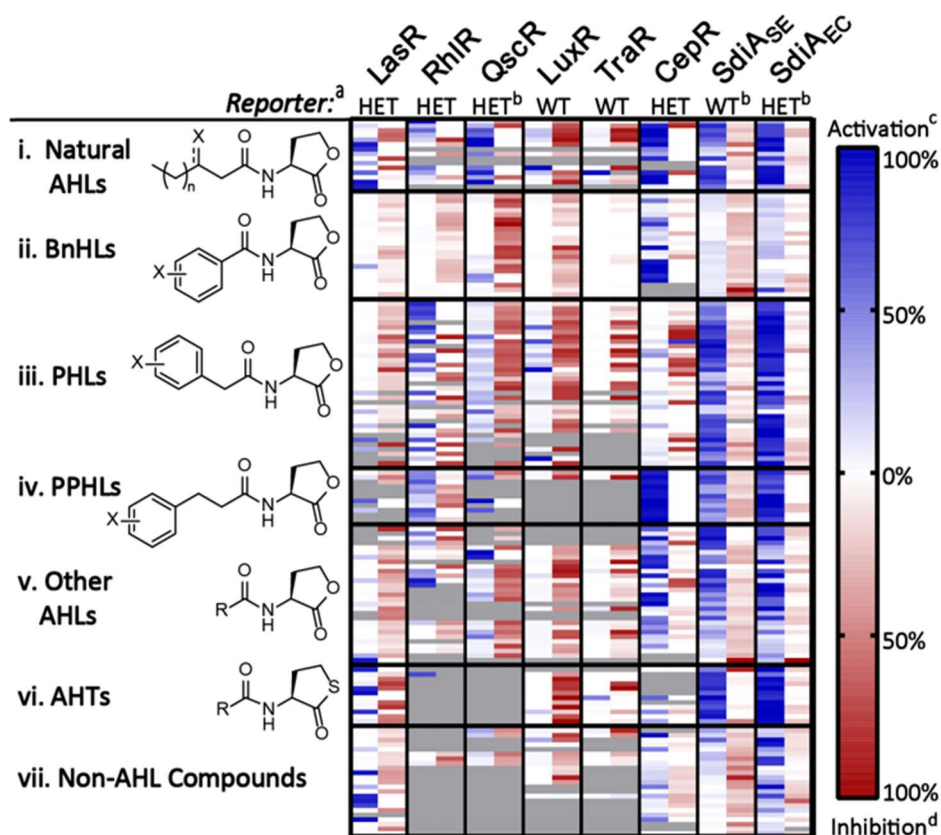


Figure I.2 Activity heatmap of AHL and AHL analogs in various LuxR-type receptors. Heatmap representation of the activity of a set of AHLs and AHL analogues in LuxR-type receptors from prior studies and the current study as measured using reporter gene assays (see Table I.S1 for further details and references). Compounds are grouped by type (i–vii) in rows; agonism (left, trending blue) and antagonism (right, trending red) data for each compound are shown in adjacent columns for each receptor. ^aReporter gene assay details: receptor expressed at wild-type levels in the native organism (WT) or from a pBAD promoter in *E. coli* Δ sdiA (HET). ^bOrphan receptor; compound **1** and **2** used as the “native ligand” for QscR and SdiA, respectively. ^c100% activation in an agonism assay is equal to the maximum activation by native ligand and 0% is equal to the activation by vehicle (DMSO). ^d100% inhibition in an antagonism assay is equal to the activation by vehicle (DMSO) and 0% inhibition is equal to the activation by the EC₅₀ concentration of native ligand (EC₉₀ for SdiA^{SE} and SdiA^{EC}). Grey bands in the heat map indicate assay data not available.

1.2.4 The promiscuity of SdiA is conserved

As shown in Figure I.2, SdiA^{EC} and SdiA^{SE} are activated by the same compound classes—that is, AHLs, PHLs, PPHLs, other AHLs, and AHTs. Similarly, BnHLs are unable to activate either receptor. This conservation of agonists between SdiA^{EC} and

SdiA_{SE} is not surprising given their sequence similarity. However, two qualitative differences exist in the screening data: SdiA_{SE} is antagonized by a slightly greater number of compounds than SdiA_{EC}, and SdiA_{EC} is agonized by more non-lactone compounds than SdiA_{SE}. It is interesting to note that *sdiA* is a descendent of a horizontal gene transfer of *rhIR* in *P. aeruginosa*.²⁰ The RhIR receptor displays some similarities with SdiA_{EC} (see Figure I.2), including being relatively promiscuous in terms of agonists, being broadly activated by PHLs and PPHLs, and not being activated by BnHLs. These results suggest that SdiA from the other genera could likely display similar levels of promiscuity and affinity for similar chemical structures.

1.2.5 Structure-activity relationships for SdiA_{EC} agonism

We next collected agonism dose-response curves for the 28 compounds with at least 50% activity in the 10 nM agonism screen (Table I.1). Most of these compounds could be divided into four categories: aliphatic AHLs (Figure I.2i), PHLs (Figure I.2iii), PPHLs (Figure I.2iv), and non-homoserine lactone compounds, such as AHTs (Figure I.2vi). We collected agonism dose-response curves of several additional compounds to better understand the SAR of these chemical scaffolds.

Table I.1 Selected SdiA_{EC} agonism dose-response assay data.

(A) AHLs				(C) AHTs			
compound	AHL ^b	EC ₅₀ [nM] (95% CI) ^d	max. act. [%] (95% CI) ^e	compound	tail group ^c	EC ₅₀ [nM] (95% CI) ^d	max. act. [%] (95% CI) ^e
A1	C4	932 (613–1415)	123 (114–132)	F9	C1	5.33 (3.97–7.15)	89.4 (84.8–93.9)
A2	C6	2.46 (1.48–4.09)	95.3 (87.8–103)	F8	A1	6.85 (4.44–10.6)	117 (108–126)
3	3-oxo-C6	3.84 (2.24–6.60)	114 (105–123)	F7	A2	1.1 (0.86–1.42)	113 (109–117)
4	C7	2.64 (1.32–5.28)	78.2 (69.9–86.6)	F6	4	2.35 (1.53–3.61)	97 (92–103)
A3	C8	2.90 (1.88–4.47)	105 (98.8–111)	F5	A3	1.64 (1.06–2.55)	120 (113–127)
H2	3-OH-C8	8.95 (5.69–14.1)	79.2 (74.5–83.9)	F2	2	4.78(2.68–8.54)	90 (81–99)
2	3-oxo-C8	0.78 (0.51–1.19)	90.6 (85.0–96.2)	F4	A4	11.4(7.19–18.2)	113(104–123)
A4	C10	16.0 (9.47–27.0)	78.8 (73.8–83.9)	F1	1	0.80 (0.56–1.15)	74 (71–77)
A7	3-oxo-C10	3.89 (2.21–6.85)	86.6 (81.5–91.7)	F10	7	6.41(2.97–13.8)	91 (79–102)
A5	C12	15.8 (11.4–22.1)	93.7 (88.4–99.1)	F11	C14	2.11(1.50–2.97)	126 (120–133)
1	3-oxo-C12	11.8 (4.97–27.8)	111 (98.6–124)	F12	C24	5.70(3.94–8.24)	109 (103–115)
H6	3-OH-C12	231 (119–448)	86.3 (75.9–96.6)	16 ^h		32.9(21.4–50.7)	122 (112–132)
A6	C16	800 (462–1385)	91.3 (80.7–102)	RN22	E22	5.57(3.67–8.53)	92 (86–99)
H25	3-oxo-C16	191 (87.3–417)	64.3 (55.7–72.9)				
(B) PHLs				(D) other compounds ^h			
compound	<i>o</i> , <i>m</i> , <i>p</i> -X ^c	EC ₅₀ [nM] (95% CI) ^d	max. act. [%] (95% CI) ^e	compound		EC ₅₀ [nM] (95% CI) ^d	max. act. [%] (95% CI) ^e
C1		7.62 (5.04–11.5)	106 (98.2–114)	B9		23.4 (18.5–29.4)	82.1 (78.3–85.9)
C4	<i>o</i> -F	4.18 (2.41–7.26)	104 (95.2–113)	F18		2.07 (1.17–3.65)	103 (95–111)
C5	<i>p</i> -Cl	3.56 (2.44–5.19)	88.2 (82.0–94.3)	12		24.2 (9.96–58.8)	93 (83–103)
C6	<i>m</i> -Cl	1.19 (0.69–2.07)	108 (99.7–117)	E22		5.68 (3.76–8.58)	106 (99–113)
C7	<i>o</i> -Cl	17.2 (11.9–24.7)	104 (96.5–111)	E37		3.68 (2.75–4.94)	102 (98–107)
7 ^d	<i>p</i> -Br	1.86 (0.80–4.31)	93.8 (85.2–102)	17		220 (145–336)	102 (92.4–112)
B4 ^f	<i>p</i> -Br	631 (432–922)	67.4 (61.2–73.6)	23		N/A	N/A
C8	<i>m</i> -Br	1.70 (1.08–2.66)	115 (107–123)				
C11	<i>m</i> -I	1.86 (1.37–2.53)	127 (121–133)				
C13	<i>p</i> -NO ₂	3.06 (2.00–4.69)	95 (88.7–101)				
C14	<i>m</i> -NO ₂	1.60 (1.09–2.34)	118 (111–125)				
C24 ^d	<i>p</i> -OCH ₃	5.00 (4.02–6.22)	99.8 (96.6–103)				
E2	<i>m</i> -OCH ₃	1.42 (0.91–2.23)	112 (105–119)				
E1	<i>m</i> -CH ₃	3.44 (2.39–4.95)	88.8 (83.4–94.2)				
E3	<i>m</i> -CF ₃	3.92 (2.71–5.66)	94.9 (89.1–101)				
E5	<i>m</i> -CN	2.43 (1.26–4.69)	106 (96.5–116)				
E7	<i>m</i> -SCH ₃	3.09 (2.15–4.44)	102 (96.4–107)				
E10	<i>p</i> -F, <i>m</i> -CF ₃	8.28 (5.76–11.9)	97.6 (91.1–104)				
E12	naphthyl	3.86 (3.08–4.85)	109 (105–113)				

^aAll dose response curves were obtained as 3 or 4 biological replicates of technical triplicates using the WT *E. coli* SdiA_{EC} reporter strain (see SI). ^bAHLs are named based on the presence of a substituent at the 3rd carbon in the acyl tail (either a hydroxyl group or carbonyl) and the number of carbons in the acyl tail. ^cSubstituent identity and position on PHL (C1). ^dData were fit using GraphPad Prism software using a three parameter and a four parameter (varied slope) dose-response analysis. Reported values are for the three parameter fit unless the Hill slope in the four parameter fit was different than 1.0 (95% CI). The two different Hill slopes were for compounds **7** [0.64 (0.32-0.95)] and **C24** [0.81 (0.68-0.94)]. ^eThe “Max Activation” refers to the “top” parameter in the non-linear regression fit. 100% activation is defined using a positive control (10 μM **2**) and 0% is defined using a negative control (DMSO). N/A denotes that the data could not be fit to this activation model. ^fInverted stereochemistry; D-homoserine lactone head group. ^gTail groups of HTs (Figure I.2iv) indicated with the compound name for the HL analogue. ^hCompound structures shown in Figure I.S1; compound numbering matches original reports.

Several trends can be identified for the effect of the AHL acyl tail on SdiA_{EC} agonism (Table I.1A and Figure I.S3A). The optimal length of aliphatic AHL tails for SdiA_{EC} is 6–8 carbons (**A2**, **4**, and **A3**; Table I.1A). While 10–12-carbon tail lengths (**A4**, **A5**) are still well tolerated, shorter 4-carbon (**A1**) and longer 16-carbon (**A6**, **H25**) tails have much lower agonism potencies. In several cases, we see that the addition of a 3-oxo group increased potency about 4-fold (**2** (OOHL), **A7**, and **H25**), and the addition of a 3-hydroxyl group appears to decrease potency (**H2**, **H6**). These trends for aliphatic AHL agonism in SdiA_{EC} are nearly identical to those we identified previously for SdiA_{SE}.¹⁹

As we have observed for numerous other LuxR-type receptors, PHLs were an extremely active class of compounds in SdiA_{EC}.^{11, 39, 48, 52} Distinct for SdiA_{EC} was its high tolerance for alterations to the PHL scaffold (Table I.1B and Figure I.S3B). Unsubstituted PHL (**C1**) has an EC₅₀ of 7.6 nM, and a wide array of substituents were tolerated, or even improved ligand potency, at the *ortho*, *meta*, or *para* positions. Only five out of 31 PHLs (**C16**, **C18**, **C21**, **C22**, and **E9**) had less than 60% activity at 100 nM, and only a single PHL (*p*-Boc-amine PHL, **C22**) had less than 30% activity (Table I.S3). Notably, many *meta* substituents, both electron-withdrawing (e.g., nitro-**C14**, cyano-**E5**) and donating (e.g., methoxy-**E2**), gave at least a 3-fold improved potency relative to **C1** in SdiA_{EC} (Table I.1B), yielding agonists with activity comparable to the native OOHL (**2**). Multiple substitutions were not always well tolerated: for example, a single *meta* trifluoromethyl substituent (**E3**) had slightly improved potency compared to **C1** (Table I.1B), but the double *meta* substituent (**E9**) had only 48% activity at 100 nM (Table I.S3). Additionally, two large *para* substituents had less than 50% activity at 100 nM (Table

I.S3): phenyl (**C18**) and Boc-amine (**C22**). However, the naphthyl version of a PHL (**E12**) was more potent than **C1** (Table I.1B) and other large *para* substituents such as iodo (**C10**) and thiomethyl (**E6**) had more than 80% activity at 100 nM (Table I.S3). These results suggest that there is significant, but not unlimited, room for accommodation of substituents on the PHL scaffold. As with aliphatic AHLs, these SARs are very similar to those observed for PHLs for SdiA_{SE}.¹⁹

The PPHL scaffold was not as well sampled in the library as the PHLs, but we can still identify certain trends. Unsubstituted PPHL **B9** (23 nM, Table 1 I.D) has an EC₅₀ that is 3-fold higher than its one carbon shorter homolog **C1**. All 11 PPHLs tested had greater than 60% agonism activity in the 100 nM screen (Table I.S3). At 100 nM, 4 out of 6 *para* substituted PPHLs and 1 out of 3 *meta* substituted PPHLs had greater than 85% activity; only the *para* nitro PPHL (**E37**) had greater than 60% activity at 10 nM (Table I.S4) and this compound is more than 6-fold more potent than unsubstituted PPHL (**B9**). These results suggest that the PPHL scaffold is less potent overall than the PHL scaffold in SdiA_{EC}, and potentially favors substituents at the *para* rather than *meta* position.

Of the small number of compounds examined with modified linkages between the lactone and alkyl tail, compounds with a sulfone linkage (**A9**, **A13**) or α,β unsaturation (**B10**, **D18**) had less than 50% agonistic activity at 100 nM (Table I.S3). Increased steric bulk at the α -carbon was also not tolerated; all the BnHLs and **S1**, **S2**, and **S3** had less than 40% activity at 100 nM, except **R8** (Table I.S3). Several analogues with alternate head groups were sampled in the library, and a subset were found to strongly activate SdiA_{EC}. Thiolactone analogues were highly active (Table I.1C) and often had improved

potency over the parent lactone (as we have observed in other LuxR-type receptors).^{19, 43, 51, 53} Inversion of the HSL stereochemistry reduced potency but retained some agonistic activity (**B3**, **B4**, and **B5**; Table I.S3); for example, inversion of stereochemistry for *p*-Br PHL (**7** vs. **B4**) resulted in a greater than 300-fold decrease in potency (Table I.1). A comparison between the results for compound **1** and **12** suggests that switching from a HL to an unsubstituted phenyl head group only reduces agonism potency 2-fold (Table I.1). Replacement of the HSL in decanoyl HL (**A4**, Table I.1A) with a cyclopentane head group (to give **17**, Table I.1D) reduced activity dramatically; however, conversion of *meta* nitro PHL (**C12**) to the cyclopentyl head group analog (**F18**) showed no significant decrease in activity at 100 nM (Table I.S3). Finally, several non-AHL compounds—identified as potent modulators of LasR in prior screens—showed only limited activity in SdiA_{EC} (**18-22**, Table I.S3).¹²

1.2.6 Antagonism assay data in SdiA_{EC}

Despite the many new agonists uncovered, we identified only two compounds capable of SdiA_{EC} antagonism in our primary screen, **11** and **15** (Figure I.3, Table I.S5). The isothiocyanate AHL derivative **11**, also known as ITC-12, was first identified by Meijler and co-workers as a mimic of LasR's native ligand (OdDHL, **1**) and shown to act (at least in part) as a covalent inhibitor of LasR by reacting with a cysteine in its ligand-binding pocket.¹⁰ In our prior study of SdiA_{SE}, we found that **11** was capable of SdiA_{SE} antagonism in both a competitive and non-competitive manner.¹⁹ Similar to SdiA_{SE}, we discovered that **11** inhibits all AHL-dependent activity in SdiA_{EC} at 100 μ M, as well as inhibiting approximately 40% of AHL-independent activity. However, at lower

concentrations, we found that **11** displayed a very interesting activity trend in SdiA_{EC}. An agonism dose response assay (Figure I.3A, black curve) revealed that **11** has two regimes of activity. At low concentrations, it agonizes SdiA_{EC} to about 70% with an EC₅₀ of 4 nM; this is consistent with the EC₅₀ value of its parent AHL, **1** (12 nM, Table I.1). Yet, at concentrations higher than 100 nM, **11** was observed to *antagonize* SdiA_{EC} instead. In a separate antagonism assay against OOHL (**2**) at its EC₉₀, compound **11** fully inhibits SdiA_{EC} with an IC₅₀ of 256 nM (Figure I.3B, red curve). We note that **11** did not inhibit cell growth at any of the concentrations tested in these assays (see Figure I.S5).

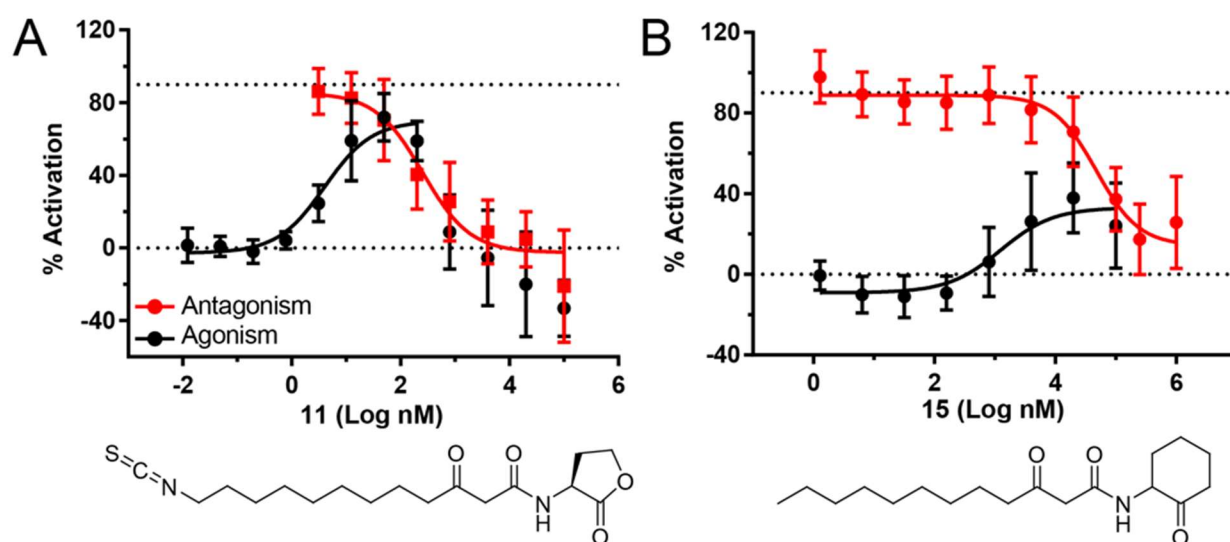


Figure I.3 Dose response curves of 11 and 15. Agonism and antagonism dose-response curves for (A) 11 and (B) 15, with chemical structures shown below the dose response curve plots. All dose response curves were obtained as 3 or 4 biological replicates of technical triplicates using the WT *E. coli* SdiA_{EC} reporter strain. 100% activation is equal to the activity of 10 μ M **2**, and 0% is equal to activation of vehicle (DMSO). Antagonism was determined in competition with **2** at its EC₉₀ (10 nM). Error bars indicate standard deviation.

The other antagonist that we identified in SdiA_{EC}, cyclohexanone **15**, had only moderate potency (IC₅₀ = 48 μM; Figure I.3B). An agonism dose response analysis revealed that **15** is actually a partial agonist with weak efficacy (33% max activity). Compound **15** was identified previously by Suga and co-workers as an inhibitor of LasR from *P. aeruginosa*;⁵⁴ it was also examined for its capability to modulate SdiA_{EC} in an *in vitro* DNA binding assay by Shimada and co-workers. Cyclohexanone **15** failed to induce DNA binding in that prior work.³⁸

Because of **11**'s interesting activity profile, most notably its high potency and efficacy as an inhibitor of SdiA_{EC} (and SdiA_{SE}),¹⁹ we further investigated its mechanism of action. We first sought to determine if the interaction between SdiA_{EC} and **11** is competitive with the interaction between SdiA_{EC} and OOHL (**2**). In SdiA_{EC} antagonism reporter assays with increasing amounts of **2**, the IC₅₀ of **11** increased, and the efficacy of inhibition at 100 μM was reduced (Figure I.S6A). In turn, we observed that the addition of **11** to an SdiA_{EC} agonism reporter assay with **2** increased the EC₅₀ and decreased the maximum activation of **2** (Figure I.S6B). These results suggest that **11** can competitively bind to SdiA_{EC}, presumably in the AHL binding pocket (as **2** has been shown to bind this site in structural studies of SdiA_{EC}).²¹⁻²² However, because of the changes to maximal inhibition and activation in these experiments, we were interested to determine if **11**'s mechanism of inhibition involved a possible covalent interaction between its electrophilic isothiocyanate and SdiA_{EC}.

I.2.7 Compound **11** reacts with C232 of SdiA_{EC}

SdiA_{EC} has three cysteines that could potentially serve as thiol nucleophiles and be covalently modified by **11** (Figure I.4A).²² We constructed a plasmid for the overexpression of SdiA from EHEC with a C-terminal His-tag (SdiA_{EHEC}H₆; see Table I.S2 for strain, plasmid, and primer details and Figure I.S7 for purification details). This tag on SdiA_{EHEC} has been shown to not disrupt AHL binding or DNA binding in prior studies,²¹⁻²² and SdiA_{EHEC} is 99% identical to SdiA_{EC} (sharing all three cysteines), allowing us to build mechanistic hypotheses for SdiA_{EC} with this tagged homolog. We next used ultra-high resolution Fourier transform ion cyclotron resonance mass spectrometry (MS)⁵⁵ to measure the intact mass of SdiA_{EHEC}H₆ that was incubated with or without **11** (10 μ M) either *in vitro* after purification or in intact *E. coli* cells (*in cellulo*) prior to purification. Unmodified and **11**-modified SdiA_{EHEC}H₆ proteoforms (SdiA_{EHEC}H₆ and **11**SdiA_{EHEC}H₆, $\Delta M=354.15$; respectively) were detected in the samples treated with **11** (see Figure I.S8 for representative MS data), suggesting covalent labeling *in vitro* and *in cellulo*. Because we observed that saturating levels of OOHL (**2**) had prevented SdiA_{EC} inhibition by **11** in the cell-based reporter assay (Figure I.S6), we also tested whether addition of saturating levels of **2** (10 μ M) could prevent covalent labeling by **11**. In samples incubated *in cellulo* with 10 μ M **11** and 10 μ M **2**, we detected little to no signal for the **11**SdiA_{EHEC}H₆ proteoform (Figure I.S9), which suggests that **2** prevented covalent labelling. We quantified the abundance of **11**SdiA_{EHEC}H₆ in the *in cellulo* **11** treated samples incubated with and without **2** (relative to SdiA_{EHEC}H₆ + **11**SdiA_{EHEC}H₆ abundance in the samples) as 0.02 ± 0.01 and 0.37 ± 0.07 , respectively (representative replicate shown in Figure I.4B; all replicates shown in Figure I.S10).

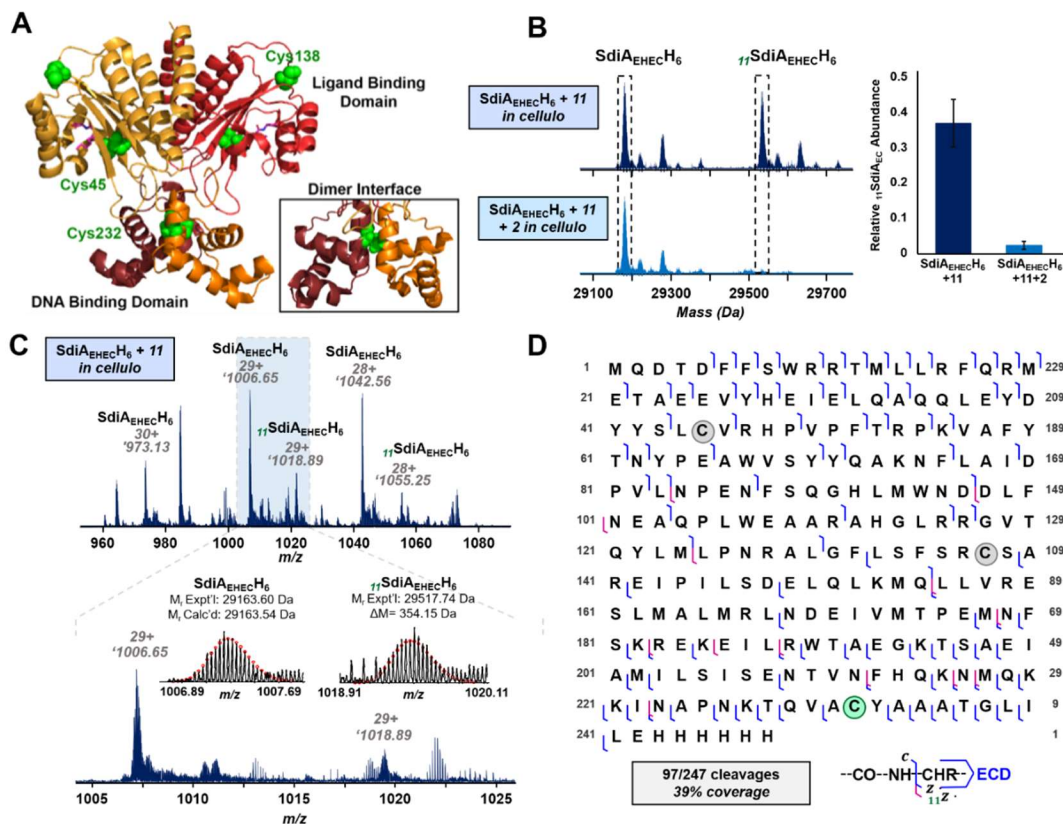


Figure I.4 Crystal Structure of SdiA_{EC} and MS analysis of 11 with SdiA_{EC}. (A) Structure of the [2-SdiA_{EHEC}H₆]₂ complex (from PDB 4y17).²² Individual monomers of SdiA_{EHEC}H₆ shown in tan/gold and red/maroon, and 2 (OHHL) shown in purple. Each cysteine in SdiA_{EHEC}H₆ is shown in green. Inset shows the dimer interface in the DNA binding domain in which C232 forms an inter-monomer disulfide. (B) (Left) Representative deconvoluted mass spectra for SdiA_{EHEC}H₆ + 11 *in cellulo* (navy) and SdiA_{EHEC}H₆ + 11 + 2 *in cellulo* (blue). (Right) Quantification of ¹¹SdiA_{EHEC}H₆ abundance relative to SdiA_{EHEC}H₆ + ¹¹SdiA_{EHEC}H₆ abundance. Relative abundance values represent average of n=3 replicates, error bars represent the standard error of the mean (SEM). (C) (top) Mass spectrum of SdiA_{EHEC}H₆ incubated *in cellulo* with 11 (quadrupole isolation of 100 *m/z* with center at 1019 *m/z*), 100 transient acquisition (2M, 0.01 s ion accumulation time). Charge states 30+, 29+, 28+ (M³⁰⁺, M²⁹⁺, M²⁸⁺) for SdiA_{EHEC}H₆ proteoforms are labelled. (bottom) Zoom-in MS region of 1005-1025 *m/z* showing SdiA_{EHEC}H₆ proteoforms (29+ charge state, M²⁹⁺), with unmodified SdiA_{EHEC}H₆ (SdiA_{EHEC}H₆) at '1006.65 *m/z* and 11-modified SdiA_{EHEC}H₆ (¹¹SdiA_{EHEC}H₆) at '1018.89 *m/z*. Experimental (Expt'l) and calculated (Calc'd) monoisotopic masses are shown for SdiA_{EHEC}H₆. Expt'l mass and mass difference between Expt'l and Calc'd monoisotopic masses from un-modified SdiA_{EHEC}H₆ are shown for ¹¹SdiA_{EHEC}H₆. (D) Sequence table showing fragment ions for two combined ECD MS/MS experiments. Blue cleavages represent detection of unmodified fragment ions and magenta cleavages represent detection of 11-modified fragment ions. Cysteine residues are circled, with C232 highlighted in green. (bottom-right) Annotation showing cleavages produced by ECD along the protein backbone and the corresponding ions.

From the sample incubated with **11** *in cellulose*, we measured the mass of SdiA_{EHEC}H₆ and ¹¹SdiA_{EHEC}H₆ with high accuracy (Figure I.4C) and subsequently isolated the ¹¹SdiA_{EHEC}H₆ proteoform for tandem MS (MS/MS) to characterize its sequence and localize the cysteine residue(s) that were modified by **11**. We achieved good sequence coverage of ¹¹SdiA_{EHEC}H₆ (39%) with 97 out of 247 protein backbone cleavages detected by electron capture dissociation (ECD),⁵⁶⁻⁵⁷ an MS/MS technique that preserves labile modifications allowing for localization (Figure I.4D). In view of the Meijler lab's report with **11** in LasR,¹⁰ we initially suspected that **11** might covalently react with the cysteine inside the SdiA_{EHEC}H₆ AHL-binding pocket (C45); however, we obtained results strongly suggestive for the modification of C232 based on the presence of z•-fragment ions at the C-terminus of the protein backbone (Figure I.4D; see Note in Figure I.S11). To probe this result further, we constructed a C232A SdiA_{EC} mutant activity reporter in *E. coli*, effectively removing the possibility for nucleophilic capture at this residue (see Table I.S2 for further details). We note that the C232A mutation reduced the overall activity of SdiA_{EC} in the cell-based reporter by more than two-thirds relative to WT (as judged by the activity of agonist **2**; Figure I.S2), suggesting that C232 plays an important role in the stability and/or activity of SdiA_{EC}. Nevertheless, and as expected, **11** was unable to inhibit C232A SdiA_{EC} activity in this reporter (tested up to 100 μM), and instead, it acted only as an agonist (Figure I.S12).

Reaction of **11** with C232 directly implies a plausible means by which **11** inhibits the AHL-dependent and AHL-independent activity of SdiA_{EC}. Based on prior structural studies of SdiA_{EHEC} and biochemical data, we predict that C232 forms an inter-monomer disulfide (see Figure I.4A inset) and potentially plays a role in the intrinsic stability and

activity of apo-SdiA_{EC}.²¹⁻²² In view of the position of C232 in SdiA_{EC}, we would suspect that covalent modification would prevent dimerization.²² In support of this hypothesis, Kim *et al.* showed that reaction of C232 with methyl methane thiosulfonate (MMTS) prevents SdiA_{EHEC} binding to DNA.²¹ Similarly, purified SdiA_{EHEC} elutes from a size-exclusion column as a dimer in the absence of a reducing agent and as a monomer in the presence of a reducing agent (data not shown), strongly suggestive of C232 forming an inter-monomer disulfide. This finding is interesting as it has broader implications; since C232 is a highly conserved residue in SdiA across *Escherichia* and other genera, **11** could serve as a general inhibitor of SdiA. This possibility is supported by its strong inhibitory activity in both SdiA_{EC} and SdiA_{SE}.

We next altered the structure of **11** to further probe its mechanism of action in SdiA_{EC} (Figure I.5). We reasoned that if the isothiocyanate of **11** was replaced with a non-electrophilic yet sterically similar moiety (e.g., an azide), it should not be able to react with C232 and inhibit SdiA_{EC}. Congruent with this hypothesis, the azide analogue of **11**, **HSL-Az-12**, acted solely as an agonist in the WT SdiA_{EC} cell-based reporter assay, with a similar EC₅₀ to its parent AHL, **1** (Figure I.6A). We note that, despite the evidence for competitive binding between **11** and **2**, the isothiocyanate of **11** could still potentially react with C232 in a manner that does not require binding to the AHL binding pocket of SdiA_{EC}. To examine this possibility, we tested the ability of butyl, octyl, and phenyl isothiocyanate to inhibit SdiA_{EC} in cell-based reporter assays; none of these compounds were able to inhibit SdiA_{EC} (Figure I.6B and Figure I.S13). These results suggest that the AHL-scaffold of **11** is important for interaction with and eventual covalent capture of SdiA_{EC}.

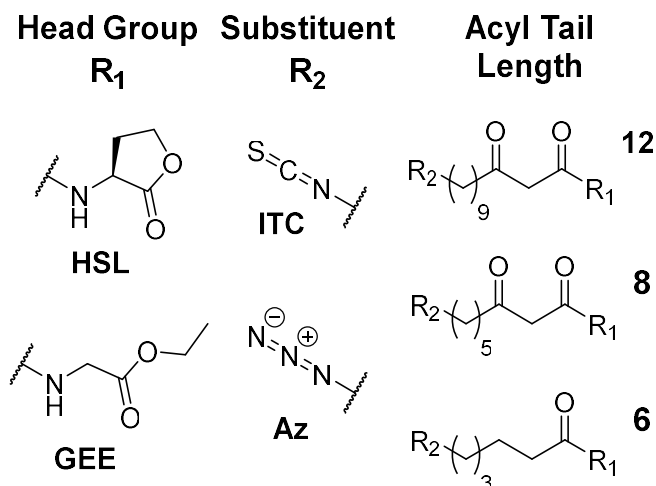


Figure I.5 Structural features of analogues of 11. Each combination of R_1 , R_2 , and acyl tail length was synthesized. Compounds are named as R_1 - R_2 -acyl tail length; for example, **11** would be **HSL-ITC-12**, and its azide analogue would be **HSL-Az-12**.

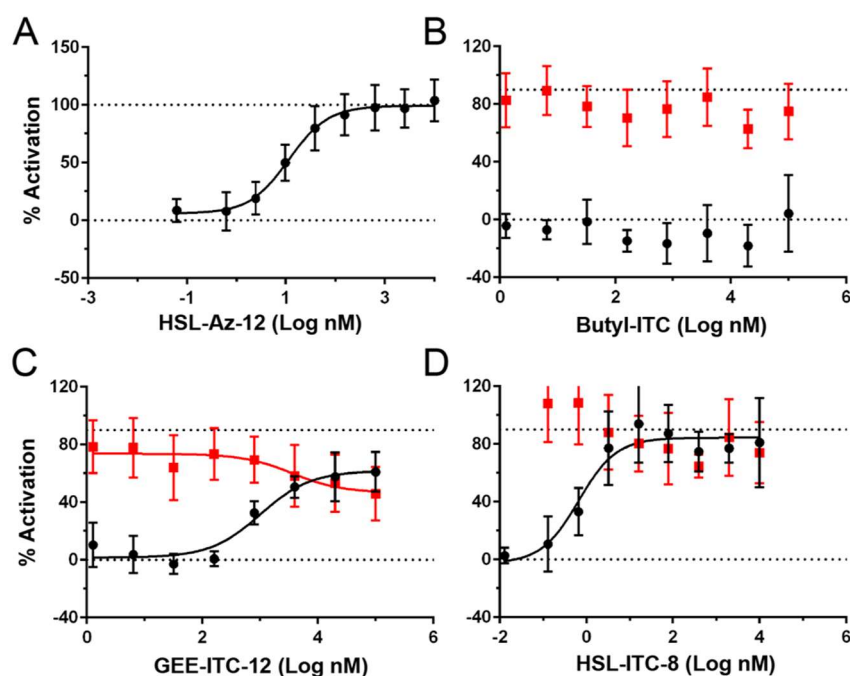


Figure I.6 Dose response curves of analogues of 11. Agonism (black) and antagonism (red) dose-response curves for (A) **HSL-Az-12**, (B) **Butyl-ITC**, (C) **GEE-ITC-12**, and (D) **HSL-ITC-8** using the JLD271-SdiA_{EC} reporter strain. All dose response curves were obtained as three or four biological replicates of technical triplicates. Error bars indicate standard deviation.

To further examine the role of the lactone head group in the interaction of **11** with SdiA_{EC}, we constructed glycine ethyl ester (GEE) headgroup analogs **GEE-ITC-12** and **GEE-Az-12**. We knew, based on our primary screening results, that a glycine ethyl ester (GEE) head group was unlikely to have a high affinity for SdiA_{EC}: the GEE analogs **F39**, **F45**, and **F47** all have less than 40% activity in the 100 nM SdiA_{EC} agonism screen (see Table I.S3). Indeed, the EC₅₀ was 250-fold higher for **GEE-ITC-12** and 400-fold higher for **GEE-Az-12** as compared to **11** and **HSL-Az-12**, respectively (Table I.S6). **GEE-ITC-12** was also a weaker antagonist of SdiA_{EC} relative to **11**, inhibiting to only 54% at 100 μM (Figure I.6C). These results with non-lactone analogs of **11** further support our hypothesis that inhibition of SdiA_{EC} by **11** is dependent on an initial non-covalent binding event dependent on the lactone headgroup, most likely in the AHL binding pocket. We also probed the effects of changing the length of the acyl tail in **11**. As SdiA_{EC} is strongly activated by AHLs with 6–8 carbon tails, we expected shorter carbon tails would generate more potent ligands. We tested **HSL-ITC-6** and **HSL-ITC-8** (and their GEE analogues) in the cell-based reporter agonism and antagonism assays. However, none of these compounds inhibited SdiA_{EC} (Figure I.6D and Figure I.S13). These results suggest that the long tail in **11** might position the isothiocyanate for productive reaction with C232 in SdiA_{EC}. Inspection of the crystal structure of SdiA_{EHEC} with **2** (Figure I.4A) suggests that the longer tail of **11** could possibly position the isothiocyanate outside of the enclosed binding pocket (beyond F59 and L77, which are thought to close the binding pocket).²² However, additional experiments will be needed to address this possibility, namely to determine (1) whether **11** remains bound to the AHL binding pocket after reaction with C232, and (2) what additional conformational changes of

SdiA_{EC} are induced by **11** to position the isothiocyanate for reaction with C232.

Biochemical and biophysical experiments to address these questions and others are ongoing in our laboratory.

1.2.8 11 reduces SdiA dependent survival of E. coli in acidic media

Lastly, we sought to investigate if the new small molecule modulators of SdiA_{EC} identified herein could affect a QS-controlled phenotype in *E. coli*. Again, SdiA_{EC} has been shown to mediate survival of *E. coli* in acidic media.^{24, 32} In these assays, *E. coli* is grown to stationary phase and then challenged with an acidic minimal medium (pH 2.5) or a neutral minimal medium (pH 7.0) for 1.5 hours; survival in the acidic medium is determined as a percentage of cells relative to those that survived in neutral medium. Using this assay protocol, we found that the $\Delta sdiA$ mutant has markedly reduced acid tolerance, but the addition of the agonist **2** to WT *E. coli* did not significantly alter survival (Figure I.7). However, antagonists **11** and **15** were found to dramatically reduce survival in the acidic medium: at 100 μ M, both antagonists reduced survival to nearly $\Delta sdiA$ levels. We note that **11** and **15** do not reduce survival in the neutral minimal medium (Figure I.S14) or in LB (Figure I.S5) and that $\Delta sdiA$ *E. coli* survival in acidic medium treated with DMSO, **2**, **11**, or **15** do not significantly differ ($p > 0.05$). We conclude from these experiments that both **11** and **15** decrease survival of *E. coli* in acidic conditions in a SdiA_{EC} dependent manner.

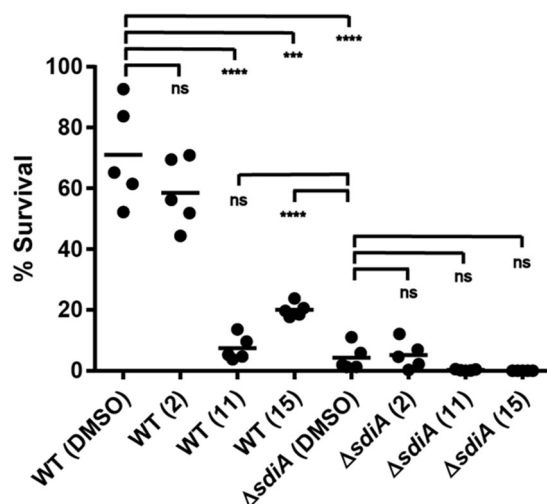


Figure I.7 Survival of WT or Δ sdiA *E. coli* in an acid challenge assay. See Methods for details. DMSO (vehicle control), **2** (10 μ M), **11** (100 μ M), or **15** (100 μ M) were added to the initial growth medium and acidic challenge media. The individual data points are shown for each condition (circles) and averages (lines) are shown representing five independent challenge wells. “ns” indicates that the means are not significantly different ($p > 0.05$). *** and **** indicate that the means are significantly different ($p = 0.0001$ and $p < 0.0001$, respectively).

1.2.9 Implications

The results of this search for non-native chemical modulators and study of AHL SAR in SdiA_{EC} have two broad implications. The first is related to the observed high promiscuity of SdiA_{EC} for AHL-type agonists. As noted above, SdiA_{EC} displays unusually high *in vitro* stability in the absence of an agonist ligand relative to other LuxR-type receptors.^{21-22, 58} Smith *et al.* proposed that the instability of most *apo*-LuxR-type receptors could serve as a kinetic screen to increase their selectivity for a specific AHL signal.⁵⁹ Under this framework, it is reasonable to speculate that *E. coli* could have evolved a stable orphan LuxR-type receptor to allow for *less* selectivity in binding and activation by exogenous AHL signals. Additionally, Huang *et al.* proposed that a

stabilized *apo*-receptor might allow the bacterium to expend less energy to maintain the ability to sense the signal and might respond more quickly to increases in signal.⁶⁰

The promiscuity of SdiA_{E_{EC}} raises questions about prior techniques used in the search for and identification of AHLs in the digestive track of cattle. Those past studies have relied primarily on bio-reporter strains based on the TraR and CviR LuxR-type receptors for the detection of AHLs.^{24, 28-31} However, SdiA_{E_{EC}} is activated not only by lower concentrations of AHL than CviR and TraR, but also by a significantly expanded array of AHLs relative to these receptors (Figure I.2). The β -galactosidase reporters for SdiA_{E_{EC}} and SdiA_{SE}, constructed in this study and in our earlier work,¹⁹ could represent valuable tools to screen for a considerably wider variety of AHLs in animal hosts or environmental samples, using thin-layer chromatography or other well-developed detection methods.⁶¹

The second implication of this study is that SdiA_{E_{HEC}} should be readily amenable to modulation with non-native molecules. Chemical tools can provide spatial and temporal control of SdiA activity, advantages not associated with common genetic approaches, such as complementation with a LuxI-type synthase.^{33, 62-63} Because SdiA_{E_{HEC}} regulates two phenotypes essential for colonization, controlling SdiA_{E_{HEC}} activity could be a means of reducing the presence of EHEC in cattle.^{24, 64} Furthermore, because SdiA_{E_{HEC}} activates one of these phenotypes and represses the other, the spatial and temporal control offered by small molecules would be useful for investigating how manipulation of SdiA_{E_{HEC}} could be used to reduce colonization and shedding of EHEC in cattle populations. Because of the pH differences throughout the bovine gastrointestinal tract, introduction of an AHL based activator or inhibitor in the rumen

(Figure I.1C) would possibly offer temporal modulation of SdiA_{EC} activity (and thus alter acid resistance) prior to entering the intestines where the lactone head group would be hydrolyzed in the alkaline pH (~8) environment of the intestines.^{24, 65} To this end, the installation of headgroups with enhanced hydrolytic stability (e.g., thiolactone or phenyl as in **F2** and **12**, respectively) could provide modulators of SdiA_{EC} activity that remain active throughout the gastrointestinal tract.

I.3 Summary and Conclusions

This study was motivated by our interest in cell-cell communication in *E. coli*, specifically in the development of chemical strategies to attenuate QS via the LuxR-type receptor SdiA_{EC}. We constructed a transcriptional reporter of SdiA_{EC} activity, screened a focused library of small molecules for activity in SdiA_{EC}, developed SARs for agonism of SdiA_{EC} by AHLs, identified highly potent non-native agonists and antagonists of SdiA_{EC}, and demonstrate that one potent antagonist (**11**) causes inhibition of SdiA_{EC} through a cysteine that is functionally important to SdiA_{EC} activity and highly conserved in SdiA from other genera. We demonstrate that SdiA_{EC} is highly promiscuous and is activated by almost all the compounds tested containing an L-homoserine lactone. Additionally, we show that SdiA_{EC} can be activated by compounds that contain head groups that are inherently more hydrolytically stable than a lactone, such as a thiolactone or phenyl, suggesting additional scaffolds that can be developed in the future as chemically robust probes of SdiA_{EC}.

Looking forward, this study lays a potential pathway for developing mechanistic rationales for not only how SdiA_{EC} is activated or inhibited by small molecules, but also

a broad range of other LuxR-type receptors. The small molecule library screened in this study consists of numerous AHL analogue scaffolds that we and others have shown to strongly activate or inhibit over 10 different LuxR-type receptors. Biochemical and biophysical studies of these LuxR-type receptors have been limited by the inability to purify the receptor in the absence of the native ligand, or a potent agonist or antagonist, and only four full-length LuxR-type receptors have been characterized by X-ray crystallography to date.¹³ In contrast, SdiA_{EC} can be purified in the absence of ligand, is readily crystallizable (as observed for SdiA_{EHEC}), and as we now show here, is strongly modulated by chemical scaffolds that have activity in many other LuxR-type receptors, the bulk of which again are largely intractable to biochemical analyses. We contend these properties make SdiA_{EC} an excellent model system for improving the understanding of the modes by which these synthetic ligand scaffolds bind to conserved features of the LuxR-type receptor binding pocket and differentially modulate the activity of this protein family.²² We also speculate that regulation of receptor dimerization via the introduction or manipulation of inter-monomer disulfides (e.g., C232 in SdiA) could provide new entry into study of LuxR-type protein function.

I.4 Supporting Information

I.4.1 Chemical and biological methods

Chemicals and compound handling

The library of compounds screened in this study is shown in Figure I.S1. These compounds were either synthesized as previously described or purchased (see Table I.S1 for additional references).¹⁹ The synthesis of the new compounds reported in this

study (i.e., the GEE/HSL library) is described later in this SI document. The β -galactosidase reporter assay substrate, *ortho*-nitrophenyl- β -D-galactopyranoside (ONPG), was purchased from DOT Scientific. Stock solutions of compounds were prepared at 10 or 100 mM in DMSO and stored at -20 °C in sealed vials.

Bacterial strains and growth conditions

The strains, plasmids, and primers used in this study are summarized in Table I.S2. All biological media and reagents were obtained from commercial sources and used according to the manufacturers' instructions. All strains were grown in lysogeny broth (LB) with the appropriate antibiotics at 37 °C with shaking (at 200 rpm) unless noted otherwise. Bacterial growth was assessed by measuring cell culture optical density by absorbance at 600 nm (OD_{600}) using a Biotek Synergy 2 plate reader. When appropriate, the following antibiotic concentrations were used for bacterial growth conditions: 10 μ g/mL gentamicin, 100 μ g/mL ampicillin, and 34 μ g/mL chloramphenicol.

Construction of *SdiA*_{EC} reporter and *SdiA*_{EHEC_{H6}} overexpression strains

Reporter (pSC11) and expression (pJN105) plasmids were constructed as described previously.¹⁹ Briefly, to make pSC11-*pgadW*, 333 base pairs of the *gadW* promoter region (-311 to $+21$) from K12 *E. coli* MG1655 (NC_000913.3) were cloned into pSC11, using the *gadW* primers listed in Table I.S2. To make pJN105-*sdiA*_{EC}, 723 base pairs of *sdiA* from K12 *E. coli* MG1655 were cloned into pJN105, using the *sdiA* primers listed in Table I.S2. To make pJN105-*sdiA*_{EC}C232A, a Gibson Assembly Cloning Kit (New England Biolabs) was used with the C232A primer listed in Table I.S1.

To make pET23b-*sdiA*_{EHEC}H₆, 720 base pairs of *sdiA* from *E. coli* 86-24 (WT EHEC serotype O157:H7) were cloned into pET23b, using the primers listed in Table I.S2. PCR-generated fragments were digested, ligated with cut vector, and transformed into *E. coli* DH5 α using standard restriction digest cloning methods as we have reported previously.⁴⁹ To construct the reporter strains, pSC11 and pJN105 were transformed into JLD271 (*E. coli* Δ *sdiA*).⁶⁶ To construct the overexpression strain, pET23b-*sdiA*_{EHEC}H₆ was transformed into BL21(DE3)-pLysS.

β -galactosidase assay reporter assay

The β -galactosidase assay using either the JLD271-SdiA_{EC} or JLD271-SdiA_{EC}C232A reporter was performed as reported previously, with minor modifications.¹⁹ The reporter strain was grown for 16–18 h (overnight) in LB medium, diluted 1:10 in fresh LB medium, and incubated until it reached an OD₆₀₀ of 0.25. Expression of SdiA_{EC} was induced by the addition of 4 mg/mL arabinose, and this subculture was incubated in 96-well plates in the presence of compounds (1% DMSO) for 4 h. For antagonism assays, the subculture was supplemented with 3-oxo-C8 AHL (OOHL, **2**) at its EC₉₀ (10 nM, 0.1% DMSO); positive and negative control wells were plated before the addition of **2** to the subculture. A 50- μ L aliquot of culture from each well was lysed in 204 μ L of Z-buffer and 8 μ L of chloroform, and a 100- μ L aliquot of this lysate was incubated with 25 μ L of 4 mg/mL ONPG for 8 min (SdiA_{EC}) or 20 min (SdiA_{EC}C232A) at 30 °C before reading absorption at 420 nm and 550 nm using a Biotek Synergy 2 plate reader.⁵⁰ Non-linear regression curve fits were generated using GraphPad Prism software (version 6) using a three parameter and a four parameter

(varied slope) dose–response analysis; all fits reported are three parameter fits (unless otherwise noted).

Purification of SdiA_{EHEC}H₆

SdiA_{EHEC}H₆ was purified as described previously.²² Briefly, BL21(DE3)-SdiA_{EHEC}H₆ was grown for 16–18 h (overnight) in LB medium. A 1:100 subculture of this overnight culture in LB medium with 100 µg/mL ampicillin was grown until an OD₆₀₀ of 0.6, chilled on ice, and then induced with 500 µM isopropyl β-D-thiogalactopyranoside (IPTG) before being incubated at 16 °C overnight. The overexpression culture was chilled on ice and then pelleted. Cells were suspended in lysis buffer (50 mM Tris (pH 8.5), 300 mM NaCl, 0.1 mM EDTA, 20 mM imidazole, and 10% glycerol) and lysed by sonication. Insoluble protein was removed by centrifugation. SdiA_{EHEC}H₆ was purified by nickel affinity chromatography (HisTrap FF 5 mL, GE Healthcare) on an FPLC (AKTA pure, GE Healthcare) via gradient elution (20 mM to 500 mM imidazole). Pure fractions were buffer exchanged (HiTrap Desalting column, GE Healthcare) into assay buffer (50 mM Tris (pH 8.5), 500 mM NaCl, 1 mM EDTA, and 10% glycerol). Samples were concentrated, quantified, and aliquots were frozen using liquid N₂ for storage at -80 °C. Note, reducing agents were not used during these purifications.

For *in vitro* compound-exposed MS samples, purified SdiA_{EHEC}H₆ was exchanged into glycerol free assay buffer and incubated with either DMSO (1%; vehicle) or compound **11** (10 µM) on ice for 30 min before precipitation with acetone at -20 °C for 4 h. Acetone was decanted, and the samples were dried under vacuum.

For intact cell (*in cellulo*) compound-exposed MS samples, prior to lysis, concentrated BL21(DE3)-SdiA_{EHEC}H₆ cells in lysis buffer were incubated with either compound **11** (10 μ M) alone or **11** (10 μ M) + **2** (10 μ M) on ice for 45 min. Cells were washed with assay buffer to remove unreacted compound and then SdiA_{EHEC}H₆ was purified as described above, exchanged into glycerol free Assay Buffer, and diluted to 10 μ M aliquots before acetone precipitation (-20 °C for 4 h). Acetone was decanted, and the samples were dried under vacuum.

Top down mass spectrometry

Acetone-precipitated protein pellets were re-suspended in 0.1% formic acid in water. The samples were further de-salted using ultracentrifugation filtration through 10 kDa molecular weight cut-off filters (Amicon). Following filtration, the samples were diluted 50% with 0.1% formic acid in MS-grade acetonitrile to aid the electrospray ionization process. The samples were directly infused into a Bruker Solarix 12 T Fourier transform ion cyclotron resonance (FTICR) mass spectrometer using a chip-based nano-electrospray source (Advion Nanomate) with gas pressure set between 0.3–0.5 psi and voltage set between 1.3–1.5 V. Skimmer voltage was set to 70 V. An excitation energy of 20% was used. For MS/MS, targeted ECD was performed. ECD parameters were varied, but electron bias between 0.6–1.0 V and pulse lengths between 15–100 ms were used. Typically, 500–2000 transients (2M) were acquired for each MS/MS experiment. MASH Suite Pro⁶⁷ was used for MS/MS data analysis, and manual validation of fragment ion matches were performed.

Acid challenge assay in *E. coli*

Survival dependent on the glutamate-dependent acid-resistance system was tested in K-12 MG1655 *E. coli* (WT or $\Delta sdiA$) as previously described.²⁴ Cells were grown overnight to stationary phase in LB medium with 0.4% glucose and either DMSO (1%; vehicle) or compound. For acid challenge, cultures were diluted 1:10 into E minimal medium (60 mM K₂HPO₄, 20 mM NaNH₄HPO₄, 9.5 mM citric acid, 800 μ M MgSO₄, pH 2.5) with 0.4% glucose, 40 μ M glutamate, and either DMSO (1%; vehicle) or compound. For a neutral challenge, an identical E minimal medium was prepared but at pH 7. Cells were incubated with either acidic or neutral E minimal medium for 1.5 h at 37 °C without shaking. CFUs were determined via plating of several dilutions (in LB medium + MOPS (pH 8)) and counting of the colony forming units (CFUs). CFU/mL was determined only from dilutions that resulted in at least 100 CFU.

Table I.S1 Details of prior small molecule screens with other LuxR-type receptors.

Receptor	Reporter type ^a	Agonism (μM) ^b	Antagonism (μM) ^c	Compounds ^d	Reference
LasR	HET	5	5	Sub-Libraries A-D	40
LasR	HET	10	10	Sub-Libraries A, E, F, H, Q-S	41-43, 45
LasR	HET	100	100	Compounds 1-22	12
QscR ^e	HET	5	5	Sub-Libraries A-D, H, Q-S	44-45
RhIR	HET	100	100	Sub-Libraries A-E	39
RhIR	HET	1000	1000	Sub-Libraries F, Q-S	47
LuxR	WT	10	10	Sub-Libraries F, Q-S	42-43, 45
LuxR	WT	200	5	Sub-Libraries A-D	46, 48
TraR	WT	10	10	Sub-Libraries A-D, F, Q-S	40, 42-43, 45
CepR	HET	100	100	All	49
SdiA _{SE} ^e	HET	1	100	All	19
SdiA _{EC} ^e	HET	0.1	100	All	This study

^aReceptor expressed at wild-type levels in the native organism (WT) or from a pBAD promoter in *E. coli* JLD271 (HET). ^bConcentration of compound used in a single concentration agonism screen. 100% activation equal to the maximum activation from native ligand; 0% equal to activation of vehicle (DMSO). ^cConcentration of compound used in a single concentration antagonism screen. 100% inhibition equal to activation of vehicle (DMSO); 0% inhibition equal to the activity of the EC₅₀ concentration of native ligand (EC₉₀ for SdiA_{SE} and SdiA_{EC}). ^dLibrary/compound names correspond to those in Figure I.S1 and our prior publications. ^eOrphan receptor; AHLs **1** and **2** used as the “native ligand” for QscR and SdiA, respectively.

Table I.S2 Strains, plasmids, and primers used in this study.^a

Strain	Description	Reference
<i>E. coli</i> DH5 α	F ⁻ , Δ 80 <i>dlacZ</i> Δ M15 Δ (<i>lacZYA-argF</i>) U169 <i>deoR recA1 endA1 hsdR17</i> (rk ⁻ , mk ⁺) <i>phoA supE44</i> λ - <i>thi-1 gyrA96 relA1</i>	Invitrogen
<i>E. coli</i> K-12 MG1655	F- λ <i>ilvG- rfb-50 rph-1</i> ; OR:H48:K-	CGSC
<i>E. coli</i> JLD271	K-12 Δ <i>lacX74 sdiA271::Cam</i> ; Cam ^R	66
<i>E. coli</i> BL21(DE3)pLysS	F ⁻ <i>ompT hsdS_B</i> (r _B ⁻ m _B ⁻) <i>gal dcm</i> (DE3) pLysS (Cam ^R)	Invitrogen
JLD271-SdiA _{EC}	JLD271 pSC11- <i>pgadW</i> pJN105- <i>sdiA_{EC}</i> ; Amp ^R , Gent ^R	This study
JLD271-SdiA _{EC} C232A	JLD271 pSC11- <i>pgadW</i> pJN105- <i>sdiA_{EC}C232</i> ; Amp ^R , Gent ^R	This study
BL21(DE3)-SdiA _{EHEC} H ₆	<i>E. coli</i> BL21(DE3) pLysS pET23b- <i>sdiA_{EHEC}H₆</i> ; Amp ^R , Cam ^R	This study
Plasmid	Description	Reference
<i>E. coli</i> 86-24 (gDNA)	Wild-type EHEC strain (serotype O157:H7)	22
pSC11-Q	Broad host range PA1897'- <i>lacZ</i> reporter; Amp ^R	39
pSC11- <i>pgadW</i>	Broad host range <i>gadW</i> '- <i>lacZ</i> reporter; Amp ^R	This study, derived from pSC11-Q
pJN105 -Q	QscR expression vector with pBAD promoter, pBBRMCS backbone; Gent ^R	68
pJN105- <i>sdiA_{EC}</i>	SdiA _{EC} expression vector with pBAD promoter, pBBRMCS backbone; Gent ^R	This study, derived from pJN105-Q
pJN105- <i>sdiA_{EC}C232A</i>	SdiA _{EC} C232A expression vector with pBAD promoter, pBBRMCS backbone; Gent ^R	This study, derived from pJN105- <i>sdiA_{EC}</i>
pET23b(+)	T7 promoter/terminator; optional C-terminal His-Tag; Amp ^R	Millipore Sigma
pET23b- <i>sdiA_{EHEC}H₆</i>	T7 inducible SdiA _{EHEC} H ₆ expression vector with C-terminal His-Tag; Amp ^R	This study, derived from pET23b(+)
Primers	Description	Reference
<i>PgadW</i> -F ^b	CATgtcgacGCCGTCTCCAGACTAATAAACCG	This study
<i>PgadW</i> -R ^b	CATggatccCACCGAGCAGACATGAGTCAT	This study
<i>sdiA_{EC}</i> -F ^b	CATgaattcATGCAGGATAAGGATTTTTTTCAGC	This study
<i>sdiA_{EC}</i> -R ^b	CATtctagaTCAAATTAAGCCAGTAGCGGC	This study
<i>sdiA_{EC}C232A</i> -R ^c	CATTCTAGATCAAATTAAGCCAGTAGCGGCCGCGTAAgc GGCAACCTGGGTC	This study; used with <i>sdiA_{EC}</i> -F
<i>sdiA_{EHEC}</i> -F ^b	CATcatatgCAGGATACGGATTTTTTTCAGCTG	This study
<i>sdiA_{EHEC}H₆</i> -R ^b	CATctcgagAATTAAGCCAGTAGCGGCCG	This study

^aAbbreviations: Cam^R, chloramphenicol resistance; Gent^R, gentamicin resistance; Amp^R, ampicillin resistance. ^bCut sites are lowercase. ^cMutated base pairs are lowercase.

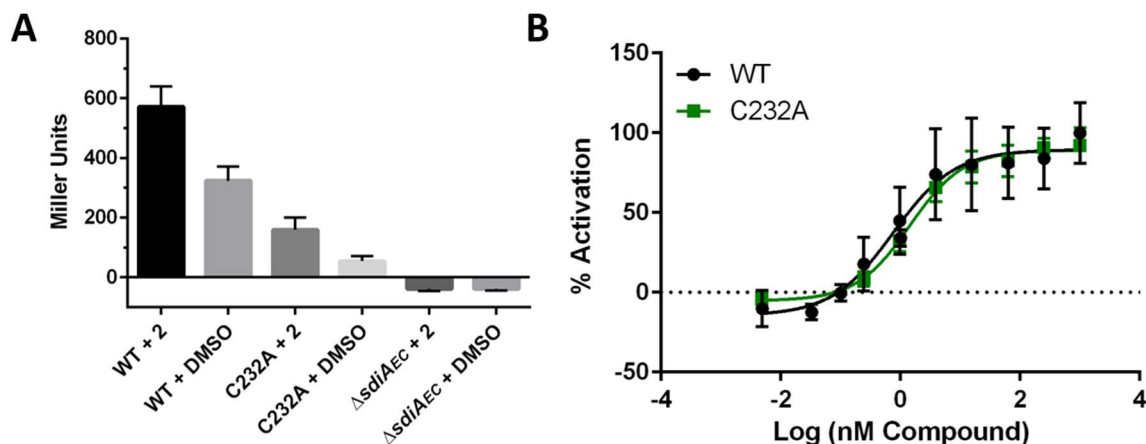


Figure I.S2 Characterization of *E. coli* SdiA_{EC} reporter strains. (A) Activity of WT (JLD271-SdiA_{EC}), C232A (JLD271-SdiA_{EC}C232A), and $\Delta sdiA_{EC}$ (JDL271-pSC11*pgadW*) reporter strains in the presence and absence of 3-oxo-C8 AHL (**2**) (at 10 μ M; DMSO as vehicle). These data represent three biological replicates of six technical replicates (n = 18): WT + **2** is 1.8-fold higher than WT + DMSO, C232A + **2** is 3.0-fold higher than C232A + DMSO, WT + **2** is 3.6-fold higher than C232A + **2**, and WT + DMSO is 6.0-fold higher than C232A + DMSO. (B) Normalized dose-response agonism assay of **2** in the WT (JLD271-SdiA_{EC}) and C232A (JLD271-SdiA_{EC}C232A) reporter strains. The EC₅₀ of **2** is 0.78 nM (0.51–1.19, 95% CI) and 1.44 nM (1.15–1.79, 95% CI) for the WT and C232A strains respectively. Both dose-response curves were obtained as three biological replicates of technical triplicates (see Methods section). 100% activity defined as the activity of 10 μ M **2**; 0% activity defined as the activity of DMSO.

Table I.S3 Primary single-concentration SdiA_{EC} agonism and antagonism screening data in the JLD271-SdiA_{EC} WT reporter.

Compound^a	Agonism^b Activity %^d	Antagonism^c Inhibition %^e
A1	34 ± 10	0 ± 16
F8	56 ± 28	1 ± 19
A2	74 ± 2	5 ± 18
F7	97 ± 12	11 ± 27
4	73 ± 14	27 ± 7
F6	90 ± 18	24 ± 11
A3	74 ± 9	29 ± 17
F5	100 ± 13	-22 ± 20
A4	117 ± 13	1 ± 15
17	38 ± 25	14 ± 8
A5	87 ± 12	4 ± 13
F4	86 ± 7	-5 ± 28
H26	108 ± 20	6 ± 12
A6	22 ± 12	9 ± 11 ^f
H2	79 ± 8	22 ± 6
H6	31 ± 4	15 ± 1
3	93 ± 14	5 ± 17
2	93 ± 11	5 ± 8
F2	81 ± 15	3 ± 15
A7	96 ± 4	-3 ± 24
1	119 ± 18	6 ± 22
H25	31 ± 9	29 ± 10
C1	75 ± 22	2 ± 15
F9	112 ± 11	-8 ± 20
C2	73 ± 5	-16 ± 10
C3	84 ± 5	15 ± 19
C4	122 ± 23	-18 ± 16
C5	92 ± 16	9 ± 6
C6	100 ± 13	16 ± 16
C7	98 ± 12	4 ± 22
7	92 ± 10	-7 ± 12
B4	81 ± 14	5 ± 10
F10	99 ± 14	21 ± 24
F39	-6 ± 7	-2 ± 9
C8	90 ± 8	2 ± 21
C9	88 ± 28	12 ± 5
C10	83 ± 19	34 ± 9
C11	100 ± 2	-7 ± 17
C12	80 ± 17	-4 ± 8
C13	82 ± 10	-18 ± 25
C14	83 ± 16	8 ± 12

F11	101 ± 14	15 ± 2
F18	99 ± 5	12 ± 6
F25	90 ± 13	11 ± 28
F40	8 ± 11	4 ± 11
C15	104 ± 13	-9 ± 13
C16	37 ± 17	-16 ± 3
C17	106 ± 11	-21 ± 9
C18	43 ± 13	6 ± 10
F13	96 ± 21	24 ± 5
E1	99 ± 4	-16 ± 19
C20	72 ± 10	34 ± 4
E3	75 ± 13	20 ± 24
C21	51 ± 9	0 ± 10
C22	-3 ± 4	3 ± 7
C23	99 ± 13	9 ± 6
C24	86 ± 15	13 ± 14
F12	99 ± 18	-13 ± 25
E2	91 ± 8	11 ± 18
C25	99 ± 19	-5 ± 3
E4	102 ± 9	-3 ± 26 ^f
E5	84 ± 1	15 ± 21
E6	81 ± 16	24 ± 29
E7	78 ± 9	26 ± 10
E8	118 ± 20	14 ± 24
E9	48 ± 4	28 ± 25
E10	111 ± 21	12 ± 26
E12	129 ± 5	13 ± 29
B9	87 ± 10	26 ± 15
8	74 ± 16	-8 ± 10
E31	65 ± 9	-7 ± 11
E32	80 ± 8	-16 ± 24
E33	61 ± 11	-7 ± 22
F45	26 ± 8	-25 ± 18
E28	103 ± 8	-3 ± 18
F47	39 ± 20	13 ± 9
9	107 ± 9	-15 ± 6
E34	113 ± 2	25 ± 16
E37	88 ± 13	23 ± 8
E38	91 ± 6	-20 ± 20
E39	74 ± 19	-18 ± 9
E15	69 ± 4	21 ± 14
E16	69 ± 22	21 ± 2
E22	107 ± 15	11 ± 22
E25	62 ± 12	-14 ± 14
RN22	99 ± 7	30 ± 11

B8	9 ± 11	-9 ± 12
B6	19 ± 13	-10 ± 24
Q2	23 ± 18	10 ± 17
Q1	12 ± 3	-4 ± 20
Q3	22 ± 10	13 ± 28
Q4	11 ± 3	12 ± 14
Q5	13 ± 6	-6 ± 7
Q6	15 ± 10	-13 ± 5
Q7	13 ± 4	25 ± 19
Q8	12 ± 8	-5 ± 7
Q12	26 ± 9	-1 ± 7
Q11	22 ± 15	23 ± 28
Q13	29 ± 18	-2 ± 23
D13	26 ± 13	14 ± 16
R3	-1 ± 6	-2 ± 13
R1	-1 ± 4	-2 ± 21
R2	8 ± 8	-3 ± 13
R4	17 ± 2	23 ± 14
R5	12 ± 12	31 ± 16
R7	7 ± 9	13 ± 23
R8	75 ± 15	25 ± 25
R9	7 ± 16	3 ± 25
S1	33 ± 5	5 ± 12
S2	25 ± 17	-11 ± 19
S3	19 ± 20	23 ± 15
A9	17 ± 14	24 ± 9
A13	22 ± 3	11 ± 9
6	90 ± 8	18 ± 20
B3	24 ± 3	10 ± 24
S5	-9 ± 3	-12 ± 24
S7	69 ± 6	29 ± 8
B11	114 ± 2	-13 ± 20
S4	16 ± 15	-16 ± 24
B12	125 ± 4	11 ± 26^f
B13	148 ± 6	23 ± 7
B14	91 ± 14	5 ± 6
B5	78 ± 16	1 ± 22
D3	61 ± 30	-3 ± 13
10	62 ± 16	-3 ± 20
16	116 ± 12	19 ± 6
5	118 ± 22	17 ± 25
H15	30 ± 17	13 ± 9
H23	81 ± 9	22 ± 18
B10	24 ± 6	20 ± 16
D4	13 ± 12	-22 ± 19

D6	54 ± 16	11 ± 8
D7	8 ± 16	-8 ± 10
D9	18 ± 13	-17 ± 15
D10	23 ± 7	9 ± 4
D16	23 ± 13	7 ± 24
D18	42 ± 11	-3 ± 8
11	24 ± 7	137 ± 25
HSL-Az-12	127 ± 18	0 ± 16
12	97 ± 9	17 ± 17
13	29 ± 11	19 ± 15
14	73 ± 4	28 ± 15
15	24 ± 5	63 ± 16
F31	15 ± 13	17 ± 12
18	45 ± 15	-12 ± 19
F55	12 ± 11	-2 ± 9
19P	-31 ± 20	17 ± 4
20	13 ± 17	-15 ± 17
21	10 ± 24	-- ^g
22	28 ± 3	20 ± 11 ^h
23	2 ± 21	24 ± 22
HSL	-2 ± 1	31 ± 9

^aCompounds listed according to order in Figure I.S1. ^bAgonism assay with 100 nM compound performed as described in the Methods section. All assays performed as a technical triplicate. ^cAntagonism assay with 100 μM compound vs. the EC₉₀ of **2** (10 nM) performed as described in the Methods section. All assays performed as a technical triplicate. ^dActivation reported as the average (±SD) of the percentage (%) of activity normalized to 10 μM **2** (100% activation) and DMSO (0% activation). ^eInhibition reported as the average (±SD) of the change in the activity (%) from 10 nM **2**. 100% inhibition equal to activation by DMSO; 0% inhibition equal to the activity of 10 μM **2**. ^fCompound had limited solubility at 10 mM in DMSO and was instead tested at 50 μM using a 5 mM DMSO stock. ^gCell growth inhibited at this compound concentration. ^hCompound yielded increased OD₆₀₀ values when tested at this concentration (possibly from precipitation).

Table I.S4 Secondary single-concentration SdiA_{EC} agonism screening data in the JLD271-SdiA_{EC} WT reporter.

Compound^a	% Activity^b Agonism
F7	87 ± 7
F6	64 ± 5
F5	90 ± 10
A4	18 ± 11
A5	14 ± 20
F4	11 ± 7
H26	18 ± 21
3	85 ± 6
2	74 ± 5
A7	52 ± 11
1	62 ± 7
F9	67 ± 7
C4	84 ± 22
C5	76 ± 18
C6	102 ± 21
C7	51 ± 25
7	56 ± 3
F10	105 ± 19
C8	67 ± 5
C9	48 ± 25
C11	92 ± 32
F11	107 ± 28
F18	66 ± 14
F25	37 ± 6
C15	41 ± 25
C17	44 ± 25
F13	49 ± 12
E1	64 ± 18
C23	38 ± 13
C24	67 ± 30
F12	91 ± 26
E2	65 ± 13
C25	27 ± 12
E4	22 ± 9
E8	48 ± 12
E10	90 ± 1
E12	88 ± 27
B9	38 ± 6
E28	18 ± 20
9	31 ± 11
E34	13 ± 13

E37	74 ± 32
E38	50 ± 25
E22	56 ± 21
RN22	59 ± 24
6	33 ± 11
B11	42 ± 14
B12	9 ± 14
B13	34 ± 21
B14	19 ± 20
16	27 ± 22
5	55 ± 10
HSL-Az-12	28 ± 13
12	13 ± 8

^aCompounds listed according to order in Figure I.S1. ^bAgonism assay with 10 nM compound performed as described in the Methods section. All assays performed as a technical triplicate. Activation reported as the average (±SD) of the percentage (%) of activity normalized to 10 μM **2** (100% activation) and DMSO (0% activation).

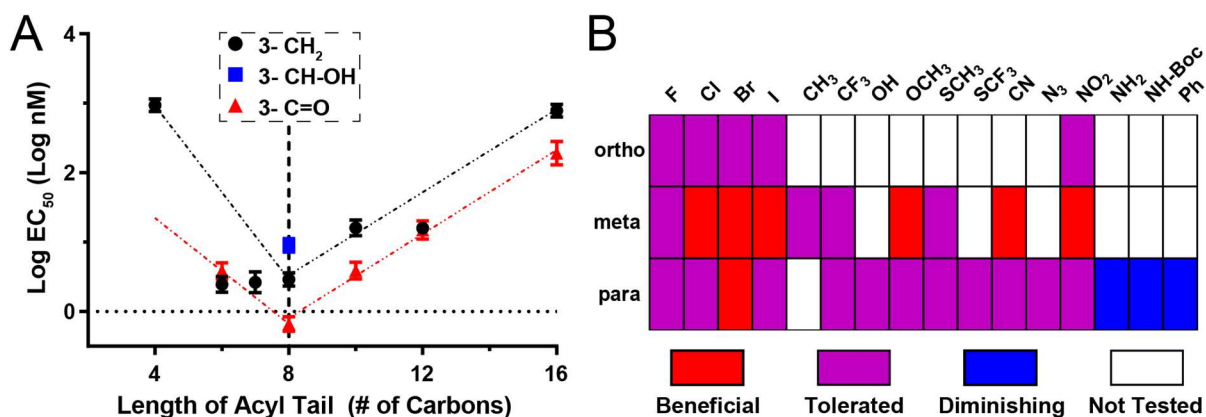
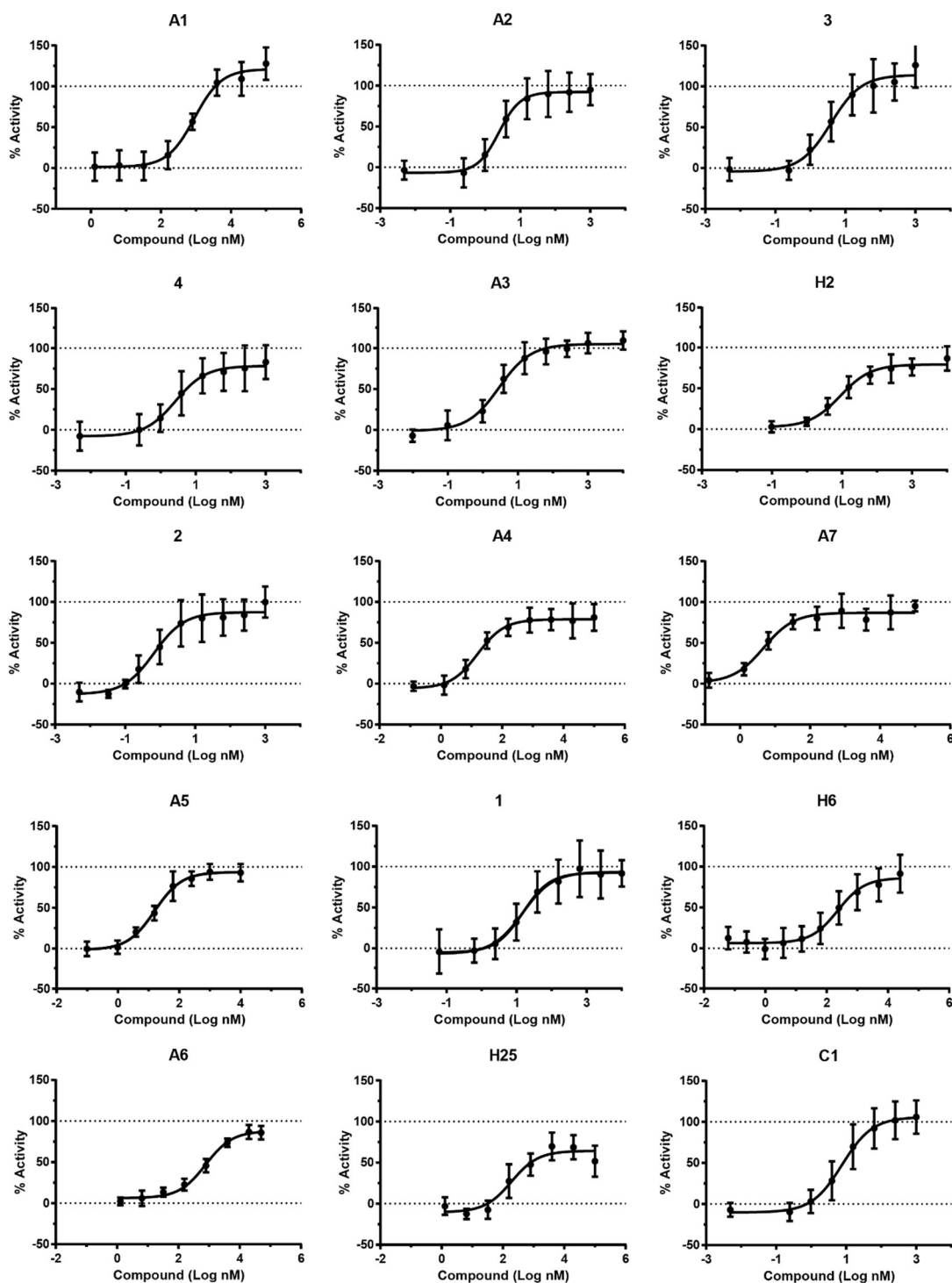
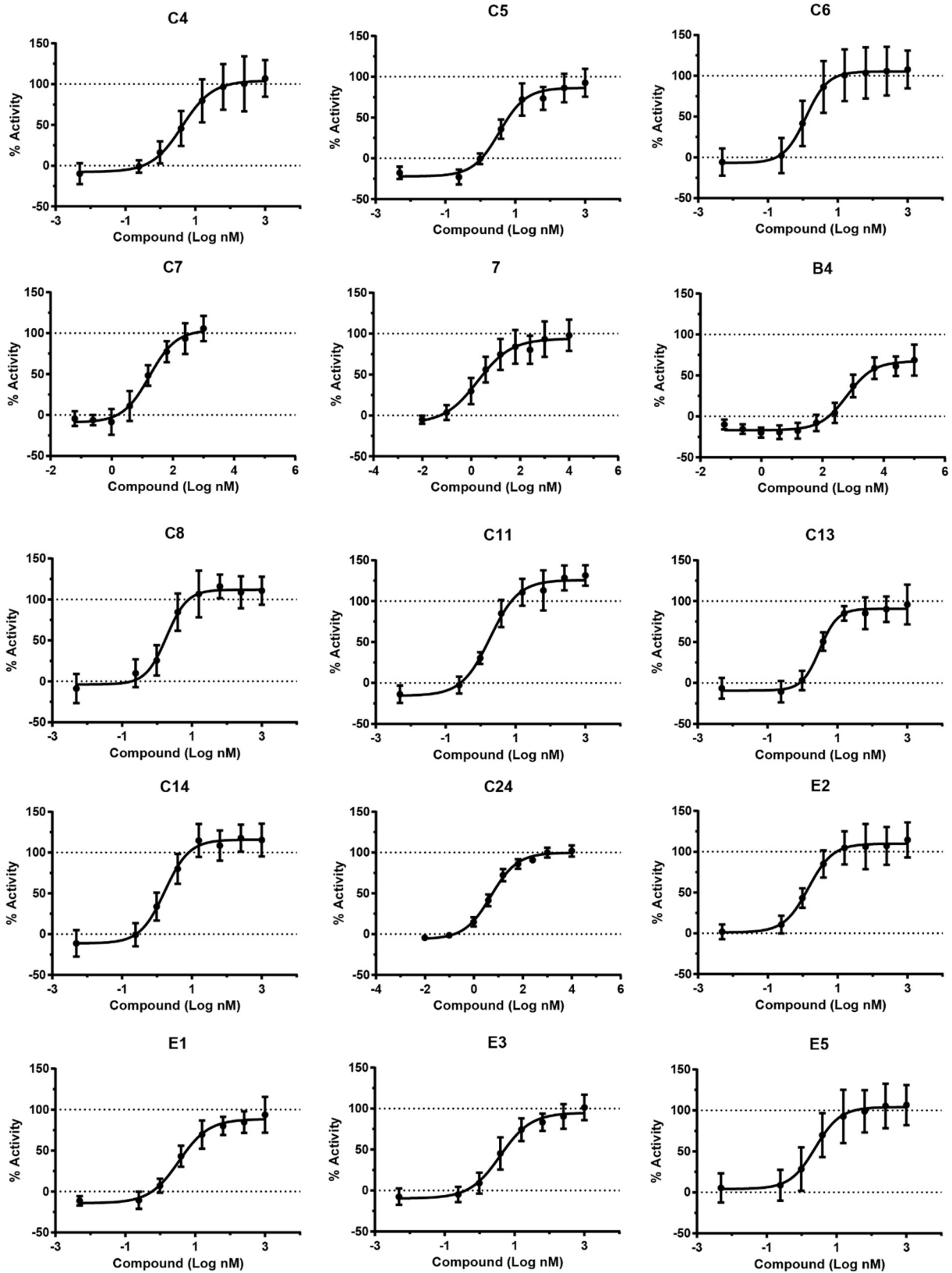
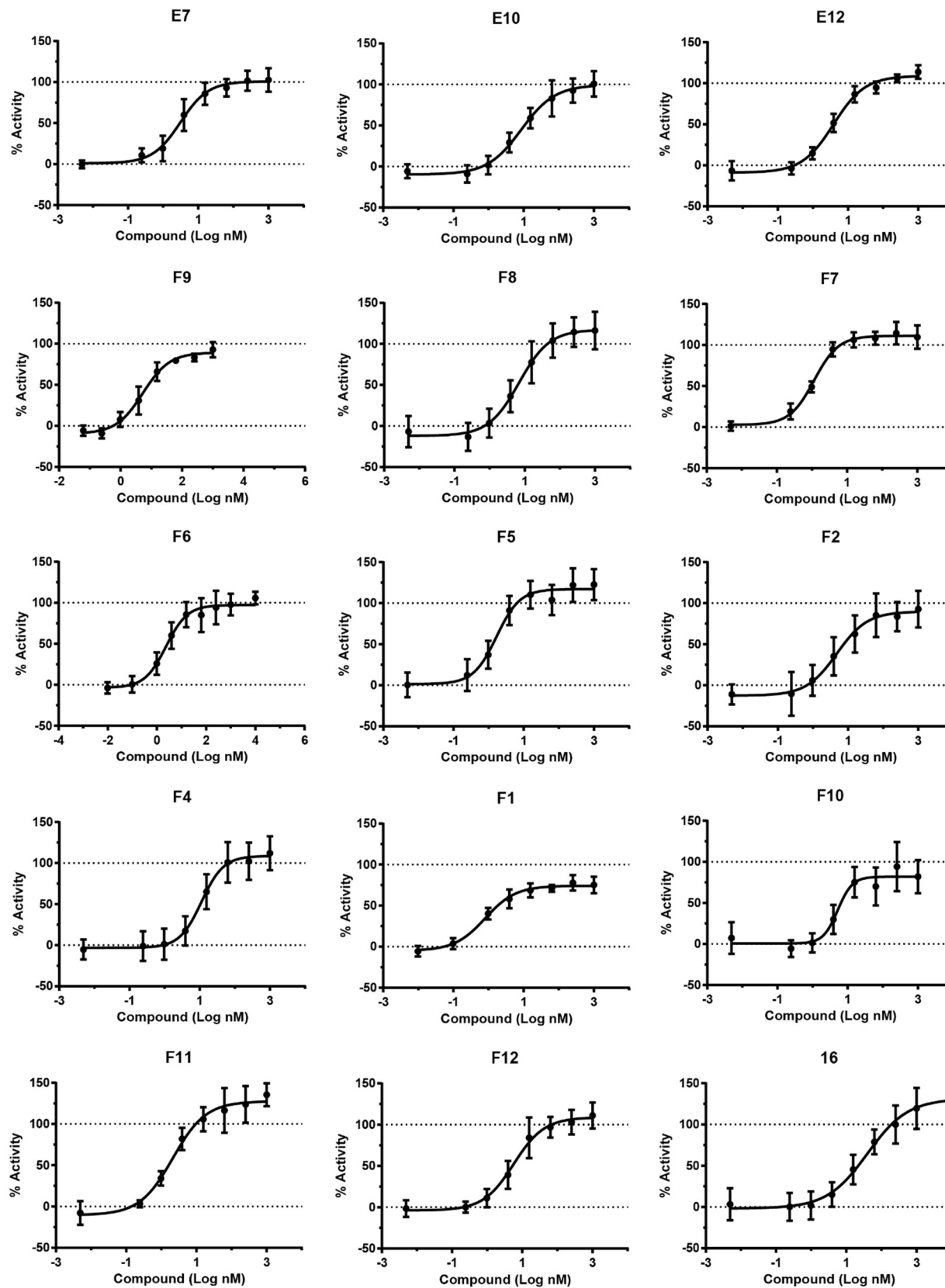


Figure I.S3 Plots of trends in SAR for AHL and PHL SdiA_{EC} agonism in the JLD271-SdiA_{EC} WT reporter. (A) Comparison of agonism potency in SdiA_{EC} for selected naturally occurring AHLs. Points represent the LogEC₅₀ of fits to dose-response data, and error bars represent the SD of these values (data from Table I.1). Dashed linear regression lines are shown to aid the eye in identifying trends. (B) Effect of an individual aryl substituent on agonism potency for all PHLs (Figure I.2iii) tested in SdiA_{EC}. Substituent identity varies across a row and position on the aryl ring varies down a column. Substituted PHLs with at least a 3-fold improvement in EC₅₀ over unsubstituted PHL (**C1**) were classified as “Beneficial” (Table I.1). Substituted PHLs with at least 60% activity at 100 nM were classified as “Tolerated” (**C1** has 75% activity at 100 nM, data from Table I.S3). Substituted PHLs with less than 60% activity at 100 nM were classified as “Diminishing” (data from Table I.S3). “Ph” = phenyl. “Boc” = tert-butyloxycarbonyl.

Figure I.S4 SdiA_{EC} agonism dose-response curve plots for compounds in Table I.1 in the main text. Compound names are indicated at the top of each plot. Assays performed as described in the Methods. All assays performed as three or four biological replicates of technical triplicates. Activation reported as the percentage (%) of activity normalized to 10 μ M **2** (100% activation) and DMSO (0% activation). Error bars show SD.







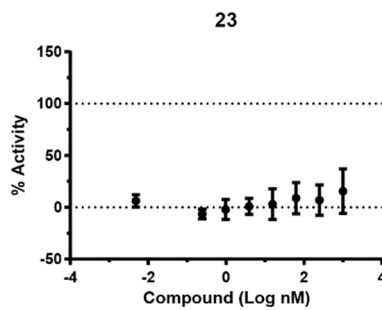
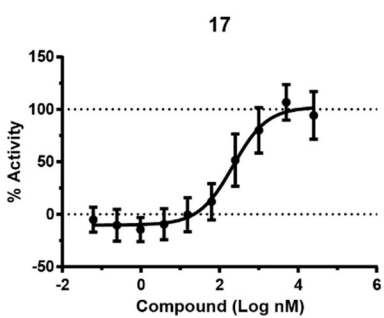
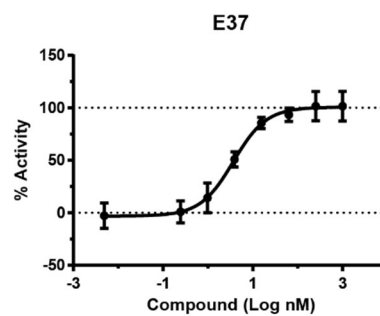
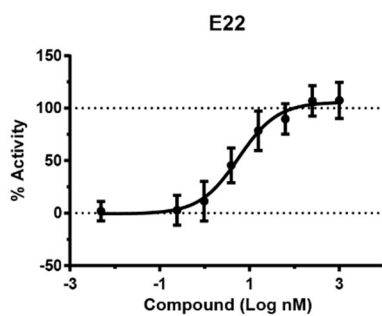
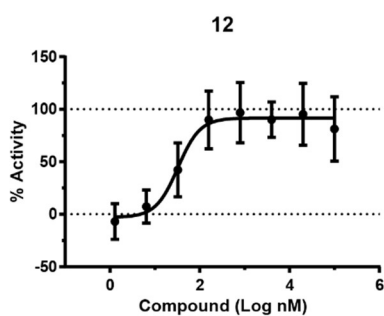
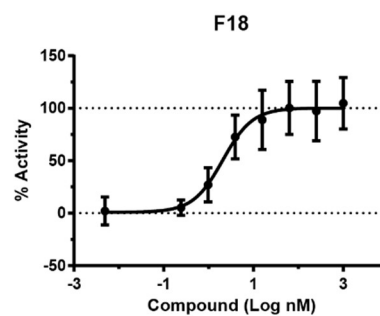
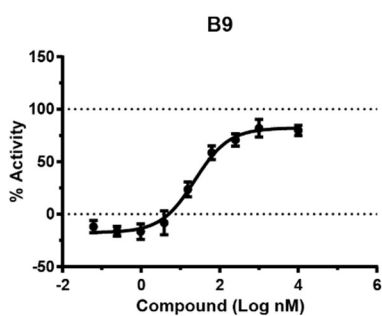
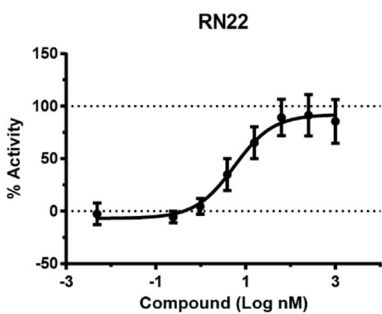


Table I.S5 SdiA_{EC} agonism and antagonism dose-response assay data for compounds 11 and 15 in the JLD271-SdiA_{EC} WT reporter.^a

Compound	Maximum Activation (%)^b (95% CI)	EC₅₀ (95% CI)	Maximum Inhibition (%)^c (95% CI)	IC₅₀ (95% CI)
11	70 (62.1–77.9)	4.03 nM (2.20–7.39)	103 (94.8–110)	256 nM (141–464)
15	33.1 (24.4–41.9)	1.25 μM (0.40–3.87)	86 (65–107)	47.8 μM (22.8–99.9)

^aAll dose response curves were obtained as three or four biological replicates of technical triplicate. ^bAgonism assay performed as described in the Methods section. The “Max Activation” refers to the “top” parameter in the non-linear regression fit. 100% activation is defined using a positive control (10 μM **2**) and 0% is defined using a negative control (DMSO). ^cAntagonism assay performed as described in the Methods section against the EC₉₀ of **2** (10 nM). The “Max Inhibition” refers to 100 – the “bottom” parameter value in the non-linear regression fit. 100% inhibition is defined using a negative control (DMSO, no AHL added to culture) and 0% inhibition is defined using a positive control (10 μM **2**).

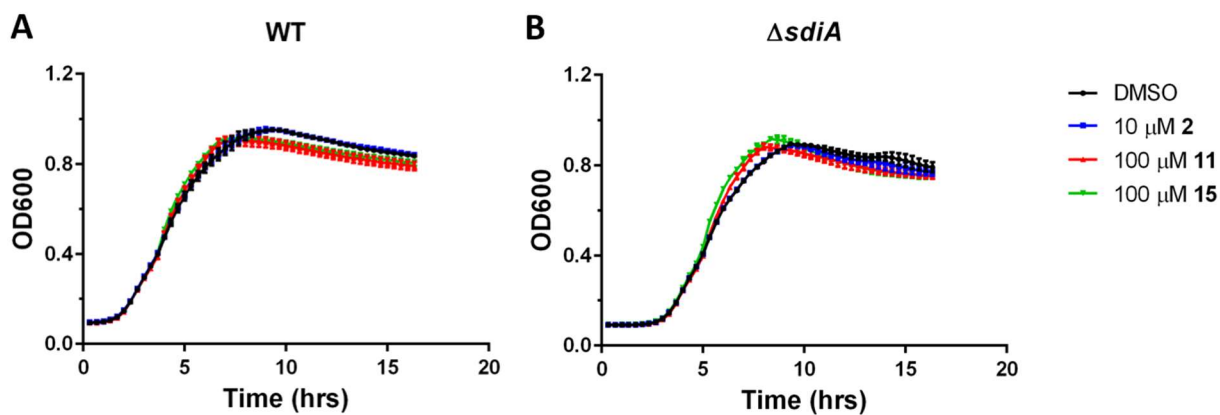


Figure I.S5 Plots of bacterial growth in the presence of compounds **2**, **11**, and **15**. (A) *E. coli* K-12 WT and (B) *E. coli* K-12 $\Delta sdiA$ (JLD271) were grown in LB medium in the presence of DMSO, **2**, **11**, or **15** overnight with shaking at 37 °C in a 96-well microtiter plate. Averages are shown and error bars represent SD (n = 4).

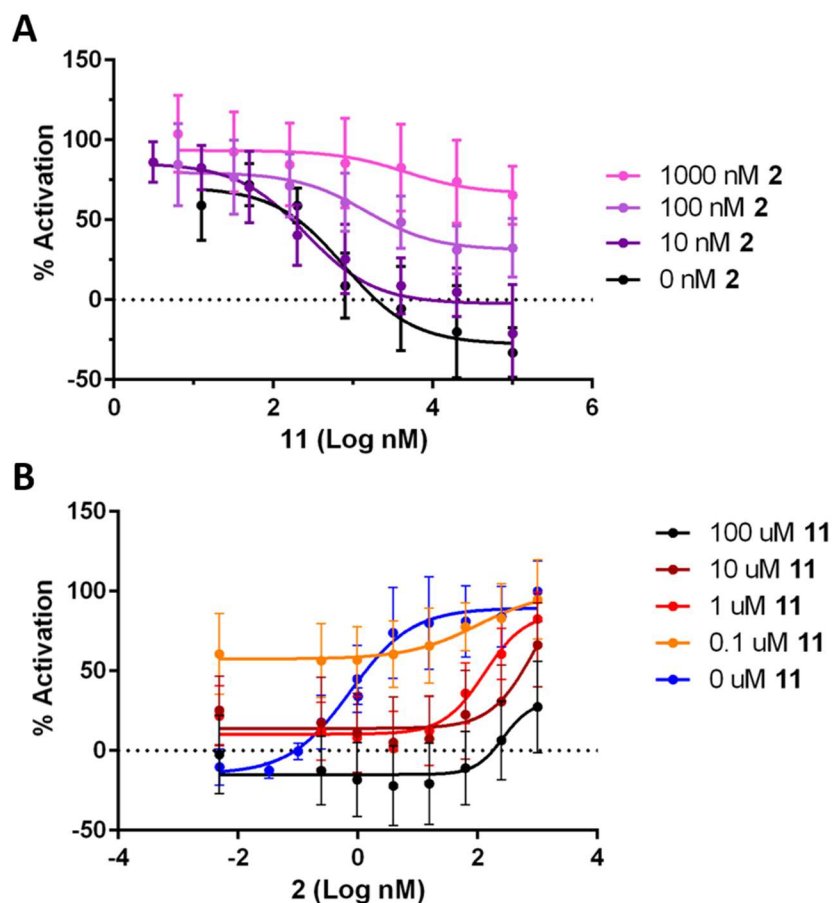


Figure I.S6 Dose-response competition curves for compounds 11 and 2. (A) Antagonism assays for **11** with varying amounts of a competing agonist, **2** (OOHL). The curve for compound **2** at 0 nM is the portion of the **11** agonism dose-response where the activity decreases. Note that at 100 μ M **11**, the activity with 0 nM and 10 nM **2** are not significantly different, but the activity with 10 nM **2** is significantly different than 100 nM and 1000 nM **2** ($p < 0.05$). (B) Agonism assays for compound **2** with varying amounts of a competing antagonist, **11**. The curve for compound **11** at 0 nM is the agonism dose-response curve for **2**. Note that at 1 μ M **2**, the activity with 0, 0.1, 1, and 10 μ M **11** are not significantly different, but the activity of 100 μ M **11** is significantly different than 0, 0.1, and 1 μ M **11** ($p < 0.05$). All dose response curves were obtained as three or four biological replicates of technical triplicates using the WT JLD271-SdiA_{EC} reporter strain (see Methods section). 100% activity is defined as the activity of 10 μ M **2** and 0% is defined as the activity of DMSO. Error bars show SD.

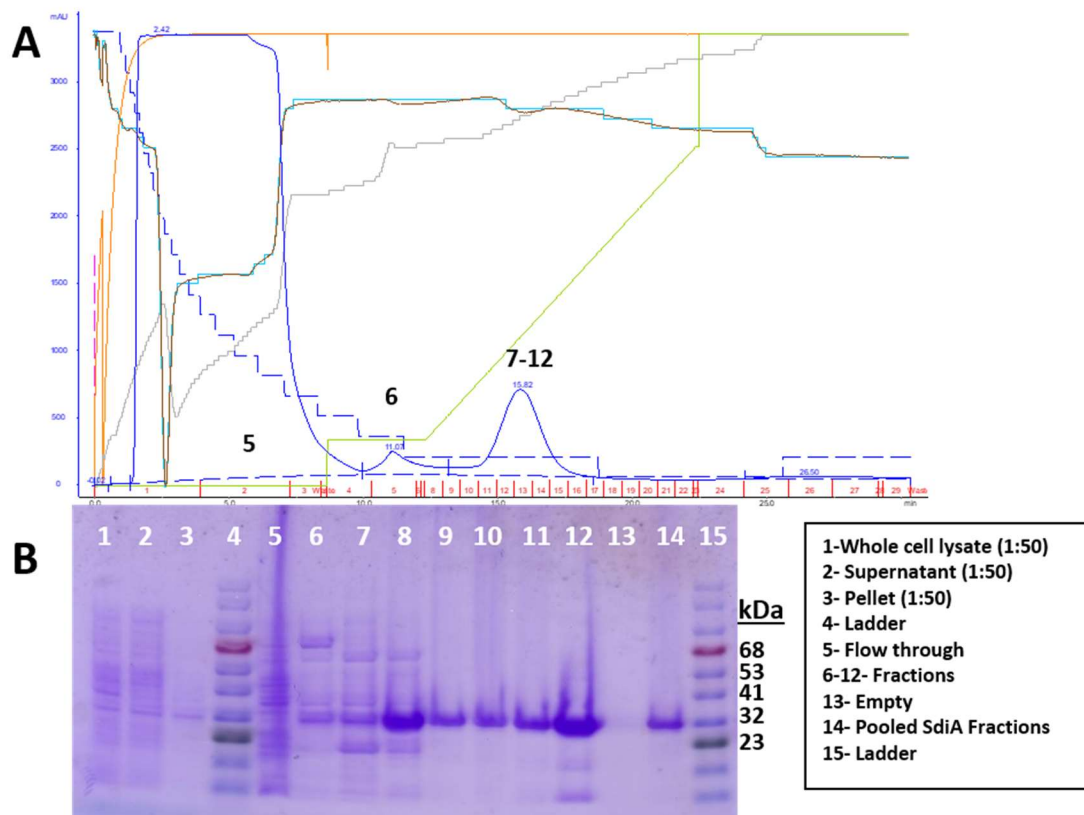


Figure I.S7 Chromatographic and SDS-PAGE data for SdiA_{EHEC}H₆. Protein was overexpressed in BL21(DE3)-SdiA_{EHEC}H₆ (see Table I.S2 for strain details) and purified as described in the Methods section. (A) FPLC chromatogram of SdiA_{EHEC}H₆ purification using a nickel affinity column. Blue trace is UV detection of protein and the bold black numbers refer to gel lanes. (B) SDS-PAGE gel image for overexpression and purification of SdiA_{EHEC}H₆. A legend at the right relates sample content to each gel lane. Dilute (1:50 dilution) whole cell lysate, supernatant with soluble protein, and pelleted insoluble protein samples were run in lanes 1–3, respectively, showing that expressed SdiA_{EHEC}H₆ was in the soluble fraction (and the pellet). FPLC fractions containing SdiA_{EHEC}H₆ are shown in lanes 7–12; these fractions were pooled and are shown in lane 14 indicating pure SdiA_{EHEC}H₆.

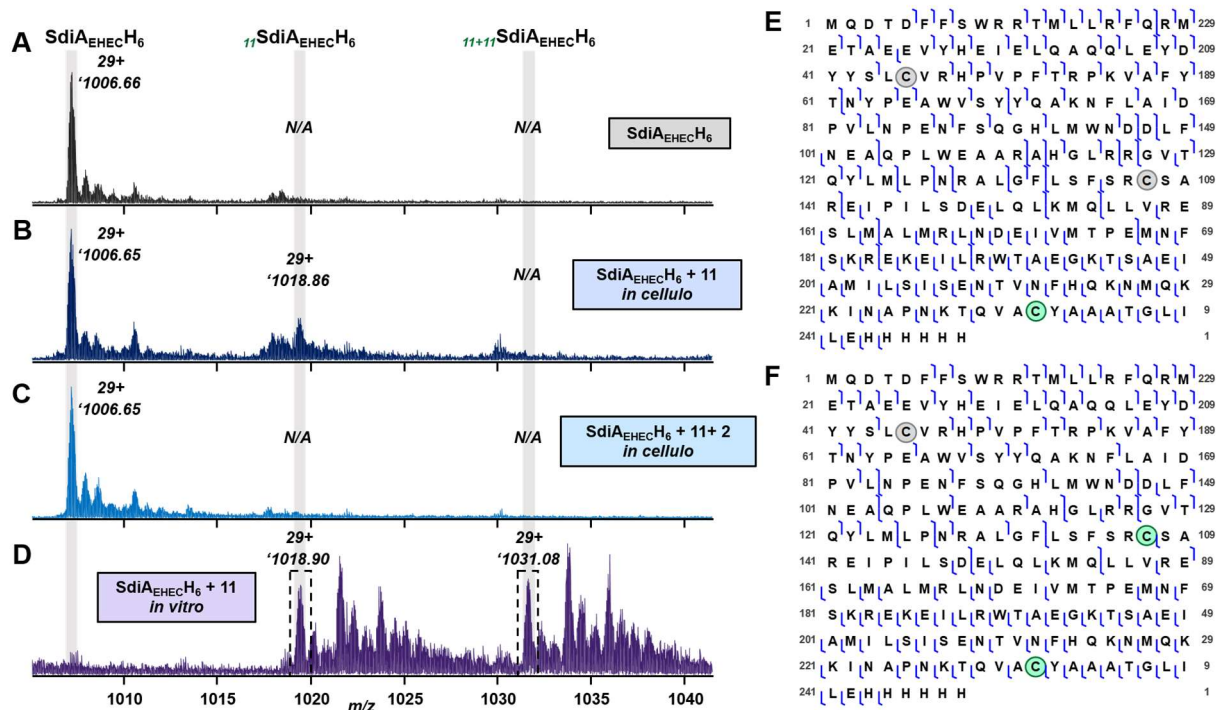


Figure I.S8 Representative nano-ESI FTICR mass spectra and MS/MS sequence tables for SdiA_{EHEC}H₆ treated with compound. Nano-ESI FTICR mass spectra for (A) purified SdiA_{EHEC}H₆ (black), (B) SdiA_{EHEC}H₆ + 11 in cells (navy), (C) SdiA_{EHEC}H₆ + 11 + 2 in cells (blue), and (D) purified SdiA_{EHEC}H₆ + 11 (purple). The singly 11-modified SdiA_{EHEC}H₆ (11SdiA_{EHEC}H₆) and doubly 11-modified SdiA_{EHEC}H₆ (11+11SdiA_{EHEC}H₆) in the 29+ charge state (M²⁹⁺) are labelled. N/A indicates the MS signal is below detection limit. The MS signals for 11SdiA_{EHEC}H₆ and 11+11SdiA_{EHEC}H₆ from the SdiA_{EHEC}H₆ + 11 *in vitro* sample [(D)] in the 29+ charge state (M²⁹⁺) were isolated for MS/MS (ECD 1.0 V). Sequence tables for (E) 11SdiA_{EHEC}H₆ and (F) 11+11SdiA_{EHEC}H₆ show protein backbone cleavages with modifications localized to cysteine residues indicated in green.

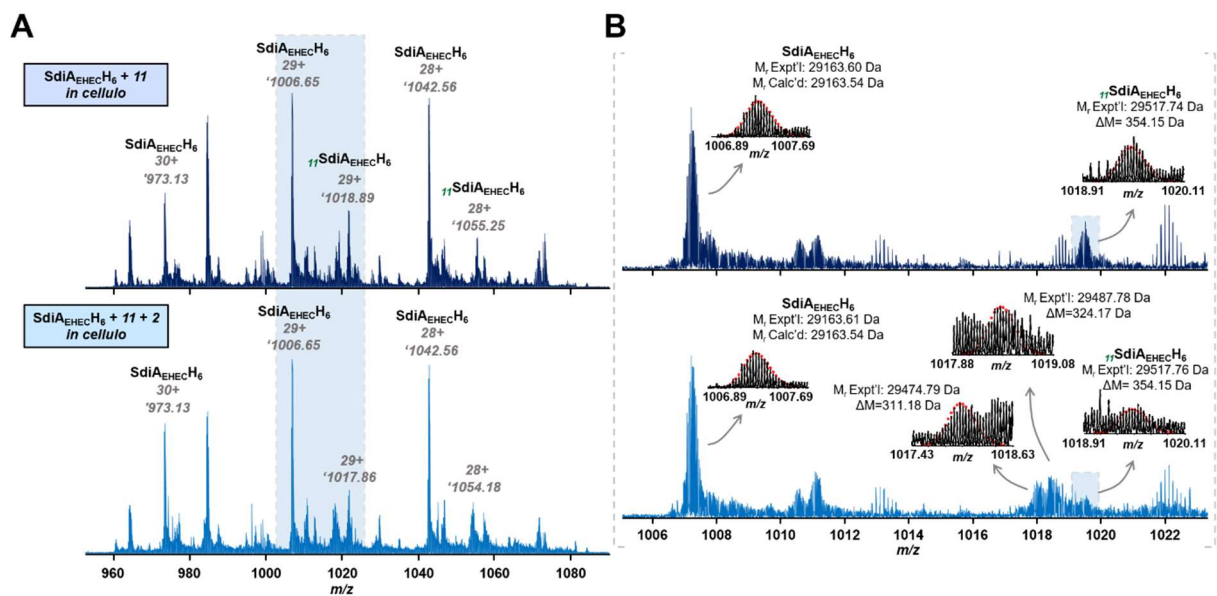


Figure I.S9 Mass spectral data for SdiA_{EHEC}H₆ incubated with compound 11 or compounds 11 + 2 in cells. (A) Nano-electrospray ionization FTICR mass spectra for SdiA_{EHEC}H₆ incubated with 10 μM 11 in cells (top) and SdiA_{EHEC}H₆ incubated with 10 μM 11 and 10 μM 2 in cells (bottom). The 30+, 29+, and 28+ charge states (M^{30+} , M^{29+} , M^{28+}) for un-modified SdiA_{EHEC}H₆ and the 29+ and 28+ charge states (M^{30+} , M^{29+}) for the 11-modified SdiA_{EHEC}H₆ (¹¹SdiA_{EHEC}H₆) are labeled in grey. (B) Zoom-in of the mass spectra to show the 29+ charge state cluster (1006-1022 m/z). Experimental (Expt'l) and calculated (Calc'd) monoisotopic masses are shown for SdiA_{EHEC}H₆. Expt'l monoisotopic masses and delta mass relative to the unmodified SdiA_{EHEC}H₆ are also shown. Experimental isotopic envelopes with theoretical isotopes are depicted for each mass shown.

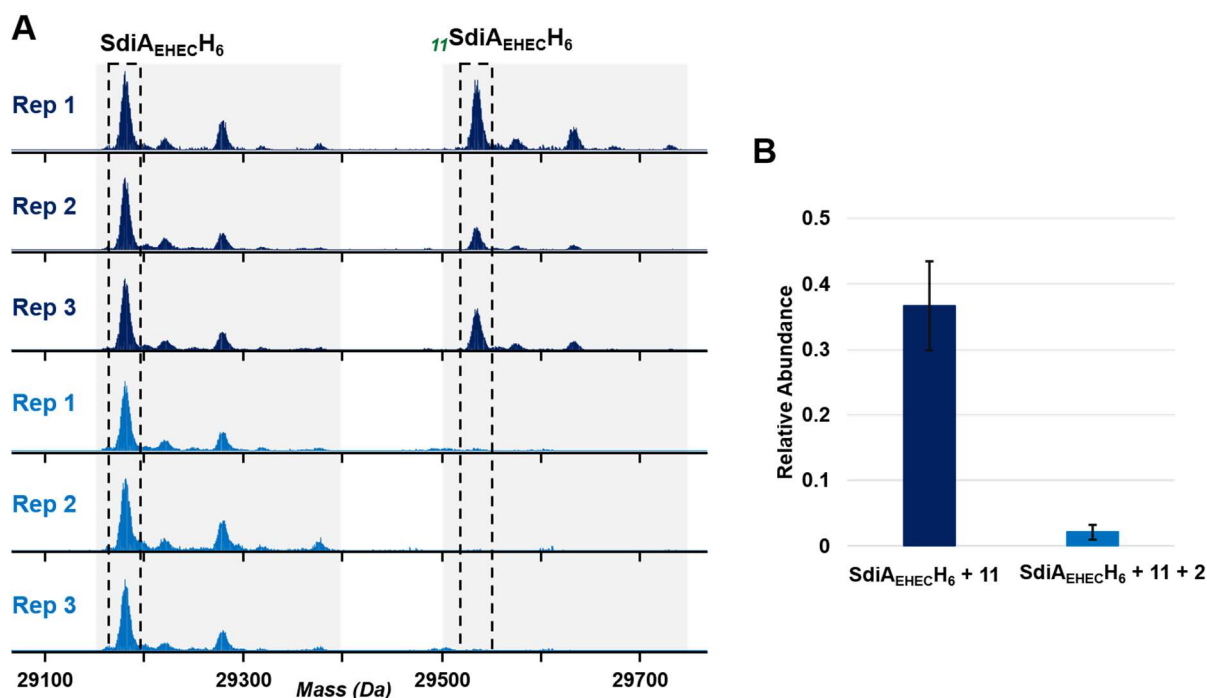


Figure I.S10 Quantification of the relative amounts of SdiA_{EHEC H6} and ¹¹SdiA_{EHEC H6}. (A) Deconvoluted mass spectra for technical replicate preparations of SdiA_{EHEC H6} incubated in cells with **11** (n=3; dark blue, top) and with **11 + 2** (n=3; light blue, bottom). SdiA_{EHEC H6} and **11**-modified SdiA_{EHEC H6} (¹¹SdiA_{EHEC H6}) peaks are outlined in black boxes with dashed lines. The other peaks in the spectrum represent salt and acetone adducts. (B) ¹¹SdiA_{EHEC H6} abundance relative to ¹¹SdiA_{EHEC H6} + SdiA_{EHEC H6}. Values represent an average of n=3 technical replicates; error bars represent standard error of the mean (SEM).

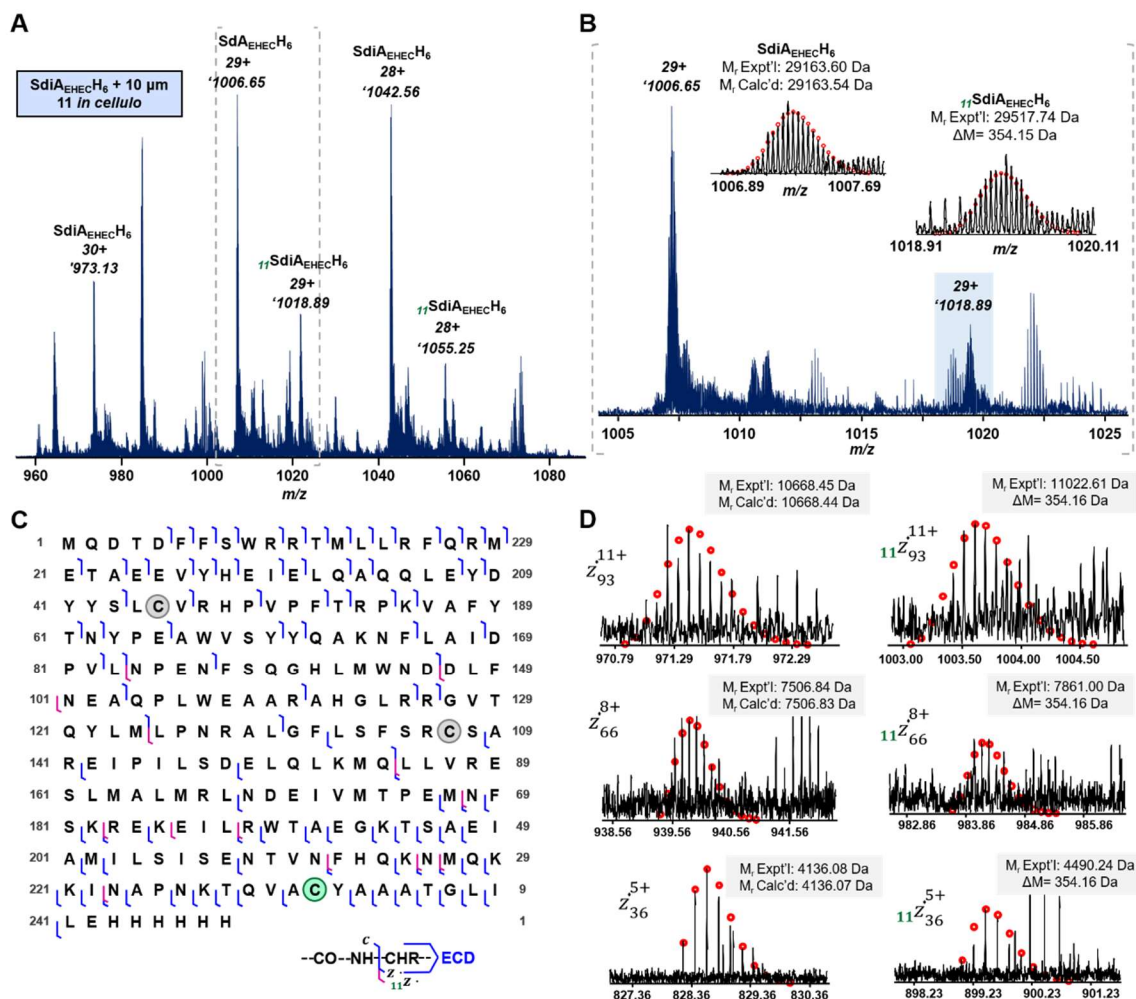


Figure I.S11 Fragmentation of SdiA_{EHEC}H₆ proteoforms for MS/MS. (A) Mass spectrum of SdiA_{EHEC}H₆ incubated in cells with **11** (Q isolation of 100 *m/z* with center 1019 *m/z*), 100 transient acquisition (2M, 0.01 s ion accumulation time). Charge states 30+, 29+, 28+ (M^{30+} , M^{29+} , M^{28+}) for SdiA_{EHEC}H₆ proteoforms are labelled. (B) Zoom-in showing SdiA_{EHEC}H₆ proteoforms (29+ charge state, M^{29+}), with unmodified SdiA_{EHEC}H₆ at '1006.65 *m/z* and **11**-modified SdiA_{EHEC}H₆ ($_{11}$ SdiA_{EHEC}H₆) at '1018.89 *m/z*. Experimental and calculated monoisotopic masses are shown for SdiA_{EHEC}H₆. Expt'l and mass difference between Expt'l and Calc'd monoisotopic masses from unmodified SdiA_{EHEC}H₆ are shown for **11**-modified SdiA_{EHEC}H₆. (C) The 29+ charge state (M^{29+}) of $_{11}$ SdiA_{EHEC}H₆ was isolated for MS/MS to localize the site of modification. Sequence table representing cleavages from two ECD experiments (0.6 V and 1.0 V). Unmodified fragments are denoted in blue, and **11**-modified fragments are denoted in magenta. Cysteine residues are labeled; C232 is denoted by a green circle as the most likely modified cysteine. (D) Representative unmodified/**11**-modified *z*•-ion pairs.

Note: While the presence of **11**-modified *z*•-ions corresponding to cleavages at L83/N84, D97/D98, F99/N100, and M124/L125 support the modification of either C138 or C232, we observed *z*•-ions corresponding to 9 C-terminus cleavages that specifically support C232 modification (magenta cleavages, Figure I.4D). That said, it is possible

that both C138 and C232 are modified and both proteoforms could contribute to the singly modified ${}_{11}\text{SdiA}_{\text{EHEC}H_6}$. Neither *c*- nor *z*-ions supporting modification of C45 were observed, but they could simply be below our detection limit. The co-isolation and fragmentation of some minor $\text{SdiA}_{\text{EHEC}H_6}$ proteoforms together with the ${}_{11}\text{SdiA}_{\text{EHEC}H_6}$ proteoform produced unmodified fragment ions for comparison to the modified fragment ions.

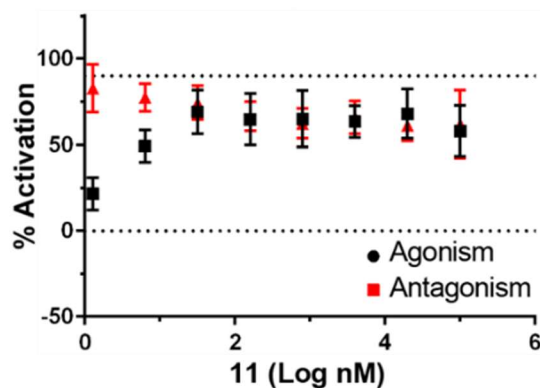


Figure I.S12 Dose-response plots for compound 11 in the *E. coli* SdiA_{EC} C232A mutant reporter strain. All data obtained as three biological replicates of technical triplicates (see Table I.S2 and Methods section for strain and assay details, respectively). All assays performed as three biological replicates of technical triplicates. Activation reported as the percentage (%) of activity normalized to 10 μM **2** (100% activation) and DMSO (0% activation). Error bars show SD.

Table I.S6 SdiA_{EC} agonism and antagonism dose-response assay data for GEE/HSL library.^a

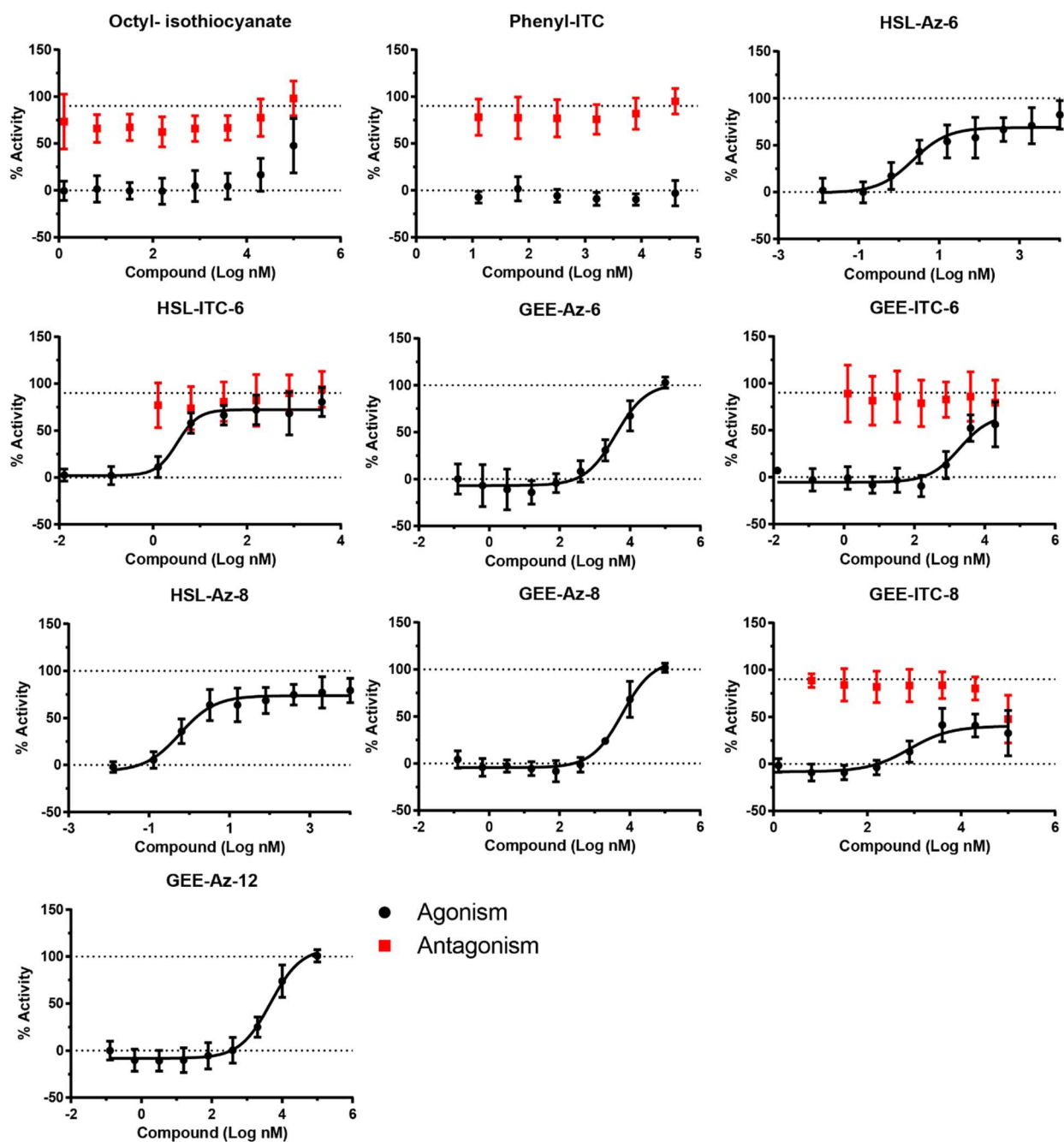
Compound ^c (R ₁ - R ₂ - # of C)	Agonism Assay		Antagonism Assay ^b	
	EC ₅₀ (95% CI)	Max Activation ^d (%, 95% CI)	IC ₅₀ (95% CI)	Max Inhibition ^e (%, 95% CI)
Butyl - ITC ^f	N/A ^g	N/A	N/A	N/A
Octyl - ITC ^f	N/A	N/A	N/A	N/A
Phenyl - ITC ^f	N/A	N/A	N/A	N/A
HSL-Az-6	2.24 nM (1.11–4.52)	69 (63–75)	N/A	N/A
HSL-ITC-6 ^f	3.30 nM (2.13–5.09)	72 (67–77)	N/A	N/A
GEE-Az-6	3.95 μM (2.28–6.83)	102 (84–120)	N/A	N/A
GEE-ITC-6 ^f	1.94 μM (0.88–4.28)	67 (52–82)	N/A	N/A
HSL-Az-8	0.592 nM (0.329–1.07)	74 (69–78)	N/A	N/A
HSL-ITC-8 ^f	0.659 nM (0.248–1.75)	84 (76–92)	N/A	N/A
GEE-Az-8	6.08 μM (4.27–8.65)	110 (96–124)	N/A	N/A
GEE-ITC-8	0.795 μM (0.336–1.88)	40 (33–47)	N/A	48 (41–55) ^h
HSL-Az-12	10.8 nM (7.09–16.4)	99 (93–106)	N/A	N/A
HSL-ITC-12 (11)	4.03 nM (2.20–7.39)	70 (62–78)	256 nM (141–464)	103 (95–110)
GEE-Az-12	4.69 μM (2.93–7.49)	109 (91–127)	N/A	N/A
GEE-ITC-12	1.02 μM (0.55–1.90)	62 (55–68)	3.63 μM (0.402–32.7)	54 (41–66)

^aAll dose response curves were obtained as three or four biological replicates of technical triplicates using the JLD271-SdiA_{EC} WT reporter strain (see Methods section).

^bAntagonism assays performed in competition with **2** at its EC₉₀ (10 nM). ^cCompound naming scheme described in Figure I.5 in the main text. ^dThe Max Activation refers to the “top” parameter in the non-linear regression fit. 100% activation defined using a positive control (10 μM **2**); 0% is defined using a negative control (DMSO). ^eThe Max Inhibition refers to 100 minus the value of the “bottom” parameter in the non-linear regression fit. 100% inhibition defined as the activity of the negative control (DMSO); 0% inhibition is defined as the activity of the positive control (10 μM **2**). ^fDenotes that at

higher concentrations, cell growth is inhibited. ^gN/A = the compound did not appear to agonize or antagonize SdiA_{EC} and the data could not be fit to an agonism or antagonism model. ^hIndicates that an antagonism model could not be fit to the data because the highest concentration did not limit the lower bound; however, at the highest concentration tested there was a statistically significant inhibition of activity.

Figure I.S13 GEE/HSL library dose-response curve plots. Data corresponds to Table I.S6. Agonism plots in black and antagonism plots in red. Compound names are indicated at the top of each plot. Assays performed as described in the Methods section. All assays performed as three or four biological replicates of technical triplicates. Activation reported as the percentage (%) of activity normalized to 10 μM **2** (100% activation) and DMSO (0% activation). Error bars show SD.



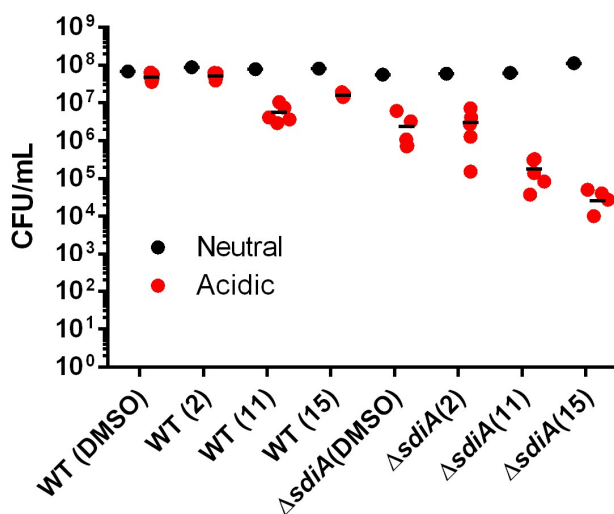


Figure I.S14 *E. coli* acid-challenge assay supporting data. CFU/mL plotted versus each condition in Figure I.7 in the main text. CFU/mL of stationary phase WT *E. coli* or $\Delta sdiA$ *E. coli* after 1:10 dilution and incubation for 1.5 h in a low glutamate (50 μ M) neutral (pH 7.0) or acidic (pH 2.5) minimal medium (see Methods section for details). DMSO (vehicle control), **2** (10 μ M), **11** (100 μ M), or **15** (100 μ M) were added to the initial growth medium and the acid challenge medium. Each point represents an individual challenge well. Black lines represent the average of acidic medium replicates (n = 5).

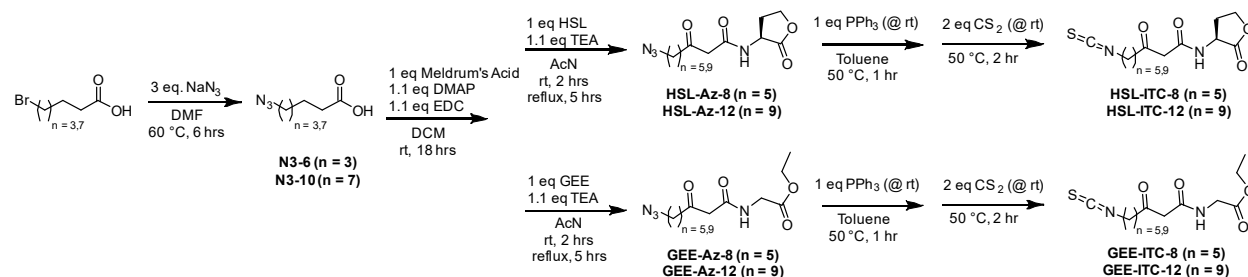
1.4.3 Synthesis of GEE/HSL compounds.

General information

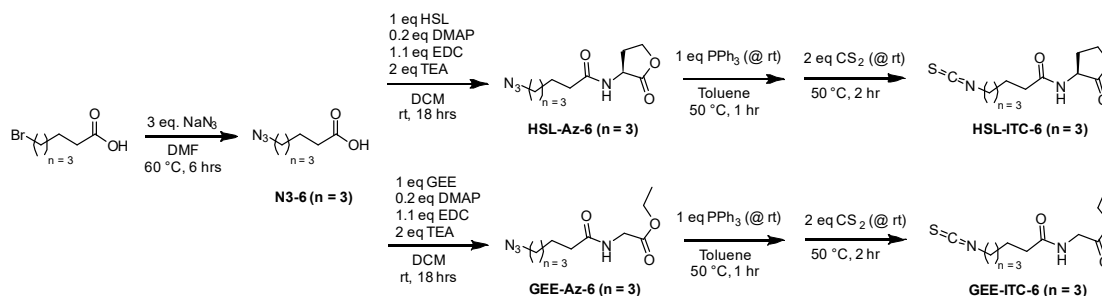
Chemical reagents and solvents were purchased from commercial sources and used without further purification, except dichloromethane (DCM) and ethyl acetate, which were each distilled and stored over activated 3 Å molecular sieves prior to use. NMR spectra were recorded in deuterated solvents at 400 MHz on a Bruker-Avance spectrometer equipped with a BFO probe, and at 500 MHz on a Bruker Avance spectrometer equipped with a DCH cryoprobe. Chemical shifts are reported in parts per million using residual solvent peaks or tetramethylsilane (TMS) as a reference. Couplings are reported in hertz (Hz). Electro spray ionization–exact mass measurement (ESI-EMM) mass spectrometry data were collected on a Waters LCT instrument.

General synthetic routes

- A.** Compounds containing a 3-oxo group (all 8 and 12 carbon tail compounds) were synthesized according to the route below. This synthetic route was used by Amara *et al.* in the initial report of **11** (HSL-ITC-12).¹⁰

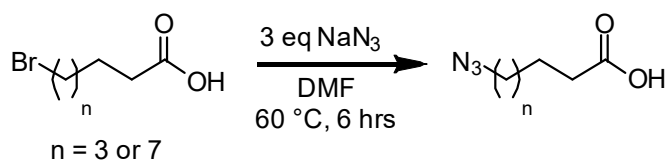


B. Compounds without a 3-oxo group (all 6 carbon tail compounds) were synthesized according to the route below.



Synthetic procedures

Compound names refer to those in routes A and B above.

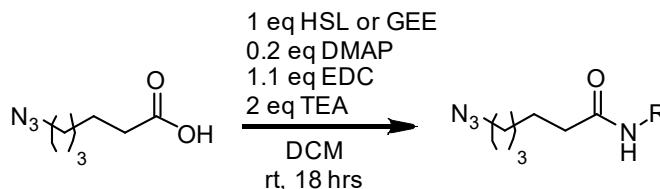


6-Azidohexanoic acid (N3-6)

6-bromohexanoic acid (0.78 g, 4.0 mmol) was dissolved in 25 mL dimethylformamide (DMF). Sodium azide (0.79 g, 12 mmol) was added, and the mixture was stirred at 60 °C for 6 hrs. The solution was cooled, diluted with 100 mL ethyl acetate, washed with 1 M HCl (5 x 10 mL) and brine (1 x 20 mL), and dried over magnesium sulfate. The mixture was then filtered and concentrated *in vacuo* to yield the crude product as a white solid (87% yield, 0.55 g). ¹H NMR (400 MHz, Chloroform-*d*): δ 3.29 (t, *J* = 6.8 Hz, 2H), 2.38 (t, *J* = 7.4 Hz, 2H), 1.65 (dp, *J* = 19.2, 7.2 Hz, 4H), 1.50–1.38 (m, 2H).

10-Azidodecanoic acid (N3-10)

10-bromodecanoic acid was reacted with sodium azide as described for **N3-6** to give **N3-10** (84% yield, 0.73 g). ^1H NMR (400 MHz, Chloroform-*d*): δ 3.26 (t, $J = 7.0$ Hz, 2H), 2.35 (t, $J = 7.5$ Hz, 2H), 1.61 (dq, $J = 14.6, 7.3$ Hz, 4H), 1.42–1.22 (m, 11H).

N-(6-Azidohexanoyl)-L-homoserine lactone (HSL-Az-6)

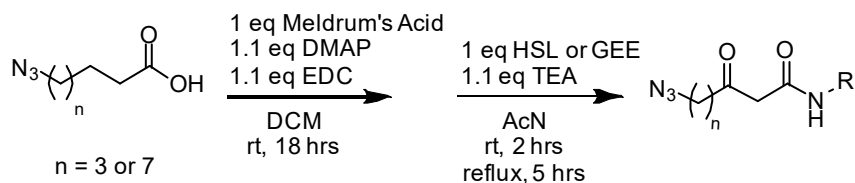
L-homoserine lactone•HBr (0.18 g, 1 mmol), *N*-(dimethylamino)pyridine (DMAP, 0.2 eq), *N*-(3-dimethylaminopropyl)-*N'*-ethylcarbodiimide hydrochloride (EDC•HCl, 1.1 eq), and **N3-6** (0.14 g, 0.88 mmol) were dissolved in 10 mL dichloromethane (DCM) with the aid of 0.28 mL of triethylamine (TEA). This mixture was stirred overnight at room temperature. The mixture was then diluted with 50 mL ethyl acetate, washed sequentially with 1 M HCl (3 x 10 mL), saturated sodium bicarbonate (3 x 10 mL), and brine (1 x 20 mL), and dried over magnesium sulfate. The mixture was filtered and concentrated *in vacuo* to yield the product as a white solid (47% yield, 99 mg). ^1H NMR (500 MHz, Chloroform-*d*): δ 6.62 (d, $J = 6.8$ Hz, 1H), 4.61 (ddd, $J = 11.4, 8.7, 6.7$ Hz, 1H), 4.46 (td, $J = 9.0, 1.4$ Hz, 1H), 4.29 (ddd, $J = 11.0, 9.2, 6.1$ Hz, 1H), 3.28 (t, $J = 6.9$ Hz, 2H), 2.75 (dddd, $J = 12.5, 8.6, 6.1, 1.4$ Hz, 1H), 2.27 (td, $J = 7.3, 1.8$ Hz, 2H), 2.25 – 2.14 (m, 1H), 1.65 (dp, $J = 29.4, 7.3$ Hz, 4H), 1.48–1.36 (m, 2H); ^{13}C NMR (126 MHz,

Chloroform-*d*): δ 175.79, 173.39, 66.09, 51.18, 49.00, 35.72, 30.00, 28.53, 26.22, 24.86;

ESI-EMM: $[M+Na]^+$ calculated 263.1115; measured 263.114; agreement 0.4 ppm.

N-(6-Azidohexanoyl)-glycine ethyl ester (GEE-Az-6)

N3-6 was reacted with glycine ethyl ester (GEE) as described for **HSL-Az-6** to produce the product as a white solid (71% yield, 151 mg). ^1H NMR (500 MHz, Chloroform-*d*): δ 6.26 (d, J = 5.4 Hz, 1H), 4.21 (q, J = 7.2 Hz, 2H), 4.02 (d, J = 5.2 Hz, 2H), 3.28 (t, J = 6.9 Hz, 2H), 2.27 (t, J = 7.5 Hz, 2H), 1.65 (dp, J = 32.8, 7.3 Hz, 5H), 1.43 (tt, J = 10.0, 6.2 Hz, 2H), 1.29 (t, J = 7.2 Hz, 3H); ^{13}C NMR (126 MHz, Chloroform-*d*): δ 172.89, 170.05, 61.44, 51.19, 41.29, 35.95, 28.55, 26.26, 24.96, 14.09; ESI-EMM: $[M+Na]^+$ calculated 265.1271; measured 265.1269; agreement 0.8 ppm.



N-(8-Azido-3-oxo-octanoyl)-L-homoserine lactone (HSL-Az-8)

Meldrum's acid (1.1 eq), *N*-(dimethylamino)pyridine (DMAP, 1.1 eq), *N*-(3-dimethylaminopropyl)-*N'*-ethylcarbodiimide hydrochloride (EDC•HCl, 1.1 eq), and **N3-6** (0.28 g, 1.7 mmol) were dissolved in 20 mL DCM. This mixture was stirred overnight at room temperature. The mixture was then diluted with 50 mL ethyl acetate, washed sequentially with 1 M HCl (3 x 10 mL) and brine (1 x 20mL), and dried over magnesium sulfate. The mixture was filtered and concentrated *in vacuo* to yield the 3-keto acid

intermediate. This intermediate was added to a solution of L-homoserine lactone•HBr (1 eq) and TEA (1.1 eq) in 10 mL acetonitrile (AcN). This mixture was stirred for 2 hrs at room temp and then refluxed for 5 hrs. The solution was cooled and the AcN was removed by vacuum. The resulting solid was diluted with 50 mL ethyl acetate, washed sequentially with 1 M HCl (3 x 10 mL), 1 M NaHSO₄ (3 x 10 mL), and brine (1 x 20mL), and dried over magnesium sulfate. The mixture was filtered and concentrated *in vacuo*, and then purified via flash silica gel chromatography (3:1 ethyl acetate:hexanes as eluent) to yield the product as a white solid (23% yield, 57 mg). ¹H NMR (500 MHz, Chloroform-*d*): δ 7.61 (d, *J* = 6.8 Hz, 1H), 4.61 (ddd, *J* = 10.8, 8.9, 7.0 Hz, 1H), 4.48 (t, *J* = 9.1 Hz, 1H), 4.34–4.24 (m, 1H), 3.47 (d, *J* = 1.6 Hz, 2H), 3.28 (t, *J* = 6.9 Hz, 2H), 2.82–2.68 (m, 1H), 2.58 (t, *J* = 7.2 Hz, 2H), 2.36–2.20 (m, 1H), 1.61 (h, *J* = 7.6 Hz, 4H), 1.47–1.32 (m, 2H); ¹³C NMR (126 MHz, Chloroform-*d*): δ 205.80, 174.98, 166.39, 65.95, 51.18, 49.07, 48.59, 43.41, 29.65, 28.63, 26.07, 22.74; ESI-EMM: [M+Na]⁺ calculated 305.1220; measured 305.1217; agreement 1 ppm.

N-(8-Azido-3-oxo-octanoyl)-glycine ethyl ester (GEE-Az-8)

N3-6 was reacted with Meldrum's acid and then GEE as described for **HSL-Az-8** and purified via flash silica gel chromatography (1:1 ethyl acetate:hexanes as eluent) to yield the product as a white solid (13% yield, 32 mg). ¹H NMR (500 MHz, Chloroform-*d*): δ 7.38 (t, *J* = 5.3 Hz, 1H), 4.22 (qd, *J* = 7.2, 1.7 Hz, 2H), 4.05 (dd, *J* = 5.5, 1.5 Hz, 2H), 3.45 (d, *J* = 1.5 Hz, 2H), 3.32–3.24 (m, 2H), 2.58 (td, *J* = 7.3, 1.6 Hz, 2H), 1.69–1.54 (m, 4H), 1.47–1.33 (m, 2H), 1.29 (t, 3H); ¹³C NMR (126 MHz, Chloroform-*d*): δ 205.78,

169.50, 165.83, 61.52, 51.17, 48.82, 43.44, 41.40, 28.62, 26.07, 22.75, 14.12; ESI-EMM: [M+H]⁺ calculated 285.1557; measured 285.555; agreement 0.7 ppm.

N-(12-Azido-3-oxo-dodecanoyl)-L-homoserine lactone (HSL-Az-12)

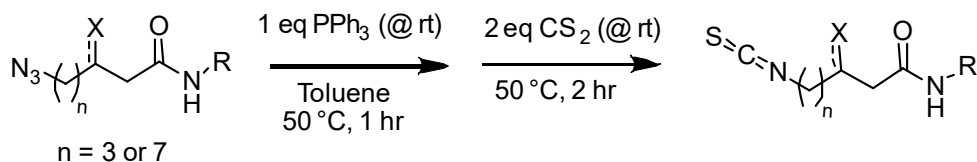
N3-10 was reacted with Meldrum's acid and then L-homoserine lactone•HBr as described for **HSL-Az-8** and purified via flash silica gel chromatography (3:1 ethyl acetate:hexanes as eluent) to yield the product as a white solid (43% yield, 0.24 g). ¹H NMR (500 MHz, Chloroform-*d*): δ 7.72 (d, *J* = 7.1 Hz, 1H), 4.62 (ddd, *J* = 11.3, 8.9, 7.0 Hz, 1H), 4.46 (td, *J* = 9.0, 1.5 Hz, 1H), 4.28 (ddd, *J* = 11.0, 9.2, 6.2 Hz, 1H), 3.47 (s, 2H), 3.26 (t, *J* = 7.0 Hz, 2H), 2.69 (dddd, *J* = 12.4, 8.2, 6.2, 1.5 Hz, 1H), 2.54 (t, *J* = 7.4 Hz, 2H), 2.29 (dtd, *J* = 12.5, 11.1, 8.9 Hz, 1H), 1.68–1.50 (m, 4H), 1.39–1.23 (m, 10H); ¹³C NMR (126 MHz, Chloroform-*d*): δ 206.07, 175.16, 166.69, 65.94, 51.39, 48.95, 48.75, 43.52, 29.30, 29.19, 29.18, 29.00, 28.88, 28.75, 26.61, 23.25; ESI-EMM: [M+H]⁺ calculated 339.2027; measured 339.2023; agreement 1.2 ppm.

N-(12-Azido-3-oxo-dodecanoyl)-glycine ethyl ester (GEE-Az-12)

N3-10 was reacted with Meldrum's acid and then GEE as described for **HSL-Az-8** and purified via flash silica gel chromatography (1:1 ethyl acetate:hexanes as eluent) to yield the product as a white solid (60% yield, 0.34 g). ¹H NMR (500 MHz, Chloroform-*d*): δ 7.50 (t, *J* = 5.5 Hz, 1H), 4.21 (q, *J* = 7.1 Hz, 2H), 4.04 (d, *J* = 5.3 Hz, 2H), 3.45 (s, 2H), 3.26 (t, *J* = 7.0 Hz, 2H), 2.55 (t, *J* = 7.3 Hz, 2H), 1.65–1.52 (m, 4H), 1.41–1.17 (m, 13H); ¹³C NMR (126 MHz, Chloroform-*d*): δ 206.27, 169.56, 166.10, 61.45, 51.46,

48.77, 43.71, 41.41, 29.24, 29.23, 29.06, 28.94, 28.82, 26.68, 23.33, 14.15; ESI-EMM:

[M+H]⁺ calculated 341.2183; measured 341.2179; agreement 1.2 ppm.



N-(6-Isothiocyanatehexanoyl)-L-homoserine lactone (HSL-ITC-6)

HSL-Az-6 (79 mg, 0.5 mmol) and triphenyl phosphine (1.1 eq) were dissolved in 10 mL toluene under nitrogen. The solution was heated to 50 °C and stirred for 1 hr. The solution was cooled to room temperature and carbon disulfide (2.5 eq) was added dropwise under nitrogen. The solution was heated to 50 °C and stirred for an additional 2 hrs. The crude mixture was concentrated under vacuum and purified via flash silica gel chromatography (ethyl acetate as eluent) to yield the product as a white solid (40% yield, 33 mg). ¹H NMR (500 MHz, Chloroform-*d*): δ 6.22 (d, *J* = 6.1 Hz, 1H), 4.58 (ddd, *J* = 11.5, 8.6, 6.0 Hz, 1H), 4.48 (td, *J* = 9.0, 1.2 Hz, 1H), 4.30 (ddd, *J* = 11.2, 9.3, 6.0 Hz, 1H), 3.54 (t, *J* = 6.5 Hz, 2H), 2.83 (dddd, *J* = 12.4, 8.6, 5.9, 1.2 Hz, 1H), 2.29 (td, *J* = 7.4, 3.0 Hz, 2H), 2.24–2.11 (m, 1H), 1.78–1.66 (m, 4H), 1.54–1.42 (m, 2H); ¹³C NMR (126 MHz, Chloroform-*d*): δ 175.54, 173.09, 66.13, 49.24, 44.86, 35.69, 30.41, 29.65, 26.10, 24.50; ESI-EMM: [M+H]⁺ calculated 257.0954; measured 257.0953; agreement 0.4 ppm.

N-(6-Isothiocyanatehexanoyl)-glycine ethyl ester (GEE-ITC-6)

GEE-Az-6 was reacted with carbon disulfide as described for **HSL-ITC-6** and purified via flash silica gel chromatography (ethyl acetate as eluent) to yield the product as a white solid (52% yield, 42 mg). ¹H NMR (500 MHz, Chloroform-*d*): δ 6.09–5.93 (m, 1H), 4.22 (q, *J* = 6.9 Hz, 2H), 4.04 (d, *J* = 5.1 Hz, 2H), 3.53 (t, *J* = 6.6 Hz, 2H), 2.28 (t, *J* = 7.4 Hz, 2H), 1.71 (dq, *J* = 12.9, 7.4 Hz, 4H), 1.53–1.42 (m, 2H), 1.29 (td, *J* = 7.1, 0.9 Hz, 3H); ¹³C NMR (126 MHz, Chloroform-*d*): δ 172.57, 170.05, 61.57, 44.87, 41.36, 35.94, 29.71, 26.15, 24.63, 14.16; ESI-EMM: [M+H]⁺ calculated 259.1111; measured 259.1110; agreement 0.4 ppm.

N-(8-Isothiocyanateoctanoyl)-L-homoserine lactone (HSL-ITC-8)

HSL-Az-8 was reacted with carbon disulfide as described for **HSL-ITC-6** and purified via flash silica gel chromatography (3:1 ethyl acetate:hexanes as eluent) to yield the product as a white solid (3% yield, 1 mg). This low yield for **HSL-ITC-8** reflects an issue with separation; further optimization of separation conditions using aromatic solvents would likely lead to increased product yields. ¹H NMR (500 MHz, Chloroform-*d*): δ 7.48 (d, *J* = 6.9 Hz, 1H), 4.58 (ddd, *J* = 11.5, 8.7, 6.5 Hz, 1H), 4.48 (td, *J* = 9.1, 1.4 Hz, 1H), 4.28 (ddd, *J* = 11.1, 9.3, 6.0 Hz, 1H), 3.53 (t, *J* = 6.5 Hz, 2H), 3.47 (s, 2H), 2.78 (dddd, *J* = 12.6, 8.6, 5.9, 1.2 Hz, 1H), 2.58 (t, *J* = 7.2 Hz, 2H), 2.23 (dtd, *J* = 12.7, 11.4, 8.9 Hz, 1H), 1.75–1.68 (m, 2H), 1.64 (p, *J* = 7.3 Hz, 2H), 1.47–1.39 (m, 2H); ¹³C NMR (126 MHz, Chloroform-*d*): δ 205.67, 174.63, 166.03, 65.87, 49.14, 48.346, 44.81, 43.45, 29.95, 29.72, 25.93, 22.37; ESI-EMM: [M+Na]⁺ calculated 321.0880; measured 321.0876; agreement 1.2 ppm.

N-(8-Isothiocyanateoctanoyl)-glycine ethyl ester (GEE-ITC-8)

GEE-Az-8 was reacted with carbon disulfide as described for **HSL-ITC-6** and purified via flash silica gel chromatography (ethyl acetate as eluent) to yield the product as a white solid (19% yield, 5 mg). ^1H NMR (500 MHz, Chloroform-*d*): δ 7.28 (s, 1H), 4.22 (q, $J = 7.1$ Hz, 2H), 4.05 (d, $J = 5.3$ Hz, 2H), 3.52 (t, $J = 6.6$ Hz, 2H), 3.45 (s, 2H), 2.59 (t, $J = 7.2$ Hz, 2H), 1.71 (dt, $J = 14.3, 6.8$ Hz, 2H), 1.64 (p, $J = 7.3$ Hz, 2H), 1.47–1.39 (m, 2H), 1.29 (t, $J = 7.2$ Hz, 4H); ^{13}C NMR (126 MHz, Chloroform-*d*): δ 205.57, 169.47, 165.65, 61.58, 48.87, 44.81, 43.38, 41.43, 29.71, 25.94, 22.39, 14.15; ESI-EMM: $[\text{M}+\text{Na}]^+$ calculated 323.1036; measured 323.1031; agreement 1.5 ppm.

N-(12-Isothiocyanatedodecanoyl)-L-homoserine lactone (HSL-ITC-12)

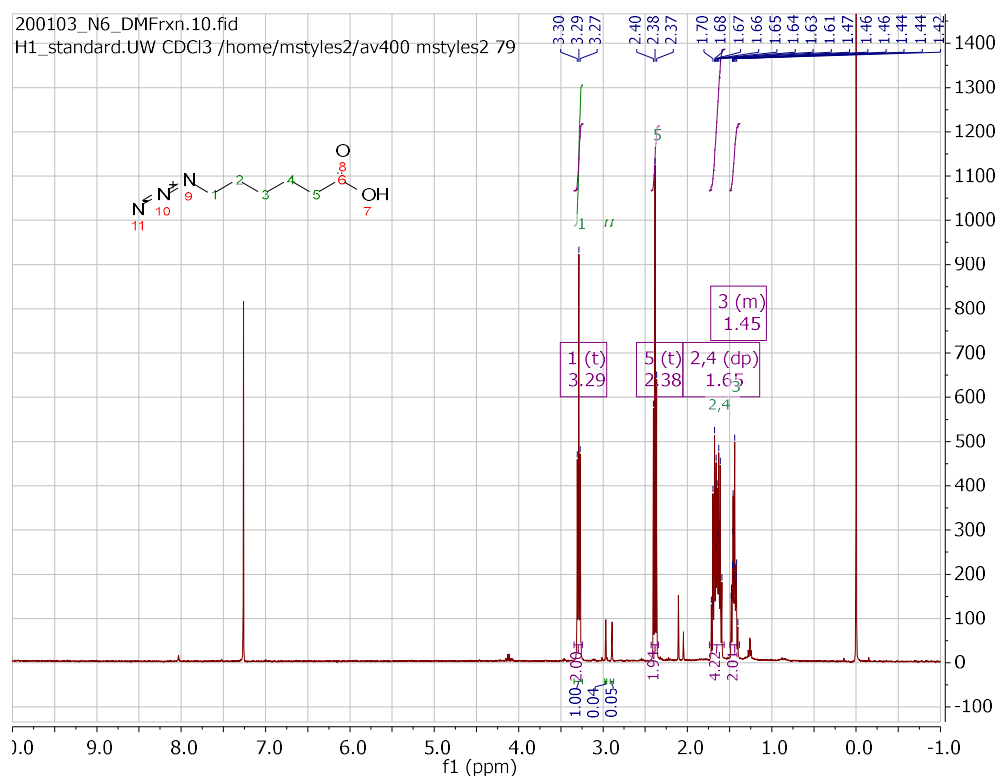
HSL-Az-12 was reacted with carbon disulfide as described for **HSL-ITC-6** and purified via flash silica gel chromatography (ethyl acetate as eluent) to yield the product as a white solid (46% yield, 93 mg). ^1H NMR (500 MHz, Chloroform-*d*): δ 7.67 (d, $J = 6.8$ Hz, 1H), 4.61 (ddd, $J = 11.4, 8.8, 6.8$ Hz, 1H), 4.48 (td, $J = 9.1, 1.4$ Hz, 1H), 4.28 (ddd, $J = 11.0, 9.2, 6.1$ Hz, 1H), 3.51 (t, $J = 6.6$ Hz, 2H), 3.47 (s, 2H), 2.73 (dddd, $J = 12.5, 8.1, 6.2, 1.4$ Hz, 1H), 2.54 (t, $J = 7.3$ Hz, 2H), 2.34–2.20 (m, 1H), 1.69 (p, $J = 6.9$ Hz, 2H), 1.58 (t, $J = 7.3$ Hz, 2H), 1.41 (p, $J = 6.9$ Hz, 2H), 1.30 (s, 8H); ^{13}C NMR (126 MHz, Chloroform-*d*): δ 206.32, 174.93, 166.45, 65.92, 49.02, 48.39, 45.04, 43.73, 29.89, 29.64, 29.14, 29.11, 28.86, 28.66, 26.48, 23.26; ESI-EMM: $[\text{M}+\text{H}]^+$ calculated 355.1686; measured 355.1683; agreement 0.8 ppm.

N-(12-Isothiocyanatedodecanoyl)-glycine ethyl ester (GEE-ITC-12)

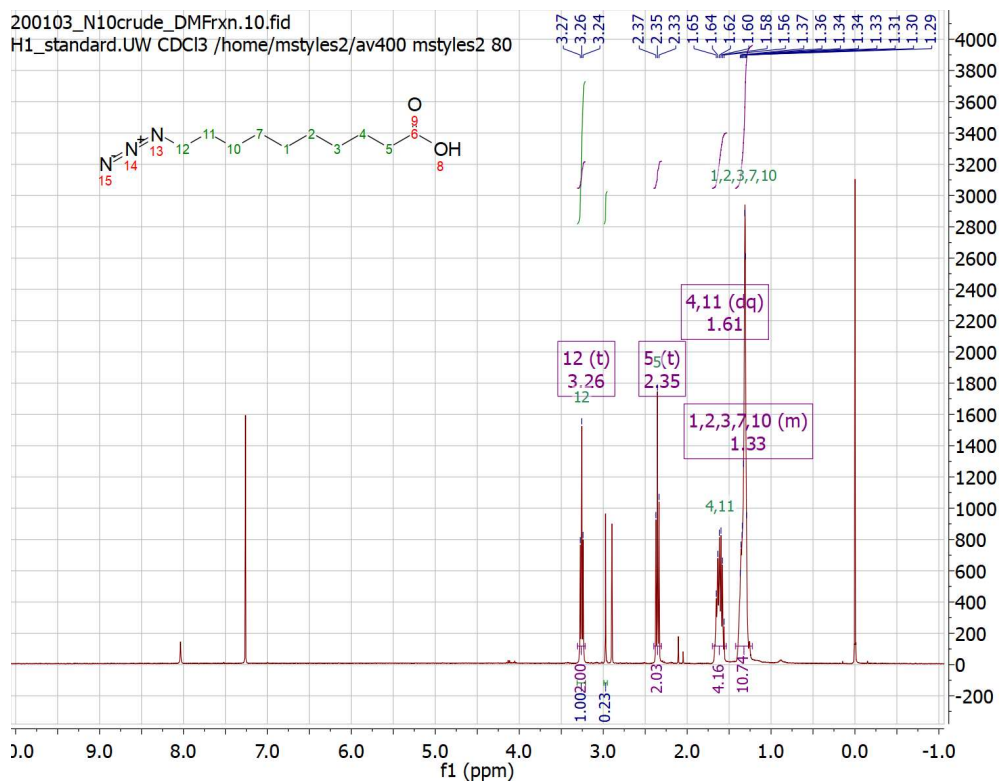
GEE-Az-12 was reacted with carbon disulfide as described for **HSL-ITC-6** and purified via flash silica gel chromatography (ethyl acetate as eluent) to yield the product as a white solid (57% yield, 162 mg). ^1H NMR (500 MHz, Chloroform- d): δ 7.46 (t, J = 5.6 Hz, 1H), 4.22 (q, J = 7.1 Hz, 2H), 4.05 (d, J = 5.4 Hz, 2H), 3.51 (t, J = 6.6 Hz, 2H), 3.45 (s, 2H), 2.55 (t, J = 7.3 Hz, 2H), 1.69 (p, J = 6.8 Hz, 2H), 1.59 (p, J = 7.3 Hz, 2H), 1.40 (dd, J = 9.9, 5.2 Hz, 2H), 1.35–1.23 (m, 11H); ^{13}C NMR (126 MHz, Chloroform- d): δ 206.33, 169.51, 165.95, 61.48, 48.63, 45.04, 43.77, 41.39, 29.91, 29.15, 29.12, 28.88, 28.67, 26.49, 23.29, 14.14; ESI-EMM: $[\text{M}+\text{H}]^+$ calculated 357.1843; measured 357.1838; agreement 1.4 ppm.

1.4.4 NMR spectra for new compounds.

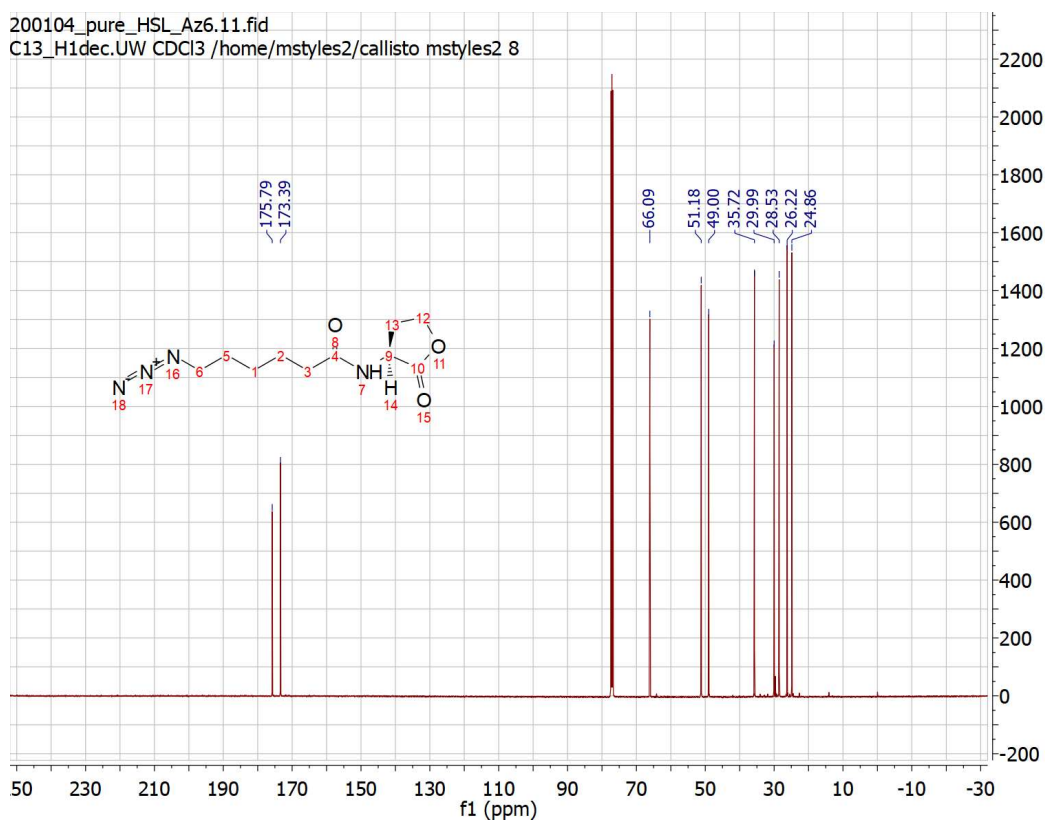
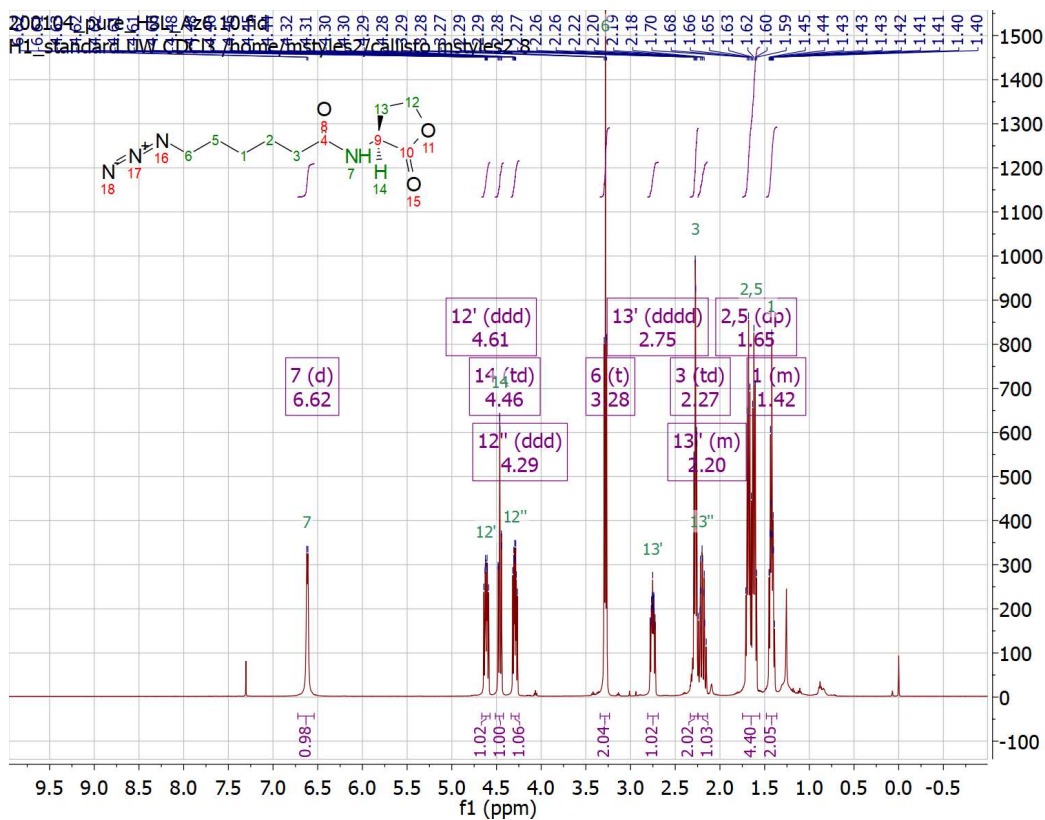
N3-6 intermediate



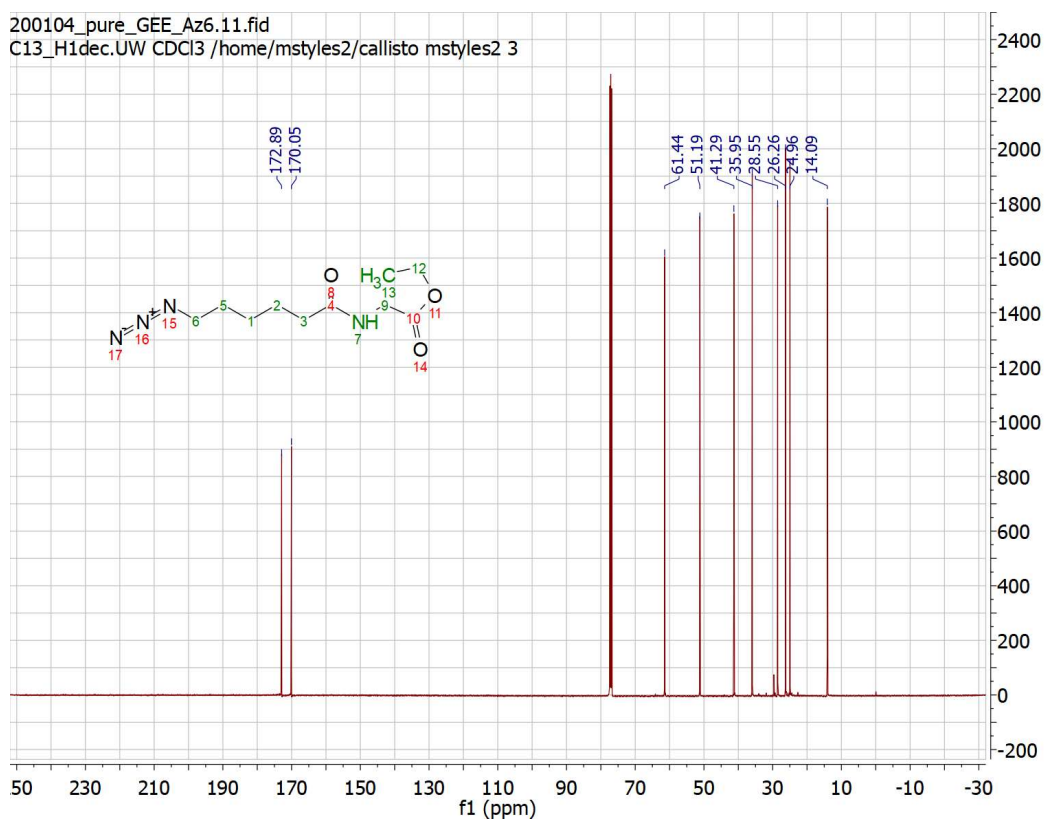
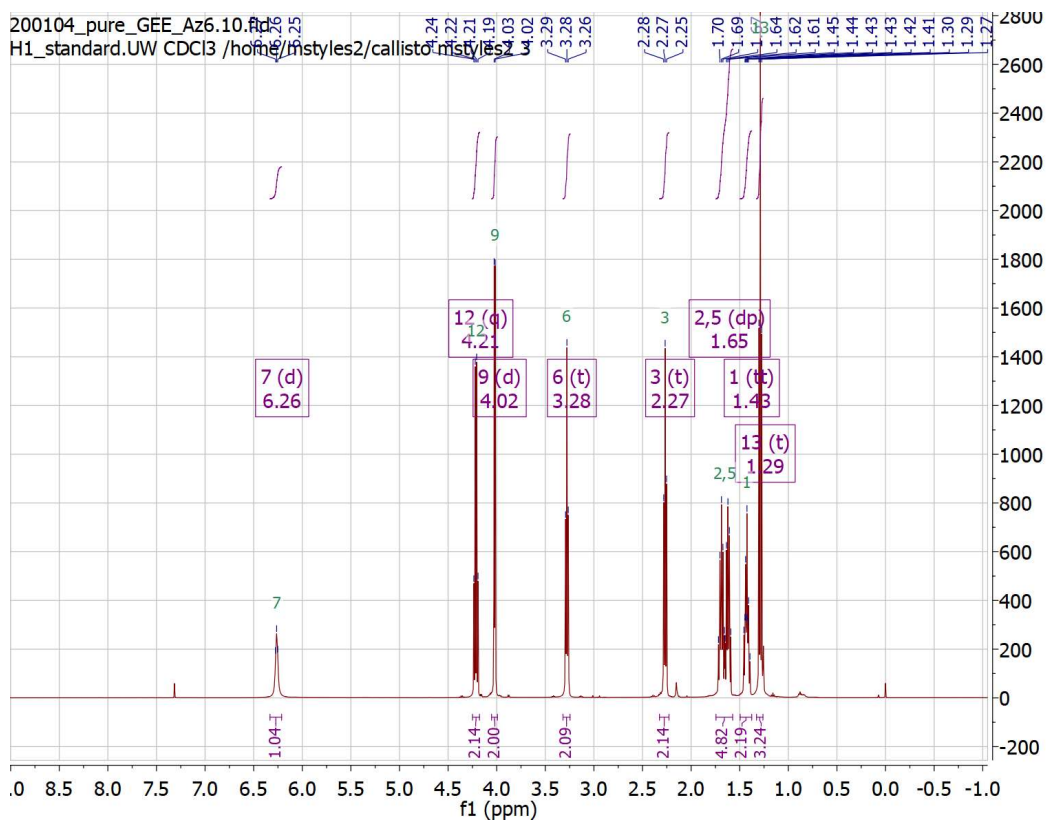
N3-10 intermediate



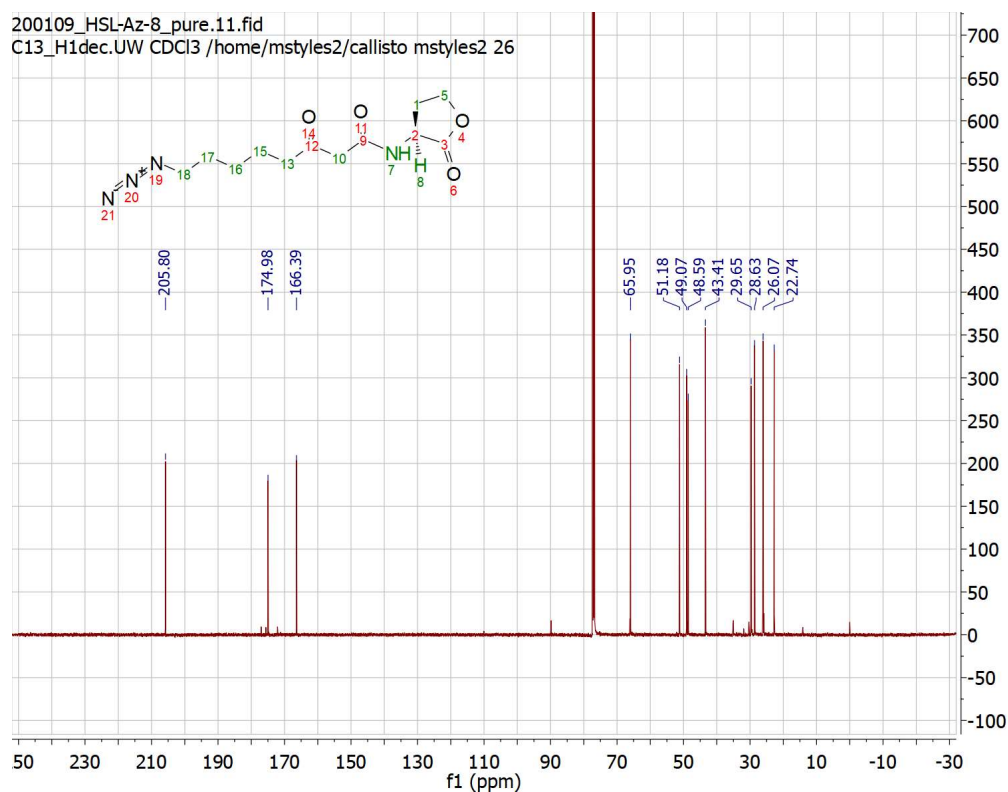
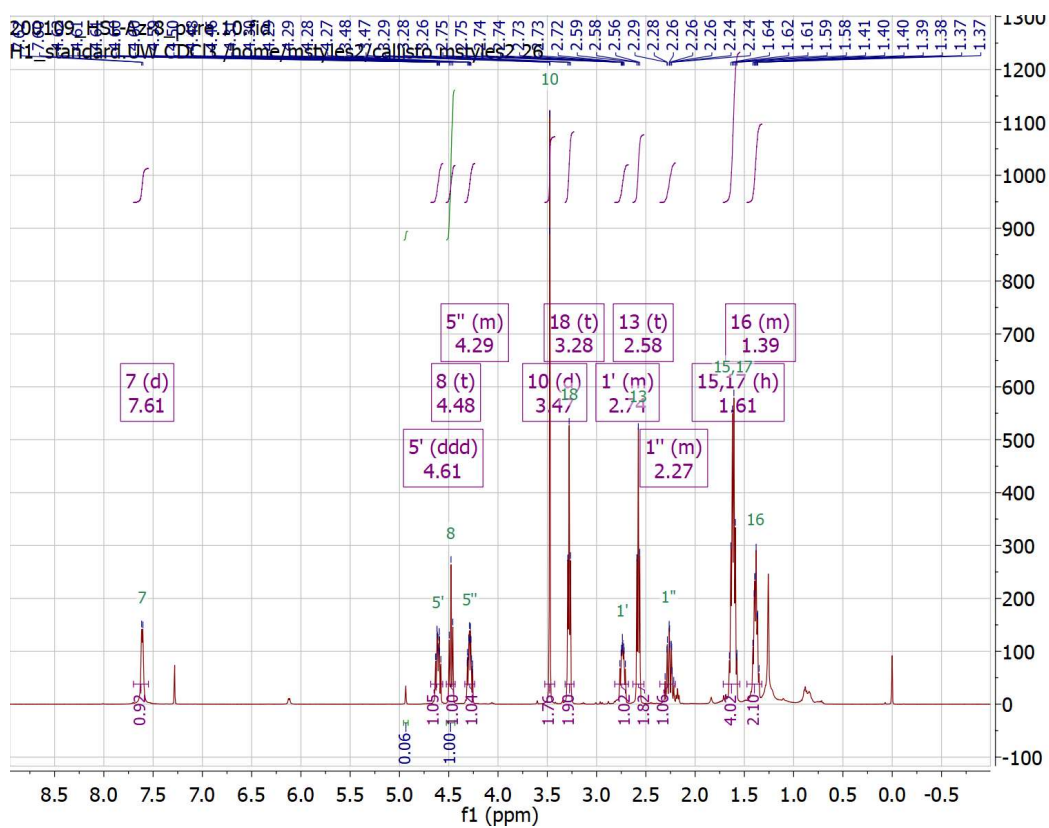
HSL-Az-6



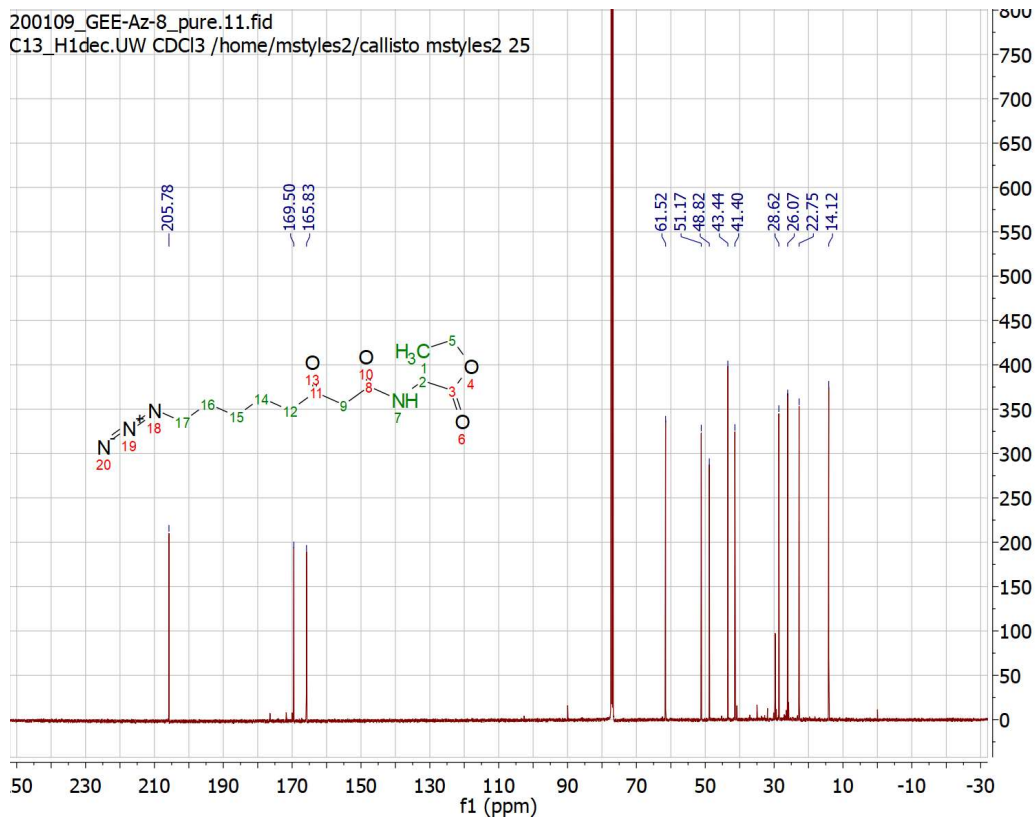
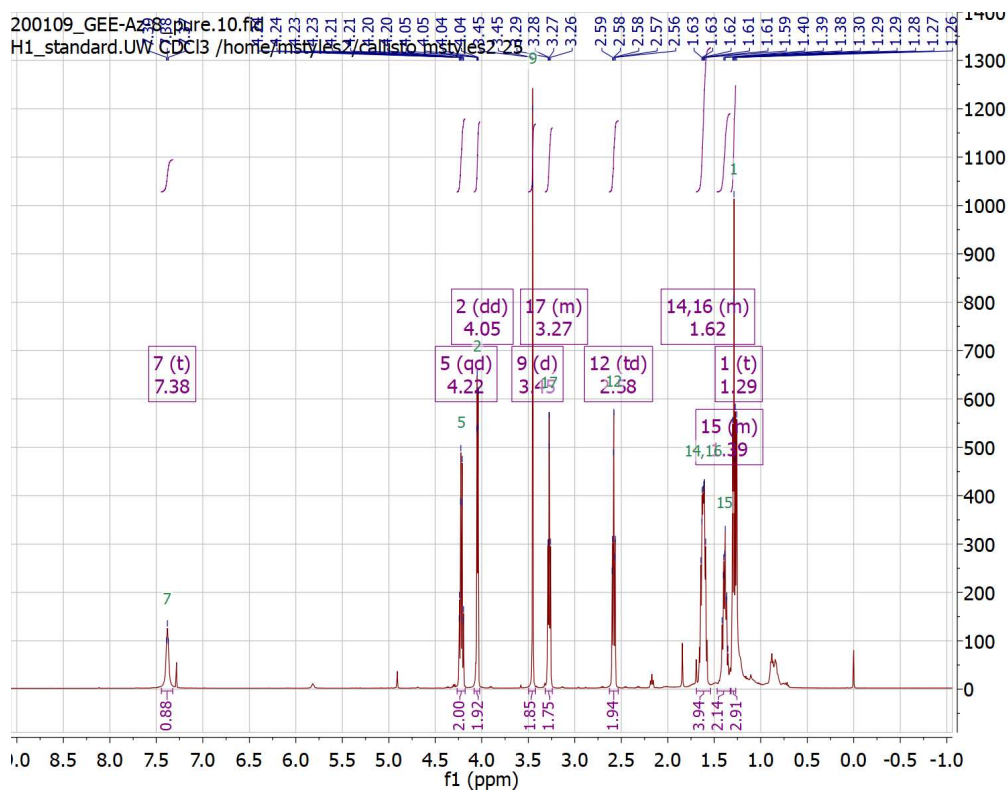
GEE-Az-6



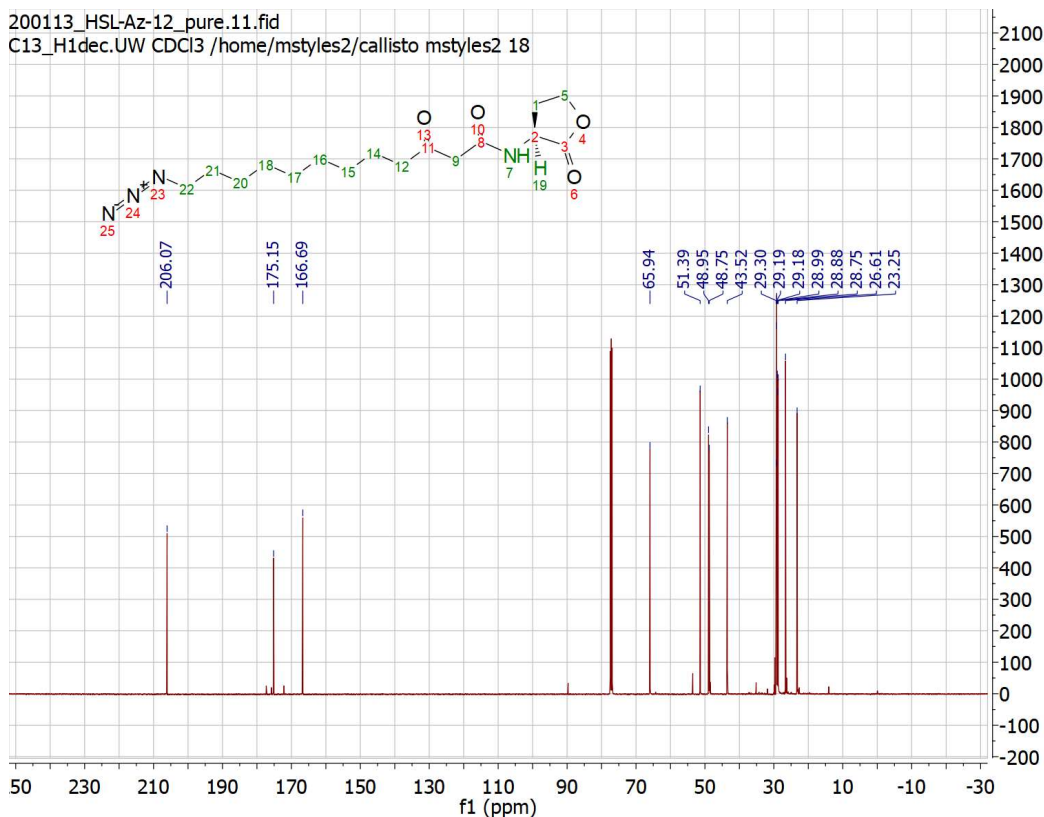
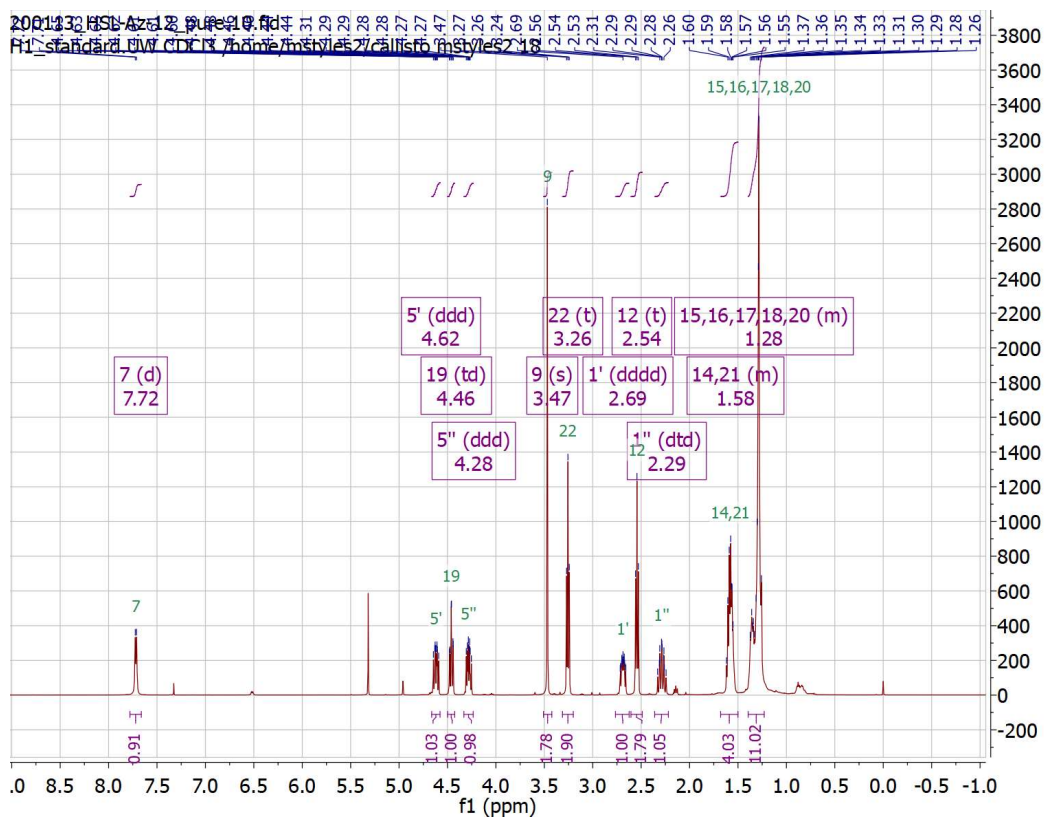
HSL-Az-8



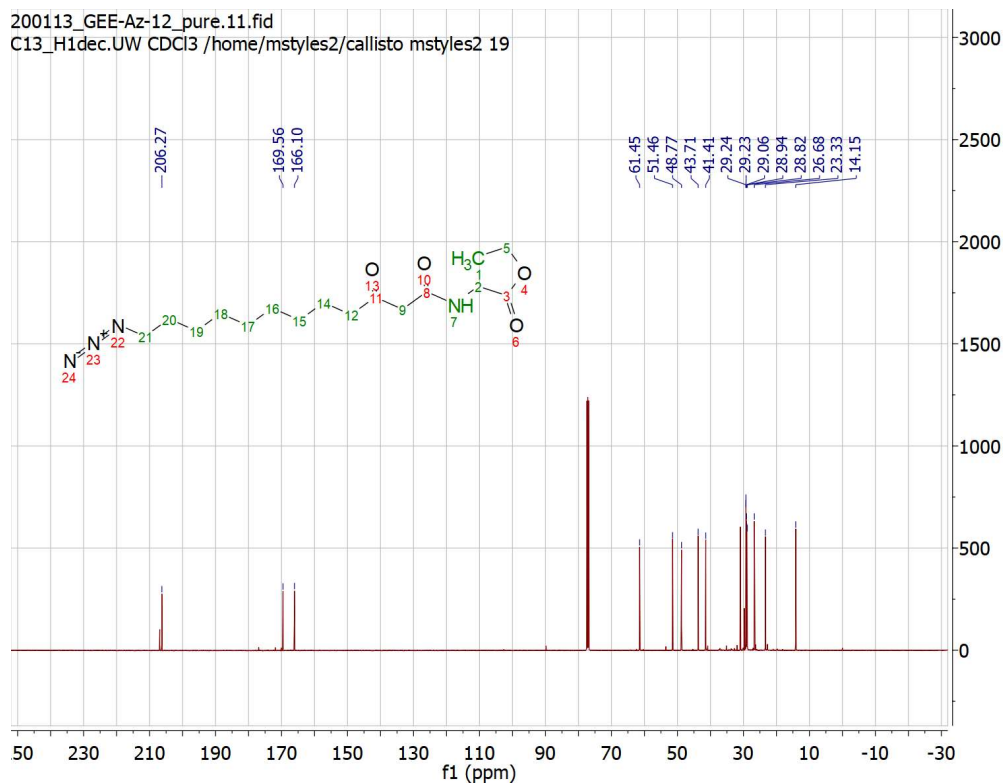
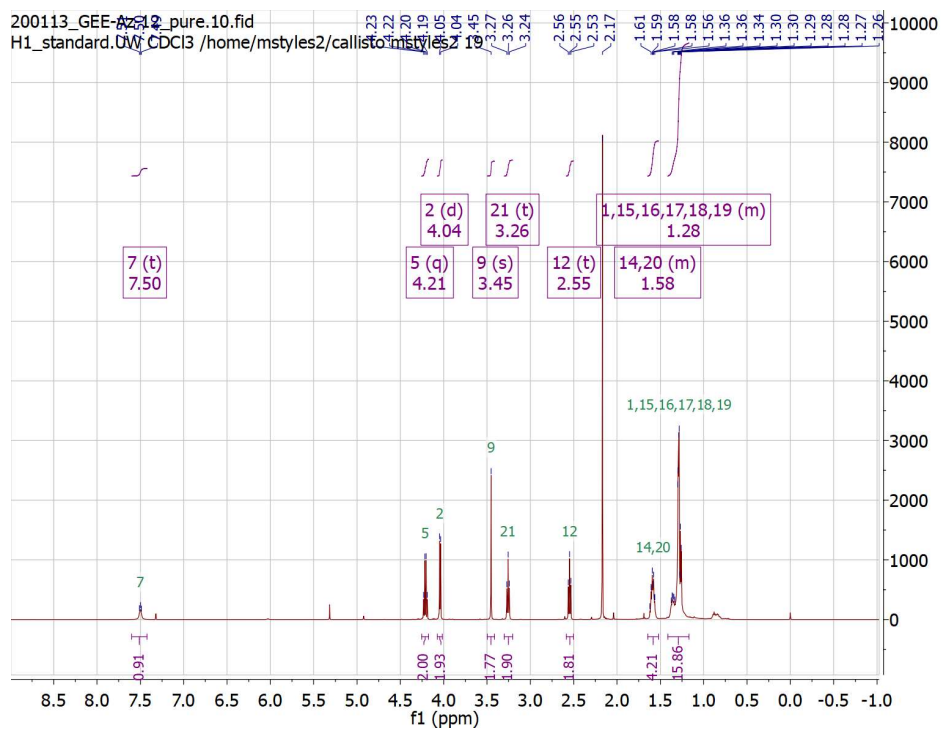
GEE-Az-8



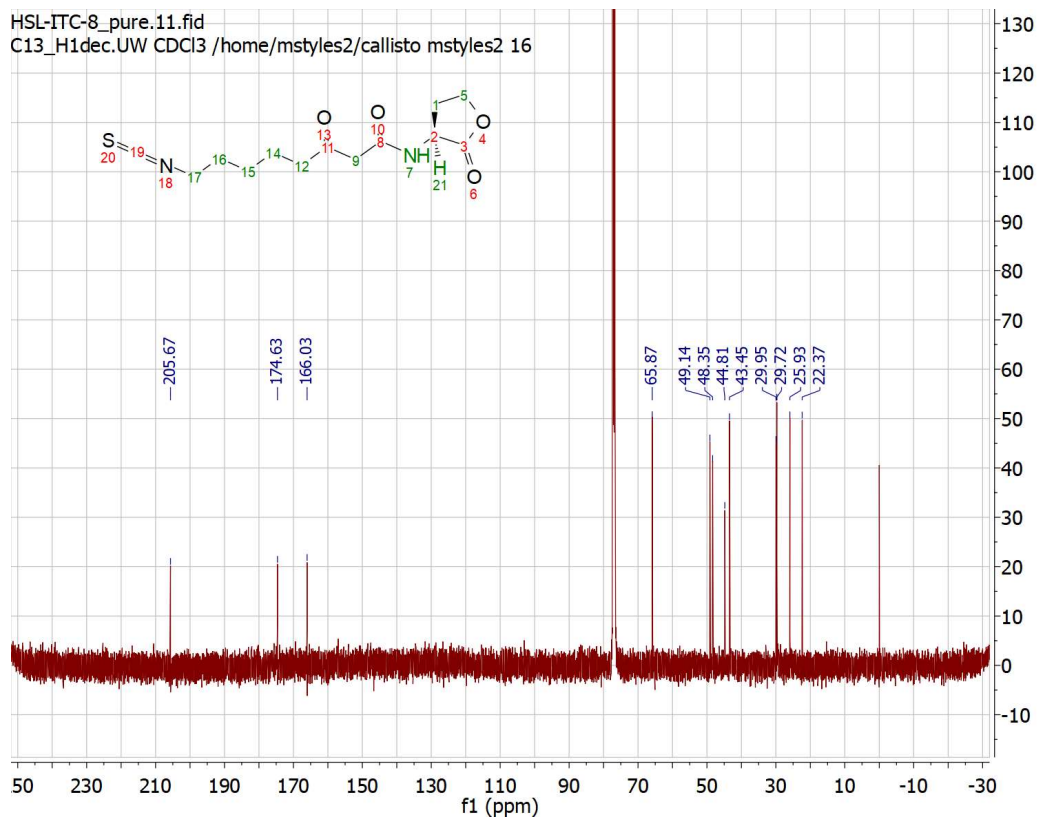
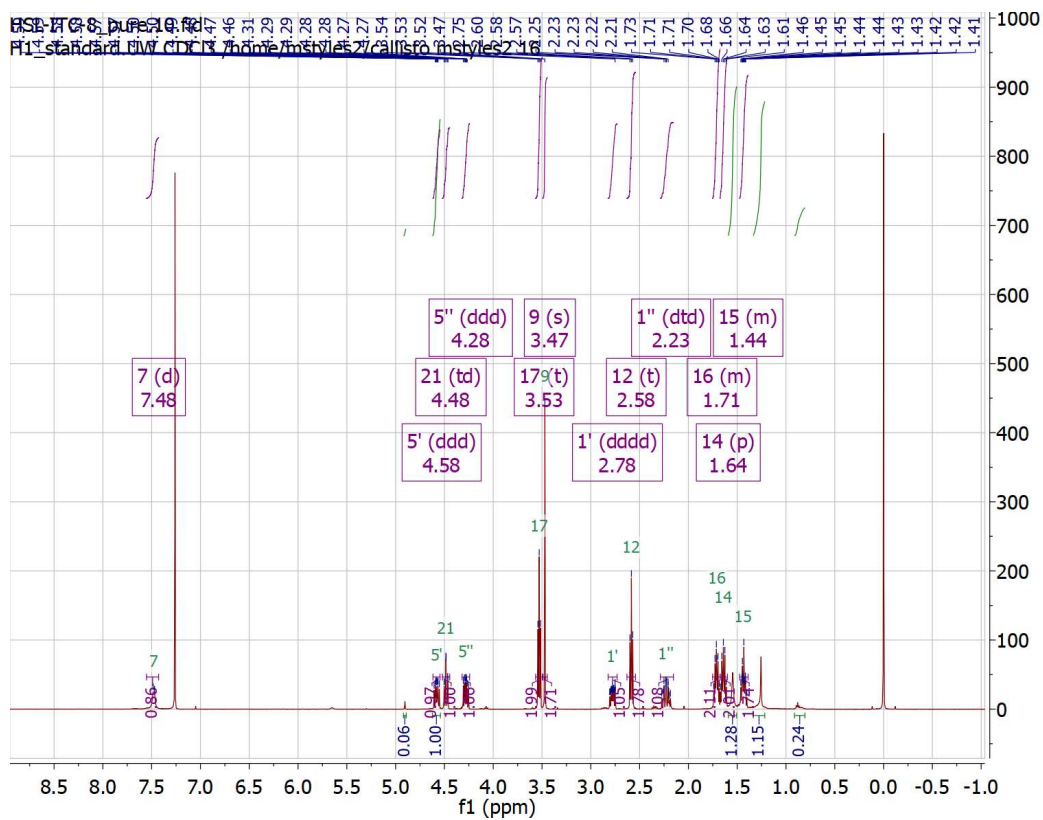
HSL-Az-12



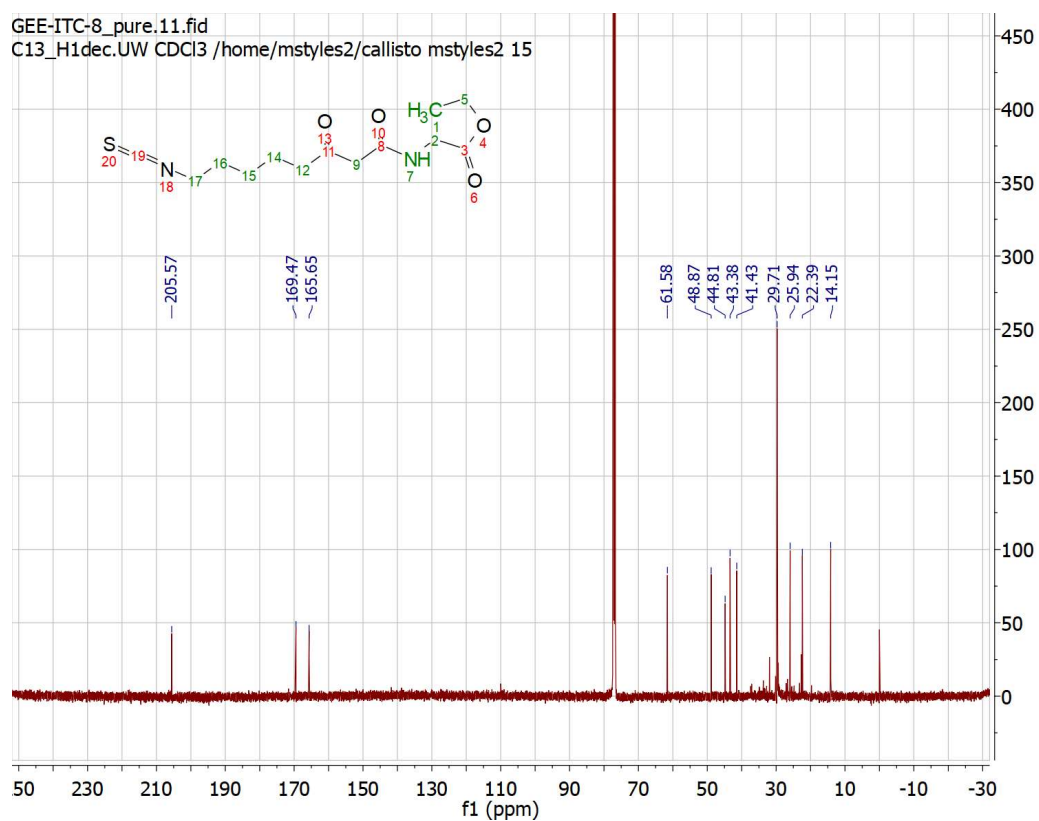
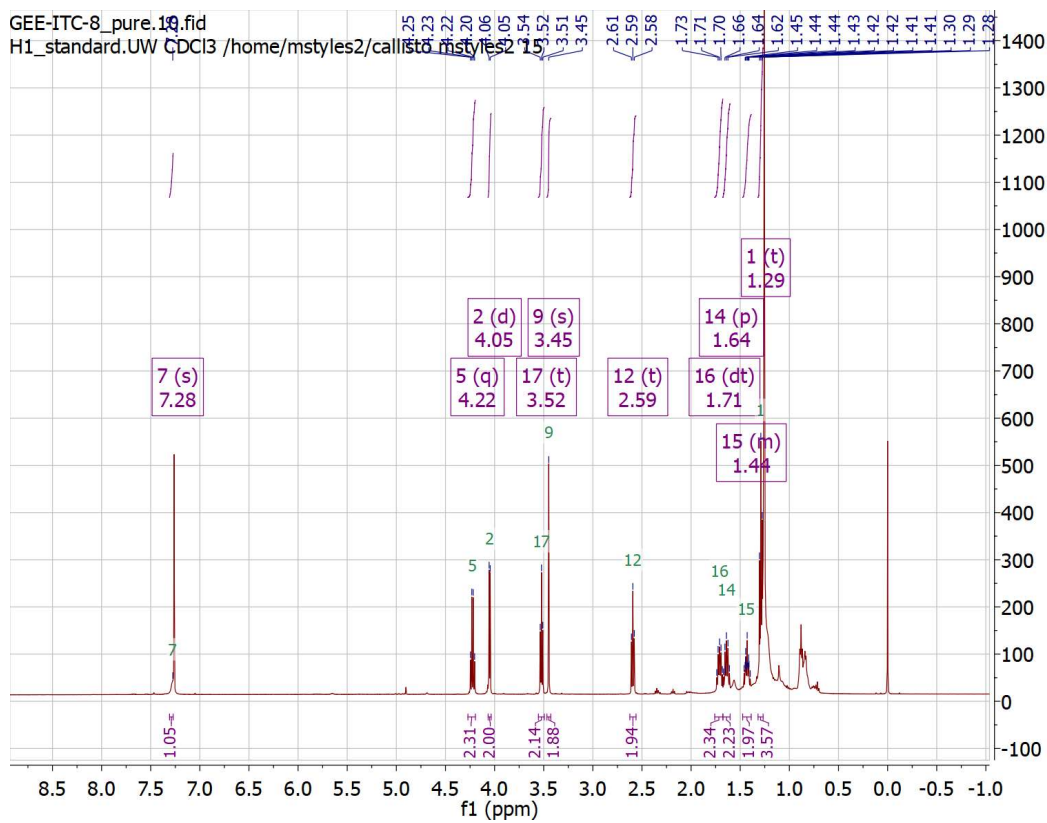
GEE-Az-12



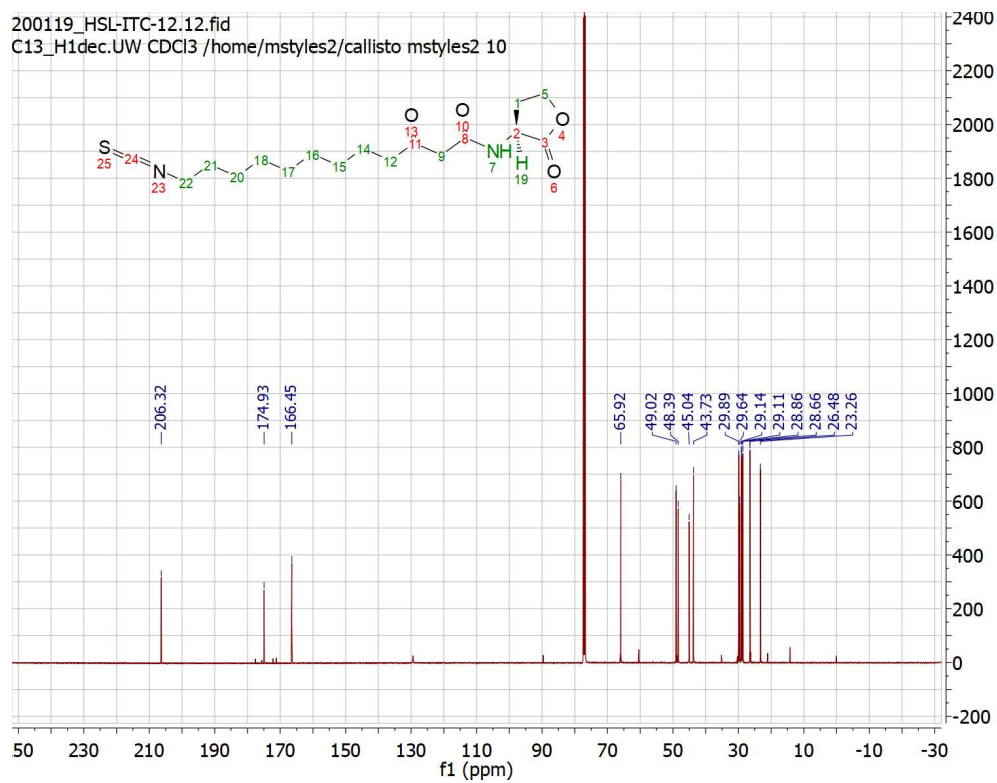
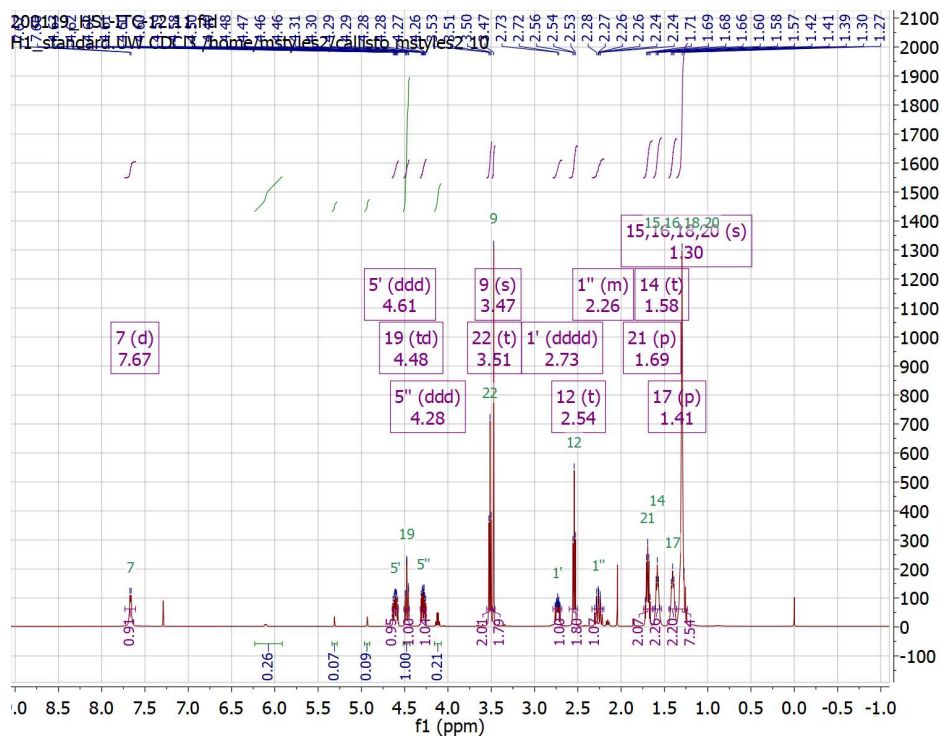
HSL-ITC-8



GEE-ITC-8



HSL-ITC-12



I.5 Acknowledgements

Financial support for this work was provided by the NIH (R01 GM109403). M.J.S. was supported in part by the UW–Madison NIH Biotechnology Training Program (T32 GM008349) and an NSF GRFP (DGE-1747503). Any opinions, findings, and conclusions or recommendations expressed in this material are those of the author(s) and do not necessarily reflect the views of the NSF. T.T. and K.H.J.W. were supported in part by the UW–Madison NIH Chemistry–Biology Interface Training Program (T32 GM008505). We gratefully acknowledge Prof. Vanessa Sperandio (UT–Southwestern) for donating *E. coli* 86-24 genomic DNA (WT EHEC serotype O157:H7).

I.6 References

1. Donaldson, G. P.; Lee, S. M.; Mazmanian, S. K., Gut biogeography of the bacterial microbiota. *Nature reviews. Microbiology* **2016**, *14* (1), 20-32.
2. Baumler, A. J.; Sperandio, V., Interactions between the microbiota and pathogenic bacteria in the gut. *Nature* **2016**, *535* (7610), 85-93.
3. Rasko, D. A.; Sperandio, V., Anti-virulence strategies to combat bacteria-mediated disease. *Nat. Rev. Drug Discov.* **2010**, *9* (2), 117-28.
4. Kendall, M. M.; Sperandio, V., What a Dinner Party! Mechanisms and Functions of Interkingdom Signaling in Host-Pathogen Associations. *mBio* **2016**, *7* (2), e01748.
5. Clatworthy, A. E.; Pierson, E.; Hung, D. T., Targeting virulence: a new paradigm for antimicrobial therapy. *Nature chemical biology* **2007**, *3* (9), 541-548.
6. Whiteley, M.; Diggle, S. P.; Greenberg, E. P., Progress in and promise of bacterial quorum sensing research. *Nature* **2017**, *551*, 313.
7. Kaper, J. B.; Sperandio, V., Bacterial cell-to-cell signaling in the gastrointestinal tract. *Infection and immunity* **2005**, *73* (6), 3197-209.
8. Waters, C. M.; Bassler, B. L., Quorum sensing: cell-to-cell communication in bacteria. *Annu. Rev. Cell Dev. Biol.* **2005**, *21*, 319-46.
9. Miller, M. B.; Bassler, B. L., Quorum sensing in bacteria. *Annu. Rev. Microbiol.* **2001**, *55*, 165-99.
10. Amara, N.; Mashiach, R.; Amar, D.; Krief, P.; Spieser, S. A.; Bottomley, M. J.; Aharoni, A.; Meijler, M. M., Covalent inhibition of bacterial quorum sensing. *J. Am. Chem. Soc.* **2009**, *131* (30), 10610-9.
11. Geske, G. D.; O'Neill, J. C.; Miller, D. M.; Mattmann, M. E.; Blackwell, H. E., Modulation of bacterial quorum sensing with synthetic ligands: systematic evaluation of N-acylated homoserine lactones in multiple species and new insights into their mechanisms of action. *J. Am. Chem. Soc.* **2007**, *129* (44), 13613-25.
12. Moore, J. D.; Rossi, F. M.; Welsh, M. A.; Nyffeler, K. E.; Blackwell, H. E., A Comparative Analysis of Synthetic Quorum Sensing Modulators in *Pseudomonas aeruginosa*: New Insights into Mechanism, Active Efflux Susceptibility, Phenotypic Response, and Next-Generation Ligand Design. *Journal of the American Chemical Society* **2015**, *137* (46), 14626-14639.

13. Welsh, M. A.; Blackwell, H. E., Chemical probes of quorum sensing: from compound development to biological discovery. *FEMS Microbiol. Rev.* **2016**, *40* (5), 774-94.
14. Chen, G.; Swem, L. R.; Swem, D. L.; Stauff, D. L.; O'Loughlin, C. T.; Jeffrey, P. D.; Bassler, B. L.; Hughson, F. M., A strategy for antagonizing quorum sensing. *Molecular cell* **2011**, *42* (2), 199-209.
15. O'Loughlin, C. T.; Miller, L. C.; Siryaporn, A.; Drescher, K.; Semmelhack, M. F.; Bassler, B. L., A quorum-sensing inhibitor blocks *Pseudomonas aeruginosa* virulence and biofilm formation. *Proceedings of the National Academy of Sciences of the United States of America* **2013**, *110* (44), 17981-6.
16. Galloway, W. R.; Hodgkinson, J. T.; Bowden, S.; Welch, M.; Spring, D. R., Applications of small molecule activators and inhibitors of quorum sensing in Gram-negative bacteria. *Trends in microbiology* **2012**, *20* (9), 449-58.
17. Michael, B.; Smith, J. N.; Swift, S.; Heffron, F.; Ahmer, B. M., SdiA of *Salmonella enterica* is a LuxR homolog that detects mixed microbial communities. *Journal of bacteriology* **2001**, *183* (19), 5733-42.
18. Venturi, V.; Ahmer, B. M. M., Editorial: LuxR Solos are Becoming Major Players in Cell-Cell Communication in Bacteria. *Frontiers in cellular and infection microbiology* **2015**, *5*, 89.
19. Styles, M. J.; Blackwell, H. E., Non-native autoinducer analogs capable of modulating the SdiA quorum sensing receptor in *Salmonella enterica* serovar Typhimurium. *Beilstein J. Org. Chem.* **2018**, *14*, 2651-2664.
20. Sabag-Daigle, A.; Ahmer, B. M., Expl and PhzI are descendants of the long lost cognate signal synthase for SdiA. *PLoS one* **2012**, *7* (10), e47720.
21. Kim, T.; Duong, T.; Wu, C. A.; Choi, J.; Lan, N.; Kang, S. W.; Lokanath, N. K.; Shin, D.; Hwang, H. Y.; Kim, K. K., Structural insights into the molecular mechanism of *Escherichia coli* SdiA, a quorum-sensing receptor. *Acta crystallographica. Section D, Biological crystallography* **2014**, *70* (Pt 3), 694-707.
22. Nguyen, Y.; Nguyen, N. X.; Rogers, J. L.; Liao, J.; MacMillan, J. B.; Jiang, Y.; Sperandio, V., Structural and mechanistic roles of novel chemical ligands on the SdiA quorum-sensing transcription regulator. *mBio* **2015**, *6* (2).
23. Kaper, J. B.; Nataro, J. P.; Mobley, H. L., Pathogenic *Escherichia coli*. *Nature reviews. Microbiology* **2004**, *2* (2), 123-40.
24. Hughes, D. T.; Terekhova, D. A.; Liou, L.; Hovde, C. J.; Sahl, J. W.; Patankar, A. V.; Gonzalez, J. E.; Edrington, T. S.; Rasko, D. A.; Sperandio, V., Chemical

- sensing in mammalian host-bacterial commensal associations. *Proceedings of the National Academy of Sciences of the United States of America* **2010**, *107* (21), 9831-6.
25. Price, S. B.; Wright, J. C.; DeGraves, F. J.; Castanie-Cornet, M. P.; Foster, J. W., Acid resistance systems required for survival of *Escherichia coli* O157:H7 in the bovine gastrointestinal tract and in apple cider are different. *Applied and environmental microbiology* **2004**, *70* (8), 4792-9.
 26. Dziva, F.; van Diemen, P. M.; Stevens, M. P.; Smith, A. J.; Wallis, T. S., Identification of *Escherichia coli* O157 : H7 genes influencing colonization of the bovine gastrointestinal tract using signature-tagged mutagenesis. *Microbiology (Reading, England)* **2004**, *150* (Pt 11), 3631-3645.
 27. Sharma, V. K.; Bearson, S. M., Evaluation of the impact of quorum sensing transcriptional regulator SdiA on long-term persistence and fecal shedding of *Escherichia coli* O157:H7 in weaned calves. *Microbial pathogenesis* **2013**, *57*, 21-6.
 28. Sheng, H.; Nguyen, Y. N.; Hovde, C. J.; Sperandio, V., SdiA aids enterohemorrhagic *Escherichia coli* carriage by cattle fed a forage or grain diet. *Infection and immunity* **2013**, *81* (9), 3472-8.
 29. Yang, Y.; Zhou, M.; Hardwidge, P. R.; Cui, H.; Zhu, G., Isolation and Characterization of N-acyl Homoserine Lactone-Producing Bacteria From Cattle Rumen and Swine Intestines. *Frontiers in cellular and infection microbiology* **2018**, *8*, 155.
 30. Edrington, T. S.; Farrow, R. L.; Sperandio, V.; Hughes, D. T.; Lawrence, T. E.; Callaway, T. R.; Anderson, R. C.; Nisbet, D. J., Acyl-homoserine-lactone autoinducer in the gastrointestinal [corrected] tract of feedlot cattle and correlation to season, *E. coli* O157:H7 prevalence, and diet. *Current microbiology* **2009**, *58* (3), 227-32.
 31. Erickson, D. L.; Nsereko, V. L.; Morgavi, D. P.; Selinger, L. B.; Rode, L. M.; Beauchemin, K. A., Evidence of quorum sensing in the rumen ecosystem: detection of N-acyl homoserine lactone autoinducers in ruminal contents. *Canadian journal of microbiology* **2002**, *48* (4), 374-8.
 32. Dyszel, J. L.; Soares, J. A.; Swearingen, M. C.; Lindsay, A.; Smith, J. N.; Ahmer, B. M., *E. coli* K-12 and EHEC genes regulated by SdiA. *PloS one* **2010**, *5* (1), e8946.
 33. Nguyen, Y. N.; Sheng, H.; Dakarapu, R.; Falck, J. R.; Hovde, C. J.; Sperandio, V., The acyl-homoserine lactone synthase YenI from *Yersinia enterocolitica*

- modulates virulence gene expression in enterohemorrhagic *Escherichia coli* O157:H7. *Infection and immunity* **2013**, *81* (11), 4192-9.
34. Sharma, V. K.; Bearson, S. M.; Bearson, B. L., Evaluation of the effects of sdiA, a luxR homologue, on adherence and motility of *Escherichia coli* O157 : H7. *Microbiology (Reading, England)* **2010**, *156* (Pt 5), 1303-12.
 35. Hoyland-Kroghsbo, N. M.; Maerkedahl, R. B.; Svenningsen, S. L., A quorum-sensing-induced bacteriophage defense mechanism. *mBio* **2013**, *4* (1), e00362-12.
 36. Lu, Y.; Zeng, J.; Wang, L.; Lan, K.; E, S.; Wang, L.; Xiao, Q.; Luo, Q.; Huang, X.; Huang, B.; Chen, C., Antibiotics Promote *Escherichia coli*-*Pseudomonas aeruginosa* Conjugation through Inhibiting Quorum Sensing. *Antimicrobial agents and chemotherapy* **2017**, *61* (12).
 37. Lu, Y.; Zeng, J.; Wu, B.; E, S.; Wang, L.; Cai, R.; Zhang, N.; Li, Y.; Huang, X.; Huang, B.; Chen, C., Quorum Sensing N-acyl Homoserine Lactones-SdiA Suppresses *Escherichia coli*-*Pseudomonas aeruginosa* Conjugation through Inhibiting tral Expression. *Frontiers in cellular and infection microbiology* **2017**, *7*, 7.
 38. Shimada, T.; Shimada, K.; Matsui, M.; Kitai, Y.; Igarashi, J.; Suga, H.; Ishihama, A., Roles of cell division control factor SdiA: recognition of quorum sensing signals and modulation of transcription regulation targets. *Genes to cells : devoted to molecular & cellular mechanisms* **2014**, *19* (5), 405-18.
 39. Eibergen, N. R.; Moore, J. D.; Mattmann, M. E.; Blackwell, H. E., Potent and Selective Modulation of the RhIR Quorum Sensing Receptor by Using Non-native Ligands: An Emerging Target for Virulence Control in *Pseudomonas aeruginosa*. *ChemBioChem* **2015**, *16* (16), 2348-56.
 40. Geske, G. D.; O'Neill, J. C.; Miller, D. M.; Wezeman, R. J.; Mattmann, M. E.; Lin, Q.; Blackwell, H. E., Comparative Analyses of N-Acylated Homoserine Lactones Reveal Unique Structural Features that Dictate Their Ability to Activate or Inhibit Quorum Sensing. *Chembiochem : a European journal of chemical biology* **2008**, *9* (3), 389-400.
 41. Gerdt, J. P.; Wittenwyler, D. M.; Combs, J. B.; Boursier, M. E.; Brummond, J. W.; Xu, H.; Blackwell, H. E., Chemical Interrogation of LuxR-type Quorum Sensing Receptors Reveals New Insights into Receptor Selectivity and the Potential for Interspecies Bacterial Signaling. *ACS Chemical Biology* **2017**, *12* (9), 2457-2464.
 42. McInnis, C. E.; Blackwell, H. E., Design, synthesis, and biological evaluation of abiotic, non-lactone modulators of LuxR-type quorum sensing. *Bioorganic & medicinal chemistry* **2011**, *19* (16), 4812-4819.

43. McInnis, C. E.; Blackwell, H. E., Thiolactone modulators of quorum sensing revealed through library design and screening. *Bioorg. Med. Chem.* **2011**, *19* (16), 4820-8.
44. Mattmann, M. E.; Geske, G. D.; Worzalla, G. A.; Chandler, J. R.; Sappington, K. J.; Greenberg, E. P.; Blackwell, H. E., Synthetic ligands that activate and inhibit a quorum-sensing regulator in *Pseudomonas aeruginosa*. *Bioorg. Med. Chem. Lett.* **2008**, *18* (10), 3072-5.
45. Mattmann, M. E.; Shipway, P. M.; Heth, N. J.; Blackwell, H. E., Potent and selective synthetic modulators of a quorum sensing repressor in *Pseudomonas aeruginosa* identified from second-generation libraries of N-acylated L-homoserine lactones. *ChemBioChem* **2011**, *12* (6), 942-9.
46. Geske, G. D.; O'Neill, J. C.; Blackwell, H. E., N-Phenylacetanoyl-L-Homoserine Lactones Can Strongly Antagonize or Superagonize Quorum Sensing in *Vibrio fischeri*. *ACS chemical biology* **2007**, *2* (5), 315-319.
47. Boursier, M. E.; Moore, J. D.; Heitman, K. M.; Shepardson-Fungairino, S. P.; Combs, J. B.; Koenig, L. C.; Shin, D.; Brown, E. C.; Nagarajan, R.; Blackwell, H. E., Structure-Function Analyses of the N-Butanoyl L-Homoserine Lactone Quorum-Sensing Signal Define Features Critical to Activity in RhIR. *ACS Chem. Biol.* **2018**, *13* (9), 2655-2662.
48. Palmer, A. G.; Streng, E.; Jewell, K. A.; Blackwell, H. E., Quorum Sensing in Bacterial Species that Use Degenerate Autoinducers Can Be Tuned by Using Structurally Identical Non-native Ligands. *Chembiochem : a European journal of chemical biology* **2011**, *12* (1), 138-147.
49. Slinger, B. L.; Deay, J. J.; Chandler, J. R.; Blackwell, H. E., Potent modulation of the CepR quorum sensing receptor and virulence in a *Burkholderia cepacia* complex member using non-native lactone ligands. *Sci. Rep.* **2019**, *9* (1), 13449.
50. Miller, J. H., *Experiments in Molecular Genetics*. Cold Spring Press: Plainview, NY, 1972.
51. Janssens, J. C.; Metzger, K.; Daniels, R.; Ptacek, D.; Verhoeven, T.; Habel, L. W.; Vanderleyden, J.; De Vos, D. E.; De Keersmaecker, S. C., Synthesis of N-acyl homoserine lactone analogues reveals strong activators of SdiA, the *Salmonella enterica* serovar Typhimurium LuxR homologue. *Applied and environmental microbiology* **2007**, *73* (2), 535-44.
52. Stacy, D. M.; Welsh, M. A.; Rather, P. N.; Blackwell, H. E., Attenuation of Quorum Sensing in the Pathogen *Acinetobacter baumannii* Using Non-native N-Acyl Homoserine Lactones. *ACS Chemical Biology* **2012**, *7* (10), 1719-1728.

53. Boursier, M. E.; Combs, J. B.; Blackwell, H. E., N-Acyl L-Homocysteine Thiolactones Are Potent and Stable Synthetic Modulators of the RhIR Quorum Sensing Receptor in *Pseudomonas aeruginosa*. *ACS Chem. Biol.* **2019**, *14* (2), 186-191.
54. Smith, K. M.; Bu, Y.; Suga, H., Induction and inhibition of *Pseudomonas aeruginosa* quorum sensing by synthetic autoinducer analogs. *Chemistry & biology* **2003**, *10* (1), 81-9.
55. Marshall, A. G.; Hendrickson, C. L.; Jackson, G. S., Fourier transform ion cyclotron resonance mass spectrometry: a primer. *Mass spectrometry reviews* **1998**, *17* (1), 1-35.
56. Kelleher, N. L.; Zubarev, R. A.; Bush, K.; Furie, B.; Furie, B. C.; McLafferty, F. W.; Walsh, C. T., Localization of labile posttranslational modifications by electron capture dissociation: the case of gamma-carboxyglutamic acid. *Anal Chem* **1999**, *71* (19), 4250-3.
57. Ge, Y.; Lawhorn, B. G.; ElNaggar, M.; Strauss, E.; Park, J. H.; Begley, T. P.; McLafferty, F. W., Top down characterization of larger proteins (45 kDa) by electron capture dissociation mass spectrometry. *Journal of the American Chemical Society* **2002**, *124* (4), 672-8.
58. Yao, Y.; Martinez-Yamout, M. A.; Dickerson, T. J.; Brogan, A. P.; Wright, P. E.; Dyson, H. J., Structure of the *Escherichia coli* quorum sensing protein SdiA: activation of the folding switch by acyl homoserine lactones. *Journal of molecular biology* **2006**, *355* (2), 262-73.
59. Smith, C.; Song, H.; You, L., Signal discrimination by differential regulation of protein stability in quorum sensing. *Journal of molecular biology* **2008**, *382* (5), 1290-7.
60. Huang, X.; Duddy, O. P.; Silpe, J. E.; Paczkowski, J. E.; Cong, J.; Henke, B. R.; Bassler, B. L., Mechanism underlying autoinducer recognition in the *Vibrio cholerae* DPO-VqmA quorum-sensing pathway. *The Journal of biological chemistry* **2020**, *295* (10), 2916-2931.
61. Shaw, P. D.; Ping, G.; Daly, S. L.; Cha, C.; Cronan, J. E., Jr.; Rinehart, K. L.; Farrand, S. K., Detecting and characterizing N-acyl-homoserine lactone signal molecules by thin-layer chromatography. *Proceedings of the National Academy of Sciences of the United States of America* **1997**, *94* (12), 6036-41.
62. Dyszel, J. L.; Smith, J. N.; Lucas, D. E.; Soares, J. A.; Swearingen, M. C.; Vross, M. A.; Young, G. M.; Ahmer, B. M., *Salmonella enterica* serovar Typhimurium

- can detect acyl homoserine lactone production by *Yersinia enterocolitica* in mice. *Journal of bacteriology* **2010**, 192 (1), 29-37.
63. Noel, J. T.; Joy, J.; Smith, J. N.; Fatica, M.; Schneider, K. R.; Ahmer, B. M.; Teplitski, M., Salmonella SdiA recognizes N-acyl homoserine lactone signals from *Pectobacterium carotovorum* in vitro, but not in a bacterial soft rot. *Molecular plant-microbe interactions : MPMI* **2010**, 23 (3), 273-82.
 64. Nguyen, Y.; Sperandio, V., Enterohemorrhagic *E. coli* (EHEC) pathogenesis. *Frontiers in cellular and infection microbiology* **2012**, 2, 90.
 65. Mao, S.; Zhang, M.; Liu, J.; Zhu, W., Characterising the bacterial microbiota across the gastrointestinal tracts of dairy cattle: membership and potential function. *Scientific reports* **2015**, 5, 16116.
 66. Lindsay, A.; Ahmer, B. M., Effect of sdiA on biosensors of N-acylhomoserine lactones. *Journal of bacteriology* **2005**, 187 (14), 5054-8.
 67. Cai, W.; Guner, H.; Gregorich, Z. R.; Chen, A. J.; Ayaz-Guner, S.; Peng, Y.; Valeja, S. G.; Liu, X.; Ge, Y., MASH Suite Pro: A Comprehensive Software Tool for Top-Down Proteomics. *Molecular & cellular proteomics : MCP* **2016**, 15 (2), 703-14.
 68. Lee, J. H.; Lequette, Y.; Greenberg, E. P., Activity of purified QscR, a *Pseudomonas aeruginosa* orphan quorum-sensing transcription factor. *Molecular microbiology* **2006**, 59 (2), 602-9.